

# **A Validated Molecular Docking Study of Lipid–Protein Interactions**

Rajyalakshmi Gaddipati

College of Engineering and Science

Victoria University

Submitted in fulfillment of the requirements of the degree of

Doctor of Philosophy

September, 2015

To my mother, father, husband, mother-in-law and children, with all  
my love and respect

## **Abstract**

The interaction of proteins with lipids is an important aspect of research as it plays a main role in various biological responses such as metabolic pathways, signal transduction and in drug discovery. Proteins that take part in the treatment of different diseases act as drug targets and hence research is ongoing to find new series of ligands of medicinally significant proteins. Few such proteins, peroxisome proliferator activated receptors (PPARs), retinoid receptors, cannabinoid receptors (CB1 and CB2), lipoxygenase (LOX), cyclooxygenases (COXs) were selected for the author's study due to their therapeutic role to act as pharmacological targets. The existing ligands for these protein targets are causing some side effects. For example, thiazolidinediones are the currently used ligands for PPARs. Thiazolidinediones bind to PPARs and used in the treatment of diabetes. However, this treatment results in obesity. Similarly, the use of Nonsteroidal Anti-inflammatory Drugs (NSAIDs) like aspirin and ibuprofen lead to stomach or gastrointestinal ulcers, heartburn, headache and dizziness. Hence, a set of ligands which have a significant role in the treatment of diseases were selected and compared for their binding affinities towards the design of a new series of drugs.

In order to find the new series of ligands of the above proteins, three groups of lipid ligands— tocotrienols ( $\alpha$ ,  $\beta$ ,  $\gamma$  and  $\delta$  tocotrienols), omega 3 fatty acids (Docosahexaenoic acid (DHA), Eicosapentaenoic acid (EPA)) and endocannabinoids (anandamide and 2-arachidonyl glycerol)—were tested for their ability to bind to PPARs, CBs and COX-2. Two molecular docking programs, AutoDock and Glide, were used to study the above lipid-protein interactions. The stability of docked complexes was tested through molecular dynamic simulations. Further, the *in silico* results were validated with *in vitro* experimental results.

The three groups of lipid ligands were provided same conditions in both *in vitro* and *in silico* experiments. Still, omega 3 fatty acids have shown strong interactions with PPARs and retinoid receptors. This is because of the ligand binding cavity of PPARs and retinoid receptors that accommodates polyunsaturated fatty acids better than the other ligands. Among the fatty acids, omega 3 fatty acids possess most potent immunomodulatory activities and among omega 3 fatty acids DHA and EPA are biologically more potent. Furthermore, DHA and EPA have anti-inflammatory and cancer preventing properties.

COX-2 also has shown strong binding interactions with DHA in both virtual and wet laboratory experiments compared to the other ligands. Next to omega 3 fatty acids, endocannabinoids have exhibited strong affinity with COX-2. Tocotrienols did not show favorable binding interactions with cyclooxygenases due to their orientation and structure which failed to fit into the binding pocket of cyclooxygenases. The ligand binding cavity of COX-2 is larger than COX-1 and hence COX-2 has shown strong binding interactions with the ligands compared to COX-1. Endocannabinoids have shown strong binding interactions with both cannabinoid receptors compared to the other two groups of lipid ligands.

A web-based validated tool, *Lipro Interact* was developed with the results of all the above lipid-protein interactions. The purpose of *Lipro Interact* was to provide the author's study of 80 lipid-protein interactions for global use. *Lipro Interact* provided the detailed information on the binding affinities of each lipid-protein interaction along with the microscopic atomic interactions, bond distances and ligand binding sites. The advantage of *Lipro Interact* is that all the lipid-protein interacting studies included were downloadable in image form. Further, *Lipro Interact* allows the users to download the PDB files of the above lipid-protein interactions. Future versions of *Lipro Interact* can calculate the binding affinity for any pair of protein and ligand.

## **Student Declaration**

“I, Rajyalakshmi Gaddipati, declare that the PhD thesis entitled “**The Study of Lipid-Protein Interactions towards the Design of Lipro Interact- A Validated Web based Tool**” is no more than 100,000 words in length including quotes and exclusive of tables, figures, appendices, bibliography, references and footnotes. This thesis contains no material that has been submitted previously, in whole or in part, for the award of any other academic degree or diploma. Except where otherwise indicated, this thesis is my own work”.

Signature: Rajyalakshmi. G

Date: 03/09/2015

## **Acknowledgements**

First, I would like to thank my Master and God for everything. I would like to thank my husband who was with me all the times providing his support. My full respect and thanks to my mother and mother-in-law who helped me in looking after my kids during my PhD studies. I would like to thank my daughters who did not ever disturb me while I am studying. I would like to extend my deep thanks and gratitude to all the people who contributed to enrich my knowledge and improve my competencies.

I am grateful to my principal supervisor Dr. Gitesh Raikundalia who guided me throughout my project and provided me with his valuable comments and advises. Further, I would like to thank my co-supervisor Dr. Michael Mathai without whose encouragement and support, this research would not have been completed. I would like to thank Dr. John Orbell for his valuable guidance provided at the beginning stages of my project. I would like to extend my deep thanks to Dr. Mike Kuiper for providing his suggestions required for the entire project. I would like to thank Dr. Elizabeth Yuriev for her help in guiding me in molecular docking techniques.

I would like to extend my thanks to Dr. Phil Beart for giving me permission to work with Howard Florey Laboratories. I would like to thank Dr. Linda Lau for supervising my project for the period of my wet laboratory experiments at Howard Florey Institute. I would like to thank Victoria University for giving me the scholarship for my project. I would like to thank Howard Florey Institute for allowing me to conduct my wet laboratory experiment in Beart lab. Finally, I would like to thank all my peers, for all the fun we have had together in the last four years.

## List of Publications

Gaddipati, R.S., Raikundalia, G.K., & Mathai, M.L. (2012). Towards the Design of PPAR Based drugs Using Tocotrienols as Natural Ligands. Paper presented at the International Conference on Engineering and Science, Beijing.

Gaddipati, R.S., Raikundalia, G.K., & Mathai, M.L. (2014). Dual and selective lipid inhibitors of cyclooxygenases and lipoxygenase: a molecular docking study. *Medicinal Chemistry Research*, 23 (7), 3389-3402.

Gaddipati, R.S, Raikundalia, G.K., & Mathai, M.L. (2014). Comparison of AutoDock and Glide towards the Discovery of PPAR Agonists. *International Journal of Bioscience, Biochemistry and Bioinformatics*, 4 (2), 100-105.

## Table of Contents

<b>Chapter 1 : Thesis overview.....</b>	<b>21</b>
<i>1.1. Introduction.....</i>	<i>21</i>
<i>1.2. Research Question.....</i>	<i>25</i>
<i>1.2.1. Gaps and Limitations of Previous Research.....</i>	<i>27</i>
<i>1.3. Aims of this Research .....</i>	<i>30</i>
<i>1.4. Originality and Uniqueness of the Research.....</i>	<i>32</i>
<i>1.5. Significance of the Research .....</i>	<i>34</i>
<i>1.6. Organization of the Thesis .....</i>	<i>36</i>
<b>Chapter 2 : Literature Review.....</b>	<b>39</b>
<i>2.2. Ligand-Receptor Interactions.....</i>	<i>41</i>
<i>2.3. Lipid Ligands.....</i>	<i>42</i>
<i>2.3.1. Tocotrienols .....</i>	<i>43</i>
<i>2.3.2. Omega 3 Fatty Acids.....</i>	<i>48</i>
<i>2.3.3. Endocannabinoids.....</i>	<i>52</i>
<i>2.4. Target Proteins.....</i>	<i>56</i>
<i>2.4.1. Therapeutic Proteins and Their Significance .....</i>	<i>58</i>
<i>2.4.2. Mutations in Target Proteins .....</i>	<i>61</i>
<i>2.4.2.1. Mutations in PPAR-<math>\alpha</math> .....</i>	<i>63</i>
<i>2.4.2.2. Mutations in PPAR-<math>\gamma</math> isoform1 .....</i>	<i>63</i>
<i>2.4.2.3. Mutations in PPAR-<math>\gamma</math> isoform2 .....</i>	<i>64</i>

<i>2.4.2.4. Mutations in SXR .....</i>	64
<i>2.4.2.5. Mutations in RXR-<math>\alpha</math>.....</i>	64
<i>2.4.2.6. Mutations in RXR-<math>\gamma</math>.....</i>	65
<i>2.4.2.7. Mutations in RAR-<math>\alpha</math>.....</i>	65
<i>2.4.2.8. Mutations in FXR.....</i>	65
<i>2.4.3. Pathways of Target Proteins.....</i>	66
<i>2.4.4. Active Sites of Target Proteins.....</i>	68
<i>2.5. Bioinformatics Tools to Assess the Lipid-Protein Interactions.....</i>	71
<i>2.5.1. Lipid Structural Databases and Tools .....</i>	72
<i>2.5.2. Protein Structural Databases.....</i>	74
<i>2.5.3. Bioinformatics Tools to Study the Active Site of Proteins.....</i>	76
<i>2.5.4. Molecular Docking Tools for the Study of Lipid-Protein Interactions .....</i>	78
<i>2.5.5. Molecular Dynamic Simulations.....</i>	82
<i>2.5.6. Experimental Validation .....</i>	83
<i>2.6. Novelty and Uniqueness of Contribution .....</i>	84
<i>2.7. Conclusion.....</i>	86
<b>Chapter 3: Bioinformatic and Biochemical Methods to Create <i>Lipro Interact</i> Software .....</b>	<b>88</b>
<i>3.1. Introduction .....</i>	88
<i>3.2. Methodology Framework .....</i>	89
<i>3.2.1. Biochemical Component .....</i>	91
<i>3.2.2. <i>Lipro Interact</i> .....</i>	91
<i>3.3. Selection of Molecular Docking Tool.....</i>	92
<i>3.4. Molecular Docking Studies using AutoDock.....</i>	93

<i>3.4.1. Ligand Preparation.....</i>	<i>94</i>
<i>3.4.2. Protein Preparation .....</i>	<i>95</i>
<i>3.4.3. Receptor Grid Generation .....</i>	<i>99</i>
<i>3.4.4. Docking with AutoDock .....</i>	<i>100</i>
<i>3.5. Molecular Docking Studies using Glide.....</i>	<i>104</i>
<i>3.5.1. Ligand Preparation.....</i>	<i>105</i>
<i>3.5.2. Protein Preparation .....</i>	<i>106</i>
<i>3.5.3. Receptor Grid Generation .....</i>	<i>107</i>
<i>3.5.4. Docking Studies.....</i>	<i>108</i>
<i>3.5.5. Validation of Docking Results.....</i>	<i>108</i>
<i>3.6. Molecular Dynamic Simulations.....</i>	<i>109</i>
<i>3.6.1. Theory of MD Simulations .....</i>	<i>109</i>
<i>3.6.2. System Building.....</i>	<i>111</i>
<i>3.6.3. Minimization .....</i>	<i>113</i>
<i>3.6.4. Molecular Dynamics .....</i>	<i>115</i>
<i>3.7. Scintillation Proximity Assay .....</i>	<i>115</i>
<i>3.7.1. Preparation of SPA System .....</i>	<i>116</i>
<i>3.7.2. Normalization and Standardization of MicroBeta Trilux .....</i>	<i>116</i>
<i>3.7.3. Saturation Binding Assay.....</i>	<i>117</i>
<i>3.7.4. Competitive Binding Assay .....</i>	<i>119</i>
<i>3.8. Developing Lipro Interact.....</i>	<i>120</i>
<i>3.9. Conclusion.....</i>	<i>121</i>

**Chapter 4 : Potential Ligands of PPARs and Retinoid Receptors ..... 123**

<i>4.1. Introduction .....</i>	<i>124</i>
<i>4.2. DHA and EPA as Potential PPAR agonists .....</i>	<i>125</i>
<i>    4.2.1. Redocking as a Docking Validation Method.....</i>	<i>127</i>
<i>    4.2.2. Molecular Docking of PPARs with Lipid Ligands using AutoDock .....</i>	<i>130</i>
<i>    4.2.3. Molecular Docking of PPARs with Lipid Ligands using Glide .....</i>	<i>130</i>
<i>    4.2.4. MD Simulation of Top Ranked Poses of PPARs .....</i>	<i>142</i>
<i>4.3. Comparison of AutoDock and Glide .....</i>	<i>149</i>
<i>4.4. RAR-<math>\gamma</math> and RXR-<math>\alpha</math> .....</i>	<i>156</i>
<i>    4.4.1. Current Retinoid Therapies and their Limitations .....</i>	<i>157</i>
<i>    4.4.2. New Series of Ligands for RAR-<math>\gamma</math> and RXR-<math>\alpha</math> .....</i>	<i>158</i>
<i>4.5. Comparison of AutoDock and Glide Docking Results .....</i>	<i>168</i>
<i>4.6. Conclusion .....</i>	<i>170</i>

**Chapter 5 : Dual and Selective Lipid Ligands of Cyclooxygenase and Lipoxygenase ..... 173**

<i>5.1. Introduction .....</i>	<i>174</i>
<i>5.2. Towards the Discovery of Anti-Inflammatory Drugs .....</i>	<i>175</i>
<i>    5.2.1. Molecular Docking Studies using AutoDock .....</i>	<i>176</i>
<i>    5.2.2. Molecular Docking Studies using Glide .....</i>	<i>180</i>
<i>    5.2.3. Ligand Binding Sites of COX-1 and COX-2 .....</i>	<i>186</i>
<i>    5.2.4. Receiver Operating Characteristic Curve .....</i>	<i>189</i>
<i>    5.2.5. Molecular Dynamic Simulations.....</i>	<i>192</i>
<i>5.3. Comparison of AutoDock and Glide Docking Results .....</i>	<i>197</i>

<i>5.4. Conclusion</i> .....	202
------------------------------	-----

## **Chapter 6 : Poteintial Ligands of Cannabinoid Receptors .....** 204

<i>6.1. Introduction</i> .....	204
--------------------------------	-----

<i>6.2. Cannabinoid Receptors as Therapeutic Targets</i> .....	206
--	-----

<i>6.3. New Series of Cannabinoid Ligands</i> .....	207
---	-----

<i>6.3.1. Findings of AutoDock</i> .....	207
--	-----

<i>6.3.2. Findings of Glide Docking</i> .....	210
---	-----

<i>6.4. Comparison of AutoDock and Glide for CB1 and CB2</i> .....	216
--	-----

<i>6.5. Conclusion</i> .....	219
------------------------------	-----

## **Chapter 7 : Scintillation proximity Assay.....** 221

<i>7.1. Introduction</i> .....	221
--------------------------------	-----

<i>7.1.1. Principle of the Assay</i> .....	222
--	-----

<i>7.1.2. Development of Assay</i> .....	224
--	-----

<i>7.2. Results and Calculations</i> .....	225
--	-----

<i>7.2.1. Binding Theory: The Law of Mass Action</i> .....	228
--	-----

<i>7.2.2. Saturation Binding Analysis</i> .....	231
---	-----

<i>7.2.3. Competitive Binding Analysis</i> .....	238
--	-----

<i>7.3. Discussion</i> .....	246
------------------------------	-----

<i>7.4. Conclusion</i> .....	255
------------------------------	-----

## **Chapter 8 : The Design of *Lipro Interact* .....** 257

<i>8.1. Introduction</i> .....	257
--------------------------------	-----

<i>8.2. Development Methodology</i> .....	258
---	-----

<i>8.2.1. Hardware Requirements .....</i>	259
<i>8.2.2. Software System Attributes.....</i>	259
<i>8.2.3. Performance Requirements.....</i>	259
<i>8.3. Review of Implementation Issues .....</i>	260
<i>8.3.1. Implementation Environment.....</i>	260
<i>8.3.2. Development Platform .....</i>	260
<i>8.3.3. Windows Platform Framework (.NET) and Programming Language (C#).....</i>	261
<i>8.3.4. Front End UI Framework (.NET Tool kit) .....</i>	262
<i>8.3.5. Programming Environment.....</i>	263
<i>8.4. Design of Lipro Interact.....</i>	264
<i>8.4.1. Software Architecture .....</i>	266
<i>8.4.2. Design of Lipro Interact.....</i>	266
<i>8.4.3. Results Analysis in Bioinformatic Component.....</i>	276
<i>8.4.4. Results Analysis in Biochemical Component .....</i>	285
<i>8.4.5. Code Used to Develop Lipro Interact .....</i>	286
<i>8.4.6. Data Exceptions .....</i>	289
<i>8.5. Structure of Lipro Interact.....</i>	289
<i>8.6. Conclusion .....</i>	290
<b>Chapter 9 : Conclusions and Future Work .....</b>	<b>292</b>
<i>9.1. Introduction .....</i>	292
<i>9.2. Key Contributions of the Research.....</i>	294
<i>9.3. Future Work.....</i>	298
<i>Abbreviations.....</i>	302

<i>References</i> .....	304
<i>Appendices</i> .....	328
<i>Appendix-A</i> .....	328
<i>Appendix-B</i> .....	329
<i>Appendix-C</i> .....	330
<i>Appendix-D</i> .....	332
<i>Appendix-E</i> .....	334
<i>Appendix-F</i> .....	336
<i>Appendix-G</i> .....	337
<i>Appendix-H</i> .....	339
<i>Appendix-I</i> .....	341
<i>Appendix-J</i> .....	342
<i>Appendix-K</i> .....	362
<i>Appendix-L</i> .....	397
<i>Appendix-M</i> .....	423

## Table of Figures

Figure 2.1 Structure of $\alpha$ -tocotrienol .....	43
Figure 2.2 Structure of $\beta$ -tocotrienol.....	44
Figure 2.3 Structure of $\delta$ -tocotrienol.....	44
Figure 2.4 Structure of $\gamma$ -tocotrienol.....	45
Figure 2.5 Known Targets of tocotrienols with different targets and enzymes .....	48
Figure 2.6 Structure of DHA.....	49
Figure 2.7 Structure of EPA.....	49

Figure 2.8 Known targets of omega 3 fatty acids with different targets and enzymes .....	52
Figure 2.9 Structure of anandamide .....	53
Figure 2.10 Structure of 2AG .....	53
Figure 2.11 Known targets of endocannabinoids with different targets and enzymes .....	56
Figure 2.12 Screen shot of downloading three dimensional lipid structures .....	74
Figure 3.1 Methodology Framework .....	90
Figure 3.2 System Building of LOX-BTT .....	112
Figure 3.3 Minimization of LOX-BTT .....	114
Figure 4.1 Redocking of PPAR- $\alpha$ with Crystal Ligand CTM.....	127
Figure 4.2 Redocking of PPAR- $\delta$ with Crystal Ligand D-32 .....	128
Figure 4.3 Redocking of PPAR- $\gamma$ with Crystal Ligand CTM.....	129
Figure 4.4 Interaction of PPAR- $\alpha$ with DHA .....	130
Figure 4.5 Interaction of PPAR- $\alpha$ with $\alpha$ -tocotrienol .....	132
Figure 4.6 Interaction of PPAR- $\delta$ with EPA.....	134
Figure 4.7 Interaction of PPAR- $\delta$ with $\delta$ -tocotrienol.....	135
Figure 4.8 Interaction of PPAR- $\gamma$ with EPA.....	136
Figure 4.9 Interaction of DHA with PPAR- $\alpha$ .....	138
Figure 4.10 Ligplot diagram of PPAR- $\alpha$ with DHA.....	139
Figure 4.11 Interaction of PPAR- $\delta$ with DHA.....	140
Figure 4.12 LigPlot diagram of PPAR- $\gamma$ with DHA.....	141
Figure 4.13 Interaction of PPAR- $\gamma$ with DHA.....	142
Figure 4.14 RMSD curve of PPAR- $\alpha$ with DHA in 2ns time period.....	143
Figure 4.15 RMSD curve of PPAR- $\alpha$ with DHA in 4ns time period.....	144
Figure 4.16 RMSF curve of PPAR- $\alpha$ with DHA .....	144
Figure 4.17 RMSD curve of PPAR- $\beta$ with DHA.....	146
Figure 4.18 RMSF curve of PPAR- $\beta$ with DHA .....	147
Figure 4.19 RMSD curve of PPAR- $\gamma$ with DHA.....	148
Figure 4.20 RMSF curve of PPAR- $\gamma$ with DHA.....	149

Figure 4.21 Comparison of Binding Energies of PPAR- $\alpha$ in AutoDock and Glide .....	154
Figure 4.22 Comparison of Binding Energies of PPAR $\delta$ in AutoDock and Glide .....	155
Figure 4.23 Comparison of Binding Energies of PPAR- $\gamma$ in AutoDock and Glide .....	155
Figure 4.24 Binding of RAR- $\gamma$ with DHA .....	160
Figure 4.25 Binding of RXR- $\alpha$ with DHA .....	161
Figure 4.26 Binding of RAR- $\gamma$ with DHA .....	162
Figure 4.27 LigPlot diagram of RAR- $\gamma$ with DHA .....	163
Figure 4.28 Binding of RXR $\alpha$ with DHA .....	164
Figure 4.29 LigPlot of RXR $\alpha$ with DHA .....	164
Figure 4.30 RMSD curve of the docked complex RAR- $\gamma$ -DHA .....	166
Figure 4.31 RMSF plot of the docked complex RAR- $\gamma$ -DHA .....	167
Figure 4.32 RMSD curve of the docked complex RXR- $\alpha$ -DHA .....	167
Figure 4.33 RMSF plot of the docked complex RXR- $\alpha$ -DHA .....	168
Figure 4.34 Comparing AutoDock and Glide for RAR- $\gamma$ and RXR- $\alpha$ .....	169
Figure 4.35 RAR- $\gamma$ : AutoDock Vs Glide .....	169
Figure 4.36 RXR- $\alpha$ : AutoDock Vs Glide .....	170
Figure 5.1 Interaction of COX-1 with EPA .....	177
Figure 5.2 Interaction of COX-2 with DHA .....	178
Figure 5.3 Interaction of LOX with $\beta$ -tocotrienol .....	179
Figure 5.4 Ligand Interaction: COX-1-EPA .....	181
Figure 5.5 Ligand Interaction: COX-2-DHA .....	185
Figure 5.6 Ligand Interaction: LOX- $\beta$ tocotrienol .....	185
Figure 5.7 Ligand Binding Site of COX-1 .....	187
Figure 5.8 Ligand Binding Site of COX-2 .....	188
Figure 5.9 LigPlot imgage of COX-1 binding to DHA .....	188
Figure 5.10 LigPlot imgage of COX-1 binding to DHA .....	189
Figure 5.11 ROC curve for the enzyme COX-1 .....	191
Figure 5.12 ROC curve for the enzyme COX-2 .....	191

Figure 5.13 ROC curve for the enzyme LOX .....	192
Figure 5.14 RMSD Plot of COX-1-EPA Docked Complex .....	193
Figure 5.15 RMSF Plot of COX-1-EPA Docked Complex .....	194
Figure 5.16 RMSD Plot of COX-2-DHA Docked Complex .....	194
Figure 5.17 RMSF Plot of COX-2-DHA Docked Complex .....	195
Figure 5.18 RMSD Plot of LOX- $\beta$ TT Docked Complex.....	195
Figure 5.19 RMSF Plot of LOX- $\beta$ TT Docked Complex .....	196
Figure 5.20 COX-1, COX-2 & LOX: AutoDock Vs Glide .....	197
Figure 5.21 COX-1: AutoDock Vs Glide .....	200
Figure 5.22 COX-2: AutoDock Vs Glide .....	201
Figure 5.23 LOX: AutoDock Vs Glide.....	201
Figure 6.1 Binding of Anandamide to CB1 .....	208
Figure 6.2 Binding of anandamide to CB2 .....	210
Figure 6.3 Binding of 2AG to CB1.....	211
Figure 6.4 Interactions of 2AG with CB1.....	212
Figure 6.5 Binding of Anandamide with CB2 .....	213
Figure 6.6 Interactions of 2AG with CB2.....	214
Figure 6.7 Comparison of AutoDock and Glide for CB1 and CB2 .....	216
Figure 6.8 Comparison of AutoDock and Glide for all the ligands with CB1.....	216
Figure 6.9 Comparison of AutoDock and Glide for all the ligands with CB2.....	217
Figure 7.1 SPA using flash plates .....	223
Figure 7.2 Error values in the calculation of $K_d$ and $K_i$ .....	230
Figure 7.3 Total binding of PPAR- $\gamma$ with C <sup>14</sup> DHA .....	232
Figure 7.4 Specific binding of PPAR- $\gamma$ with C <sup>14</sup> DHA.....	234
Figure 7.5 Saturation binding of COX-2 with C <sup>14</sup> DHA at different times .....	236
Figure 7.6 Total binding of COX-2 with C <sup>14</sup> DHA.....	236
Figure 7.7 Specific binding of COX-2 with C <sup>14</sup> DHA .....	238
Figure 7.8 Binding of C <sup>14</sup> EPA to PPAR- $\gamma$ in presence of unlabeled DHA.....	241

Figure 7.9 Competitive binding of PPAR- $\gamma$ .....	242
Figure 7.10 Competitive binding of COX-2 with labelled DHA and unlabeled arachidonic acid .....	243
Figure 7.11 Competitive binding of COX-2 with labelled DHA and unlabeled arachidonic acid .....	245
Figure 7.12 COX-2-Competitive Binding .....	246
Figure 7.13 K <sub>i</sub> values from AutoDock .....	247
Figure 8.1 Downloading the information from <i>Lipro Interact</i> .....	264
Figure 8.2 Functionality of <i>Lipro Interact</i> .....	265
Figure 8.3 Architecture of <i>Lipro Interact</i> .....	266
Figure 8.4 Welcome Page of <i>Lipro Interact</i> .....	267
Figure 8.5 Instructions on welcome page .....	268
Figure 8.6 Instructions on welcome page .....	268
Figure 8.7 List of proteins in the bioinformatic component of <i>Lipro Interact</i> .....	269
Figure 8.8 List of ligands in the bioinformatic component of <i>Lipro Interact</i> .....	270
Figure 8.9 List of protein-ligand interactions in the bioinformatic component of <i>Lipro Interact</i> .....	270
Figure 8.10 The Bioinformatic component of <i>Lipro Interact</i> .....	271
Figure 8.11 List of protein in the biochemical component of <i>Lipro Interact</i> .....	272
Figure 8.12 List of validated options in the biochemical component of <i>Lipro Interact</i> .....	272
Figure 8.13 Experimental validation of <i>Lipro Interact</i> .....	273
Figure 8.14 Binding information about PPARs .....	274
Figure 8.15 Comparing the AutoDock and Glide for Cannabinoid Receptors .....	275
Figure 8.16 Downloading PDB files.....	275
Figure 8.17 Using AutoDock binding energy in <i>Lipro Interact</i> .....	276
Figure 8.18 Using Glide Score as binding energy in <i>Lipro Interact</i> .....	277
Figure 8.19 Preparing the protein structure using VMD.....	277
Figure 8.20 Different drawing methods of VMD .....	278
Figure 8.21 Preparing ligand structure using VMD .....	279
Figure 8.22 Interacting amino acids of protein with ligand .....	280
Figure 8.23 Labelling the atoms of protein and ligand .....	281

Figure 8.24 Adjusting the image lay out.....	281
Figure 8.25 Importing the protein-ligand docked structure into Maestro suite .....	282
Figure 8.26 Generating the ligand interaction diagram .....	282
Figure 8.27 Preparing the image using LigPlot .....	283
Figure 8.28 Preparing the bar chart using Excel sheet.....	284
Figure 8.29 Comparison of AutoDock results with SPA.....	285
Figure 8.30 Comparison of Glide results with SPA.....	286
Figure 8.31 XML Source code.....	287
Figure 8.32 Code used to develop <i>Lipro Interact</i> .....	288

## **Table of Tables**

Table 2.1 Therapeutic role of targets .....	57
Table 2.2 Computational tools and databases of lipids.....	73
Table 2.3 Computational tools and databases of proteins.....	75
Table 2.4 Computational tools and databases for the study of ligand binding site of proteins.....	77
Table 2.5 Computational tools and databases for the study of lipid-protein interaction.....	80
Table 3.1 Target proteins and lipid ligands.....	91
Table 3.2 Protein Input Structure Information.....	106
Table 4.1 Lowest Binding Energies of PPAR- $\alpha$ calculated by AutoDock .....	131
Table 4.2 Binding affinities of PPAR- $\beta$ with lipid ligands calculated by AutoDock .....	132
Table 4.3 Binding affinities of PPAR- $\gamma$ with Lipid Ligands calculated by AutoDock.....	135
Table 4.4 Glide Score of PPAR- $\alpha$ with Lipid Ligands .....	138
Table 4.5 Glide Score of PPAR- $\delta$ with Lipid Ligands .....	140
Table 4.6 Glide Score of PPAR- with lipid ligands .....	141
Table 4.7 Interacting amino acids of PPARs with lipid ligands in AutoDock and Glide .....	151
Table 4.8 Binding Affinities of RAR- $\gamma$ and RXR- $\alpha$ in AutoDock.....	159
Table 4.9 Glide Score of RAR- $\gamma$ and RXR- $\alpha$ .....	162
Table 5.1 Binding affinities of COX-1 with lipid ligands in AutoDock.....	177

Table 5.2 Binding affinities of COX-2 with lipid ligands in AutoDock.....	179
Table 5.3 Binding affinities of LOX with lipid ligands in AutoDock .....	180
Table 5.4 Glide score of COX-1 with eight lipid ligands .....	180
Table 5.5 Glide Score of COX-2 with eight lipid ligands.....	183
Table 5.6 Glide Score of LOX with eight lipid ligands .....	186
Table 5.7 Common Interacting amino acids in AutoDock and Glide.....	198
Table 6.1 Binding Affinities of CB1 with eight lipid ligands in AutoDock .....	208
Table 6.2 Binding Affinities of CB2 with eight lipid ligands in AutoDock .....	209
Table 6.3 Glide Score of CB1 with lipid ligands.....	212
Table 6.4 Glide Score of CB2 with lipid ligands.....	215
Table 6.5 Interacting amino acids of CB1 and CB2 in both AutoDock and Glide.....	218
Table 7.1 Total binding of PPAR- $\gamma$ with C <sup>14</sup> DHA.....	232
Table 7.2 Specific binding of PPAR- $\gamma$ with C <sup>14</sup> DHA.....	233
Table 7.3 Total binding of COX-2 with C <sup>14</sup> DHA.....	237
Table 7.4 Specific binding of COX-2 with C <sup>14</sup> DHA .....	237
Table 7.5 Binding of C <sup>14</sup> EPA to PPAR- $\gamma$ in presence of unlabeled DHA.....	240
Table 7.6 Competitive binding of COX-2 with labelled DHA and unlabeled arachidonic acid.....	243
Table 7.7 Difference between AutoDock K <sub>i</sub> and experimental K <sub>i</sub> .....	248
Table 7.8 Validation of Glide docking with SPA results.....	250
Table 8.1 Hardware Specification.....	259

# Chapter 1

## Thesis Overview

### 1.1. Introduction

Two or more atoms join together to form molecules. If these molecules are present in a living organism, they are termed as *biomolecules*. Biomolecules can be either large (macro molecules) or small. Usually, macromolecules have a complex three-dimensional structure. Proteins, lipids, carbohydrates and nucleic acids are some of the biomolecules present in a living organism. The structure, properties and function of these biomolecules is important in maintaining proper health. However, the structure, properties and function of biomolecules change when they interact with each other. Physical or chemical interaction between two biomolecules is called *a biomolecular interaction*.

When two of the above mentioned biomolecules bind together or interact with each other, they trigger biological responses which play an important role in clinical research. Hence it is necessary to understand the mechanism involved in the binding of two biomolecules. Moreover, due to the complex three dimensional structures of biomolecules, studying their interaction needs more focus. Depending on the strength and significance of binding between two biomolecules, their interaction is used in different research areas like drug discovery, clinical research, health informatics etc. (Huber & Muller, 2006). The significance of any

biomolecular interaction is determined by the role played by these biomolecules in health and disease.

Proteins are macromolecules and are one of the building blocks of life. The three-dimensional structure of protein is complex with many amino acids. Proteins are used as drug targets due to their significant role in the metabolic or signalling pathway specific to a disease condition. Basically, a *drug* is an organic molecule that activates or inhibits the function of a protein. In order to design drugs, proteins are either activated or inhibited with small molecules known as *ligands*. Therefore, to design a new series of drugs, the study of protein-ligand interactions plays a crucial role. Drugs are designed based on the ligand binding site which either activate or inhibit the protein function (Anderson, 2003). Designing drugs using a ligand-based approach is called *ligand-based drug design* (Aparoy et al., 2012). If the ligand is a lipid binding to protein, this is a *lipid-protein interaction* which is ultimately used for the design of a new generation of drugs.

In order to consider a particular lipid-protein interaction for the drug designing the mechanism of this lipid-protein interaction has to be analyzed further. To achieve this, the effect of lipid-protein interaction should be studied *in vivo*. To consider a particular ligand as an effective drug candidate, the action of ligand has to be studied *in vivo*. Further the mechanism of action of ligand and the effect of ligand on a particular biological reaction has to be analyzed. The metabolism of ligand-protein interaction has to be studied.

Lipids are a group of organic compounds that are insoluble in water and soluble in organic solvents. Lipids, commonly known as fats are a group of naturally occurring biomolecules. Fatty acids, waxes, fat soluble vitamins A, D, E and K belong to lipids. Lipids are one of the energy reserves of the body and supply it when the body is in need. They also play an important role in signalling by interacting with various enzymes and receptors. Tocotrienols,

omega 3 fatty acids and endocannabinoids are three important groups of lipids in health and disease. These three classes of lipids have a relationship between them in terms of their binding affinities to the same enzyme or receptor, yet they induce very different biological outcomes. This commonality of binding makes it important to be able to determine the affinity of lipids within each of these lipid classes to different signalling targets. The research on the interactions of these classes of lipids with different receptors is interesting as the three lipid groups play a vital role in cancer research, bone health, atherosclerosis and other cardiovascular diseases.

Ligand-receptor interactions play an important role in many biological processes as well as in the treatment of many diseases (Bongrand, 1999). The strength of ligand-receptor binding depends on several factors including the structures of the ligand and receptors. The type of ligand-receptor interaction is based on the type of biomolecules involved. For example, if the ligand is protein and the receptor is also a protein then it is protein-protein interactions. Similarly, if the ligand is a lipid and the receptor is protein then it is termed as lipid-protein interaction. However, in the case of enzymes the ligand is usually considered as a substrate and this type of interaction is known as enzyme-substrate interaction. Whatever is the type of interaction, a detailed mechanism involved in binding of both the molecules has to be more focussed.

Ligand-receptor interactions have become the fundamental basis for the design of drugs. Drug designing is also known as ligand designing, because it involves the design of a small molecule that binds tightly to its target (Tollenaere, 1996). The strength of binding between ligand and receptor is measured in terms of binding affinity between them. In other words binding affinity or binding energy is the direct measure of the strength of binding between ligand and receptor. Furthermore, the binding affinity between the ligand and receptor are

calculated through various biological experiments. However, the microscopic atomic interactions are better studied using bioinformatic techniques.

There are two fundamental events that influence ligand-receptor binding. First, there must be an interaction between ligand and receptor which result in the binding of ligand to receptor. This is called the affinity. Second, the effect of ligand on the receptor to initiate a biological response, which is termed as efficacy (Strange, 2008). Agonist is a small molecule (ligand) which is usually a chemical binds to a receptor and activates the receptor resulting in a biological response. Antagonist is also a ligand that blocks the action of a receptor. An agonist can be a full agonist, partial agonist or inverse agonist. Full agonists are the compounds that bind to the receptor and result in the activation of receptor and elicit the maximal response of the receptor system (Guzman, 2015). In the other words full agonists have high efficacy and produce full response while occupying a relatively low portion of receptors. Partial agonists have lower efficacy than full agonists. Partial agonists also activate the receptor and produce sub-maximal response (Guzman, 2015). Inverse agonists bind to the receptor at the same site where agonist binds and result in the opposite pharmacological effect to that of the agonist (Guzman, 2015). Antagonists bind to the receptor and inhibit the action of receptor. The author's study was focused on the affinity of ligand with the receptor.

With the development of computer technology, understanding the biological association of two biomolecules has now become easy. The complex three dimensional structure of proteins and ligands are now available. Hence, the atomic interactions between ligand and protein are studied in close proximity. There are different bioinformatic techniques available to study the ligand-receptor interactions. To name a few are virtual screening, molecular docking and molecular dynamic simulations (MD simulations). Comparing the virtual results with wet laboratory results improves the accuracy of results.

## 1.2. Research Question

There are several drugs available these days to treat diseases like cancer, diabetes, atherosclerosis, etc. However, there are public concerns about the side effects of drugs which are currently in use these days. For example thiazolidinediones (TZDs), the widely used anti-diabetic drugs cause some side effects such as obesity and cardiovascular risks (Malapaka et al., 2012). The use of Nonsteroidal Anti-inflammatory Drugs (NSAIDs) like aspirin and ibuprofen lead to stomach or gastrointestinal ulcers, heartburn, headache and dizziness (Smith et al., 2000). Hence the research problem is identified as the lack of effective drugs that can treat the above mentioned diseases with few or no side effects.

Furthermore, the design of a new series of drugs starts with the finding of new molecular targets. The strong binding affinity and the microscopic atomic interactions are important to analyze if a particular ligand molecule can be a potential drug candidate. At the same time virtual computational results need to be validated with the wet laboratory experimental results, because the virtual results alone are not sufficient to discover new drug targets. This implies the need of a study that provides both the microscopic atomic interactions of ligand-receptors and wet laboratory experimental validations.

Moreover, proteins such as Retinoid Xenobiotic Receptor (RXR) and Peroxisome Proliferator Activated Receptor- $\delta$  (PPAR) are biologically significant and have great medicinal values as discussed in detail in Chapter 2 Section 2.4. Finding the agonists of these targets is already in research. Still, there is a need to investigate further on these proteins for their agonism/antagonism of different ligands (Evans et al., 2004; Germain et al., 2006b).

Some ligand molecules act on two or more proteins at the same time, resulting in unwanted side effects. For example, aspirin, the most commonly used anti-inflammatory drug, blocks both Cyclooxygenase-1 (COX-1) and Cyclooxygenase-2 (COX-2), which disturbs the stomach

and kidneys (Goodsell, 2000). So there is a need to find a selective inhibitor of COX-2 which does not act on COX-1, because inhibition of COX-1 results in gastrointestinal damage. Similarly, some ligands have to act on more than one protein. For instance, if arachidonic acid does not bind to COX-2, then arachidonic acid metabolism might shunt to the Lipoxygenase (LOX) pathway, resulting in the formation of leukotrienes, and leading to inflammation and cardiovascular diseases (Hudson et al., 1993; Laufer, 2001; Rainsford, 1987; Rainsford, 1999). Hence, there is a need to find a dual inhibitor of both COX-2 and LOX.

In order to discover new series of ligands, a set of different targets need to be examined with a set of different ligands. Further, the binding affinities between each protein and ligand should be studied and their microscopic interactions have to be analyzed in detail. In addition, the binding affinity of different ligands for each protein is to be compared to find the strongest potential molecular target.

Hence the research question is

*“To identify the molecular mechanism of binding of the ligands of interest to the chosen proteins on the basis of both the characteristics of the binding/active sites and the chemical structure of the ligands”.*

The three groups of lipids—tocotrienols, omega 3 fatty acids and endocannabinoids—have commonalities of binding to different proteins. These lipid ligands have significant medicinal values and hence the study of their interaction with different proteins plays an important role in drug discovery. Moreover, these ligands being natural cause fewer side effects than synthetic ligands (Nesto et al., 2003). Furthermore, the research question is supported by the gaps and limitations of the previous research as explained in the following section.

### ***1.2.1. Gaps and Limitations of Previous Research***

The gaps and limitations of the previous research were identified as follows.

The binding site of PPARs with Docosahexaenoic acid (DHA) was studied previously through molecular docking and computer simulations (Gain & Style, 2008). However, this study performed by Gani & Style lack the experimental validation. Li et al., and Oster et al., have conducted experiments on the biological binding of PPAR- $\gamma$  with DHA (Li et al., 2005; Oster et al., 2010) in a wet laboratory experiment. Both the studies have focused only on PPAR- $\gamma$  and not on other PPARs. Hence, a comparison between three types of PPARs was missing. Moreover, the study of Li et al. did not reveal the microscopic atomic interactions between PPAR- $\gamma$  and DHA. The study by Oster et al., 2010 has concluded that further work is needed to establish the mechanism of action of PPAR- $\gamma$  with DHA and EPA and the differences in the mechanism of DHA and EPA involving PPAR- $\gamma$  (Oster et al., 2010). The author's study has filled this gap of a study that compares both microscopic atomic interactions with wet laboratory experimental validations. Furthermore, the author's study is extended to some other lipid ligands and proteins along with DHA and PPARs. Stone et al., have examined the binding of PPAR- $\gamma$  with  $\gamma$ -tocotrienol (Stone et al., 2005). However, the author's study has extended to other proteins and lipid ligands apart from  $\gamma$ -tocotrienol.

RXR heterodimers are involved in multiple signalling pathways and the potential of RXR-targeted pharmacology is to be clarified. Still, there is a need for further RXR research to find out whether or not any ligands exist that can activate RXRs (Germain et al., 2006b).

PPAR- $\alpha$  is the molecular target for lipid-lowering fibrate drugs. However, the use of fibrates is limited due to low potency and restricted selectivity (Sierra et al., 2007). The anti-diabetic drugs-TZDs use PPAR- $\gamma$  as a molecular target (Malapaka et al., 2012). However, TZDs cause side effects like obesity and cardiovascular diseases (Malapaka et al., 2012). A potential

therapeutic target of PPAR- $\delta$  is under investigation (Kroemer et al., 2004). Similarly, there are limitations in current retinoid therapies. For example, Bexarotene is the first approved RXR agonist which can be used to treat all stages of cutaneous T-cell lymphoma (Zhang & Duvic, 2003). However, some adverse effects like hypertriglyceridemia, hypercholesterolemia, central hypothyroidism and headache have also been reported (Lowe & Plosker, 2000).

COX-2 and PPARs were tested previously for their binding affinities. The binding affinity of COX-2 was tested with plant secondary metabolites and not with lipid ligands as in the author's study (Huss et al., 2002). Similar to the author's study, Huss et al., also have conducted enzymatic SPA to find new COX-2 inhibitors. The study of Huss et al., has evaluated ubiquitous plant constituents for the inhibition of COX-2 catalyzed prostaglandin E2 biosynthesis. COX-2 activity was determined for 49 plant metabolites during this study.

There is an emerging need for the research on COX-LOX dual inhibitors because of their significant role in variety of cancers including prostate cancer (Pommery et al., 2004; Skelly & Hawkey, 2003). Hence, the author's study has focussed on finding dual and selective inhibitors of COX and LOX. Chronic use of COX-2 inhibitors (eg. Vioxx scandal) is linked to heart attack and stroke leading to death. Further research is needed to find selective inhibitors of COX-2 (Brown et al., 2005).

Anandamide and other endocannabinoid ligands were studied before through molecular docking (Padgett et al., 2008). The study of Padgett et al. is similar to the author's study in comparing the molecular docking results with experimental results. However, Padgett et al.'s study is different from the author's in the choice of ligands. Padgett's study has concluded that during docking, anandamide adapted certain conformations which are analogous to arachidonic acid, the substrate of COX-2. Moreover, the study was limited to the binding of

anandamide and its analogues only with CB1. The author's study included CB2 and other lipid ligands.

$\Delta 9$ -THC is the widely used synthetic cannabinoid that binds actively to cannabinoid receptors. This synthetic cannabinoid is used to treat vomiting, nausea associated with chemotherapy and as a stimulate of appetite in AIDS (Mackie, 2006). It has some analgesic properties and causes some side effects like dizziness, ataxia and blurred vision (Noyes et al., 1975). Hence there is a need to discover the new cannabinoid agonist because of the limitation of  $\Delta 9$ -THC use.

Tocotrienols have a similar structure to rosiglitazone (one of TZDs) which is a synthetic ligand of PPARs, in having a chromanol ring. TTs and rosiglitazone also resemble each other in exhibiting anti-inflammatory properties (Fang et al., 2010). The presence of polar head group and a hydrophobic tail in the structure of DHA and EPA make them act as natural agonists of PPARs (Sheu et al., 2005). It is well known through previous research done so far on cannabinoid receptors that 2AG and anandamide are endogenous ligands (Di Marzo et al., 2000 ; Padgett et al., 2008). This opens a channel to test these ligands further to be the ligands of both CB1 and CB2. There were different *in vitro* experiments conducted to study the binding of DHA and EPA with PPARs and cyclooxygenases (Funahashi et al., 2008; Hawcroft et al., 2010; Oster et al., 2010; Yang et al., 2004). Hence, it is interesting to study the microscopic atomic interactions of DHA, EPA with PPARs and cyclooxygenases using *in silico* experiments. Furthermore, these three groups (tocotrienols, omega 3 fatty acids and endocannabinoids) of lipid ligands relate to each other in their chemical structures and biological properties.

Considering the gaps and limitations of previous research, the author's research study was designed with the aims discussed in the following section.

### ***1.3. Aims of this Research***

The research in this thesis focused on lipid-protein interactions. One of the important roles of lipids is to store the energy and supply to the body whenever there is a need. Lipids are large and diverse group of naturally occurring molecules that include fats, waxes, sterols, and fat soluble vitamins such as vitamins A, D, E, K, glycerides and many more. These lipids when taken in the right amounts act as the body's energy reserves to maintain proper health. The association of these lipids with different proteins is further significant in many biological pathways, signal transductions and metabolism.

Three groups of lipids were selected as ligand molecules for the current study.

- Tocotrienols

Vitamin E is made up of four types of tocopherols and four types of tocotrienols. All four types of tocotrienols ( $\alpha$ ,  $\beta$ ,  $\gamma$  and  $\delta$ ) were included in the current study.

- Omega 3 Fatty acids

Docosahexaenoic acid (DHA) and Eicosapentanoic acid (EPA) were considered as lipid ligands for the current study.

- Endocannabinoids

From the group of endocannabinoids, 2Arachidonyl Glycerol (2AG) and anandamide were selected for the current study.

Three groups of proteins were chosen to study the interactions.

- Nuclear Receptor Family

Five targets—PPAR- $\alpha$ , PPAR- $\beta$ , PPAR- $\gamma$ , RXR- $\alpha$ , Retinoic Acid Receptor (RAR- $\gamma$ ) were considered to study their interaction with the above mentioned lipid ligands.

- Enzymes

Three enzymes, COX-1, COX-2 and LOX were selected for the current study.

- Cannabinoid Receptors

Both Cannabinoid Receptor1 (CB1) and Cannabinoid Receptor1 (CB2) were chosen to study the lipid-protein interactions.

The importance of each ligand and protein were discussed in detail in Chapter 2. In total, there are ten proteins and eight lipid ligands. Hence, the study aims on 80 lipid-protein interactions. Furthermore, the purpose of this thesis is discussed below:

1. The aim is to study the 80 lipid-protein interactions in terms of
  - their binding affinities,
  - microscopic atomic interactions between the protein and ligand,
  - the ligand binding pocket of the proteins,
  - the active site amino acids of the protein which interact with the ligand,
  - the intermolecular interactions between the ligand and protein,
  - the cross reactivity of each ligand with each protein
  - the potentiality of each ligand to be the drug candidate for each protein.
2. All the proteins selected for the current study are already involved in the design of certain drugs. For example, PPARs are the drug targets for TZDs (antidiabetic drugs); COXs are the drug targets for NSAIDs (anti-inflammatory drugs) and so on. However, these drugs have some side effects (discussed in detail in Chapters 4-6) and so the current study was designed to find new series of ligands that can act as drug candidates and cause few or no side effects. The aim is to study the potential of each ligand to be an effective drug candidate.
3. There are various molecular docking techniques available today to study the ligand-receptor interactions. However, selecting a suitable docking technique remains as a

challenge. Hence, a comparison study was conducted between two molecular docking techniques. The study was aimed to use molecular dynamic simulations to support the molecular docking results.

4. Virtual results need an experimental validation. Hence, the study conducted a wet laboratory experiment. Then, an evaluation study determined the accuracy of molecular docking by comparing the results with that of wet laboratory experimental results.
5. Finally, the aim of the study is to develop a web-based tool—*Lipro Interact*—that further illustrates all 80 lipid-protein interactions. The purpose of *Lipro Interact* is to make all the lipid-protein interactions accessible for the future research. *Lipro Interact* is designed in such a way that the binding data (for example, the binding affinity, the ligand binding site of protein, the amino acids of the protein interacting with ligand, PDB files<sup>1</sup> of protein bound to ligand etc) of all the 80 lipid-protein interactions are available for the future use by researchers.

#### ***1.4.Originality and Uniqueness of the Research***

The literature review conducted throughout this research study was used to determine the originality of this thesis. First and foremost there is no software available that provides the same information as *Lipro Interact*. Further, *Lipro Interact* proves its uniqueness in providing the detailed mechanism of lipid-protein interactions which do not exist anywhere else. The results included in *Lipro Interact* are from the author's research. After performing molecular docking, PDB files were generated for each protein binding with each ligand. These PDB files contain the ligand bound to protein at the active site. Hence, this information is useful in assessing the ligand binding pocket of each protein. Further, they are useful in understanding

---

<sup>1</sup> Protein Data Bank (PDB) format provides a standard representation of macromolecular structure

the microscopic atomic interactions between the protein and ligand. *Lipro Interact* also provides the binding affinities and interactions of the proteins with lipid ligands. These informative images were prepared as a result of this research. Moreover, the virtual results of *Lipro Interact* were validated with wet laboratory experiment, conducted as a part of this research.

The selection of proteins and lipid ligands is based on their biological significance as discussed in Chapter 2, Sections 2.3 and 2.4. After observing the studies similar to the author's, it was identified that the combination of these lipid ligands and proteins was not used in the previous research so far (Chapter 2, Section 2.6). Furthermore, this thesis study presents a novel approach to study lipid-protein interactions. Now-a-days there are many bioinformatic tools available to perform molecular docking and molecular dynamic simulations. This research study has performed a review on the available docking programs. Furthermore, the study explained a step-by-step procedure to study the ligand-receptor interactions using bioinformatic tools.

Sometimes the structure of proteins gets altered because of mutations (an alteration in the gene sequence that causes a change in protein structure). The altered protein structure results in difference in binding affinity of proteins. Hence it is worthwhile to study the possible mutations associated with each protein before considering them for drug designing. The study of this thesis has identified all possible mutations related to the proteins and were shown in the form of figures. The effects of each mutation were included in different tables for different proteins. Each figure depicts the mutations associated with each protein and the tables were provided for the detailed information on this mutation.

The methodology for this research study was designed based on the literature review performed. The docking procedure depends on the structure of each protein and ligand.

Further, the importance of any molecular docking procedure lies in the selection of active site at which the ligand binds. Hence, a detailed literature review was conducted to study the structure of protein, ligand and the active site information. Further, molecular dynamic simulations were performed with the results of docking.

A new series of ligands were proposed for the proteins based on the virtual and wet laboratory experimental results. These experimental results were shown in Figures and Tables as an evidence of originality of this thesis. Furthermore, dissociation constant ( $K_d$ ) and inhibition constant ( $K_i$ ) values for all the proteins were derived from detailed calculation (Chapter 7, Section 7.2) that determined the novelty of this research study. Nonetheless, the comparison studies were conducted between AutoDock and Glide and between virtual experimental results and wet laboratory experimental results. The comparison studies were supported by unique bar charts which are drawn from the author's experimental results.

The lipid-protein interactions were analyzed in detail from the findings of AutoDock and Glide conducted in this study. These results were further validated with the wet laboratory experiment. The conclusions and the key contributions of the author's study were derived from these experimental results.

## ***1.5. Significance of the Research***

The lipid ligands and proteins considered for this study are biologically significant to maintain proper health and control the disease (Chapter 2, Section 2.3 and 2.4). These proteins were already in use to treat several diseases like cancer, diabetes, atherosclerosis, etc. Hence, the pharmaceutical industry is paying more attention to the research of finding new series of drug candidates for these proteins. This thesis answers the questions to the binding mechanisms of these proteins with different lipid ligands. Furthermore, this study fulfilled the gaps from the previous research as it was explained in Section 1.2.1.

The importance of this research study is determined by the following reasons.

- Research on agonists of PPARs is significant as PPARs play key roles in the regulation of energy homeostasis and inflammation (Kroemer et al., 2004).
- From the discovery of synthetic compounds that activate the RXR-RXR homodimers different rexinoids have been reported. Still there is no single rexinoid with apparent subtype selectivity (Germain et al., 2006b). This issue has now become a challenge due to the presence of conserved residues in RXR Ligand Binding Pocket (LBP).
- Arachidonic acid metabolism is mediated by LOX, and would further contribute to the side effect profile observed for NSAIDs in osteoarthritis (Burnett et al., 2012). Moreover, LOXs are found to play a role in cardiovascular diseases. Hence, a single inhibitory agent that acts on both COXs and LOX is of interest to medicinal chemistry (Zheng et al., 2006).
- Cannabinoid receptors are the attractive targets for the design of therapeutic ligands, because CB1 and CB2 receptors act as the substrates for several endogenous ligands, enzymes and transporter proteins of neuromodulatory system (Mackie, 2006).
- Tocotrienols are chemically more active than tocopherols because of the unsaturated tail. Tocopherols and tocotrienols also differ in the number of methyl groups present on the chromanol ring. A previous study performed by Aggarwal, et al., suggested that tocotrienols have positive health effects on bone health, brain health, blood sugar metabolism and cancer (Aggarwal et al., 2010).
- Omega 3 fatty acids are the natural ligands of PPARs because of the presence of polar head group and a hydrophobic tail in their structures (Sheu et al., 2005). Omega 3 fatty acids prevent cancer by arresting the cell cycle and inducing apoptosis by activating phosphatase (Rafat et al., 2004). The UK dietary guidelines for

cardiovascular diseases acknowledge the importance of long-chain omega-3 fatty acids in reducing the risk of heart diseases (Ruxton et al., 2004).

- Endocannabinoids, due to their capacity in reducing inflammation, cell proliferation and cell survival could be used in cancer treatment (Sarfaraz et al., 2008). The binding of endocannabinoids to COX-2 results in various events which include cell viability, mobilization of calcium and modulation of synaptic transmission (Fowler, 2007). They alter synaptic transmission, cardiovascular system and immune system through CB1 and CB2 (Chávez et al., 2010).

Further, the microscopic interactions found from this study are the fundamental basis for the design of PPAR-based, COX-based and cannabinoid-based drugs. Moreover, the study is useful as it proposes potential ligands for several proteins. The atomic interactions between the proteins and lipid ligands are useful in analyzing the active site amino acids of each protein for each ligand. Nonetheless, *Lipro Interact* was developed from this study that provides the information on all the 80 lipid-protein interactions. Through *Lipro Interact* the study is made available for future research.

## ***1.6. Organization of the Thesis***

A detailed literature review was conducted and was explained in Chapter 2. Through literature review the biological and medicinal values of each ligand and proteins were identified. The literature review was performed to find appropriate lipid ligands and proteins for this study. Different mutations associated with proteins were identified and depicted in figures. The available bioinformatic tools and techniques for the study of lipid-protein interactions were explained in this Chapter. Furthermore, a suitable research methodology for the study was designed through the literature review. The literature review has identified the need of *Lipro Interact* software.

Chapter 3, “Bioinformatic and Biochemical Methods to Create *Lipro Interact* Software” explains the research methodology of the thesis. This Chapter discussed the significance of each method selected for the current study. Further, the thesis framework was described in this Chapter. A step-by-step procedure for each method was given in detail in this Chapter. Both the bioinformatic and biochemical methods in the study of ligand-receptor interactions were explained.

The results of molecular docking and molecular dynamic simulations were discussed from Chapter 4-6. Chapter 4, “Potential Ligands of PPARs and Retinoid Receptors” illustrated the findings from molecular docking of nuclear receptors (PPARs, RAR- $\gamma$  and RXR- $\alpha$ ) with eight lipid ligands. The Chapter discussed the side effects of existing PPAR-based, RAR and RXR-based drugs and the potentiality of eight lipid ligands to be the drug candidates of PPARs, RAR- $\gamma$  and RXR- $\alpha$ ). The Chapter also explained the comparison of molecular docking results used for the study.

Chapter 5, “Dual and Selective Lipid Ligands of Cyclooxygenase and Lipoxygenase” covered the results of molecular docking of the three enzymes COX-1, COX-2 and LOX with eight lipid ligands. The Chapter outlined the side effects of current COX and LOX-based drugs. Further, the Chapter explained the dual and selective lipid ligands of COXs and LOX.

The binding affinities of CB1 and CB2 with eight lipid ligands were discussed in Chapter 6, “Potential Ligands of Cannabinoid Receptors”. The current cannabinoid-based drugs and their side effects were also described. Further, the comparison studies of molecular docking techniques for both CB1 and CB2 with each lipid ligand were explained.

Chapter 7, “Scintillation Proximity Assay” covered the wet laboratory experiment (SPA) conducted. The Chapter was focussed on the comparison of SPA results with the molecular docking results. The binding affinities of ligand-receptors were calculated from the wet

laboratory experiment and evaluated with molecular docking results. Furthermore, the Chapter described the possibility of each ligand to be a potential drug candidate for the proteins.

The detailed design and development of *Lipro Interact* was explained in Chapter 8, “The Design of *Lipro Interact*”. The Chapter explains how the results from both the biochemical and bioinformatic components were converted into a software tool. Furthermore, this Chapter illustrated the use of *Lipro Interact*.

Chapter 9, “Conclusions” concluded the finding of the current study. The major findings from both the biochemical and bioinformatic experimental approaches were explained in this Chapter. The prospective future work of the current study was also described in this Chapter.

# Chapter 2

## Literature Review

### ***2.1. Introduction***

Lipids are group of biomolecules that store energy. They act as the structural components of cell membranes. Proteins are one of the building blocks of life. The body needs both lipids and proteins for its growth, maintenance and repair. The interaction of lipids with proteins is of high importance since they are involved in the treatment of various diseases. Due to the role of lipid-protein interactions in designing drugs for different diseases like cancer, diabetes and atherosclerosis, medicinal chemistry research is focussing more on lipid-protein interactions. The complex three dimensional structures of lipids and proteins have now become available with the recent development of bioinformatics tools and advancements in experimental techniques. Apart from the several studies performed before on different lipid-protein interactions there is still a need for further research due to the tremendous need for the pharmaceutical industry to design drugs for cancer, diabetes, atherosclerosis, obesity and inflammatory diseases. There are a number of lipids and proteins available that play a role in health and disease and different combinations of lipid versus protein interactions are yet to be studied.

Moreover, the public are concerned about the side effects of drugs which are currently in use these days. For example TZDs, the widely used anti-diabetic drugs cause some side effects such as obesity and cardiovascular risks (Malapaka et al., 2012). The use of NSAIDs like aspirin and ibuprofen lead to stomach or gastrointestinal ulcers, heartburn, headache and dizziness (Smith et al., 2000). Considering the side effects of these drugs current research has focussed on the discovery of natural agonists/antagonists that can be used in designing the new generation of drugs.

This chapter provides a comprehensive literature review for the selected ligand-protein interactions and their significance in the field of biomedicine. The literature review was aimed at three important, interesting components.

- *Lipid Ligands.* Three important groups of lipids were selected based on their chemical activity and biochemical importance. The structural features of the selected lipids were studied. The health significance of these lipids and their effective role in the treatment of different diseases were analyzed.
- *Selection of Bioinformatics Tools.* In order to specify lipid ligands as drug candidates the chemistry behind these lipid-protein interactions should be analyzed. There are many bioinformatics tools available to study the binding abilities of biomolecules. A suitable bioinformatics tool has to be selected prior to the study of lipid-protein interactions.
- *Target Proteins.* The target proteins were selected based on their medicinal significance. All the selected proteins from the current study have significant effects on the treatment of several diseases. Hence, the pharmaceutical industry is paying more attention to their research. To assess if a particular protein-lipid interaction can lead to a potential drug development the strength of their binding must be studied. In

order to select a particular protein for drug designing, the action of that drug may not be the same as predicted in the case of any mutations of the protein. Mutations associated with proteins sometimes change their structure and function, thereby greatly influencing the binding mechanism of that particular protein with a specific ligand. Hence, the mutations of the selected proteins were reviewed before dealing with the binding mechanism of the proteins.

Section 2.2 explains the history behind the ligand-receptor research. The structural features, along with the research done so far on the interaction of three groups of lipid ligands, including their limitations, were discussed in Section 2.3. The selected target proteins were reviewed for their biomedical importance and were given in detail in Section 2.4. A detailed study was conducted on the mutations connected with the structure of target proteins and was explained in Section 2.4.2. Section 2.5 is a review performed on various bioinformatics tools available to study the lipid-protein interactions. Section 2.6 explained the importance of the author's study and section 2.7 elucidated the conclusions from this chapter.

## ***2.2. Ligand-Receptor Interactions***

A *ligand* (the lipid in the study of the author) is a small chemical molecule that forms a complex with a macromolecule by binding at its active site and initiates a biological response. The macromolecule in whose binding pocket the ligand binds is called a *receptor* (protein). Since ligand-receptor binding results in a biological purpose, the study is important in many aspects. The research into ligand-receptor interactions was initially improved by three main lines of research. The structures of the majority of the ligand-receptors were available with X-ray crystallography and genetic engineering. Next, the complex mechanism of ligand-receptor interactions were easily understood with the help of computer power and simulation tools. Finally, various techniques like atomic microscopy, hydrodynamic flow and

magnetic fields made the understanding of single ligand-receptor bonds possible (Bongrand, 1999).

There are various bioinformatics tools and algorithms available to measure the binding affinity between the ligand and the receptor. Hence, there is a need for the user to select the best suitable technique for the study. Virtual screening was extensively used in the 1970s and 1980s, however, did not fulfil expectations due to its failure in computational screening of new ligands based on their structure (Shoichet, 2004). The advanced studies in the fields of computational chemistry and protein structure determination have concentrated on virtual screening and rapid mechanical docking methods. With the advent of two-dimensional and three-dimensional structures of receptors, docking methods were used more extensively (Schneider et al., 2002). The constant maintenance and update of structural databases have made the three dimensional structure of some of the proteins and lipids available. Bioinformatics tools to locate the ligand binding pocket of a protein are available now. The microscopic atomic movement of the protein during its interaction with the ligand can be studied using molecular dynamic simulations. The computer simulations can then be compared with the results of laboratory experiments.

The three groups of lipids—tocotrienols, omega 3 fatty acids and endocannabinoids—are chemically active and by binding to different proteins they initiate physiological and biological responses. Some of these lipid-protein interactions are also significant in the design of drugs for various diseases.

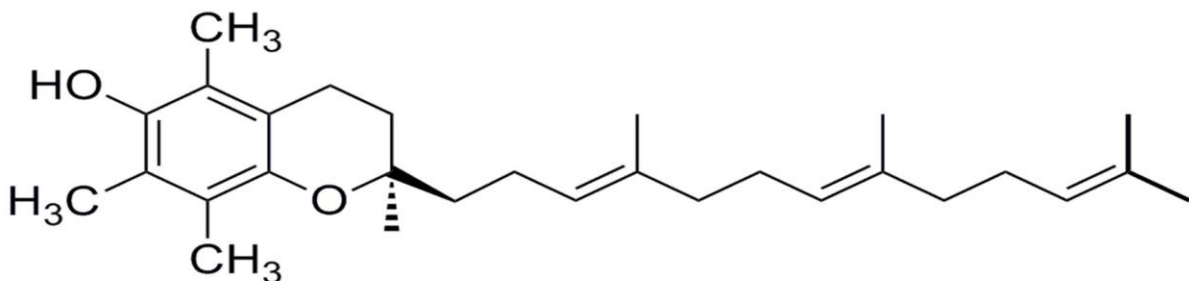
### **2.3. Lipid Ligands**

Three specific groups of lipids were selected based on their structural similarities. These three groups of lipids are related to each other in terms of their binding affinities to the same enzymes and receptors, yet they induce very different biological outcomes (Gaddipati, 2012;

Gaddipati et al., 2014ab). This commonality of binding makes it important to be able to determine the affinity of lipids within each of these lipid groups. The interaction of these three groups of lipids with various proteins plays an important role in drug discovery.

### **2.3.1. Tocotrienols**

Vitamin E exists in eight isoforms.  $\alpha$ ,  $\beta$ ,  $\gamma$  and  $\delta$  tocopherols and  $\alpha$ ,  $\beta$ ,  $\gamma$  and  $\delta$  tocotrienols. Tocopherols and tocotrienols have similar structures in possessing a chromanol ring. However, the unsaturated farnesyl side chain of tocotrienols makes them more active than tocopherols which have a saturated phytol side chain. Tocopherols and tocotrienols also differ in the number of methyl groups present on the chromanol ring (Sen et al., 2006). Tocopherols do not have double bonds in the phytol side chain, whereas tocotrienols have three double bonds in the farnesyl side chain. Tocotrienols are chemically more active than tocopherols because of the unsaturated tail. Hence, the current research focuses on  $\alpha$ ,  $\beta$ ,  $\gamma$  and  $\delta$  tocotrienols.

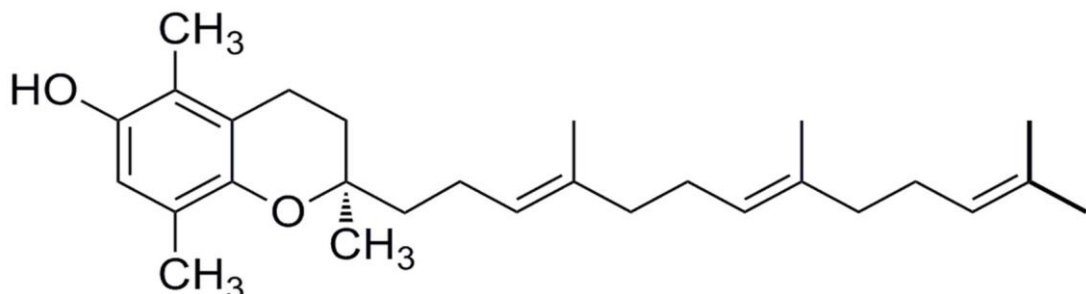


**Chemical Formula:** C<sub>29</sub>H<sub>44</sub>O<sub>2</sub>  
**Molecular Weight:** 424.66

**Figure 2.1 Structure of  $\alpha$ -tocotrienol**

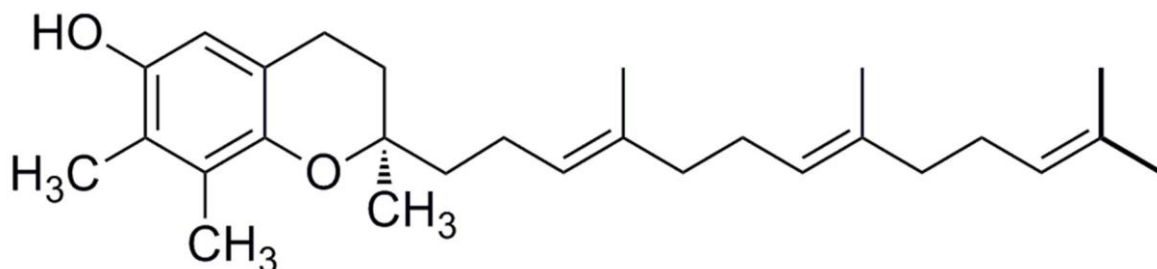
$\alpha$ ,  $\beta$ ,  $\gamma$  and  $\delta$  tocotrienols are similar in structure. However, the difference lies in the number of methyl groups on the chromanol ring. Tocotrienols are basically composed of a chromanol ring with one chiral centre, which is attached to the farnesyl side chain with three double

bonds.  $\alpha$ -tocotrienol has three methyl groups at 5, 7, 8 positions of the aromatic ring as shown in Figure 2.1.  $\beta$ -tocotrienol has two methyl groups at 5, 8 of the aromatic ring as shown in Figure 2.2.



**Chemical Formula:** C<sub>28</sub>H<sub>42</sub>O<sub>2</sub>  
**Molecular Weight:** 410.63

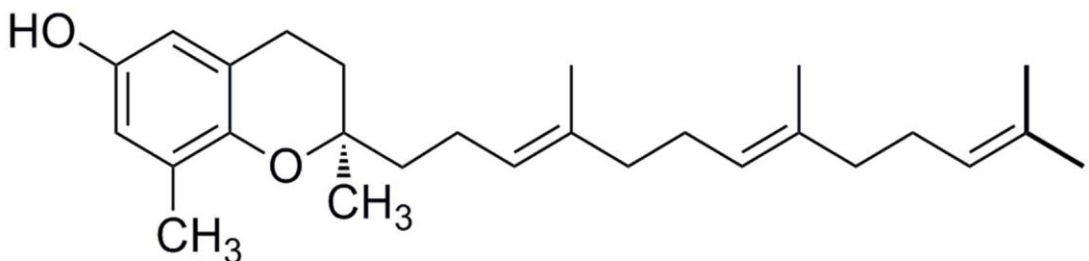
**Figure 2.2 Structure of  $\beta$ -tocotrienol**



**Chemical Formula:** C<sub>28</sub>H<sub>42</sub>O<sub>2</sub>  
**Molecular Weight:** 410.63

**Figure 2.3 Structure of  $\gamma$ -tocotrienol**

$\gamma$ -tocotrienol has two methyl groups at 7, 8 positions as depicted in Figure 2.3.  $\delta$ -tocotrienol has only one methyl group at position 8 which is represented in Figure 2.4. The difference in the number and position of methyl groups is the reason for the existence of four different isoforms of tocotrienols. This difference leaves a significant change in their binding affinities with the same receptors.



**Chemical Formula:** C<sub>27</sub>H<sub>40</sub>O<sub>2</sub>  
**Molecular Weight:** 396.61

**Figure 2.4 Structure of  $\delta$ -tocotrienol**

### 2.3.1.1. Metabolism of Tocotrienols

Evidence of tocotrienols metabolism in the body is relatively limited compared to tocopherols (Gee, 2011). According to the experiments conducted by Fairus et al., after the administration of 1011mg of Tocotrienol Rich Fraction (TRF) in healthy subjects, tocotrienols were transported in triacyl glycerol rich fractions (Fairus et al., 2006). In this study it was observed that considerable amounts of  $\alpha$ ,  $\gamma$  and  $\delta$ -tocotrienols were detected in both plasma and lipoproteins. In another clinical study it was found that higher concentrations of tocotrienols were observed in adipose tissue surrounding benign than malignant breast cancer tumour (Nesaretnam et al., 2007). Recently Fu et al. revealed through their experiments that tocotrienols disappeared from plasma after 24 hours of administration due to the low affinity of  $\alpha$ -Tocopherol Transport Protein ( $\alpha$ -TTP) for tocotrienols (Fu et al., 2014). Another study has suggested that tocotrienols might be metabolized by an alternate independent  $\alpha$ -TTP pathway (Gee, 2011).

### 2.3.1.2. Biological Activity of Tocotrienol

Tocotrienols are capable of preventing cancer development and reduce the risk of atherosclerosis (Hendrich et al., 1994). It was indicated from the past *in vitro* research that tocotrienols can be used in the treatment of breast cancer (Guthrie et al., 1997). In another

study it was noticed that TRF obtained from rice bran oil has remarkably reduced the risk of cardiovascular diseases by inhibiting cholesterol synthesis (Qureshi et al., 1997). A previous study performed by Aggarwal, et al., suggested that tocotrienols have positive health effects on bone health, brain health, blood sugar metabolism and cancer (Aggarwal et al., 2010).

The findings of a study performed in patients with hyperlipidemia and carotid stenosis concluded that the anti-oxidation properties of tocotrienols may influence the course of carotid atherosclerosis (Tomeo et al., 1995). Tomeo et al., have investigated the anti-oxidation role of  $\alpha$  and  $\gamma$  tocotrienols in patients with carotid atherosclerosis. The effect of tocotrienols on hepatocarcinogenesis is tested in rats as a part of research performed previously by Ngah et al. The results from this experiment suggested that tocotrienol administered in rats reduced the severity of hepatocarcinogenesis (Ngah et al., 1991). It was identified in another study that  $\gamma$  tocotrienol is the most potent inhibitor of cholesterol synthesis and helps in lowering serum cholesterol in hypercholesterolemic patients (Qureshi et al., 1991). This study has concluded that tocotrienols, being the natural food products can be easily administered and accepted by humans, and may well prove to have fewer side effects than do many other medications (Qureshi et al., 1991). The medicinal values of tocotrienols imply the need for further research on them.

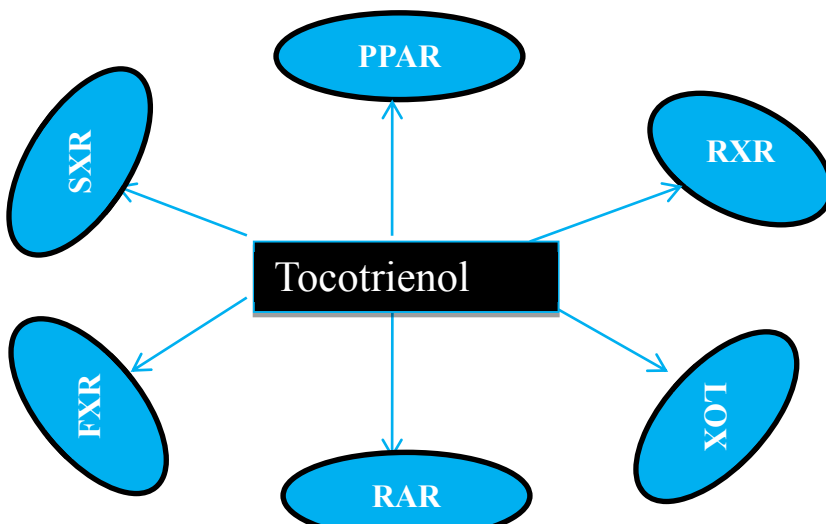
### ***2.3.1.3. Interactions of Tocotrienols with Different Proteins***

Naturally occurring tocotrienols exhibit anti-carcinogenic properties due to the presence of isoprenoid (2-methyl-1,3-butadiene) units in the lypophilic side chain (Packer et al., 2001). The unique structure of tocotrienols helps them to enter easily into cells and confer their better anti-oxidant properties (Richard, 2014).

The recent research on diabetic mice has shown that after binding to peroxisome proliferator activated receptor (PPAR), tocotrienols can regulate the PPAR target genes and improve

the consumption of whole body glucose and insulin sensitivity (Fang et al., 2010). Steroid Xenobiotic Receptor (SXR) binds to tocotrienols resulting in the activation of gene expression by forming a tocotrienol-SXR-RXR complex. It was noticed in an *in silico* docking study that  $\alpha$ -tocotrienol binds to the opening cavity close to the active site of 12-LOX and hinders the access of arachidonic acid to the catalytic site (Khanna et al., 2003). These studies lend further support to  $\alpha$ -tocotrienol as a neuroprotective form of vitamin E. The docking of all four tocotrienols along with all four tocopherols was performed and the study selected the adenosine triphosphate (ATP) binding site of P-glycoprotein (Upadhyay, 2009). The data from this study has revealed that  $\alpha$  and  $\delta$  tocotrienols have highest affinity at the ATP site of P-glycoprotein. The interaction of  $\alpha$ -tocopherol transfer protein, tocopherol associated protein, human serum albumin, and P-glycoprotein with tocotrienols and tocopherols present valuable information about their binding mode during metabolism, absorption, transport and efflux. The unsaturated side chain of tocotrienols makes them more potent than tocopherol (Upadhyay, 2009). The binding of tocotrienols with Farnesoid Xenobiotic Receptor (FXR) and RAR still needs to be tested.

It was observed in a recent study that tocotrienols are more potential cancer agents than tocopherols (Ling et al., 2012). Tocotrienols could be used as potential anti-cancer therapeutic agents as they were shown to have chemosensitization and anti-cancer stem cell effects. The research is now focusing on tocotrienols for future chemoprevention and cancer treatment, because of the disappointing results of tocopherols in previous clinical studies. Although the medicinal importance of tocotrienols was proved by previous research, the action of tocotrienol as a potential drug target is studied less (Ling et al., 2012).

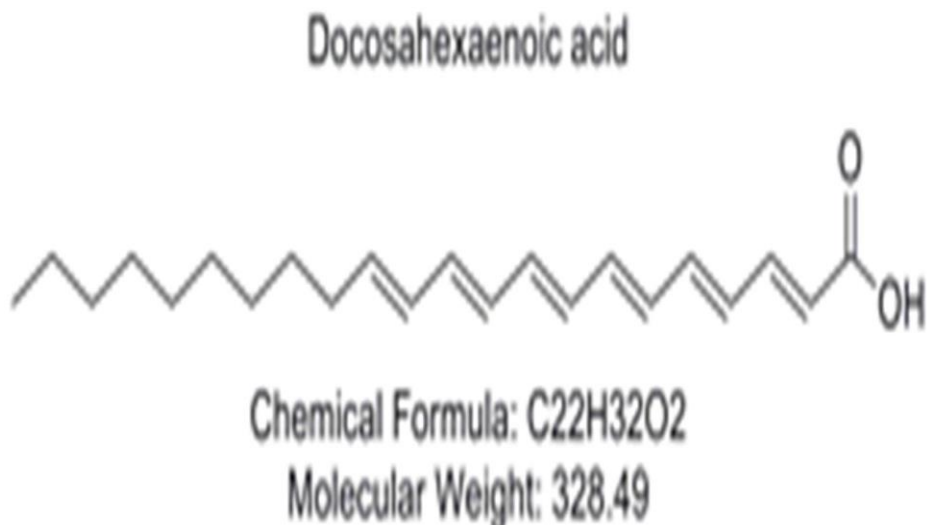
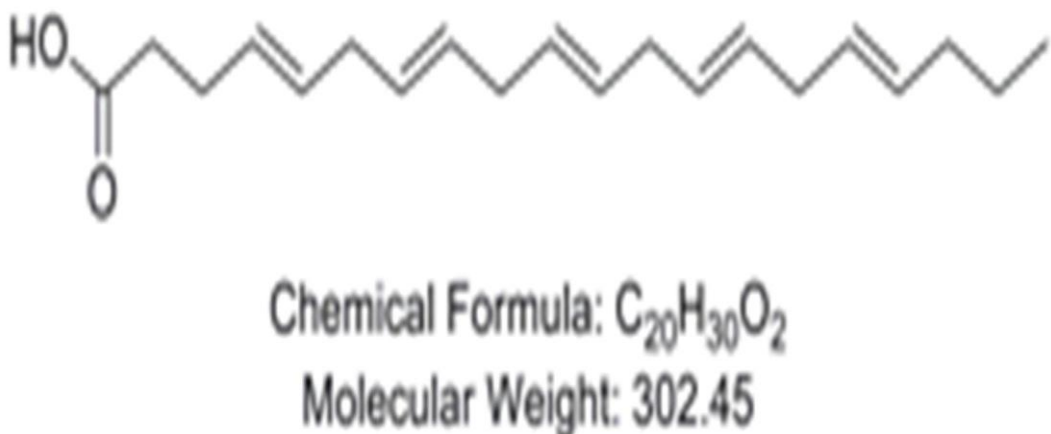


**Figure 2.5 Known Targets of tocotrienols with different targets and enzymes**

After performing a thorough literature review, PPARs, RAR, RXR, LOX were predicted to have a strong binding affinity with tocotrienols. Interestingly, all the receptors selected for the current study have medicinal value and so the ability of tocotrienols to act as their ligands is further tested in the current research. Figure 2.5 depicted the known targets of tocotrienols with different targets and enzymes.

### 2.3.2. *Omega 3 Fatty Acids*

Omega 3 fatty acids are PolyUnsaturated Fatty Acids (PUFAs) with a double bond at the third carbon atom. The fatty acids have two ends with carboxylic acid (COOH) on one end and methyl group on the other end as shown in Figures 2.6 and 2.7. The carboxylic end is considered as the beginning of the fatty acid chain, whereas the methyl end is the tail. Since omega 3 fatty acids have a double bond at the third carbon from the methyl end ( $\omega$  end) they are named as omega 3 fatty acids. DHA and EPA are selected for the current study from the group of omega 3 fatty acids. They were selected because they are chemically active and play an important role in pharmacology due to their health significance.

**Figure 2.6 Structure of DHA****Figure 2.7 Structure of EPA**

DHA has 6 double bonds with 22 carbon atoms as shown in Figure 2.6, whereas EPA has 5 double bonds with 20 carbon atoms (Figure 2.7). The first double bond in both DHA and EPA starts at the third carbon from the methyl or  $\omega$  end.

### **2.3.2.1. Metabolism of DHA and EPA**

Omega 3 fatty acids as such are not produced in the body and hence must be supplied through diet. Fish oil is rich in both DHA and EPA. It was not much known about the metabolism of

DHA and EPA in the body (Li et al., 2005). It was found in a study that EPA can get incorporated into phospholipid bilayer (Hawcroft et al., 2010). Further, in phospholipid bilayer EPA competes with the active site of COX-2 enzyme. After activating COX-2, EPA metabolizes into prostaglandin-E3 and acts efficiently in reducing human lung and pancreatic cancer (Funahashi et al., 2008; Yang et al., 2004). Consumption of fish oil rich in DHA and EPA was identified to improve the prognosis of diseases such as atherosclerosis, psoriasis and rheumatoid arthritis (Clark et al., 1993; Simopoulos, 2002).

### ***2.3.2.2. Biological Activity of Omega 3 Fatty Acids***

The medical importance of DHA and EPA along with a few antirheumatic drugs and other drugs have been shown to be effective in treating diseases like ulcerative colitis, hyperlipidemia, and skin lesions and also in decreasing the toxicity of cyclosporine in patients with psoriasis (Simopoulos, 1991). Moreover, omega 3 fatty acids are required for the normal functional development of the retina and brain, predominantly in premature infants (Simopoulos, 1991). They also help in preventing cancer by arresting the cell cycle and inducing apoptosis by activating phosphatase (Rafat et al., 2004). Omega 3 fatty acids have also been suggested to play an important role in the pathophysiology and treatment of bipolar disorder (Stoll et al., 1999). Animal studies suggest that omega 3 fatty acids exert protective effects against breast, colon and prostate cancers. In patients with colorectal cancer DHA and EPA decrease cell proliferation and maintain the balance between colonic cell proliferation and apoptosis (Simopoulos, 2003). Among the fatty acids, omega 3 fatty acids possess most potent immunomodulatory activities and among omega 3 fatty acids DHA and EPA are biologically more potent (Simopoulos, 2002). Animal experiments and clinical intervention indicate that because of anti-inflammatory properties omega 3 fatty acids can be used in the treatment of autoimmune diseases (Simopoulos, 2002). The UK dietary guidelines for cardiovascular diseases acknowledge the importance of long-chain omega-3 fatty acids in

reducing the risk of heart diseases (Ruxton et al., 2004). The deficiency of omega 3 fatty acids in a normal diet leads to harmful effects on synaptic functions and emotional behaviour (Lafourcade et al., 2011).

### ***2.3.2.2. Interactions of Omega 3 Fatty Acids with Different Proteins***

Computational docking and molecular simulation studies performed in the previous research indicated that DHA binds to PPARs and RXRs with high affinity (Gani & Style, 2008). Unfortunately, there is no experimental evidence for the binding of DHA with PPAR (Gani & Style, 2008). Due to high affinity, EPA occupies the ligand binding pocket of PPAR (Xu et al., 1999). DHA and EPA activate the cannabinoid receptors and express their endocannabinoid's nature (Brown et al., 2010). DHA and EPA are the novel ligands of transient receptor potential vanilloid receptor (TRPV1) which is an ion channel expressed in neurons and brain (Lafourcade et al., 2011).

The beneficial health effects of DHA and EPA relate to their anti-inflammatory properties, the exact mechanism is unknown (Balvers et al., 2010). The mechanism behind the binding of omega 3 fatty acids to G protein-coupled receptor 120 (GPR120) is also not clear, however, it results in broad anti-inflammatory effects (Oh et al., 2010). Platelet aggregation is caused by the interaction of Cyclooxygenase (COX) with omega 3 fatty acids (Hu et al., 2002). The beneficial effects on lipid metabolism are because of the selective regulation of FXR caused by the binding of omega 3 fatty acids to FXR (Zhao et al., 2004). The binding of RAR with omega 3 fatty acids result in the expression of genes involved in synaptic plasticity (Buaud et al., 2010).

The target targets and enzymes were predicted from the literature review and are shown in Figure 2.8. The research done so far on omega 3 fatty acids suggests that they could be the potential drug candidates to design drugs for diseases like cancer, heart diseases and

behavioural disorders. The interaction of DHA and EPA with different biological proteins is significant and needs to be further tested.

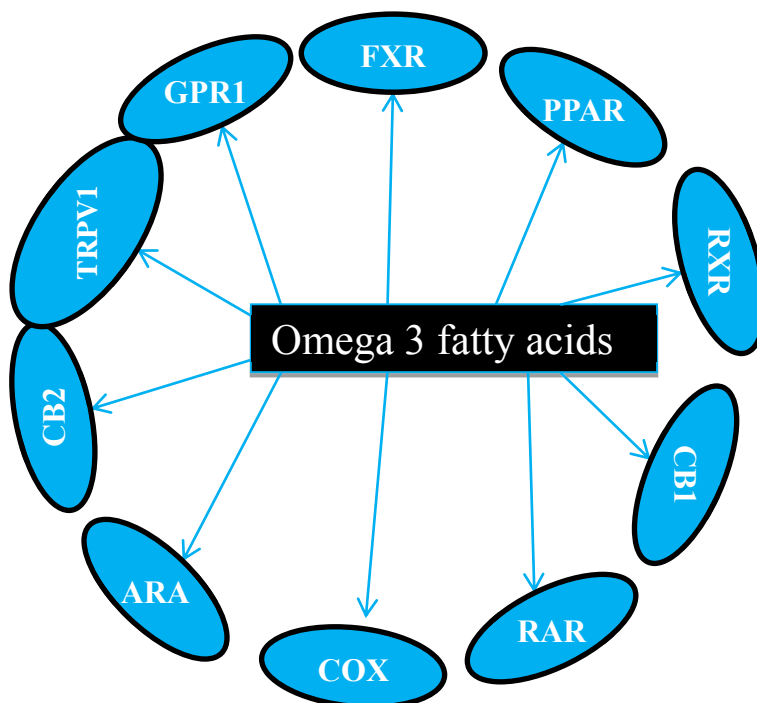


**Figure 2.8 Known targets of omega 3 fatty acids with different targets and enzymes**

### 2.3.3. Endocannabinoids

The endogenous cannabinoids—anandamide and 2AG—were selected for the study from endocannabinoids. Anandamide is the ethanolamine amide of arachidonic acid. It has 22 carbon atoms with four double bonds (Figure 2.9). The first double bond is in the sixth position from the  $\omega$  end (omega 6 fatty acids). The structure of anandamide is similar to arachidonic acid.

Arachidonic acid attached to ethanol amide (amide formed from carboxylic acid) is the structure of anandamide (also called arachidonyl ethanolamide). 2AG is another endogenous cannabinoid formed from arachidonic acid and diacylglycerol. It is an ester with 23 carbon atoms and four double bonds (Figure 2.10). Similar to anandamide the first double bond in 2AG is located at the sixth position from  $\omega$  end as shown in Figure 2.10.

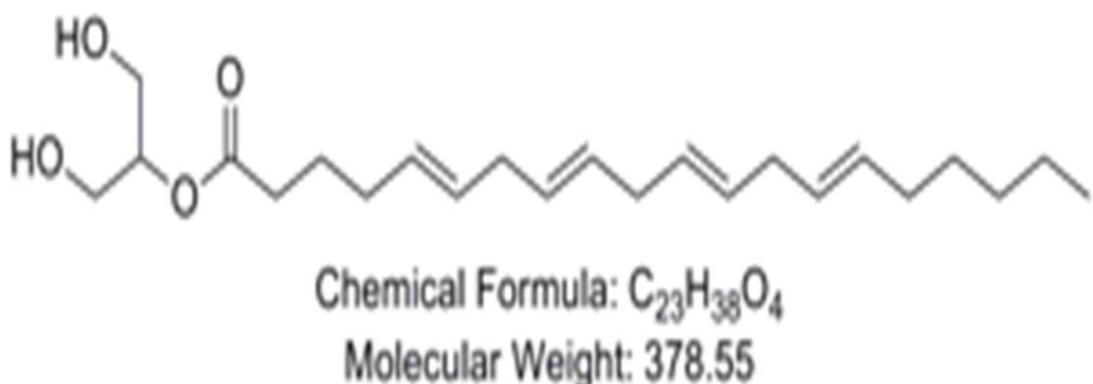


**Figure 2.9 Structure of anandamide**

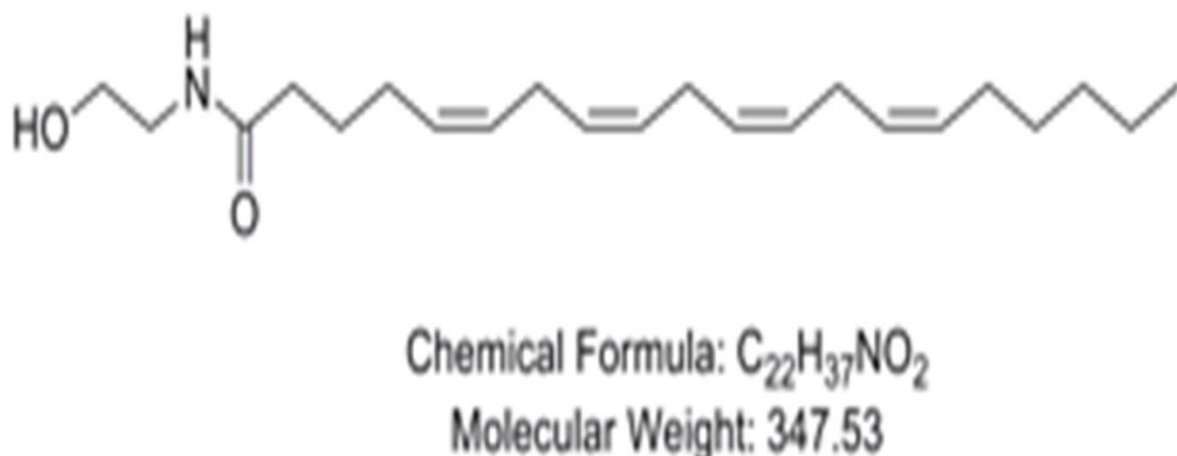


**Figure 2.10 Structure of 2AG**

### 2.3.3.1. Metabolism of Endocannabinoids

Mostly anandamide is metabolized by the enzyme Fatty Acid Amide Hydrolase (FAAH) and 2AG is metabolized by monoacyl glycerol lipase (Jhaveri et al., 2007). However, sometimes 2AG is also metabolized by FAAH (Jhaveri et al., 2007). Both 2AG and anandamide can be metabolized by COX-2 (Kozak et al., 2000, 2004). Furthermore, it was believed that 2AG and anandamide were transported to cells that contributed to the termination of the bioavailability of endocannabinoids (Hillard & Jarrahian, 2005; Ortega-Gutiérrez et al., 2004).

### ***2.3.3.2. Biological Activity of Endocannabinoids***

Endocannabinoid research was greatly accelerated two decades ago with the discovery of cannabinoid receptors (Kano et al., 2009). The research carried out on endocannabinoids over the last seven years has concluded that pharmacological antagonists could be used in the treatment of obesity and as an aid to the cessation of smoking (Jonsson et al., 2006). Endocannabinoids, due to their capacity in reducing inflammation, cell proliferation and cell survival could be used in cancer treatment (Sarfaraz et al., 2008). Further research on endocannabinoids suggests that the endocannabinoid system in the skin is involved in biological processes like growth differentiation, proliferation and apoptosis (Bíró et al., 2009).

The endocannabinoid system plays a major role in a broad range of diseases from mood and anxiety disorders, movement disorders such as Parkinson's and Huntington's disease, neuropathic pain, multiple sclerosis and spinal cord injury, to cancer, atherosclerosis, myocardial infarction, stroke, hypertension, glaucoma, obesity/metabolic syndrome, and osteoporosis (Pacher et al., 2006). Although several clinical studies and preclinical trials were performed before on the novel therapeutic approaches of the endocannabinoid system, current treatments do not fully address the patient's need (Pacher et al., 2006). The currently used inhibitors of endocannabinoid metabolizing enzyme in pain have caused some unexpected complexities and hence there is a need for better understanding on the pathophysiological role of endocannabinoids (Pacher et al., 2013). Cannabinoid treatment was observed to be beneficial in viral infections. Past research has indicated that cannabinoid drugs may be useful in treating meningitis (Reiss, 2010). The synthetic cannabinoid HU-211 has been experimentally tested on rats for its effective treatment of pneumococcal meningitis (Bass et al., 1996). This experiment has revealed that HU-211 has positive effects in the therapy of meningitis.

The use of cannabinoid drugs has been always controversial due to their adverse side effects (Harris & Brown, 2013). More importance is given to the synthetic cannabinoids that minimize the psychoactive effects (Fattore & Fratta, 2011). The author's study falls in line with the recent issues regarding the role of cannabinoids in the treatment of meningitis, which hit the news with a segment "Cannabis oil: Raided for helping their son". As per the recent televised show, (telecasted in 'Sunday Night', 20<sup>th</sup> July 2014 at 8.15pm on Channel 7, Australia) cannabis oil has played a tremendous role in treating epilepsy associated with meningitis ("Cannabis oil: Raided for helping their son", 2014). The author's study of thesis is also in the same context in supporting the use of cannabinoids in health and disease.

### ***2.3.3.2. Interactions of Endocannabinoids with Different Proteins***

The interaction of endocannabinoids with different proteins and enzymes is shown in Figure 2.11. Endocannabinoids have significant influence on PPARs. Anandamide activates RXR that heterodimerises with PPAR (Sun et al., 2007). The binding of endocannabinoids to COX-2 results in various events which include cell viability, mobilization of calcium and modulation of synaptic transmission. They also interact with LOX and produce biologically active compound (Fowler, 2007). They alter synaptic transmission, cardiovascular system and immune system through CB1 and CB2. TRPV1 mediates pain sensation mainly found in the peripheral nervous system and brain. TRPV1 interacts with endocannabinoids and regulates synaptic strength (Chávez et al., 2010).

There are several innovative therapeutic approaches of the endocannabinoid system as a result of past decades of research on plant cannabinoids (Di Marzo et al., 2004). Although most of them have advantages, the disadvantages of cannabinoid-based drugs lead a path to the current research. There was extensive research on the interaction of endocannabinoids

with different proteins and enzymes. However, the side effects of cannabinoid-based drugs and satisfying the patient needs are still a gap in the previous research.

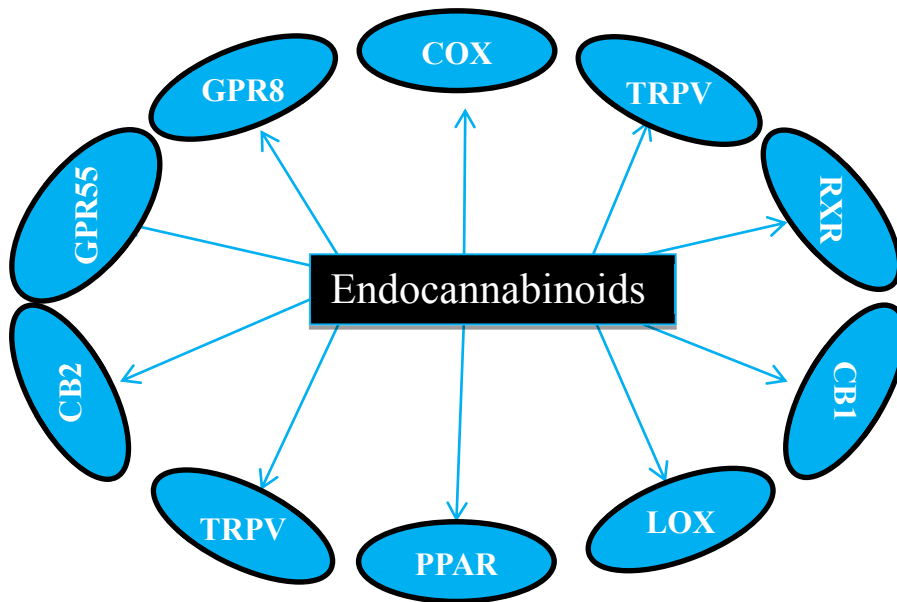


**Figure 2.11 Known targets of endocannabinoids with different targets and enzymes**

These lipid ligands differ structurally in the functional groups in their structures. For example, the position of the methyl group on the chromanol ring forms four different isomers of tocotrienols, which is the reason for their binding differences with the same receptor molecules. DHA has six double bonds, whereas EPA has five double bonds, which could be the reason for DHA to have a stronger affinity with many targets than EPA. Anandamide and 2AG have four double bonds. However, the functional group in anadamide is ethanolamide whereas in 2AG the functional group is glycerol. This is the reason for the difference in their binding energies with the same targets. Since these lipid ligands have a significant role in health and diseases and their chemistry with other molecules is interesting, this particular group of lipid ligands was selected for the study of this thesis.

## 2.4. Target Proteins

Tocotrienols, omega 3 fatty acids and endocannabinoids are three important groups of lipids that have a vital role in health and disease.

**Table 2.1 Therapeutic role of targets**

<b>Target Receptor</b>	<b>Drugs in use</b>	<b>Action on</b>	<b>Side Effects</b>
PPAR- $\alpha$	Fibrates	Cholesterol lowering Drugs	Low potency and restricted selectivity (Sierra et al., 2007)
PPAR- $\gamma$	Thiazolidinediones	Diabetes	Cardiovascular risks and obesity (Malapaka et al., 2012)
PPAR- $\beta/\delta$	PPAR- $\beta/\delta$ drugs are under investigation	Metabolic syndrome	Weight Gain (Luquet et al., 2005)
RAR- $\gamma$	Acitretin	Psoriasis	Loss of consciousness, sudden change in behavior (Katz et al., 1999)
RXR- $\alpha$	Etodolac	Inflammation	Constipation, blurred vision, diarrhea (Porro et al., 1991)
COX 1 & 2	NSAIDs (Aspirin & Ibuprofen)	Inflammation	Stomach or gastrointestinal ulcers, heartburn, headache, and dizziness (Smith et al., 2000)
LOX	Zileuton	Asthma, inflammation, arthritis and psoriasis	Headache, heartburn, diarrhea, rash, nausea, itching, flu like symptoms (Parnes & Chuma, 2000)
Cannabinoid Receptors 1 &2	Nabilone	Nausea and vomiting caused by cancer chemotherapy	Sleep Problems, anxiety, depression, fast heartbeat, drowsiness and dizziness (Steele et al., 1979)

The interaction of these three groups of lipids with different proteins and enzymes play an important role in drug discovery.

A detailed literature review was performed (as discussed in Section 2.3) on the possible binding sites of the above three groups of lipids with different proteins. The proteins that were predicted to have strong binding affinities with the above lipid ligands were selected for the study. Further, the proteins selected for the study have great pharmacological significance

in terms of designing drugs for different diseases like cancer, diabetes, atherosclerosis and inflammatory diseases.

Interestingly, all the receptors selected for the current research are already in use as drug targets for the treatment of above mentioned diseases. However, these drugs cause some side effects and hence the pharmaceutical industry is paying more attention to the natural agonists of these proteins which cause little or no side effects. Therefore, the current study, which is aimed to find a suitable natural ligand of therapeutic target proteins, is novel.

Table 2.1 lists the selected proteins. The author's study is aimed to find the potential ligands for these proteins which can result in few or no side effects. The detailed therapeutic significance of target proteins was discussed in Section 2.4.1.

#### ***2.4.1. Therapeutic Proteins and Their Significance***

Due to the regulatory role of PPARs, in the expression of genes associated with various diseases such as cancer, diabetes, atherosclerosis and obesity, the pharmaceutical industry is actively investigating PPARs and their binding mechanism with different ligands. The agonists of PPAR- $\alpha$ ,  $\beta$  /  $\delta$  and  $\gamma$  are used to design drugs for high levels of cholesterol, diabetes and inflammation, respectively. However, these drugs have some side effects and limitations. Therefore, there is still a need to find the potential pharmacological targets for PPARs. After binding to ligands, PPARs act as transcription factors and control lipid and glucose metabolism (Collino et al., 2008). The search is on for the design of novel therapeutic signalling targets as the currently available therapies have proven to be highly unsatisfactory. Recent research suggests that PPARs play an important role in the pathophysiology of various disorders of the central nervous system (Collino et al., 2008).

The limitations of currently used PPAR-based drugs have laid a foundation for the current docking study of finding the new ligands that activate PPARs. PPAR-based anti-diabetic and hypolidemic drugs cannot be used in patients with high lipid levels (Gani et al., 2008). PPAR- $\gamma$  is the molecular target for TZDs which are widely used anti-diabetic drugs. TZDs are effective in treating diabetes if they don't cause any side effects like obesity and cardiovascular risks (Malapaka et al., 2012). PPAR- $\alpha$  based lipid-lowering fibrate drugs are limited in their efficacy due to restricted selectivity (Sierra et al., 2007). Therefore, there is a need to find potential agonists of PPAR-  $\alpha$  and  $\gamma$  that cause little or no side effects. Moreover, the dual agonists of PPAR- $\alpha$  and  $\gamma$  are of interest to the pharmaceutical industry. Although a similar docking study was conducted previously for the binding affinities of PPARs, the study was limited to DHA (Gani et al., 2008). PPAR  $\delta$  reduces the level of triglycerides and low density lipo-proteins and increases the level of high density lipo-protein cholesterol. A potential therapeutic target for PPAR  $\delta$  is to be investigated (Staels et al., 2005). Previous research also suggested that PPAR- $\gamma$  has a therapeutic potential to treat inflammatory diseases and certain cancers (Murphy et al., 2000).

RXR  $\alpha$  and RAR  $\gamma$  regulate retinoic acid target genes. RXR  $\alpha$  forms a heterodimeric complex with PPAR- $\gamma$  and used in the treatment of breast cancer. It was observed in an *in vitro* study that PPAR-RXR selective ligands can be used in cancer therapy (Crowe et al., 2004). The combined therapy of PPAR and RXR ligand for breast cancer treatment is under research. An *in vitro* study suggested that RXR selective ligands are capable of inhibiting the proliferation of breast cancer cells and caused regression of the disease (Crowe et al., 2004). It holds the therapeutic potential for the treatment of metabolic diseases (Pérez et al., 2012). The therapeutic role of RARs and RXRs can be modulated by ligand which binds to RAR and RXR. Although the powerful anticancer drugs are targeted by these receptors, their use is

limited by toxicity. This implies the need of more selective ligands that might overcome such problems (de Lera et al., 2007).

COX inhibitors play a role in reducing the risks of pancreatic cancer as they can induce apoptosis (cell death). It was observed in a research study that the risk of pancreatic cancer is 60% lower in people who use aspirin (NSAID acts as a COX inhibitor) six or more times a week (Ding et al., 2003). NSAIDs use arachidonic acid as the substrate of COX-1 and COX-2. However, NSAIDs cause some side effects like dyspepsia (stomach upset), edema (swelling of the skin due to alteration in kidney function) and gastric irritation (Krönke et al., 2009). Chronic use of COX-2 inhibitors (eg. Vioxx scandal) is linked to heart attack and stroke leading to death. Further research is needed to find selective inhibitors of COX-2 (Brown et al., 2005).

Different types of Lipoxygenases (5-LOX, 8-LOX, 12-LOX, and 15-LOX), after binding to arachidonic acid and other substrates, form several intermediate products which are involved in the development and progression of human cancers and atherosclerosis (DeWitt, 1999). Moreover, elevated levels of LOX metabolites are observed in lung, prostate, breast, colon and skin cancer cells (Kuhn, 2005). The inhibitors of LOX (eg. Zileuton- a LOX based drug used to treat asthma) can be used in the treatment of asthma, inflammation, arthritis and psoriasis (Kuhn, 2005). The use of dual inhibitors is an interesting approach as both COX and LOX derivatives are also involved in cancer proliferation apart from inflammation (Leval et al., 2002). There is a need for further research to explain the role of LOX in reducing the risk of pancreatic cancer (Ding et al., 2003). Research is being carried out actively to find the dual inhibitors of both COX and LOX.

Cannabinoid Receptors in hippocampus of the brain play an important role in learning and memory formation. The research done so far on endocannabinoid system has identified

$\Delta 9$ -tetrahydrocannabinol ( $\Delta 9$ -THC), HU-210, CP55940, R-(+)-WIN55, 212-2 and anandamide as the agonists of cannabinoid receptor 1 and 2 (Davies et al., 2002).  $\Delta 9$ -THC is the most widely used cannabinoid drug. However,  $\Delta 9$ -THC causes some psychotropic side effects like sleepiness, euphoria, anxiety, confusion, nausea, dizziness (Naef et al., 2003). Hence there is still a need to find potential agonists of cannabinoid receptors, which result in few or no side effects. CB1 and CB2 receptors are attractive targets for the design of therapeutic ligands. Several endogenous ligands, for which cannabinoid receptors are the substrates, were already discovered as a result of the past research (Pavlopoulos et al., 2006).

#### ***2.4.2. Mutations in Target Proteins***

During the author's study of lipid-protein interactions, it was noticed that the protein structure might be altered, sometimes because of mutations, affecting the binding affinities. Mutation is a sudden or spontaneous change that occurs in the nucleotide sequence naturally or through mutagens. Sometimes the change in the DNA results in the alteration of the amino acid sequence ultimately causing a defect in the protein product structurally and functionally. Mutations play an important role in the binding mechanism and reveal new facts in discovering drugs for a series of diseases like diabetes, lipidemia, cancer and so forth (Yue et al., 2005). Mutations play a vital role in the calculation of ligand binding affinities. The ligand binding domain of the receptor would be altered due to mutation. Since the amino acid sequence is changed, the ligand might not bind to the receptor in some situations, resulting in abnormal function. This would lead to a difference in binding affinities. Hence, it is important to study the possible mutations related to targets.

Nuclear receptors regulate various physiological activities from reproduction and development, to homeostasis and metabolism, through ligand dependent transcription (Modica et al., 2009). Among all the nuclear receptors, the following receptors interact with

the above three groups of lipid ligands. In this chapter, the occurrence of different mutations in nuclear receptors in the human gene is discussed. Missense, nonsense and point mutations are naturally occurring. In some cases the proteins were experimentally mutated in other's research on drug discovery. The change in the amino acid sequence, causes the structural conformation of the mutated protein differs from the normal protein. If the mutation occurs in the ligand binding domain of the protein, this would greatly affect the binding affinity of that protein during the ligand-receptor interaction and so the author's study is focussed on the mutations occurring in the ligand binding domain of the protein. Therefore, the author's study of mutations in nuclear receptors is novel in a way of understanding the interaction of these receptors with different ligands. Since most of the drugs act through nuclear receptors, the review on protein mutations is helpful in studying their interaction with different drugs. The amino acid sequence and the binding regions of DNA and various ligands of targets are taken from the National Centre for Biotechnology Information (NCBI) web site (<http://www.ncbi.nlm.nih.gov/>).

The author's study of mutations was performed in order to support the present research on the interaction of nuclear receptors with different ligands. All the mutations studied were depicted graphically, where a horizontal black line indicates the protein chain with the total number of amino acids. A blue block represents the DNA binding domain and an orange block shows the ligand binding domain. The effect of each mutation is shown in tabular form along with the type of mutation. The tables and figures about mutations are found in the Appendix from A-H. Mutations discussed are in the ligand binding site. Although all the mutations are not contextualized by dangerous disease, the ones that alter the protein structure and have an impact on the ligand binding site were discussed.

### ***2.4.2.1. Mutations in PPAR- $\alpha$***

PPAR is a transcription regulation factor that functions in cellular differentiation, development and metabolism. There are three types of PPARs: PPAR- $\alpha$ , PPAR- $\delta$  and PPAR- $\gamma$ . Due to the significant role of PPAR- $\gamma$  in extracellular lipid metabolism, glucose homeostasis and adipocytes differentiation (Ng et al., 2002), it was studied more extensively than the other two types.

There are 468 amino acids in PPAR- $\alpha$ . It can bind to DNA within the region of 101 to 184 amino acids. The ligand binding domain is from 201-467 amino acids. The mutations are marked according to the number of amino acids on which they are occurring. For example, phenylalanine at 273<sup>rd</sup> position is mutated to Alanine and is represented as F273A. F273A mutation in the ligand binding domain of PPAR- $\alpha$  is similar to F282A in PPAR- $\gamma$ . In both the cases phenylalanine is mutated to alanine, which enlarges the ligand binding pocket of the receptor (Ng et al., 2002). Refer to Appendix A for the possible mutations in PPAR- $\alpha$ .

### ***2.4.2.2. Mutations in PPAR- $\gamma$ isoform1***

Recent studies suggest that PPAR- $\gamma$  can be used as a molecular target in drug discovery techniques for a series of diseases like diabetes and dyslipidaemia (Evans et al., 2001). There are 477 amino acids in PPAR- $\gamma$  isoform1. Mutations in PPAR- $\gamma$  isoform 1 and 2 are studied individually as they are high in number. The DNA binding domain is about 83 amino acids starting from 110-193. The ligand binding domain is from amino acids 209 to 476. The mutations occurring in the ligand binding domain influence the binding affinity. The effect of each mutation along with its type is mentioned in Appendix B.

### ***2.4.2.3. Mutations in PPAR- $\gamma$ isoform2***

There are 505 amino acids in PPAR- $\gamma$  isoform2. The DNA binding domain is from position 138 to 221. The ligand binding domain is from 237 to 504 amino acids. The extra 28 amino acids in the N-terminus of PPAR- $\gamma$  isoform2 make its ligand-independent activation 5-10 folds more effective than that of PPAR- $\gamma$  isoform1 (Deeb et al., 1998). The mutations like P12A, S112A and P113Q would not affect its binding capacity with other ligand. Many of the mutations occurring in both isoforms of PPAR- $\gamma$  result in insulin resistance (Appendix C). Y355X and R358X are nonsense mutations. In this instance ‘X’ refers to the nonsense or stop codon leading to the termination of protein chain synthesis. The substitution of proline with alanine at 12th position (P12A) due to a missense mutation in this protein causes variations in body mass index as mentioned in Appendix C.

### ***2.4.2.4. Mutations in SXR***

This protein has 434 amino acids. The DNA binding domain is from 40 to 127 amino acids. The mutations in this region would affect its binding to DNA and reduce the transcriptional activity. The ligand binding domain is from 236 to 428 amino acids. Most of the mutations in SXR are missense mutations. The mutation (H407Q) in the ligand binding domain of the protein results in increased levels of constitutive activity (the activity displayed by the receptor despite the absence of ligand). This literature review has identified all the mutations occurring in the ligand binding domain of SXR. Refer to Appendix D for the mapping of mutations (Figure 2.7) in SXR along with their effect (Table 2.4).

### ***2.4.2.5. Mutations in RXR- $\alpha$***

There are three types of RXRs: RXR- $\alpha$ , RXR- $\beta$  and RXR- $\gamma$ . The significant mutations have only been reported for RXR- $\alpha$  and RXR- $\gamma$  as mentioned below. The protein sequence of

RXR- $\alpha$  consists of 463 amino acids, where DNA binds to the region of 133 to 209 amino acids. RXR- $\alpha$  form a heterodimer with PPAR to initiate transcription. The mutations within the ligand binding domain of RXR are studied, the majority being experimental mutations. At position 313, phenylalanine (Phe) can be substituted with valine (Val), isoleucine (Ile), serine (Ser) or alanine (Ala). Substitution with different amino acids resulted in different effects as depicted in Table 2.5 (Appendix E). Three mutations are shown at the position of amino acid 421 in Figure 2.8 (Appendix E), where arginine was mutated to Leucine, Glycine or Alanine. The change of R $\rightarrow$ A is a missense mutation which occurred naturally. The other two (R $\rightarrow$ L and R $\rightarrow$ G) are experimental substitutions. All mutations and their effects are shown in Appendix E.

#### ***2.4.2.6. Mutations in RXR- $\gamma$***

RXR- $\gamma$  has 463 amino acids. A sequence of 68 amino acids makes up the DNA binding domain and the ligand binding domain consists of 208 amino acids. However, only three mutations have been observed so far in this protein are shown in Appendix F.

#### ***2.4.2.7. Mutations in RAR- $\alpha$***

There are 462 amino acids in RAR- $\alpha$ . The binding location of DNA is from 82 to 166 amino acids. The ligand binding domain is from 186-416 amino acids. All the mutations in these proteins were derived experimentally except for R272G and M297L. Both the natural and experimental substituted mutations are mapped in Figure 2.10 (Appendix G). Their effects are shown in Table 2.7 (Appendix G).

#### ***2.4.2.8. Mutations in FXR***

There are 472 amino acids in this protein with the DNA binding domain comprising from 124 to 211 and the ligand binding domain from 251 to 471 amino acids. The study of mutations in

FXR has provided information on physiological or pharmacological modulation of FXR. All the mutations in FXR are observed from a single study. Mutations are marked in Figure 2.11 (Appendix H). Table 2.8 (Appendix H) depicts their significant effect.

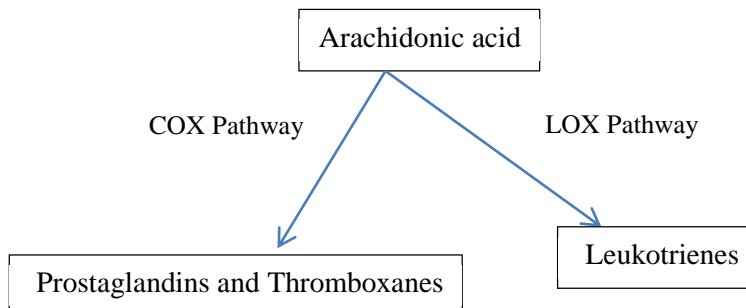
All the figures in the above mentioned appendices are helpful in locating a mutation, whether it is in the DNA binding domain or in the ligand binding pocket of a receptor. It is observed from the figures and tables (Appendix A-H) that mutations in the DNA binding domain affect the rate of transcription (Tate et al., 1995). Mutations in the ligand binding domain change the shape of the ligand binding pocket and reduce the receptor activation by different ligands (Wang et al., 2006). Change in a single amino acid of a receptor protein alters the whole structure and function of that receptor as depicted in the tables and figures. The data provided in this review could be used in the discovery of drugs that bind to the above mentioned nuclear receptors. This literature review also opens a channel to carry out in silico mutations of these nuclear receptors.

### ***2.4.3. Pathways of Target Proteins***

This Section describes various pathways in which the target proteins are involved in.

The up regulation of PPAR- $\alpha$  is associated with the up regulation of RXR- $\alpha$ . PPAR- $\alpha$  forms heterodimers with RXR- $\alpha$  (Konstandi et al., 2013). Then PPAR- $\alpha$ -RXR- $\alpha$  complex binds to PPAR response element in the promoter of target genes and stimulates their transcription (Chan & Wells, 2009). After binding to ligands, PPARs act as transcription factors and control lipid and glucose metabolism (Collino et al., 2008). PPARs are also involved in signalling pathway, glucose homeostasis, lipid metabolism and adipocyte differentiation (Lemberger et al., 1996). PPARs were found to regulate diverse aspects of lipid metabolism including fatty acid oxidation, fat cell development, lipoprotein metabolism and glucose homeostasis (Li & Glass, 2004).

Cyclooxygenases catalyze the conversion of arachidonic acid to prostaglandins. COX-1 is mainly responsible for arachidonic acid conversion in homeostatic regulation while COX-2 is primarily involved in prostaglandin production in internal stimuli (Dubois et al., 1998). COX-1 and COX-2 show major differences in mRNA splicing, stability and translational efficiency. Although both COX-1 and COX-2 catalyze identical reactions, they are regulated by two independent different systems (Dubois et al., 1998). The major precursor of eicosanoids is arachidonic acid and the pathways leading to the synthesis of eicosanoids are known as arachidonate cascade. There are three pathways within this cascade, including cyclooxygenase and lipoxygenase pathways (Smith et al., 1991). Prostanoids that include prostaglandins and thromboxanes are formed via cyclooxygenase pathway. LOX pathway is the production of leukotrienes by the action of LOX on arachidonic acid (Smith et al., 1991).



It was found in an experiment conducted by Liu et al., that CB1 receptors inhibit N-methyl-D-aspartic Acid (NMDA)-mediated calcium influx and cell death via inositol triphosphate (IP3) signaling pathway (Liu et al., 2009). Cannabinoid receptors get activated by the synthetic cannabinoid ligand, WIN ([2,3-dihydro-5-methyl-3-(4-morpholinylmethyl)pyrrolo[1,2,3-de]-1,4-benzoxazin-6-yl]-1-naphthalenylmethanone ). WIN after binding to cannabinoid receptors triggers IP3 signaling pathway and activates the release of calcium ions from intracellular stores (Liu et al., 2009). CB1 receptors couple with

G-protein coupled receptors (GPCRs) and then the same GPCRs activate different signaling pathways after activation by different ligands (Drake et al., 2008).

#### ***2.4.4. Active Sites of Target Proteins***

The characteristic feature of PPAR ligand binding cavity is its size which is 3-4 times larger than that of the other nuclear receptors. Due to this large binding cavity PPARs can accommodate a variety of natural and synthetic ligands (Grygiel-Górniak, 2014). Omega 3 fatty acids are the natural ligands of PPARs because of the presence of polar head group and a hydrophobic tail in their structures (Sheu et al., 2005).

The ligand binding domain of PPAR- $\gamma$  is comprised of three layer antiparallel  $\alpha$ -helix. The ligand binding cavity of PPAR- $\gamma$  is in three arms ‘Y’ shape providing with large binding cavity to ligands (Sheu et al., 2005). Sheu et al., have conducted experiments on the active site of PPAR- $\gamma$  using a technique called uniform mapping (Sheu et al., 2005). In this study they have examined the ligand binding domain of PPAR- $\gamma$  and found the active site regions for six different agonists. These agonists are rosiglitazone, farglitazar, tesaglitazar, ragaglitazar, GW409544 and GW0072. Apart from these synthetic ligands, phytanic acid is a natural agonist of PPAR- $\gamma$  (Grygiel-Górniak, 2014).

The surrounding amino acids observed in the binding mode of rosiglitazone bound to PPAR- $\gamma$  in Sheu et al., study were Phe 282, Cys 285, Gln 286, Ser 289, His 323, Tyr 327, Phe 363, His 449, Leu 469 and Tyr 473. In the case of the agonist GW0072 the active site amino acids identified were Arg 288, Glu 291, Ala 292, Glu 295, Met 329 and Glu 343. Tesaglitazar bound to PPAR- $\gamma$  at the region of Ser 255, Glu 259, Phe 264, His 266, Val 277, Ala 278 and Arg 280. The amino acids of Val 450, Leu 453, Glu 454, Lys 457, Met 463, Leu 465 and Glu 470 of PPAR- $\gamma$  have interacted with agonist GW40944. Likewise ragaglitazar bound to PPAR- $\gamma$  at the amino acids Pro 366, Glu 369, Phe 370, Lys 373 and Asp 441. The amino

acids Glu 276, Ile 279, Arg 357, Phe 360, Met 364 and Glu 460 were the active site amino acids interacted with farglitazar (Sheu et al., 2005).

The ligand binding site of PPAR- $\alpha$  is located on the centre of the ligand bind domain flanked by helices 3, 5, 7, 11 and 12. The ligand binding domain of PPAR- $\alpha$  starts with the amino acid residues 199 and ends with the amino acid 468. The ligand binding cavity of PPAR- $\alpha$  is similar to PPAR- $\gamma$  and is situated in a large T-shaped cavity (Cronet et al., 2001). The synthetic ligand AZ 242 was tested in a study conducted by Cronet et al., for its binding with PPAR- $\alpha$ . It was found in this study that AZ 242 has interacted with the amino acids Tyr 280, Thr 279, Met 330, Val 332, Ile 339, Leu 344, Met 355, Cys 275 and Cys 276 (Cronet et al., 2001). The author's selection of the active site amino acids of PPAR- $\alpha$  (as Cys 275, Cys 276, Met 330 and Met 355) was based on this study as well. Fibrates such as clofibrate, fenofibrate, and bezafibrate are synthetic ligands of PPAR- $\alpha$  (Nakamura et al., 2000).

The ligand binding pocket of PPAR- $\delta$  was studied by Batista et al., and found that it is in 'Y' shape similar to PPAR- $\gamma$  (Batista et al., 2012). In this study the synthetic ligand GW0742 was tested for its binding with PPAR- $\delta$  and identified that the amino acids Phe 246, Cys 249, His 287, Phe 291, Ile 327, His 413, Leu 433 and Tyr 437 have formed hydrogen and hydrophobic bonds with the ligand GW0742 (Batista et al., 2012).

RXR- $\alpha$  has 'L' shaped hydrophobic ligand binding cavity (Haffner et al., 2004). Different agonists of RXR- $\alpha$  were tested in a study conducted by Haffner et al., for their binding sites and found that most of the agonists have interacted with the amino acids Gln 275, Ala 2721, Leu 309, Leu 326, Phe 313, Ile 268, Ala 272, Val 349, Cys 269, Cys 432 and Val 342 (Haffner et al., 2004). In another study by Egea et al., the agonist 9 cis retinoic acid was tested for its binding with RXR- $\alpha$  and identified that the amino acids Cys 432, Leu 326, His 435, Ala 327, Gln 275, Ala 721, Ala 272, Val 349, Leu 309, Phe 313 and Cys 269 have

interacted with the ligand (Egea et al., 2000). After examining the above two studies in terms of maximum number of hydrogen and hydrophobic interactions the amino acids Cys 269, Val 349, Ala 271, Ala 272, and Cys 432 were selected as the active site amino acids for the author's study. The ligand binding domain of RAR- $\gamma$  was studied by Lamour et al., while observing the binding site of the agonist all trans retinoic acid (Lamour et al., 1996). In this study they revealed that the amino acids Arg 278, Arg 273, Leu 233, Cys 235 and Leu 271 have interacted with the ligand forming hydrogen and hydrophobic interactions (Lamour et al., 1996). Lamour et al., have also studied the mutations related with agonist and antagonist binding and reported that the single amino acid mutation of Arg 276 and Arg 394 to Alanine decreased agonist or antagonist binding. Mutation of Arg 272 to Ala did not have considerable effect on ligand binding. The two mutations Arg 217 and Arg 294 to Ala have increased the binding efficiency for antagonists and did not have an effect for agonists (Lamour et al., 1996).

The crystal structures of COXs were analyzed from different studies (Kurumbail et al., 1997; Luong et al., 1996; Picot et al., 1994). It was identified from these studies that the amino acids Arg 120, Tyr 355, His 513 (Arg 513 in COX-2) and Glu 524 act as an entry point for the COX active site. Further the examination of both COX-1 and COX-2 revelled that a hydrophobic cavity is present at the entrance of COX active site. This cavity contains a large number of non-conserved residues such as Thr 89 (Val 89 in COX-2), Leu 92 (Ile 92 in COX-2), Ile 112 (Leu 92in COX-2), Leu 115 (Tyr 115 in COX-2), Val 119 (Ser 119 in COX-2) and Leu 357 (Phe 357) (Llorens et al., 1999). COX-2 has large number of aromatic and polar amino acid residues compared to COX-1. This is the reason for the large ligand binding site of COX-2 which is also observed in author's study and explained in Chapter 5 under Section 5.2.3. The author's choice of active site amino acids in COXs was based on this review and crystal structure analysis.

In the case of mutations in CB1 such as Cys 257 to Ser, Cys 264 to Ser, Cys 257 and Cys 264 to Ser, Cys 257 to Ala, and Cys 264 to Ala, CB1 may fail to bind to the synthetic ligand CP55940 (Shire et al., 1996). The synthetic ligand CP55940 has bound to the amino acids Phe 174, Lys 192, Val 196, Phe 200, Glu 258, Leu 260 and Gln 261 (Shim et al., 2003). The ligand binding domain of CB2 was examined with different synthetic ligands and found that the amino acids Cys 275, Cys 257, Ser 112, Ala 118, Val 155 and Gly 304 have interacted with the ligands (Pei et al., 2008; Shim et al., 2003).

## ***2.5. Bioinformatics Tools to Assess the Lipid-Protein Interactions***

Lipids play an important role in the storage of energy, cell-cell communication and in maintaining the structure of cell membranes. Biological processes such as carbohydrate metabolism signal transduction and inflammatory responses are regulated in part by lipids. Lipids play a significant role in cellular communication. Moreover, lipids regulate carbohydrate metabolism, inflammatory response and neuronal signal transmission. As a result of the above roles of lipids, they are known to be involved in the potential therapy of different disease states like asthma, Alzheimer's disease, rheumatoid arthritis, malaria and cancer (Cotter et al., 2006).

Lipids, when interacting with proteins, result in different physiological and biological actions. If lipids are proven to have strong interaction with proteins like PPAR, then COX and LOX could be the potential candidates in the design of drugs for diseases like cancer, asthma, arthritis, atherosclerosis and inflammation. However, testing lipid-protein interactions using wet laboratory experiments involves high cost, effort and time. Moreover, it is not possible for the detailed analysis like the atomic bonds, bond distances and molecular interactions.

This is the main benefit of bioinformatics tools, where the affinity of lipid-protein interactions can be tested initially using advanced computational techniques like molecular

docking and molecular dynamic simulations. The interactions which are proven to have strong affinity can be validated using laboratory techniques like ligand binding assays or enzyme assays depending on the type of receptor molecule. The first step in this kind of study is to collect the three dimensional structure of lipids (ligands), and the crystal structures of proteins (receptors or enzymes).

### ***2.5.1.Lipid Structural Databases and Tools***

There are different databases which store collections of lipid structures in two dimensional and three dimensional forms. The following databases are some examples of lipid structural databases. ‘LIPIDAT’ is a lipid related database that has a collection of lipids, which are classified according to their type, backbone, chain, head group, etc. This database was started in the early 1990s and is still operational however, not updated after 1997. ‘LIPIDAT’ is useful in studying the physicochemical properties of lipids, and the use of lipids in the formulation of foods and pharmaceuticals (Caffrey et al., 1992).

Lipid Bank is an open access database that has a collection of more than 6000 natural lipids, including fatty acids, glycerolipids, sphingolipids, steroids and also different vitamins. This database contains the information of common and International Union of Pure and Applied Chemists names of lipids, their unique molecular structure along with the literature information (Watanabe et al., 2000). This database was started in 1989 and was last updated in the year 2007. ‘Cyber Lipid Center’ is another lipid database that contains the information of various lipids. Unlike other databases, this has a complete explanation of the lipid properties, structure, health benefits, and the source of lipids, chemical isolation methods and the history of each lipid with publications. The start date of this database is not known exactly, however, it was last updated on 2012.

‘LMSD’ – Lipid Maps Structure Database is a relational database that has a huge collection of lipid structures available to download in different formats. This database also gives the structural and physicochemical properties of lipids. This is a lipid only database that has both texts based and structure based search options (Fahy et al., 2007). This database was created in 2003 and updated in 2012.

**Table 2.2 Computational tools and databases of lipids**

Name of tool	Type of tool	URL
LIPIDAT	Database	<a href="http://www.lipidat.tcd.ie/">http://www.lipidat.tcd.ie/</a>
Lipid Bank	Database	<a href="http://lipidbank.jp/">http://lipidbank.jp/</a>
Cyber Lipid Center	Database	<a href="http://www.cyberlipid.org/">http://www.cyberlipid.org/</a>
LMSD	Database	<a href="http://www.lipidmaps.org/">http://www.lipidmaps.org/</a>
The Lipid Library	Database	<a href="http://lipidlibrary.aocs.org/">http://lipidlibrary.aocs.org/</a>
PubChem	Database	<a href="http://pubchem.ncbi.nlm.nih.gov/">http://pubchem.ncbi.nlm.nih.gov/</a>
ChEBI	Database	<a href="http://www.ebi.ac.uk/chebi/">http://www.ebi.ac.uk/chebi/</a>
Chemsketch	Software	<a href="http://www.acdlabs.com/resources/freeware/chemsketch/">http://www.acdlabs.com/resources/freeware/chemsketch/</a>
Chemdraw	Software	<a href="https://www.cambridgesoft.com/Ensemble_for_Chemistry/ChemDraw/">https://www.cambridgesoft.com/Ensemble_for_Chemistry/ChemDraw/</a>
Open Babel	Software	<a href="http://openbabel.org">http://openbabel.org</a>

While all the above databases focus on the structure and properties of lipids, ‘LMPD’-Lipid Maps Proteome Database is organized to explain the association of lipids with different proteins and genes. Different computational tools and databases available for the study of lipid structures are shown in Table 2.2. The three dimensional structure (3D) of lipids can be downloaded from the PubChem web site. The search for a desired lipid molecule displays all the available result structures. The target structure appears in two dimensional (2D) and 3D format in two different tabs as shown in Figure 2.4. Also, there are other bioinformatics tools named Chemdraw and ‘Chemsketch’ which can be used to draw the chemical structures of biomolecules including lipids.

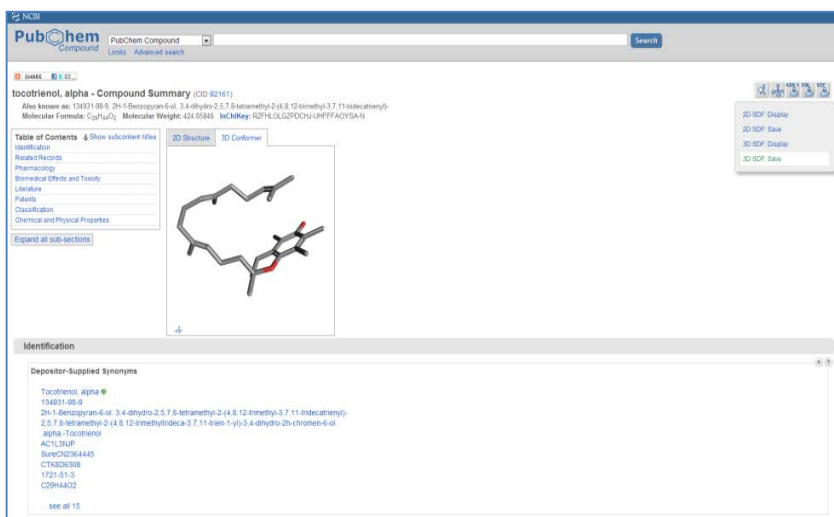


**Figure 2.12 Screen shot of downloading three dimensional lipid structures**

### 2.5.2. Protein Structural Databases

Protein structures are very complex and can be studied in three dimensional or two dimensional forms. The crystal structures of proteins can be downloaded in different formats from Protein Data Bank (PDB). In this database each entry of a protein is represented by a code which is usually called a PDB code. The same protein can be represented by multiple PDB codes. However, each PDB code is unique for each protein structure. The structures vary from each other in having different crystallographic resolutions, ligands, co-factors, crystallization conditions, etc.

The continuous research in the field of bioinformatics has developed easy access to almost all protein structures. The complex three dimensional structures of the proteins can either be downloaded from the structural databases or modelled using model databases. Usually structural databases have the collection of protein structures which are determined by X-ray Crystallography or Nuclear Magnetic Resonance or any other experimental procedure. The following are some structural databases.

The Protein Data Bank in Europe (PDBe) provides high quality protein molecule structures and related data by working in collaboration with worldwide Protein Data Bank (wwPDB)

partners, the Research Collaboratory for Structural Bioinformatics (RCSB) and BioMegResBank (BMRB) in the USA and the Protein Data Bank of Japan (PDBj). All the protein structures of PDB can further be analyzed using another pictorial database, PDBsum. PDBsum is a web-based database that gives an overview and the key information about each protein structure deposited in the PDB.

**Table 2.3 Computational tools and databases of proteins**

Name of tool	Type of tool	URL
PDB	Database	<a href="http://www.rcsb.org/pdb/home/home.do">http://www.rcsb.org/pdb/home/home.do</a>
PDBe	Database	<a href="http://www.ebi.ac.uk/pdbe/index.html#m=0&amp;h=0&amp;e=0&amp;r=0&amp;l=0&amp;a=0&amp;w=0">http://www.ebi.ac.uk/pdbe/index.html#m=0&amp;h=0&amp;e=0&amp;r=0&amp;l=0&amp;a=0&amp;w=0</a>
PDBsum	Database	<a href="http://www.ebi.ac.uk/pdbsum/">http://www.ebi.ac.uk/pdbsum/</a>
Swiss-Model	Online Tool	<a href="http://swissmodel.expasy.org/">http://swissmodel.expasy.org/</a>
SCOP	Online Tool	<a href="http://scop.mrc-lmb.cam.ac.uk/scop/">http://scop.mrc-lmb.cam.ac.uk/scop/</a>
HMMSTR	Online Tool	<a href="http://www.bioinfo.rpi.edu/~bystrc/hmmstr/server.php">http://www.bioinfo.rpi.edu/~bystrc/hmmstr/server.php</a>
Israel Science and Technology	Protein Sequence Database	<a href="http://www.science.co.il/biochemical/Protein-Databases.asp">http://www.science.co.il/biochemical/Protein-Databases.asp</a>
RasMol	Molecular Graphics Visualization Program	<a href="http://rasmol.org/">http://rasmol.org/</a>
Pymol	Molecular Graphics Visualization Program	<a href="http://pymol.org/">http://pymol.org/</a>
Chimera	Molecular Structure Visualization Program	<a href="http://www.cgl.ucsf.edu/chimera/">http://www.cgl.ucsf.edu/chimera/</a>
Visual Molecular Dynamics	Molecular Visualization Program	<a href="http://www.ks.uiuc.edu/Research/vmd/">http://www.ks.uiuc.edu/Research/vmd/</a>
Swiss-Pdbviewer	Multiple Protein Structure Analysis Tool	<a href="http://spdbv.vital-it.ch/">http://spdbv.vital-it.ch/</a>

Model databases are built manually to store the collection of protein structures determined based on the sequence of proteins. For example, HMMSTR (Hidden Markov Model for local

sequence-Structural correlations in proteins) or the Rosetta prediction server is model databases that can predict the protein structure from its sequence.

The list of various protein sequence databases is stored in Israel Science and Technology database. If the protein structure is not available in PDB or could not be predicted using its sequence, then the homology modelling of the protein can be performed using Swiss-Model server. Further, the computational tools and data bases for the study of protein structures are listed in Table 2.3

### ***2.5.3. Bioinformatics Tools to Study the Active Site of Proteins***

If the ligand binding site and shape in the protein structure is known, *in silico* or experimental procedures can be performed to determine the ligand type and the protein function (Glaser et al., 2006). The structure and function of a protein play an important role in the design of safe and efficient therapeutics. The SMAP Web Service is an interesting, user-friendly web interface which is suitable to predict the ligand binding pocket of a protein and to compare the 3D ligand binding sites. SMAP-WS can also be used to predict the side effects of drugs and repurpose the existing drugs for new indications. SMAP-WS is a parallel web service for structural proteome-wide ligand-binding site comparison.

‘The Lipid Library’ is another database useful for lipid research. Along with the basic structure and properties of lipids it will also explain the chemistry, biological properties, and their function, biochemistry of plant and animal lipids in detail. Apart from the above lipid exclusive databases, the lipid ligand structures can be downloaded from the databases like PubChem, ChemSpider, ChEBI, etc. There is another database named SCOP (Structural Classification of Proteins) in which proteins are classified according to their structure and sequence.

After downloading the structure of protein from the database, it can be viewed using different molecular graphical tools mentioned below.

- RasMol
- Pymol
- Chimera
- Visual Molecular Dynamics
- Swiss-Pdbviewer.

These software tools are useful to alter the protein structures, produce publication quality images, study the amino acid sequence of a protein, preparing the protein structures for molecular docking (a computational method used to predict the orientation of one molecule to another) and to compare and align the similar proteins. The available tools for the study of ligand binding site are shown in Table 2.4.

**Table 2.4 Computational tools and databases for the study of ligand binding site of proteins**

Name of tool	Type of tool	URL
MetaPocket	Active Site Finding Tool	<a href="http://projects.biotech.tu-dresden.de/metapocket/">http://projects.biotech.tu-dresden.de/metapocket/</a>
CASTp	Binding Pocket Tool	<a href="http://sts.bioe.uic.edu/castp/">http://sts.bioe.uic.edu/castp/</a>
BBCB	Web Interface	<a href="http://computing.bio.cam.ac.uk/">http://computing.bio.cam.ac.uk/</a>
BindingDB	Web Accessible Database	<a href="http://www.bindingdb.org/bind/index.jsp">http://www.bindingdb.org/bind/index.jsp</a>
JCB	Web site	<a href="http://ppi.fli-leibniz.de/">http://ppi.fli-leibniz.de/</a>

The PDB code of the protein or the PDB file of a protein can be used as an input for these tools. The output explains about the active site and pocket of the protein with a three dimensional pictorial representation.

Apart from the above mentioned bioinformatics tools there are also other methods like (SURFNET- Consurf) to predict the binding site of the protein. To make this easier, the Bioinformatics and Computational Biology services (BBCB) have put together all the available techniques for the study of proteins. These techniques are designed for binding site

prediction, protein binding pocket identification, binding affinity prediction and protein interaction with different ligands. There is another public, web-accessible database, BindingDB that has the measured binding affinities of a collection of proteins bound with ligands. It also contains the crystal structures of protein-ligands. This database mainly focuses on the proteins which can act as drug targets.

#### **2.5.4. Molecular Docking Tools for the Study of Lipid-Protein Interactions**

Once the crystal structures of protein and lipid are available, the next step is to study the interaction between lipid and protein. *Molecular Docking* is the virtual experiment used to measure the strength of binding between two molecules. The three dimensional structure of both the ligand and the protein are the inputs to perform docking. There are various docking tools available. Some are commercial whereas some of them are free to download.

Since particular docking tools work best for the specific targets, it is good practice to use more than one docking tool in order to obtain accurate results (Lape et al., 2010). Each docking tool varies from the other in the type of scoring function, it uses to perform molecular docking. The *scoring function* is a mathematical algorithm that is used to calculate the strength of non-covalent interactions, which can also be termed as binding affinity (Halperin et al., 2002). There are three types of scoring functions.

- 1) Knowledge based scoring functions
- 2) Empirical scoring functions
- 3) Force field, scoring functions.

All three scoring functions calculate binding affinity between two molecules by using a different algorithm.

The JCB (Jena Center for Bioinformatics) protein-protein interaction website discusses the various docking software available to study protein-ligand and protein-protein interactions. The website Click2Drug provides the information about all the available bioinformatics tools

to study the ligand binding sites, databases that have structural information of proteins and ligands and various docking tools. AutoDock 4.2 is a widely used molecular docking technique for which the quality of assessment (of protein-ligand binding affinity prediction) was determined (Kim et al., 2008). Glide is another docking tool developed by Schrodinger that predicts protein-ligand binding modes and ranks the ligands via high-throughput screening. Glide docking tool uses two scoring functions: Standard Precession (SP) and Extra Precession (XP). To dock multiple lipid ligands with single protein, Glide can be used. Also, there are web-based docking tools available like Docking Server, Hex Server, and Swiss Dock. These tools accept the input of protein and ligand in the form of PDB files. The output is generated from the server very quickly, from which the user can analyze the results of docking.

The results of docking could be further analyzed using software tools like Pymol, Swiss PDB, Chimera, and LigPlot. Usually the strength of binding between the protein and lipid is measured in terms of the binding energy. Binding energy is based on the intermolecular interactions between the protein and ligand. The types of bonds can be hydrogen bonds, hydrophobic interactions, electrostatic interactions and van der Waal interactions (Ross et al., 1981). The distance and type of bond between the ligand and the receptor determine the strength of binding where the lower the binding energy the stronger the affinity between the ligand and the receptor (Kim et al., 2008).

Docking is also useful in computer aided drug design. Section 2.3 discussed about the health importance of three groups of lipids. These three groups of lipids were shown to bind to different molecular targets which are used in the design of drugs. For example, tocotrienol as a pharmacological target for PPAR can be used to treat cancer, diabetes and cardiovascular diseases. It was proved through docking that tocotrienols have a strong affinity with PPARs (Gaddipati, 2012). Further use of bioinformatics tools is discussed below.

The docking tools can be used in this aspect to find how strongly a ligand can bind to its receptor (protein or enzyme). The development of bioinformatics tools is also significant in the field of drug discovery. The molecular docking of tocotrienol with antiperoxidative enzymes was carried using Autodock4.0 as the docking program (Khan et al., 2011). This *in silico* docking is also supported by an *in vivo* experiment and investigated the protective role of tocotrienol against infection and inflammation. The binding of tocotrienols with antioxidant enzymes was observed through molecular docking (Khan et al., 2011).

Another docking tool-Molegro Virtual Docker can be used to study the enzyme inhibition (Khan et al., 2011). The binding of PUFAs with Brain-Derived Neurotrophic Factor (BDNF) was studied through molecular docking. The results of this study suggested that the physical interaction of PUFAs with BDNF can modulate insulin resistance and regulate food intake and body weight (Vetrivel et al., 2012). The interaction of endocannabinoids with CB1 and CB2 were studied using bioinformatics tools like quantitative structural-activity relationships (a computational method that correlates the structure or property of a protein with activities), docking and molecular dynamic simulations (Reggio, 2010).

**Table 2.5 Computational tools and databases for the study of lipid-protein interaction**

Name of tool	Type of tool	URL
Click2Drug	Web site	<a href="http://www.click2drug.org/">http://www.click2drug.org/</a>
DockingServer	Web-Based Docking Tool	<a href="http://www.dockingserver.com/web">http://www.dockingserver.com/web</a>
Hex Server	Web-Based Docking Tool	<a href="http://hexserver.loria.fr/">http://hexserver.loria.fr/</a>
Swiss Dock	Web-Based Docking Tool	<a href="http://swissdock.vital-it.ch/docking">http://swissdock.vital-it.ch/docking</a>
Ligplot	Software	<a href="http://www.ebi.ac.uk/thornton-srv/software/LIGPLOT/">http://www.ebi.ac.uk/thornton-srv/software/LIGPLOT/</a>
MD tools	Website	<a href="http://www.ks.uiuc.edu/Development/MDTools/">http://www.ks.uiuc.edu/Development/MDTools/</a>

The inhibitory activities of endocannabinoids are studied by using flexible docking procedures (Romani et al., 2011). Various bioinformatics tools involved in the study of lipid-protein interactions were shown in Table 2.5.

### ***2.5.4.1. Limitations of Molecular Docking***

Calculation of lowest binding energy or binding affinity depends on how well the ligand binds to the protein (Sousa et al., 2006). Docking protocols are the combination of search algorithm and scoring functions. There is relatively a large number of scoring functions and search algorithms available today. In order to include the true binding modes between protein and ligand, the search algorithm should allow the degree of freedom of the protein-ligand system (Sousa et al., 2006). The two critical elements of any search algorithm are fast and effectiveness. Logically, the effectiveness of any docking protocol lies in combining the best search algorithm with the best scoring function. However, several studies have confirmed that the performance of most docking tools depends on the binding site and the ligand to be investigated (Clark et al., 1993; Kuntz et al., 1982; Schulz-Gasch & Stahl, 2003).

Sometimes, inaccuracies in the energy models used to score potential ligand-receptor complexes lead to the differences in binding energies. Some docking experiments might fail due to the inability of docking method to account for conformational changes that occur during the binding process of ligand and protein (Teodoro et al., 2001). Furthermore, predicting receptor structural rearrangements is a complex problem.

Current docking methods follow the lock and key theory proposed by Emil Fischer in 1890 (Cramer, 1994). So the protein structures were considered as rigid entities and the ligand changes its three dimensional structures during the binding process to fit into protein binding site. Later in 1958 Koshland proposed induced fit theory to explain the mechanism of interaction between protein and ligand (Koshland, 1995). According to this theory both protein and ligand structures are flexible and both the structures change their conformation when they interact to form a complex to form a minimum energy fit. Unfortunately, the computational capability is limited to follow the exact modeling of the flexibility available to

protein during binding process (Teodoro et al., 2001). Modeling the full flexibility of protein requires 1000 degrees of freedom whereas conventional ligand techniques can handle up to 30 degrees of freedom approximately (Teodoro et al., 2001). This problem can be solved with MD simulations as MD simulations take into account of all the degrees of freedom available to the protein (Teodoro et al., 2001). Accurate energy calculations can also be carried out using MD simulations. However, MD simulations are computationally expensive.

The author's study of molecular docking was supported by both MD simulations and wet laboratory experimental validations.

### ***2.5.5. Molecular Dynamic Simulations***

Molecular dynamics are computer simulations that give the view of physical motion of atoms. It is complex to understand the molecular mechanism while two macromolecules are interacting with each other. Molecular dynamic simulations are useful to understand the structural properties and the microscopic interaction between macromolecules such as proteins (Allen, 2004). MD simulations play an important role in drug discovery. When small molecules like drugs (a lipid or any other ligand) bind to their target (protein), the ligand will come across a macromolecule in constant motion. Also, the ligand brings a conformational change to the protein structure. Molecular dynamics play a significant role here by simulating the receptor motion and providing information about these movements.

Alder and Wainwright have demonstrated molecular dynamic simulations while studying the interaction of hard spheres (hard sphere model is used to mimic the motion of molecules or atoms in a container) in the late 1950's (Alder et al., 1957). The use of MD simulation was very low in 1950's. However, this is not the case today. There is tremendous research done on MD simulations not only for proteins, but also for lipid systems. Computer aided drug design has used MD simulations for many years to calculate binding energies. MD

simulations are rapidly progressing with the improvement in simulation methodology and increasing accuracy of biomolecular force fields (Hansson et al., 2002). For example, the biological function of vitamin E was understood easily with molecular dynamic simulations of  $\alpha$ -tocopherol that provided the structural and kinetic properties of this vitamin E isomer (Qin et al., 2009). Its importance can be seen by the various forms in which it can be applied to study an interaction. For example, MD simulations were used to study the effects of  $\alpha$ -tocopherol on the stability and lipid dynamics of model membranes imitating the lipid composition of plant chloroplast membranes (Hincha, 2008). The structure and dynamics of the endocannabinoid N-archidonylethanolamine (anandamide) in a phospholipid bilayer were probed using MD simulations (Lynch et al., 2005). The analysis suggested that the shape of anandamide is complementary to cholesterol (Furse et al., 2006). MD simulations were used to explore the behavior of the COX-1 and COX-2 enzyme isoforms bound to arachidonic acid (Di Pasquale et al., 2009). Different simulation tools available are listed on the website of the Theoretical and Computational Biophysics Group of Illinois University. Based on the type of receptor molecule and nature of the ligand a particular simulation tool can be selected.

### ***2.5.6.Experimental Validation***

Simulations form a bridge between the theory and experiment. A theory can be tested by performing simulations using the same model and the model can be compared with the experimental results. Also, computer simulations that are difficult or even impossible in the laboratory (Reggio, 2010) can be performed. After the study of lipid-protein interactions using in silico techniques like molecular docking and molecular dynamic simulations, the results can be compared with the laboratory experimental results. The best pairs of proteins and ligands which have stronger affinities can further be tested using biological experiments. The lipid-protein interactions which are important to health can be considered for computer-aided drug design in the future.

## ***2.6. Novelty and Uniqueness of Contribution***

This section discusses about the similar research to author's study along with the limitations and gaps in the past research. Although the binding site of PPARs with DHA was studied previously through molecular docking and computer simulations (Gani & Style, 2008). The author's study is extended to some other lipid ligands and proteins along with DHA and PPARs. The protein PPAR and the ligand DHA are same in both Author's study and the study conducted by Gani & Style. However, Gani & Style have used ICM molecular docking technique and AMBER molecular dynamic simulations which are different from the ones used by the author. Due to this difference the binding affinities yielded by both the studies cannot be compared.

Later, in 2009, the molecular docking study of tocotrienols was performed by Upadhyay with the similar approach as the author's study (Upadhyay, 2009). The ligands used in this study are entirely different from the ligands considered for author's study. Moreover, this study was limited to the binding of tocotrienols with P-glycoprotein (Section 2.3.1.1) whereas the author's study focused on many other proteins. P-glycoprotein also known as permeability glycoprotein or multidrug resistance protein is an important protein of cell membrane that pumps many foreign substances out of the cell.

Tocotrienols and tocopherols were examined previously for their inhibitory action on COX-2 and found that  $\gamma$ -tocotrienol is an inhibitor of COX-2 (Stone et al., 2005). Further, Stone et al., have revealed that tocotrienols and tocopherols activate PPAR- $\gamma$ . Stone et al., have examined the binding of PPAR- $\gamma$  with  $\gamma$ -tocotrienol. The author's study has extended to other proteins and lipid ligands. The study of Stone et al. has used western blot analysis to determine the binding of tocotrienols with PPAR- $\gamma$  and COX-2 whereas the author's study

has used SPA. Hence, the binding affinities obtained from these two studies cannot be compared.

SPA of PPARs with thiazolidinediones was conducted and the  $K_d$  of PPARs was calculated (Sun et al., 2005). The study conducted by Sun et al., has used darglitazone as a ligand and none of the ligands from the author's study were used.

Anandamide and other endocannabinoid ligands were studied before using molecular docking (Padgett et al., 2008). The study of Padgett et al. is similar to the author's study in comparing the molecular docking results with experimental results and is contrast in the choice of ligands. Padgett's study has concluded that during docking, anandamide has adapted to certain conformations which are analogous to arachidonic acid, the substrate of COX-2. Moreover, the study was limited to the binding of anandamide and its analogues only with CB1. The author's study included CB2 and other lipid ligands.

COX-2 and PPARs were tested for their binding affinities before. The binding affinity of COX-2 was tested with plant secondary metabolites and not with lipid ligands as in the author's study (Huss et al., 2002). Similar to the author's study, Huss et al., also have conducted enzymatic SPA to find new COX-2 inhibitors. This study has evaluated ubiquitous plant constituents for the inhibition of COX-2 catalyzed prostaglandin E2 biosynthesis. COX-2 activity was determined for 49 plant metabolites during this study.

The binding affinities of anandamide and 2AG were calculated experimentally using different assay methods (Adams et al., 1998; Adams et al., 1995; Gonsiorek et al., 2000). The studies have used different methods such as *in vitro* receptor binding (Adams et al., 1998), antinociception assay (Adams et al., 1995) and intact cell radioligand binding (Gonsiorek et al., 2000). All these methods involved the calculation of binding affinities of anadamide and 2AG with cannabinoid receptors. However, the methodological differences reflected in

different binding affinities (Herkenham et al., 1991). Hence, the binding affinity values, from the author's study, differ from the determinations from the above mentioned studies.

It can be concluded from the above similar studies that, even though there are some experimentally-determined and computationally predicted binding affinities for the target proteins and ligands, these values cannot be compared with the values determined from the author's study. This is because of the different sets of parameters and methodologies considered for each study with different combinations of proteins and ligands.

Nevertheless, there is no similar web based tool to *Lipro Interact* that can provide the binding affinities and microscopic binding information of the target lipid-protein interactions as in the author's study. Although, there are many bioinformatics tools available for the interaction studies of lipids and proteins as discussed in Section 2.5, *Lipro Interact* is unique in its function and design. Moreover, *Lipro Interact* facilitates the biological future researchers with binding data related to the target receptors and ligands. The PDB files available to download from *Lipro Interact* were generated as a result of author's study and they do not exist anywhere else. These PDB files are ready to use for the further studies.

After reviewing all the relevant research studies, it is concluded that the author's study is novel and unique and does not overlap with the similar studies of the past.

## **2.7. Conclusion**

The literature review has focused on three groups of lipid ligands: tocotrienols, omega 3 fatty acids and endocannabinoids. These three groups of lipids are chemically active and biochemically significant. The interaction of these lipid ligands with different proteins was studied extensively. The proteins which are currently used as drug targets were selected for

the current study. With the advent of computer technology, understanding the three dimensional structure of protein and ligand and their interaction has now become easy.

The lipid-protein interactions mentioned in the current study would be further useful in designing drugs for different diseases like cancer, diabetes, and atherosclerosis, inflammatory and behavioural disorders. The currently available treatments are not up to the patient needs and are also causing some side effects. Hence, the current research was focussed on finding the potential targets for the above mentioned diseases. As the lipid ligands are naturally occurring they might cause few or no side effects. Individually, both the ligands and receptor targets considered for the current research are biologically significant and medicinally important; their interaction would be useful in the design of a new generation of drugs.

This chapter summarized the past research carried out with regards to the selected ligands and receptor interactions along with their pharmacological significance. There is a knowledge gap in the previous research regarding:

- i) the lack of experimental validations for significant lipid-protein interactions
- ii) the study of mutations of target proteins
- iii) particular software that could predict the binding affinities of the selected ligands and receptors.

Identifying this research need, the author has focused researching on these topics. Consequently, the research presented in the coming chapters of this thesis is an effort to address these knowledge gaps pertaining to target lipid-protein interactions and their use in drug designing.

The literature review discussed in this chapter is the fundamental basis to design the bioinformatics and biochemical experimental methodology described in chapter 3.

## Chapter 3

# Bioinformatic and Biochemical Methods to Create *Lipro Interact* Software

### 3.1. Introduction

The study of the three dimensional (3D) structure of a protein and ligand was complex before the development of computer technology. There has been an incredible amount of research in the last few years to understand the affinity of the related ligand-receptor system. The improvement of computer power and simulation techniques allowed for an extended exploration of the interaction of realistic macromolecules (Bongrand, 1999). The strength of an interaction between the ligand and the receptor is called binding energy. There are many computational, as well as theoretical methods available for calculating the binding energies between the ligand and the receptor. The problems raised in the design of bioactive compounds, particularly in the area of computer-aided drug designing, have motivated the development of computational tools. With the advancement in biomolecular X-ray crystallography, the 3D structures of some proteins are available today.

The entry of bioinformatics tools into the existing biological world has created a new chapter in the field of biomedical research. Experiments for research, which were once costly and

time-consuming, have found great value in bioinformatics tools due to their low expenditure and rapid results. The use of computer power in the biological world is tremendous. The computational methods used for this purpose are docking and MD simulations (Bissantz et al., 2000). The recognition (*Docking*) process between a ligand and its receptor plays an important role in virtually all biological processes (Mangoni et al., 1999). MD simulations are used to study the stability of a docked protein-ligand complex. Molecular docking and MD simulations need experimental validation. However, the results of *in silico* techniques provide guidance for the wet laboratory techniques, and save time and effort.

In this Chapter, Section 3.2 discussed the selection of a particular docking tool based on the specific target. The reason for selecting AutoDock and Glide was explained in Section 3.3. Section 3.4 and Section 3.5 described the molecular docking tools (*AutoDock* and *Glide*) performed to study the binding between target lipids and proteins. Through molecular docking, the top ranked ligands are identified as the strongest lipid ligands of the target proteins. The stability of the docked lipid-protein complex was studied using MD simulation and is explained in Section 3.6. As virtual methods require experimental validation, SPA is conducted to study the biological binding of the target lipid-proteins. Section 3.7 specifies the procedure of SPA. The findings from all of the above sections are applied to the design of the software and a brief explanation is included in Section 3.8. Section 3.9 concludes all the above Sections of Chapter 3.

## **3.2. Methodology Framework**

The methodology of this thesis involved both biochemical and bioinformatic techniques. The following Figure 3.1 represents different steps carried as a part of this methodology.

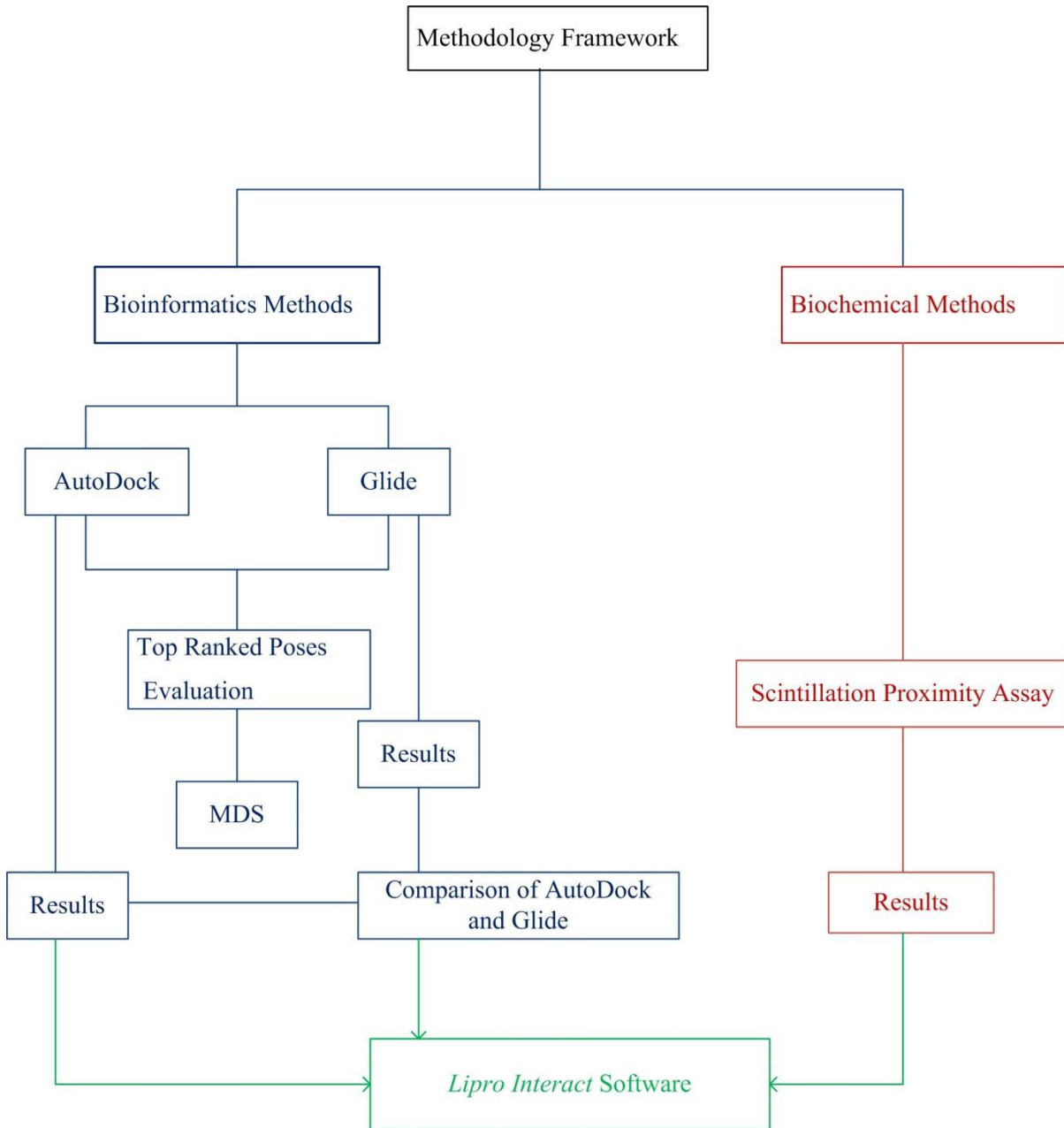


**Figure 3.1 Methodology Framework**

### 3.2.1. Bioinformatic Component

The bioinformatic component of thesis methodology was shown in blue colour in the above Figure 3.1. Total ten proteins and eight lipid ligands shown in the Table 3.1 were selected for the study. AutoDock and Glide docking were performed for all the ten proteins with eight lipid ligands. Each protein was docked with eight ligands and their binding affinities were

calculated for all the 80 lipid-protein interactions in both AutoDock and Glide docking programs. The results of both AutoDock and Glide were compared in terms of binding affinities and intermolecular interactions. The top ranked docking poses for each protein were then subjected to MD simulation, which further evaluated the stability of docked complexes.

**Table 3.1 Target proteins and lipid ligands**

Protein	Ligand
PPAR- $\gamma$	$\alpha$ -tocotrienol
PPAR- $\alpha$	$\beta$ -tocotrienol
PPAR- $\delta$	$\gamma$ -tocotrienol
RAR- $\gamma$	$\delta$ -tocotrienol
RXR- $\alpha$	DHA
COX-1	EPA
COX-2	2AG
LOX	Anandamide
CB1	-
CB2	-

### **3.2.2. Biochemical Component**

The biochemical component of the project was shown in brown colour in the Figure 3.1. From the above ten proteins PPARs, RAR and RXR belong to the nuclear receptor family. COX-1, COX-2 and LOX are enzymes, whereas, CB1 and CB2 are the members of G-protein coupled receptor family. Five proteins were selected with at least one protein from each family—PPAR- $\gamma$ , PPAR- $\alpha$ , COX-2, CB1 and CB2—to perform the wet laboratory experiment, SPA. These five proteins were selected based on AutoDock and Glide docking results. SPA was conducted in two phases. 1. Saturation binding analysis 2. Competitive binding analysis and is explained in detail in Section 3.7.

### **3.2.3. Lipro Interact**

The development of *Lipro Interact* involved the collaboration of both bioinformatic and biochemical components of the project and was shown in green in the Figure 3.1. As a final

step, the results from AutoDock and Glide as well as the SPA results were further taken to develop *Lipro Interact* Software.

### ***3.3. Selection of Molecular Docking Tool***

The formation and dissociation of specific non-covalent interactions between varieties of macromolecules play a crucial role in the function of a biological system. Molecular docking is useful to study the ligand-receptor interactions where the ligand binding domain of a particular protein can be identified, and binding affinities can be predicted. Selecting a particular docking tool for the study of ligand-receptor interactions is always a challenge. There are many docking tools available like AutoDock (Morris et al., 2009), FlexX (Kramer et al., 1999), Dock (Ewing et al., 2001), Gold (Verdonk et al., 2003), Glide (Glide, 2011), etc. Each docking program uses a different scoring function. Scoring functions estimate interaction energies between small ligands and receptors, and rank docking results according to the relative binding affinities of different ligands. They enable a virtual screening of compound libraries and the design of ligands with improved affinities.

It is always difficult to judge the best docking tool, as particular tools work better for specific targets (Lape et al., 2010). The author's study has selected *AutoDock* and *Glide* as docking tools to examine the target ligand-receptor interactions. The selection of these docking tools is based on a literature review conducted by Cross et al., 2009 on the proteins and ligands. AutoDock 4.2 (Morris et al., 2009) and Glide (Glide, 2011) are identified as suitable docking tools for the current study. Using more than one docking tool, and comparing their outcomes, further improves the accuracy of the results. The bioinformatics tool selection was based on the literature review performed, which is explained in Section 2.4 of Chapter 2.

A review was conducted by Sousa et al., to evaluate the available docking programs (Sousa et al., 2006). The combination of the best search algorithm (Lamarckian Genetic Algorithm)

and the best scoring function (empirical scoring function) is the example of accurate results of AutoDock. The statistical analysis performed by Sousa et al., has revealed that AutoDock has occupied the highest percentage (48%) of citations compared to other docking programs. AutoDock was used in a structure based drug design of potential protein kinase inhibitors and the study has concluded that AutoDock is a flexible ligand-docking method (Ali et al., 2011). Another recent study has also used both AutoDock and Glide to compare the suitability for the docking and predicting the anticancer agents (Adeniyi & Ajibade, 2013).

In a review carried out on different docking tools, it was discovered that Glide docking yields the most accurate results compared to the other docking tools like GOLD and ICM (Krovat et al., 2005). In another study conducted by Friesner et al., Glide was identified as a novel docking tool for the protein-ligand binding affinities (Friesner et al., 2006). Further, Glide was used in another study to calculate the binding affinities (Chang et al., 2010). Deb et al., have conducted molecular docking and receptor-specific studies with Glide docking tool and the results are successful (Deb et al., 2012). The performance of Glide docking was evaluated by Vass et al., in a sequential multiple-ligand docking paradigm predicting the binding modes of 129 protein-ligand complexes (Vass et al., 2012). For the above reasons and due to the budget constraints of the project, the author has chosen AutoDock and Glide as molecular docking techniques.

### ***3.4. Molecular Docking Studies using AutoDock***

With the development of computer technology over the years, a number of docking algorithms have been made publicly available. Compared to the other fast docking algorithms, it was identified in an evaluation study (Buzko et al., 2002) that AutoDock offered a considerable combination of accuracy and speed as opposed to other methods. AutoDock is an automated procedure designed to predict the interaction of ligands with

biomolecular targets. The docking procedure is explained in the following sections. AutoDock uses an empirical scoring function and Lamarckian Genetic Algorithm (Morris et al., 1998).

### **3.4.1. Ligand Preparation**

The 3D structures of the eight selected ligands were downloaded from the PubChem website (Chapter 2, section 2.5, Table 2.2). Although there are several other databases that have a collection of lipid structures, the PubChem website is growing with the contribution of 80 other database vendors, and is a reliable source for ligand structures. Refining the structure of the ligands was carried out using *Chimera* software, as all the atoms, bonds and molecules can be clearly viewed and adjusted according to the needs (Pettersen et al., 2004). During this step the ligand structures were minimized. AutoDock accepts the ligand structure in either MOL2 format or PDB format. After adding hydrogens using AutoDock Tools (ADT), the MOL2 or PDB format of the file was converted to a PDBQT file, which was the actual input to the docking procedure. Ligand flexibility was achieved by choosing a root atom. This root atom acts as the centre of rotation during coordinate transformation in the docking simulation (Morris et al., 2009).

The protonation states have to be determined for the rigid ligands with macro cyclic rings and exotic chemical groups (Cosconati et al., 2010). However, the eight lipid ligands used in this study are flexible. Hence, the default protonation states set by AutoDock were used. By using the protonation states set by AutoDock, ADT can convert coordinates into the form required for AutoDock calculations (Cosconati et al., 2010). Hence, adding hydrogens atoms and charges, merging non-polar hydrogen atoms onto their retrospective heavy atoms, assigning atom types in the docking process were performed by using ADT (Cosconati et al., 2010).

### **3.4.2. Protein Preparation**

The crystal structures of all the target proteins were downloaded from the PDB ([www.pdb.org](http://www.pdb.org)). These structures were refined by deleting the existing ligand using *Chimera* software. The Graphical User Interface (GUI) of ADT was used to prepare the PDBQT file by adding polar hydrogens and partial charges to the protein molecule. PDB codes 3FEI, 3GZ9 and 3FEJ were used for the crystal structures of PPAR- $\alpha$ , - $\beta$  and - $\gamma$  respectively.

The crystal structures were selected based on the crystal resolution. Resolution is the measure of the quality of data which was collected on the crystal containing the protein. When all the proteins in a crystal are aligned in an identical way, they result in the formation of a very perfect crystal and all of the proteins will scatter the X-rays the same way (Berman et al., 2000). On the other hand the diffraction pattern does not contain much information when the proteins in the crystal are slightly different due to local flexibility or motion. Hence, resolution is considered as a level of detail present in the diffraction pattern and the level of detail that would be seen in an electron density map calculation (Berman et al., 2000). It is easy to see every atom in the electron density map in case of high resolution structures with minimum resolution values. Considering this the PDB codes with minimum resolution values were selected as a first step. Then these PDB codes were filtered based on the publication. Some PDB codes were already published indicating the positive results in molecular docking whereas others are yet to publish. Later, the crystal structures with the selected PDB codes were examined to check for the presence of mutations and the complete side chains. The PDB codes with incomplete side chains were disregarded. Finally, before confirming a particular PDB code for the current molecular docking study, the structures were observed for the correct three dimensional conformations. The structures were also filtered based on the presence of ligands, crystalline waters and cofactors.

The active site of the amino acid was selected based on the crystal ligand binding site. For example, the crystal ligand CTM binds to the protein PPAR- $\alpha$  at the amino acids, Cys 275, Cys 276, Met 330 and Met 355 and to PPAR- $\gamma$  at the amino acids, Met 364, Cys 285, Met 348 and Gly 284. This information was taken from the published article about the X-ray crystal structure of CTM bound to PPAR- $\alpha$  and PPAR- $\gamma$  (Grether et al., 2009). The same set of amino acids was considered for the author's study as the binding site of the protein. The active site selection was based on an experiment in which PPARs were tested for their binding affinity with 26 ligands where CTM was identified as strong affinity dual agonist of PPAR  $\alpha$  and  $\gamma$  (Grether et al., 2009). Hence, the author's study was aimed to compare the binding affinities of eight lipid ligands with CTM. Similarly a literature review was conducted on the crystal ligand binding site of protein. After analyzing the active sites suitable to eight lipid ligands the binding site of the protein was selected for each target protein.

The amino acids Cys 275, Cys 276, Met 330 and Met 355 were considered as the active site for the protein PPAR- $\alpha$  (Grether et al., 2009). For PPAR- $\delta$ , the combination of amino acids His 323, His 449, Tyr 473, Cys 285 and Thr 288 is the active site (Connors et al., 2009). Met 364, Cys 285, Met 348 and Gly 284 were the active site amino acids for PPAR- $\gamma$  (Grether et al., 2009). In the case of RXR- $\alpha$ , the PDB code 1FBY was used with the active site amino acids Cys 269, Val 349, Ala 271, Ala 272, and Cys 432 (Egea et al., 2000). The PDB file 3LBD was downloaded from the PDB website for the crystal structure of RAR- $\gamma$ . Amino acids Leu 233, Ser 289, Arg 273 and Leu 271 were considered as the active site amino acids for RAR  $\gamma$  (Klaholz et al., 1998). Prior to the selection of active site for a particular target protein a thorough literature was conducted as discussed in Chapter 2 Section 2.4.4 to study the different binding sites of the protein. Then the selection was based on the successful results from the previous publications.

The crystal structures with PDB codes 3N8Y, 1CVU and 3V99 were used for the enzymes COX-1, COX-2 and LOX respectively. A typical PDB file consists of heavy atoms, water, co-factors and metal ions, and can be multimeric. AutoDock needs a refined protein structure as an input file. Hence, the imported protein crystal structures were refined using Chimera. All three enzymes used in this study have two identical side chains: chain A and chain B. The active sites of COX-1, COX-2 and LOX are located on chain A hence chain B was removed from the crystal structures in order to simplify the multimeric complex. Amino acids—Arg 120, Tyr 355, Tyr 385, Ser 530 and Asn 375—were chosen as the active site amino acids for COX-1 (Rowlinson et al., 1999). The same active site (Arg 120, Tyr 355, Tyr 385, Ser 530 and Leu 531) was considered for COX-2, except for a single amino acid difference (Vecchio et al., 2010). The catalytic domain is present in the N-terminus of LOX. Amino acids Met 239, Tyr 359, Gln 358, Asn 308 and Ala 542 were considered as the active site amino acids (Madeswaran et al., 2012).

The X-ray crystal structures of CB1 and CB2 are not available on the PDB website. Hence, the structural sequences of these two receptors were downloaded from the Uniprot (<http://www.uniprot.org>) website and submitted to the I-TASSER server (<http://zhanglab.ccmb.med.umich.edu/I-TASSER/>). Uniprot is an open accessible website that provides comprehensive, high quality protein sequences and functional information. I-TASSER server was selected to predict the 3D structure of cannabinoid receptors. I-TASSER server is ranked as the best method in the server section of the 7th critical Assessment of Structure Prediction to predict the 3D structure of a protein from amino acid sequence (Zhang, 2008). In a study performed by Roy et al., I-TASSER was recognised as a unified platform for automated protein structure and function (Roy et al., 2010). It was found in another study that the performance of I-TASSER is better than the rest of online servers that can predict the protein structures (Roy et al., 2012).

After submitting the protein sequence, I-TASSER used ten templates that were very similar to the submitted protein sequence. I-TASSER modelling used LOMETS which identified the structure templates from the PDB library (Roy et al., 2012). LOMETS is a meta-server threading approach that contains multiple threading programs where each program generates tens of thousands of templates. Then I-TASSER used Z-Score to sort the templates of highest significance in the threading alignments. Z-score was calculated by the difference between the raw and average scores in the unit of standard deviation. LOMETS threading program selected the top ten templates. Here each threading program selected one or two templates with highest Z-score. The threading programs were sorted by the average performance in the large-scale benchmark test experiments (Roy et al., 2010).

I-TASSER simulations generated tens of thousands conformations (that are called decoys) for each target. To select the final models, I-TASSER clustered all the decoys based on the pair-wise structure similarity with the help of SPICKER program (Roy et al., 2010). SPICKER is a clustering algorithm to identify the near native models from a pool of protein structure decoys. After these I-TASSER generated 5 models that corresponds to the 5 largest structure clusters. According to Monte Carlo theory the largest clusters represent the states of the largest partition function or lowest free energy and hence have the highest confidence. C-score was used to quantitatively measure each model (Roy et al., 2012). C-score is a confidence score for estimating the quality of predicted models by I-TASSER. It was calculated based on the significance of threading template alignments and the convergence parameters of the structure assembly simulations. The top 5 models generated by I-TASSER were ranked by the cluster size. So the top ranked models have a higher C-score (Roy et al., 2010).

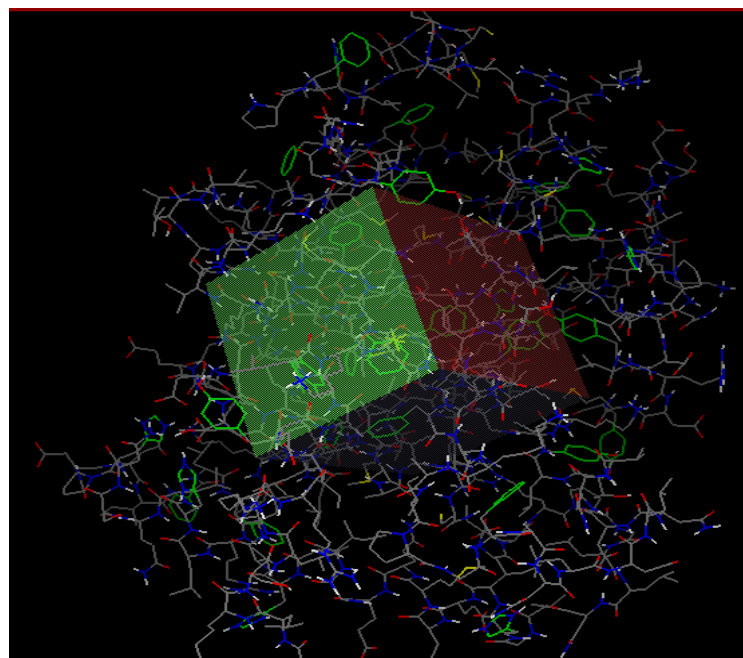
Then, I-TASSER used TM-align program to match the first I-TASSER model to all structures in the PDB library. TM-align program is based on the TM-score or RMSD. TM-score is a

proposed score to measure the structural similarity of two structures (Zhang & Skolnick, 2004). By using TM-score I-TASSER sorted 5 models based on top 10 proteins from PDB that have closest structural similarity. These proteins often have similar function due to the similarity in structure (Zhang, 2008).

The 5 models generated were evaluated using the NIH MBI Laboratory servers (<http://nihserver.mbi.ucla.edu/SAVES/>). NIH MBI Laboratory servers use ERRAT protein structure verification algorithm which is especially designed for the evaluation of crystallographic model building and refinement. ERRAT program analyzes the statistics of non-bonded interactions between different atom types. This program compares the statistics from highly refined structures and the error values were calibrated to give the confidence limits (Colovos & Yeates, 1993). The best model was selected based on the results generated from NIH MBI laboratory servers. Amino acids Met 240, Trp 241, Trp 356, Leu 359, Leu 360 and Ala 283 (Mahmoudian, 1997) were considered to be the active site amino acids of CB1 for the grid generation. For CB2, Ser 112, Phe 117, Leu 255, Cys 257, Trp 194 and Trp 258 were treated as the active site amino acids (Montero et al., 2005).

### ***3.4.3. Receptor Grid Generation***

The receptor grid was generated for the active site amino acids of the protein. The active site of the protein was embedded in a 3D grid. The grid preparation for one of the proteins (PPAR- $\alpha$ ) is shown in Figure 3.2. The 3D grid is shown in the center of the protein structure with X, Y and Z dimensions of 45.916, 33.192 and 35.476 respectively. AutoGrid pre-calculates the grid maps for each atom type present in the docked ligand. This further helps with fast docking calculations.

**Figure 3.2 Grid formations for PPAR- $\alpha$** 

### ***3.4.4. Docking with AutoDock***

After preparing the protein and ligand files, performing molecular docking is the next step.

The docking procedure using AutoDock requires the following files as an input:

- a grid map file, that is generated by AutoGrid, as discussed in Section 3.4.3,
- a PDBQT file for the ligand (Section 3.4.1),
- a docking parameter file which specifies the files and parameters for the docking calculation. ADT is used to generate the docking parameter file.

The final docked coordinates were written by AutoDock in a docking log file (DLG). The docking protocol was set as follows.

#### ***3.4.4.1. Conformation Search***

Lamarckian Genetic Algorithm, Genetic Algorithm, Simulated Annealing and Local Search are the different search methods available in AutoDock for performing the conformation search. Of these conformations, Lamarckian Genetic Algorithm was used for the author's

study since it is the most efficient one (Morris et al., 1998). The hybrid of genetic algorithm with the adaptive local search method forms Lamarckian Genetic Algorithm (LGA). It was observed in an experiment that LGA works better than genetic algorithm and local search methods (Morris et al., 1998). The performance of LGA is based on the empirical scoring function. This program determines the docking poses with the interacting energies between random pairs of ligand and various selected portions of protein (Tiwari et al., 2009). LGA uses an empty grid affinity for the conformational search. These conformations tend to bury hydrophobic portions inside and form internal hydrogen bond interactions (Morris et al., 2009). Further, LGA can handle the ligands with more degrees of freedom than simulated annealing, genetic algorithm and local search and hence considered as most efficient, reliable and successful of the other three search algorithms (Morris et al., 1998).

#### ***3.4.4.2. Number of Evaluations***

The above search methods include parameters for determining the amount of computational effort used in the search. The default number of evaluations was considered for the author's docking studies, as it is sufficient based on the protein and ligand structures (Hetényi & van der Spoel, 2002).

#### ***3.4.4.3. Redocking as a Validation Method of Docking***

Redocking was performed as a validation method for protein-ligand complexes. The 3D structures of the crystal ligands were obtained by removing the crystal ligand from protein crystallographic complexes. The crystal ligands were then redocked with all the proteins using AutoDock. Root Mean Square Deviation (RMSD) values between the crystal ligand and the predicted conformations were calculated using Pymol software (Chapter 4, Section 4.2.3).

### ***3.4.4.4. Evaluating the Results of Docking***

At the end of a docking simulation, the clustering information and the internal energies were written by AutoDock into a DLG file. AutoDock performed the cluster analysis of the different docked conformations. The number of runs was set based on the structure of ligand and protein. Initially AutoDock was run using the default parameters for docking. After analyzing the results, if the docked complexes did not yield binding poses with lowest binding affinities and active site amino acid interactions, the parameters were modified as follows.

Some protein-ligand complexes yielded lowest binding energy conformations within 10 runs while some complexes took 50-100 runs. For example, tocotrienols when docked with PPARs did not produce the conformations in ten runs. So, the number of runs was increased from 10 to 100 in a step wise manner. Finally after analyzing the results, the lowest binding energy conformation was observed for tocotrienols-PPAR complexes in 100 runs. Likewise, DHA and EPA when docked with LOX did not yield the lowest binding energy conformations until 50 docking runs. After 50 docking runs the complex started generating positive binding energies. Since positive binding energies are the measure of false results the docking was stopped at 50 runs. On the other hand endocannabinoids (2AG and anandamide) produced the lowest binding energy conformations within 10 runs when docked with cannabinoid receptors. After ten runs the complexes generated positive binding energies. Thus, the sufficient sampling required for molecular docking was provided based upon the trial docking experiments conducted. The sufficient sampling depends on the ligand structure and the number of torsions in the ligand structure (Morris et al., 2009).

The minimum energy found in each run was reported as a histogram from the DLG file, which also includes a table of RMSD values within each cluster. The results were analyzed

using ADT and Visual Molecular Dynamics (VMD). The similar structure ligands resulted in less difference in their binding affinities.

#### ***3.4.4.5. Analyzing AutoDock Results***

The DLG file is opened and observed with the help of ADT. The interactions between the docked conformation of the ligand and the receptor were studied during this step. By default, ADT showed the ligand as a ball and stick surrounded by a molecular surface. The colored surface distinguishes the regions that were in contact with the receptor from gray colored regions that were not in contact. Portions of the receptor that were in contact with the ligand were shown with the ball-and-stick. Hydrogen bonds were shown as a string of small spheres. VMD (<http://www.ks.uiuc.edu/Research/vmd/>) was also used to analyze the results of AutoDock. The resultant PDB files generated for the docked protein-ligand complexes were opened using VMD, and the bond distances and bond lengths from protein to ligand were analyzed. The amino acids of the protein within a 4Å distance around the ligand were shown in the images drawn from VMD.

#### ***3.4.4.6. Selection of the Best Docked Pose***

The results from each run were analyzed from the DLG file generated by AutoDock. For each run the conformation instance can be found from the DLG file. Each conformation was represented as a specific set of ligand atoms that were in the interaction with the protein. For each conformation AutoDock computed intermolecular energy and torsional energy. The combination of both intermolecular energy and torsional energy gives the binding energy between the protein and ligand. When there were 100 runs for the complex of tocotrienols and PPARs 100 conformations were generated. All 100 conformations were viewed using the GUI of ADT. The conformations with the ligand binding to the active site of the protein and with the maximum number of intermolecular interactions were then viewed using VMD and

Pymol (<http://www.pymol.org/>). During this step, the conformations were studied from the lowest binding energy, to the highest binding energy. Hydrogen bonds, van der Waal interactions and electrostatic interactions of the ligand with proteins were identified and grouped into the result data. Then, these conformations were again analyzed for the lowest binding energies and the rest of them were disregarded. From this list of conformations, the pose in which the ligand bound to the binding pocket of protein with maximum number of van der Wall and electrostatic interactions and lowest binding energy was chosen as top ranked binding pose (Morris et al., 2009).

Later, Pymol and VMD were used to record the interacting amino acids of the protein within a 4Å distance of the ligand. Pymol is a molecular graphic tool which is used to view the 3D structure of the proteins in different conformations. This tool was utilized to locate the possible interactions between the receptor and ligand, and also the length of the bond. Publication quality images are produced using Pymol. VMD is 3D graphical molecular visualization program used to analyze large biomolecular systems. LigPlot (<https://www.ebi.ac.uk/thornton-srv/software/LIGPLOT/>) software was used to study the hydrogen bonds and hydrophobic interactions between the ligand and protein.

### **3.5. Molecular Docking Studies using Glide**

Glide docking tool is a product of Schrödinger (Schrödinger, LLC, New York, 2011), designed to study the ligand-receptor interactions. Glide is a new approach that can search for favorable interactions of proteins with more than one ligand. Therefore, Glide docking provides an opportunity to compare the binding mode and affinity of multiple ligands with the protein. *Ligand pose* can be defined as the position and orientation of a ligand with respect to the protein, along with its conformation in flexible docking. The ligand poses generated by Glide docking are usually evaluated by a series of hierarchical filters. Glide uses

‘ChemScore empirical scoring function’. This algorithm recognizes favorable hydrophobic and hydrogen-bonding interactions between the protein and ligand. Glide is ranked number one among the currently available docking tools through different evaluative experiments (Kellenberger et al., 2004). In a review performed on different docking tools, it was noticed that Glide docking yields the most accurate results compared to the other docking tools like GOLD and ICM (Krovat et al., 2005).

### ***3.5.1.Ligand Preparation***

Glide accepts the 3D PDB format of the ligand structure as an input file for the ligand preparation. The 3D structures of all eight ligands ( $\alpha$ -tocotrienol,  $\beta$ - tocotrienol,  $\gamma$ -tocotrienol,  $\delta$ -tocotrienol, DHA, EPA, 2AG, anandamide) were downloaded from the PubChem website. Glide modifies the torsional internal coordinates of the ligand during docking. The Schrodinger ligand preparation product, LigPrep, is used to prepare the ligand molecule for Glide docking. The LigPrep (LigPrep, 2011) process consists of a series of steps that refine the ligand structure. Removing unwanted structures, adding hydrogens, optimizing and minimizing ligand structures were carried out through LigPrep. The ligand structures were minimized using OPLS-2005 force field due to its improved parameterization and greater coverage (Sudha et al., 2011). Furthermore, OPLS-2005 force field was recommended for grid generation because of its handling capacity of metals among the other force fields (LigPrep, 2011). As a result, a single low energy 3D structure with correct chiralities was produced.

LigPrep is designed to produce high quality 3D structures by introducing variations in chemical structures such as stereochemistry or the protonation state (LigPrep, 2011). Hence, the protonation states for all the ligands were set using LigPrep. If the structural data is available, the protonation states of the ligand can be deduced from the structure of the ligand

(Friesner et al., 2006). The structural data is available for all the ligands and the protein active site was also selected prior to conducting molecular docking. Hence, the correct protonation states were assigned with a binding mode of the ligand (Friesner et al., 2006).

### **3.5.2. Protein Preparation**

The 3D structures of all the proteins were downloaded from the PDB. Table 3.2 refers to the PDB codes and crystal ligands used for the current study. A typical PDB file consists of heavy atoms, waters, co-factors, and metal ions, and can be multimeric. Glide docking needs a refined protein structure as an input file. Hence, the imported protein crystal structures were refined using the Protein Preparation Wizard of Maestro (Suite2011, Maestro Version 9.2). The multimeric complex structure of the protein is simplified, as the minimum number of atoms in the complex structure is desirable for computer efficiency. All the crystallographic water molecules, except for those that have bridged interactions between the protein and the ligand, are removed from the 3D structure of the receptor molecules.

**Table 3.2 Protein Input Structure Information**

<b>Protein</b>	<b>PDB code</b>	<b>Crystal Ligand</b>
PPAR $\alpha$	3FEI	CTM
PPAR $\beta/\delta$	3GZ9	D32
PPAR $\gamma$	3FEJ	CTM
COX-1	3N8Y	Diclofenac
COX 2	1CVU	Arachidonic acid
LOX	3V99	Arachidonic acid
RAR $\gamma$	3LBD	Retinoic Acid
RXR $\alpha$	1FBY	Retinoic Acid

The water molecules were usually allowed to spin and toggle on and off (Verdonk et al., 2005). Toggling a water molecule on would introduce an entropic penalty and may result in change of binding energies (Cambridge Crystallographic Data Centre, 2011). Hence, these water molecules were deleted before conducting molecular docking. This is in contrast in the

case of the water molecules that have bridging interactions between protein and ligand. These water molecules play an important role in mediating hydrogen-bonding interactions and are the key for facilitating tight binding (Huggins & Tidor, 2011). Hence, the water molecules that formed bridging interactions between protein and ligand were retained in the structures.

The Protein Preparation Wizard is efficient in adjusting the protein, metal ions and cofactors. The wizard repairs any missing residues near the active site of the protein. The ligand bond orders and formal charges were adjusted. Following these steps, restrained minimization of the protein was carried out with the Impact Refinement module (Impref, 2011).

The resulting protein structures were reviewed to examine the refined ligand/protein/water structures to ensure the correct formal charges, bond orders, protonation states, and the required final adjustments were made. The prepared protein structures were then used to generate receptor grid files.

### ***3.5.3. Receptor Grid Generation***

The shape and properties of the receptor were represented on a grid by several different sets of fields that provide progressively more accurate scoring of the ligand poses. The receptor grid is one of the input files to perform ligand docking. Receptor grid generation requires a prepared structure (an all atom structure with appropriate bond orders and formal charges), which is achieved from the previous step (Section 3.4.2). The receptor grid for all the proteins was set up and generated from a Receptor Grid Generation panel. The options from this panel were used to define the receptor structures. During this step, co-crystallized ligands were removed, and the position and size of the active site was determined, as it will be represented by receptor grids. The ligands in the crystal structures (as mentioned in Table 3.1) were used to determine the active site of the receptor. The force field OPLS\_2005 was used to allow a proper treatment of metals and a wide range of atom types defined.

### ***3.5.4. Docking Studies***

Previously calculated receptor grids and ligand structures prepared through LigPrep were required to perform Glide ligand docking. The ligand docking panel from Glide was used to perform the docking in two steps by selecting XP mode in the first step and SP mode in the second step. The flexible docking option with default settings was selected from the ligand docking panel as this directs the docking process to generate conformations internally. Glide measured the ligand-receptor binding affinity in terms of Glide score. The Glide score is the sum of all the ligand interactions with the protein, like van der Waal interactions, hydrogen bonds, hydrophobic interactions, and the electrostatic interactions that approximate the ligand binding free energy (Friesner et al., 2006). The performance of the docking method was evaluated by drawing a Receiver Operator Characteristic (ROC) curve.

### ***3.5.5. Validation of Docking Results***

The results of Glide docking were validated using a ROC curve (Huang et al., 2006). The docking results generated from both XP and SP modes of docking were subjected to enrichment studies (studies used to validate the performance of a particular method). The plot was drawn by considering sensitivity on the X-axis, and specificity on the Y-axis. Sensitivity (true positives) is the ability of the eight known ligands (actives) to react with the target proteins. Specificity (false positives) is the binding result of the eight known ligands combined with 200 decoys (random). The decoys were downloaded from the Schrodinger website ([www.schrodinger.com](http://www.schrodinger.com)). The docking of eight known and two hundred unknown ligands was performed using both XP and SP modes of Glide docking. This output file was used as the input file for enrichment studies. The best ligand poses isolated from the docking output files of XP and SP docking were the actives for the enrichment calculation. The enrichment results were used to plot the ROC curve. The ROC plot was generated between

the known versus unknown ligands (Chapter 5, Section 5.2.3). The known ligands were ranked as actives among the total ligands used.

## ***3.6. Molecular Dynamic Simulations***

Molecular dynamics is a computer simulation technique where the time evolution of a set of interacting atoms is followed by numerical integration of Newton's equation of motion (Li, 2005). MD simulations need high performance computing and longer periods of simulation time. Hence, MD simulations were conducted only for the top ranked pose of protein-ligand combinations considering the budget constraints and available resources. Further, the reason for performing MD simulation is to study the stability of docked complexes and to ensure that molecular docking has yielded accurate results. The stability of a docked complex is usually identified with its RMSD and RMS fluctuations during the period of simulation. MD simulations were performed for the strongest binding affinity complexes as follows.

### ***3.6.1. Theory of MD Simulations***

Science is based on the experimental results. The chemical machinery of life can be understood with the experimental results. The structure and elucidation of the function of large biomolecules was determined by the experimental techniques such as X-ray diffraction and nuclear magnetic resonance. However, the experiment was possible only in conjunction with models and theories (Meller, 2010). The effect of experiment and theory has been altered by the computer simulations. Simulation uses computer to model the physical system. The machine interprets the results in terms of physical properties with the calculations implied by a mathematical model. It can be classified as a theoretical method as computer simulation deals with models.

Through MD simulations basic physical theories can be applicable to biological phenomena such as quantum, classical and statistical mechanics lead to equations which cannot be solved analytically exactly (Meller, 2010). The algorithm of MD simulations is based on the time evolution of a set of interacting particles followed via the solution of Newton's equation of motion as shown in the following equation.

$$F_i = m_i \frac{d^2 r_i(t)}{dt^2} \quad (\text{Meller, 2010})$$

where  $F_i$  is the force acting on the  $i$ th particle due to interaction at time  $t$ ,  $m_i$  is the mass of the particle,  $r_i(t) = (X_i(t), Y_i(t), Z_i(t))$  is the position vector of  $i$ th particle.

Particles in the above equation correspond to the atoms. They may represent any distinct entities such as chemical groups. The description of time evolution at phase space and the position and velocity vectors define MD trajectories (Meller, 2010).

The force acting on interacting atoms recomputes at each step to update the position and velocities in the step wise numerical integration procedure. Hence, the repeated calculation of forces defines the overall complexity of the MD algorithm. According to statistical mechanics the average configurations of the system represent physical quantities. MD trajectories provide a set of configurations and the conservation energy is implied by Newtonian dynamics (Meller, 2010). Therefore, physical quantity can be measured by taking the average of values calculated from MD trajectories. However, MD simulations have some limitations such as quantum effects, reliability of the interatomic potentials, time and size (Meller, 2010).

Some biologically important processes such as oxygen binding to haemoglobin, catalytic cleavage of the peptide bond by chymotrypsin involve quantum effects. These quantum effects include changes in chemical bonding and the presence of important noncovalent

intermediates. For this kind of phenomena straight forward atomic force field simulations cannot be used (Meller, 2010). Moreover, quantum MD simulations were impractical for large systems.

The results of MD simulations will be realistic only if the potential energy mimics the forces experienced by the real atoms. In order to speed up the evolution of forces potential should have a simple functional form.

One of the most severe problems in MD simulations is the time limitation. For example, the conformational transition in haemoglobin takes tens of microseconds while protein folding may take few minutes. However, the time step in numerical integrations could be limited to one femto second due to the presence of significant fast motions. Thus, following the allosteric transition in haemoglobin requires tens of billions of steps for a system of 10,000 atoms (Meller, 2010). In case of strong interactions of macromolecules with their water and lipid environments, the desired length of simulations places a limit on the increasing size (Meller, 2010).

### **3.6.2. System Building**

To test the docking parameters and results, MD simulation using *Desmond* software was performed (Bowers et al., 2006; Guo et al., 2010; Shivakumar et al., 2010). Desmond allows the users to examine biological and pharmaceutical events with speed and accuracy (Wang et al., 2013). With the possibility of long time scale of MD simulation, Desmond provides comprehensive setup, simulation and analysis tools (Wang et al., 2013). MD simulation were performed for docking complexes PPAR- $\alpha$ -DHA, PPAR- $\beta$ -DHA, PPAR- $\gamma$ -DHA, COX-1-EPA, COX-2-2AG, LOX-BTT, RAR- $\gamma$ -DHA, RXR- $\alpha$ -DHA, CB1-Anandamide, and CB2-Anandamide with the lowest binding energy to evaluate the stability and conformational

changes. MD simulations were carried out using a Desmond module of Schrodinger (Desmond, 2012).

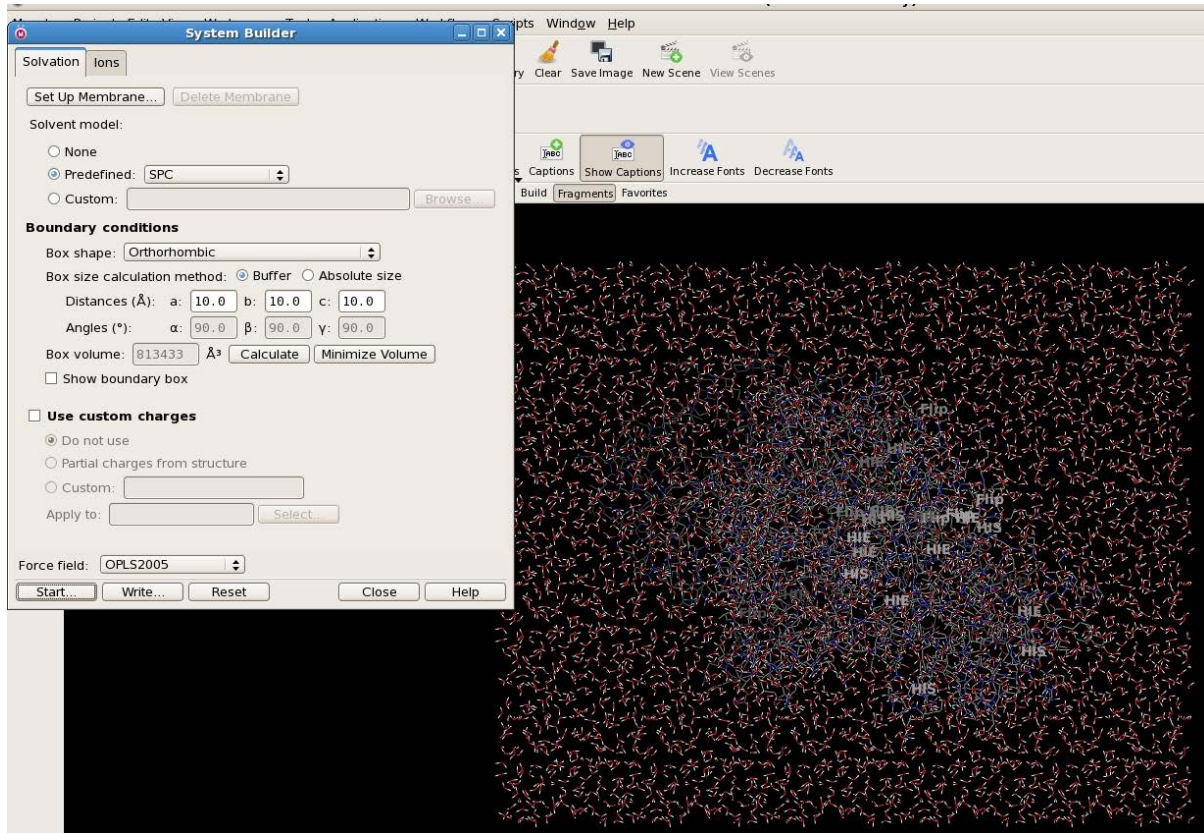


**Figure 3.2 System Building of LOX-BTT**

The system building was achieved using a simple point charge water model, and neutralized by replacing solvent molecules with  $\text{Na}^+$  ions. The orthorhombic water box has a volume of:

- $312735 \text{ \AA}^3$  for PPAR  $\alpha$ ,
- $330827 \text{ \AA}^3$  for PPAR  $\beta$ ,
- $350599 \text{ \AA}^3$  for PPAR  $\gamma$ ,
- $1547723 \text{ \AA}^3$  for COX-1-EPA,
- $678693 \text{ \AA}^3$  for COX-2-2AG,
- $813433 \text{ \AA}^3$  for LOX-BTT,

- $300980 \text{ \AA}^3$  for RAR  $\gamma$ -DHA,
- $286817 \text{ \AA}^3$  for RXR  $\alpha$ -DHA,
- $935946 \text{ \AA}^3$  for CB1,
- $50093 \text{ \AA}^3$  for CB2

and a distance of  $10 \text{ \AA}$  buffer region between protein atoms and box sides as shown in the Figure 3.2. The OPLS-2005 force field is used in the system building for protein interactions.

### ***3.6.3. Minimization***

Minimizing the number of atoms in the complex system structure removed unfavorable contracts which would otherwise crash the simulation during force evaluations in MD. Hence, the final system was minimized as follows with approximately:

- 30134 atoms in PPAR- $\alpha$ ,
- 31610 atoms in PPAR- $\beta$ ,
- 33774 atoms in PPAR- $\gamma$ ,
- 108748 atoms in COX-1-EPA,
- 65889 atoms in COX-2-2AG,
- 813433 atoms in LOX-BTT,
- 28086 atoms in RAR- $\gamma$ -DHA,
- 27591 atoms in RXR  $\alpha$ -DHA,
- 72564 atoms in CB1-Anandamide,
- 53251 atoms in CB2,

were subjected to simulation. In brief, the full system was minimized using a maximum of 2000 iterations with steepest descent and limited memory Broyden–Fletcher– Goldfarb–

Shanno algorithms, with a convergence threshold of 50.0kcal/mol/Å<sup>2</sup>. This is followed by a similar unrestrained minimization with a convergence threshold of 5.0kcal/mol/Å<sup>2</sup>. The minimized system is relaxed with three short span simulations.

- NVT ensemble (constant number of atoms (N), volume (V), and temperature (T)) for a simulation time of 12 picoseconds (ps) restraining all non-hydrogen solute atoms.
  - NPT (constant number of atoms (N), pressure (P), and temperature (T)) ensemble for a simulation time of 24 ps restraining all non-hydrogen solute atoms.
  - NPT ensemble, without restraints, for a simulation time of 24 ps.

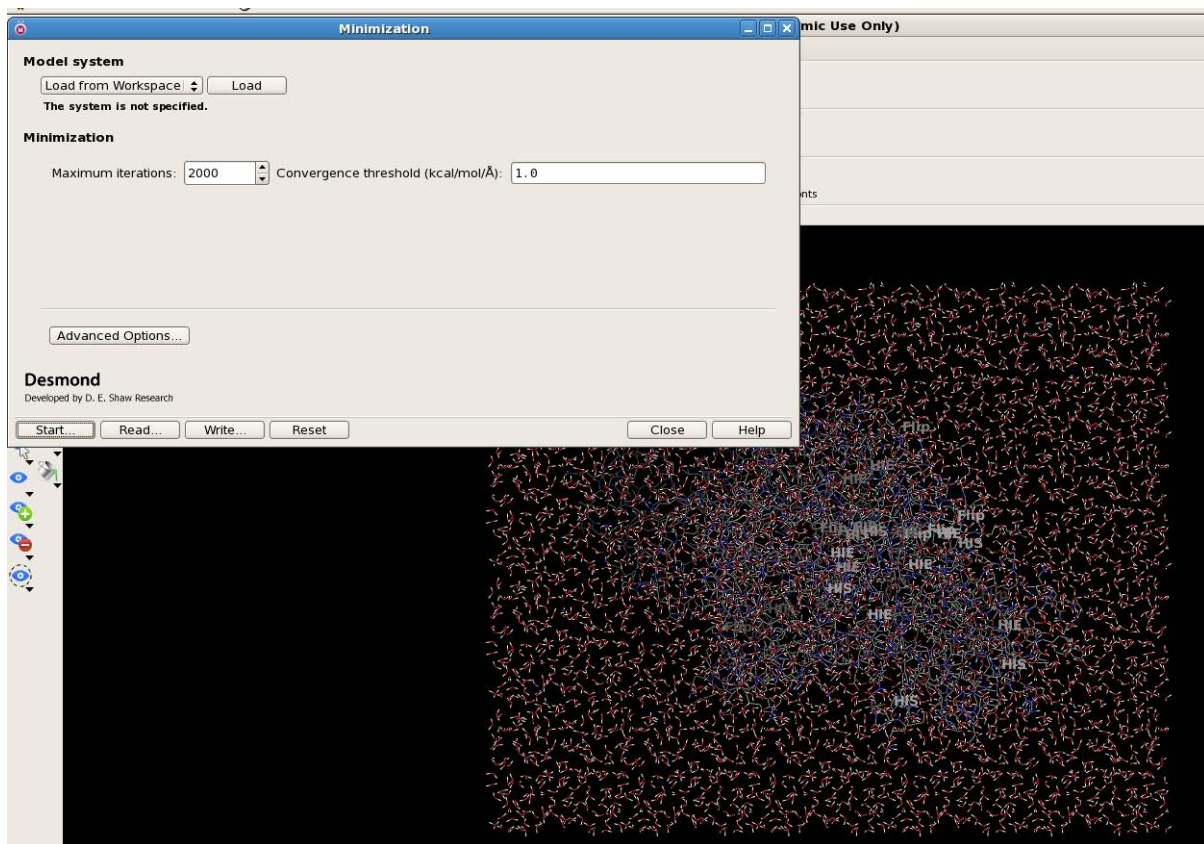


**Figure 3.3 Minimization of LOX-BTT**

The three simulations were performed with default parameters of time steps, temperature, and velocity in a Berendsen thermostat. These initial minimization and simulations were

implemented to prepare the model for a simulation time of 2ns. As an example, the minimization of LOX-BTT complex is shown the Figure 3.3.

### ***3.6.4. Molecular Dynamics***

The model was then simulated for 2ns, with a time step of 2 femtoseconds (fs) NPT ensemble using a Berendsen thermostat at 310K, and velocity resampling for every 1ps. The simulated system was analyzed for stability of the docking complex. Energy fluctuations and RMSD of each complex was analyzed with respect to simulation time. RMSF (Root Mean Square Fluctuations) of the backbone of all the docked complexes were analyzed.

## ***3.7. Scintillation Proximity Assay***

SPA was conducted for the proteins PPAR- $\alpha$ , PPAR- $\gamma$ , COX-2, CB1 and CB2 with all eight ligands. The binding between the proteins and target ligands is studied by conducting both saturation and competitive binding experiments. The protein binding with different concentrations of radiolabelled ligand was observed during saturation binding. In the competitive binding assay, a single concentration of radiolabelled ligand was taken along with different concentrations of unlabeled ligands, and was tested for their binding ability with proteins. SPA is explained in detail in Chapter 7.

The proteins PPAR- $\alpha$ , PPAR- $\gamma$ , COX-2, CB1 and CB2, and the unlabeled ligands were supplied by Sapphire Bioscience <sup>2</sup>. DHA and EPA were labelled by using C<sup>14</sup> radioisotope, whereas 2AG and anandamide were labelled with H<sup>3</sup> radioisotope and were supplied by Bio scientific Pty Ltd <sup>3</sup>. 96-well WGA coated flash plates were supplied by Perkin Elmer <sup>4</sup>. The instrument used to read the radioactivity was MicroBeta Trilux.

---

<sup>2</sup> Sapphire Bioscience Pty Ltd, Australia (<http://www.sapphirebioscience.com/>)

<sup>3</sup> Bio scientific Pty Ltd (<http://www.biosci.com.au/>)

### ***3.7.1.Preparation of SPA System***

The initial step in the procedure was pre-coating the flash plates with coating buffer. The coating buffer was prepared with 0.015M sodium carbonate and 0.035M sodium bicarbonate at a pH of 9.6. Flash plates were stored at 4<sup>0</sup>C. The steps involved in preparing the SPA system were as follows:

- The coating buffer with a volume of 200 $\mu$ l was added into each well.
- The plates were shaken at room temperature for 1 hour and the buffer was discarded.
- The dry plates were stored at -20<sup>0</sup>C

The assay buffer was made up with 10% glycerol, 25mM HEPES, 12.5mM MgCl<sub>2</sub>, 50mM KCl, and 1mM DTT.

### ***3.7.2. Normalization and Standardization of MicroBeta Trilux***

MicroBeta Trilux is a multi-detector instrument used for liquid scintillation counting. Each detector comprises two photomultiplier (PM) tubes, with one of the PM tubes disabled to read the flash plates. The calibration procedure for the performance of PM tubes is called *normalization*. Preparing a counting protocol and correcting the counting efficiency using the normalization parameters is called *standardization*. The normalization and standardization protocols for the flash plates were performed by the following steps (Software version 3.0):

- The sample was taken in G11.
- A new normalization was created.
- The window settings of normalization protocol were changed to 175-360 for H<sup>3</sup> and 175-650 for C<sup>14</sup>.

---

<sup>4</sup> PerkinElmer, Australia (<http://www.perkinelmer.com/>)

- The protocol was saved and the same parameters were used to create a counting protocol.
- The efficiency of the instrument was calculated after running the protocol.

### ***3.7.3. Saturation Binding Assay***

Saturation binding was performed by taking the increasing concentrations of radiolabelled ligand, with a constant concentration of unlabeled ligand. The aim of this assay was to find the dissociation constant ( $K_d$ ) of the radiolabelled ligand with the protein. Saturation binding was performed in two steps. The first step was to find the total binding of the protein with a ligand, and the second step was to find the non-specific binding. By subtracting the non-specific binding from total binding, the specific binding was measured and  $K_d$  was calculated from the saturation curve. The radiolabelled ligand was taken in four different concentrations. The concentration of  $C^{14}$  DHA and  $C^{14}$  EPA were 50nM, 75nM, 100nM and 150nM, whereas, for  $H^3$ 2AG and  $H^3$ anandamide the concentrations are 10nM, 15nM, 20nM and 25nM. The optimum concentration of each protein to generate a saturation curve varies. The final assay concentration of PPAR- $\alpha$  and  $\gamma$  were  $\sim$ 13 picograms, whereas for CB1 and CB2 the concentration is  $\sim$  9.75picograms, and for COX-2 the concentration was  $\sim$  6.75picograms. The steps of measuring the non-specific binding were the same as that of total binding, except for the incubation time and the concentration of unlabeled ligand. The concentration of unlabeled ligand during the total binding analysis was only 5 $\mu$ M, whereas during the non-specific binding study, the unlabeled ligand concentration was increased to 30 $\mu$ M. The different concentrations of radiolabelled ligands were added along with the increased concentration of unlabeled ligand and incubated for 3 hours. With the excess concentration of unlabeled ligand and prolonged incubation time, unlabeled ligand occupies all the specific binding sites of the protein. Hence, the radiolabelled ligand occupied only the non-specific

binding sites of the protein. When the plate was read in MicroBeta, counts per minute (CPM) indicates the non-specific binding of the radiolabelled ligand.

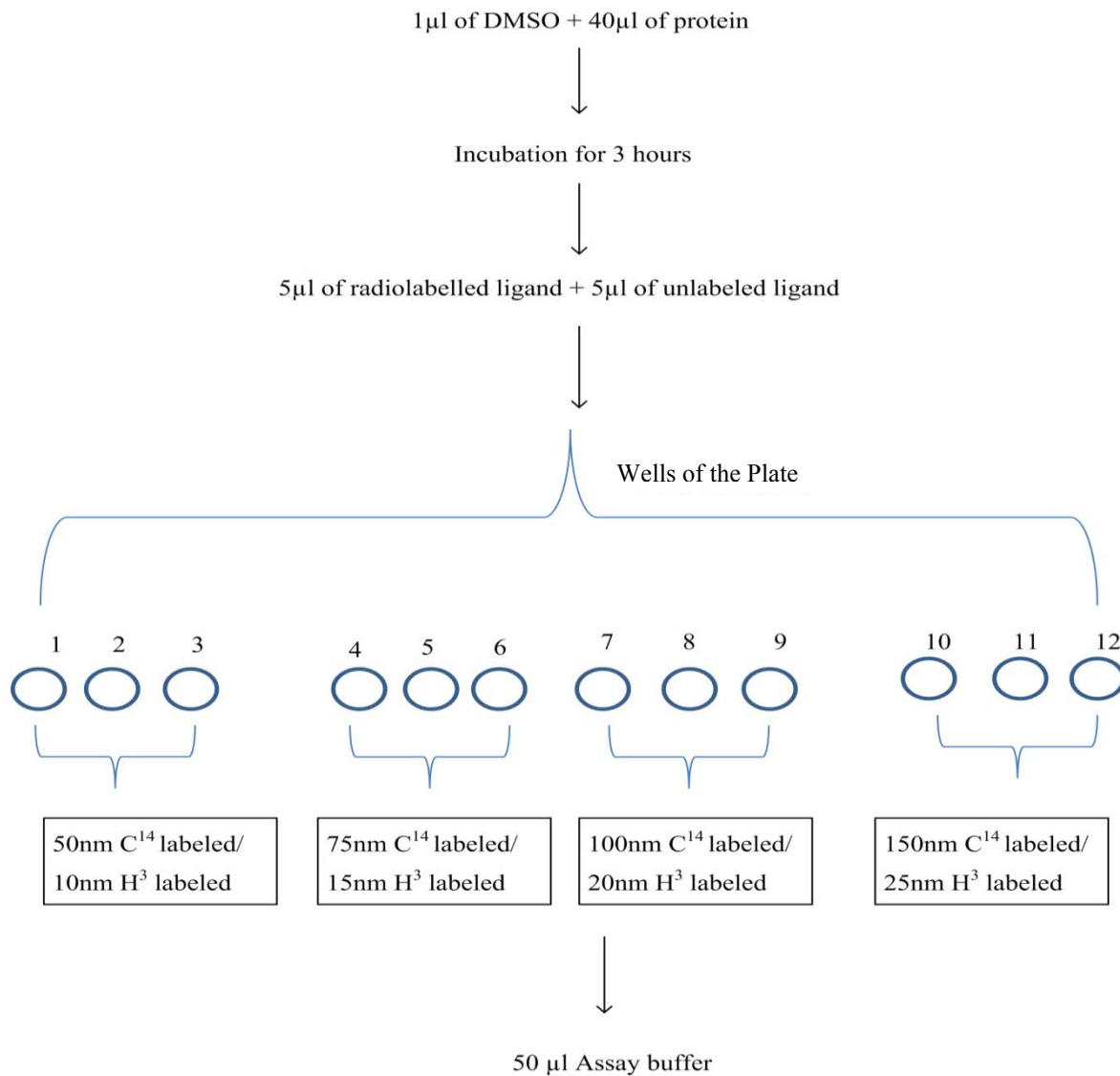


**Figure 3.4 Procedure of saturation binding analysis**

The steps for measuring the total binding were as follows as shown in the Figure 3.4.

After adding all the ingredients, the plate was shaken for 15 minutes and incubated at room temperature for 1 hour. Finally, the plate was read in MicroBeta using the counting protocol created for the sample.

A saturation curve was plotted by taking the radiolabelled ligand concentration on the X-axis and CPM on the Y-axis. Both total and non-specific binding are plotted on the same graph to calculate the specific binding. The software Graph pad prism 6.04 (<http://www.graphpad.com/>) was used to plot the graphs (Chapter 7, Section 7.2.2 and Section 7.2.3).

### ***3.7.4. Competitive Binding Assay***

Competitive binding assay was performed by taking the increased concentrations of unlabeled ligand with a constant concentration of radiolabelled ligand. This type of assay was used to calculate the binding strength of unlabeled ligands with the protein. The aim was to find the inhibition constant of unlabeled ligands for the proteins. During the assay, the increasing amounts of unlabeled ligand compete with the constant concentrations of radiolabelled ligand for the specific binding sites of the protein. The excess amounts of unlabeled ligands were more likely to occupy the active sites of the protein, leaving very few sites for the radiolabelled ligand.

The radioligand concentration was constant (50nM for C<sup>14</sup> labeled and 20nM for H<sup>3</sup> labeled) for the whole competitive binding assay. The assay was conducted with the steps shown in the Figure 3.5. Unlike saturation binding, in competitive binding assay the labeled and unlabeled ligands were mixed in the Eppendorf as shown above. From the Eppendorf 10µl of stock mix of labeled and unlabeled ligands was added into the wells. Then the plate was shaken for well 15mins followed by a 3 hour incubation time. Finally, the plate was read in Microbeta Trilux using the standardized protocol prepared with the sample prior to the assay.

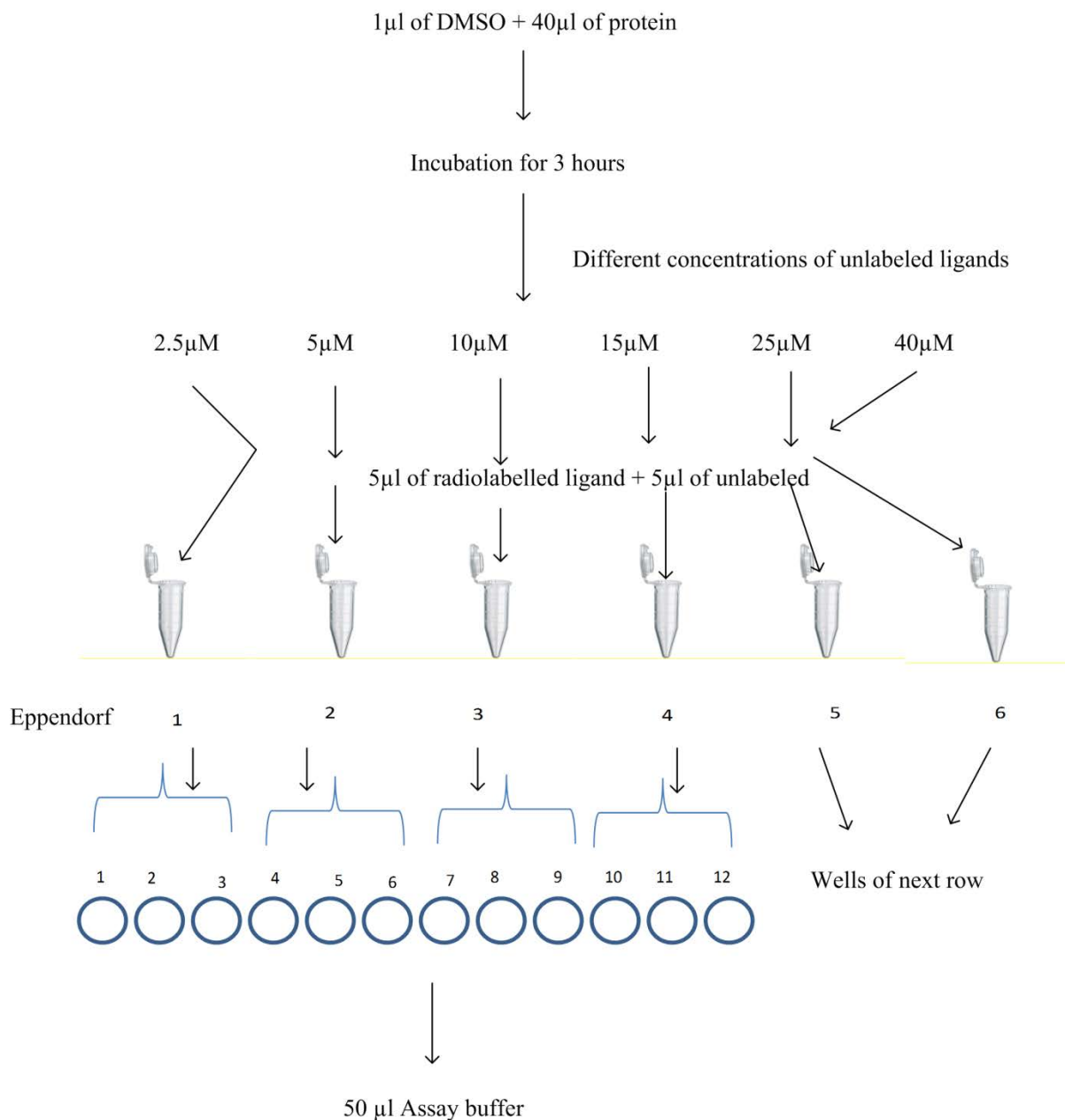


**Figure 3.5 Procedure of competitive binding analysis**

### 3.8. Developing Lipro Interact

The author's web-based *Lipro Interact* software was developed with the results of AutoDock, Glide and SPA. The main aim of creating this software was to make all the studied lipid-protein interactions available to existing research. As of now, there is no such software to study the binding energies of lipid-protein interactions. *Lipro Interact* provides an

opportunity to both the biochemical and bioinformatic researchers to access the microscopic interactions visually. *Lipro Interact* conveniently supports the researchers in providing the binding data of target lipids and proteins. The software greatly helps to enhance the future research on lipid-protein interactions.

The software also allows the user to download the PDB files and lipid-protein interacting images that provide information about the protein active sites, bond lengths and bond distances of lipid ligands with the respective protein. *Lipro Interact* is totally web-based and was developed using .Net framework. The detailed design and development of the software is explained in Chapter 8.

### **3.9. Conclusion**

This methodology chapter has presented a step-by-step procedure to study lipid-protein interactions. The comparison made between AutoDock and Glide is useful to select a suitable docking technique for the target proteins and ligands. The dissociation constant ( $K_d$ ) value generated from AutoDock is more suitable to compare the docking results with those of laboratory experiments. However, generating the output based on the grid-based energy evaluation is a major limitation of AutoDock (Morris et al., 2009). For the complex protein structures, generating a grid map file was not as easy as for the simple proteins. Moreover, in some cases the grid parameter file with grid dimensions more than 60Å did not yield satisfactory results. The atoms included in the protein must be treated as rigid.

Glide analyzes the results with publication quality images without the need for any other software tools. However, Glide generates binding energy in terms of Glide score and not the  $K_i$  which is a major limitation of Glide docking. Since, the  $K_i$  is an indirect measure of binding energy, the SPA results and Glide results are compared in terms of binding energies.

*Lipro Interact* software fulfils the emerging need for a lipid-protein interacting tool in the field of biomedicine.

PPARS, RXR- $\alpha$  and RAR- $\gamma$  belong to one family, which is a nuclear receptor family. Hence, the interacting mechanism of nuclear receptors (PPARs, RXR- $\alpha$ , and RAR- $\gamma$ ) with different lipid ligands were discussed in Chapter 4.

# Chapter 4

## Potential Ligands of PPARs and Retinoid Receptors

*Publications pertaining to this chapter:*

1. *Gaddipati, RS, Raikundalia GK, Mathai ML. Towards the Design of PPAR based Drugs using tocotrienol as natural ligands-A Docking Analysis. Paper presented at the International Conference on Engineering and Applied Sciences, Beijing, China, 2012, 352-59 (2012 ICEAS July 24-27)*
2. *Gaddipati, RS, Raikundalia GK, Mathai ML. (2014). Comparison of AutoDock and Glide towards the discovery of PPAR agonists. Paper presented at the International Conference on Bioscience, Biochemistry and Bioinformatics, Melbourne, Australia, 2014, published in International Journal of Bioscience, Biochemistry and Bioinformatics.*

## 4.1. Introduction

Peroxisome Proliferator Activated Receptors (PPARs) are members of the nuclear receptor family. They exist in three isoforms: PPAR- $\alpha$ , PPAR- $\beta/\delta$  and PPAR- $\gamma$ . Three isoforms of PPARs have different active sites in their ligand binding domains and hence bind to different ligands. These ligands can be potential candidates for the drugs that can treat abnormal metabolic homeostasis (Oyama et al., 2009). PPARs regulate the gene expression of different diseases like cancer, diabetes, atherosclerosis and obesity (Oyama et al., 2009). PPARs regulate energy metabolism by each carrying out a unique function and serve as therapeutic targets to treat obesity and homeostasis (Evans et al., 2004).

Retinoic acid Receptor (RAR) and Retinoic Xenobiotic receptors (RXR) are also members of the nuclear receptor family, each exists in three different isoforms  $\alpha$ ,  $\beta$  and  $\gamma$ . Among all these retinoids, RAR- $\gamma$  and RXR- $\alpha$  were considered for the current study due to their biological significance and biochemical specificity. RAR- $\gamma$ -RXR- $\alpha$  heterodimers are necessary for growth arrest (and hence play role in cancer therapy) and endodermal differentiation (Germain et al., 2006a). Retinoids are the active metabolites of Vitamin A during development, cell differentiation and homeostasis (Klaholz et al., 1998).

RAR-RXR heterodimers mediate the physiological function of natural retinoids (Mark et al., 2006). They are attractive targets for drug discovery since they allow dual ligand input (de Lera et al., 2007). In order to reduce toxicity in the current retinoid therapy, there is a need for the research of selective modulators of retinoids. Moreover, the tissue distribution of retinoid receptors is not uniform to elicit more specific biological responses (de Lera et al., 2007). RXR heterodimers were involved in multiple signalling pathways and the potential of RXR-targeted pharmacology is to be clarified. Still, there is a need for further RXR research to find out whether or not any ligands exist that can activate RXRs (Germain et al., 2006b).

Three groups of lipid ligands were tested for their capacity to bind PPARs, RAR-and RXR- $\alpha$ . There are four isomers of tocotrienols—tocotrienol- $\alpha$ ,  $\beta$ ,  $\gamma$  and  $\delta$ —, omega 3 fatty acids (DHA and EPA), endocannabinoids (2-Arachidonyl glycerol and anandamide. The above ligands were selected since fatty acids and eicosanoids are natural agonists of PPARs (Kliwer et al., 1997). Moreover, these ligands being natural cause fewer side effects than synthetic ligands (Nesto et al., 2003). The positive health effects of these lipid ligands were discussed in detail in Chapter 2, Section 2.3.

All the eight lipid ligands used in the current study are chemically active and medically significant. It was discussed in Chapter 3 that two different docking tools, AutoDock 4.2 (Morris et al., 2009) and Glide (Glide, 2011) were used.

This chapter explains the binding affinities of three isomers of PPARs with eight lipid ligands. The docking validation method of redocking was discussed in Section 4.2.1. Section 4.2.2 describes the ability of DHA and EPA to act as potential agonists of PPARs through AutoDock and Glide docking methods in Section 4.2.3. MD simulation studies were elucidated in Section 4.2.4. Section 4.3 illuminates the comparison of the results of two docking methods. The binding affinities of RAR- $\gamma$  and RXR- $\alpha$  were discussed in Section 4.4. Further, Section 4.4 explains the potential agonists of retinoid receptors, which include the findings of AutoDock, Glide and MD simulations. Section 4.5 is about comparing the docking results for RAR- $\gamma$  and RXR- $\alpha$ . Finally, Section 4.6 concludes this Chapter.

## ***4.2. DHA and EPA as Potential PPAR agonists***

PPARs are lipid-sensors that can be activated by both dietary fatty acids and their metabolic derivatives in the body (Evans et al., 2004). The long and medium chain unsaturated fatty acids are the most abundant ligands of PPARs (Fang et al., 2010). PPAR- $\alpha$  and  $\gamma$  are expressed in liver and adipose tissue, respectively. PPAR- $\delta$  is expressed throughout the body

and low levels in liver. PPAR- $\gamma$  acts as a molecular target for the anti-diabetic drugs thiazolidinediones (TZDs). PPAR- $\gamma$  also has a potential to treat inflammatory diseases and certain cancers (Murphy et al., 2000). PPAR- $\alpha$  is the molecular target for lipid-lowering fibrate drugs. The metabolic regulatory role of PPAR- $\delta$  is recently recognized and clinical trials for PPAR- $\delta$  agonists are to be investigated (Evans et al., 2004). The limitations of currently used PPAR-based drugs are explained in Chapter 2.

Research on agonists of PPARs is significant as PPARs play key roles in the regulation of energy homoeostasis and inflammation (Kroemer et al., 2004). The agonists of PPARs are currently used therapeutically. The dual agonists of PPAR- $\alpha$  and  $\gamma$  are used in the treatment of diabetes and dyslipidemia and hence are of high importance. The anti-diabetic drugs thiazolidinediones (TZDs) use PPAR- $\gamma$  as a molecular target (Malapaka et al., 2012). However, TZDs cause side effects like obesity and cardiovascular diseases (Malapaka et al., 2012). A potential therapeutic agonist of PPAR- $\delta$  is under investigation (Kroemer et al., 2004). Considering the medicinal importance of PPARs in the treatment of different diseases like diabetes, atherosclerosis and cancer, they are docked with eight lipid ligands to test their potentiality as PPAR agonists. Table 4.1 shows their binding affinities with PPARs calculated using AutoDock.

Out of all the eight lipid ligands, DHA, followed by EPA have shown a strong binding affinity with both PPAR- $\alpha$  and PPAR- $\gamma$ . Therefore, DHA can be considered as a dual agonist of PPAR- $\alpha$  and  $\gamma$ . The crystal ligand 2S-3-(4-[2-(4-chlorophenyl)-1, 3-thiazol-4-yl] methoxy-2-methylphenyl)-2-ethoxypropanoic acid (CTM) was considered as a potential dual agonist of both PPAR- $\alpha$  and PPAR- $\gamma$  (Grether et al., 2009). Furthermore, DHA, EPA and all four types of tocotrienols have expressed a strong affinity with PPAR- $\alpha$  and PPAR- $\gamma$  than CTM as shown in Table 4.1. Crystal ligand-D32 was considered for PPAR- $\delta$  (PDB code 3GZ9). PPAR- $\delta$  also showed stronger binding with DHA and EPA than with the crystal ligand-D32.

However, PPAR- $\delta$  has poor affinity with tocotrienols and endocannabinoids than with the crystal ligand-D32. The crystal structure information of all the three types of PPARs was discussed in Chapter 3.

#### **4.2.1. Redocking as a Docking Validation Method**

Redocking is the most significant validation method to evaluate the accuracy of the docking procedure (Tripathi et al., 2012). Redocking determined how closely the lowest binding energy pose resembles the experimental binding mode determined by X-ray crystallography. The docking procedure was validated by removing the crystal ligand (CTM for PPAR- $\alpha$  and  $\gamma$  and D32 for PPAR- $\delta$ ) from the binding site and redocking it to the binding site of PPAR- $\alpha$  (PDB code: 3FEI), PPAR- $\gamma$  (PDB code: 3FEJ) and PPAR- $\delta$  (PDB code: 3GZ9). The alignment of PPAR- $\alpha$ , PPAR- $\beta$  and PPAR- $\gamma$  with crystal ligand is depicted in Figure 4.1, 4.2 and 4.3 respectively where the redocked ligand is shown in red color.

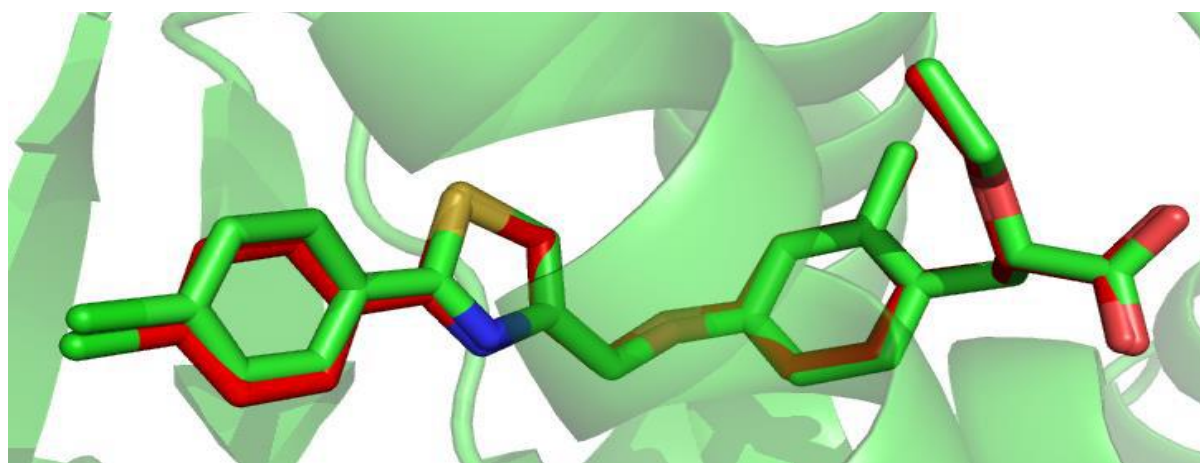


**Figure 4.1 Redocking of PPAR- $\alpha$  with Crystal Ligand CTM**

The crystal ligand was removed from the binding site and was superimposed with X-ray crystal structures of PPARs to calculate RMSD values. RMSD between the predicted conformation and the observed binding mode for all three isoforms of PPARs was less than 2 $\text{\AA}$  as shown in Table 4.7. RMSD values between the crystal ligand and the predicted

conformation is an indicator of whether or not correct docking was obtained from a particular docking method (Kroemer et al., 2004). RMSD less than 2Å is the cut-off of correct docking, perhaps because the resolution in an X-ray crystallography is often about 2Å and higher precision than the resolution of crystal structure analysis is not meaningful (Tripathi et al., 2012). Therefore the docking procedure in the current study was considered to be successful as the RMSD between the crystal ligand and predicted conformation was less than 2Å.

**Table 4.1 RMSD values**

Protein	Crystal Ligand	RMSD AutoDock	RMSD Glide
PPAR- $\alpha$	CTM	0.160	0.169
PPAR- $\delta$	D32	0.203	0.123
PPAR- $\gamma$	CTM	0.165	0.162

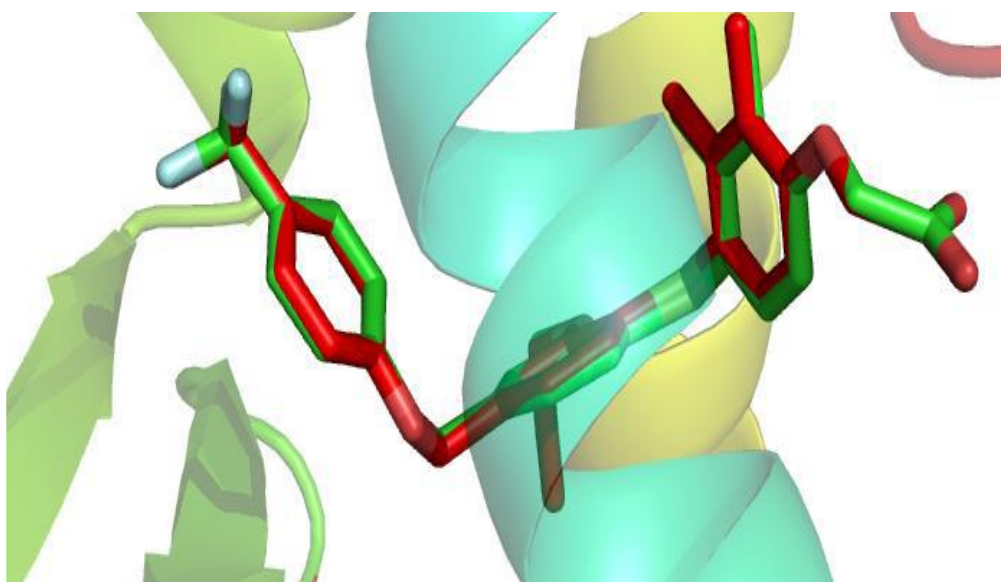


**Figure 4.2 Redocking of PPAR- $\delta$  with Crystal Ligand D-32**

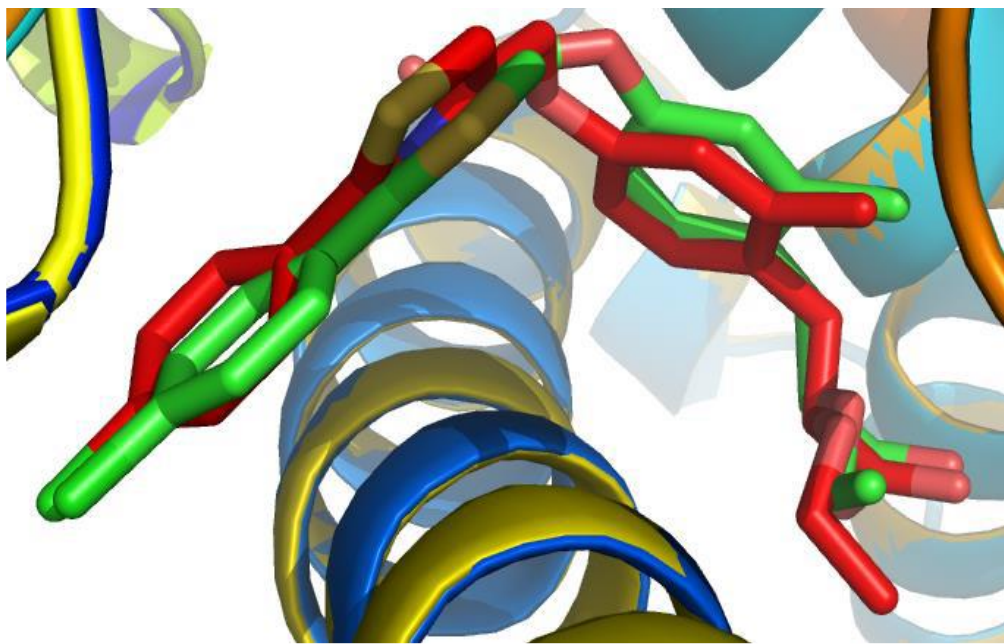


**Figure 4.3 Redocking of PPAR- $\gamma$  with Crystal Ligand CTM**

The 3D structure of the crystal ligands CTM and D32 are shown in Figures 4.1-4.3. CTM and D32 are the co-crystal structures of the PDB files considered for molecular docking. The binding site at which these ligands bound to the protein was considered as target's active site for molecular docking. The binding site for crystal ligands and eight lipid ligands was considered as the same during the procedure of molecular docking. Hence, redocking was conducted with known conformation and orientation of crystal ligands at target's active site (Hevener et al., 2009). The alignment of crystal ligands before and after docking determined the quality of docking procedure. Further, the rotatable chemical bonds in eight lipid ligands are similar to CTM and D32. Redocking the crystal ligand as docking validation method was used in several studies previously (Bajda et al., 2014; Hevener et al., 2009; Kalva et al., 2014; Kroemer et al., 2004; Tripathi et al., 2012). The author's study of redocking was based on the procedure from these publications.

#### 4.2.2. Molecular Docking of PPARs with Lipid Ligands using AutoDock

Interaction between protein and ligand were studied in terms of their binding energies. The highest bond strength between protein and ligand results in the lowest binding energy. PPAR- $\alpha$  has shown a strong binding affinity with DHA. The interacting amino acids around 4Å distance amino acids are shown in Figure 4.4. Figure 4.4 was captured using LigPlot software. Hydrogen bonds along with bond distances are represented in green color in Figure 4.4. The amino acids Cys 276, Thr 279, Ser 280, Tyr 334, and Val 332 have formed hydrophobic interactions with the ligand. EPA has expressed binding energy of -10.1cal/mol.

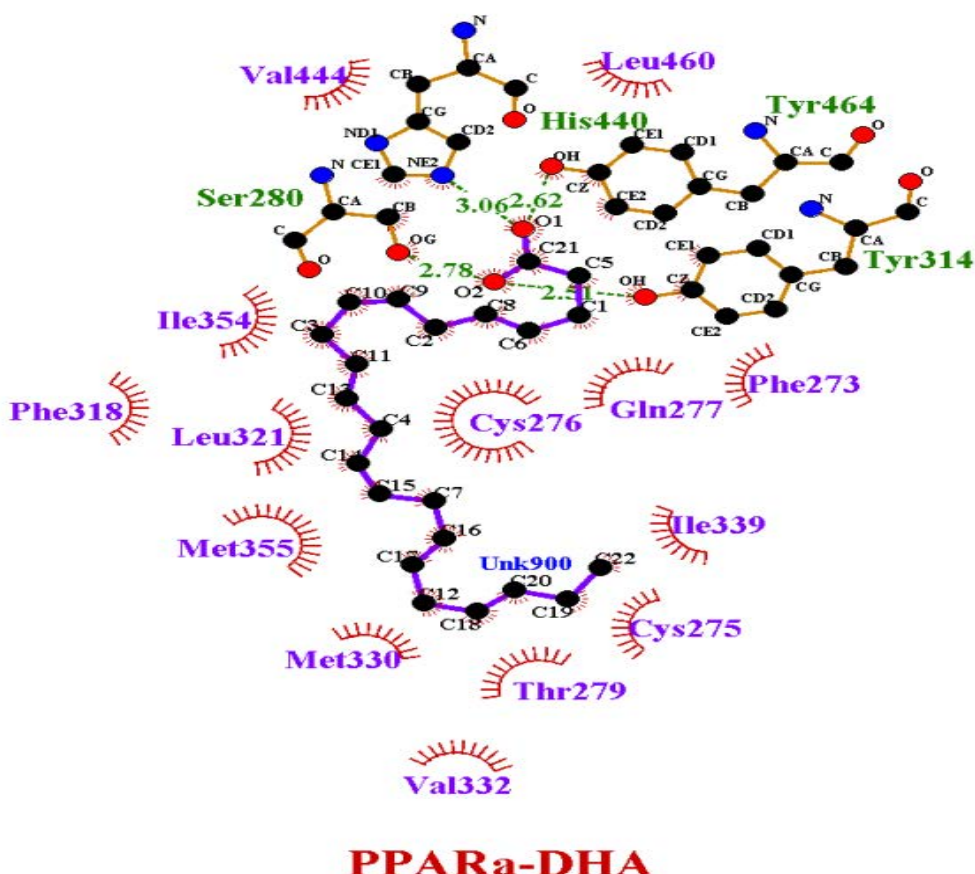


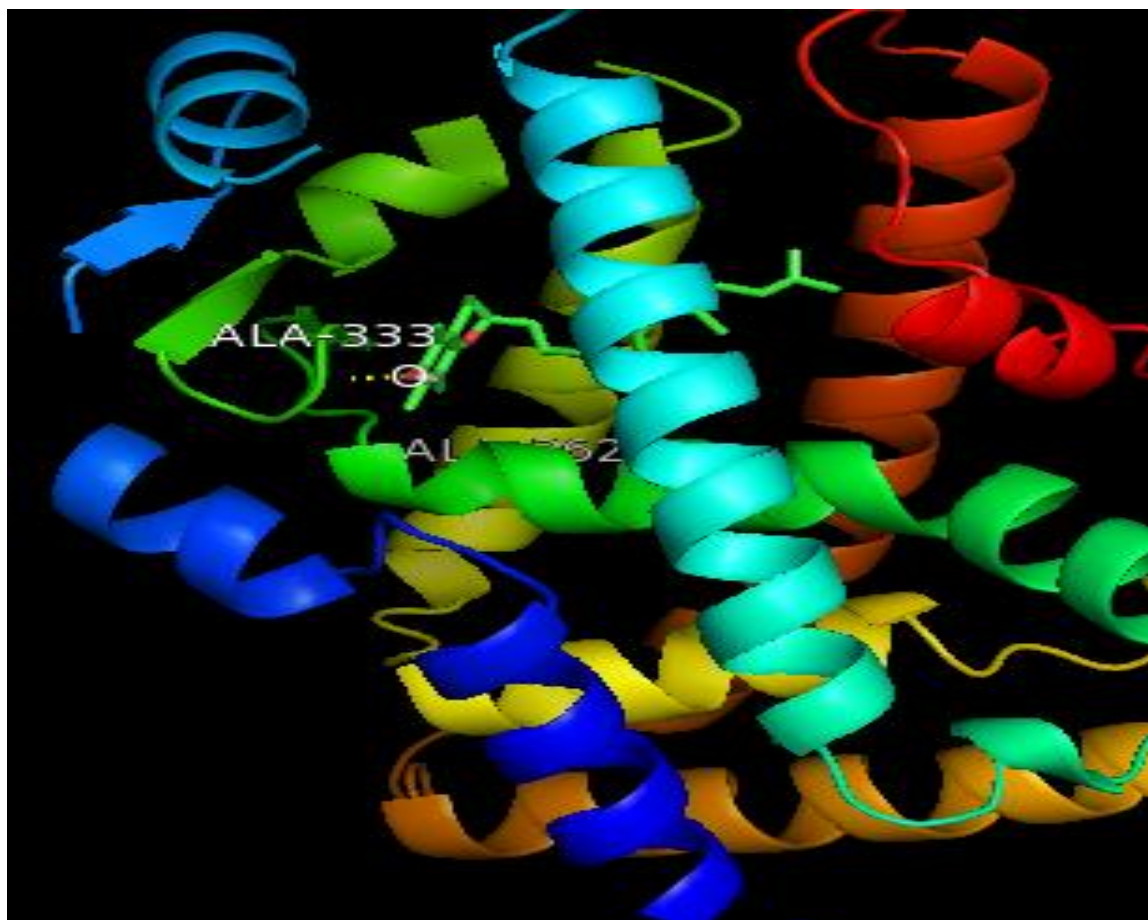
Figure 4.4 Interaction of PPAR- $\alpha$  with DHA

Compared to tocotrienols and omega 3 fatty acids, 2AG and anandamide have shown less affinity with PPAR- $\alpha$ . All the eight lipid ligands have shown a strong binding affinity with PPAR- $\alpha$  than with the crystal ligand CTM as shown in Table 4.2.

**Table 4.1 Lowest Binding Energies of PPAR- $\alpha$  calculated by AutoDock**

Ligand	AutoDock-Lowest binding energy (kcal/mol)
DHA	-11.5
EPA	-10.1
2AG	-7.69
Anandamide	-6.57
$\alpha$ -tocotrienol	-9.87
$\beta$ -tocotrienol	-9.98
$\gamma$ -tocotrienol	-8.44
$\delta$ -tocotrienol	-9.53
CTM	-7.72

Among tocotrienols, the lowest binding energy (-8.44 kcal/mol) was observed between PPAR- $\alpha$  and  $\gamma$ -tocotrienol as shown in Table 4.2. Hydrogen is donated by amino (NH) group of Ala 333 of PPAR- $\alpha$  to hydroxyl group present on C6 of  $\beta$ -tocotrienol thereby forming a bond with 2.1 $\text{\AA}$  distance (Figures 4.5). Ala 333 was present within 4 $\text{\AA}$  of the active site amino acids. Amino acids Leu 331, Val 332, Cys 275, Ser 280, Phe 273, Gln 277, Leu 456, Leu 460, Tyr 464, His 440, Met 355, Cys 276, Met 330 and Ala 333 of PPAR- $\alpha$  formed hydrophobic interaction with the ligand. Amino acids Cys 275, Cys 276, Met 330 and Met 355 were considered to be the active binding site of the ligand (Grether et al., 2009). Figure 4.5 shows the binding of PPAR- $\alpha$  with  $\beta$ -tocotrienol which was a snapshot of Pymol software (Pymol, Version 1.5.0.4).

**Figure 4.5 Interaction of PPAR- $\alpha$  with  $\alpha$ -tocotrienol****Table 4.2 Binding affinities of PPAR- $\beta$  with lipid ligands calculated by AutoDock**

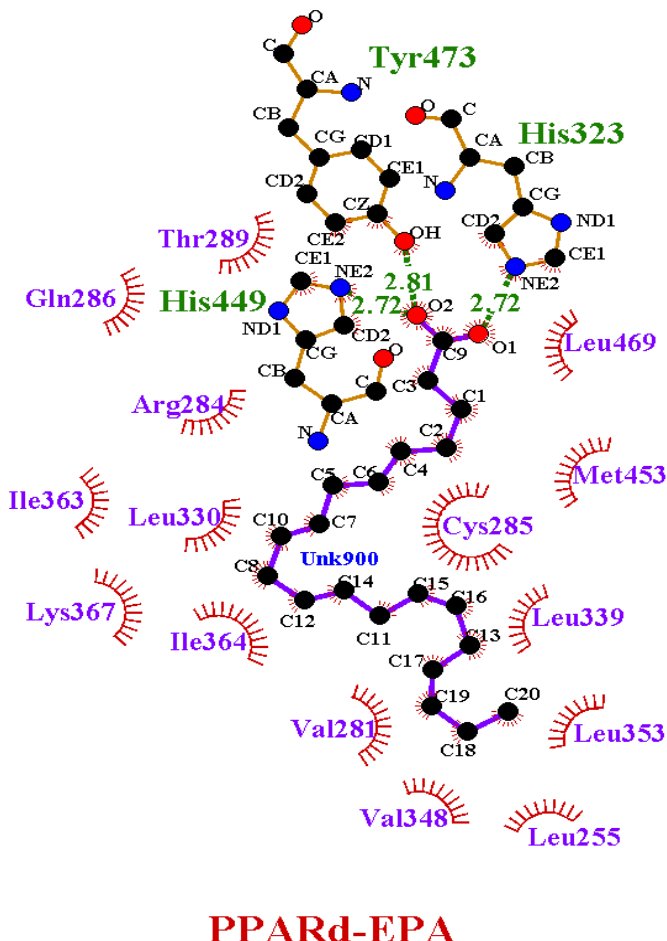
Ligand	AutoDock-Lowest binding energy (kcal/mol)
DHA	-11.40
EPA	-10.93
2AG	-9.22
Anandamide	-8.67
$\alpha$ -tocotrienol	-9.20
$\beta$ -tocotrienol	-9.97
$\gamma$ -tocotrienol	-9.09
$\delta$ -tocotrienol	-9.31
D-32 crystal ligand	-10.2

Although the protein (PPAR- $\alpha$ ) is the same, four types of tocotrienols have shown different binding energies due to different R groups present on the chromanol ring which might affect the aromaticity and conformation of ligand structure in docking. Further, four types of tocotrienols bound to PPARs at different sites resulting in the variation of binding energies.

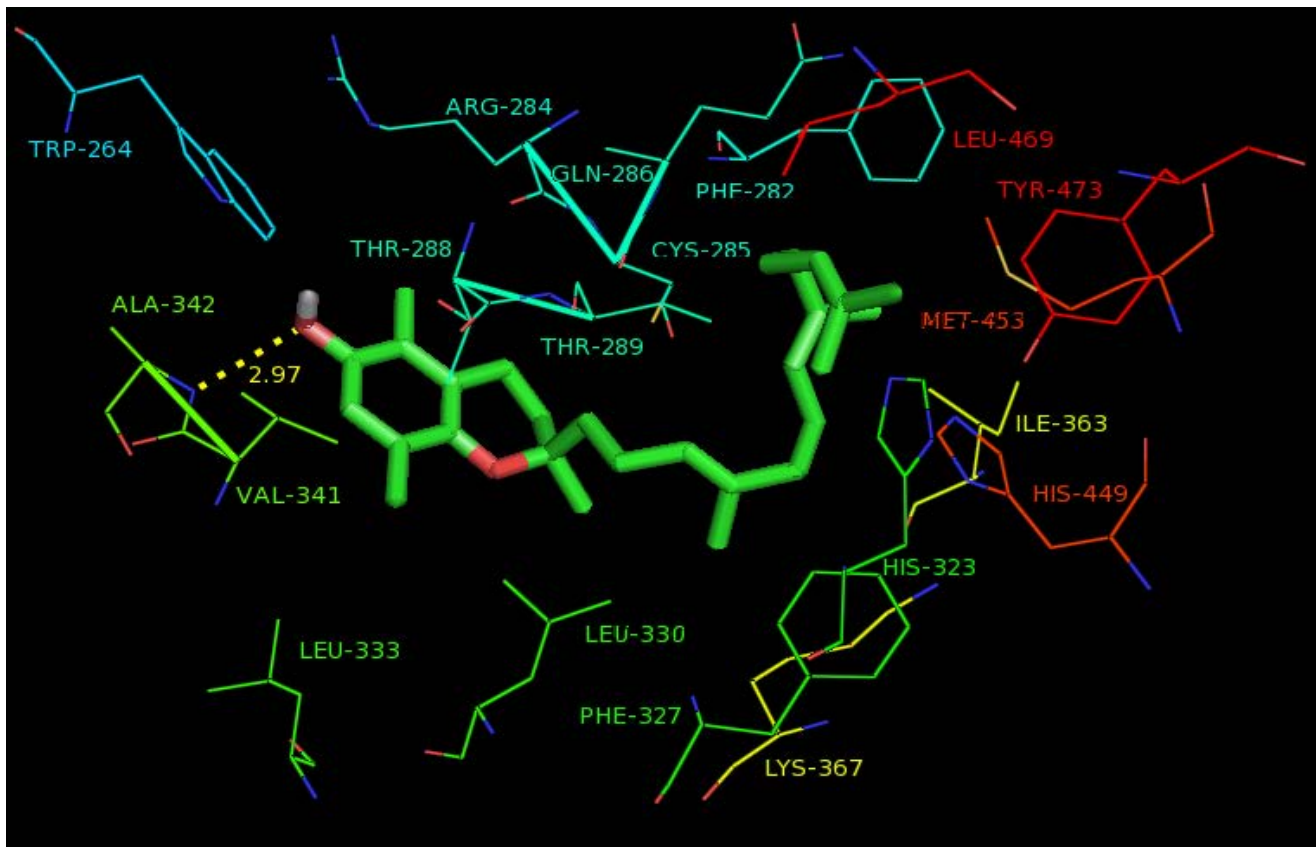
Ala 333 of PPAR- $\alpha$  has formed either hydrogen or hydrophobic bonds with all four types of tocotrienols. In the case of DHA and EPA Ser 280, Tyr 464 and Tyr 314 of PPAR- $\alpha$  have interacted with the ligand. The difference in the active site of the protein and the amino acids that are forming bonds with ligand vary due to the orientation of ligand that fit into the ligand binding pocket of the protein during docking procedure (Morris et al., 2009). The change is also because of the number of rotatable bonds present in each ligand which in turn depend on the structure of ligand (Morris et al., 2009).

PPAR- $\beta/\delta$  also have shown strong binding affinity with DHA (-11.40 kcal/mol) and EPA (-10.93 kcal/mol) as shown in Table 4.3. DHA and EPA are the potential ligands of PPAR- $\beta/\delta$  due to their strong affinity compared to the crystal ligand-D32. The amino acids around 4Å distance from the active site of the protein were shown in the following Figure 4.6. Anandamide (-8.67kcal/mol) and 2AG (-9.22kcal/mol) have also shown considerable strength of binding with PPAR- $\beta/\delta$ . However, the binding affinity is less when compared to the crystal ligand-D32.

Interestingly, the other three types of tocotrienols ( $\alpha$ ,  $\gamma$  and  $\delta$ ) also have shown a strong affinity with PPAR- $\delta$  (Table 4.3). Amino acids Leu 333, Leu 330, Lys 367, Ile 363, Leu 469, Phe 327, His 449, His 323, Tyr 473, Thr 289, Gln 286, Cys 285, Met 453, Phe 282, Thr 288, Trp 264 and Ala 342 have formed hydrophobic interactions with the ligand.

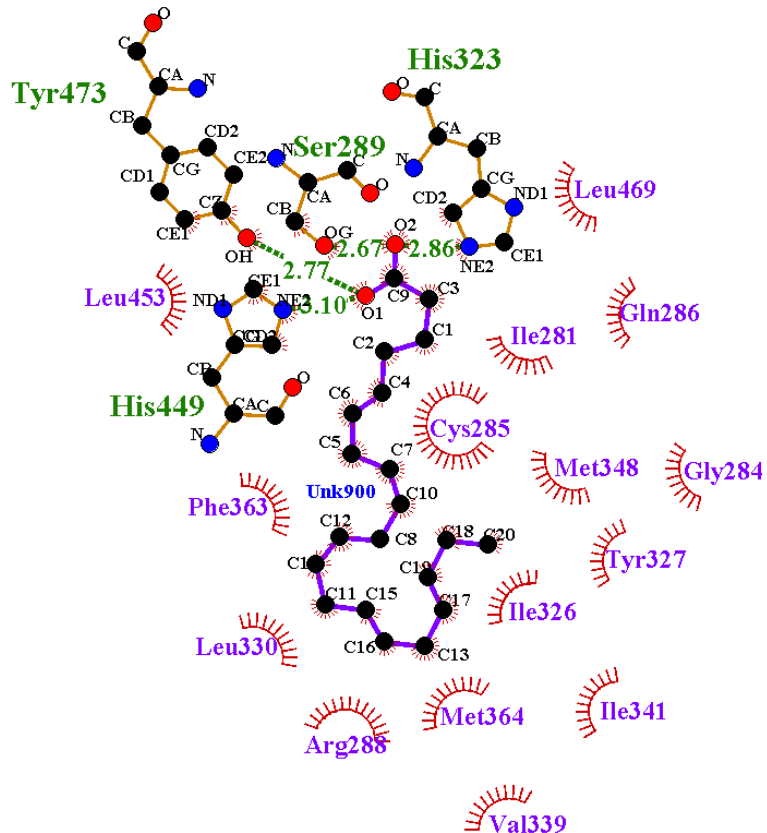
**Figure 4.6 Interaction of PPAR- $\delta$  with EPA**

The active site for PPAR- $\delta$  was predicted to be a combination of amino acids His 323, His 449, Tyr 473, Cys 285, and Thr 288 (Connors et al., 2009). The presence of the same amino acids such as Cys, Leu, Met, Phe, Val, Ser, Tyr, Gln, His and Ala in the hydrophobic pocket of the Ligand Binding Domain (LBD) of both PPAR- $\alpha$  and  $\delta$  could be the reason for similar binding affinities of these two proteins with the same ligands. Most of the agonists, e.g., TIPP -703 (phenylprionic acid-type pan agonist) and  $\alpha$ -ethoxy-phenyl propionic acid have similar binding affinities with PPAR- $\alpha$  and  $\gamma$  (Grether et al., 2009). In the case of tocotrienols, PPAR- $\alpha$  and  $\delta$  have similar binding affinities.

**Figure 4.7 Interaction of PPAR- $\delta$  with  $\delta$ -tocotrienol****Table 4.3 Binding affinities of PPAR- $\gamma$  with Lipid Ligands calculated by AutoDock**

Ligand	AutoDock-Lowest binding energy (kcal/mol)
DHA	-11.71
EPA	-10.22
2AG	-7.74
Anandamide	-6.29
$\alpha$ tocotrienol	-8.93
$\beta$ tocotrienol	-8.95
$\gamma$ tocotrienol	-9.66
$\delta$ tocotrienol	-9.68
CTM	-8.0

Except for anandamide and 2AG, all the other six lipid ligands (DHA, EPA,  $\alpha$ ,  $\beta$ ,  $\gamma$  and  $\delta$  tocotrienols) have expressed a strong affinity with PPAR- $\gamma$  in comparison to the crystal ligand CTM. The binding energies of PPAR- $\gamma$  with lipid ligands were shown in Table 4.4. The binding of EPA with PPAR- $\gamma$  is shown in Figure 4.8.

**PPAR $\gamma$  EPA****Figure 4.8 Interaction of PPAR- $\gamma$  with EPA**

The amino acids Cys 285, His 449, Ser 289, Tyr 327, His 323, and Tyr 473 of PPAR- $\gamma$  have formed hydrophobic interactions with the ligand EPA. DHA also has shown similar kind of interactions with PPAR- $\gamma$  due to their structural similarities. Compared to omega 3 fatty and tocotrienols, anandamide and 2AG have poor affinity with PPAR- $\gamma$ .  $\gamma$ -tocotrienol has a strong affinity with PPAR- $\gamma$  with the lowest binding energy (-9.66 Kcal/mol) compared to the other three types of tocotrienols.  $\gamma$ -tocotrienol is the hydrogen donor to His 323 (amino acid from the active site) of PPAR- $\gamma$  (Iwata et al., 2001).  $\delta$ -tocotrienol showed the binding energy of (-9.68kcal/mol) with PPAR- $\gamma$ . Arg 288 donated hydrogen to  $\delta$ -tocotrienol to form a bond.  $\beta$ -tocotrienol has a relatively poor affinity (binding energy of -8.95kcal/mol) with PPAR- $\gamma$ .

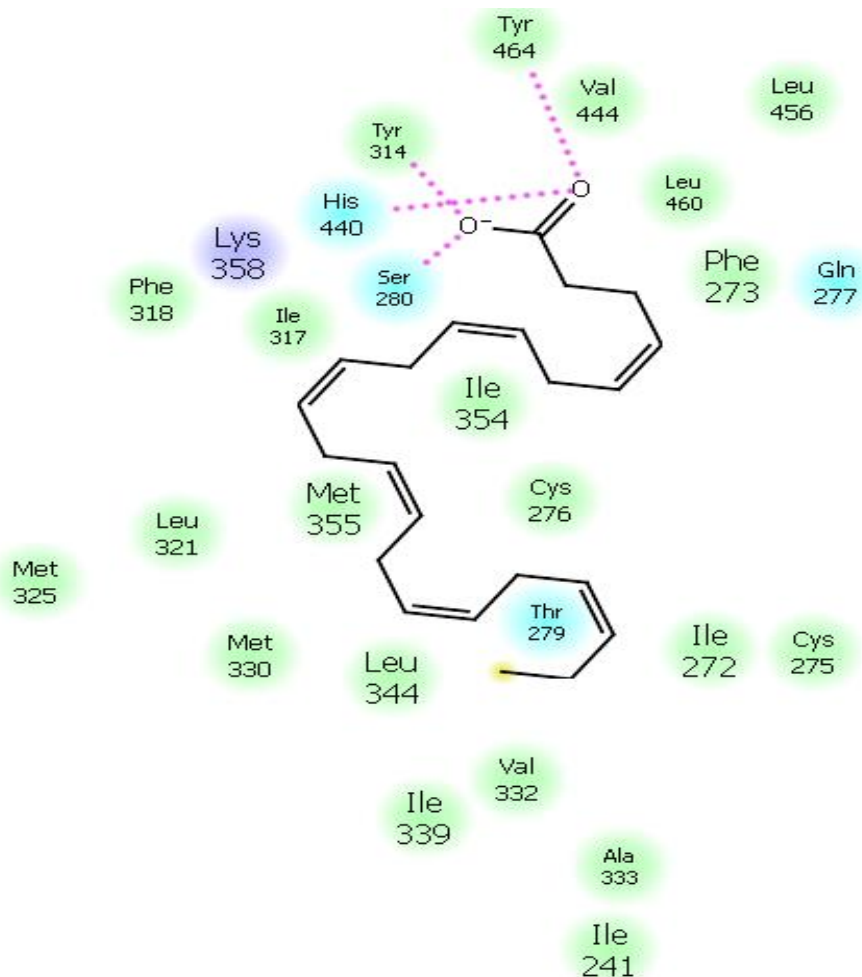
compared to the other two isoforms of PPARs. A similarly low affinity (binding energy of -8.93kcal/mol) was observed between PPAR- $\gamma$  and  $\alpha$ -tocotrienol.

The presence of three methyl groups in the chromanol ring of  $\alpha$ -tocotrienol might cause steric hindrance resulting in the highest binding energy (Comitato et al., 2009). Arg 280, Glu 259, Met 348, Ile 341, Met 364, Ile 281, Cys 285, Gly284 have formed hydrophobic interactions with the ligand. The active site of the protein was predicted to be Met 364, Cys 285, Met 348 and Gly 284 (Grether et al., 2009).

#### ***4.2.3. Molecular Docking of PPARs with Lipid Ligands using Glide***

DHA and EPA have expressed strong binding with PPAR- $\alpha$  in terms of their Glide score. The following Figure 4.9 is a ligand generation diagram from Glide. It was observed from Figure 4.9 that the amino acids Tyr 464, Val 444, Ser 280 and His 440 have formed bonds with the ligand. The active site amino acids Met 355, Cys 275, Met 330 and Cys 276 were closely interacting with the ligand DHA. EPA also has formed similar kind of interactions with PPAR- $\alpha$ .

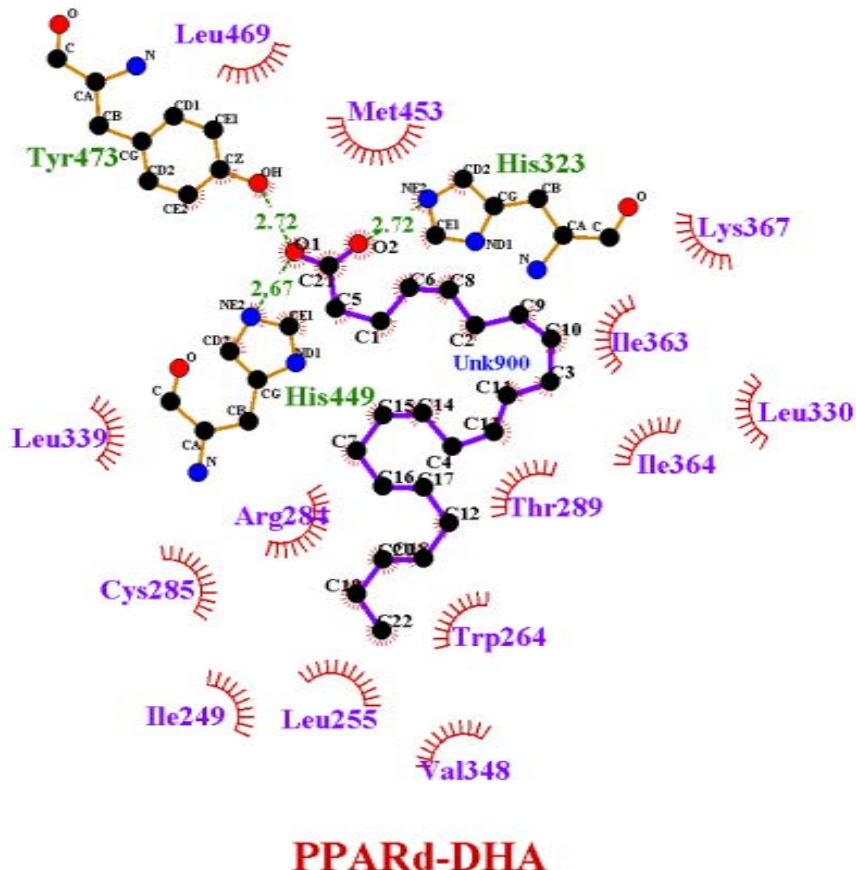
The interactions of DHA with PPAR- $\alpha$  are shown Figures 4.9 and 4.10. PPAR- $\alpha$  has formed hydrophobic interactions with the active site amino acids Cys 275, Cys 276, Met 330 and Met 355 (Figure 4.10). Oxygen (O) 1 located on carbon (C) 21 of DHA has formed two bonds with His 440 and Tyr 464 with bond distances 3.06 $\text{\AA}$  and 2.62 $\text{\AA}$  respectively. Ser 280 and Tyr 314 have formed bonds with O2 of C21 on DHA with bond distances 2.78 $\text{\AA}$  and 2.51 $\text{\AA}$  as shown in Figure 4.10. The figure was generated with the output file of DHA with PPAR- $\alpha$  using LigPlot software (Wallace et al., 1995). The hydrophobic interactions were shown in red colored spikes pointing towards the ligand whereas the hydrogen bond interactions are represented in green color. The ligand is located in the center.

**Figure 4.9 Interaction of DHA with PPAR- $\alpha$** 

After DHA and EPA, 2AG has considerable affinity with PPAR- $\alpha$ . The binding energy of  $\beta$ -tocotrienol and  $\delta$ -tocotrienol is the same as that of the crystal ligand CTM. Anandamide and  $\gamma$ - tocotrienol have shown poor affinity with  $\alpha$ -tocotrienol, compared to CTM as shown in Table 4.5.

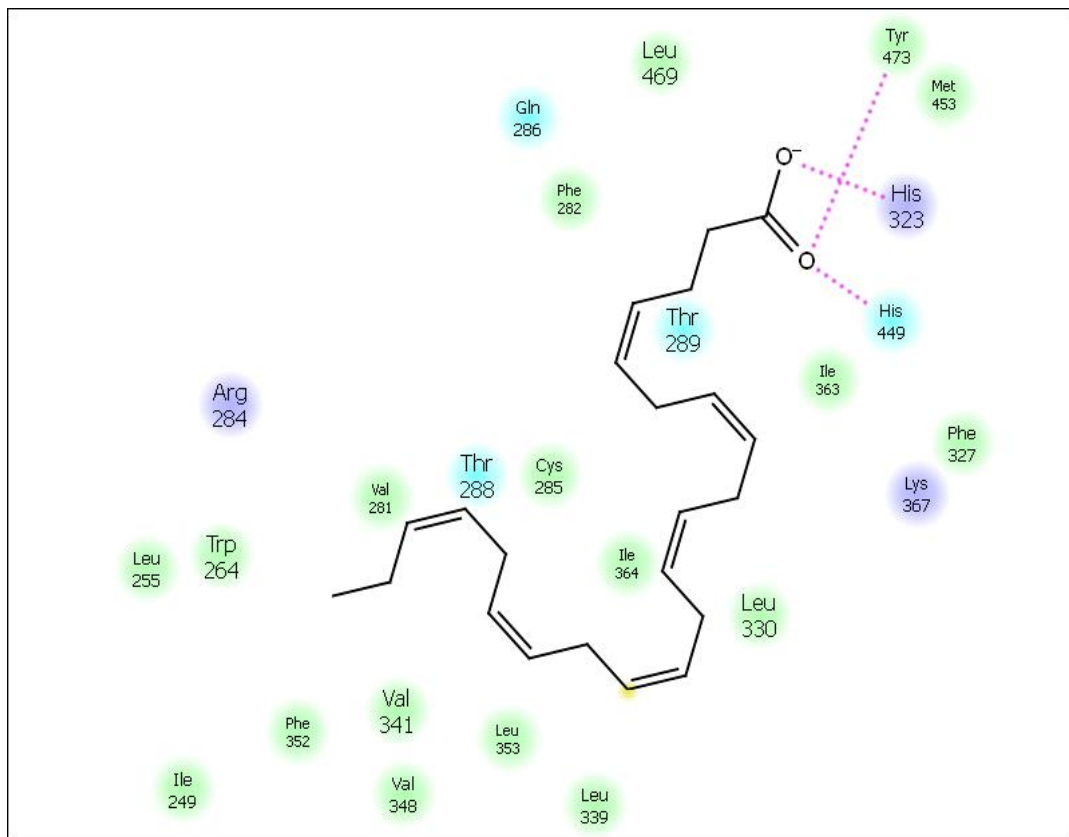
**Table 4.4 Glide Score of PPAR- $\alpha$  with Lipid Ligands**

Ligand	Glide Score (kcal/mol)
DHA	-10.2
EPA	-9.3
2AG	-8.0
Anandamide	-5.6
$\alpha$ tocotrienol	-7.1
$\beta$ tocotrienol	-7.5
$\gamma$ tocotrienol	-7.3
CTM	-7.5



**Figure 4.10 Ligplot diagram of PPAR- $\alpha$  with DHA**

Similar to PPAR- $\alpha$ , PPAR- $\beta$  also has a strong affinity with both DHA and EPA as shown in Table 4.6. Except for omega 3 fatty acids the other two groups of lipid ligands (tocotrienols and endocannabinoids) did not have strong binding affinity than the crystal ligand-D32. The active site amino acids His 323 and His 449 of PPAR- $\beta$  have formed bonds with DHA with bond distances of 2.72 Å, 2.72Å and 2.67Å, respectively (Figure 4.10). O2 on C21 of DHA formed a bond with His 323 in distance of 2.72Å. The other amino acids like Thr 289, Leu 330, Ile 364, Cys 285, Thr 288 etc were closely interacting with the ligand by forming hydrophobic interactions (Figure 4.10 and Figure 4.11).

**Figure 4.11 Interaction of PPAR- $\delta$  with DHA****Table 4.5 Glide Score of PPAR- $\delta$  with Lipid Ligands**

Ligand	Glide Score (kcal/mol)
DHA	-15.8
EPA	-14.8
2AG	-10.8
Anandamide	-9.7
$\alpha$ -tocotrienol	-9.7
$\beta$ -tocotrienol	-9.3
$\gamma$ -tocotrienol	-9.8
$\delta$ -tocotrienol	-7.7
D32-Crystal ligand	-11.7

The active site amino acids Cys 285, Met 348, met 364 and Gly 284 of PPAR- $\gamma$  have formed hydrophobic interactions with the ligand. His 449 and Tyr 473 of PPAR- $\gamma$  have formed two hydrogen bonds with O1 located on C21 of DHA with a bond distance of 3.08 $\text{\AA}$  and 2.76 $\text{\AA}$  as shown in Figures 4.12 and 4.13. Two more bonds were observed with O2 on C21 of DHA with bond a distance of 2.93 $\text{\AA}$  from His 323 and 2.70 $\text{\AA}$  from Ser 289 (Figure 4.12 and

Figure 4.13). The binding energy of EPA is somewhat close to DHA and stronger than the crystal ligand CTM as shown in Table 4.7. Next to omega 3 fatty acids, tocotrienols are the better ligands of PPAR- $\gamma$  compared to CTM. The affinity of endocannabinoids was lower than the crystal ligand CTM.

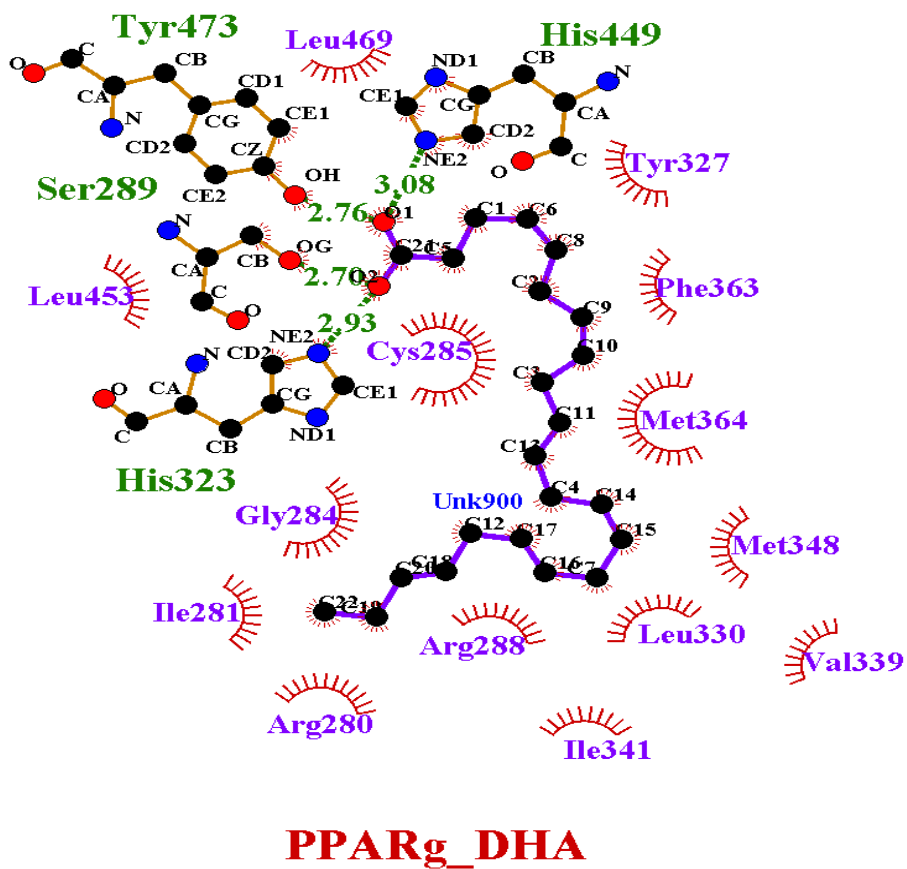


**Figure 4.12** LigPlot diagram of PPAR- $\gamma$  with DHA

**Table 4.6** Glide Score of PPAR- with lipid ligands

Ligand	Glide Score (kcal/mol)
DHA	-10.3
EPA	-9.4
2AG	-7.7
Anandamide	-5.2
$\alpha$ tocotrienol	-8.2
$\beta$ tocotrienol	-8.4
$\gamma$ tocotrienol	-8.5
$\delta$ tocotrienol	-8.5
CTM	-8.1

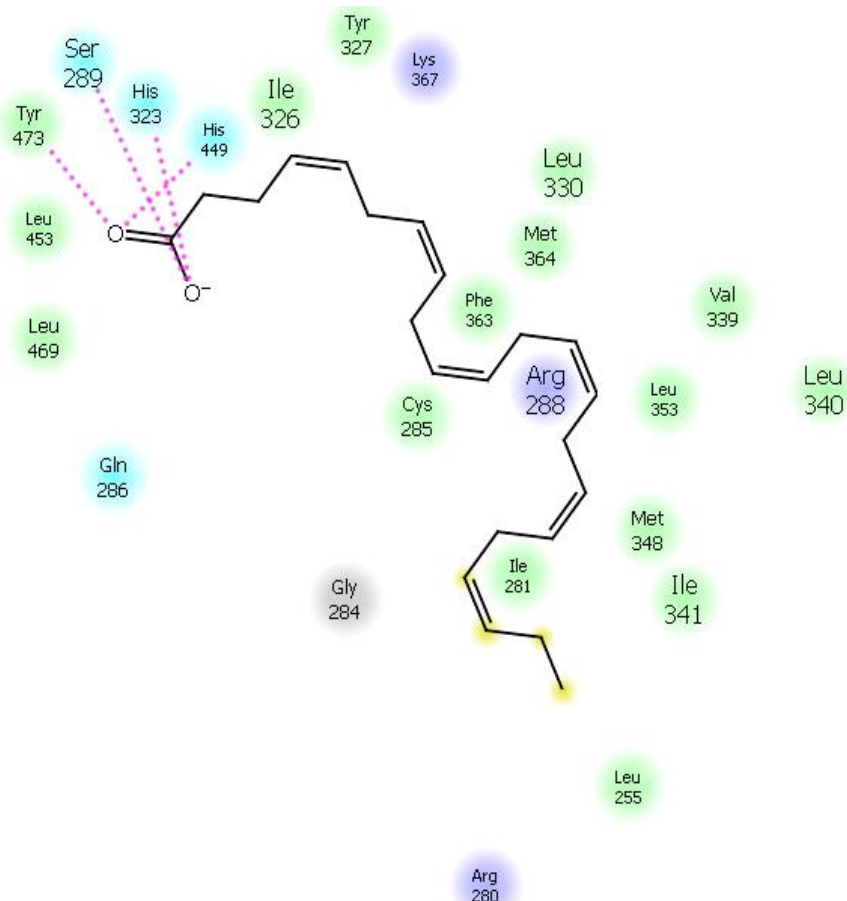


**Figure 4.13 Interaction of PPAR- $\gamma$  with DHA**

To conclude, omega 3 fatty acids are the potential ligands for all three isoforms of PPARs. Tocotrienols could be the dual agonists of PPAR- $\alpha$  and  $\gamma$ .

#### 4.2.4. MD Simulation of Top Ranked Poses of PPARs

Considering the available resources, MD simulations were performed for the docked complexes of PPAR- $\alpha$ ,  $\beta$  and  $\gamma$  with DHA as DHA has shown a strong affinity with PPARs in both AutoDock and Glide docking. The stability of the three docked complexes was studied in terms of RMSD and RMSF values generated during MD simulations. The structural diversity during MD simulations can be analyzed by calculating RMSD values (Kuzmanic & Zagrovic, 2010). RMSF values were calculated to study the thermal stability and structural flexibility (Kuzmanic & Zagrovic, 2010). RMSD was used to measure the change of protein

structure during the course of simulation. RMSD calculated the changes in Å. The changes in the order of 1-3Å were considered perfectly acceptable (Ramamoorthy et al., 2013; Rizo, 2015). RMSD is a good indicator of overall stability of any protein system (Ramamoorthy et al., 2013). The lower RMSD values during MD simulations for docked complexes showed consistent nature of docking conformations (Umamaheswari, 2011). RMSF is a measure of the average fluctuation of residues over time (Ramamoorthy et al., 2013). RMSD and RMSF values were calculated using simulation event analysis of Desmond. All frames were aligned with the starting structure prior to the calculations.

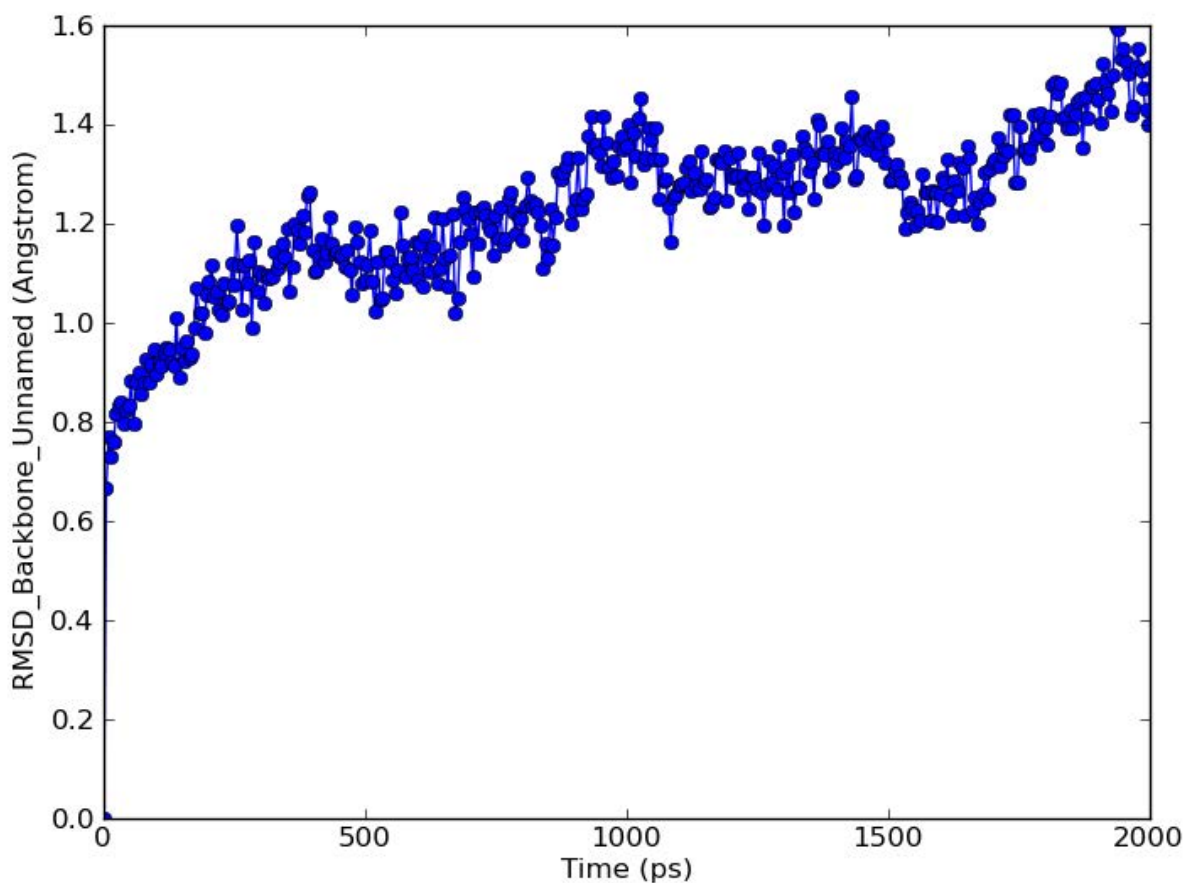


**Figure 4.14 RMSD curve of PPAR- $\alpha$  with DHA in 2ns time period**

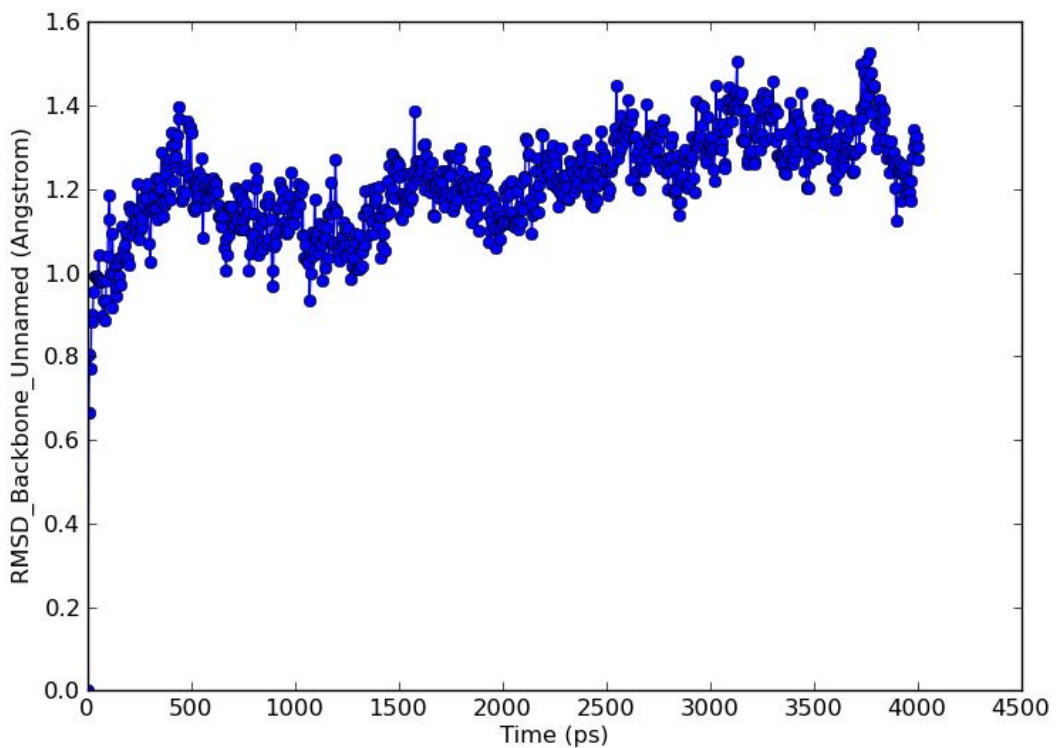


**Figure 4.15** RMSD curve of PPAR- $\alpha$  with DHA in 4ns time period

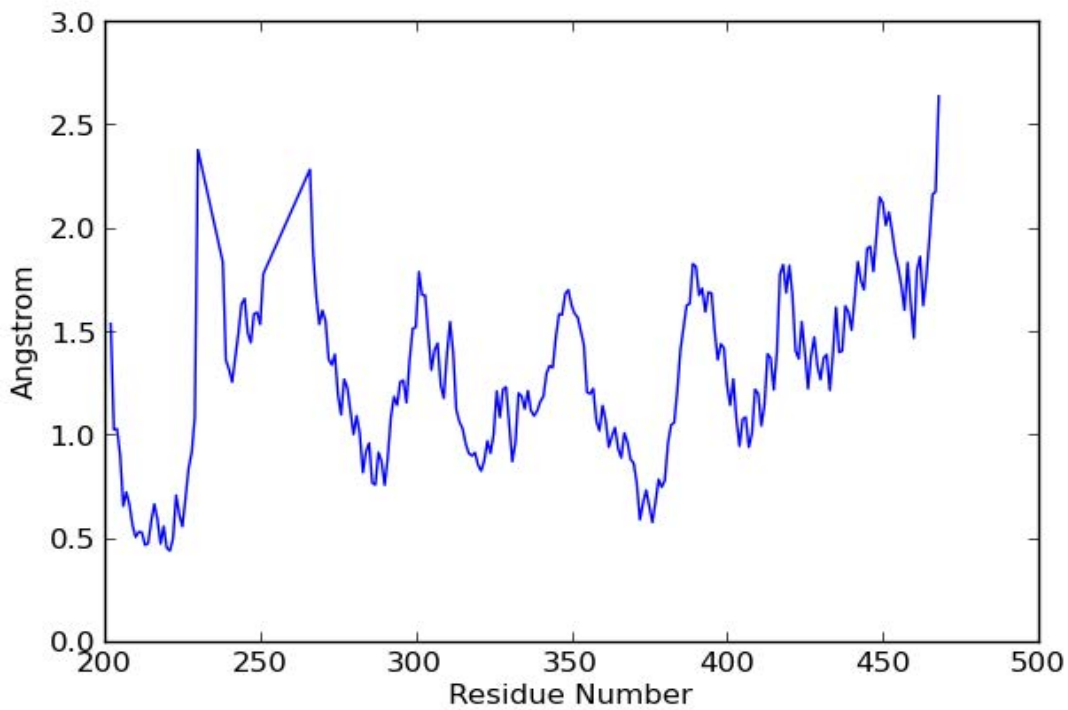


**Figure 4.16** RMSF curve of PPAR- $\alpha$  with DHA

It was observed that the three PPAR docked complexes were moderately stable during a period of 2ns simulations. The RMSD range of PPARs is within 2Å. The RMSD plot in Figure 4.14 was projecting upwards indicating that 2ns time period was not sufficient. Hence, the RMSD values for PPAR- $\alpha$ -DHA complex were also analyzed in 4ns time period and the plot is shown in Figure 4.15. During 4ns time period the RMSD values are very stable and represented the stability of the docked complex.

In case of PPAR- $\alpha$  and  $\beta$  the RMSD range is much less and is within 1.6Å (Figure 4.16 and Figure 4.20). It was slightly higher (1.8Å) for PPAR- $\gamma$  (Figure 4.21). The lower values of RMSD range indicated the consistency of docking conformations during MD simulation. Although there are some rearrangements during the period of MD simulation, overall, the docked complexes expressed considerable stability (Figures 17, 19 and 21). The graph was projecting upwards as shown in Figure 4.16. Yet the average deviation was within the range of 2Å.

The interacting amino acids of PPAR- $\alpha$  are Met 330, Met 355, Cys 275, Cys 276, Thr 279, Ser 280, Tyr 334, Ala 333, Asn 219, His 440, Val 332, Val 324, Tyr 464 and Tyr 314. For the amino acid, Asn 219, the RMSF fluctuations were recorded in between 0.5-0.7Å respectively. In the case of Cys 275, Cys 276, Thr 279 and Ser 280 the RMSF fluctuations were observed between 0.8-1Å. The fluctuation for Tyr 314, Val 324, Met 330, Val 332, Ala 333, Tyr 334 and Met 355 were from 0.8Å to 1Å. For Tyr 364 the RMSF fluctuation has come down to 0.5 Å again. So for all the interacting amino acids of PPAR- $\alpha$ , the fluctuations were within the range of 0.5Å-1Å.

The RMS fluctuations for PPAR- $\alpha$ ,  $\beta$  and  $\gamma$  are shown in Figures 4.17, 4.19 and 4.21 respectively. RMSF values were generated for the backbone. For PPAR- $\alpha$ , the RMSF values range from 0.5Å - 2.6Å (Umamaheswari, 2011). The initial fluctuations started at 1.5Å,

slowly went down to  $0.4\text{\AA}$  and have gone up to  $2.5\text{\AA}$ . The peak values were recorded at  $2.6\text{\AA}$  approximately. The active site amino acids for PPAR- $\alpha$  were numbered from 275-355 and for these amino acids the RMS fluctuation was ranging lower ( $0.5$ - $1.1\text{\AA}$  approximately). For most of the amino acids numbering from 260-440, the RMSF values were within the range of  $0.7\text{\AA}$  - $1.6\text{\AA}$  approximately. So the average RMSF range for PPAR- $\alpha$  was within  $1.6\text{\AA}$  (Figure 4.18).

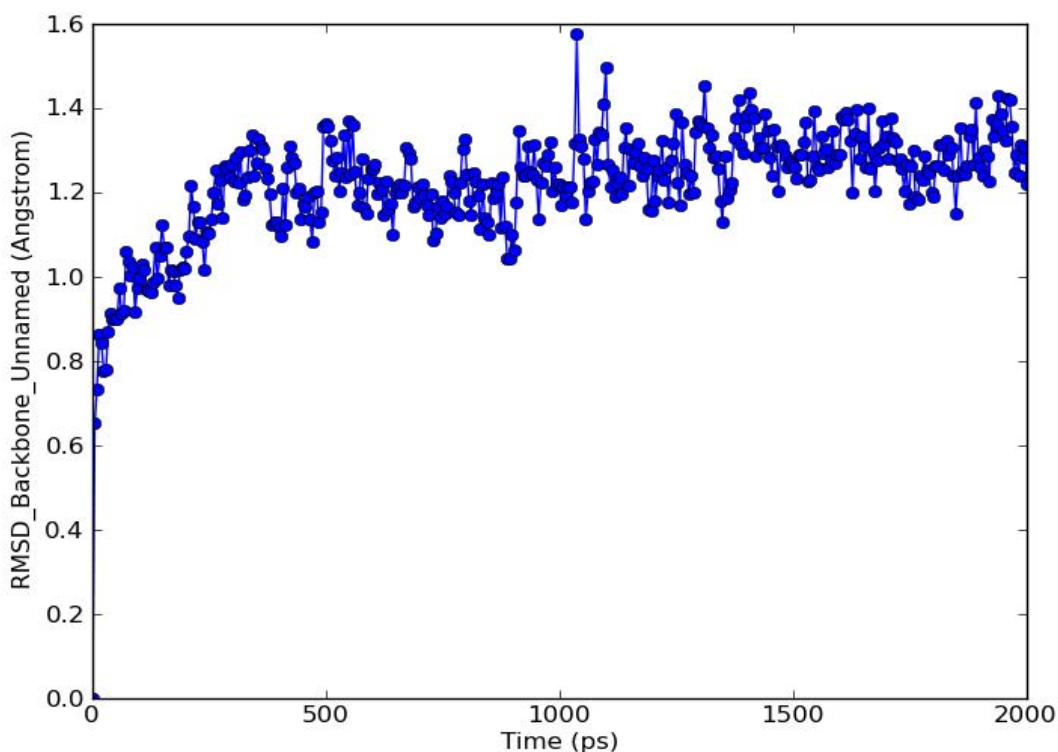


**Figure 4.17 RMSD curve of PPAR- $\beta$  with DHA**

PPAR- $\beta$  has shown RMS fluctuations within the range of  $1.0\text{\AA}$  - $2.3\text{\AA}$ . Similar to PPAR- $\alpha$  initial fluctuation were recorded at  $1.0\text{\AA}$ , moved down to  $0.5\text{\AA}$  and reached the peak at  $2.3\text{\AA}$  approximately. The active site amino acids of PPAR- $\delta$  were from the numbers 285-473. For these amino acids the RMSF values were ranging from  $1.2\text{\AA}$  - $1.4\text{\AA}$  indicating the stability of ligand in the ligand binding pocket of the protein. The majority of the amino acids

(numbering from 275-430) recorded the RMSF values within the range of  $1.2\text{\AA}$  -  $1.4\text{\AA}$  (Figure 4.19).

The interacting amino acids of PPAR- $\beta$  are His 323, His 449, Tyr 473, Ile 363, Leu 339, Ala 342, Thr 288, Phe 282, Met 453, Cys 285, Leu 330, Ile 364 and Thr 289. For the amino acids Phe 282, Cys 285, Thr 288 and Thr 289 the RMSF fluctuations were recorded between  $1.0$ - $1.2$   $\text{\AA}$ . The amino acids His 323, Leu 330, Leu 339 and Ala 342 have shown fluctuations from  $1$ - $1.5$   $\text{\AA}$ . RMSF values for Ile 363 and Ile 364 were observed at  $1.0$   $\text{\AA}$ . His 449 and Tyr 473 have fluctuated from  $1.0$ - $1.2$   $\text{\AA}$ .

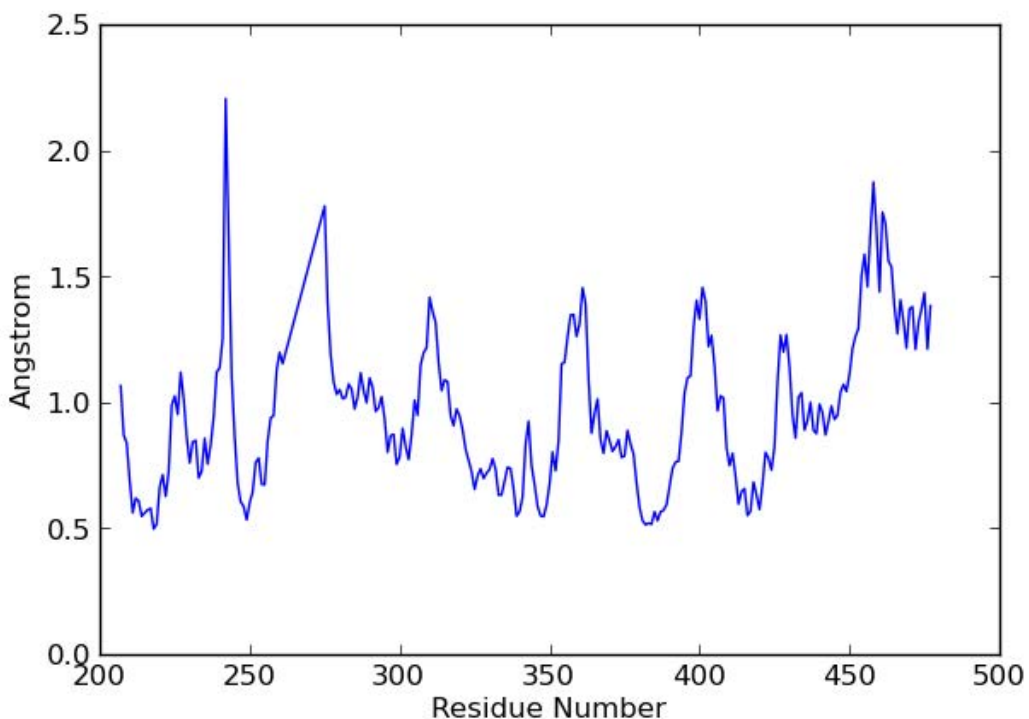


**Figure 4.18 RMSF curve of PPAR- $\beta$  with DHA**

The range of RMSF values for PPAR- $\gamma$  is from  $2.0\text{\AA}$ - $3.4\text{\AA}$  as shown in Figure 4.20. The initial fluctuations were recorded at  $2.0\text{\AA}$  and then there was a sudden fall to  $0.5\text{\AA}$ . Although the peak RMSF fluctuations were at  $3.4\text{\AA}$ , the fluctuations for the active site amino acids (from 284-364) were ranging from  $0.5\text{\AA}$  -  $1.0\text{\AA}$ . Hence, the ligand binding domain was stable

during the period of MD simulation. For the maximum number of amino acids from 275-475 the RMSF values were within the range of 2.3 Å approximately. The lower RMSF values during MD simulation in the presence of lipid ligand support the molecular docking study.

The interacting amino acids of PPAR- $\gamma$  are His 323, Cys 285, Met 364, Tyr 473, Tyr 327, Met 348, Gly 286, Leu 330, His 449, Arg 288, Ser 289, Gly 284, Arg 280, Phe 282 and Tyr 373. For the amino acids Arg 280, Phe 282, Gly 284, Cys 285, Gly 286 and Ser 289 the RMSF fluctuations were observed from 1.0 Å to 1.3 Å. The amino acids His 323, Tyr 327 Leu 330 and Met 348 have shown fluctuations between 0.4-1.4 Å. The RMSF fluctuations for Met 364 and Tyr 473 were recorded at 1.6 Å approximately. The remaining interacting amino acid His 449 of PPAR- $\gamma$  has shown fluctuations at 1.7 Å.

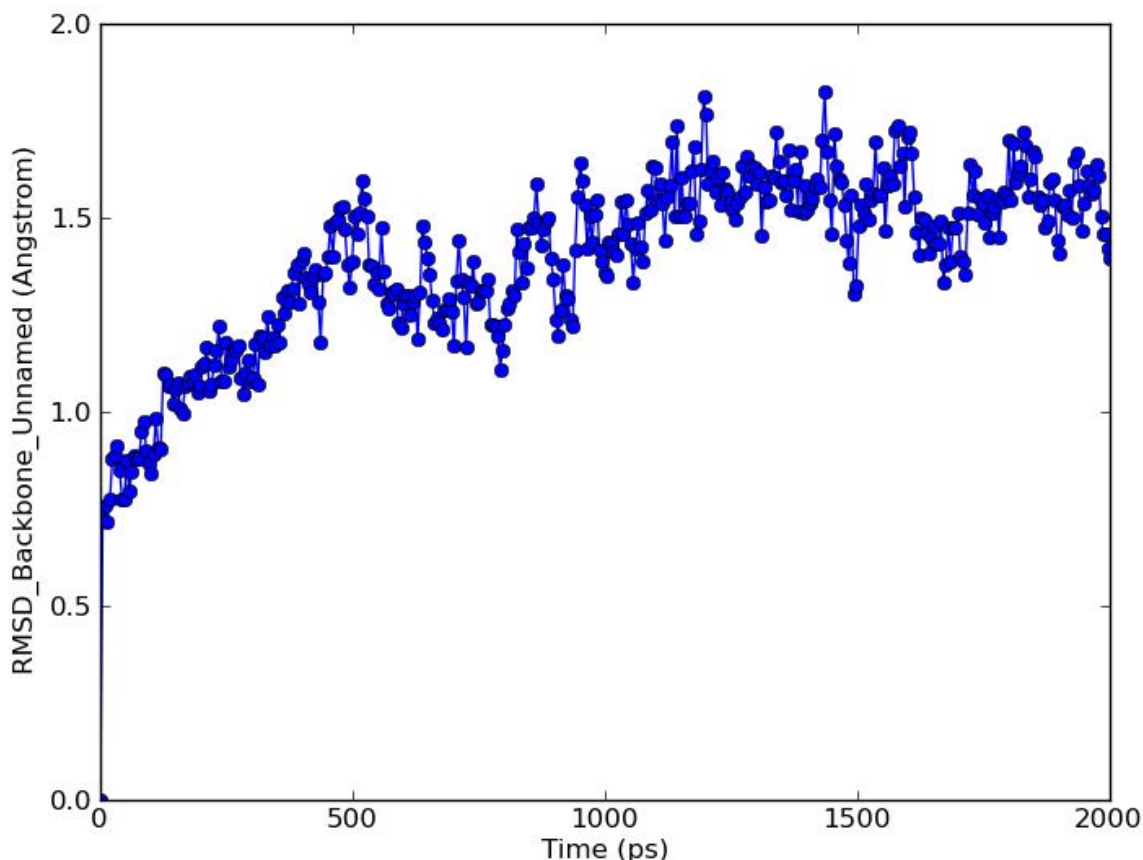


**Figure 4.19 RMSD curve of PPAR- $\gamma$  with DHA**

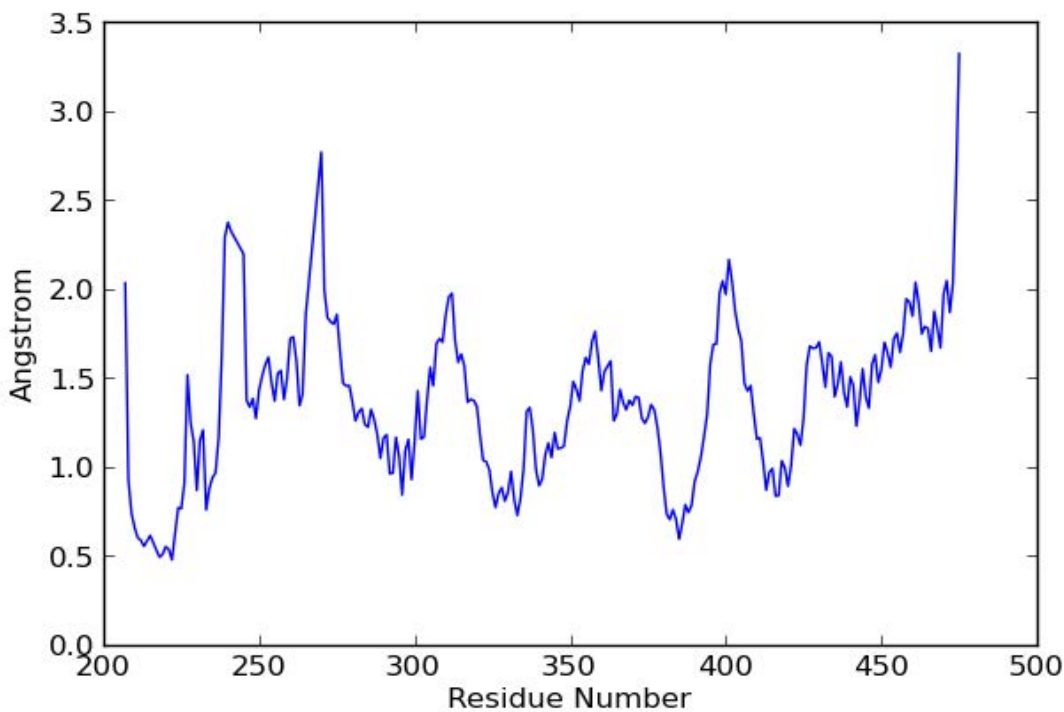


Figure 4.20 RMSF curve of PPAR- $\gamma$  with DHA

### 4.3. Comparison of AutoDock and Glide

AutoDock and Glide use two different scoring functions and search algorithm. AutoDock is based on empirical scoring function whereas Glide is based on XP scoring function. The search method in AutoDock is Lamarckian Genetic Algorithm. Glide docking uses a series of hierarchical filters to find the best possible ligand-binding locations in a pre-built receptor grid space (Tiwari et al., 2009). Prior to evaluate the energy interactions of ligand with protein, the filters include a systematic search approach that sample the positional, conformational and orientation space of the ligand (Friesner et al., 2004). Hence, the difference in search algorithm and scoring function cause difference in the binding poses and binding energies.

Furthermore, the procedure of ligand preparation and protein preparation vary in both docking techniques. AutoDock merges all non-polar hydrogens before saving file into pdbqt format. Rotatable bonds were changed into non-rotatable bonds (Tiwari et al., 2009). In case of Glide

docking ligand minimization and optimization were carried by LigPrep module of Maestro suite. In AutoDock the pdb format of protein structures were prepared with the structure preparation tool of AutoDock. During this step monomers were separated from the crystal structures. In Glide the protein coordinates were pre-processed using Protein Preparation Wizard of Maestro suite. The monomers were deleted in Glide as well. Same crystal structures and ligand binding sites were used in both AutoDock and Glide.

Based on the above differences between two docking techniques it is difficult to directly compare the results from AutoDock and Glide (Tiwari et al., 2009). Moreover, the best binding pose in both docking techniques varies since the generation of binding pose differs with the different grid parameters and number of torsions in the ligand structure. This implies that AutoDock and Glide result in different binding poses. Hence, a visual alignment of the binding poses obtained from AutoDock and Glide did not yield the RMSD values within 2Å deviation. However, the binding affinities in both docking techniques were calculated in terms of kcal/mol. Due to the same crystal structure and active site of the protein considered in both AutoDock and Glide, the intermolecular interactions in both the docking techniques are similar. Hence, the similarities between two docking techniques were studied with the help of binding affinities and intermolecular interactions.

AutoDock and Glide have generated similar binding energies for all the three isoforms of PPARs with all the eight lipid ligands docked in the author's study. In order to compare the similarity between both AutoDock and Glide, the interacting amino acids within 4Å distance from the ligand were shown in Table 4.7. The common interacting amino acids of both the docking methods were represented in bold.

**Table 4.7 Interacting amino acids of PPARs with lipid ligands in AutoDock and Glide**

Protein	Ligand	Interacting Amino acids within 4Å distance in Auto Dock	Interacting Amino acids within 4Å distance in Glide
PPAR- $\alpha$	DHA	Met 330, Met355, Cys 275, Cys 276, Thr 279, Ser 280	Met 330, Met355, Cys 275, Cys 276, Thr 279, Ser 280
PPAR- $\alpha$	EPA	Met 355, Ser 280, Met 330, Thr 279, Cys 276, Tyr 334	Met 355, Ser 280, Met 330, Thr 279, Cys 276, Tyr 314
PPAR- $\alpha$	2AG	Tyr334, Ala 333, Met 330, Cys 275, Asn 219, His 440	Tyr 334, Ala 333, Met 330,Cys 275, Asn 219, His 440
PPAR- $\alpha$	Anandamide	CYS 276, Thr 279, Tyr 334, Val 332, Met 330, Cys 375	Cys 276, Thr 279, Tyr 334, Val 332, Met 330, Tyr 464
PPAR- $\alpha$	$\alpha$ -tocotrienol	Met 330, Met 355, Cys 275, Cys 276, Ala 333, Thr 279	Met 330, Met 355, Cys 275, Cys 276, Ala 333, Val 324
PPAR- $\alpha$	$\beta$ -tocotrienol	Met 330, Met 355, Cys 275, Cys 276, Val 332, Val 324	Met 330, Met 355, Cys 275, Cys 276, Val 332, Ser 280
PPAR- $\alpha$	$\gamma$ -tocotrienol	Met 330, Met 355, Cys 276, Ser 280, Thr 279, Val 332	Met 330, Met 355, Cys 276, Ser 280, Thr 279, Val 332
PPAR- $\alpha$	$\delta$ -tocotrienol	Met 330, Met 355, Cys 275, Cys 276, Val 332, Met 320	Met 330, Met 355, Cys 275, Cys 276, Val 332, Met 320
PPAR- $\beta/\delta$	DHA	His 323, His 449, Tyr 473, Ile 363, Leu 330, Val 341	His 323, His 449, Tyr 473, Ile 363, Leu 339, Ala 342
PPAR- $\beta/\delta$	EPA	His 323, His 449, Tyr 473, Thr 288, Phe 282, Ile 364	His 323, His 449, Tyr 473, Thr 288, Phe 282, Ile 363
PPAR- $\beta/\delta$	2AG	Thr 288, Met 453, Phe 282, Cys 285, His 449, Leu 330	Thr 288, Met 453, Phe 282, Cys 285, His 449, Leu 330
PPAR- $\beta/\delta$	Anandamide	His 449, Thr 288, Ile 364, Leu 330, Ala342, Cys 285	His 449, Thr 288, Ile 364, Leu 330, Met 453, Cys 285
PPAR- $\beta/\delta$	$\alpha$ -tocotrienol	His 449, Ile 363, Ala 342, Cys 285, Ile 363, Arg 284	His 449, Ile 363, Cys 285, Thr 288, His 323, Tyr 473
PPAR- $\beta/\delta$	$\beta$ -tocotrienol	Cys 285, Tyr 473, His 449, Leu 330, Phe 282, Met 453	Cys 285, Tyr 473, Met 453, Ile 363, His 323, His 449

**Table 4.7 Continued**

Protein	Ligand	Interacting Amino acids within 4Å distance in Auto Dock	Interacting Amino acids within 4Å distance in Glide
PPAR- $\beta/\delta$	$\gamma$ -tocotrienol	<b>His 449, Tyr 473, Met 453, Thr 289, Cys 285, Ile 363</b>	<b>His 449, Tyr 473, Met 453, Thr 289, Cys 285, Ile 364</b>
PPAR- $\beta/\delta$	$\delta$ -tocotrienol	<b>His 449, Tyr 473, Met 453, Ile 364, Ala 342, Cys 285</b>	<b>His 449, Tyr 473, Met 453, Ile 363 Cys 285, His 323</b>
PPAR- $\gamma$	DHA	<b>Cys 285, Met 364, Phe 282, Met 355, Leu 330, Arg 288</b>	<b>Cys 285, Met 364, Tyr 473, Leu 330, Tyr 327, Met 348</b>
PPAR- $\gamma$	EPA	<b>Cys 285, Met 364, Ser 289, Leu 330, Tyr 327, Arg 288</b>	<b>Cys 285, Gly 286, Met 364, Leu 330, His 449, Arg 288</b>
PPAR- $\gamma$	2AG	<b>Cys 285, Gly 286, Met 364, Leu 330, His 449, Arg 288</b>	<b>Cys 285, Leu 330, Met 364, Tyr 473, His 449, Ser289</b>
PPAR- $\gamma$	Anandamide	<b>Cys 285, Leu 330, Met 364, Tyr 473, His 449, Ser289</b>	<b>Cys 285, Met 348, Met 364, Gly 284, Arg 288, Leu 330</b>
PPAR- $\gamma$	$\alpha$ -tocotrienol	<b>Cys 285, Met 348, Met 364, Gly 284, Arg 288, Leu 330</b>	<b>Cys 285, Met 348, Met 364, Gly 284, Arg 280, His 449</b>
PPAR- $\gamma$	$\beta$ -tocotrienol	<b>Cys 285, Met 348, Met 364, Gly 284, Arg 288, His 449</b>	<b>Cys 285, Met 348, Met 364, Gly 284, Phe 282, Tyr 373</b>
PPAR- $\gamma$	$\gamma$ -tocotrienol	<b>Cys 285, Met 348, Met 364, Gly 284, Phe 282, Tyr 327</b>	<b>Cys 285, Met 348, Met 364, Gly 284, His 449, Tyr 473</b>
PPAR- $\gamma$	$\delta$ -tocotrienol	<b>Cys 285, Met 348, Met 364, Gly 284, His 323, Tyr 473</b>	<b>Cys 285, Met 348, Met 364, Gly 284, Tyr 373, Tyr 473</b>

The active site was confirmed for PPARs since ligands occupied the same binding site in both AutoDock and Glide programs. Although AutoDock and Glide use different scoring functions, they resulted in generating the similar binding energies.

Apart from the slight difference in the binding energies generated from AutoDock and Glide docking tools, the interaction of protein with ligand was similar in both the methods. Using

two different methods of docking that resulted in a similar interaction of target proteins with ligands indicated the accuracy of the docking procedure.

The binding modes of protein with ligand were compared with the help of data from Table 4.7. In the case of PPAR- $\alpha$ , the active site amino acids in AutoDock were Met 330, Met355, Cys 275, Cys 276, Thr 279, Ser 280, Tyr 334, Ala 333, Asn 219, His 440, Val 332, Val 324 Val 332, Met 320. For the same protein the active site amino acids in Glide were observed as Met 330, Met355, Cys 275, Cys 276, Thr 279, Ser 280, Tyr 334, Ala 333, Asn 219, His 440, Val 332, Val 324, Tyr 464 and Tyr 314. The amino acid Met 320 was not seen in the active site amino acids of PPAR- $\alpha$  in AutoDock whereas Tyr 314 and Tyr 364 were not observed in the active site amino acids of PPAR- $\alpha$  in Glide. Expect this rest of the amino acids are same in both AutoDock and Glide docking techniques.

Likewise, the active site amino acids of PPAR- $\delta$  in AutoDock were identified as His 323, His 449, Tyr 473, Ile 363, Leu 330, Val 341, Thr 288, Phe 282, Ile 364, Met 453, Cys 285, Ala342, Arg 284 and Thr 289. The active site amino acids of PPAR- $\delta$  in Glide docking were observed to be His 323, His 449, Tyr 473, Ile 363, Leu 339, Ala 342, Thr 288, Phe 282, Met 453, Cys 285, Leu 330, Ile 364 and Thr 289. The amino acids Val 341 and Arg 284 were not seen in the binding mode of PPAR- $\delta$  with lipid ligands in Glide docking. The amino acid Leu 339 was not observed in AutoDock in the binding mode of PPAR- $\delta$  with lipid ligands.

In the binding mode of PPAR- $\gamma$  with lipid ligands the active site amino acids Cys 285, Met 364, Phe 282, Met 355, Arg 288, Ser 289, Tyr 327, Gly 286, Leu 330, His 449, Tyr 473, Met 348, Gly 284 and Leu 330 were observed during the docking procedure of AutoDock. In Glide docking the amino acids His 323, Cys 285, Met 364, Tyr 473, Tyr 327, Met 348, Gly 286, Leu 330, His 449, Arg 288, Ser289, Gly 284, Arg 280, Phe 282 and Tyr 373 were identified in the binding mode of PPAR- $\gamma$ . The amino acid Met 355 was not seen in the active

site of PPAR- $\gamma$  in Glide docking whereas the amino acids His 323 and Arg 280 were not present in the binding mode during the docking procedure of AutoDock. Rest of the amino acids were same in both AutoDock and Glide docking procedures.

To compare the efficiency of both AutoDock and Glide the bar graphs were drawn with the help of binding energies obtained from both the docking methods. AutoDock yielded lower binding energies for both PPAR- $\alpha$  and  $\gamma$  while Glide obtained lower binding affinities for PPAR- $\delta$  (Figure 4.22). Individual efficiency of AutoDock and Glide for the interaction of eight lipid ligands with PPAR- $\alpha$ ,  $\beta$  and  $\gamma$  was shown in Figures 4.21, 4.22 and 4.23, respectively.

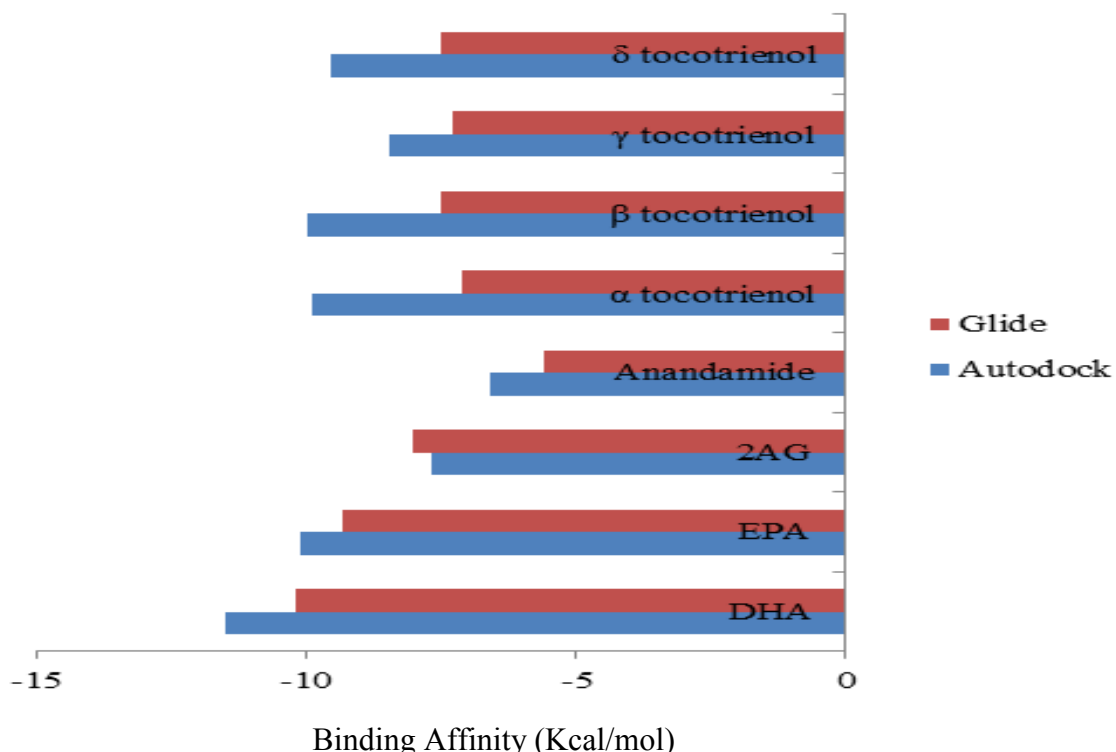


**Figure 4.21 Comparison of Binding Energies of PPAR- $\alpha$  in AutoDock and Glide**

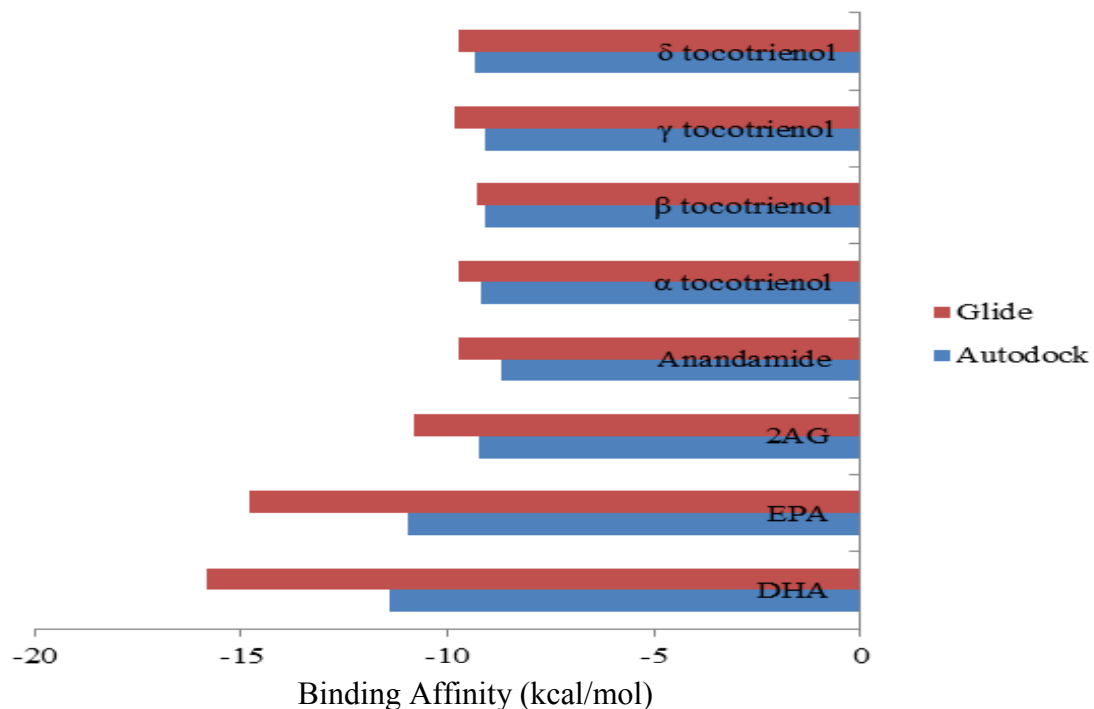


**Figure 4.22 Comparison of Binding Energies of PPAR  $\delta$  in AutoDock and Glide**



**Figure 4.23 Comparison of Binding Energies of PPAR- $\gamma$  in AutoDock and Glide**

#### **4.4. RAR- $\gamma$ and RXR- $\alpha$**

Retinoids were used in therapeutic applications in the treatment of skin diseases like psoriasis, acne and in the treatment or chemoprevention of cancers (Klaholz et al., 1998). The effects of RAR- $\gamma$  and RXR- $\alpha$  on cell growth and survival can be modulated by the small molecule ligands. Although the compounds that target these receptors are powerful anti-cancer drugs, their use is limited by toxicity (de Lera et al., 2007).

It was noticed through *in vitro* studies that RAR and RXR heterodimers bind to cognate response elements more than do RAR or RXR homodimers. Recently RAR and RXR were identified as existing pharmacological targets of cancer and metabolic disease therapies (Altucci et al., 2007). There was evidence from the past research that RAR and RXR can also be activated by PUFAs including DHA (Lengqvist et al., 2004). Fatty acids can function as true endogenous ligands of retinoids. Lengqvist et al., have concluded from their study that DHA binds to the ligand binding pocket of RXR- $\alpha$  with high affinity equal to the synthetic ligand, BMS 961.

9-*cis* and all-*trans* retinoic acid specifically bind to RARs whereas 9-*cis*-retinoic acid exclusively bind to RXRs (Klaholz et al., 1998). RXR-RAR heterodimers act as the functional units in the transduction of retinoid signal (Kastner et al., 1995). Moreover, RXRs play significant role as they also heterodimerises with the other members of the nuclear receptor family apart from RARs (Mangelsdorf et al., 1995). RXR- $\alpha$  and RAR- $\gamma$  are similar in their LBDs except for two major differences:

- Three helices, H3, H11 and H12 (the transactivation helix) undergo large conformational changes
- Helix H2 of RXR- $\alpha$  LBD was replaced by a disordered connecting peptide in an extended conformation (Egea et al., 2000).

The selective agonists of RAR- $\gamma$  were used in the treatment of emphysema (Belloni & Klaus, 2001). Emphysema is a condition in which the air sacs of the lungs are damaged and enlarged causing breathlessness. Synthetic agonists and antagonist of RARs and RXRs were used in the therapeutic applications of retinoids (Moise et al., 2007). RAR and RXR agonists and modulators were used in the treatment and chemoprevention of various forms of cancer (Chomienne et al., 1989). Although 9-cisretinoic acids identified as an agonist of RXRs, it is not a selective compound of RXRs because it has high affinity for all three isoforms of RARs (Germain et al., 2006b). Rexinoids are the synthetic compounds that recognize only RXRs. Rexinoids are very important to study the role played by RXRs and to decipher their ligand dependent activities and to know more about the relationship between the partners in RXR heterodimers.

#### ***4.4.1. Current Retinoid Therapies and their Limitations***

For the last several years, the synthetic retinoids like isotretinoin, etretinate and acitretin have been used as monotherapy or in combination to treat Cutaneous T-Cell Lymphoma (CTCL). Bexarotene is the first approved RXR agonist which can be used to treat all stages of CTCL (Zhang & Duvic, 2003). However, some adverse effects like hypertriglyceridemia, hypercholesterolemia, central hypothyroidism and headache have also been reported (Lowe & Plosker, 2000). Tretinoin (retinoid) is a drug used to treat acne and disorders of keratinization (Appa, 1999). It works well in reducing the incidence of acne. However, the irritation intolerance, erythema and peeling associated with this treatment have become an issue. Targretin (LGD 1069) is another synthetic RXR selective retinoid, investigated. A study has been conducted to observe the metabolic profile of LGD 1069 in advanced cancer patients (Rizvi et al., 1999). During this study of Rizvi et al., dose limiting toxicities like skin desquamation, hyperbilirubinemia, transaminase elevation, leukopenia, and diarrhoea were

observed. Two synthetic retinoids tazarotene (AGN190168) and adapalene (CD271) are available for the treatment of psoriasis and acne. Despite their therapeutic properties, the administration of retinoids is limited by severe toxic side effects like headache and bone toxicity (Germain et al., 2006a).

Considering the limitations and side effects of current agonists, a group of eight lipid ligands were tested for their binding ability with RAR- $\gamma$  and RXR- $\alpha$ .

#### ***4.4.2. New Series of Ligands for RAR- $\gamma$ and RXR- $\alpha$***

Crystal structures of RAR- $\gamma$  and RXR- $\alpha$  bound to various ligands reveal that the shape of the ligand binding pocket (LBP) of these receptors is different (Germain et al., 2004). After comparing the LBPs of RAR- $\gamma$  and RXR- $\alpha$ , it was observed that RXR- $\alpha$  LBP shows a more restrictive and shorter ‘L’ shape, whereas RAR- $\gamma$  LBP shows linear ‘l’ shape (Germain et al., 2006b). Depending on their flexibility the ligands can bind to both the LBPs. The distinctive structure of LBP of RXR- $\alpha$  allows the generation of ligands that discriminate between RARs and RXRs. From the discovery of synthetic compounds that activate the RXR-RXR homodimers different rexinoids have been reported. Still there is no single rexinoid with apparent subtype selectivity (Germain et al., 2006b). This issue has now become a challenge due to the presence of conserved residues in RXR LBP.

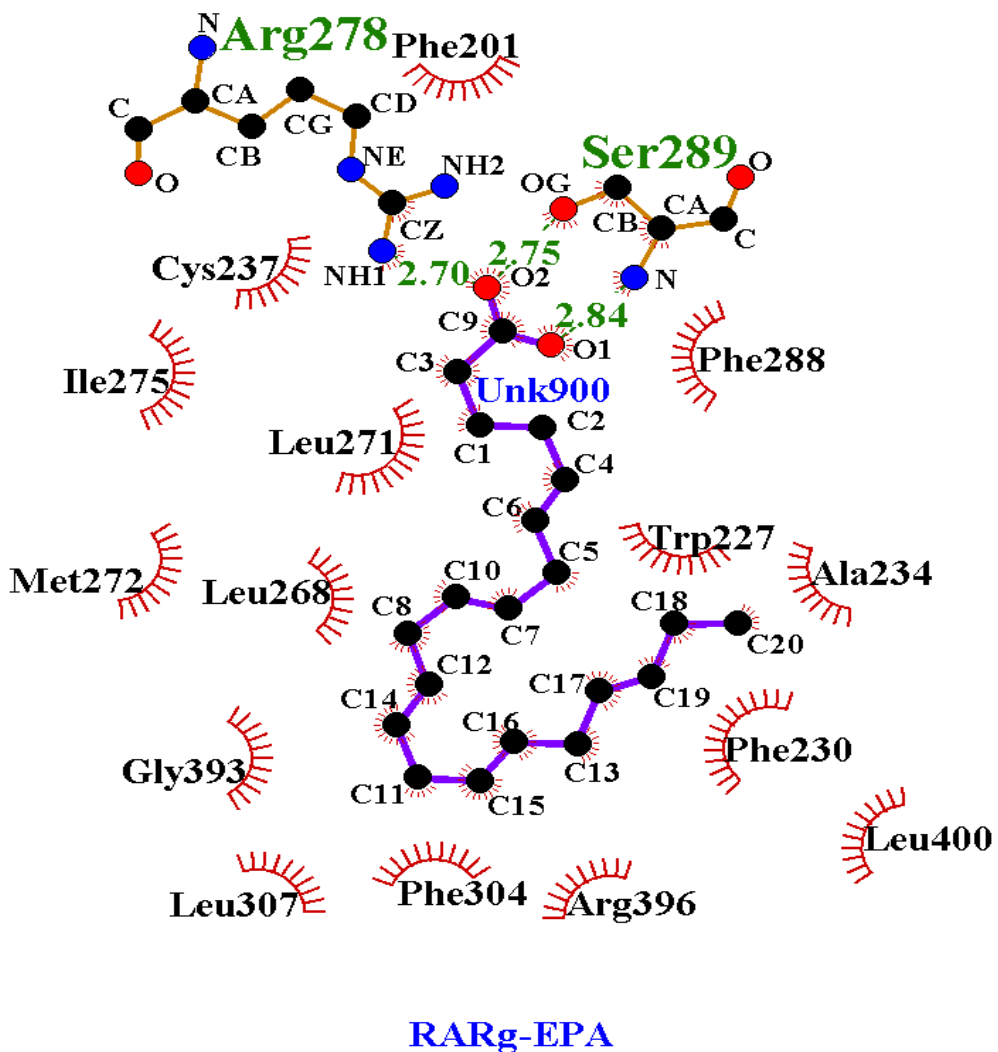
Out of all the eight lipid ligands docked, DHA has exhibited strong affinity with RAR- $\gamma$  and RXR- $\alpha$  in both AutoDock and Glide. It was found in another study (Lengqvist et al., 2004) that DHA is required for efficient RXR activation. This study also showed that DHA is a more potent ligand of RXR. The binding of RAR- $\gamma$  and RXR- $\alpha$  with other lipid ligands in AutoDock and Glide docking methods is explained in the following sections.

#### 4.4.2.1. Findings of AutoDock

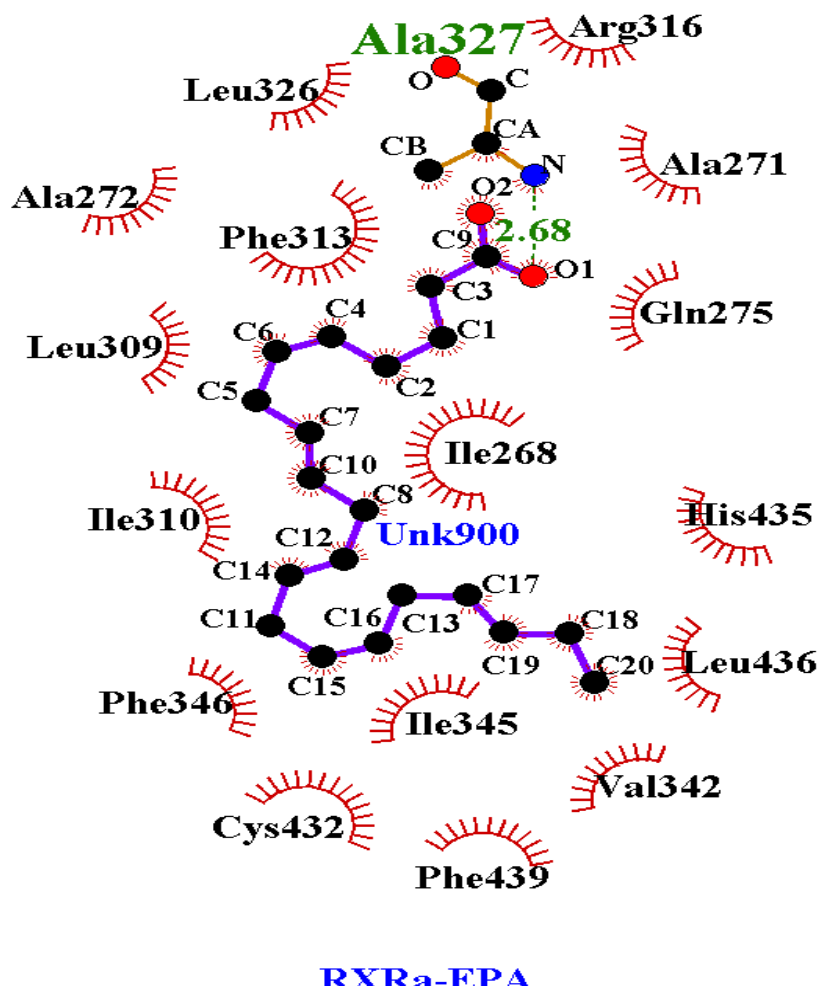
DHA and EPA have shown a strong binding affinity with RAR- $\gamma$  and RXR- $\alpha$  in AutoDock as shown in Table 4.9. DHA is similar to 9-*cis*- retinoic acid in functional properties and hence synergistically activates RXR-RAR heterodimers in combination with all-*trans*-retinoic acid (Lengqvist et al., 2004). This finding further supports the function of DHA and EPA as true RXR- $\alpha$  agonist. The active site amino acids Ser 289, Arg 278 and Leu 271 of RAR- $\gamma$  were closely interacting with EPA as shown in Figure 4.24. The binding energies of DHA and EPA are -12.51 and -10.18 kcal/mol. RAR- $\gamma$  and RXR- $\alpha$  have shown similar kind of interactions due to their structural similarities. Interestingly, RXR- $\alpha$  also has shown the binding affinity of -12.06kcal/mol with DHA. EPA has expressed a slightly stronger affinity (-11.92kcal/mol) with RXR- $\alpha$  than with RAR- $\gamma$ . The interaction of EPA with RXR- $\alpha$  is shown in Figure 4.25 where the active site amino acids Ala 327, Val 342, Ala 271, Ala 272 and Cys 432 are within 4Å distance from DHA.

**Table 4.8 Binding Affinities of RAR- $\gamma$  and RXR- $\alpha$  in AutoDock**

Protein	Ligand	Binding Energy AutoDock (kcal/mol)
RAR- $\gamma$	DHA	-12.51
RAR- $\gamma$	EPA	-10.18
RAR- $\gamma$	2AG	-10.73
RAR- $\gamma$	$\delta$ -tocotrienol	-9.03
RAR- $\gamma$	$\gamma$ -tocotrienol	-11.42
RAR- $\gamma$	Anandamide	-10.84
RAR- $\gamma$	$\beta$ -tocotrienol	-12.15
RXR- $\alpha$	$\alpha$ -tocotrienol	No Binding
RXR- $\alpha$	$\beta$ -tocotrienol	No Binding
RXR- $\alpha$	$\gamma$ -tocotrienol	-8.63
RXR- $\alpha$	$\delta$ -tocotrienol	No Binding
RXR- $\alpha$	DHA	-12.06
RXR- $\alpha$	EPA	-11.92
RXR- $\alpha$	2AG	-8.24
RXR- $\alpha$	Anandamide	-9.15

**Figure 4.24 Binding of RAR- $\gamma$  with EPA**

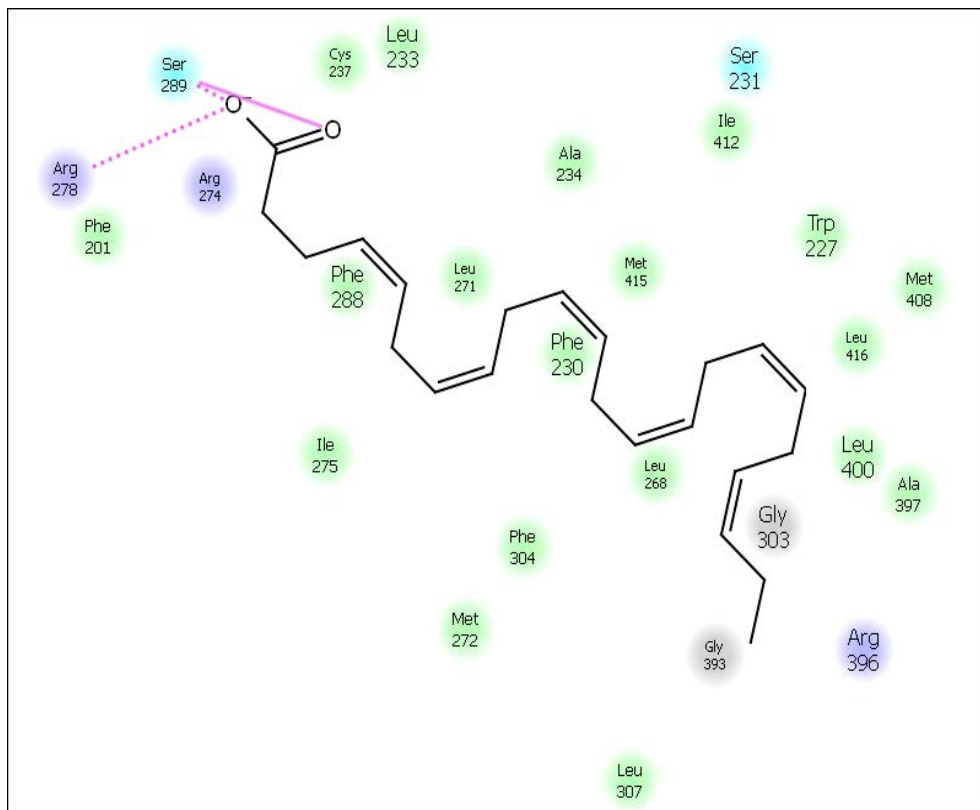
Secondary to omega 3 fatty acids, endocannabinoids (2AG and anandamide) have shown a considerable binding affinity with both RAR- $\gamma$  and RXR- $\alpha$ .  $\gamma$ -tocotrienol has expressed a stronger affinity (-11.42kcal/mol) than EPA with RAR- $\gamma$  but not with RXR- $\alpha$  (Table 4.9).  $\alpha$  and  $\delta$ -tocotrienols did not produce any binding poses with RAR- $\gamma$  and RXR- $\alpha$ .  $\beta$ -tocotrienol has shown a strong affinity with RAR- $\gamma$  (-12.15kcal/mol) but did not produce any binding poses with RXR- $\alpha$ . Figure 4.24 and 4.25 are the screen shots prepared using LigPlot (Wallace et al., 1995).

**Figure 4.25 Binding of RXR- $\alpha$  with EPA**

#### **4.4.2.2. Findings of Glide**

The Glide score generated for each pair of the receptor (RAR- $\gamma$  and RXR- $\alpha$ ) and the ligand is shown in Table 4.10. As in the procedure of AutoDock, both RAR- $\gamma$  and RXR- $\alpha$  have shown strong binding affinity with DHA (-16.0 kcal/mol and -15.4 kcal/mol respectively). The interaction of DHA with RAR- $\gamma$  is shown in Figure 4.26 which is the ligand interaction diagram generated using Glide.

It was observed from the Figures 4.26 and 4.27 that O1 and O2 located on C21 have formed hydrogen bonds with Ser 289 and Arg 278 of RAR- $\gamma$  with bond distances 2.85 Å and 2.75 Å respectively.

**Figure 4.26 Binding of RAR- $\gamma$  with DHA****Table 4.9 Glide Score of RAR- $\gamma$  and RXR- $\alpha$** 

<b>Protein</b>	<b>Ligand</b>	<b>Glide Score (kcal/mol)</b>
RAR- $\gamma$	DHA	-16.0
RAR- $\gamma$	EPA	-14.7
RAR- $\gamma$	2AG	-12.9
RAR- $\gamma$	DTT	-12.1
RAR- $\gamma$	GTT	-11.2
RAR- $\gamma$	Anandamide	-10.7
RAR- $\gamma$	$\beta$ -tocotrienol	-10.3
RAR- $\gamma$	$\alpha$ -tocotrienol	No Binding
RXR- $\alpha$	$\alpha$ -tocotrienol	No Binding
RXR- $\alpha$	$\beta$ -tocotrienol	No Binding
RXR- $\alpha$	$\gamma$ -tocotrienol	-10.9
RXR- $\alpha$	$\delta$ -tocotrienol	No Binding
RXR- $\alpha$	DHA	-15.4
RXR- $\alpha$	EPA	-14.3
RXR- $\alpha$	2AG	-9.6
RXR- $\alpha$	Anandamide	-11.6

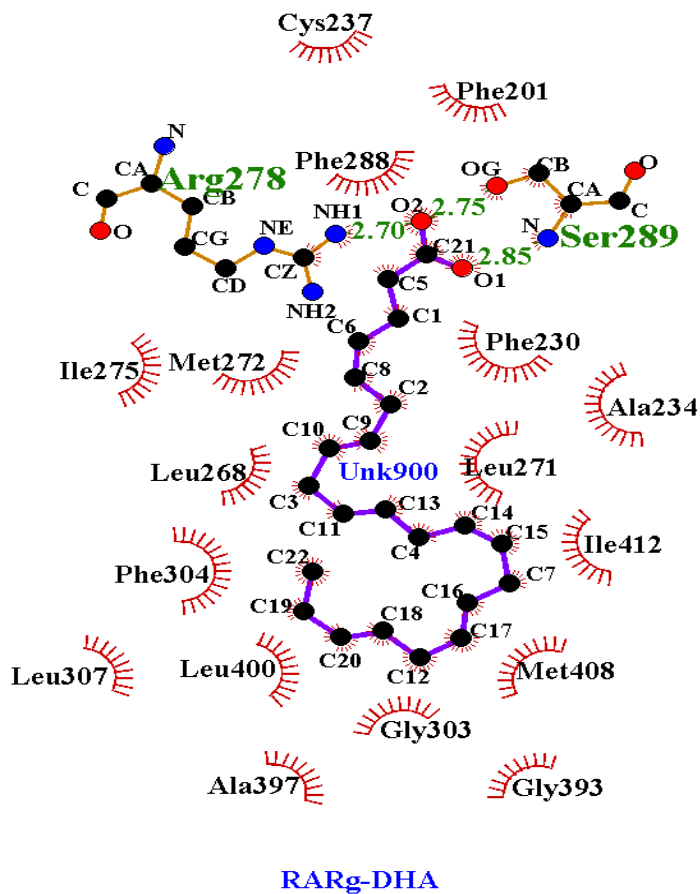


**Figure 4.27 LigPlot diagram of RAR- $\gamma$  with DHA**

The other active site amino acids like Leu 233, Leu 271 and Arg 273 have formed hydrophobic interactions with DHA. EPA has expressed strong bond strength of -14.7kcal/mol as shown in Table 8 indicating that omega 3 fatty acids are ligands of RAR- $\gamma$ . Among endocannabinoids 2AG has expressed strong binding affinity (-12.9kcal/mol) with RAR- $\gamma$  whereas anandamide has shown the bond strength of -10.7kcal/mol. Comparatively tocotrienols have expressed poor affinity than DHA, EPA and 2AG.  $\delta$ -tocotrienol (-12.1kcal/mol) and  $\gamma$ -tocotrienol (-11.2kcal/mol) have shown a stronger affinity than anandamide while  $\alpha$ -tocotrienol did not produce any binding poses with RAR- $\gamma$ .

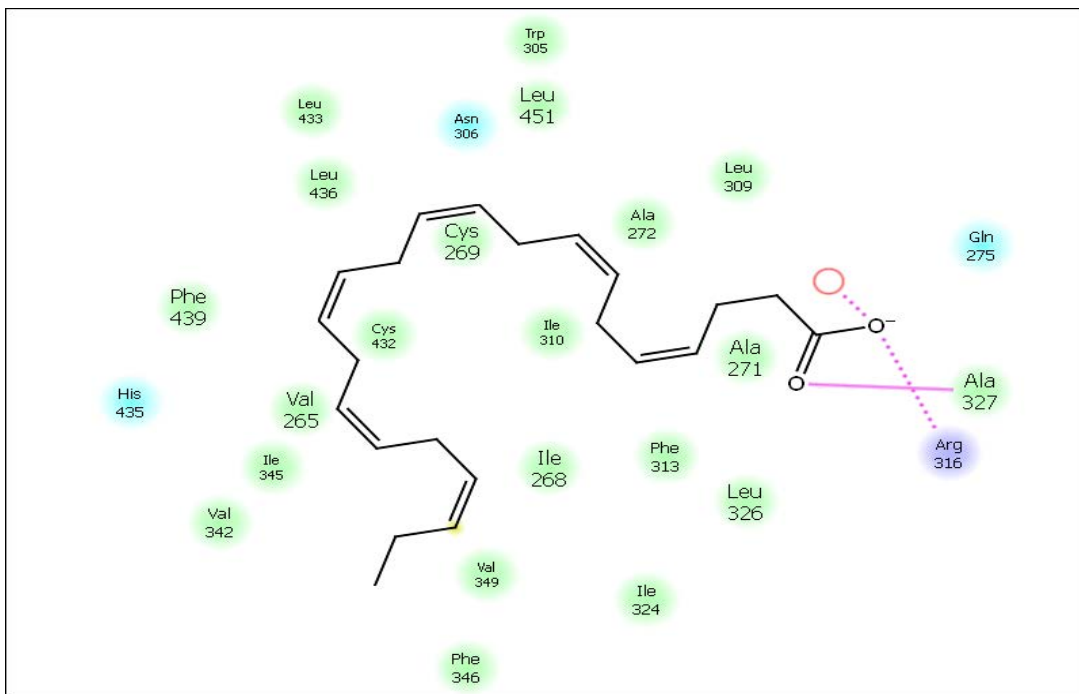


**Figure 4.28 Binding of RXR  $\alpha$  with DHA**

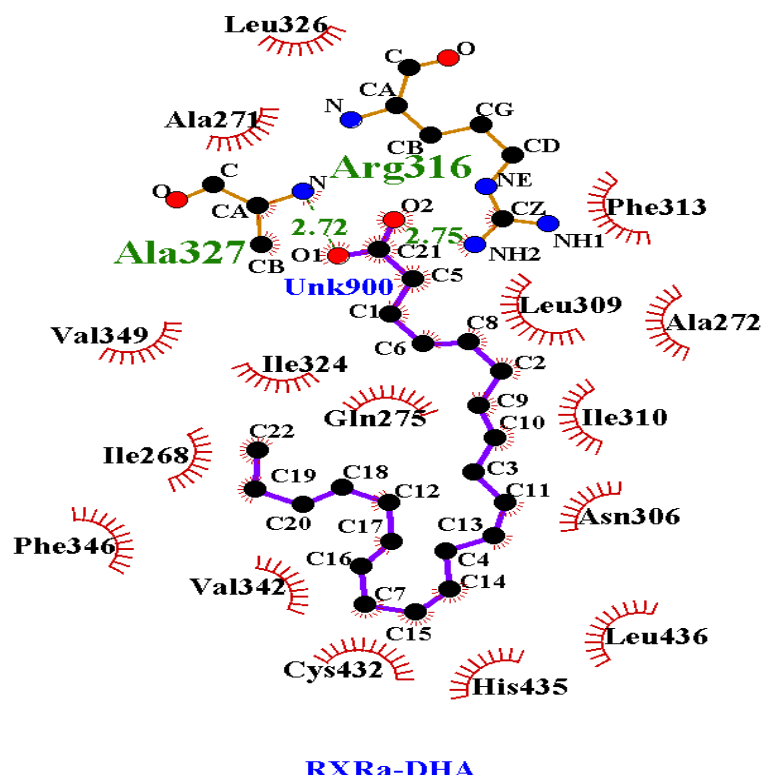


**Figure 4.29 LigPlot of RXR  $\alpha$  with DHA**

The interaction of DHA with RXR- $\alpha$  is shown in the Figures 4.27 and 4.28. As it is shown in both the Figures 4.27 and 4.28, O1 and O2 located on C21 of DHA have formed hydrogen bonds with Ala 327 and Arg 316 with bond distances 2.72 $\text{\AA}$  and 2.75 $\text{\AA}$  respectively. Active site amino acids Ala 271, Ala 272, Cys 269, Cys 432 and Val 349 have formed hydrophobic interactions with the ligand DHA.

The other omega 3 fatty acid EPA which is structurally similar to DHA, has shown strong interaction (-14.3kcal/mol) with RXR- $\alpha$ . Unlike RAR- $\gamma$ , RXR- $\alpha$  has expressed a strong binding affinity (-11.6kcal/mol) with anandamide than with 2AG (-9.6kcal/mol). Among the four types of tocotrienols only  $\gamma$ -tocotrienol has shown a strong affinity with RXR- $\alpha$  whereas  $\alpha$ ,  $\beta$  and  $\delta$ -tocotrienols did not produce any binding poses.

#### ***4.4.2.3. MD Simulation of RAR- $\gamma$ and RXR- $\alpha$ with strongest affinity ligands***

After performing AutoDock and Glide, the stability of top ranked docked complexes (RAR- $\gamma$ -DHA and RXR- $\alpha$ -DHA) were further subjected to MD simulations. Simulations were run for 2ns and the stability was studied with the help of RMSD and RMSF plots generated as a result of MD simulations (Figures 4.30 to 4.33). The RMSD and RMSF values within 2 $\text{\AA}$  indicate a stable complex (Hayes et al., 2011; Shu et al., 2011). The RMSD range for the docked complex RAR- $\gamma$ -DHA was from 0.6 $\text{\AA}$  to 1.4 $\text{\AA}$  which shows the success of docking method. The peak values (1.4 $\text{\AA}$  -Figure 4.30) were recorded at 1.5ns. The RMSF fluctuations were varying within the limit of 2.5 $\text{\AA}$  (Figure 4.30). The peak values were recorded at 2.3 $\text{\AA}$  approximately. However, the RMSF fluctuations for the active site amino acids numbering from 233-289 were ranging from 1.0 $\text{\AA}$  - 1.8 $\text{\AA}$  respectively. The initial fluctuations were recorded at 1.5 $\text{\AA}$  and followed by a sudden fall in 0.4 $\text{\AA}$  after a few conformational changes. For most of the amino acids the fluctuations were noticed within the range of 0.4 $\text{\AA}$  -1.4 $\text{\AA}$  as shown in Figure 4.31.

RMSD and RMSF plots for the docked complex RXR- $\alpha$ -DHA are shown in Figures 4.31 and 4.32. The initial RMSD values were recorded at 0.7 $\text{\AA}$  and after 2ns of MD simulations the values were within the limit of 2 $\text{\AA}$ . Peak values were obtained at 1.5ns. The lower RMSD values throughout MD simulations indicate the stability of the docked complex. The RMS fluctuations are ranging from 1.5 $\text{\AA}$  - 2.6 $\text{\AA}$  approximately. The RMSD curve in Figure 4.32 is drifting upwards until 1.4ns and started drifting downwards at 2ns.

The RMSF values for the active site amino acids numbering from 269-349 were recorded from 1.3 $\text{\AA}$  – 1.8 $\text{\AA}$  approximately. For the majority of amino acids the RMS fluctuations were within the limit of 2 $\text{\AA}$ .

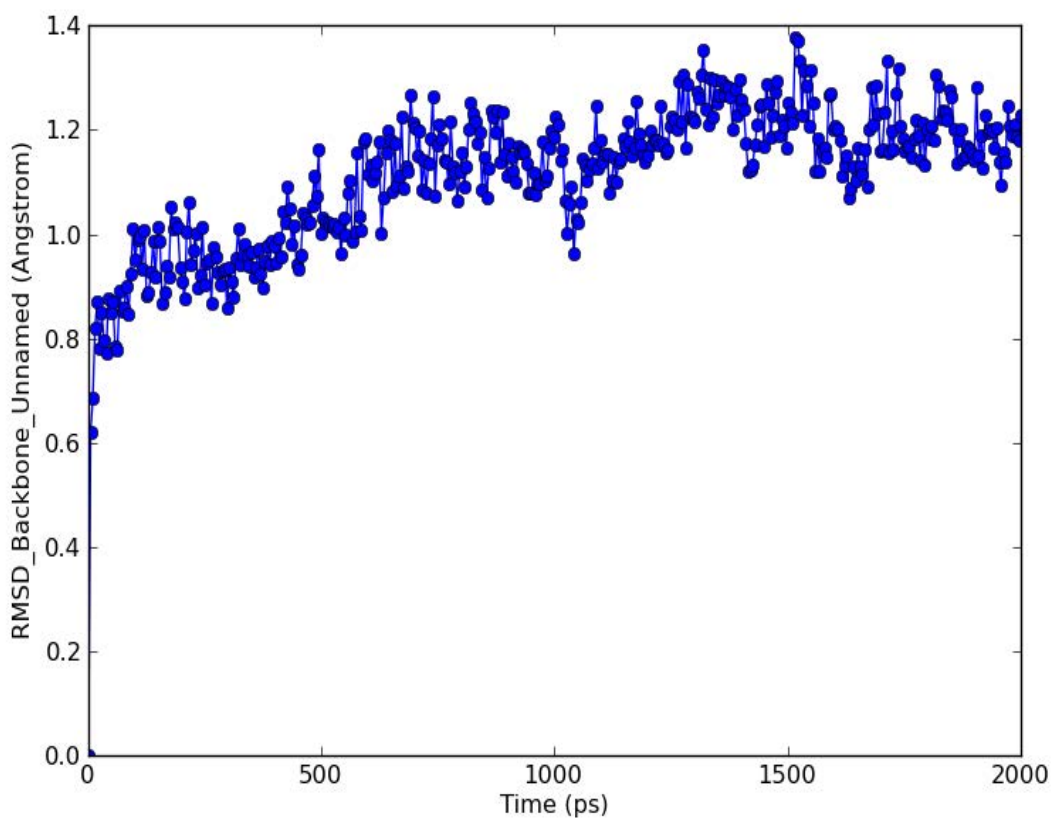


**Figure 4.30 RMSD curve of the docked complex RAR- $\gamma$ -DHA**

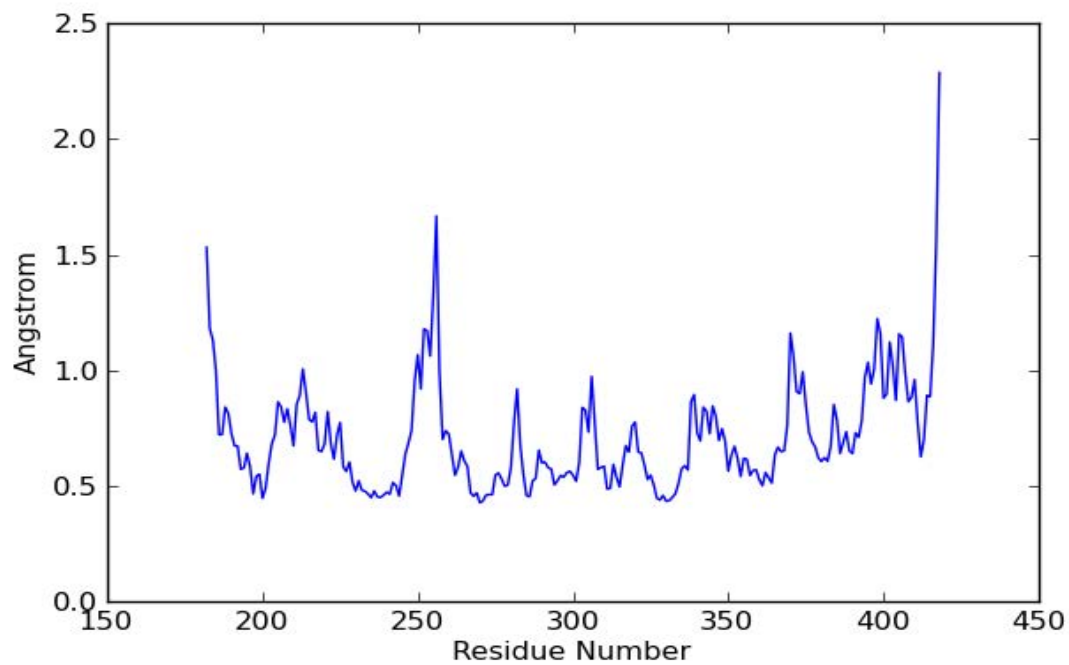


**Figure 4.31 RMSF plot of the docked complex RAR- $\gamma$ -DHA**

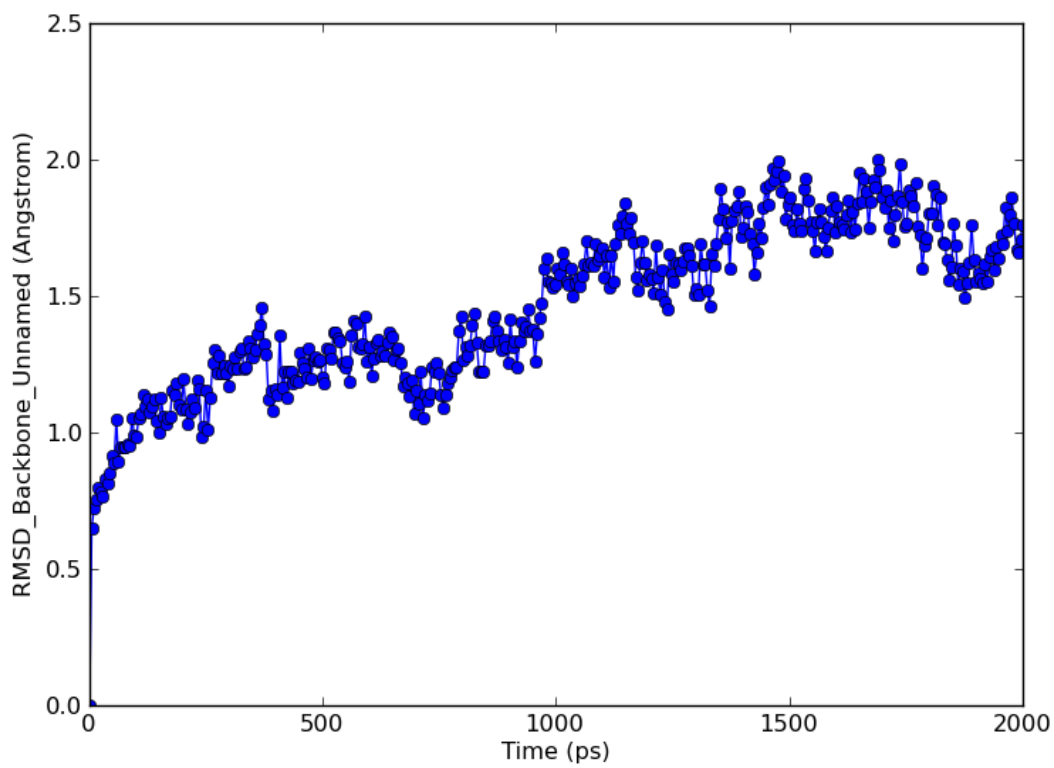


**Figure 4.32 RMSD curve of the docked complex RXR- $\alpha$  -DHA**

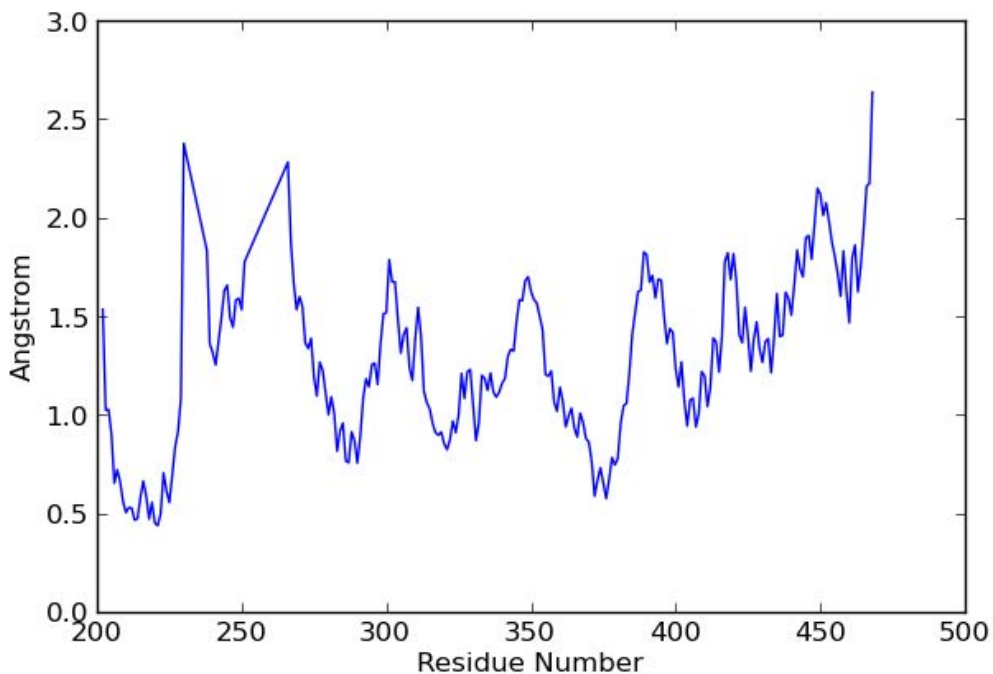
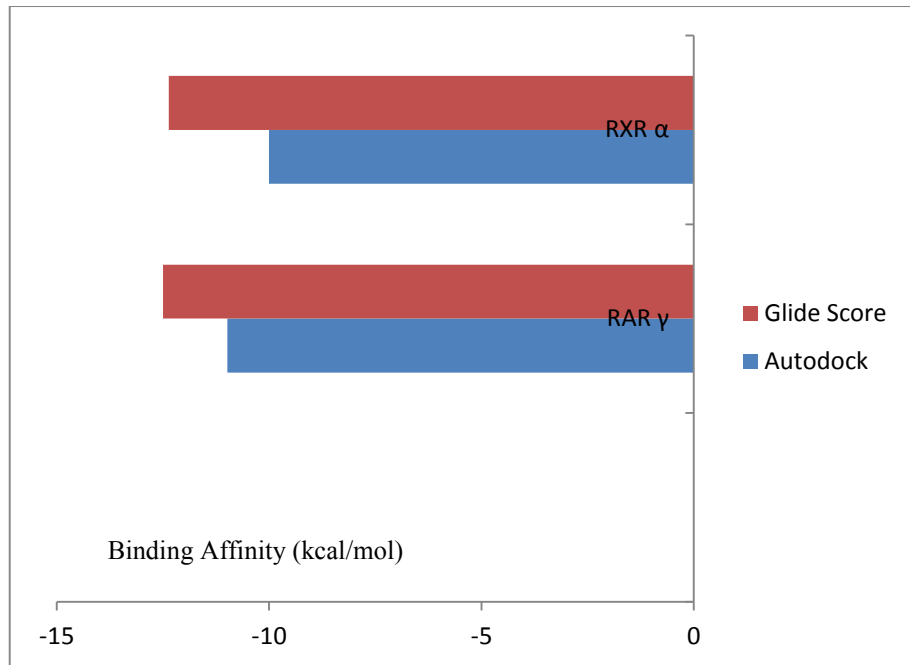


**Figure 4.33 RMSF plot of the docked complex RXR- $\alpha$ -DHA**

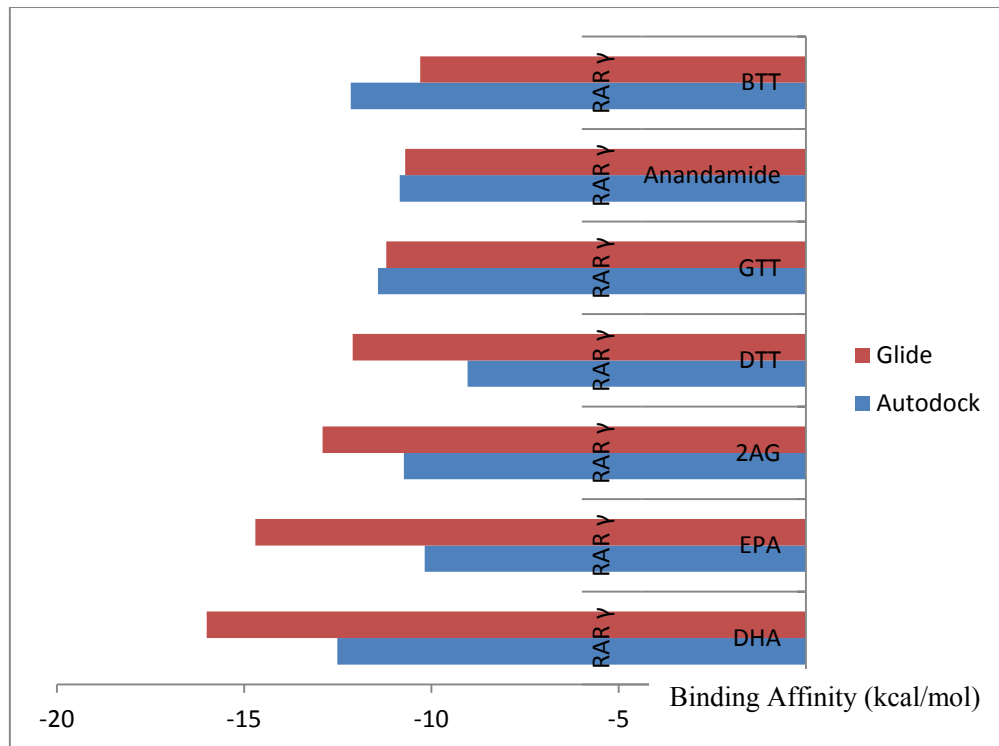
#### 4.5. Comparison of AutoDock and Glide Docking Results

AutoDock and Glide docking techniques have yielded similar results. In both the cases DHA is the top ranked ligand for RAR- $\gamma$  and RXR- $\alpha$ . There was a slight difference in the binding energies obtained from the two techniques as shown in Figure 4.34. Apart from the docking score the interactions between the receptors and ligands were clearly studied from Glide than from AutoDock.

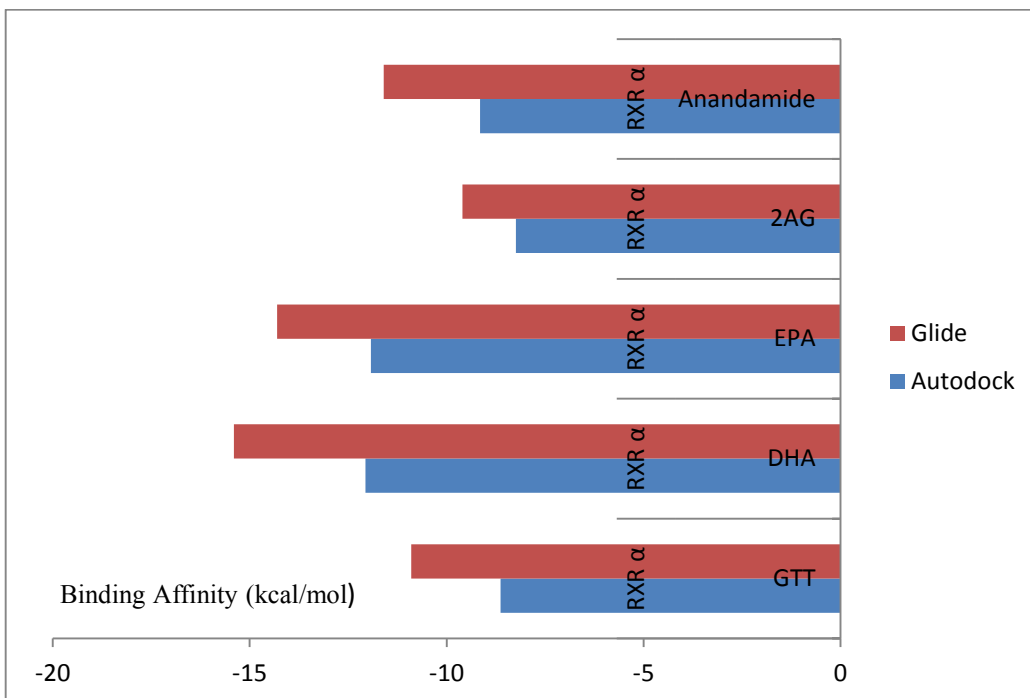
Individual receptor plots (Figures 4.35 and 4.36) were drawn in order to compare the binding affinities generated from AutoDock and Glide. The ligands DHA, EPA, 2AG and  $\delta$ -tocotrienol have shown significant differences between AutoDock and Glide in terms of their binding energies, whereas  $\gamma$ -tocotrienol and anandamide have expressed a very slight difference as shown in Figure 4.35.



**Figure 4.34 Comparing AutoDock and Glide for RAR- $\gamma$  and RXR- $\alpha$**



**Figure 4.35 RAR- $\gamma$ : AutoDock Vs Glide**

**Figure 4.36 RXR- $\alpha$ : AutoDock Vs Glide**

RXR- $\alpha$  did not show considerable binding with  $\alpha$ ,  $\beta$  and  $\delta$ - tocotrienols in both AutoDock and Glide. Although both the docking tools use different algorithms their performance is identical in ranking the ligands according to their binding affinity with the target proteins.

## 4.6. Conclusion

The side effects of current PPAR-based and retinoid-based drugs are the fundamental basis of the author's study. After studying the binding affinities, the study has proposed a new series of ligands for both PPARs and retinoids.

During AutoDock, all the eight ligands have shown strong affinity with PPAR- $\alpha$  compared to the crystal ligand CTM. Tocotrienols have shown similar binding affinities with PPAR- $\alpha$  and PPAR- $\delta$ . DHA and EPA are observed as the dual agonists of PPAR- $\alpha$  and  $\gamma$ . Tocotrienols and omega 3 fatty acids have shown a strong binding affinity with PPAR- $\alpha$  and  $\gamma$  compared to the

crystal ligand CTM. PPAR- $\delta$  has shown a strong binding affinity with omega 3 fatty acids compared to the other two groups of lipid ligands.

It was found in Glide docking that 2 AG has shown strong affinity with PPAR- $\alpha$  compared to tocotrienols. Although, anandamide belong to the same group of lipids as 2AG, there was a considerable difference in their binding affinities. In the case of PPAR- $\delta$  and PPAR- $\gamma$ , only omega 3 fatty acids have shown strongest affinity compared to the crystal ligand-D32. Interestingly, the ranking of three groups of lipid ligands according their binding affinities with PPARs is the same in both AutoDock and Glide. Omega 3 fatty acids were ranked as one followed by tocotrienols and endocannabinoids.

Redocking was performed as a validation method of AutoDock and Glide. It was observed from redocking studies that the docking procedure is accurate. MD simulation studies were performed for the docked complexes with lowest binding energies. The lower RMSD and RMSF values of PPARs during 2ns periods of MD simulations have confirmed the stability of the docked complexes. In both AutoDock and Glide the ligands have occupied the same binding pocket generating the similar docking poses.

Unlike PPARs, RAR- $\gamma$  and RXR- $\alpha$  have shown strong binding affinity with both omega 3 fatty acids and endocannabinoids. Comparatively, tocotrienols have expressed less affinity. The binding of DHA with both RAR- $\gamma$  and RXR- $\alpha$  was almost similar. However, EPA has shown strong affinity with RXR-  $\alpha$  compared to RAR- $\gamma$ . Among tocotrienols,  $\gamma$ -tocotrienol has exhibited favorable interactions with RAR- $\gamma$  and RXR- $\alpha$ . In the group of endocannabinoids, anadamide has shown strong binding affinity with RAR- $\gamma$  and RXR- $\alpha$  compared to 2AG.

Retinoid receptors are one of the interesting drug targets. From the above molecular docking studies using AutoDock and Glide software, it is concluded that DHA is the potential ligand

for both RAR- $\gamma$  and RXR- $\alpha$ . Hence, DHA can be further tested for its pharmacological efficiency to act as a drug target of RAR- $\gamma$  and RXR- $\alpha$ . MD simulation studies have further tested the stability of the top ranked docked complexes RAR- $\gamma$ -DHA and RXR- $\alpha$ -DHA.

Similar to the nuclear receptor family the enzymes COX-1, COX-2 and LOX are interesting to study in terms of their binding affinities with the same lipid ligands. The interaction mechanism of these three enzymes, with eight lipid ligands is discussed in Chapter 5.

## Chapter 5

# Dual and Selective Lipid Ligands of Cyclooxygenase and Lipoxygenase

*Publication pertaining to this chapter:*

*Gaddipati, R.S., Raikundalia, G. K., & Mathai, M. L (2014). Dual and selective lipid inhibitors of cyclooxygenases and lipoxygenase: a molecular docking study. Medicinal Chemistry Research, 1-14.*

## 5.1. Introduction

Cyclooxygenase (COX) and Lipoxygenase (LOX) are important enzymes which play an important role in arachidonic acid metabolism. There is an emerging need for the research on COX-LOX dual inhibitors because of their significant role in variety of cancers including prostate cancer (Pommery et al., 2004; Skelly & Hawkey, 2003). Hence, the author's study has focussed on finding the dual and selective inhibitors of COX and LOX.

COX exists in two isoforms: COX-1 and COX-2. The expression of COX-1 is constitutive and the expression of COX-2 is induced in response to inflammation (Vane et al., 1998). They are the major targets of non-steroidal anti-inflammatory drugs (NSAIDs), such as aspirin and ibuprofen (Mifflin et al., 2001). However, the use of NSAIDs can result in side effects like stomach or gastrointestinal ulcers, heartburn, headache, and dizziness (Smith et al., 2000). NSAIDs should not be used in patients with renal failure; therefore, there is a need to find a potential inhibitor for COX-1 and COX-2 that can be used to treat inflammation and pain. Dual inhibition of COX and LOX has two advantages. First, dual inhibitors act on two major arachidonic acid metabolic pathways and retain a wide range of anti-inflammatory activity. Second, dual inhibitors reduce gastric toxicity, which is the most troublesome side effect of COX inhibitors (Leval et al., 2002). This demonstrates the need to find potential inhibitors for the actions of COXs, which would aid in reducing the number of side effects. The current study is designed to observe the binding of COX-1 and COX-2 with different substrates that would cause little or no side effects.

The structure and enzymatic activity of COX-1 and COX-2 are very similar, yet they have different substrate and inhibitor selectivity (Ding et al., 2003). Lipoxygenases are iron-containing enzymes that catalyze the oxidation of polyunsaturated fatty acids. There are different types of LOXs (5-LOX, 8-LOX, 12 LOX, and 15-LOX) based on the number of

carbon atoms they act on, or based on the incorporation of oxygen (Ding et al., 2003). Different types of LOXs are categorized based on their positional specificity of arachidonic acid activation. The crystal structure of 12-LOX is used for the current molecular docking stud. They are widely found in plants, animals, and fungi (Brash, 1999). LOX is a monomeric protein that has an N-terminal  $\beta$ -barrel domain, and C-terminal catalytic site containing a single non-heme iron atom.

The eight ligands used in this study have substantial health benefits, and so they were docked with COX-1, COX-2, and LOX to observe their inhibitory activities. The current molecular docking experiment is useful to identify lipid ligands that are dual inhibitors and selective inhibitors of both COX and LOX. Selective inhibitors act on COX-2 and LOX without acting on COX-1. Selective inhibition is beneficial, because the inhibition of COX-1 results in gastrointestinal disturbance, unlike COX-2.

This chapter explains the molecular docking experiments conducted to find the potential ligands of COX-1, COX-2, and LOX. The results of AutoDock and Glide were discussed in Sections 5.2.1 and 5.2.2 respectively. The stability of these docked complexes is studied using molecular dynamic simulations, and is described in Section 5.2.5. In order to find suitable docking technique for COX-1, COX-2, and LOX, comparison studies were conducted and explained in Section 5.4. Finally, Section 5.5 concludes the contents of this Chapter.

## ***5.2. Towards the Discovery of Anti-Inflammatory Drugs***

There is widespread concern about the side effects of NSAIDs used to treat inflammatory conditions. NSAIDs inhibit the actions of COXs which are involved in the formation of prostaglandins and thromboxanes from arachidonic acid. However, the inhibition of COXs by NSAIDs could shunt the arachidonic acid metabolism towards the LOX pathway, which

could further cause the increased formation of leukotrienes, leading to inflammation and NSAIDs induced side effects like asthma and gastrointestinal damage (Hudson et al., 1993; Laufer, 2001; Rainsford, 1987, 1993, 1999). Arachidonic acid metabolism is mediated by LOX, and would further contribute to the side effect profile observed for NSAIDs in osteoarthritis (Burnett et al., 2012). Moreover, LOXs are found to play a role in cardiovascular diseases. Hence, a single inhibitory agent that acts on both COXs and LOX is of interest to medicinal chemistry (Zheng et al., 2006). The current molecular docking study is an attempt to find such dual inhibitory agents to both COX and LOX.

Essential fatty acids like linoleic acid and arachidonic acid are metabolized to eicosanoids by the enzymes COX and LOX. These fatty acids have a significant role in the progress of pancreatic cancer. The level and activity of both COX and LOX are observed to be abnormal in pancreatic cancer (Ding et al., 2003). Hence, potential inhibitors of these enzymes might be useful in the treatment of pancreatic cancer. COX converts arachidonic acid to prostaglandin precursors, which are used by other enzymes to form prostaglandins that cause pain and inflammation. The pharmacological inhibition of cyclooxygenase gives relief from pain and inflammation. Inhibition of the enzyme LOX has positive health effects in the case of arthritis and inflammation (Rainsford, 1993, 1999). Potential inhibitors of LOX can be used in the treatment of asthma, inflammation, and respiratory disease (Kalva et al., 2011).

### ***5.2.1. Molecular Docking Studies using AutoDock***

The binding energies of all three enzymes (COX-1, COX-2, and LOX) with eight lipid ligands are shown in Table 5.1, 5.2 and 5.3 respectively. As per the results of AutoDock, EPA has expressed a strong affinity (-11.88kcal/mol) with the enzyme COX-1. The interaction of EPA with COX-1 is shown in Figure 5.1. The amino acid Ser 530 has formed a bond with the oxygen atom of DHA, with a bond distance of 2.2Å. The amino acids Val 349,

Ala 527, Ile 345, Leu 351, and Ala 527 etc. have formed hydrophobic interactions with EPA. DHA has less affinity (-8.42 Kcal/mol) with COX-1 compared to EPA. Tocotrienols did not show remarkable binding with COX-1. Following DHA and EPA, endocannabinoids (2AG and anandamide) were identified as ligands of COX-1.

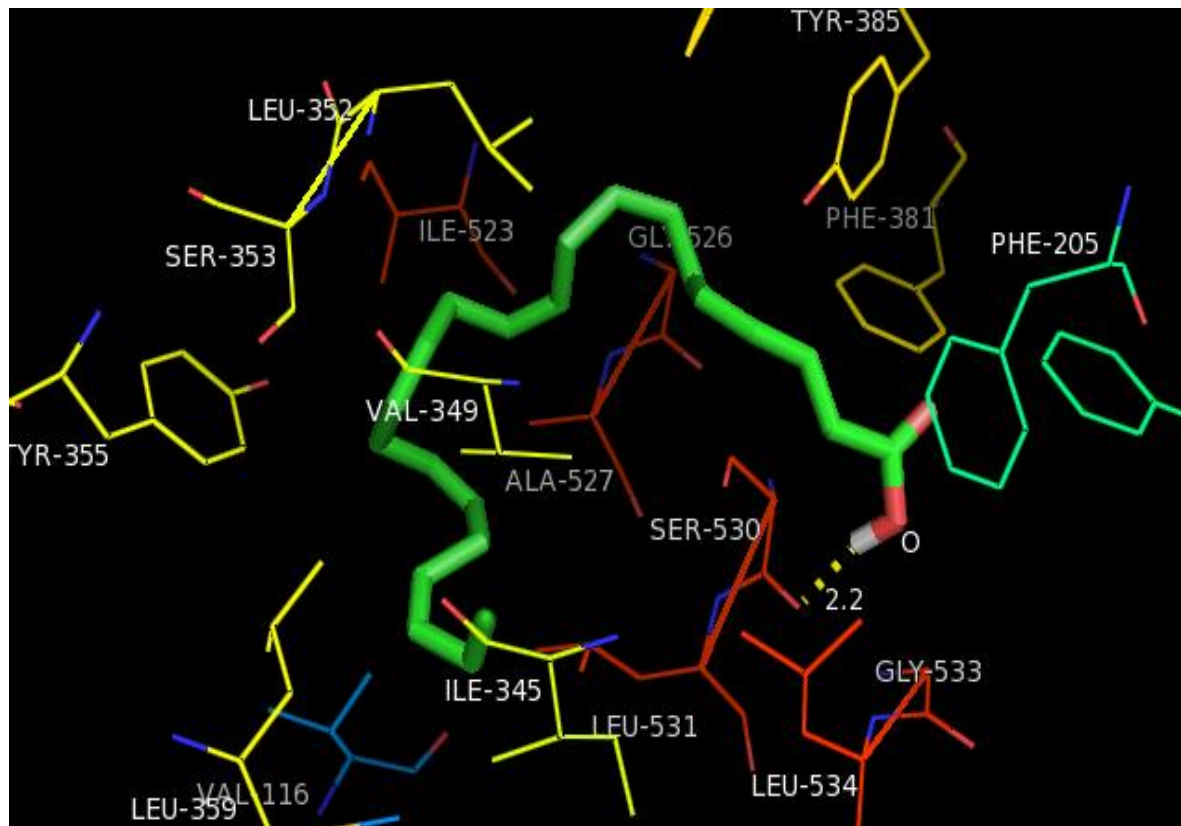


**Figure 5.1 Interaction of COX-1 with EPA**

**Table 5.1 Binding affinities of COX-1 with lipid ligands in AutoDock**

Ligand	Lowest Binding energy (kcal/mol) AutoDock
DHA	-8.42
EPA	-11.88
2AG	-8.32
Anandamide	-8.86
ATT	-4.23
BTT	-6.15
DTT	-5.80
GTT	-4.88
DIF	-7.20

Omega 3 fatty acids and endocannabinoids are the potential ligands of COX-1, as they have a stronger affinity with COX-1 than with the crystal ligand diclofenac.

COX-2 has shown a strong affinity with DHA (-12.51 kcal/mol); their interaction is depicted in Figure 5.2. The ligand binding pocket of COX-1 varies from COX-2 due to change of Ile 523 (present in COX-1) to Val 523 in COX-2. As Val 523 is structurally smaller than Ile 523, COX-2 actively binds to the ligands in place of COX-1 (Vane et al., 1998). COX-1 and COX-2 also vary in their gene expression and biological roles.

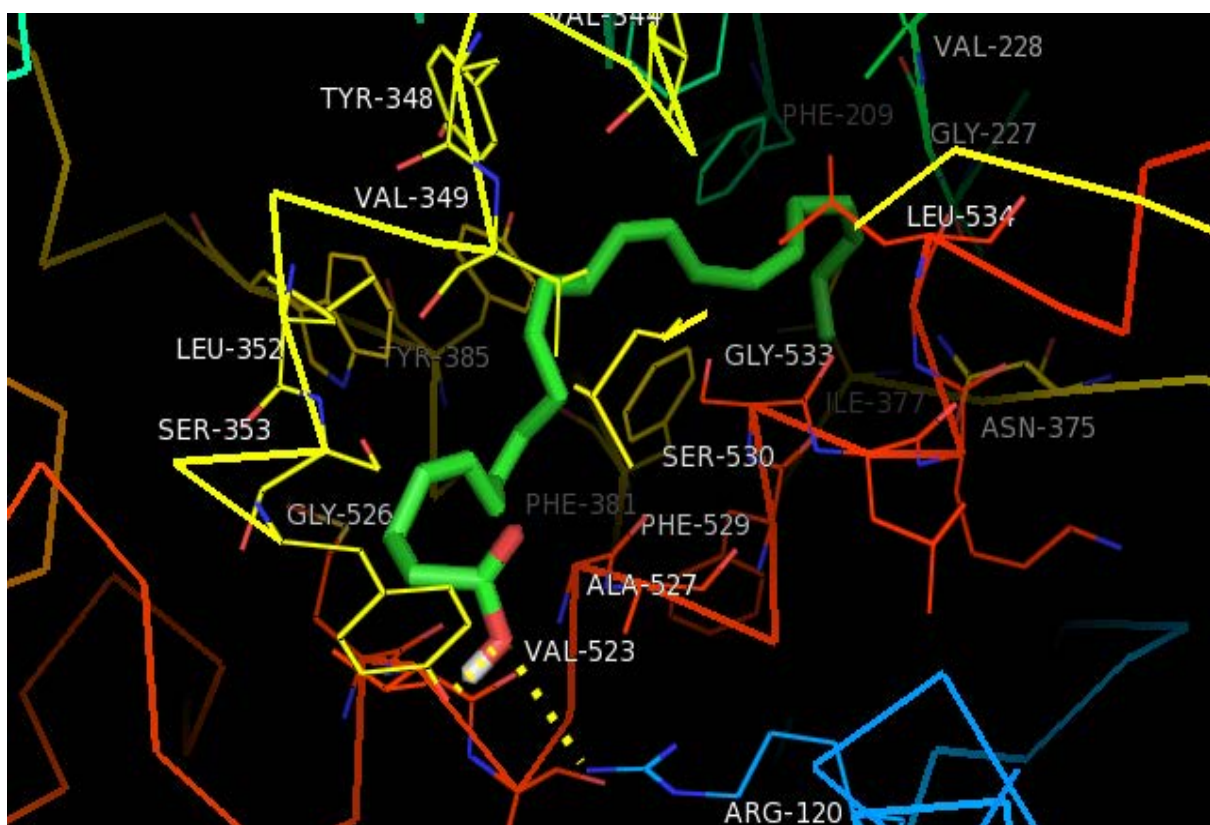


**Figure 5.2 Interaction of COX-2 with DHA**

Both COX-1 and COX-2 are heme-containing homodimeric enzymes. The amino acid sequences of the enzymes have a similarity of 63 % (Mifflin et al., 2001). COX-1 has an 8-amino acid insertion at the amino terminus, while COX-2 has an 18-amino acid insertion at the carboxyl terminus (Mifflin et al., 2001). After DHA,  $\alpha$ -tocotrienol (-11.98 kcal/mol) and

2AG (-11.90 kcal/mol) have shown higher affinity with COX-2. This is also in contrast to COX-1, where COX-1 did not produce any binding poses with  $\alpha$ -tocotrienol. EPA and anandamide are considered as the next level of ligands to COX-2, with binding affinities of -9.16 kcal/mol and -8.74 kcal/mol respectively (Table 5.2). Except for  $\gamma$ -tocotrienol, the rest of the seven lipid ligands have a stronger affinity with COX-2 than arachidonic acid.

**Table 5.2 Binding affinities of COX-2 with lipid ligands in AutoDock**

Ligand	Lowest Binding energy (kcal/mol) AutoDock
DHA	-12.51
EPA	-9.16
2AG	-11.90
Anandamide	-8.74
ATT	-11.98
BTT	-8.14
DTT	-9.51
GTT	-7.93
ARA	-8.10

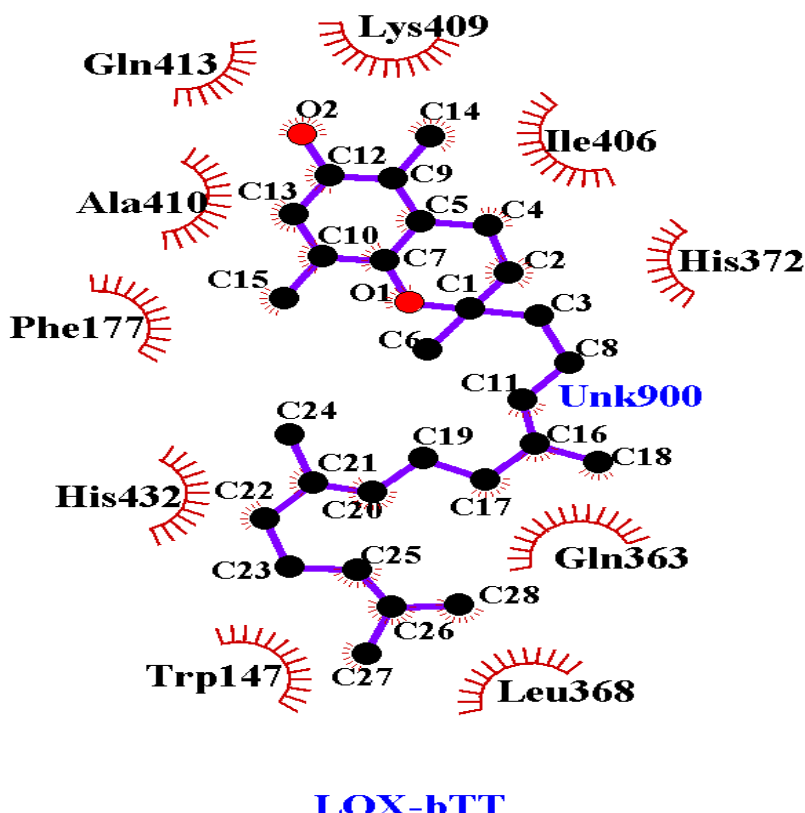


**Figure 5.3 Interaction of LOX with  $\beta$ -tocotrienol**

LOX has shown strong interaction with  $\beta$ -tocotrienol, as shown in Figure 5.3 and Table 5.3. Phe 177, Gln 413, and Ala 410 formed bonds with the ligand, with bond distances of 2.2 $\text{\AA}$ , 2.0 $\text{\AA}$  and 1.8 $\text{\AA}$  respectively. The other amino acids like Leu 368, His 372, Leu 409, Ile 406, Gln 363, and Trp 147 etc. are closely interacting with the ligand  $\beta$ -tocotrienol. Except for all four tocotrienols, the remaining ligands (DHA, EPA, 2AG and Anandamide) did not show considerable binding with LOX when compared to the crystal ligand arachidonic acid.

**Table 5.3 Binding affinities of LOX with lipid ligands in AutoDock**

Ligand	Lowest Binding energy (kcal/mol) AutoDock
DHA	-4.05
EPA	-5.76
2AG	-3.38
Anandamide	-4.79
ATT	-7.72
BTT	-7.80
DTT	-7.20
GTT	-7.29
ARA	-6.20

### 5.2.2. Molecular Docking Studies using Glide

**Table 5.4 Glide score of COX-1 with eight lipid ligands**

Ligand	Glide Score (kcal/mol)
DHA	-8.3
EPA	-9.8
2AG	-7.5
Anandamide	-8.4
ATT	-3.2
BTT	-5.4
DTT	-6.7
GTT	-3.5
DIF	-8.0

The binding site of crystal ligand diclofenac is considered to be the active site for the grid generation of COX-1 (Sidhu et al., 2010). Diclofenac is one of the commonly used NSAIDs

that have anti-inflammatory, anti-analgesic, and anti-pyretic properties. However, the action of diclofenac goes beyond COX inhibition, and includes other novel actions like the inhibition of PPAR- $\gamma$ , and alteration of interleukin-6 production (Gan, 2010). Due to the structural differences between COX-1 and COX-2, it was believed that EPA can only bind to COX-2 (Vane et al., 1998). However, the author's molecular docking study has identified that EPA is the best ligand for the enzyme COX-1 out of the eight ligands used in the *in silico* experiment (Table 5.4). EPA formed two bonds with the amino acids Ser 530 and Tyr 385, as shown in Figure 5.4.

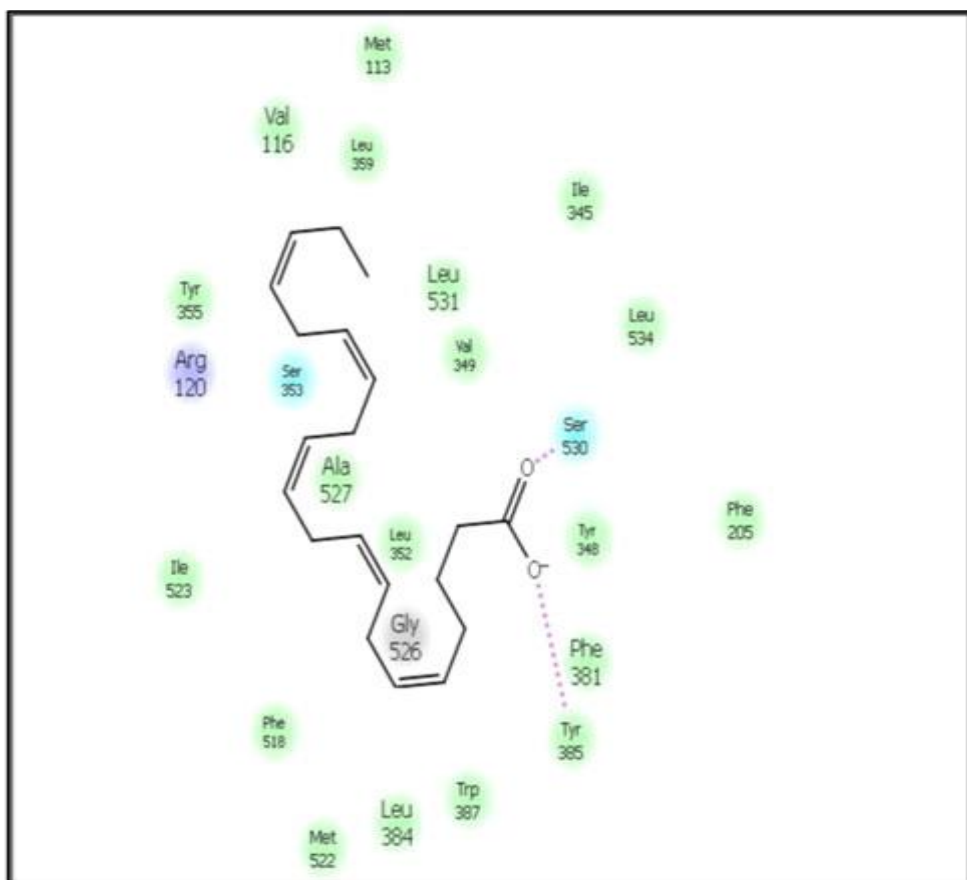


**Figure 5.4 Ligand Interaction: COX-1-EPA**

The hydroxyl (OH) group of the carboxylic acid located on C1 of EPA donates a hydrogen atom to the hydroxyl group located on C4 of the amino acid tyrosine. A hydrogen atom is also donated by the OH group on C1 of EPA, to the hydroxyl group of Ser 530, resulting in a

bond. The hydrophobic interactions were observed with Tyr 348, Phe 381, Phe 205, Ile 345, Leu 534, Leu 531, Val 349, and Ala 527 (Figure 5.4). Hydrophobic interactions are shown in a green color, polar amino acids are represented in blue, hydrogen bonds are illustrated with pink dots, and a purple color indicates positively charged amino acids.

The rest of the three successful ligands, DHA, 2AG, and anandamide, have shown almost similar docking scores with COX-1 (Table 5.4). Compared to the other four ligands,  $\beta$ ,  $\gamma$  and  $\delta$ -tocotrienols generated a slightly higher Glide score with COX-1.  $\alpha$ -tocotrienol did not produce any considerable binding poses, indicating no binding with COX-1. This could be due to the orientation of  $\alpha$ -tocotrienol, which might have failed to fit into the small ligand-binding pocket of COX-1 (Mifflin et al., 2001; Vane et al., 1998). Hence, it is concluded from this study that  $\alpha$ -tocotrienol is a selective inhibitor of COX-2. This outcome of the current work supports the search to find effective drugs that can act only on COX-2 without binding to COX-1 (Goodsell, 2000). Aspirin, the most commonly used anti-inflammatory drug, blocks both COX-1 and COX-2, which disturbs the stomach and kidneys since the normal levels of prostaglandins are disturbed.

The action of COX-2 is to bind to arachidonic acid and produce prostaglandins which cause inflammation. Thus, there is a need to find ligands of COX-2 which can compete with arachidonic acid for the active site of this enzyme. This would block the synthesis of prostaglandins, thereby preventing pain and inflammation. Hence, this research focuses on finding the ligands of COX-2 that can compete with arachidonic acid. It is observed in this study that COX-1 and COX-2 resulted in different docking scores with the same lipid ligands. This might be due to the change of the active site amino acid Ile to Val in COX-2 at positions 434 and 523 (Vane et al., 1998).

**Table 5.5 Glide Score of COX-2 with eight lipid ligands**

Ligand	Lowest Binding energy (kcal/mol) AutoDock
DHA	-11.2
EPA	-10.6
2AG	-11.7
Anandamide	-10.9
ATT	-11.0
BTT	-8.2
DTT	-10.8
GTT	-9.7
ARA	-10.5

2AG has shown the lowest Glide score, indicating stronger binding with COX-2 (-11.7 kcal/mol) than the remaining ligands as shown in Table 5.5. All the lipid ligands in this study, except for  $\beta$ -tocotrienol (-8.2 kcal/mol) and  $\gamma$ -tocotrienol (-9.7 kcal/mol), were observed as stronger ligands of COX-2 than the crystal ligand arachidonic acid in terms of the Glide score (-10.5 kcal/mol). Since these ligands were shown to fit into the binding pocket of COX-2 with strong affinity, they can be used in the prevention of cancer as COX-2 selective inhibitors, as suggested by Brown and DuBois (Brown, et al., 2005). According to Subbaramaiah and Dannenberg (Subbaramaiah and Dannenberg, 2003), the level of COX-2 was observed to be higher in cancer patients, indicating a link between increased COX-2 activity and tumorigenesis. This is supported by the author's study, which is underway to determine if the selective COX-2 inhibitors can be used in the prevention and treatment of cancer. COX-1, COX-2, and LOX are involved in the treatment of testicular cancer, as supported by Matsuyama and Yoshimura (Matsuyama & Yoshimura., 2009). It was found in the current study that the ligands DHA, EPA, anandamide, 2AG, and  $\delta$ -tocotrienol bind to all three enzymes, and can be used as common ligands for the above three enzymes. Since these lipid ligands are naturally occurring and chemically active, they might result in fewer or no side effects.

DHA has formed a bond with Tyr 385 and Ser 530. EPA and 2AG have generated a similar docking score with COX-2. Comparatively, anandamide resulted in a higher docking score than the other three lipid ligands. If arachidonic acid does not bind to COX-2, then arachidonic acid metabolism might shunt to the LOX pathway, resulting in the formation of leukotrienes, and leading to inflammation and cardiovascular diseases (Hudson et al., 1993; Laufer, 2001; Rainsford, 1987; Rainsford, 1999). Hence, finding a dual inhibitor for both COX-2 and LOX, which can prevent arachidonic acid from binding to these two enzymes, would help in designing the drugs for inflammation. It was found in the author's study that all the eight lipid ligands have shown interaction with the enzyme LOX.

$\beta$ -tocotrienol resulted in the lowest Glide score, indicating that it has strong binding with LOX (Table 5.6). Hydrogen was donated by the carboxyl group of Gln 413, to the hydroxyl group present on C6 of  $\beta$ -tocotrienol. Hydrophobic interactions were observed with the amino acids Ile 406, Phe 177, Ala 410, Leu 368, Leu 373, Val 436, Phe 151, Trp 147, and Phe 151.  $\beta$ -tocotrienol competed with arachidonic acid and occupied the active site of the enzyme because of this strong interaction between LOX and  $\beta$ -tocotrienol.

The amino acids around a 4 $\text{\AA}$  distance from the ligand are shown in Figure 5.5. The crystal ligand arachidonic acid is considered for the receptor grid generation of LOX. All eight target ligands have shown a better Glide score with LOX than with arachidonic acid (-5.3 kcal/mol). Endocannabinoids (2AG and anandamide) have shown a similar Glide score with tocotrienols. The ligands DHA, EPA, 2AG, and anandamide are the common inhibitors of both COX and LOX enzymes, and hence, are used to treat cancer and inflammation (Shureiqi et al., 2001). It was identified in author's study that  $\alpha$ -tocotrienol bound to both COX-2 and LOX without binding to COX-1.

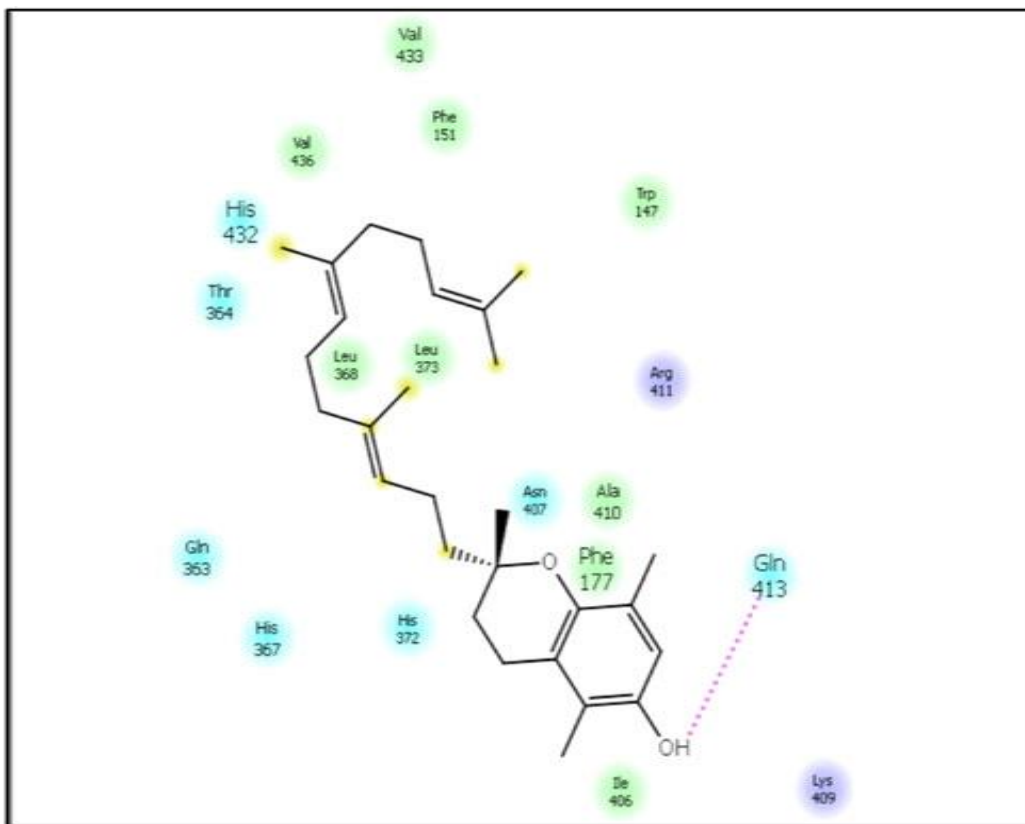


Figure 5.5 Ligand Interaction: COX-2-DHA

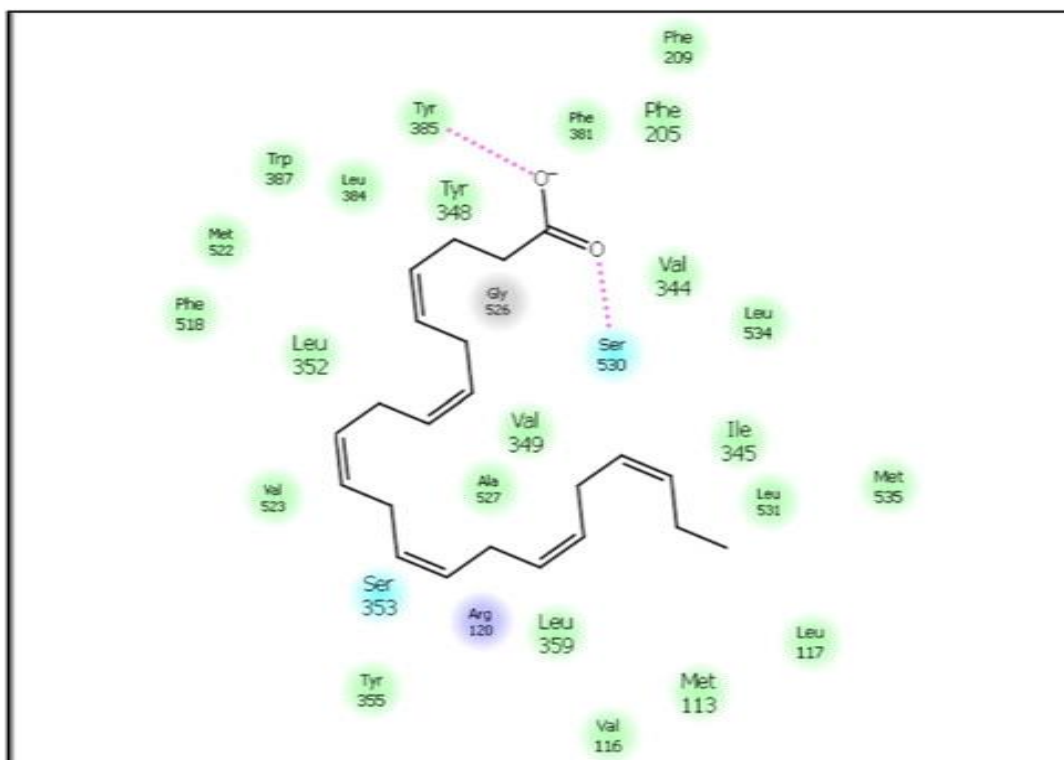


Figure 5.6 Ligand Interaction: LOX- $\beta$  tocotrienol

**Table 5.6 Glide Score of LOX with eight lipid ligands**

Ligand	Lowest Binding energy (kcal/mol) AutoDock
DHA	-5.5
EPA	-5.8
2AG	-7.2
Anandamide	-6.7
ATT	-7.2
BTT	-8.0
DTT	-6.2
GTT	-7.1
ARA	-5.5

Inhibition of LOX is also associated with cell growth inhibition and apoptosis (Shureiqi et al., 2000). LOX inhibitors have anticarcinogenic effects, and can also be used to treat inflammatory diseases. The lipid ligands in this study can be used to develop new cancer chemo preventive approaches targeted on LOX activity (Shureiqi et al., 2001).

For the enzymes COX-2 and LOX, the ligands used in the author's study are potential ligands than arachidonic acid. Moreover, these lipid ligands bind to both COX-2 and LOX, and hence, can be used as the dual inhibitors of COX-2 and LOX. Tocotrienols generally have a low binding affinity for COX-1 compared to COX-2 and LOX. In particular,  $\alpha$ -tocotrienol is most selective for COX-2 and LOX, as it did not produce any binding poses with COX-1. Apart from the similar structures of COX-1 and COX-2, the large binding pocket of COX-2 resulted in binding with more ligands than COX-1.

### **5.2.3. Ligand Binding Sites of COX-1 and COX-2**

A single amino acid difference in the active site of COX-1 and COX-2 makes COX-2 selective to some drugs (Simmons et al., 2004). As mentioned earlier Val 523 in COX-2 is replaced with Ile 523 in COX-1 as shown in the following Figures 5.7 and 5.8. This single difference opens a hydrophobic pocket in COX-2 which can be accessed by some selective

drugs (Simmons et al., 2004). There are some other changes near the active site as shown in the Figures 5.7 and 5.8 (captured using Pymol).

Tyr 385 and Ser 530 have formed bonds with COX-2 where as in COX-1 only Tyr 385 has formed bond and not Ser 530. Ser 530 was not seen in the active site of COX-1 with in 4Å distance from the active site of COX-1. Further, Arg 120, Trp 387, Leu 359, Val 344 and Tyr 348 have closely interacted with both COX-1 and COX-2. The ligand also interacted with the amino acids Gly 526 and Ala 527 of COX-2 which were not seen in the active site of COX-1. The interaction of more amino acids in COX-2 than in COX-1 demonstrated the enlarged binding site of COX-2. This change in the interacting amino acids in both COX-1 and COX-2 resulted in the differences in the binding affinities when they interact with the same ligands.

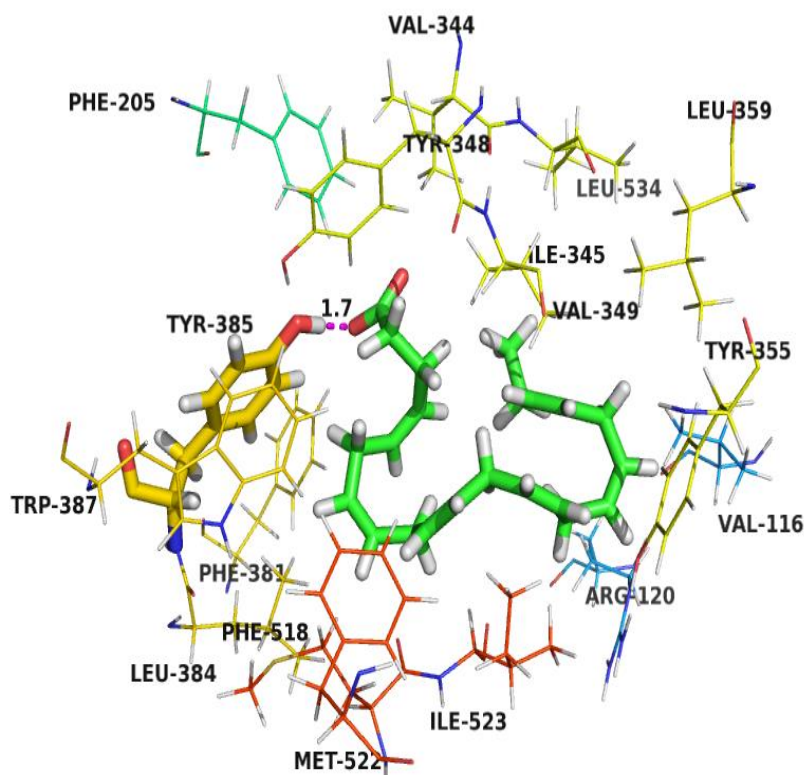


**Figure 5.7 Ligand Binding Site of COX-1**

The differences in the ligand binding site and sequence of amino acids in COX-1 and COX-2 resulted in the differences of binding affinities of DHA, EPA and other lipid ligands as well.

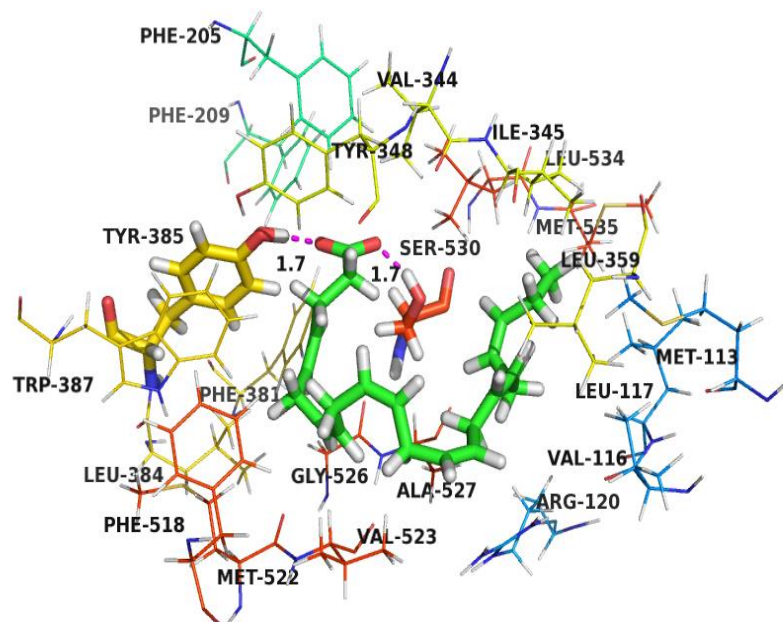


**Figure 5.8 Ligand Binding Site of COX-2**

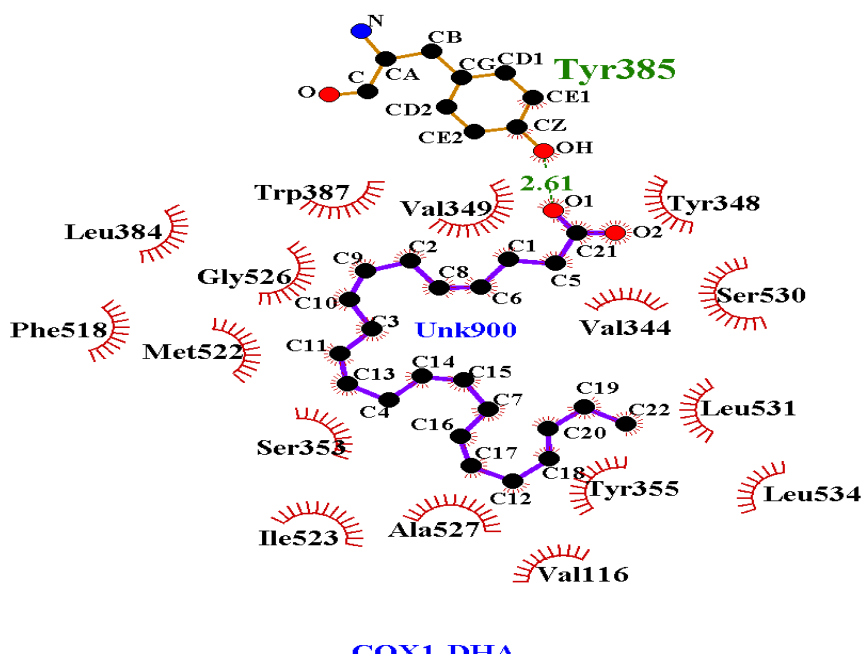


**Figure 5.9 LigPlot image of COX-1 binding to DHA**

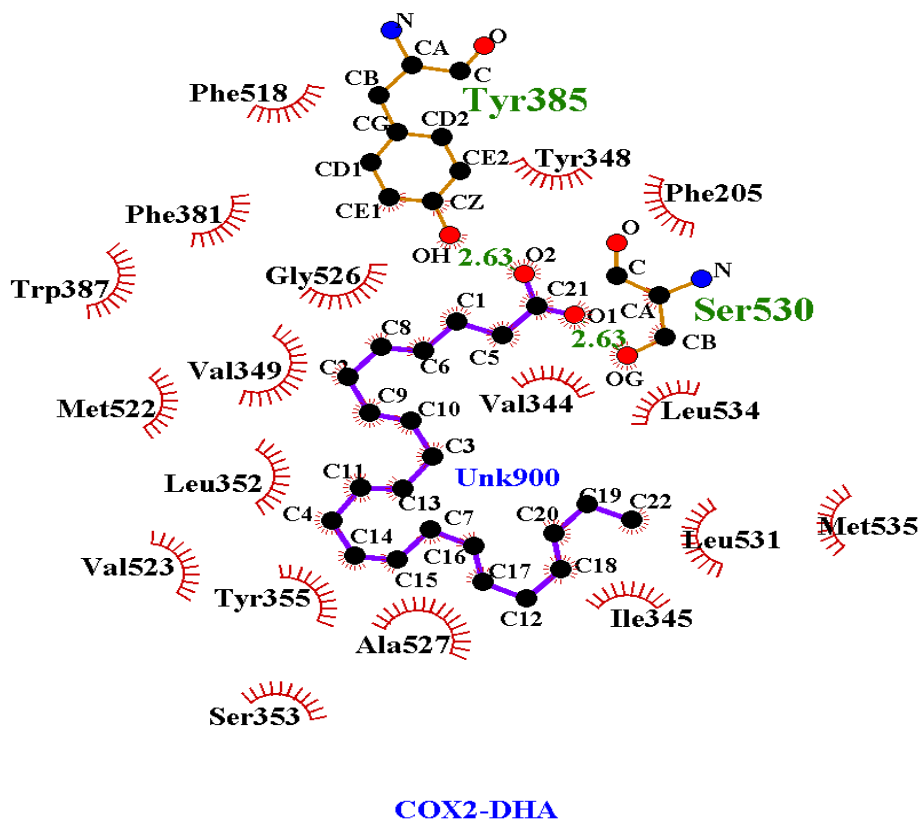


**Figure 5.10 LigPlot image of COX-1 binding to DHA**

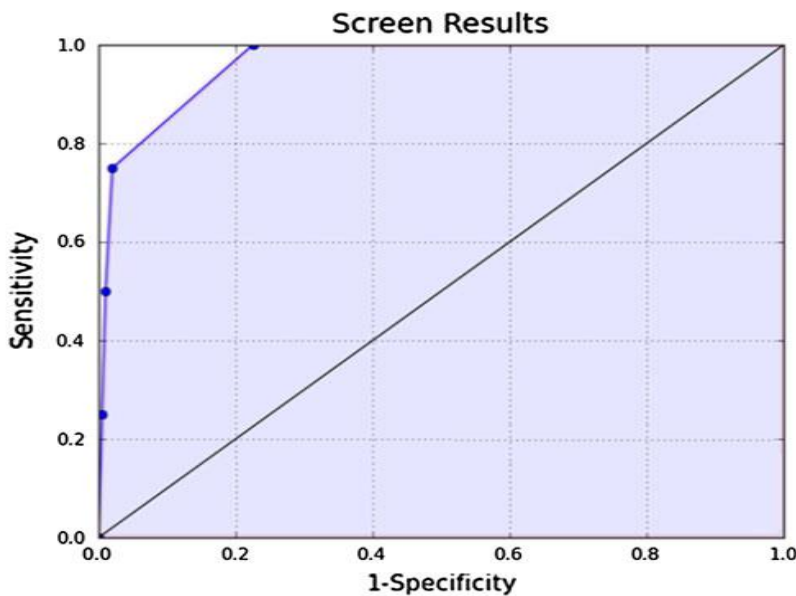
It was observed from Figures 5.9 and 5.10 that Ile 523 has formed a hydrophobic interaction with COX-1 whereas Val 523 in COX-2 is forming a hydrophobic interaction with DHA. Tyr 385 has formed a hydrogen bond with both COX-1 and COX-2 with bond distances 2.61 Å and 2.63 Å respectively. Ser 530 has formed a hydrogen bond in COX-2 with a bond distance of 2.63 Å and hydrophobic interaction in COX-1. Val 349, Gly 526, Tyr 355, Ala 527, Ser 353, Val 344 have formed hydrophobic interactions in both COX-1 and COX-2.

#### 5.2.4. Receiver Operating Characteristic Curve

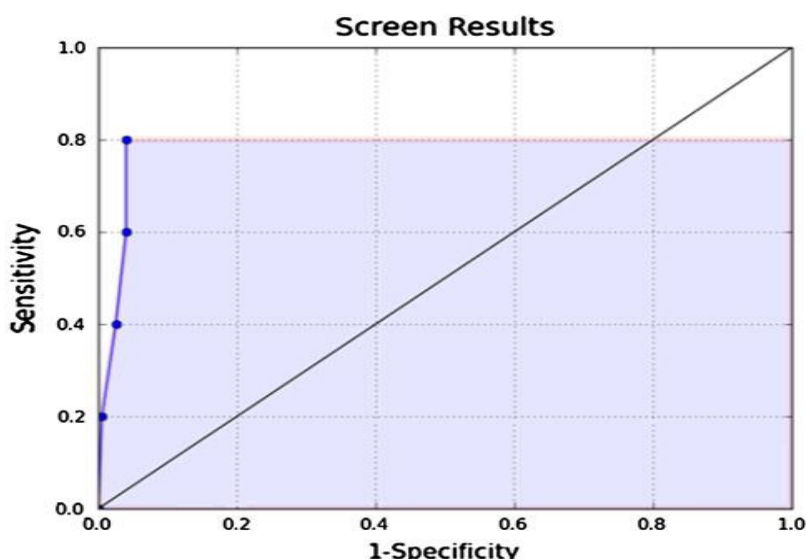
The ROC curve for the ligands was generated using the enrichment calculator of Maestro v9.2. ROC curve was used to check if the docking program was able select the active ligands amongst the inactive ligands. The set of decoys were downloaded from Schrodinger web site

([www.Schrodinger.com](http://www.Schrodinger.com)). Three compound sets that were previously used for docking validation studies were used in this study (Friesner et al., 2004; Halgren et al., 2004). ROC curves are independent of the number of actives in the decoy set and they include information on sensitivity and specificity (Hevener et al., 2009). Enrichment studies were conducted previously using the same decoy set of ligands (Friesner et al., 2004; Gatica & Cavasotto, 2011; Halgren et al., 2004; Hevener et al., 2009). Hence, even if COX-1 and COX-2 target non-polar ligands, the results were not affected. Moreover, the decoys in Schrödinger web site were designed to meet all kinds of targets such as enzymes, nuclear receptors and GPCRs etc. The decoys were designed to match with the physical chemistry of ligands on a target-by-target basis by the properties of polar, non-polar, number of rotatable bonds, hydrogen bond donors and acceptors (Friesner et al., 2004; Halgren et al., 2004). The decoys were designed to fulfil their role as negative controls. Hence, the chances of flaw results are very less.

Out of the eight ligands used in the author's study, only four of them (DHA, EPA, 2AG, and anandamide) were recognized as displaying strong binding with COX-1, and the remaining four ( $\alpha$ ,  $\beta$ ,  $\gamma$  and  $\delta$ -tocotrienols) were weak binders. In the ROC curve for the enzyme, COX-1 was above the diagonal near to the Y-axis (sensitivity), indicating better docking enrichment (Huang et al., 2006). The area under the accumulation curve (AUC value) is  $0.98 \text{ \AA}^\circ$ , which is very close to the theoretically perfect performance ( $1.0 \text{ \AA}$ ) (Deng et al., 2008). Accuracy was measured by the area under the ROC curve. The area under the ROC curve demonstrates the ability of the method in differentiating the true positives from the false positives. The following figures 5.11, 5.12, and 5.13 are the ROC curves of the enzymes COX-1, COX-2 and LOX respectively.

**Figure 5.11 ROC curve for the enzyme COX-1**

It was identified through the docking results that there are six inhibitors (DHA, EPA, 2AG, anandamide,  $\gamma$ , and  $\delta$ -tocotrienol) of the enzyme COX-2 out of the eight ligands considered for the study. Hence, the ROC curve was generated for these 6 ligands, with the combination of 200 unknown ligands. The curve is close to the X-axis as shown in the Figure 5.12. With XP mode of docking, the AUC is 0.92 for the enzyme COX-2. This shows the ability of the docking method to avoid false positives and false negatives (Deng et al., 2008).

**Figure 5.12 ROC curve for the enzyme COX-2**

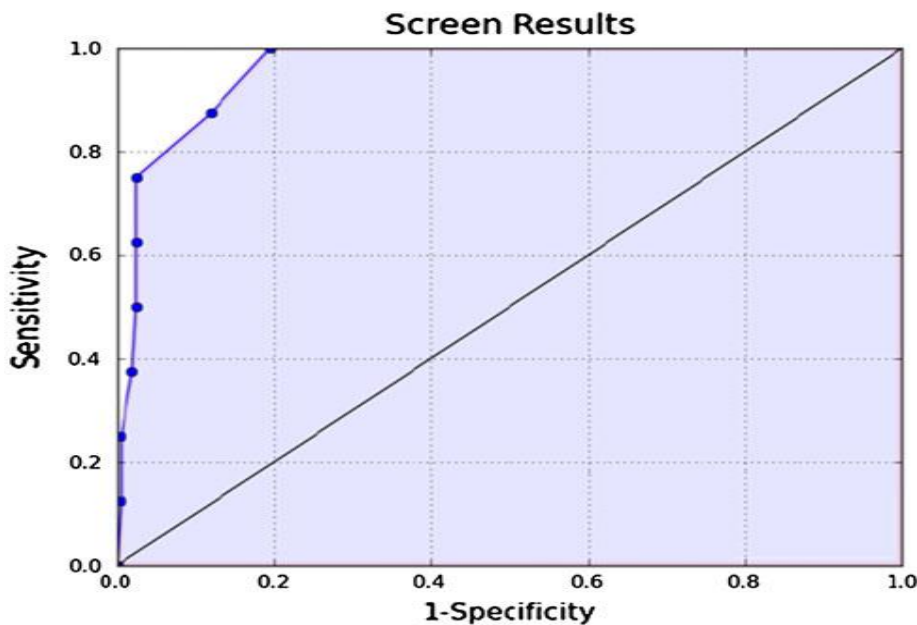


**Figure 5.13 ROC curve for the enzyme LOX**

Unlike COX-1 and COX-2, the ROC curve was generated for all the eight ligands in the case of LOX. The ROC curve is above the diagonal and is close to the true positives (X-axis), as can be seen in Figure 5.13. The AUC is  $0.99 \text{ \AA}$  in the case of LOX, which is almost equal to the theoretical perfect performance ( $1.0 \text{ \AA}^\circ$ ), indicating the accuracy of the results (Deng et al., 2008). For the enzyme LOX, all the eight ligands have been recognized as inhibitors during the enrichment calculation, as shown in the ROC curve (Figure 5.13).

### 5.2.5. Molecular Dynamic Simulations

MD simulations for the docked complexes of COX-1-EPA, COX-2-DHA, and LOX- $\beta$ -tocotrienol were performed. The docked protein-ligand complexes that have the higher affinities were subjected to MD simulation studies. The RMSD and RMSF plots for the enzymes COX-1, COX-2, and LOX are shown in Figures 5.14-5.19. It was observed from Figures 5.14, 5.16 and 5.18 that all three docked complexes, after performing MD simulations, were relatively stable during a 2ns MD simulation period (after a small rearrangement from the initial conformation). RMSD plots of COX-1 (Figure 5.14), COX-2

(Figure 5.16), and LOX (Figure 5.18) suggested that the backbone atoms have expressed a significant stability during the course of MD simulations.

The RMSD range of COX-1 backbone atoms was limited within 2.5 Å, whereas for COX-2 and LOX, the RMSD values were within 2 Å. The lower RMSD values during the entire MD simulations for docked complexes COX-1-EPA, COX-2-2AG, and LOX-BTT showed the consistent nature of docking conformations. RMSF values were calculated by the atomic fluctuations for the backbone atoms of COX-1, COX-2 and LOX (Figures 5.15, 5.17, and 5.19). RMSF values for most of the residues in the COX-1-EPA complex were within the limit of 2.5 Å.

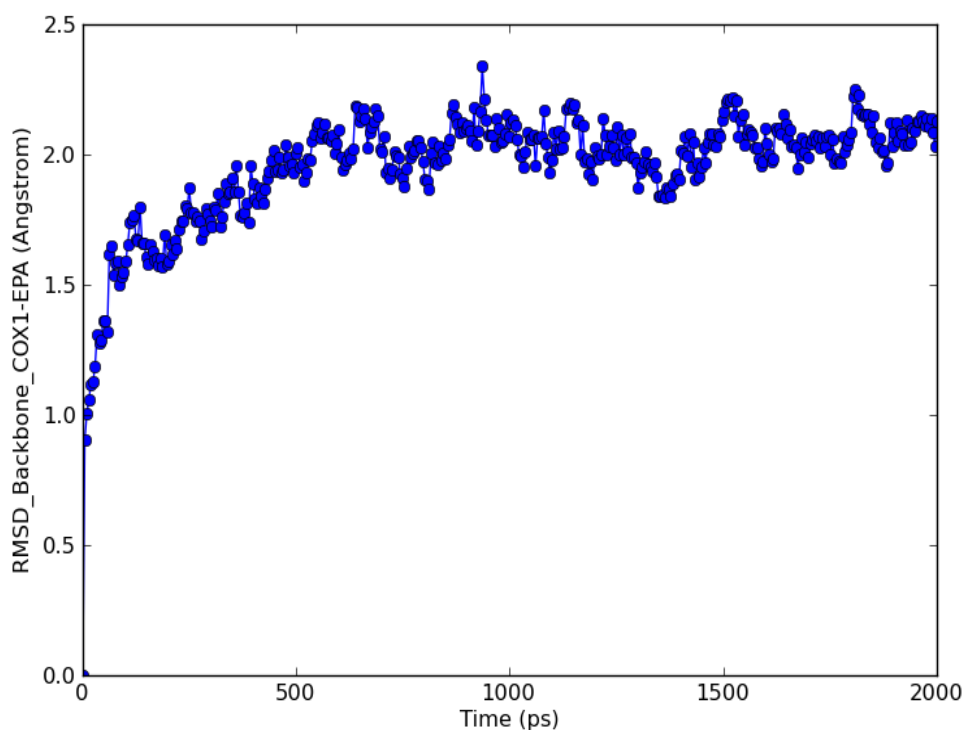


**Figure 5.14 RMSD Plot of COX-1-EPA Docked Complex**

The amino acids, Val 349, Tyr 348, Ala 527, Phe 205, Ser 530, Leu 352, Gly 526, Ile 523, Leu 531, Arg 120, Glu 524, Val 116, Val 119, and Leu 534 of COX-1 have interacted with

the ligand. Val 116, Val 119 and Arg 120 have shown RMSF fluctuations between 0.7-1.0 Å approximately. For the interacting amino acid Phe 205 the fluctuations were recorded at 1.0-1.3 Å. Val 349 and Leu 352 have shown RMSF fluctuations were ranging from 1.3 Å to 1.5 Å. For the remaining interacting amino acids Ile 523, Glu 524, Gly 526, Ala 527 Ser 530 and Leu 531 the RMSF fluctuations were identified between 0.7-1.0 Å.

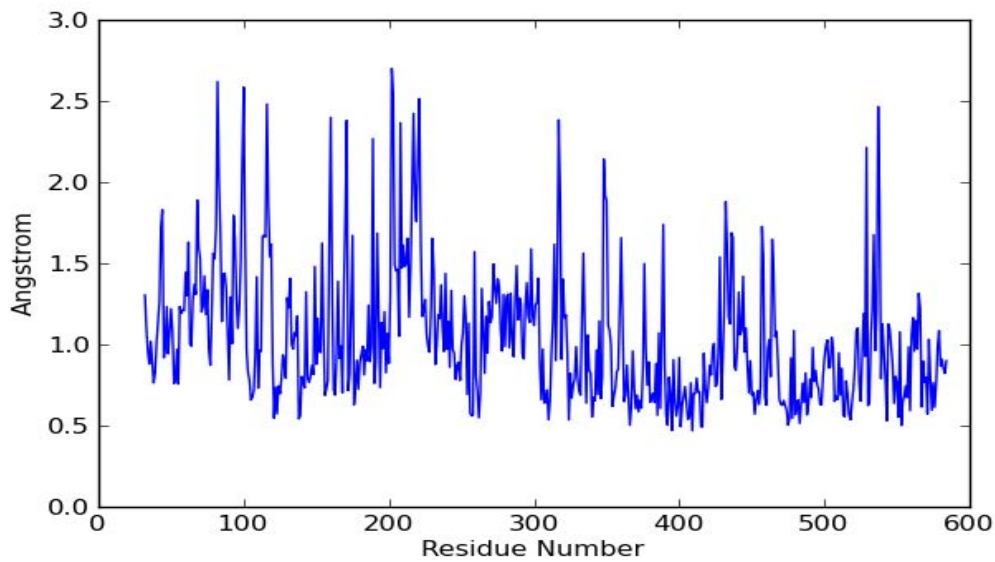


**Figure 5.15 RMSF Plot of COX-1-EPA Docked Complex**

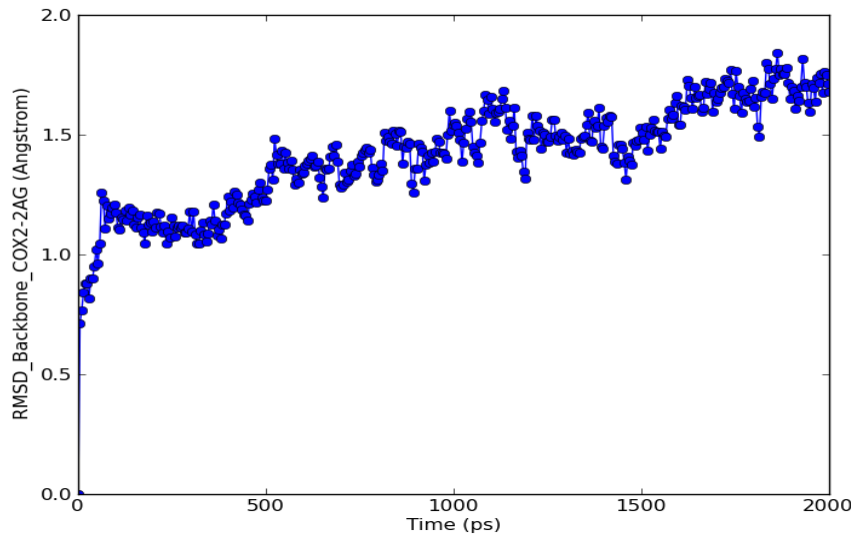


**Figure 5.16 RMSD Plot of COX-2-DHA Docked Complex**

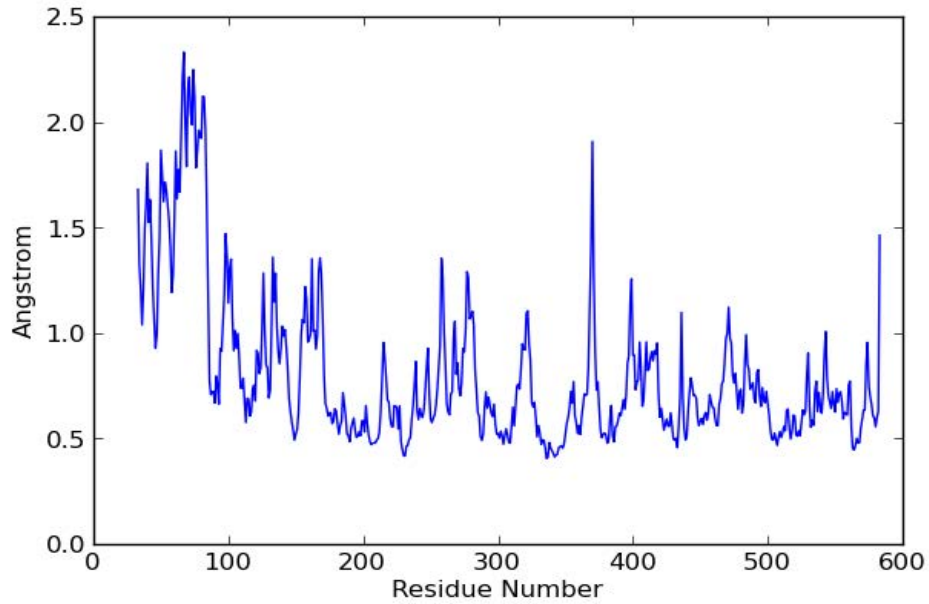


**Figure 5.17 RMSF Plot of COX-2-DHA Docked Complex**

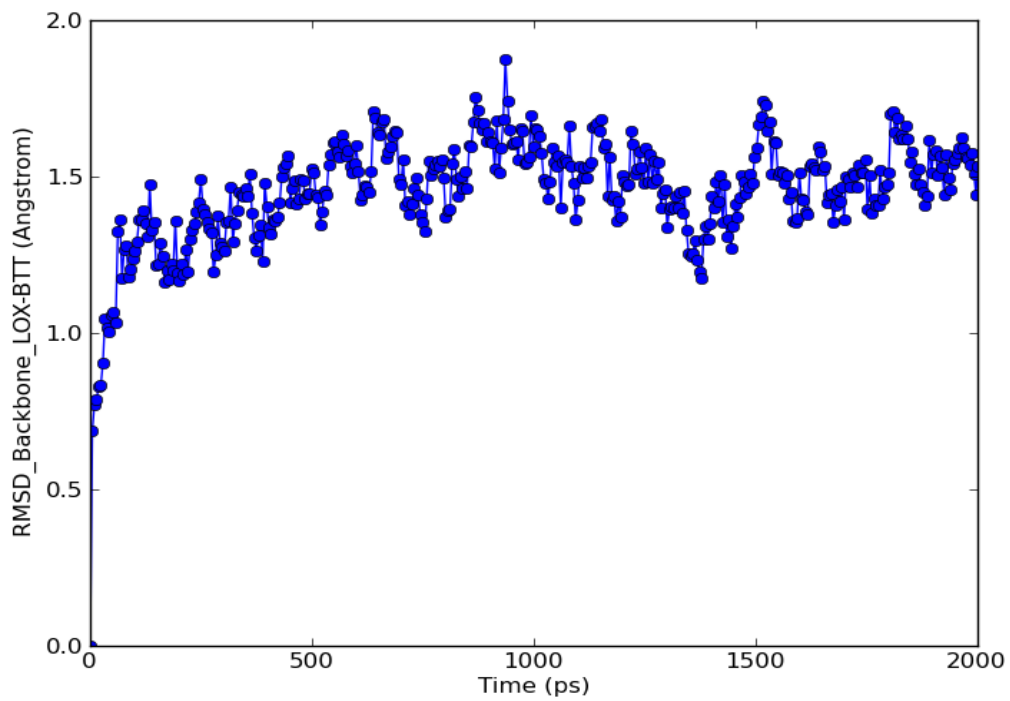


**Figure 5.18 RMSD Plot of LOX- $\beta$ TT Docked Complex**

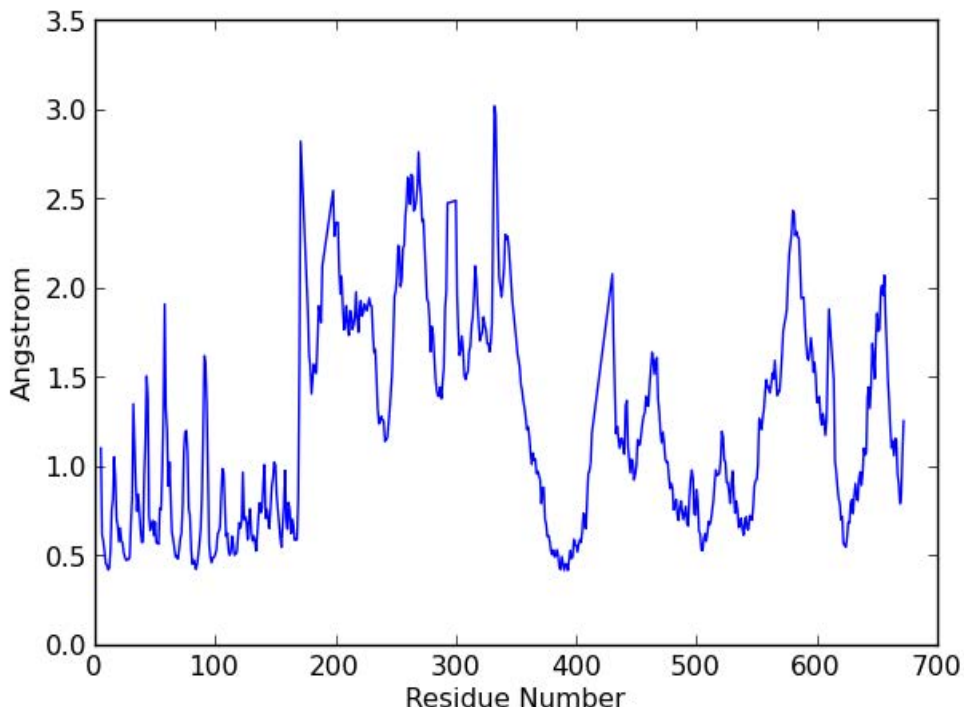


**Figure 5.19 RMSF Plot of LOX- $\beta$ TT Docked Complex**

For the enzyme COX-2, the RMS fluctuations ranged from 0.5 to 1.5 Å for many residues (Figure 5.15). The interacting amino acids of COX-2 were Tyr 385, Ser 530, Val 349, Leu 531, Tyr 348, Phe 381, Val 523, Gly 526, Phe 205, Leu 352, Ala 527, Arg 120, Leu 534 and Leu 352. The amino acid Arg 120 has fluctuated between 0.5-0.7 Å. The amino acids, Tyr 348, Val 349, Leu 352 and Phe 381 have shown fluctuations that were ranging from 0.6-0.8 Å. RMSF fluctuations for the rest of the interacting amino acids, Val 523, Gly 526, Ala 527, Leu 531 and Leu 534 were recorded at a range of 0.5-0.9 Å.

In the case of LOX, the RMSF values were within 3.0 Å. The lower atomic fluctuations for the backbone atoms of COX-1, COX-2, and LOX indicated small conformational change (Hayes et al., 2011; Shu et al., 2011). The binding pose of LOX with ligands showed the interacting amino acids as Arg 596, His 600, Gln 413, Ala 410, Phe 177, Ala 603, Ile 406, Phe 432, Val 604, Leu 607, His 372, Leu 368, Leu 373, His 367, and Phe 359. The RMSF fluctuations for the amino acid Phe 177 were recorded at 0.8 Å approximately. For the amino

acids Phe 359, His 367, Leu 368, His 372 and Leu 373 the fluctuations were ranging from 1.5-1.8 Å. The interacting amino acids Ile 406, Ala 410, Gln 413 and Phe 432 have shown fluctuations from 1.5-2 Å. The remaining interacting amino acids, Arg 596, His 600, Ala 603 Val 604 and Leu 607 have shown fluctuations between 1.8-2 Å approximately.

The active site amino acids for the proteins COX-1, COX-2, and LOX were ranging from the residue number 355 to 530 (approximately), where the RMS fluctuations were observed to be less than 2Å , indicating more stability of the lipid ligand. Even in the presence of lipid inhibitor, the RMSD and RMSF values were observed to be lower, and reached the equilibrium before 2Å approximately.

### **5.3. Comparison of AutoDock and Glide Docking Results**

The interacting amino acids of COX-1, COX-2 and LOX with the target ligands were studied in both AutoDock and Glide (Table 5.7). The common amino acids around a 4 Å distance from the ligand were represented in bold in Table 5.7. It was identified from the table that there were at least three amino acids in common in both the docking methods. In some cases, the hydrogen bonds and hydrophobic interactions were also similar in both AutoDock and Glide, for example, the hydrogen bond between COX-1 and EPA, the hydrophobic interactions between LOX and β-tocotrienol.

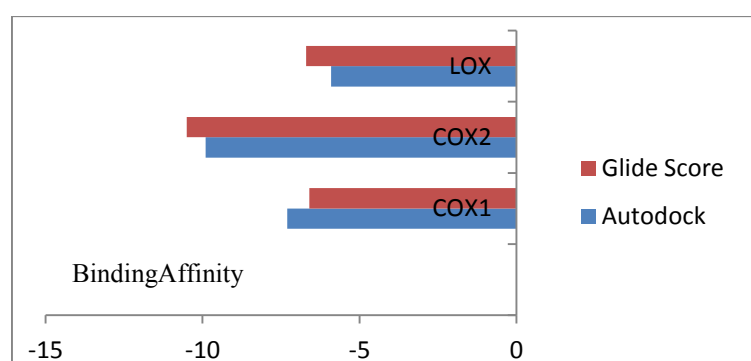


**Figure 5.20 COX-1, COX-2 & LOX: AutoDock Vs Glide**

**Table 5.7 Common Interacting amino acids in AutoDock and Glide**

Protein	Ligand	Interacting amino acids	
		AutoDock	Glide
COX-1	DHA	Ser 530, Val 349, Tyr 385, Ala 527, Phe 205	Val 349, Tyr 348, Ala 527, Phe 205, Gly 526
COX-1	EPA	Ser 530, Tyr 385, Val 349, Ala 527, Ile 523	Ser 530, Leu 352, Gly 526, Val 349, Ile 523
COX-1	2AG	Arg 120, Tyr 355, Glu 520, Glu 524, Ile 523	Ser 530, Leu 531, Arg 120, Glu 524, Val 116
COX-1	Anandamide	Tyr 355, Ser 353, Val 349, Leu 352, Leu 534	Ser 530, Leu 531, Val 349, Val 119, Leu 534
COX-2	DHA	Tyr 385, Ser 530, Ala 527, Val 523, Val 349	Tyr 385, Ser 530, Val 349, Leu 531, Tyr 348
COX-2	EPA	Tyr 385, Ser 530, Leu 531, Val 523, Val 349	Tyr 385, Ser 530, Leu 531, Val 349, Phe 381
COX-2	2AG	Ser 530, Gly 526, Val 349, Val 523, Ala 527	Tyr 385, Ser 530, Leu 531, Val 523, Gly 526
COX-2	Anandamide	Tyr 385, Tyr 348, Leu 531, Val 523, Val 349	Tyr 385, Phe 205, Leu 531, Val 349, Leu 352,
COX-2	DTT	Leu 531, Gly 526, Ala 527, Val 349, Leu 352	Ala 527, Val 349, Arg 120, Leu 534, Leu 352
LOX	DHA	Ala 410, Asn 407, Ile 406, Phe 177, Gln 413	Arg 596, His 600, Gln 413, Ala 410, Phe 177
LOX	EPA	His 600, Arg 596, Ala 603, Phe 177, Gln 363	His 600, Arg 596, Ala 603, Phe 177, Ala 410
LOX	2AG	Asn 407, Ile 406, Phe 177, His 372, Ala 410	Ile 406, Ala 410, His 600, Phe 432, Ala 603
LOX	Anandamide	Gln 413, Phe 177, Val 178, Ala 410, Leu 368,	Phe 177, Val 604, Leu 607, Ala 603, Ala 410
LOX	ATT	Gln 413, Val 178, Phe 177, Ala 410, Leu 368	Ile 406, Phe 177, Ala 410, His 372, Ala 603

**Table 5.7 Continued**

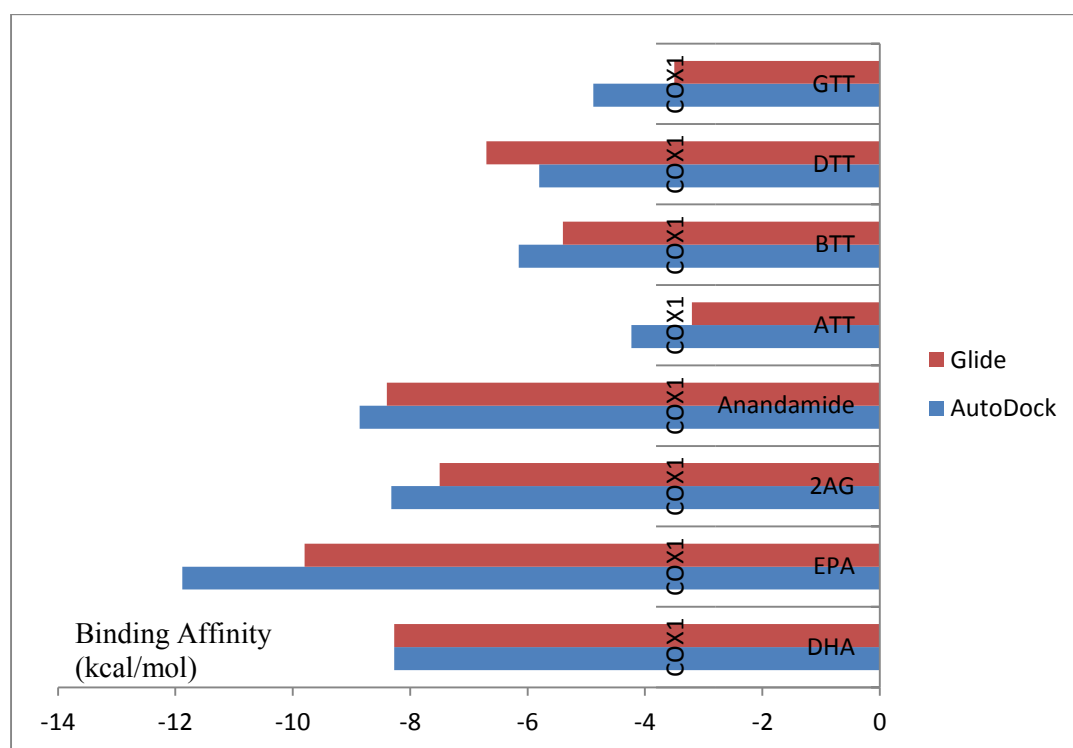
<b>Protein</b>	<b>Ligand</b>	<b>Interacting amino acids</b>	
		<b>AutoDock</b>	<b>Glide</b>
LOX	DTT	<b>Gln 413, Phe 177, Ile 406, Ala 410, Leu 368</b>	<b>Gln 413, Ile 406, Phe 177, His 372, Leu 368</b>
LOX	BTT	<b>Gln 413, Phe 177, Leu 368, Leu 373, Ala 410</b>	<b>Phe 177, Ile 406, Ala 410, Leu 368, Leu 373</b>
LOX	GTT	<b>Gln 413, Ala 410, Phe 177, Leu 368, Val 178</b>	<b>Gln 413, Ala 410, Phe 177, His 367, Phe 359</b>

The interacting amino acids of COX-1 observed during the procedure of AutoDock were Ser 530, Val 349, Tyr 385, Ala 527, Phe 205, Ile 523, Arg 120, Tyr 355, Glu 520, Glu 524, Tyr 355, Ser 353, Leu 352 and Leu 534. During Glide docking, the amino acids, Val 349, Tyr 348, Ala 527, Phe 205, Ser 530, Leu 352, Gly 526, Ile 523, Leu 531, Arg 120, Glu 524, Val 116, Val 119, and Leu 534 of COX-1 have interacted with the ligand. The amino acids Val 349, Ser 530, Ala 527, Phe 205, Leu 352, and Glu 524 were commonly observed in both the procedures.

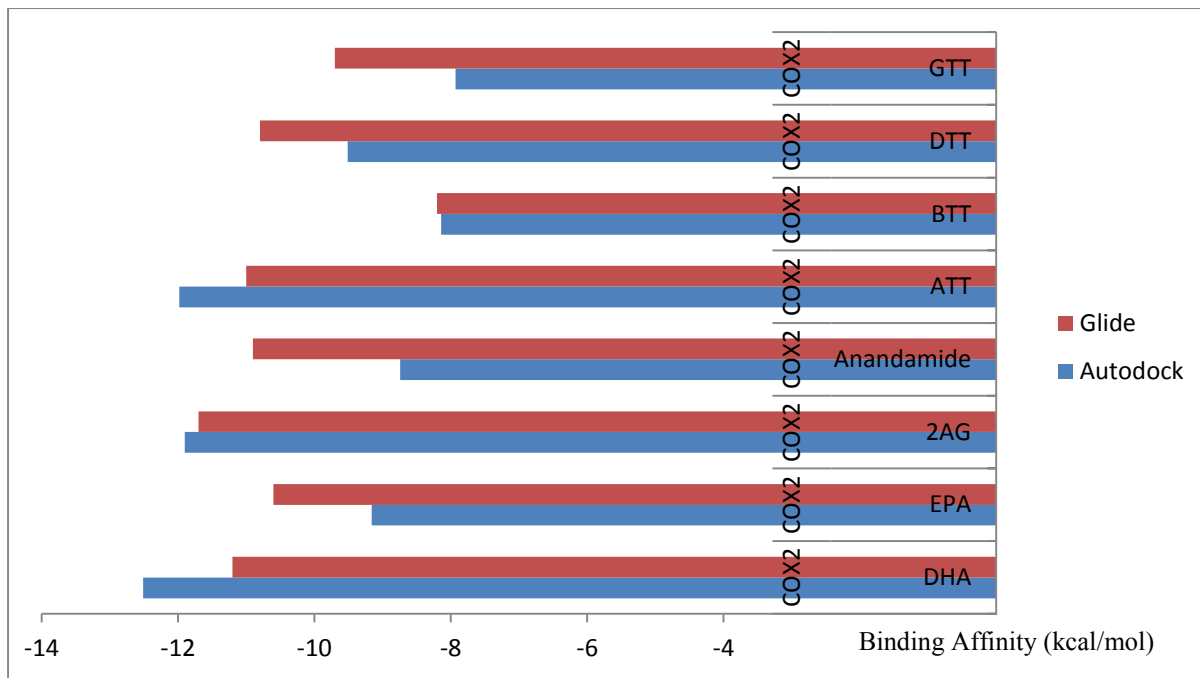
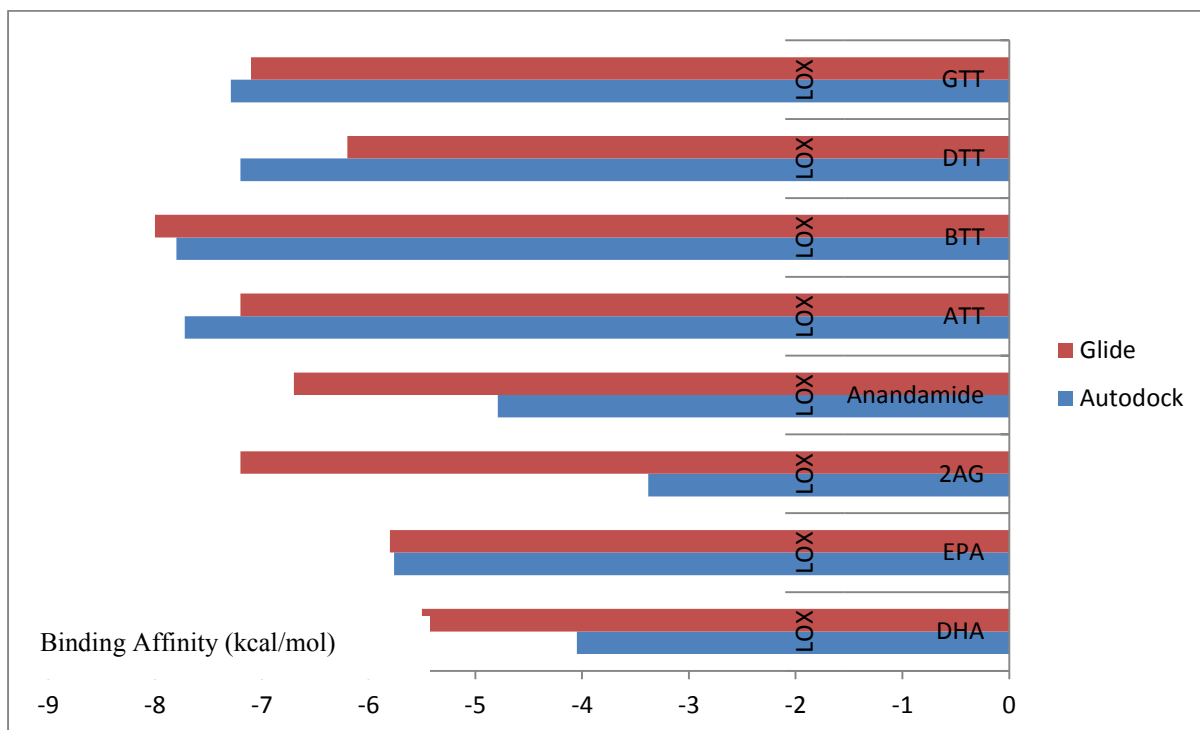
In the case of COX-2 the interacting amino acids identified in the docking procedure of AutoDock were Tyr 355, Ser 353, Val 349, Leu 352, Leu 534, Ser 530, Ala 527, Val 523, Val 349, Leu 531, Gly 526 and Tyr 348. The interacting amino acids observed in Glide were Tyr 385, Ser 530, Val 349, Leu 531, Tyr 348, Val 349, Phe 381, Val 523, Gly 526, Phe 205, Leu 352, Ala 527, Arg 120, Leu 534 and Leu 352. The amino acids, Val 349, Ser 530, Tyr 348, Ala 527, Val 523, Gly 526, Leu 531 and Leu 352 were common in both AutoDock and Glide docking procedures. Tyr 355, Ser 353, Leu 534 were observed as interacting amino acids in the docking procedure of AutoDock and not in Glide docking. Likewise, amino acids, Tyr

385, Val 349, Phe 381, Phe 205, and Arg 120 were Leu 534 interacting with ligand in Glide docking and not in AutoDock.

In the binding mode of LOX with eight lipid ligands the amino acids Gln 413, Phe 177, Ile 406, Ala 410, Leu 368,Leu 373, Val 178, Asn 407, His 600, Arg 596, Ala 603, Gln 363 and His 372 were observed in the docking procedure of AutoDock. During Glide docking the amino acids Arg 596, His 600, Gln 413, Ala 410, Phe 177, Ala 603, Ile 406, Phe 432,Val 604, Leu 607, His 372, Leu 368, Leu 373,His 367, and Phe 359 were identified as interacting amino acids. The amino acids Gln 413, Phe 177, Ile 406, Ala 410, Leu 368, Arg 596, Leu 373, His 600, Ala 603 and His 372 were commonly observed in both the docking procedures. The amino acids Val 178, Asn 407, Gln 363 have shown interactions in the docking procedure of AutoDock. In the case of Glide docking Phe 432, Val 604, Leu 607, Leu 373, His 367, and Phe 359 were identified as interacting amino acids.



**Figure 5.21 COX-1: AutoDock Vs Glide**

**Figure 5.22 COX-2: AutoDock Vs Glide****Figure 5.23 LOX: AutoDock Vs Glide**

Interestingly, in both AutoDock and Glide, COX-1 has shown a strong binding affinity with EPA, COX-2 with DHA, and LOX with  $\beta$ -tocotrienol, indicating the accuracy of the docking

procedure. The average scores of AutoDock and Glide for COX-1, COX-2 and LOX were plotted in Figure 5.20. As shown in this figure, AutoDock has yielded lower binding energies for COX-1, whereas Glide resulted in lower binding affinities for COX-2 and LOX. The individual AutoDock and Glide scores for COX-1, COX-2, and LOX with the eight lipid ligands were depicted in Figures 5.21-5.23. AutoDock has generated strong affinity for COX-1 with all the ligands except for  $\delta$ -tocotrienol. Glide score obtained stronger affinity than AutoDock in the case of  $\delta$ -tocotrienol.

The other three ligands,  $\alpha$ ,  $\gamma$  and  $\delta$ -tocotrienols, have yielded strong binding with LOX in AutoDock in comparison to Glide.

## **5.4. Conclusion**

From the literature review conducted (Chapter 2), it was identified that there is need to find the potential inhibitors of the enzymes COX and LOX. Medicinal chemistry research is focusing more on finding the selective inhibitors of these enzymes, because of the side effects of currently used COX and LOX-based drugs (NSAIDS). As per the molecular docking results, out of the eight lipid ligands (DHA, EPA, 2AG, anandamide and the four tocotrienols) docked with the three enzymes COX-1, COX-2, and LOX, COX-1 has expressed a higher affinity with EPA, whereas COX-2 has shown a strong binding affinity with 2AG. LOX has shown strong interaction with  $\beta$ -tocotrienol. Interestingly,  $\alpha$ -tocotrienol has shown strong binding affinity with COX-2 and LOX but not with COX-1. However, molecular docking techniques do not provide accurate binding energies. Based on the fact that virtual methods need experimental validations the binding abilities of lipid ligands were also compared with the wet laboratory experimental results. The binding affinities derived from both AutoDock and Glide docking techniques were not consistent since molecular docking techniques never predict the binding energies accurately. This is the reason the

results were also discussed in terms of binding poses and interacting amino acids apart from binding affinities. The main advantage of molecular docking is the speed and the guidance it provides to perform wet laboratory experiments. The microscopic atomic interactions can be studied in much better way even though they do not produce accurate binding energies.

MD simulation and ROC curve have further improved the accuracy of molecular docking results. The stability of the docked complexes was cross-examined with the results of MD simulation. ROC curve has evaluated the docking parameters.

The same eight lipid ligands were then examined for their binding abilities with cannabinoid receptors. The binding mechanism of cannabinoid receptors with lipid ligands is discussed in Chapter 6.

# Chapter 6

## Potential Ligands of Cannabinoid Receptors

### ***6.1. Introduction***

Cannabinoid receptors are part of the cannabinoid system present in the human brain. Two types of cannabinoid receptors, CB1 and CB2 have been discovered so far. They were named so as they were derived from the cannabis plant first. They belong to the G-protein coupled receptor (GPCR) family. CB1 and CB2 receptors activate cannabinoids thereby suppressing the behavioral responses. Higher amounts of CB1 are expressed in brain and lower amounts in lungs, liver and kidneys whereas CB2 is expressed in the immune system. Cannabinoid receptors play an important role in memory, appetite, pain sensation and mood. Three classes of ligands—endocannabinoids, amino alkyl indole and eicosanoid derivatives—activate cannabinoid receptors (Howlett, 1995). CB1 and CB2, being the members of GPCR family, are characterised by seven hydrophobic transmembrane helices (Montero et al., 2005).

CB1 and CB2 exhibit 48% amino acid sequence identity. Cannabinoid receptors are the attractive targets for the design of therapeutic ligands, because CB1 and CB2 receptors act as the substrates for several endogenous ligands, enzymes and transporter proteins of neuromodulatory system (Mackie, 2006). Cannabinoid receptors respond to the cannabinoid

drugs such as Δ9-Tetra Hydro Cannabinol (THC). They also bind to the endogenous ligands like anandamide and 2-AG (Howlett et al., 2002). The other agonists of CB1 and CB2 are Δ8-THC which is a psychotropic plant cannabinoid whereas 11-hydroxy-Δ8-THC-dimethylheptyl (HU-210) and desacetyl-L-nantradol are synthetic cannabinoids (Howlett et al., 2002). These agonists are already proved *in vivo* and *in vitro* for their response on cannabinoid receptors. CP-55,940 is another potent cannabinoid agonist by which it was shown that cannabinoids could inhibit adenylate cyclase in neuroblastoma cells (Howlett et al., 1988). WIN55212 is also a cannabinoid agonist.

SR141716A is identified as a selective antagonist of CB1 receptor while SR144528 is the selective antagonist of CB2. It was proved *in vitro* that SR141716A antagonises the inhibitory effects of cannabinoid receptor agonists on adenylate cyclase activity in rat brain (Rinaldi-Carmona et al., 1994). The effect of SR141716A on food intake and body weight is studied in another experiment and observed that brain cannabinoid receptors are involved in the regulation of appetite and body weight (Colombo et al., 1998). Studies using inverse agonist SR141716A suggest that endogenous cannabinoids activate numerous presynaptic cannabinoid receptors (Schlicker & Kathmann, 2001). A number of biochemical assays were carried out to study the antagonism of SR144528 on CB2 receptors and it was noticed that SR144528 has antagonised all the agonists of CB2 (Griffin et al., 1999). SR144528 extends and increases the pain behavior produced by tissue damage (Calignano et al., 1998).

In this chapter, molecular docking studies of CB1 and CB2 with lipid ligands α-, β-, γ- and δ-tocotrienols, DHA, EPA, 2AG and anandamide are discussed in Section 6.2. A new series of potential cannabinoid ligands are discussed in Section 6.3. Section 6.3.1 describes the binding mechanism of cannabinoid receptors with the above lipid ligands through AutoDock. Glide docking studies are included in section 6.3.2. A comparison study is conducted between

AutoDock and Glide docking result and is explained in Section 6.4. Section 6.5 concludes the findings of the study on cannabinoid receptors.

## ***6.2. Cannabinoid Receptors as Therapeutic Targets***

CB1 and CB2 receptors are the primary targets of many endogenous ligands and play a significant role in endocannabinoid metabolism. They play an important role in pain, memory, anxiety, bone growth and immune function by binding to ligands. Hence, CB1 and CB2 receptors have become the attractive targets for the design of therapeutic ligands. Δ9-THC is the widely used synthetic cannabinoid that binds actively to cannabinoid receptors. This synthetic cannabinoid is used to treat vomiting, nausea associated with chemotherapy and as a stimulant of appetite in AIDS (Mackie, 2006). It has some analgesic properties and causes some side effects like dizziness, ataxia and blurred vision (Noyes et al., 1975). Out of all the drugs that affect the endocannabinoid system, CB1 antagonists are of major interest to clinical studies due to their significance in metabolic effects and as an anti-obesity drug.

The first CB1 antagonist reported was Rimonabant, also known as SR141716 or Acomplia. It has nano molar affinity for CB1 and very little affinity for CB2 (Rinaldi-Carmona et al., 1994). It was revealed through clinical trials that Rimonabant may induce the symptoms like anxiety and depression and may cause some psychiatric side effects (Moreira & Crippa, 2009). Another CB1 antagonist AM251 has high affinity and is commercially available. The obese patients who use AM251 had reported psychopathological disorders and depression (Shearman et al., 2003). LY320135 is another inverse agonist which is less selective and has poor bioavailability (Felder et al., 1998).

CB2 selective agonists such as AM1241, HU308 and JWH133 are already used therapeutically and they are devoid of known psychoactivity. It was proved through several

studies that CB2 agonists are effective in chronic pain models (Mackie, 2006). CB2 agonists are analgesic in some neuropathic pain models and peripheral inflammatory models (Hohmann et al., 2004). CB2 agonists have strong potential for the treatment of pain, osteoporosis and cardiovascular diseases. HU308 is a CB2 agonist that decreases bone loss and may lead to the development of an analgesic drug that used for pain relief (Mackie, 2006). The efficacy of CB2 agonists in treating neuropathic pain over a period of months still needs to be determined. Further, a better understanding on the physiological role of cannabinoid receptors is needed for the proper pharmacological use of CB1 and CB2 receptor agonists and antagonists. The research is ongoing to design drugs targeting cannabinoid receptors. The current experiment was designed to study the binding mechanism of cannabinoid receptors with different lipid ligands including endocannabinoids.

### ***6.3. New Series of Cannabinoid Ligands***

In order to find new series of cannabinoid ligands, eight lipid molecules were examined for their interactions with CB1 and CB2. Two molecular docking programs, AutoDock and Glide, were applied to study the interactions between cannabinoid receptors and lipid ligands. An interesting cross-reactivity was observed in the binding affinities of lipid ligands and cannabinoid receptors and is discussed in the following sections.

#### ***6.3.1. Findings of AutoDock***

After performing the molecular docking studies using AutoDock and Glide docking tools, the results were tabulated in Table 6.1 and 6.2. The binding affinities of CB1 and CB2 receptors with different lipid ligands were shown in that table. Anandamide has shown strong affinity (-11.83kcal/mol) with CB1. The other endocannabinoid 2AG has a binding energy of -11.28kcal/mol to CB1. Anandamide has formed favorable binding interactions within the binding pocket of CB1 as shown in Figure 6.1. The active site amino acids Trp 356 and

Leu 359 have formed bonds with the ligand. The distance between the surrounding amino acids and the ligand was shown in pink dots (Figure 6.1) which were less than 4Å indicating close interaction with the ligand. Anandamide is similar to the synthetic ligand Δ9-THC in most of its pharmacological properties and hence has more potential to act as an agonist of cannabinoid receptors (Adams et al., 1998).

**Table 6.1 Binding Affinities of CB1 with eight lipid ligands in AutoDock**

Ligand	Lowest Binding Energy AutoDock(kcal/mol)
DHA	-10.55
EPA	-10.46
2AG	-11.28
Anandamide	-11.83
α-tocotrienol	-8.35
β-tocotrienol	-9.76
γ-tocotrienol	-9.46
δ-tocotrienol	-9.11

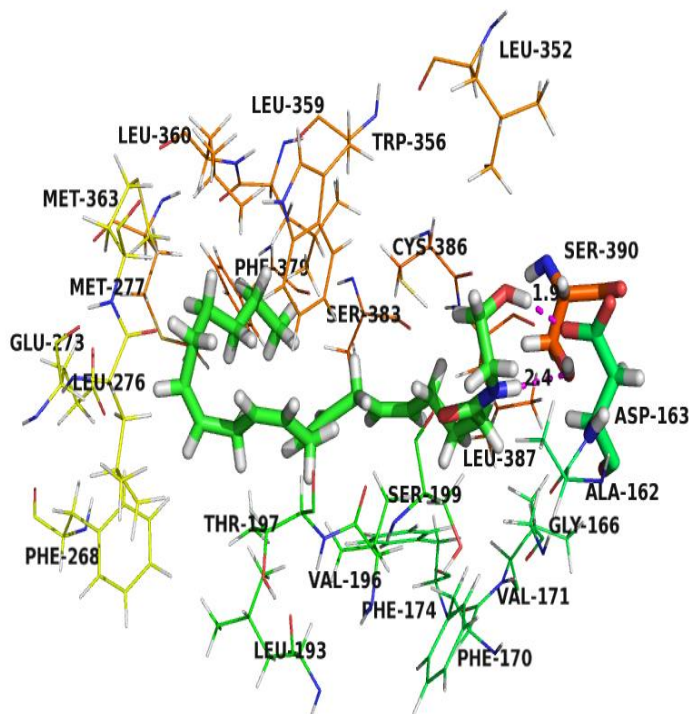


**Figure 6.1 Binding of Anandamide to CB1**

Cannabinoid receptors have the flexibility to accept multiple biologically relevant conformations (Padgett et al., 2008). It is well known through the research done so far on cannabinoid receptors that 2AG and anandamide are endogenous ligands (Di Marzo et al., 2000 ; Padgett et al., 2008). This opens a channel to test these ligands further to be the ligands of both CB1 and CB2. Although there is much difference in the binding affinities of tocotrienols compared with the rest of the ligands, there are considerable interactions between CB1 and tocotrienols.

Furthermore, CB2 has shown strong affinity with anandamide (-11.24kcal/mol and -11.03kcal/mol) and 2AG (Table 6.2). Experiments were already conducted in another study to observe the effect of anandamide on cannabinoid receptors. It was found during this study that anandamide has depressed spontaneous activity and produced hypothermia followed by immobility in mice (Adams et al., 1998). Although DHA and EPA have fit into the ligand binding pocket of CB2 with -10.88kcal/mol and -9.33kcal/mol of binding energy, the bond strength is lesser than with CB1. Ser 390 and Asp 163 of CB1 have formed bonds with anandamide with distances 2.4 Å and 1.9 Å respectively. According to the Figure 6.1 the amino acids Ser 390, Asp 163, Leu 387, Ser 199, Thr 197, Phe 379 and Ser 383 make up the ligand binding site of CB1.

**Table 6.2 Binding Affinities of CB2 with eight lipid ligands in AutoDock**

Ligand	Lowest Binding Energy AutoDock(Kcal/mol)
DHA	-10.88
EPA	-9.33
2AG	-11.03
Anandamide	-11.24
$\alpha$ -tocotrienol	-8.2
$\beta$ -tocotrienol	No Binding
$\gamma$ -tocotrienol	-7.42
$\delta$ -tocotrienol	-7.33

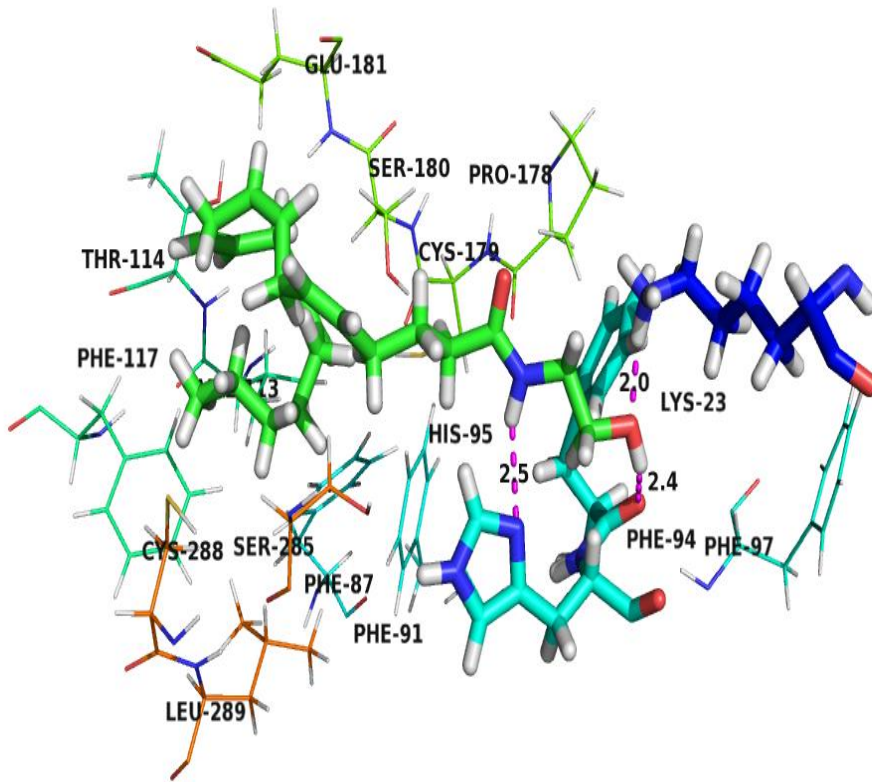


**Figure 6.2 Binding of anandamide to CB2**

During AutoDock CB1 has actively interacted with the target lipid ligands compared to CB2 (Table 6.2). Tocotrienols have shown very poor affinity with CB2 unlike with CB1. The structural differences between CB1 and CB2 might be the reason for this. His 95, Phe 94 and Lys 23 of CB2 have formed bonds with anandamide with bond distances 2.5Å, 2.4Å and 2.0Å respectively as shown in Figure 6.2. Apart from these three amino acids Cys 179, Thr 114, Phe 117, Cys 288 and Leu 289 were also observed as the ligand binding sites of CB2 (Figure 6.2).

### 6.3.2. Findings of Glide Docking

During Glide docking 2-AG and anandamide have similar binding affinities with CB1. Figures 6.3 and 6.4 illustrate the interactions of CB1 and 2AG. The oxygen atom located on

C15 of 2AG has formed bonds with Asp 163 and Ser 203 with the bond distances 2.70 Å and 2.97 Å, respectively (Figure 6.4). The rest of the active site amino acids-Trp 356, Leu 359 and Leu 360 have closely interacted with the ligand as shown in Figures 6.3 and 6.4. DHA and EPA also have similar binding affinities with CB1.  $\alpha$ - and  $\beta$ -tocotrienols have poor affinity with CB1 compared to the other ligands.  $\gamma$ - and  $\delta$ -tocotrienols have moderate affinity with CB1 as shown in Table 6.3.

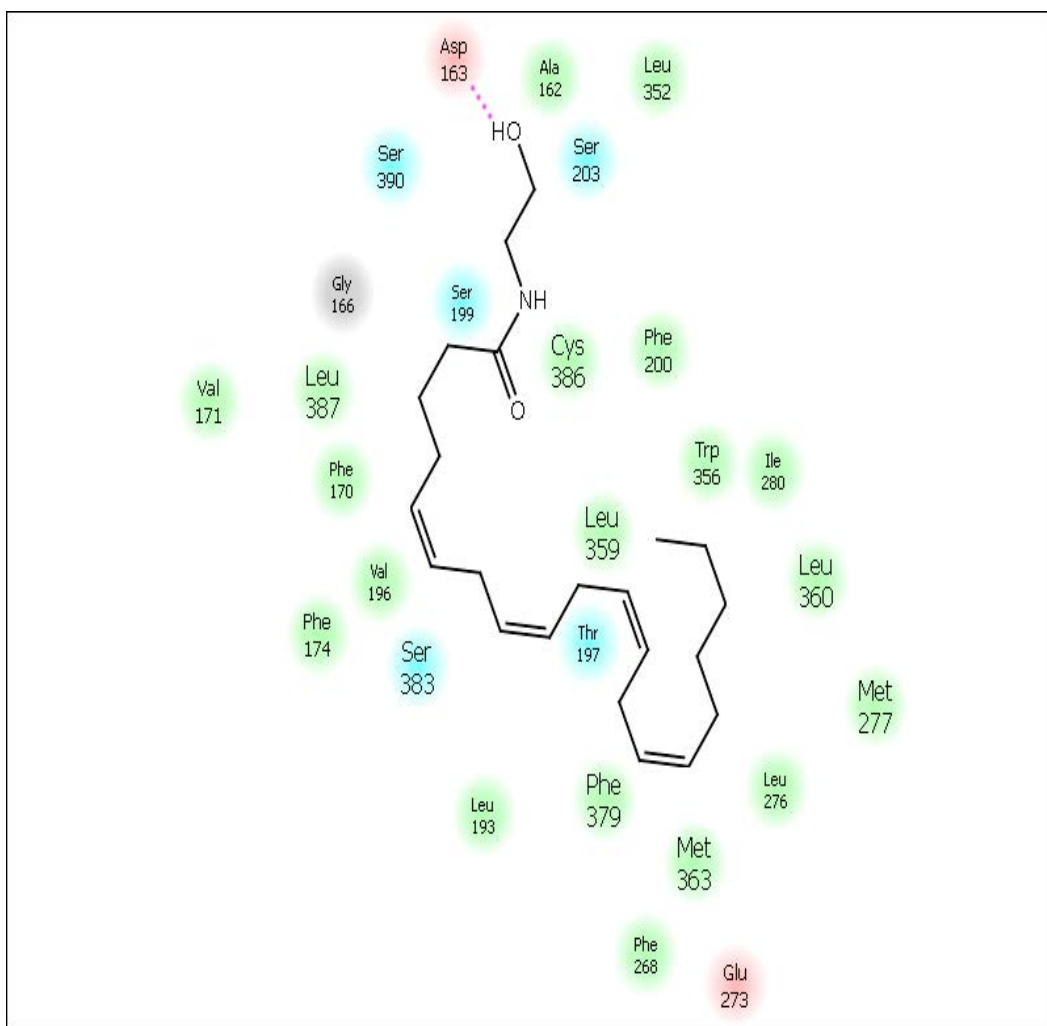


**Figure 6.3 Binding of 2AG to CB1**

Table 6.3 Glide Score of CB1 with lipid ligands

Ligand	Glide Score (Lowest Binding Energy in Kcal/mol)
DHA	-9.9
EPA	-9.8
2AG	-10.2
Anandamide	-10.1
$\alpha$ -tocotrienol	-7.5
$\beta$ -tocotrienol	-7.8
$\gamma$ -tocotrienol	-8.6
$\delta$ -tocotrienol	-8.0

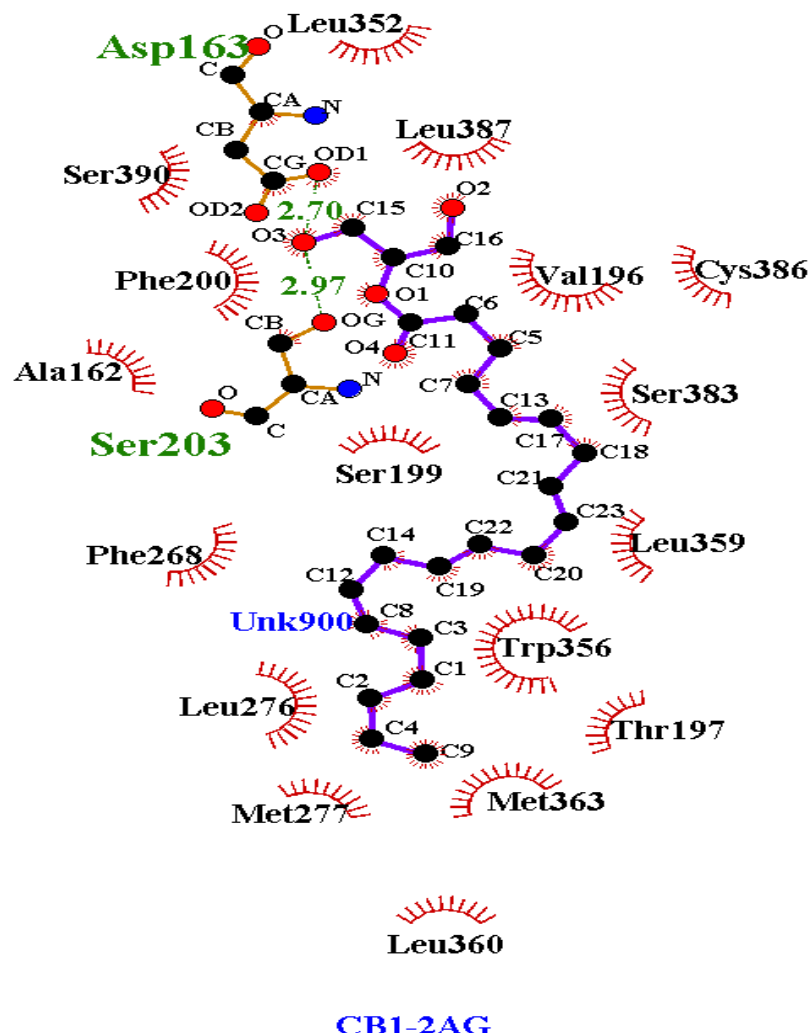
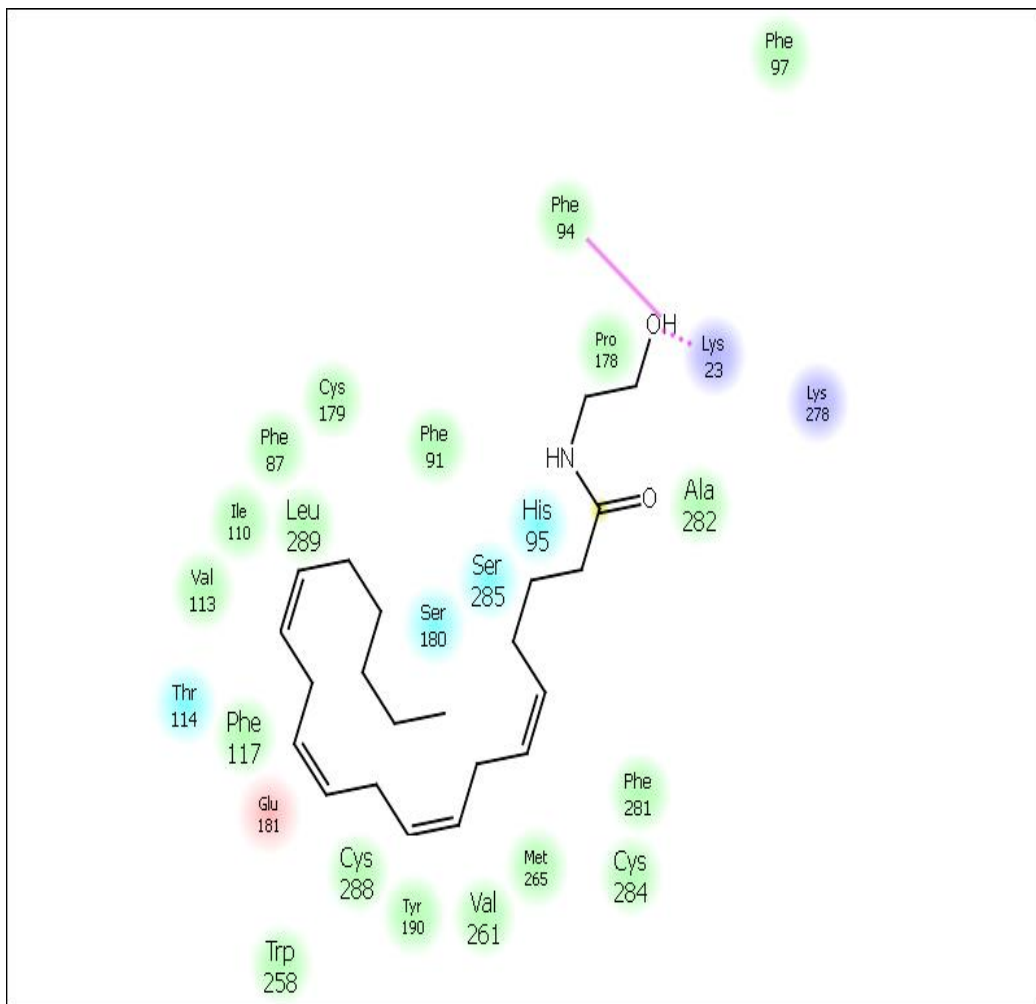
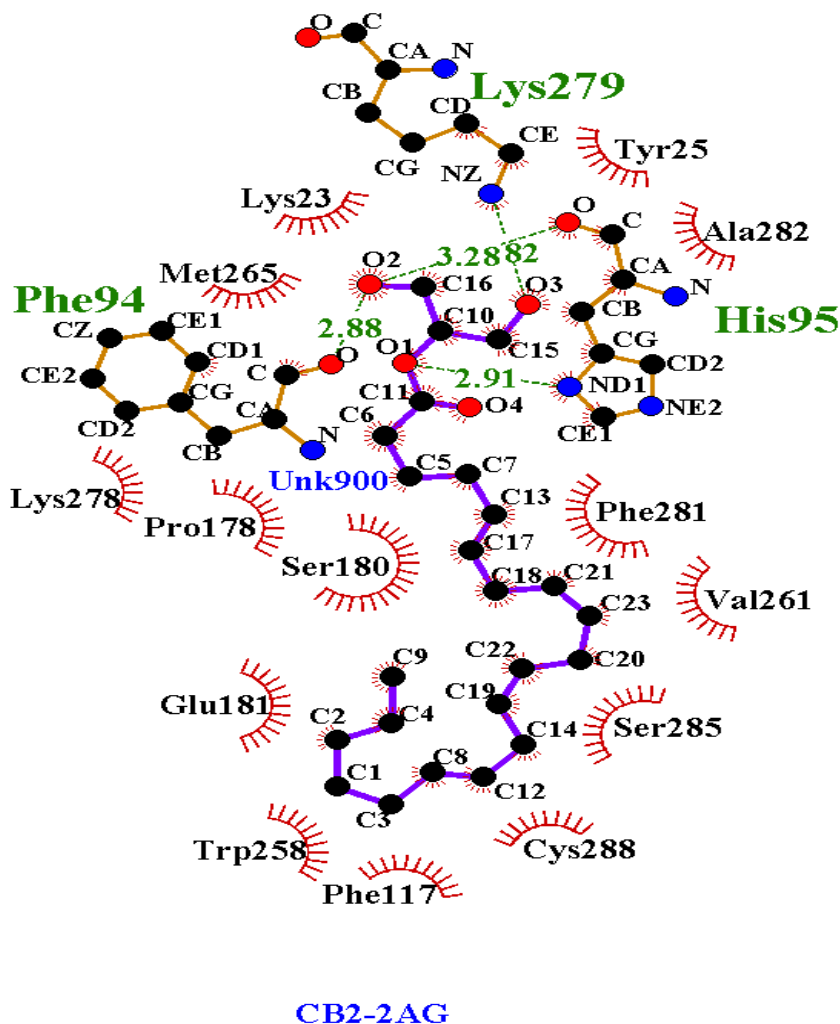


Figure 6.4 Interactions of 2AG with CB1

**Figure 6.5 Binding of Anandamide with CB2**

The binding of anandamide with CB2 is shown in Figure 6.5. The hydroxyl group located on C22 of anandamide has formed one hydrogen bond with Phe 94 with a bond distance of 3.10 Å and another hydrogen bond with Lys 23 with a bond distance of 2.89 Å (Figure 6.5). The active site amino acids Phe 117, Cys 179, Trp 258 were closely interacting with the ligand within 4 Å distance. The binding of 2AG with CB2 is shown in Figure 6.6. O1 located on C11 of 2AG has formed a hydrogen bond with His 95 with a bond distance of 2.91 Å. O2 located on C16 of 2AG has formed hydrogen bond with Phe 94 with a bond distance of 2.88 Å. O3 located on C15 of 2AG has formed hydrogen bond with Lys 279 with a bond distance of 3.28 Å (Figure 6.6). Hydrophobic and the other interactions are represented in Figure 6.6.

**Figure 6.6 Interactions of 2AG with CB2**

Unlike CB1, CB2 did not produce any bonding interactions with  $\beta$  tocotrienol and CB2 expressed very poor affinity with  $\gamma$  and  $\delta$  tocotrienols. Interestingly, both 2AG and anandamide have shown equal affinity (-10.7kcal/mol) with CB2 (Table 6.4). However, there is experimental evidence which proved that 2AG is the strongest agonist for cannabinoid receptors among a number of naturally occurring molecules (Sugiura et al., 2000). In another experiment it was shown that 2AG is a full agonist of cannabinoid receptors and is more potent than anandamide (Gonsiorek et al., 2000). This could be one of the limitations of molecular docking which failed to identify the binding energy differences between similar structures. The structure of 2AG and anandamide are similar except for the number of carbon

atoms. There are 23 carbon atoms in 2AG and 22 carbon atoms in anandamide. Apart from this both the structures have four double bonds with the first double bond located at the 6<sup>th</sup> carbon from  $\omega$  end. AutoDock is limited to identify this close similarity between 2AG and anandamide and hence resulted in the same binding energies.

**Table 6.4 Glide Score of CB2 with lipid ligands**

Ligand	Glide Score (Lowest Binding Energy in kcal/mol)
DHA	-9.5
EPA	-9.1
2AG	-10.7
Anandamide	-10.7
$\alpha$ -tocotrienol	-7.0
$\beta$ -tocotrienol	No Binding
$\gamma$ -tocotrienol	-7.0
$\delta$ -tocotrienol	-8.01

As it was mentioned in the conclusion of Chapter 5, molecular docking results are not always accurate. The binding energies yielded from AutoDock and Glide docking techniques have shown differences indicating inconsistency. However, this difference is as predicted before due to different parameters considered in both the docking techniques. These differences are explained in detail in Chapter 4 under Section 4.3. DHA and EPA have shown similar binding affinities with CB1 and not with CB2. Further, the difference in the binding affinities of DHA and EPA with both CB1 and CB2 is the example of selectivity and specificity of these ligands with cannabinoid receptors. 2AG and anandamide have exhibited similar binding affinities due to their structural similarities as explained above in Section 6.3.2.  $\beta$ -tocotrienols did not show any binding with CB1. The predicted free binding energies for the remaining three tocotrienols were too close to each other. This could be because of the similar structure of tocotrienols with only one methyl group variation.

## 6.4. Comparison of AutoDock and Glide for CB1 and CB2

AutoDock has yielded higher binding affinities compared to Glide (Figure 6.7). Two docking techniques are almost similar with less difference in the binding affinities. Further, they are similar in terms of having common interacting amino acids and interactions with the ligand. The ranking of ligands in both the docking techniques is almost the same except for anandamide (which is rank 1 in AutoDock and rank 2 in Glide) and tocotrienols.

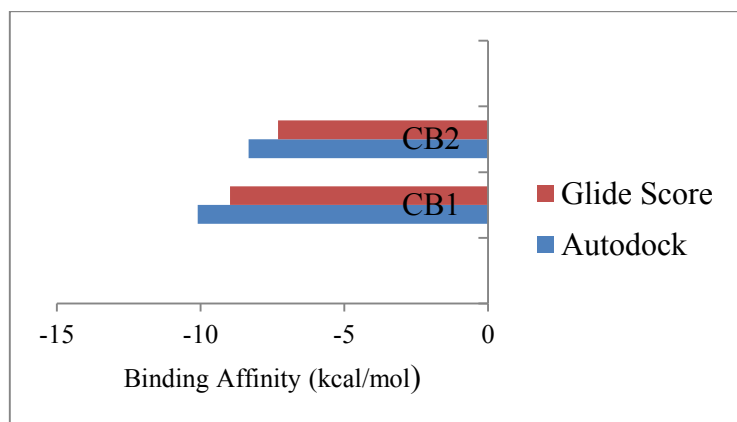


**Figure 6.7 Comparison of AutoDock and Glide for CB1 and CB2**

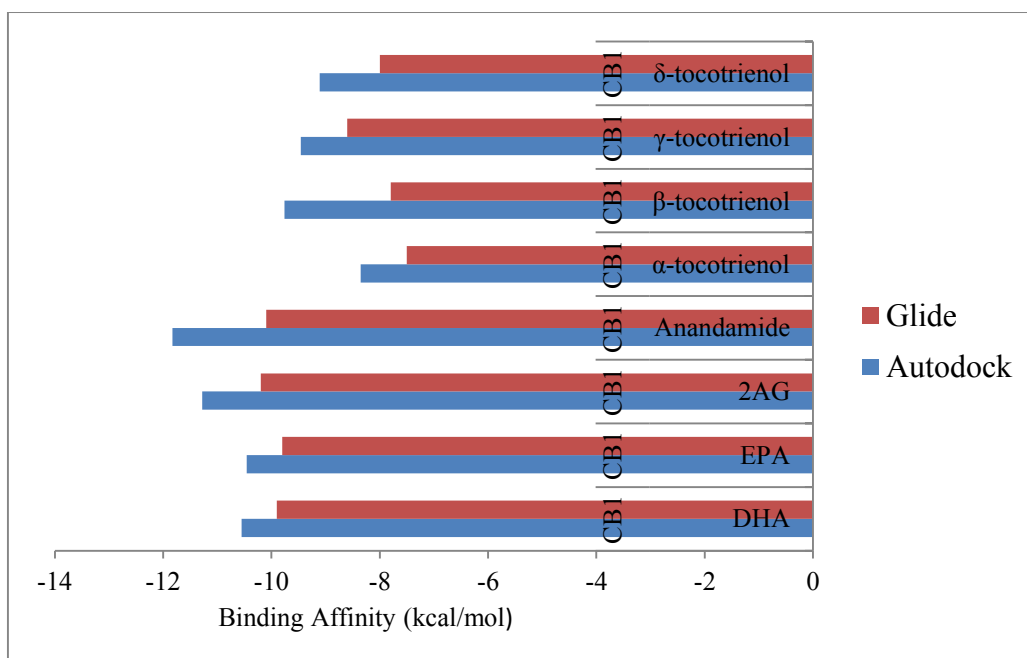


**Figure 6.8 Comparison of AutoDock and Glide for all the ligands with CB1**

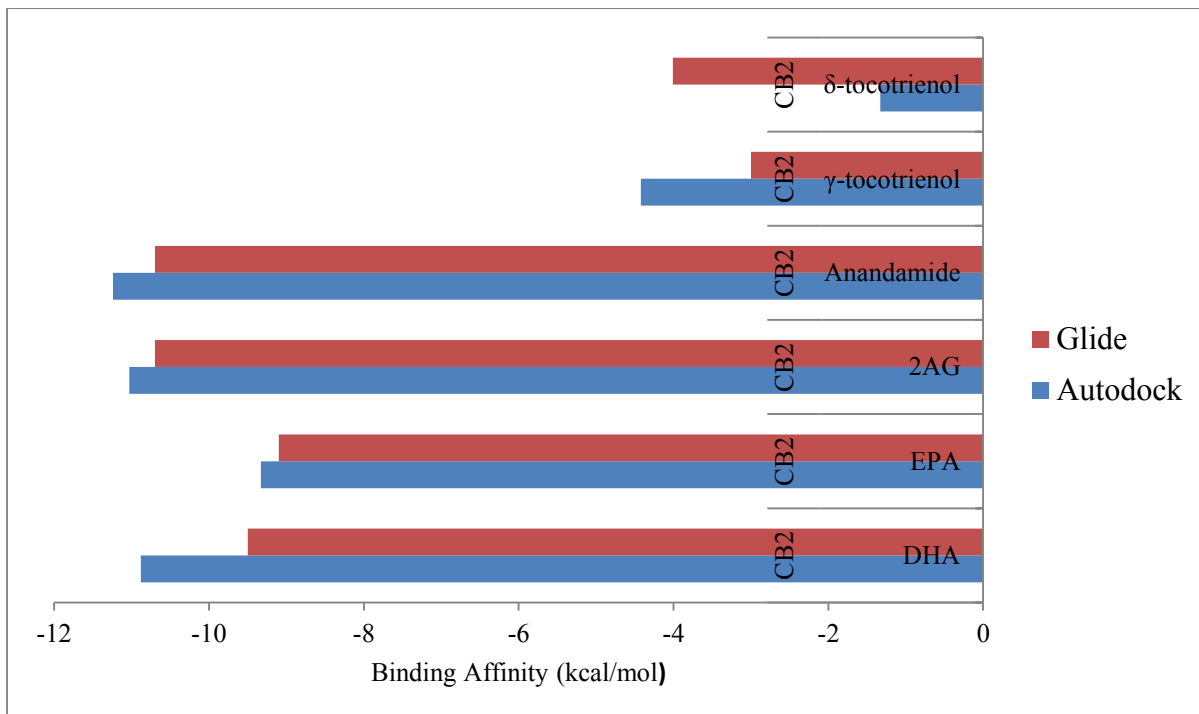


**Figure 6.9 Comparison of AutoDock and Glide for all the ligands with CB2**

The comparison of results of AutoDock and Glide for each ligand with CB1 and CB2 is shown in the above Figures 6.8 and 6.9. In the case of CB1 all the eight lipid ligands have shown strong interaction during AutoDock compared to Glide. Anandamide and  $\beta$ -tocotrienol have shown difference between AutoDock and Glide binding energies. Remaining ligands have shown slighter difference in their binding energies of AutoDock and Glide (Figure 6.8). In the case of CB2,  $\alpha$  and  $\beta$ -tocotrienols did not produce any binding poses during AutoDock whereas Glide has shown poor affinity with  $\beta$ -tocotrienol and no binding with  $\alpha$ -tocotrienol. Hence,  $\alpha$  and  $\beta$ -tocotrienols are not included in the comparison. Ligands DHA, EPA, 2AG, anandamide and  $\gamma$ -tocotrienol have generated more binding affinity with CB2 during AutoDock than during Glide docking.  $\gamma$ -tocotrienol has shown difference between AutoDock and Glide whereas EPA has shown a very slight difference (Figure 6.9). Unlike other ligands  $\delta$ -tocotrienol has shown strong binding affinity during Glide docking than during the procedure of AutoDock with much difference in their binding energies.

**Table 6.5 Interacting amino acids of CB1 and CB2 in both AutoDock and Glide**

Protein	Ligand	Interacting amino acids	
		AutoDock	Glide
CB1	$\alpha$ -tocotrienol	<b>Ser 383, Leu 387, Leu 276, Met 277</b>	<b>Leu 276, Met 277, Ser 383, Cys 286</b>
CB1	$\beta$ - tocotrienol	<b>Leu 276, Met 277, Val 196, Thr 197</b>	<b>Thr 197, Val 196, Leu 276, Phe 268</b>
CB1	$\gamma$ - tocotrienol	<b>Phe 268, Glu 273, Leu 276, Met 277</b>	<b>Phe 268, Glu 273, Met 277, Leu 276</b>
CB1	$\delta$ - tocotrienol	<b>Phe 268, Glu 273, Met 363, Leu 360</b>	<b>Met 363, Leu 360</b> <b>Glu 273, Cys 286</b>
CB1	DHA	<b>Thr 197, Val 196, Phe 91, Phe 94</b>	<b>Leu 359, Cys 286, Thr 197, Val 196</b>
CB1	EPA	<b>Ser 383, Leu 387, Val 196, Phe 174</b>	<b>Ser 383, Leu 387, Leu 193, Phe 174</b>
CB1	2AG	<b>Thr 197, Phe 379, Ser 383, Leu 387</b>	<b>Phe 379, Met 363, Thr 197, Ser 199</b>
CB1	Anandamide	<b>Ser 199, Phe 379, Ser 383, Leu 387</b>	<b>Leu 387, Ser 383, Met 277, Leu 276</b>
CB2	$\alpha$ -tocotrienol	<b>Cys 179, Ser 180</b> Ser 285, Cys 288	<b>Cys 179, Ser 180, His 95 , Ala 282</b>
CB2	$\gamma$ - tocotrienol	<b>Glu 181, Ser 180, Phe 117, Thr 114</b>	<b>Cys 288, Leu 289</b> <b>Phe 117, Thr 114</b>
CB2	$\delta$ - tocotrienol	<b>Ser 285, Cys 288, Cys 179, Glu 181</b>	<b>Ser 285, Cys 288 , Cys 179 , Glu 181</b>
CB2	DHA	<b>Cys 179 , Ser 180 , His 95, Lys 23</b>	<b>Phe 117, Val 113, His 95, Lys 23</b>
CB2	EPA	<b>His 95, Lys 23 , Phe 91 ,Phe 87</b>	<b>Ile 110, Val 113, Lys 23, Phe 87</b>
CB2	2AG	<b>Ser 285, Cys 288, His 95 , Lys 23</b>	<b>Ser 285, Cys 288, Phe 94, His 95</b>
CB2	Anandamide	<b>Phe 117, Thr 114 , Ser 285 , Cys 288</b>	<b>Val 113, Thr 114, Ser 285 , Cys 288</b>

Further both the docking techniques were compared in term of interacting amino acids as shown in Table 6.5. The common active site amino acids in both the procedures are shown in bold in Table 6.5. During the procedure of AutoDock, the binding pose of CB1 with the ligands has shown the interacting amino acids as Ser 383, Leu 387, Leu 276, Met 277, Val 196, Thr 197, Phe 268, Glu 273, Met 363, Leu 360, Phe 174, Phe 379 and Ser 199. In the case of Glide docking the amino acids Leu 276, Met 277, Ser 383, Cys 286, Thr 197, Val 196,

Phe 268, Glu 273, Met 363, Leu 360, Leu 359, Leu 387, Leu 193, Phe 174, Phe 379 and Ser 199 have interacted with the ligand. All the interacting amino acids which were observed in the docking procedure of AutoDock were also observed in Glide docking. However, the amino acids Cys 286, Leu 359, and Leu 193 were identified only during Glide docking.

In the case of CB2, the interacting amino acids in the docking procedure of AutoDock were identified as Cys 179, Ser 180, Ser 285, Cys 288, Glu 181, Phe 117, Thr 114, His 95, Lys 23, Phe 91, Phe 94 and Phe 87. The amino acids Cys 179, Ser 180, His 95, Ala 282, Cys 288, Leu 289, Phe 117, Thr 114, Ser 285, Glu 181, Val 113, His 95, Lys 23, Phe 87, Phe 94 and His 95 were observed as interacting with the ligand in Glide docking. The amino acid Phe 91 was interacting with the ligand during the procedure of AutoDock and not in Glide docking. The amino acids, Ala 282, Leu 289, Val 113 and Phe 94 were observed as interacting amino acids in Glide docking and not in the procedure of AutoDock.

## ***6.5. Conclusion***

Cannabinoid receptors are very important for mental health and play a significant role in many biological processes. The discovery of synthetic agonists and antagonists of CB1 and CB2 is a major area of research to be explored. The limitations and disadvantages of the present synthetic agonists is the background for the current research. The binding of cannabinoid receptors was examined with eight lipid ligands. The findings suggested that omega 3 fatty acids were potential ligands of cannabinoid receptors. Molecular docking was conducted using AutoDock and Glide docking. The results of both the molecular docking techniques were compared in terms of binding affinities and interacting amino acids.

The molecular docking results of cannabinoid receptors were further validated with the wet laboratory experiment (SPA). The evaluation of virtual molecular docking results with SPA results for cannabinoid receptors, PPARs and COX-2 is discussed in Chapter 7.

# Chapter 7

## Scintillation Proximity Assay

### 7.1. Introduction

Scintillation proximity assay (SPA) was used to study the binding between the biological molecules such as between an enzyme and its substrate or a ligand and a receptor. It is a versatile receptor binding assay and has advantages over other assay methods as there is no need for a filtration step (to separate unbound ligand from free ligand). In 1979 Hart and Greenwald pioneered this technique (Hart & Greenwald, 1979) and it has become an important technique in high-throughput screening (HTS) due to its speed, sensitivity and reliability (Wu & Liu, 2005). Ligand binding reactions can be monitored more rapidly than other methods using SPA (Udenfriend et al., 1987).

SPA has broad applications in monitoring ligand-receptor interactions and enzyme reactions due to its simplicity and high-throughput format (Mallari et al., 2003). The drug screening applications and wide range of molecular interactions were conducted in SPA system which allows a fast and sensitive assay (Berry et al., 2012). For the above reasons, SPA has been selected to study the ligand-receptor interactions in the current study. In the current study SPA was performed in saturation binding and competitive binding formats.

Five targets—PPAR- $\alpha$ , PPAR- $\gamma$ , COX-2, CB1 and CB2—have been selected to be examined under the SPA system. These five proteins were selected based on the molecular docking results, their biochemical significance and the project budget constraint. The binding affinities of these five proteins with eight lipid ligands were studied using the molecular docking experiments and were discussed in detail in Chapters 4, 5 and 6. Since the virtual experiments always need an experimental validation, the binding affinities were also studied using SPA. The results of SPA were then compared with the results of molecular docking.

In this chapter, Section 7.2 discusses the results and calculations of SPA. The procedure of SPA was conducted in two phases: saturation binding assay and the competitive binding assay. The saturation binding assay was performed with different concentrations of radiolabeled ligand and with a single concentration of unlabeled ligand. In contrast, competitive binding assay was carried out with a single concentration of radiolabeled ligand and with different concentrations of unlabeled ligands. The detailed procedure is discussed in Sections 7.2.2 and 7.2.3. Furthermore, there is a slight difference in the procedure of SPA for receptors and enzymes. Since the enzyme-substrate reactions are very rapid compared to the receptor-ligand reactions, the results were analyzed according to time. This time-dependent strategy is applied only for COX-2. The validation studies of molecular docking results with SPA results are discussed in Section 7.3 whereas Section 7.4 concludes this chapter.

### ***7.1.1. Principle of the Assay***

The ligand that is tagged with radiolabeled atoms ( $H^3$ ,  $C^{14}$ ,  $P^{32}$ , and  $I^{125}$ ) is used to perform SPA. The receptor is immobilized either to a scintillation bead or to a flash plate that is coated with scintillate material. When radiolabeled ligand binds to the receptor, it emits light in the form of  $\beta$ -particles which can be read as counts per minute (CPM) on a  $\beta$ -counter. The close proximity of radioisotope to scintillate material coated on the flash plates allows

transfer of the radiation energy that is read through a  $\beta$ -counter. The energy from unlabeled ligands is dissipated into the aqueous media and is too weak to be detected (Wu et al., 2005).

Different kinds of  $\beta$ -counters like TopCount<sup>5</sup>, Microbeta<sup>6</sup>, Liquid Scintillation counter <sup>7</sup> and LEAD seeker<sup>8</sup> are currently available.

The author's study has used wheat germ agglutinin (WGA) coated flash plates to conduct SPA. The flash plates are scintillate coated and the protein binds to the walls of flash plate (during incubation) as shown in Figure 7.1. After the ligand is added, some ligands bind to the protein and are shown in green color in Figure 7.1, whereas some ligands do not bind and are shown in grey color in Figure 7.1.

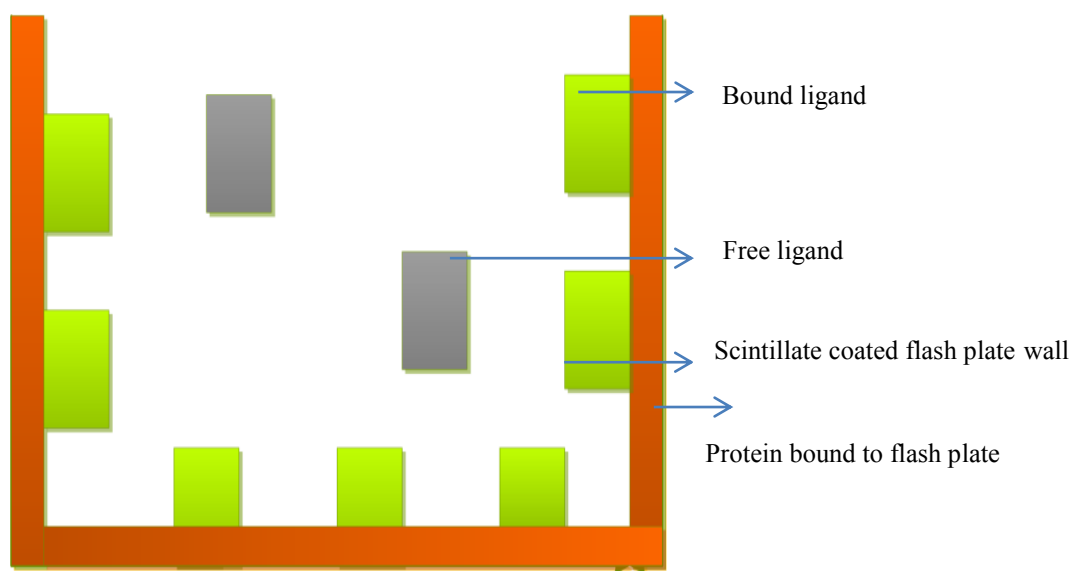


**Figure 7.1 SPA using flash plates**

<sup>5</sup> Top Count (<http://www.perkinelmer.com/catalog/family/id/topcount>)

<sup>6</sup> Microbeta (<http://www.perkinelmer.com/catalog/family/id/microbeta>)

<sup>7</sup>LiquidScintillationCounter([http://www.perkinelmer.com/resources/technicalresources/applicationsupportknowledgebase/radiometric/liquid\\_scint.xhtml](http://www.perkinelmer.com/resources/technicalresources/applicationsupportknowledgebase/radiometric/liquid_scint.xhtml)),

<sup>8</sup>LEADseeker([https://www.gelifesciences.com/gehcls\\_images/GELS/Related%20Content/Files/1314729545976/litdocLSTCSBS01\\_20141013150148.pdf](https://www.gelifesciences.com/gehcls_images/GELS/Related%20Content/Files/1314729545976/litdocLSTCSBS01_20141013150148.pdf))

### 7.1.2. Development of Assay

Reagents required for the assay are:

- Radiolabelled Ligands
- Membrane bound/ partially purified/solubilized/biotinylated receptors
- Microplate / Flash Plate of 96/ 384 wells
- WGA / Streptavidin /Poly-L-lysine Scintillation beads with the use of microplate (not required with Flash Plate)
- Assay Buffer

The choice of radio ligand and receptor was the first step in setting up the SPA system. Although, different radiolabeled atoms like H<sup>3</sup>, C<sup>14</sup>, I<sup>125</sup>, P<sup>33</sup>, and S<sup>35</sup> are available H<sup>3</sup> and I<sup>125</sup> are known to be the most suitable for SPA due to their low risk levels, high specific activity and shorter β-emission path length. However, for few ligand structures, custom radiolabeling of H<sup>3</sup> and I<sup>125</sup> may not be available. The radioisotope C<sup>14</sup> could be the next choice in this instance. The selection of receptor was dependent on the type of beads or plates selected for the study. Instead of scintillation beads, micro plates coated with scintillate or flash plates can be used. Flash Plates are available in 96 or 384 wells. For WGA scintillation beads or WGA coated flash plates, membrane bound receptors or partially purified receptors or solubilized receptors are suitable. WGA binds to the carbohydrate moiety (N-acetyl glucosamine) of the protein and helps immobilize the protein to the walls of the plate. If streptavidin beads or streptavidin coated flash plates are used biotinylated receptors must be selected as avidin can bind to the biotin coupled to the receptor protein. However, either WGA or streptavidin are useful only to stabilize the receptor onto the matrix bead or plate wall and does not actually test the binding affinity between the receptor and ligand.

The format of the assay can be achieved with the selection of bead type, plate type, order of adding the reagents, nonspecific binding (Auld et al., 2004). If the scintillation beads are used to conduct the assay, it is preferable to add the beads, radiolabeled ligand and the receptor and incubate it. When using beads, the optimum membrane to bead ratio must be maintained for the successful assay. If flash plates are used, it is better to add the receptor and incubate it for 3-15 hours so that the receptor couples to the WGA or streptavidin. After the incubation time the radiolabeled and unlabeled ligands were added and incubated for another hour to get a stable signal. It was observed during the experiment that the signal lasts overnight.

The assay buffer (10% Glycerol, 25mM HEPES, 12.5mM MgCl<sub>2</sub>, 50mMKCl, 1mMDTT) should be a combination of inhibitors, salts, cofactors and agents that reduce nonspecific binding. The pH must be adjusted to 7.6 after preparing the buffer. The preparation of assay buffer was discussed in the Appendix-I. Assay conditions like incubation time, receptor concentration, radiolabeled and unlabeled ligand concentrations, the amount of SPA bead (if used) are dependent on the type of ligand and receptor selected for the study. If the dissociation constant ( $K_d$ ) of the protein is known it is suggested to dilute the radio ligand close to the  $K_d$  of the receptor of interest. The advantage of SPA is that it doesn't need a filtration step and it reduces the volume of liquid radioactive waste.

## **7.2. Results and Calculations**

SPA was applied for saturation binding and competitive binding. Competitive binding assay was used to study the inhibition constant ( $K_d$ ) using unlabeled ligands. To find the ideal radio ligand for the study to compete with unlabeled ligand, the  $K_d$  of each ligand for each protein was determined using saturation binding analysis. The molarity of radiolabeled ligands is calculated as follows.

The specific activity of C<sup>14</sup>DHA = 55 mci/mmol or 0.055ci/mmol.

Concentration of C<sup>14</sup>DHA = 0.1 μci/ml.

Molarity = Concentration (μci/ml) / Specific Activity (ci/mmol)

$$= 0.1/0.055$$

$$= 1.818\text{mM or } 1818.1\mu\text{M}.$$

The specific activity and concentration of C<sup>14</sup>EPA are same as that of C<sup>14</sup>EPA. Therefore, the molarity of C<sup>14</sup>EPA is also 1818.1 μM.

Specific activity of H<sup>3</sup>2AG = 40ci/mmol

Concentration of C<sup>14</sup>DHA = 0.1mcCi/ml

Molarity = Concentration (mcCi/mM) / Specific Activity (ci/mM)

$$= 0.1/40$$

$$= 0.0025\text{mM or } 2.5\mu\text{M}.$$

The molarity of H<sup>3</sup>2AG = 2.5μM.

Specific activity of H<sup>3</sup>Anandamide = 200ci/mM.

Concentration of C<sup>14</sup>DHA = 1mcCi/ml.

Molarity = Concentration (mcCi/mM) / Specific Activity (ci/mM)

$$= 1/200$$

$$= 0.005\text{mM or } 5\mu\text{M}$$

The molarity of H<sup>3</sup>Anandamide = 5μM.

The output from microbeta or scintillation counter is the number of photons detected per unit time, typically expressed in counts per minute (CPM). The ratio between CPM detected by the instrument and actual disintegrations per minute (DPM) of the radio isotope is defined as *efficiency* (Sittampalam et al., 2012). This efficiency for each radioisotope was calculated during the normalization. The procedure of normalization was explained in Chapter 3 under Section 3.7.2. In order to measure the specific binding of ligand to the protein in terms of  $\mu\text{M}/\text{mg}$  the CPM must be converted into  $\mu\text{M}/\text{mg}$ . For this conversion the specific activity of the radiolabel ligands should be converted to CPM/fmol. The amount of radioactivity per unit mole of a radioligand is referred to as the *specific activity* (Sittampalam et al., 2012). Usually the units of specific activity are given in Ci/mM by the manufacturer. However, the raw data from the assay using radioactivity are in either CPM or DPM. Hence, the conversion of CPM/fM or DPM/fM is more convenient for the data analysis. The efficiency of each radiolabeling must be calculated during the normalization of MicroBeta detectors (Kahl et al., 2004).

Equation to convert specific activity (Ci/mM) into CPM/fmol:

Conversion factor:  $1\text{Ci} = 2.22 \times 10^{12} \text{ DPM}$

$$10^{12} \text{ fM} = 1\text{mM}$$

$$\begin{aligned} \text{CPM/fM} &= [\text{SA (Ci/mM)} \times [2.22 \times 10^{12} \text{ DPM/Ci}] \times [\text{mM}/10^{12}\text{fM}]] \times \text{Efficiency (CPM/DPM)} \\ &= \text{SA} * \text{Eff} * 2.22 \end{aligned}$$

The efficiency of MicroBeta for  $\text{C}^{14}$  labelling isotopes = 0.90 or 90%

The specific activity of  $\text{C}^{14}\text{DHA}$  and  $\text{C}^{14}\text{EPA}$  given by the manufacturer =  $55\mu\text{Ci}/\text{mM}$ .

Converting  $\mu\text{Ci}$  into Ci:

$$55 \mu\text{Ci} = 0.055\text{Ci.}$$

To convert the specific activity of  $\text{C}^{14}\text{DHA}$  and  $\text{C}^{14}\text{EPA} = 0.055 \times 0.90 \times 2.22$

$$= 0.10989 \text{ CPM/fM}$$

The efficiency of MicroBeta for  $\text{H}^3$  labelling = 0.95 or 95%.

The specific activity of  $\text{H}^3\text{2AG}$  given by the manufacturer = 40Ci.

Converting the specific activity of  $\text{H}^3\text{2AG} = 40 \times 0.95 \times 2.22$

$$= 84.36 \text{ CPM/fM.}$$

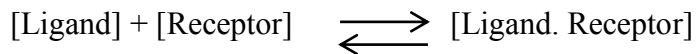
The specific activity of  $\text{H}^3$  anandamide given by the manufacturer = 200Ci.

Converting the specific activity of  $\text{H}^3\text{Anandamide} = 200 \times 0.95 \times 2.22$

$$= 421.8 \text{ CPM/fM.}$$

### **7.2.1. Binding Theory: The Law of Mass Action**

The process of receptor-ligand binding assays is complex due to the conformational changes and multiple noncovalent bonds. Apart from this complexity, most of the radioligand binding experiments use the law of mass action. According to the law of mass action the rate of any chemical reaction is equal to the product of the masses of reactants (ligand and the receptor).



- The association of ligand and receptor occurs when they are in the correct orientation and when they have sufficient energy to collide with each other. The rate of

association equals  $[ligand] \times [receptor] \times K_{on}$  where  $K_{on}$  is the association rate constant.

- After the ligand binds to the receptor they remain bound together for a random amount of time. The rate of dissociation constant equals to  $[ligand, receptor] \times K_{off}$  where  $K_{off}$  is the dissociation constant.
- After dissociation the ligand and receptor are same as before binding.

Equilibrium is reached when the rate of formation of  $[ligand, receptor]$  complexes equal the rate of dissociation. At equilibrium

$$[ligand] \times [receptor] \times K_{on} = [ligand, receptor] \times K_{off} \text{ (Motulsky, 1996)}$$

If the above equation is rearranged to define the equilibrium dissociation or dissociation constant ( $K_d$ ).

$$\frac{[ligand] \times [receptor]}{[ligand, receptor]} = \frac{K_{off}}{K_{on}} = K_d$$

The units of  $K_d$  are expressed in moles/liter or molar concentration of ligand. The maximum amount of receptor binding is called the  $B_{max}$ . The concentration of ligand that occupies half of the receptors at equilibrium or in other words half of the  $B_{max}$  is called  $K_d$ . Although the term dissociation constant is less commonly used, it is directly related to the affinity of a compound. Low  $K_d$  (in nanomoles or pico molar) indicates that the low amount of ligand is sufficient to occupy the binding sites of receptor and hence the affinity is high. If  $K_d$  is high, high amounts of the ligand are required to occupy the receptor and hence the affinity is low.

### **7.2.1.1. Fractional Occupancy**

Fractional occupancy is used to describe the fraction of receptors occupied at a particular concentration of radiolabeled ligand. In other words fraction of all receptors bound to ligand.

As per the law of mass action, fractional occupancy is the function of radio ligand concentration at equilibrium (Motulsky, 1996).

$$\text{Fractional Occupancy} = \frac{[\text{ligand. receptor}]}{[\text{receptor}]} = \frac{[\text{ligand. receptor}]}{[\text{receptor}] + [\text{ligand. receptor}]}$$

After simplifying the equation using algebra:

$$\text{Fractional Occupancy} = \frac{[\text{ligand}]}{([\text{ligand}] + K_d)} \quad (\text{Motulsky, 1996})$$

	A	B
1	log(inhibitor) vs. response -- Variable slope	
2	Best-fit values	
3	BOTTOM	13.20
4	TOP	57.56
5	LOGIC50	1.142
6	HILLSLOPE	-2.995
7	IC50	13.87
8	Span	44.35
9	Std. Error	
10	BOTTOM	2.652
11	TOP	1.596
12	LOGIC50	0.02876
13	HILLSLOPE	0.5968
14	Span	3.532
15	95% Confidence Intervals	
16	BOTTOM	1.793 to 24.61
17	TOP	50.69 to 64.42
18	LOGIC50	1.018 to 1.266
19	HILLSLOPE	-5.563 to -0.4264
20	IC50	10.43 to 18.45
21	Span	29.15 to 59.55
22	Goodness of Fit	
23	Degrees of Freedom	2
24	R <sup>2</sup>	0.9964
25	Absolute Sum of Squares	5.987
26	Sy.x	1.730
27	Number of points	
28	Analyzed	6

Figure 7.2 Error values in the calculation of  $K_d$  and  $K_i$

The  $K_d$  and  $K_i$  values in saturation and competitive binding analysis were calculated by Graph Pad. Graph pad considers the standard error values and confidence intervals while calculating  $K_d$  and  $K_i$  values as shown in Figure 7.2. Figure 7.2 is a screen shot taken from Graph pad software to show the example of  $K_i$  calculation of CB2. Figure 7.2 show that Graph Pad software considers the error values while calculating  $K_d$  and  $K_i$  values in both saturation binding analysis and competitive binding analysis.

### ***7.2.2. Saturation Binding Analysis***

Saturation binding is performed for PPAR- $\gamma$ -C<sup>14</sup>DHA, PPAR- $\gamma$ -C<sup>14</sup>EPA, PPAR- $\alpha$ -C<sup>14</sup>DHA, PPAR- $\alpha$ -C<sup>14</sup>EPA, CB1-H<sup>3</sup>2AG, CB1-H<sup>3</sup>Anandamide, CB1-C<sup>14</sup>DHA, CB1-C<sup>14</sup>EPA, CB2-H<sup>3</sup>2AG, CB2-H<sup>3</sup>Anandamide, CB2-C<sup>14</sup>DHA, CB2-C<sup>14</sup>EPA, and COX-2-C<sup>14</sup>DHA. The results are discussed in the following sections.

#### ***7.2.2.1. PPAR- $\gamma$ with C<sup>14</sup> Labeled DHA***

During the three hours of incubation time PPAR- $\gamma$  bonds to the scintillate coated wells of the flash plate. After adding C<sup>14</sup>DHA and unlabeled DHA, they both bound to the protein resulting in total binding. The radiolabeled ligand binds to the specific and nonspecific binding sites of the protein and hence, this type of binding is called the total binding. Later, homologous competitive binding assay is conducted in order to exclude the nonspecific binding from the total binding. The nonspecific binding is read by incubating the protein for longer time periods in excess of unlabeled ligand and increasing concentrations of radiolabelled ligand. The excess of unlabeled ligand binds to the specific binding sites of the protein, leaving nonspecific binding sites of the protein for radiolabeled ligand. By subtracting the nonspecific binding counts from total binding the specific binding was calculated. The total, specific and nonspecific bindings of PPAR- $\gamma$ -DHA are shown in Table 7.1.

The graph shown in Figure 7.2 is drawn by taking the radioligand concentration on X-axis and CPM generated from MicroBeta on Y-axis. The graph shows the total, specific and nonspecific binding of PPAR- $\gamma$  with C<sup>14</sup>DHA.

**Table 7.1 Total binding of PPAR- $\gamma$  with C<sup>14</sup>DHA**

Radio ligand Concentration (nM)	Total Binding in (CPM)	Specific Binding (CPM)	Nonspecific Binding (CPM)
50	902	752	150
75	1170	967	203
100	1376	1082	294
150	1403	1078	325

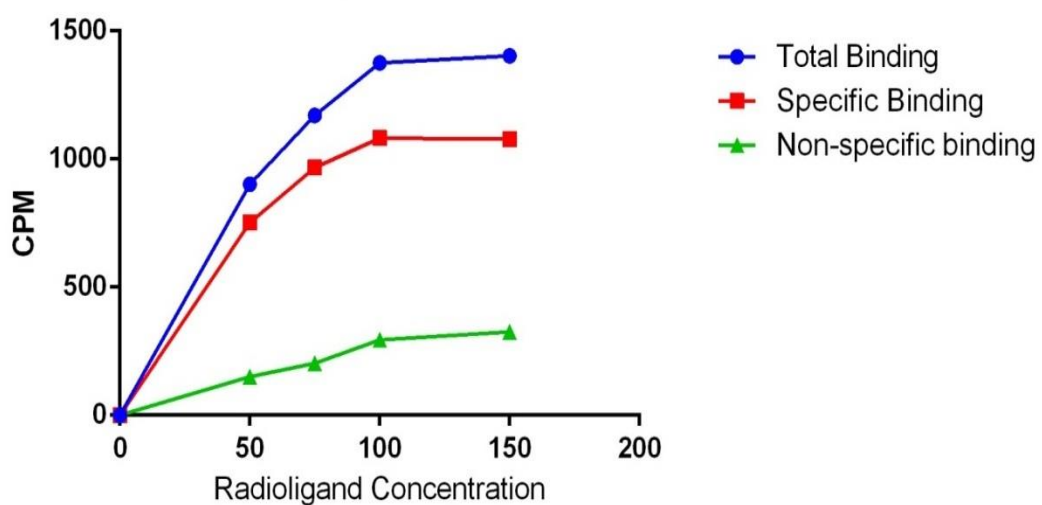


**Figure 7.3 Total binding of PPAR- $\gamma$  with C<sup>14</sup>DHA**

An equilibrium saturation binding measures total and nonspecific binding at various radioligand concentrations. Table 7.2 shows the specific binding only. The specific binding is now converted from CPM to Pico molar. By dividing the Pico molar or micromoles of the protein with the stock concentration of protein (the stock concentration of PPAR- $\gamma$  is 1.17mg/ml) the specific binding is converted to  $\mu$ M/mg of protein as shown below.

Equation to convert CPM to pM (pico molar):

$$pM = CPM/SA \text{ (CPM in fmol) / Vol (in ml)}$$

Total volume is a 100 $\mu$ l aliquot of a stock mix.

**Table 7.2 Specific binding of PPAR- $\gamma$  with C<sup>14</sup>DHA**

Radio ligand Concentration (nM)	Specific Binding (CPM)	Specific Binding ( $\mu$ M)	Specific Binding ( $\mu$ M/mg)
50	752	0.068	0.058
75	967	0.087	0.074
100	1082	0.098	0.083
150	1078	0.098	0.083

Specific binding is converted into  $\mu$ mol/mg using the following steps.

- Equation to convert CPM to pM (pico molar) (Auld et al., 2004) :

$$pM = CPM/SA \text{ (CPM in fmol) / Volume (in ml)} \text{ (Auld et al., 2004)}$$

- Pico molar are converted to micromoles.
- Micromoles of specific binding are converted to  $\mu$ M/mg by dividing the micromoles with mg of protein (PPAR- $\gamma$  stock concentration is 1.17mg/ml).

According to the above equation dividing the CPM by specific activity of C<sup>14</sup>DHA in fmol:

$$1. \quad 752 \text{ CPM} / 0.10989 \text{ CPM/fmol} = 6843.2$$

Now, dividing this values by the assay volume (100 $\mu$ l) in ml

$$6843.2 / 0.1 \text{ ml} = 68432 \text{ pM or } 0.068 \text{ } \mu\text{M}$$

The steps are followed for the CPMs at remaining three concentrations of radioligand.

$$2. \quad 967 / 0.10989 \text{ CPM/fmol} / 0.1 \text{ ml}$$

$$= 87997 \text{ pM or } 0.087 \text{ } \mu\text{M}$$

$$3. \quad 1082 / 0.10989 \text{ CPM/fmol} / 0.1 \text{ ml}$$

$$= 98462 \text{ pM} \text{ or } 0.098 \mu\text{M}$$

$$4. \quad 1078/0.10989 \text{ CPM/fmol /0.1ml}$$

$$= 98098 \text{ pM} \text{ or } 0.098 \mu\text{M}$$

After converting the CPMs into  $\mu\text{M}/\text{mg}$  of protein a graph is drawn by taking the radio ligand concentration on X-axis and specific binding on Y-axis as shown Fig 7.4.

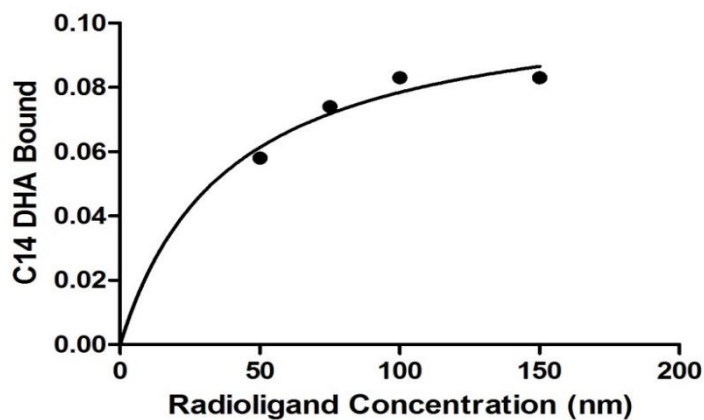


**Figure 7.4 Specific binding of PPAR- $\gamma$  with C¹⁴DHA**

Specific binding at equilibrium is equal to fractional occupancy multiplied by the maximum receptor binding ( $B_{max}$ ) and depends on the concentration of radioligand ( $[L]$ ).

$$\text{Specific Binding} = \text{Fractional occupancy} \times B_{max} = \frac{B_{max} \times [L]}{[L] + K_d}$$

The  $B_{max}$  and  $K_d$  were calculated by using Graph Pad prism versions 5.0 and 6.0 ([www.graphpad.com](http://www.graphpad.com)). For PPAR- $\gamma$  and DHA the  $B_{max}$  is  $0.1089 \mu\text{M}/\text{mg}$  and  $K_d$  is  $38.75 \text{nM}$ . At  $38.75 \text{nM}$  ( $K_d$ ) the specific binding is  $0.057 \mu\text{M}/\text{mg}$  which is approximately half of  $B_{max}$ .

The  $K_d$  and Bmax for PPAR $\gamma$ -EPA were calculated the same way as that of PPAR- $\gamma$  and DHA. The best fit Bmax and  $K_d$  values generated for PPAR- $\gamma$ -EPA are 0.1047  $\mu\text{M}$  and 46.96nM, respectively.

According to the graph at  $K_d$  46.7nM specific binding  $Y = 0.0525 \mu\text{M}/\text{mg}$  which is approximately equal to half of the Bmax. The detailed calculations regarding the binding of PPAR- $\gamma$ -EPA are in Appendix-J

The best fit Bmax and  $K_d$  values generated for PPAR $\alpha$ -DHA are 0.1032  $\mu\text{M}$  and 41.23nM, respectively. The best fit Bmax and  $K_d$  values generated for PPAR $\alpha$ -EPA are 0.1047  $\mu\text{M}$  and 46.96nM respectively. According to the graph at  $K_d$  46.7nM specific binding  $Y=0.0525 \mu\text{M}/\text{mg}$  which is approximately equal to half of the Bmax. The calculations for PPAR $\alpha$ -DHA and PPAR $\alpha$ -EPA were included in Appendix-J.

The binding of CB1 was tested with H<sup>3</sup>2AG, C<sup>14</sup> DHA and C<sup>14</sup> EPA. The  $K_d$  and Bmax were calculated from the graphs (Appendix-J).

- Bmax of CB-H<sup>3</sup>2AG = 477.1pM/mg and  $K_d$  = 29.90nM.
- Bmax of CB1-C<sup>14</sup> DHA = 0.1805  $\mu\text{M}/\text{mg}$  and  $K_d$  = 37.22nM.
- Bmax of CB1-C<sup>14</sup> EPA = 0.1952  $\mu\text{M}/\text{mg}$  and  $K_d$  = 40.95nM.

The best fit Bmax is 79.40 pM/mg and  $K_d$  is 34.43nM. The Bmax and  $K_d$  values of CB2-H<sup>3</sup>2AG, C<sup>14</sup> DHA and C<sup>14</sup> EPA were calculated and the detailed calculations and relevant graphs are in Appendix-J.

- Bmax of CB2-H<sup>3</sup>2AG = 365.1pm/mg  $K_d$  = 38.86nM.
- Bmax of CB2-C<sup>14</sup> DHA = 0.1989 $\mu\text{M}/\text{mg}$   $K_d$  = 46.51nM.
- Bmax of CB2-C<sup>14</sup> EPA = 0.1678 $\mu\text{m}/\text{mg}$   $K_d$  = 49.19nM.

### 7.2.2.2. COX-2 with C<sup>14</sup> Labeled DHA

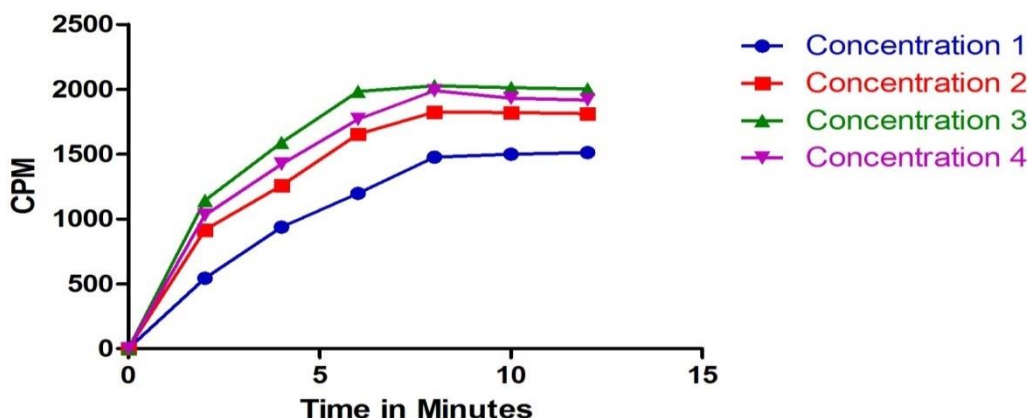


**Figure 7.5 Saturation binding of COX-2 with C<sup>14</sup>DHA at different times**

Unlike the above proteins, the enzyme action is very rapid and the reaction takes place within minutes after adding the ligand. Hence, the CPM readings are taken for 2 minutes time period at different concentrations of COX-2. Figure 7.5 is the graph drawn by taking time on X-axis and CPM on Y-axis.

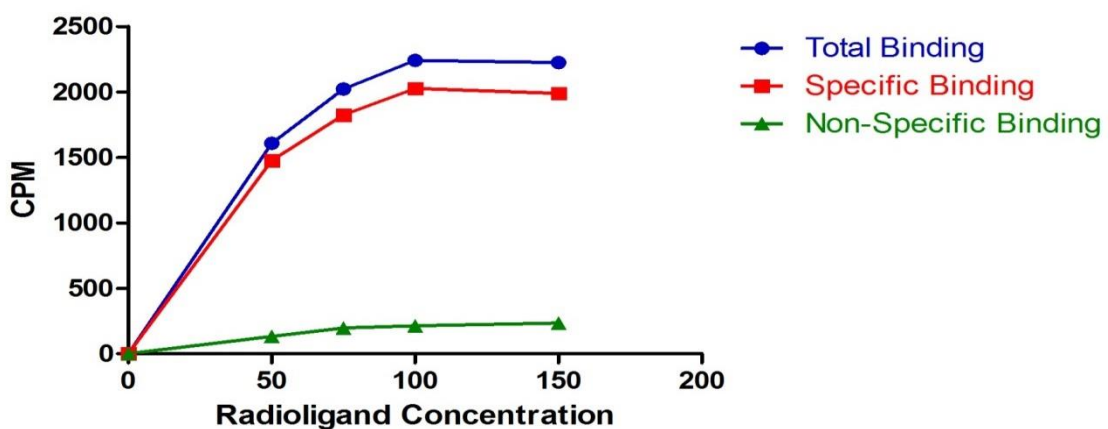


**Figure 7.6 Total binding of COX-2 with C<sup>14</sup>DHA**

For the enzyme COX-2, the binding of different concentrations of radiolabelled ligand are read in 2-5 minute time periods. Time dependent binding is considered for COX-2. The peak

CPM values from the Figure 7.5 are considered to plot the graph of total, specific and nonspecific bindings in Figure 7.6.

**Table 7.3 Total binding of COX-2 with C<sup>14</sup>DHA**

Radio ligand Concentration (nM)	Total Binding (CPM)	Specific Binding (CPM)	Nonspecific Binding (CPM)
50	1607	1475	132
75	2021	1825	196
100	2240	2026	214
150	2223	1989	234

The specific binding in CPM from Table 7.3 is converted into the specific binding in  $\mu\text{M}/\text{mg}$  as shown in Table 7.4.

**Table 7.4 Specific binding of COX-2 with C<sup>14</sup>DHA**

Radio ligand Concentration (nM)	Specific Binding in CPM	Specific Binding ( $\mu\text{M}$ )	Specific Binding ( $\mu\text{M}/\text{mg}$ )
50	1475	0.134	0.60
75	1825	0.166	0.75
100	2026	0.184	0.83
150	1989	0.180	0.81

$$1. \quad 1475 \text{ CPM} / 0.10989 \text{ CPM/fmol} / 0.1\text{ml}$$

$$= 134225 \text{ pM or } 0.134 \text{ } \mu\text{M}$$

$$2. \quad 1825 \text{ CPM} / 0.10989 \text{ CPM/fmol} / 0.1\text{ml}$$

$$= 166075 \text{ pM or } 0.166 \text{ } \mu\text{M}$$

$$3. \quad 2026 \text{ CPM} / 0.10989 \text{ CPM/fmol} / 0.1\text{ml}$$

$$= 184366 \text{ pM or } 0.184 \text{ } \mu\text{M}$$

$$4. \quad 1989 \text{ CPM} / 0.10989 \text{ CPM/fmol} / 0.1\text{ml}$$

$$= 180999 \text{ pM or } 0.180 \text{ } \mu\text{M}$$

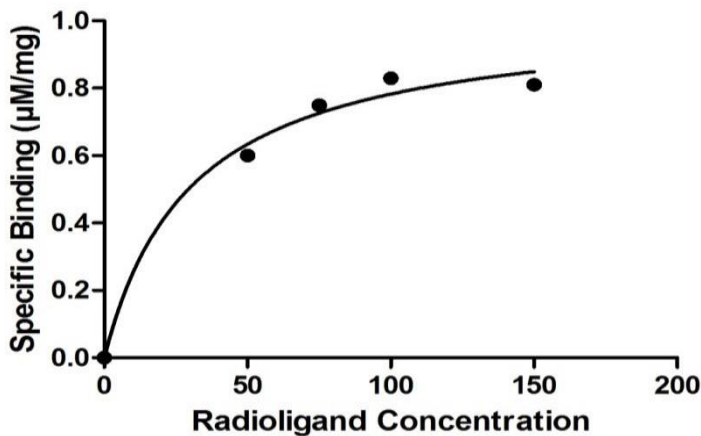


**Figure 7.7 Specific binding of COX-2 with  $\text{C}^{14}\text{DHA}$**

The  $V_{\max}$  is  $0.1034\mu\text{M}/\text{mg}$  and  $K_m$  is  $30.66\text{nM}$  as per the calculations from the graph shown in Figure 7.7.

### 7.2.3. Competitive Binding Analysis

Competitive binding assay was performed with a single concentration of radioligand in the presence of different concentrations of unlabeled ligand. If the radioligand competes with the same unlabeled ligand, it is called homologous competition binding. If the radioligand competes with different unlabeled ligand it is heterologous competitive binding. Competitive binding assay is advantageous over saturation binding assay as it requires only small amounts of radioligand. Moreover, this type of assay can be applied to screen thousands of drugs which are predicted to have similar affinities with the target receptor. Competitive binding assay is faster and easier than the other screening methods. The ideal concentration of radioligand in a competitive binding assay is usually less than or equal to its  $K_d$  which is determined during saturation binding analysis. The incubation time should be more than the saturation binding experiment, because higher concentrations of unlabeled ligands take longer time periods to reach equilibrium (Motulsky & Neubig, 2001).

The concentration of unlabeled ligand that blocks half of the specific binding is called inhibitory concentration ( $IC_{50}$ ) or effective concentration ( $EC_{50}$ ).  $IC_{50}$  or  $EC_{50}$  is the concentration of unlabeled ligand that results in radioligand binding halfway between the upper and lower plateaus. The aim of competitive binding assay is to determine the equilibrium dissociation constant ( $K_i$ ) of the receptor for the competing unlabeled ligand.  $K_i$  of the unlabeled drug is proportional to the  $IC_{50}$ . If the  $IC_{50}$  is low the  $K_i$  also is low and the affinity is high.  $K_i$  of the receptor for the unlabeled ligand can be calculated from Cheng and Prusoff equation as follows (Cheng & Prusoff, 1973).

$$K_i = \frac{EC_{50}}{1 + \frac{[L]}{K_i}}$$
(Cheng & Prusoff, 1973)

- $K_i$  is the equilibrium dissociation constant for the unlabeled compound
- $EC_{50}$  is the concentration causing 50% inhibition of binding
- $[L]$  is the concentration of radioligand
- $K_i$  is the equilibrium dissociation constant for the radioligand (calculated from Saturation Binding Experiment)

#### **7.2.3.1. $K_i$ of PPAR- $\gamma$ with $C^{14}$ Labeled EPA and Unlabeled DHA**

The  $K_i$  for PPAR- $\gamma$  was calculated for the unlabeled ligands EPA, DHA,  $\alpha$ ,  $\gamma$  and  $\delta$ -tocotrienols through competitive binding assay in which  $C^{14}$ EPA is the radiolabeled ligand. The concentration of  $C^{14}$ EPA is 50nM (close to its  $K_d$  from saturation binding analysis) and was maintained constant to compete with the above mentioned unlabeled ligands. The concentration of unlabeled ligands is as high as 100times from the saturation binding

analysis. The incubation time was increased to 3 hours from the saturation binding analysis. Initially a homologous competitive binding assay is conducted by radiolabeled ( $C^{14}$ ) EPA and unlabeled EPA. Later heterologous competitive binding assay is conducted with DHA,  $\alpha$ ,  $\gamma$  and  $\delta$ -tocotrienols using the same concentration of  $C^{14}$ EPA.

$EC_{50}$  was determined by using a sigmoidal dose-response (variable slope), which is also known as a four-parameter logistic nonlinear regression analysis using GraphPad Prism (<http://www.graphpad.com/scientific-software/prism/>) as shown in the equation below:

$$Y = \text{Bottom} + \frac{\text{Top}-\text{Bottom}}{(1 + 10^{(\log EC_{50}-X) * \text{Hill slope}})}$$

(Motulsky, 1996)

**Table 7.5 Binding of  $C^{14}$ EPA to PPAR- $\gamma$  in presence of unlabeled DHA**

Unlabeled Ligand ( $\mu$ M)	$C^{14}$ EPA Bound (CPM)	$C^{14}$ EPA Bound ( $\mu$ M)	$C^{14}$ EPA Bound ( $\mu$ M/mg)
0	3070	0.279	0.238
5	2856	0.259	0.221
10	938	0.085	0.072
20	754	0.077	0.065

1.  $3070\text{CPM} / 0.10989 \text{ CPM/fmol} / 0.1\text{ml} (100\mu\text{l aliquot of stock mix})$

$$= 279370\text{pM} \text{ or } 0.279 \mu\text{M}$$

2.  $2856\text{CPM} / 0.10989 \text{ CPM/fmol} / 0.1\text{ml} (100\mu\text{l aliquot of stock mix})$

$$= 259896\text{pM} \text{ or } 0.259 \mu\text{M}$$

3.  $938\text{CPM} / 0.10989 \text{ CPM/fmol} / 0.1\text{ml} (100\mu\text{l aliquot of stock mix})$

$$= 85358\text{pM} \text{ or } 0.085 \mu\text{M}$$

4.  $856\text{CPM} / 0.10989 \text{ CPM/fmol} / 0.1\text{ml} (100\mu\text{l aliquot of stock mix})$

$$= 77896\text{pM} \text{ or } 0.077 \mu\text{M}$$

The competitive binding of PPAR- $\gamma$  with all the above five ligands is shown in Figure 7.8. The CPM readings were converted to  $\mu\text{M}/\text{mg}$  as shown in Table 7.5. After converting the CPM into  $\mu\text{M}/\text{mg}$ , the values were plotted on the Y- axis and the log [unlabeled ligand concentrations] is taken on X-axis in graph as shown in the Figure 7.8.

$$\text{EC}_{50} = 6.571.$$

The equilibrium dissociation constant for the unlabeled compound ( $K_i$ ) was calculated using the Cheng-Prusoff equation (Lazareno et al., 1993).

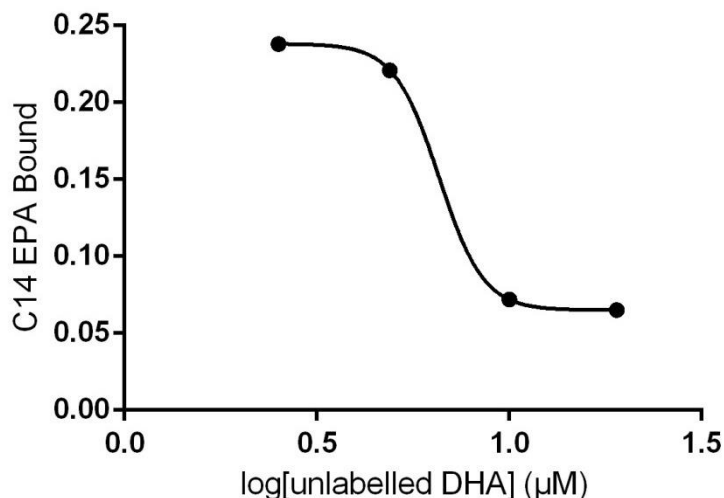


**Figure 7.8 Binding of  $\text{C}^{14}\text{EPA}$  to PPAR- $\gamma$  in presence of unlabeled DHA**

$$K_i = \text{EC}_{50} / [1 + ([L] / K_d)]$$

$$\text{So } K_i = 6.571 / [1 + (50 / 46.96)]$$

$$= 6.571 / 1 + 1.06$$

$$= 6.571 / 2.06$$

$$= 3.189 \mu\text{M}.$$

The  $\text{EC}_{50}$  and  $K_i$  values were also demonstrated for unlabelled EPA,  $\alpha$ -tocotrienol,  $\gamma$ -tocotrienol and  $\delta$ -tocotrienol. The graphs and calculations were described in Appendix-K. It is interesting to note that the  $K_i$  of  $\gamma$ -tocotrienol and  $\delta$ -tocotrienol is same for PPAR- $\gamma$  with a

slight difference in their EC<sub>50</sub>. The Figure 7.9 represents the binding of all the tested unlabelled ligand in the order of their K<sub>i</sub> values.

- EC<sub>50</sub> of PPAR- $\gamma$ -EPA = 7.4 and K<sub>i</sub> = 3.59  $\mu\text{M}$ .
- EC<sub>50</sub> of PPAR- $\gamma$ - $\alpha$ -tocotrienol = 7.667 and K<sub>i</sub> = 3.72  $\mu\text{M}$ .
- EC<sub>50</sub> of PPAR- $\gamma$ - $\gamma$ -tocotrienol = 7.904 and K<sub>i</sub> = 3.95  $\mu\text{M}$ .
- EC<sub>50</sub> of PPAR- $\gamma$ - $\delta$ -tocotrienol = 8.15 and K<sub>i</sub> = 3.95  $\mu\text{M}$ .

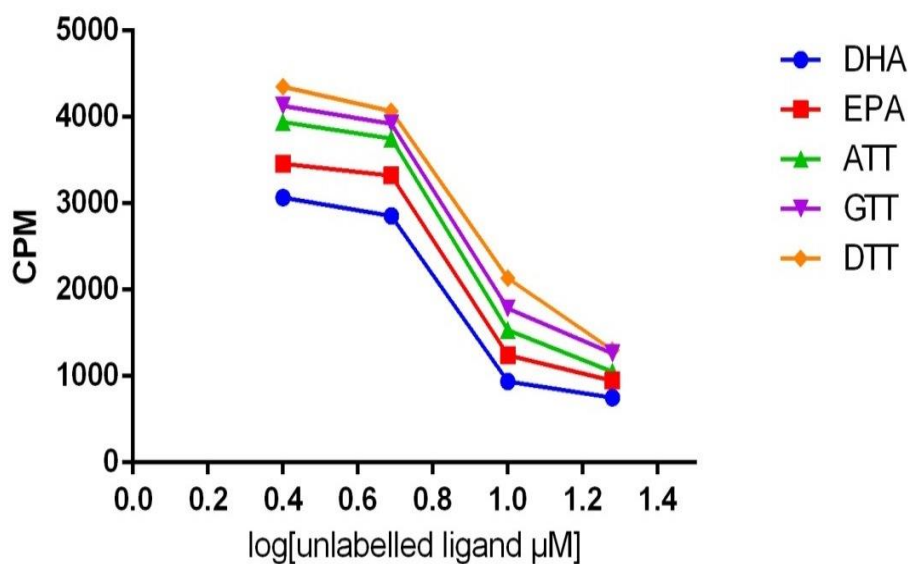


**Figure 7.9 Competitive binding of PPAR- $\gamma$**

The competitive binding analysis was performed for PPAR- $\alpha$  and unlabeled  $\alpha$ ,  $\delta$  and  $\gamma$ -tocotrienols, anandamide and 2AG. The parameters of the assay are same as that of the above mentioned PPAR- $\alpha$  and DHA. The calculations and graphs were included in Appendix-K.

- EC<sub>50</sub> of PPAR- $\alpha$ - $\alpha$ -tocotrienol = 11.86 and K<sub>i</sub> = 5.36  $\mu\text{M}$ .
- EC<sub>50</sub> of PPAR- $\alpha$ -Anandamide = 12.49 and K<sub>i</sub> = 5.65  $\mu\text{M}$ .
- EC<sub>50</sub> of PPAR- $\alpha$ - $\gamma$ -tocotrienol = 13.45 and K<sub>i</sub> = 6.08  $\mu\text{M}$ .
- EC<sub>50</sub> of PPAR- $\alpha$ - $\delta$ -tocotrienol = 14.22 and K<sub>i</sub> = 6.43  $\mu\text{M}$ .
- EC<sub>50</sub> of PPAR- $\alpha$ -2AG = 14.83 and K<sub>i</sub> = 6.71  $\mu\text{M}$ .

Similarly, the EC<sub>50</sub> and K<sub>i</sub> values for α, δ and γ-tocotrienols were calculated after conducting the competitive binding assay with CB1 and H<sup>3</sup>labelled anandamide. The detailed calculations were included in Appendix-K.

- EC<sub>50</sub> of CB1-α-tocotrienol = 12.48 and K<sub>i</sub> = 5.97 μM.
- EC<sub>50</sub> of CB1-γ-tocotrienol = 13.39 and K<sub>i</sub> = 6.4 μM.
- EC<sub>50</sub> of CB1-δ-tocotrienol = 14.08 and K<sub>i</sub> = 6.73 μM.

#### **7.2.3.2. K<sub>i</sub> of COX-2 with C<sup>14</sup> Labeled DHA and Unlabeled Arachidonic acid**

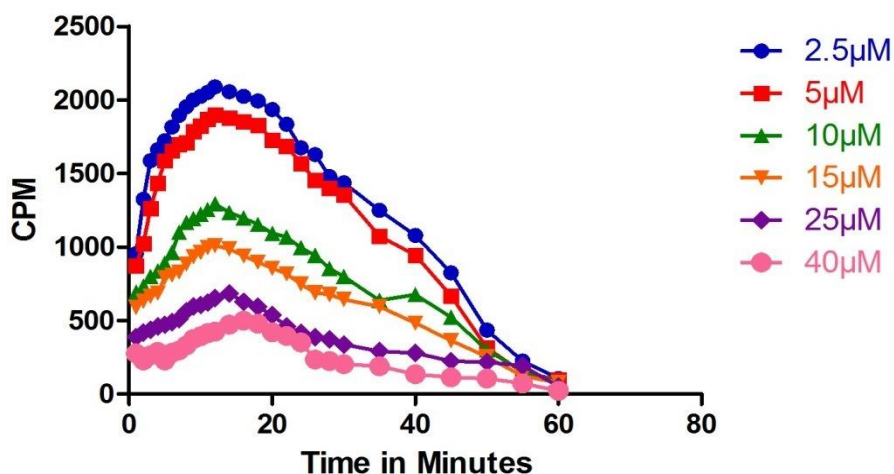


**Figure 7.10 Competitive binding of COX-2 with labelled DHA and unlabeled arachidonic acid**

**Table 7.6 Competitive binding of COX-2 with labelled DHA and unlabeled arachidonic acid**

Unlabeled Ligand (μM)	C <sup>14</sup> DHA Bound (CPM)	C <sup>14</sup> DHA Bound (μM)	C <sup>14</sup> DHA Bound (μM/mg)
2.5	1672.	0.152	0.69
5	1566.	0.142	0.64
10	923.	0.083	0.37
15	551.	0.050	0.22
25	337.	0.030	0.13
40	294.	0.026	0.11

Similar to saturation binding analysis of COX-2, competitive binding is also analyzed based on time. Figure 7.10 shows the time dependant competitive binding of COX-2 to C<sup>14</sup> labeled DHA at different concentrations of unlabeled arachidonic acid. Table 7.6 shows the amount of labelled DHA bound to COX2 and Figure 7.11 represent these values in graph.

1. 1672CPM/ 0.10989 CPM/fmol /0.1ml (100μl aliquot of stock mix)

$$= 152152 \text{ pM} \text{ or } 0.152 \mu\text{M}$$

2. 1566CPM/ 0.10989 CPM/fmol /0.1ml

$$= 142506 \text{ pM or } 0.142 \mu\text{M}$$

3. 923CPM/0.10989 CPM/fmol /0.1ml

$$= 83993 \text{ pM or } 0.083 \mu\text{M}$$

4. 551CPM/0.10989 CPM/fmol /0.1ml

$$= 50141 \text{ pM or } 0.050 \mu\text{M}$$

5. 337CPM/0.10989 CPM/fmol /0.1ml

$$= 30667 \text{ pM or } 0.030 \mu\text{M}$$

6. 294CPM/0.10989 CPM/fmol /0.1ml

$$= 26754 \text{ pM or } 0.026 \mu\text{M}$$

$\text{IC}_{50} = 10.29$  (calculated from the graph shown in Figure 7.13)

$$K_i = \frac{\text{IC}_{50}}{[S/(K_m + 1)]} \quad (\text{Cer et.al, 2009})$$

$$[S/(K_m + 1)]$$

Substituting IC<sub>50</sub>, Substrate Concentration and Km in the above equation:

$$= \frac{9.43}{[75/(30.66+1)]}$$

$$= \frac{9.43}{(75/31.66)}$$

$$= 9.43/ 2.36$$

$$= 3.99 \mu\text{M.}$$

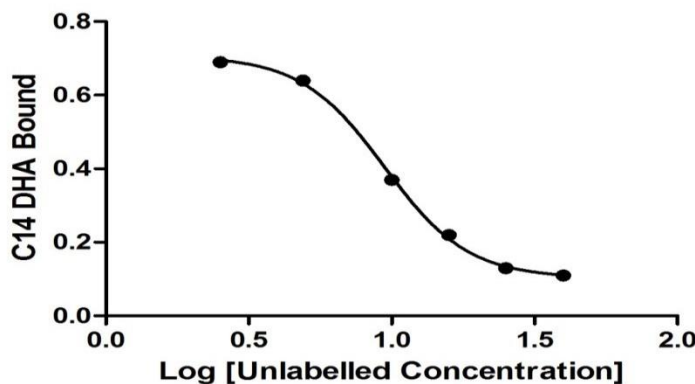


**Figure 7.11 Competitive binding of COX-2 with labelled DHA and unlabeled arachidonic acid**

The other unlabelled ligands—anandamide,  $\alpha$ - and  $\gamma$ -tocotrienols—and 2AG were also examined for their binding abilities with COX-2. The assay procedure for these ligands is same as that of COX-2 with EPA and arachidonic acid as mentioned above. The order of ligands according to their binding strength is shown in Figure 7.12. The detailed calculations and graphs were included in Appendix-K.

- EC<sub>50</sub> of COX-2- $\alpha$ -tocotrienol = 11.75 and K<sub>i</sub> = 4.97  $\mu$ M.
- EC<sub>50</sub> of COX-2-Anandamide = 12.02 and K<sub>i</sub> = 5.09  $\mu$ M.
- EC<sub>50</sub> of COX-2-2AG = 12.89 and K<sub>i</sub> = 5.46  $\mu$ M.
- EC<sub>50</sub> of COX-2- $\gamma$ -tocotrienol = 13.41 and K<sub>i</sub> = 5.68  $\mu$ M.

The competitive binding analysis for the enzyme COX-2 is slightly modified by reading the plate for every 1 minute during the first 12 mins and for every 2 mins from 12-30 mins and for every 5 mins from 30-60 mins. All the readings are plotted in graphs and are included in Appendix-K. Care was taken such that the only enzyme-substrate binding was read before the product formation. The peak readings are plotted in graphs (Appendix-K) and were considered to calculate the K<sub>i</sub> of unlabeled ligand.

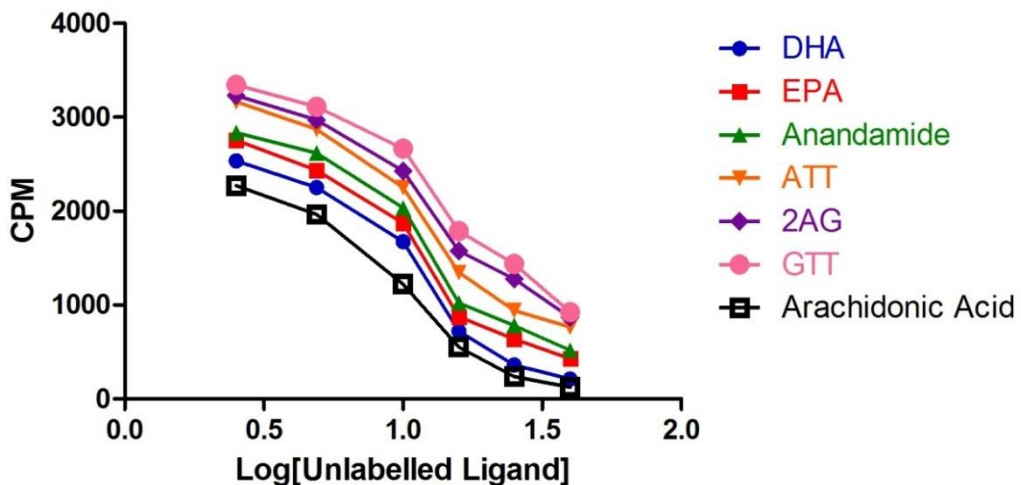


Figure 7.12 COX-2-Competitive Binding

## 7.3. Discussion

SPA is performed to validate the molecular docking results. The findings from this study along with the validations are discussed in the following section.

### 7.3.1. Validation of AutoDock Results with SPA Results

Following Figure 7.13 is a screenshot taken from AutoDock output file (dlg file) of PPAR  $\gamma$ -DHA after molecular docking. Figure 7.13 shows that the estimated binding free energy is -11.71kcal/mol (Chapter 4, Table 4.7). The binding energy/binding affinity is calculated by AutoDock. AutoDock calculates the binding energy by adding final intermolecular energy (shown as (1) in Figure 7.14), final total internal energy ((2) in Figure 7.14) and torsional free energy ((3) in Figure 7.14) and by subtracting unbound system's energy ((4) in Figure 7.14) (Morris et al., 2009).  $K_i$  values were not calculated manually to avoid micro molar differences. They were calculated by AutoDock as shown in Figure 7.14 (Morris et al., 2009). Following screen shot shows the  $K_i$  value as  $2.21\mu M$  for PPAR- $\gamma$ -DHA which is represented in Table 7.7. The same procedure was followed for the rest of the

protein-ligand combinations. This  $K_i$  value is compared with the experimentally determined  $K_i$  value.

```
file) for outputting.
```

```
MODEL      2
USER      Run = 2
USER      Cluster Rank = 1
USER      Number of conformations in this cluster = 1
USER
USER
USER      Estimated Free Energy of Binding      = -11.71 kcal/mol
[=(1)+(2)+(3)-(4)]
USER      Estimated Inhibition Constant, Ki      = 2.21 uM
(micromolar) [Temperature = 298.15 K]
USER
USER      (1) Final Intermolecular Energy      = -12.19 kcal/mol
USER      vdW + Hbond + desolv Energy      = -12.18 kcal/mol
USER      Electrostatic Energy      = -0.01 kcal/mol
USER      (2) Final Total Internal Energy      = -1.31 kcal/mol
USER      (3) Torsional Free Energy      = +4.47 kcal/mol
USER      (4) Unbound System's Energy  [=(2)] = -2.68 kcal/mol
USER
-----
```

**Figure 7.13  $K_i$  values from AutoDock**

The  $K_i$  values obtained from SPA are in excellent agreement with the  $K_i$  values obtained from AutoDock. The difference between  $K_i$  values calculated by AutoDock and SPA is less than one order of magnitude in each case of protein-ligand pair tested as shown in Table 7.8 (Marshall et al., 2006). Chen et al, in 2004 has used molecular modelling prior to chemical synthesis to predict the reactivity of newly designed radiolabeled molecules with their targeted DNA molecules. In this experiment, Chen et al., have compared the binding free energy and inhibition constant ( $K_i$ ) with experimentally determined values (Chen et al., 2004). In 2005, Toprakci & Yelekci have performed AutoDock to estimate  $K_i$  of monoamine oxidase-B inhibitors and compared these values with those of experimental values (Toprakçı & Yelekçi, 2005).

**Table 7.7 Difference between AutoDock  $K_i$  and experimental  $K_i$** 

<b>Combinations</b>	<b>Protein-Ligand Pair</b>	<b><math>K_i</math> calculated by AutoDock (<math>\mu M</math>)</b>	<b><math>K_i</math> calculated from Experiment (<math>\mu M</math>)</b>	<b>Difference in fold</b>
1.	PPAR $\gamma$ -DHA	2.1	3.18	1.5
2.	PPAR $\gamma$ -EPA	2.07	3.59	1.7
3.	PPAR $\gamma$ -ATT	2.05	3.72	1.8
4.	PPAR $\gamma$ -GTT	3.22	3.95	1.22
5.	PPAR $\gamma$ -DTT	3.24	3.65	1.12
6.	PPAR $\alpha$ -DHA	4.34	5.28	1.21
7.	PPAR $\alpha$ -ATT	4.36	5.36	1.22
8.	PPAR $\alpha$ - Anandamide	3.85	5.65	1.37
9.	PPAR $\alpha$ -GTT	3.22	6.08	1.22
10.	PPAR $\alpha$ -DTT	5.69	6.43	1.13
11.	PPAR $\alpha$ -2AG	4.14	6.71	1.60
12.	CB1-Anandamide	3.99	5.36	1.34
13.	CB1-ATT	3.54	5.97	1.68
14.	CB1-GTT	3.28	6.40	1.95
15.	CB1-DTT	5.09	6.73	1.32
16.	CB2-Anandamide	9.69	7.77	0.80
17.	CB2-ATT	5.68	8.41	1.48
18.	CB2-GTT	6.44	8.53	1.32
19.	CB2-DTT	6.28	8.77	1.39
20.	COX-2-EPA	3.29	4.36	1.32
21.	COX-2-Anandamide	3.66	4.97	1.36
22.	COX-2-ATT	4.27	5.09	1.19
23.	COX-2-2AG	3.76	5.46	1.45
24.	COX-2-GTT	4.52	5.68	1.25

An excellent agreement was observed (the difference is only 1.1-1.2 fold) between AutoDock estimated  $K_i$  values of combinations 4, 5, 6, 7, 9, 10, 16, 22 and 24 and the experimental  $K_i$  values as shown in Table 7.7 (Binda et al., 2003). Reasonable values (the difference is between 1.3 and 1.4) were obtained from the combinations 8, 12, 15, 18-21 and 23 (Ooms et al., 2003). The difference for the rest of the combinations is within 2folds which is acceptable (Toprakçı & Yelekçi, 2005).

All the combinations, except 16 have lower  $K_i$  values than that of the experimental  $K_i$  values. Some combinations have highly favorable results with only 1.1-1.2 fold difference, whereas

some are acceptable with 2folds difference. This might be because of the simplifications used in AutoDock procedure such as deleting the explicit water molecules and not considering the solution and entropic effects (Toprakçí & Yelekçi, 2005). The orientation of ligand in the binding site of protein along with their  $K_i$  values is also important to be considered in rational drug design. AutoDock results discussed in Chapters 4-8 reveal that in some of the cases the ligand position in the active site of the protein is reasonably well.

### ***7.3.2. Validation of Glide Results with SPA Results***

Unlike AutoDock, Glide does not calculate  $K_i$  values. Both the results are shown in Table 7.8. The Glide score or docking score is an estimate of the binding affinity and is accurate up to only few kcal/mol. Hence, the use of Glide score is limited to distinguish nanomolar concentrations from micro molar (Schrodinger, 2011). This implies to the fact that converting Glide score into  $K_i$  would not give accurate results. Furthermore, Glide has been designed to achieve docking accuracy and it is difficult to produce strong correlations with experimental binding energies because of the approximations used in Glide (Schrodinger, 2011). Hence, Glide docking results were given a ranking according to their Glide Scores of binding affinity. Similarly, SPA results were ranked according to their  $K_d$  and  $K_i$  values.

It was observed from the Table 7.8 that in some of the cases (Combinations 1, 2, 6, 7, 15, 16, 20-26, 29, 30) the Glide ranking and SPA ranking is same. Interestingly, for CB2 receptor protein, the Glide ranking is exactly the same as that of SPA (Combinations 20-26 from Table 7.8). DHA and EPA have shown same ranking order with all the proteins except for the enzyme COX-2. The Glide ranking order of tocotrienols is same as that of SPA only for CB2 and at rest each case the order is jumbled slightly. Although, the Glide ranking order for the combinations 13 and 14 is not the same as that of SPA, the difference in their Glide scores

(Combination 13 Glide Score is -10.02kcal/mol and Combination 14 Glide Score is -10.01kcal/mol) is very less.

**Table 7.8 Validation of Glide docking with SPA results**

Combinations	Glide Ranking	SPA Ranking
1.	PPAR $\gamma$ -DHA	PPAR $\gamma$ -DHA
2.	PPAR $\gamma$ -EPA	PPAR $\gamma$ -EPA
3.	PPAR $\gamma$ -GTT	PPAR $\gamma$ -ATT
4.	PPAR $\gamma$ -ATT	PPAR $\gamma$ -GTT
5.	PPAR $\gamma$ -DTT	PPAR $\gamma$ -DTT
6.	PPAR $\alpha$ -DHA	PPAR $\alpha$ -DHA
7.	PPAR $\alpha$ -EPA	PPAR $\alpha$ -EPA
8.	PPAR $\alpha$ -2AG	PPAR $\alpha$ -ATT
9.	PPAR $\alpha$ -DTT	PPAR $\alpha$ - Anandamide
10.	PPAR $\alpha$ -GTT	PPAR $\alpha$ -GTT
11.	PPAR $\alpha$ -ATT	PPAR $\alpha$ -DTT
12.	PPAR $\alpha$ - Anandamide	PPAR $\alpha$ -2AG
13.	CB1-2AG	CB1-Anandamide
14.	CB1-Anandamide	CB1-2AG
15.	CB1-DHA	CB1-DHA
16.	CB1-EPA	CB1-EPA
17.	CB1-GTT	CB1-ATT
18.	CB1-DTT	CB1-GTT
19.	CB1-ATT	CB1-DTT
20.	CB2-Anandamide	CB2-Anandamide
21.	CB2-2AG	CB2-2AG
22.	CB2-DHA	CB2-DHA
23.	CB2-EPA	CB2-EPA
24.	CB2-ATT	CB2-ATT
25.	CB2-GTT	CB2-GTT
26.	CB2-DTT	CB2-DTT
27.	COX-2-2AG	COX-2-DHA
28.	COX-2-DHA	COX-2-EPA
29.	COX-2-Anandamide	COX-2-Anandamide
30.	COX-2-ATT	COX-2-ATT
31.	COX-2-EPA	COX-2-2AG
32.	COX-2-GTT	COX-2-GTT

### 7.3.3. Findings from Molecular Docking and SPA

It was determined from Section 7.3.1 and 7.3.2 that the docking results are correlated very well with SPA results. SPA was performed for the proteins PPAR- $\alpha$ , PPAR- $\gamma$ , CB1, CB2 and COX-2. Hence, the lipid ligand interactions of the above proteins are important for the

rational drug design. The prospective benefits of these interactions are discussed in the following sections.

### ***7.3.3.1. Interactions of PPARs with Lipid Ligands***

Both PPAR- $\alpha$  and PPAR- $\gamma$  have shown strong potential with DHA and EPA (Gaddipati et al., 2014a). PPARs are the ligand-activated transcription factors. They regulate genes that play an important role in cell differentiation and various metabolic processes (Sethi et al., 2002). PPAR- $\gamma$  plays a significant role in lipid-protein metabolism, adipogenesis and insulin sensitivity. PPAR- $\alpha$  is implicated in fatty acid metabolism. From the author's study, it was observed that PUFAs such as DHA and EPA bind to PPARs. On the other hand, DHA and EPA improve the prognosis of anti-inflammatory diseases (Sethi et al., 2002). The author's study has also determined that DHA and EPA have shown strong interactions with targets compared to the other lipid ligands tested in this study. The distinct, important bioactive properties of omega 3 fatty acids make them significant in the interaction with other biomolecules (Deckelbaum et al., 2006).

DHA and EPA have an effect on the expression of several key proteins related to inflammation, lipid metabolism and energy utilization (Deckelbaum et al., 2006). However, DHA and EPA can up regulate or down regulate the expression of proteins in different tissues (Lee & Hwang, 2002). A diet enriched with DHA/EPA reduces the expression of PPAR- $\alpha$  in adipose tissue without affecting the expression of PPAR- $\gamma$  (Deckelbaum et al., 2006). Whereas, it was noticed in an insulin-resistant mouse model that the expression of both PPAR- $\alpha$  and PPAR- $\gamma$  is induced in the arterial wall (Ton et al., 2005). DHA and EPA dynamically modulate PPAR-mediated gene expression and cellular responses and DHA suppressed the activity of PPARs in a colon tumor cell line (Lee & Hwang, 2002). DHA and EPA alter membrane fluidity and interact with PPARs and improve cardiovascular health by

altering lipid metabolism (Cottin et al., 2011). DHA and EPA decrease triacyl glycerol levels and DHA increases HDL and LDL particle size. Further, DHA decreases blood pressure, heart rate and platelet aggregation (Cottin et al., 2011).

Secondary to omega 3 fatty acids, tocotrienols have shown a comparable strong interaction with PPARs. Recent studies have shown that the combined treatment of  $\gamma$ -tocotrienol with PPAR- $\gamma$  has silenced the growth of human breast cancer cells (Malaviya & Sylvester, 2014).  $\gamma$ -tocotrienol stimulates endogenous PPAR- $\gamma$  activity (Fang et al., 2010) and results in the increase of PPAR- $\gamma$  ligand 15-S-hydroxyeicosatetraenoic acid in human prostate cancer cells (Malaviya & Sylvester, 2013). Tocotrienols have cardio protective effects such as inhibiting platelet aggregation and anti-atherosclerotic (Vasantha et al., 2011). The molecular targets of tocotrienols play a significant role in cancer and diabetes (Vasantha et al., 2011). The multi-functional role of tocotrienols indicates them to be possible candidates for drug designing.

The third group of lipid ligands, endocannabinoids—anandamide and 2AG—also have shown strong affinities with PPARs. The effect of anandamide on the activity of PPAR- $\gamma$  is investigated and it was shown that anandamide induced transcriptional activation (Bouaboula et al., 2005). Anandamide, after binding to PPAR- $\gamma$ , induces cellular PPAR- $\gamma$  signalling (Bouaboula et al., 2005). Endocannabinoids mediate vasorelaxation by activating PPAR- $\gamma$  in the vasculature (O'Sullivan et al., 2009). The strong binding of endocannabinoids with PPARs examined in this thesis study further opens up a channel for the design of endocannabinoid-PPAR-based drugs.

### ***7.3.3.2. Interactions of Cannabinoid Receptors with Lipid Ligands***

From the author's study it is found that the endocannabinoids (anandamide and 2AG) are the most potent ligands of cannabinoid receptors. However, it is interesting to note that omega 3 fatty acids (DHA and EPA) also have exhibited equal potency with both CB1 and CB2.

The role of cannabinoid receptors in the treatment of obesity has provoked the development of cannabinoid receptor agonists/antagonists (Pertwee, 2012). Rimonabant (also known as SR141716A; Acomplia), the drug used to treat obesity entered European clinics in 2006 and was withdrawn in 2008 for its adverse effects on anxiety and depression (Le Foll et al., 2009). This has prompted pharmaceutical companies to develop drugs with improved benefit-to-risk ratios (Pertwee, 2009). Δ9THC (Dronabinol; Marinol) and its synthetic analogue, Nabilone (Cesamet) were licensed 25 years ago for the activation of cannabinoid receptors. However, dronabinol causes excess body weight, when it is used in AIDS patients as an appetite stimulant (Pertwee, 2012). Another cannabinoid-based drug, Sativex was licensed in Canada in 2005 and in Europe in 2010 to treat multiple sclerosis and advanced cancer. Despite a favorable benefit-to-risk ratio, Sativex also causes unwanted side effects (Pertwee, 2007). Hence, currently there is a lot of interest in the design of cannabinoid-based drugs which maximize the beneficial therapeutic effects and minimize the unwanted side effects (Pertwee, 2012). The lipid ligands tested in the author's study have shown a strong affinity with cannabinoid receptors and their  $K_i$  values were demonstrated.

Anandamide binds to cannabinoid receptors and exhibits pharmacological activity in mice similar to other psychotropic cannabinoids (Deutsch & Chin, 1993). It was identified in the previous research that 2AG activates the functional cannabinoid receptors (Van Sickle et al., 2005). The findings from other experiments prove that the action of DHA and EPA as anticancer agents is influenced by the expression of cannabinoid receptors in some tumour cells (Brown et al., 2010). Tocotrienols were shown to decrease cardiac fibrosis in response to high fat diet. Cannabinoid receptors also play an important role in cardiac fibrosis (McAinch et al., 2012). It was proved from the author's study that tocotrienols bind to cannabinoid receptors, with strong affinity; further research is required for the association of tocotrienols with cannabinoid receptors.

### 7.3.3.3. *Interactions of COX-2 with Lipid Ligands*

COX-2 has exhibited strong affinities with all the ligands examined in the author's study. It is already studied from the previous research that DHA and EPA replace the actual substrate (arachidonic acid) of COX-2 and form different mediators which are identified to be anti-inflammatory and inflammatory-resolving (Serhan et al., 2004). This was supported by the author's study in which it is observed that DHA and EPA are more or less equally competing with arachidonic acid to occupy the active site of COX-2 (Gaddipati et al., 2014ab). The amount of arachidonic acid decreases in inflammatory cell membrane with increased dietary consumption of DHA and EPA (Calder, 2006). Although arachidonic acid is the preferred substrate of COX-2, this enzyme also oxygenates other fatty acids like DHA and EPA (Vecchio et al., 2010).

In a study conducted by Shirode et al, it was found that the lower levels of celecoxib in combination with high levels of  $\gamma$ -tocotrienol have indeed enhanced the therapeutic effect (Shirode & Sylvester, 2010). According to the finding from another study  $\gamma$ -tocotrienol inhibits COX-2 (Ahn et al., 2007). COX-2 has been proven to be a suitable molecular target for the development of anti-inflammatory drugs with its best therapeutic effect (Nesaretnam & Meganathan, 2011). Celecoxib is a selective inhibitor of COX-2 that has an anti-cancer effect. However, the use of Celecoxib is limited due to toxicity reasons (Suleyman et al., 2007).

The results from a study revealed that 2AG inhibited COX-2 and prevented the excessive expression of COX-2 (Zhang & Chen, 2008). COX-2 metabolizes 2AG to prostaglandin esters and anandamide to prostaglandin ethanolamides (Kozak et al., 2000). 2AG plays a significant role in neuroinflammation by suppressing COX-2 expression (Zhang & Chen, 2008). It was identified in a study that 2AG is not only a ligand for CB1 and CB2 but also a

substrate for COX-2 and metabolized as effectively as arachidonic acid (Kozak et al., 2000). COX-2 oxygenates and inactivates endocannabinoids which represents a biologically meaningful and isoform-selective function of this enzyme (Wahn et al., 2005). Prostaglandin E2 ethanolamides are produced after COX-2 metabolizes anandamide (Kozak et al., 2004). When COX-2 mediates the oxygenation of endocannabinoids, novel lipids that are structurally related to prostaglandins are provided (Ross et al., 2002). The spectrum of prostaglandin actions is extended by these novel lipids (Kozak et al., 2004). The author's study is unique in explaining the microscopic interactions of the above mentioned proteins and lipid ligands and thus leaving a route to the design of a new generation of drugs.

#### **7.4. Conclusion**

SPA is a homogenous versatile assay to assess the ligand-receptor interactions. The results of SPA reveal that the molecular docking results are in excellent agreement with wet laboratory experiments. The current study has used WGA coated flash plates to develop the SPA system. The law of mass action was applied to study the ligand-receptor interactions using wet laboratory experiments.

SPA was conducted with both saturation binding and competitive binding methods. Saturation binding was performed for  $C^{14}$  labeled DHA and EPA with PPAR- $\gamma$  and  $\alpha$ . The binding affinity was measured in terms of their  $K_d$  values. It was found that both PPAR- $\gamma$  and  $\alpha$  have shown strong binding affinity with DHA followed by EPA. The saturation binding of CB1 and CB2 was conducted with  $C^{14}$  labeled DHA,  $C^{14}$  labeled EPA,  $H^3$  labeled anandamide and  $H^3$  labeled 2AG. The order of their  $K_d$  values is the same for both CB1 and CB2. They have shown strongest binding affinity and lowest  $K_d$  in the order of anandamide, 2AG, DHA and EPA. The assay procedure for the enzyme COX-2 was slightly modified and the enzyme kinetics was studied in different time periods due to the rapid enzyme action. The

saturation binding of COX-2 was performed with DHA and EPA. Lower  $K_d$  values were observed for DHA followed by EPA.

Competitive binding analysis was performed to study the binding affinity of unlabeled ligands. For PPAR- $\gamma$ , unlabeled ligands—DHA, EPA,  $\alpha$ -tocotrienol,  $\gamma$ -tocotrienol and  $\delta$ -tocotrienol—were used in completion with  $C^{14}$  labeled EPA. DHA has shown strong binding affinity with DHA followed by EPA,  $\alpha$ -tocotrienol,  $\gamma$ -tocotrienol and  $\delta$ -tocotrienol. The competitive binding for PPAR- $\alpha$  was performed with  $C^{14}$  labeled DHA and unlabeled  $\alpha$ ,  $\gamma$  and  $\delta$ -tocotrienols, anandamide and 2AG. The order of these ligands according to their binding affinities with PPAR- $\alpha$  is DHA,  $\alpha$ -tocotrienol, anandamide,  $\gamma$ -tocotrienol,  $\delta$ -tocotrienol and 2AG. For CB1 and CB2, the competitive binding was performed with  $H^3$  labeled anandamide and unlabeled  $\alpha$ ,  $\gamma$  and  $\delta$ -tocotrienols.  $\alpha$ -tocotrienol has shown strong affinity followed by  $\gamma$ -tocotrienol and  $\delta$ -tocotrienols. In the case of COX-2, unlabeled arachidonic acid was used as also used to compare the binding affinities of lipid ligands.

It was understood from both virtual and laboratory experiments that omega 3 fatty acids have exhibited strong affinities with PPARs, CBs and COX-2. The three groups of lipid ligands have strong potential to be the drug candidates for the above mentioned proteins. Furthermore, the microscopic interactions between these proteins and lipid ligands are already explained in the previous chapters.

The molecular interactions of the target proteins with lipid ligands are explained so far both in terms of biochemical and bioinformatic experimental results. Since, the resulting data analysis is in large volumes, a web-based tool *Lipro Interact* has been developed to make this entire dataset available for the future lipid-protein interacting research. The detailed design of *Lipro Interact* is explained in Chapter 8.

# Chapter 8

## The Design of *Lipro Interact*

### 8.1. Introduction

Eight lipid ligands were tested for their binding affinities with ten different proteins through both bioinformatic (molecular docking) and biochemical (scintillation proximity assay) methods. The virtual bioinformatic results were then validated with the biochemical experimental results. Each ligand (lipid)-receptor (protein) pair was analyzed for their binding energies, interactions,  $K_d$  and  $K_i$  values. The molecular docking results of both AutoDock and Glide were compared to find a suitable docking tool for the target proteins and ligands. The PDB file for each protein and lipid combination was created.

The lipid-protein interactions from the current study have pharmacological significance and have great impact on future research related to the ten chosen targets and eight lipid ligands. Hence, all the binding results were transformed into the form of a web based tool named *Lipro Interact*. Extracting the data of lipid-protein interactions is made simple with the use of *Lipro Interact*. For example, the software contains all 80 (ten proteins and eight lipid ligands) PDB files obtained as a result of molecular docking. A user can simply download the PDB files they are interested in by selecting the protein and lipid of relevance. In the same way,

the binding energies, the interactions, and the comparison of AutoDock and Glide etc. for all proteins and ligands can be retrieved from *Lipro Interact*.

The microscopic binding information about the studied lipid-protein interaction was conveyed in the form of different images, since images provide a clear picture of interacting atoms. Furthermore, the validation of binding results with the experimental results improves the strength of *Lipro Interact*. This tool is all about making the binding data related to 80 lipid-protein interactions available to researchers. *Lipro Interact* was uniquely developed by the author with the experimental information, and hence the data in this tool does not exist elsewhere.

The other possibility of making these interactions available is through simply uploading the data on web directly. However, this would not make 80 lipid protein interactions exclusively available. Furthermore, the users might not understand the details of each lipid-protein interaction. Hence, it was chosen to develop a web-based tool with the binding information of 80 lipid-protein interactions. This way the information was made accessible easily and *Lipro Interact* can be updated with future versions.

In this Chapter, Section 8.2 explains the design of *Lipro Interact*. Section 8.3 is about the developmental methodology of *Lipro Interact*. The choice of implementation issues are reviewed in Section 8.4. The results in *Lipro Interact* are analyzed in Section 8.5. Section 8.6 describes the structure of *Lipro Interact*. Finally, Section 8.7 concludes this chapter.

## **8.2. Development Methodology**

Development Methodology is the structure of a project that is used to plan, analyze, design, implement, and test the software. The hardware requirements, software system attributes and the performance requirements are discussed below.

### **8.2.1. Hardware Requirements**

The minimum hardware requirements are needed as an effective chunk of memory is required for performing activities. The minimum hardware requirements are shown in Table 8.1.

**Table 8.1 Hardware Specification**

Hardware	Minimum	Recommended
Computer(GHz)	1.8GHz	2.8GHz
RAM	512mb	1GB
Hard disk	5GB Free Space	80GB

### **8.2.2. Software System Attributes**

The software system attributes are as follows (Larsson, 2004):

- Reliability: The reliability of *Lipro Interact* is established by checking its functionality performance at different stages during and after the development.
- Availability: The system remains operational when it is required by the user.
- Maintainability: The system is designed such that it could be easily extendable; that is, new services can be added using the same paradigm. While developers are required to extend the system, the code to develop new services is not expected to be complex.

### **8.2.3. Performance Requirements**

Performance requirements define acceptable response times for the system functionality. However, for the project-*Lipro Interact* specific performance requirements could not be defined because, the execution time of the query result depends on the location of server and the location of end user.

## **8.3. Review of Implementation Issues**

Based on the requirement analysis and application design, the implementation environment is selected for *Lipro Interact* as discussed below.

### **8.3.1. Implementation Environment**

For the leading position in the software development environments, Sun's Java and Microsoft's .Net framework compete tremendously. They focus on facilitating the developers with an environment which assures to be fast, reliable and secure. To design *Lipro Interact*, .Net framework was selected as this is more suitable to develop fully functioning web sites with an effective performance (Webdeveloper.com, 2014). Moreover .Net framework is compatible in a Windows environment (Thai & Lam, 2003).

### **8.3.2. Development Platform**

.NET is essentially a system application that runs on Windows Operating System (Thai & Lam, 2003). The best features of .NET technology are its:

- Ease of implementation.
- Appropriate to implement for business models and is very reliable.
- Time for designing and maintenance of any application is greatly reduced; additionally the debugging part takes lesser time when compared to Java.
- .NET provides a base class library that supports innovative web development (Webdeveloper.com, 2014).

The most important component of .NET frame work is Common Language Runtime (CLR). CLR is similar to Java Virtual Machine (JVM). However, JVM supports only Java language

whereas; CLR supports any language that can be represented in its common intermediate language (Thai & Lam, 2003). Furthermore, eliminating unnecessary code and involving less code for the developers is another interesting feature of .NET (Webdeveloper.com, 2014). The resources required maintaining the functionality and to manage the websites is available within .NET framework. Nonetheless, ASP.NET is supported with multiple languages such as Visual Basic, C++, C# etc. Also, ASP.NET reduces the lines of code needed to develop large application (ido.net, 2010). Deployment is easy with ASP.NET due to built-in configuration (ido.net, 2010). Another advantage of using ASP.NET is its client side controls which are used to develop interactive grids, wizards, calendrers, etc ("Web Hosting, Design, & Coding," 2015). PHP is another script language used for the web development. ASP.NET is beneficial over PHP in having classes and name spaces ("ASP.NET vs PHP," 2015). Further ASP.NET was used to develop *Lipro Interact* as the design, project needs and requirements are suited well with ASP.NET.

*Lipro Interact* is all about providing the microscopic study of lipid-protein interactions in the form of images and PDB files. Hence, the basic project requirements are fetching the data from the XML data source and presenting this information in Graphical User Interface (GUI). The design of *Lipro Interact* is suitable to develop with .NET framework because of its functions like rendering the images. Furthermore, the availability of many ASP.NET servers within the project budget constraint makes it easy to deploy *Lipro Interact* for the global use.

### **8.3.3. *Operating System (WINDOWS)***

*Lipro Interact* Software is an application which is developed using ASP.NET and windows operating system. However, the user doesn't necessarily should have windows operating system. *Lipro Interact* runs on any operating system. Therefore, the best operating system has been chosen sensibly for the project. Candidate operating systems are Windows 7 and

Windows 8. According to W3Schools, operating system platform statistics shows that more than 80% of people are using Windows (W3Schools, 1999-2013). Windows 7 and Windows 8 versions have a higher percentage among them. Since this research project is targeting many people in the field of biotechnology (with basic computer knowledge), the author has chosen to build it on a Windows 7 platform.

### **8.3.4. Windows Platform Framework (.NET) and Programming Language (C#)**

The programming language C# adopts the features of .NET framework such as scalability, extensibility, rich GUI, security etc. The project needs rich GUI controls such as dropdown boxes, buttons, text boxes and labels which are available in .NET Frame work. Moreover, the .NET platform is compatible with a wide range of programming languages. C# has been preferred as a programming language, considering factors such as object orientation, ease of understanding, and development speed. Furthermore, the project requirements such as binding the XML data to the data set of lipid-protein interactions and the generation of appropriate output from *Lipro Interact* are suitable for the syntax of the C# programming language, as described in Section 8.5.5.

### **8.3.5. Front End UI Framework (.NET Tool kit)**

.NET framework has been integrated with a toolkit which helps in creating interfaces, text boxes, forms, chart components etc. These controls are compatible with the OS platform. This tool kit has necessary controls which are needed for the development of the application—*Lipro Interact*.

### **8.3.6. Programming Environment**

Microsoft Visual Studio 2010 Integrated Development Environment (IDE) was selected to develop *Lipro Interact*. This IDE is primarily developed by the Microsoft Corporation to support the development of applications which use the above programming language and the .NET platform. The following listed tools/frameworks were chosen for implementation.

- 1) .NET Framework 4.0
- 2) C#/ Win forms
- 3) Framework

Finally, *Lipro Interact* was verified against Jacob Neilson's 10 usability heuristics for user interface design as discussed below (Nielsen, 1995).

**Match between system and the real world:** All the word and phrases in *Lipro Interact* are familiar to the users. In order to familiarise the users with words in *Lipro Interact*, a welcome page was included with the user instructions which clearly explained the meaning and use of words.

**Consistency and standards:** *Lipro Interact* maintains consistency of the words and actions throughout. In order not to confuse the users same words were used to convey the same meaning. For example, to provide the information of interacting amino acids within 4Å distance from the ligand in AutoDock, “4Å-AutoDock” was used in *Lipro Interact*. Similarly, interacting amino acids within 4Å distance from the ligand in Glide were provided with the option 4Å-Glide.

**Recognition rather than recall:** To reduce user's memory load, the information in *Lipro Interact* is made clearly visible and retrievable whenever appropriate. The instructions are

provided in all the three pages of *Lipro Interact* to avoid the users from recalling the instructions from the first page. The information can be simply downloaded by clicking the button “Download image file” as shown in Figure 8.1.

**Aesthetic and minimalist design:** The information in *Lipro Interact* was made visible by eliminating the irrelevant information.

**Help and Documentation:** *Lipro Interact* contains a link for help and documentation as shown in Figure 8.1. By clicking this link the user can view help and documentation.

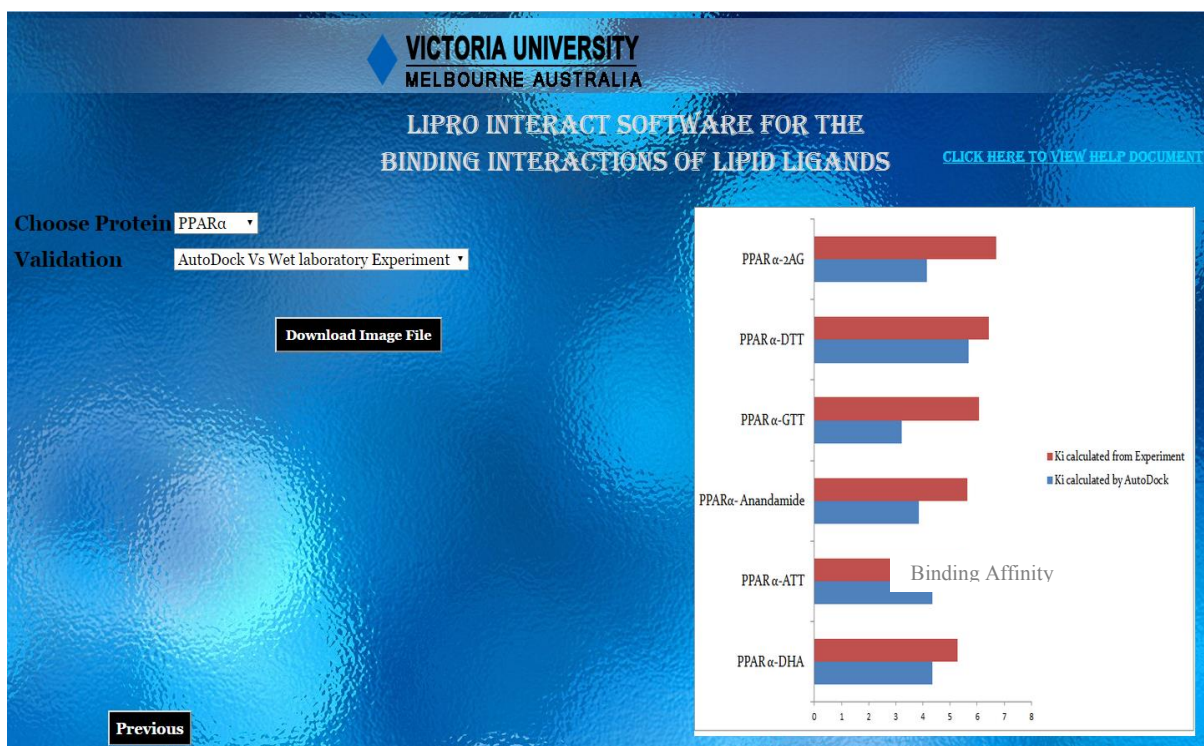


**Figure 8.1** Downloading the information from *Lipro Interact*

## 8.4. Design of *Lipro Interact*

The basic design and use of *Lipro Interact* is illustrated with the help of the use case diagram as shown in Figure 8.2. In the case of *Lipro Interact*, the actors could be students, researchers, drug designers, technicians or anyone else who is interested in the study of lipid-

protein interactions. Hence, the actor is shown as researcher in Figure 8.2. *Lipro Interact* is shown in system boundary box.

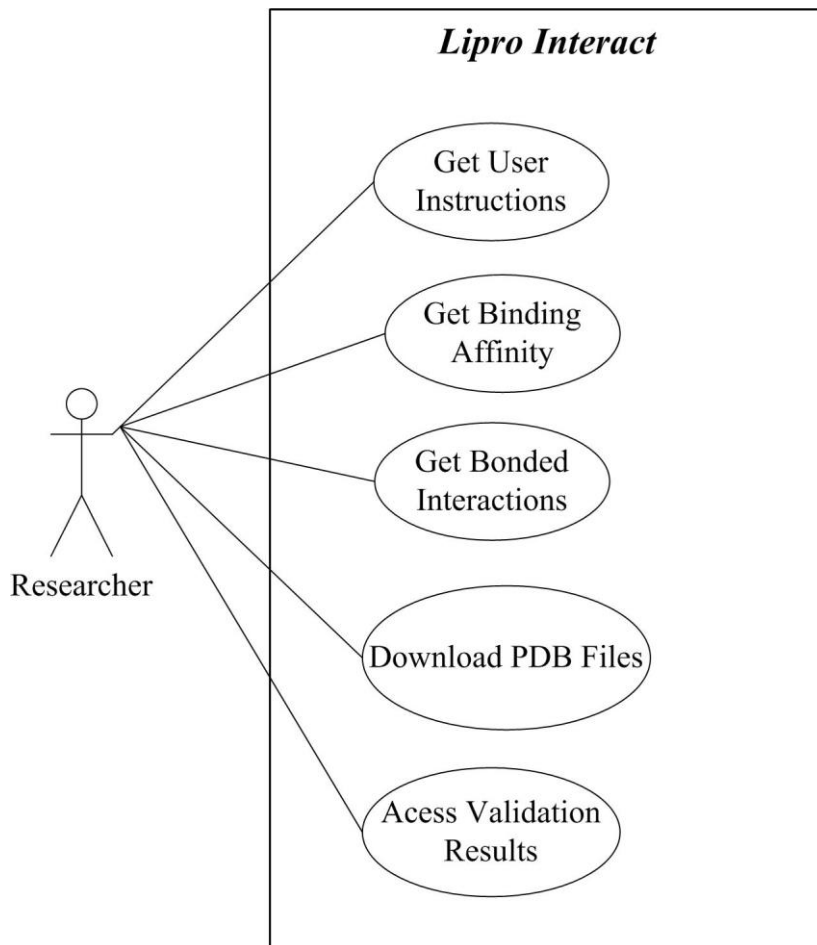


**Figure 8.2 Functionality of *Lipro Interact***

The first use case, “Get User Instructions” represents that the users can read the instructions from welcome page. The second use case “Get binding affinity”, indicates that *Lipro Interact* displays the values of binding affinities (yielded from AutoDock and Glide molecular docking techniques) on the screen. Further, the third use case “Get Interactions”, shows that *Lipro Interact* provides the interactions between the selected proteins and ligands. The fourth use case “Download PDB Files” illustrates that *Lipro Interact* allows the users to download PDB files for the selected proteins and ligands. Finally, the fifth use case “Access Validation Results” represents that *Lipro Interact* also provides the validation proof for the results.

Further, the architecture of *Lipro Interact* is shown in Figure 8.3. The design of *Lipro Interact* is explained in Section 8.5.2 and 8.5.3. The different stages in preparing the output of *Lipro Interact* are explained in detail in Section 8.5.4.

#### **8.4.1. Software Architecture**

The software architecture is shown in Figure 8.3. In order to achieve the functionalities shown in Figure 8.3, the structure of *Lipro Interact* is designed with the help of software architecture shown in Figure 8.3.

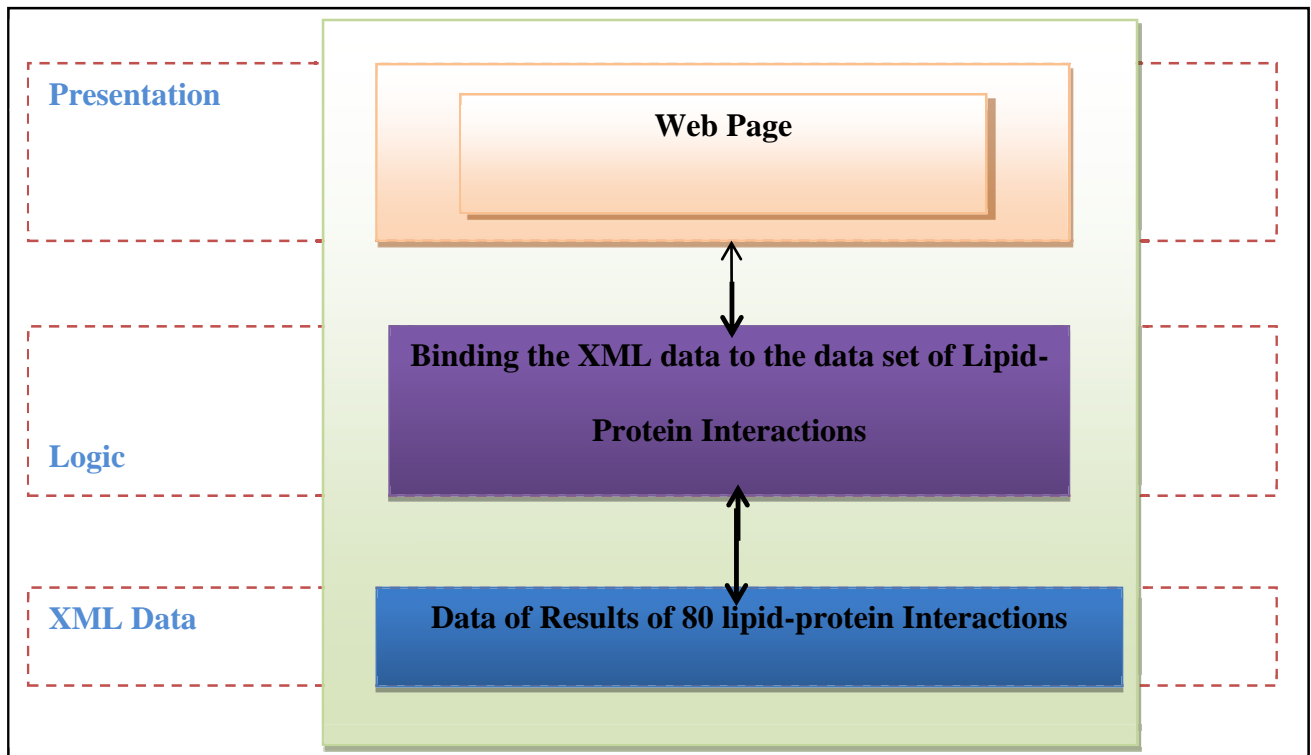


**Figure 8.3 Architecture of *Lipro Interact***

#### **8.4.2. Design of *Lipro Interact***

*Lipro Interact* contains three pages. *Lipro Interact* was provided with ‘Next’ and ‘Previous’ buttons to navigate from page to page.

**Welcome Page:** This page provides the instructions on using *Lipro Interact*. These instructions are helpful for the user to understand and download the required information. The screenshot of welcome page view is shown Figure 8.4. In order to show the instructions clearly two different screenshots were takes as shown in Figures 8.5 and 8.6. This page also has the list of references related to the development of *Lipro Interact*. If the users have any questions, they can contact the author using the contact details provided in this page.

**VICTORIA UNIVERSITY**  
MELBOURNE AUSTRALIA

LIPRO INTERACT SOFTWARE FOR THE  
BINDING INTERACTIONS OF LIPID LIGANDS

1. Select protein and ligand from 'Choose protein' and 'Choose Ligand', respectively.
2. Select the type of interaction you are interested in.
3. Binding energy provides the affinity between the selected protein and ligand as a result of AutoDock and Glide.
4. 4Å-AutoDock : The interacting amino acids of the selected protein with the selected ligand within 4Å distance in AutoDock. The images are drawn using VMD (<http://www.ks.uiuc.edu/Research/vmd/>) software. A new cartoon model is selected to represent the protein structure and VDW is selected for the ligand structure.
5. 4Å-Glide : The interacting amino acids of the selected protein with the selected ligand within 4Å distance in Glide.
6. Bonded Interactions: For the selected protein and ligand, this option displays the hydrophobic interactions and hydrogen bonds between them obtained from LigPlot software. Hydrogen bonds are represented using dashes. Hydrophobic interactions are represented by an arc with a spike pointing towards the ligand atoms.
7. Comparison of AutoDock and Glide: This option compares AutoDock and Glide from which the user can choose the best suitable docking technique for the selected protein and ligand.
8. PDB files: The PDB files are generated after docking the protein with lipid ligand. This PDB files can be downloaded which reflect the interaction between protein and ligand. These PDB files are ready to use further molecular docking or molecular dynamic simulations.

**References:**

1. Gaddipati, R.S, Raikundalia, G. K, & Mathai, ML. (2014). Comparison of AutoDock and Glide towards the Discovery of PPAR Agonists. International Journal of Bioscience, Biochemistry and Biomaterials, 4(2), 100-105.
2. Gaddipati, R. S., Raikundalia GK, Mathai ML. (2014). Dual and selective lipid inhibitors of cyclooxygenases and lipoxygenase: a molecular docking study. Medicinal Chemistry Research, 1-14.
3. Gaddipati, R. S., Raikundalia GK, Mathai ML. (2012). Towards the Design of PPAR based Drugs using tocotrienol as natural ligands-A Docking Analysis. Paper presented at the International Conference on Engineering and Applied Sciences, Beijing.

Contact:  
Rajyalakshmi Gaddipati  
[rajyalakshmi.gaddipati@live.vu.edu.au](mailto:rajyalakshmi.gaddipati@live.vu.edu.au)

Next

**Figure 8.4 Welcome Page of *Lipro Interact***

- 1.** Select protein and ligand from ‘Choose protein’ and ‘Choose Ligand’, respectively.
- 2.** Select the type of interaction you are interested in.
- 3.** Binding energy provides the affinity between the selected protein and ligand as a result of AutoDock and Glide.
- 4.** 4A-AutoDock : The interacting amino acids of the selected protein with the selected ligand within 4A distance in AutoDock. The images are drawn using VMD ([www.VMD.com](http://www.VMD.com)) software. A new cartoon model is selected to represent the protein structure and VDW is selected for the ligand structure.

**Figure 8.5 Instructions on welcome page**

- 5.** 4A-Glide : The interacting amino acids of the selected protein with the selected ligand within 4A distance in Glide.
- 6.** Bonded Interactions: For the selected protein and ligand, this option displays the hydrophobic interactions and hydrogen bonds between them obtained from LigPlot software. Hydrogen bonds are represented using dashes. Hydrophobic interactions are represented by an arc with a spike pointing towards the ligand atoms.
- 7.** Comparison of AutoDock and Glide: This option compares AutoDock and Glide from which the user can choose the best suitable docking technique for the selected protein and ligand.
- 8.** PDB files: The PDB files are generated after docking the protein with lipid ligand. These PDB files can be downloaded which reflect the interaction between protein and ligand. These PDB files are ready to use further molecular docking or molecular dynamic simulations.

**Figure 8.6 Instructions on welcome page**

- **Bioinformatic Component:** The second page of *Lipro Interact* includes the bioinformatic results of the author’s study. These results are the finding of AutoDock and Glide from the Chapters 4, 5 and 6. Further, the detailed analysis of each lipid-protein interaction was included in the form of downloadable images. There are total

seven options involved in studying all 80 lipid-protein interactions. These seven options are described in Section 8.5.2. The user has a choice of selecting protein, ligand, and the type of protein-ligand interaction in which the user has an interest. Furthermore, the ‘Download Image File’ button on this page allows the user to download any image. There are ten proteins included under the ‘Choose Protein’ option, and eight lipid ligands are included under the ‘Choose Ligand’ option. Further, there are seven options for the study of ‘Protein-Ligand Interaction’. The list of proteins available in *Lipro Interact* is shown in Figure 8.7. Figure 8.8 shows the list of ligands available within *Lipro Interact*. Finally, the list of available protein-ligand interactions is shown in Figure 8.9. An example with a selection of PPAR- $\alpha$  from the ‘Choose Protein’ option, DHA from the ‘Choose Ligand’ option and 4Å -AutoDock from the list of ‘Protein-Ligand Interaction’ is shown in Figure 8.10. Further, the detailed analysis of each protein-ligand interaction is discussed in Section 8.5.3.

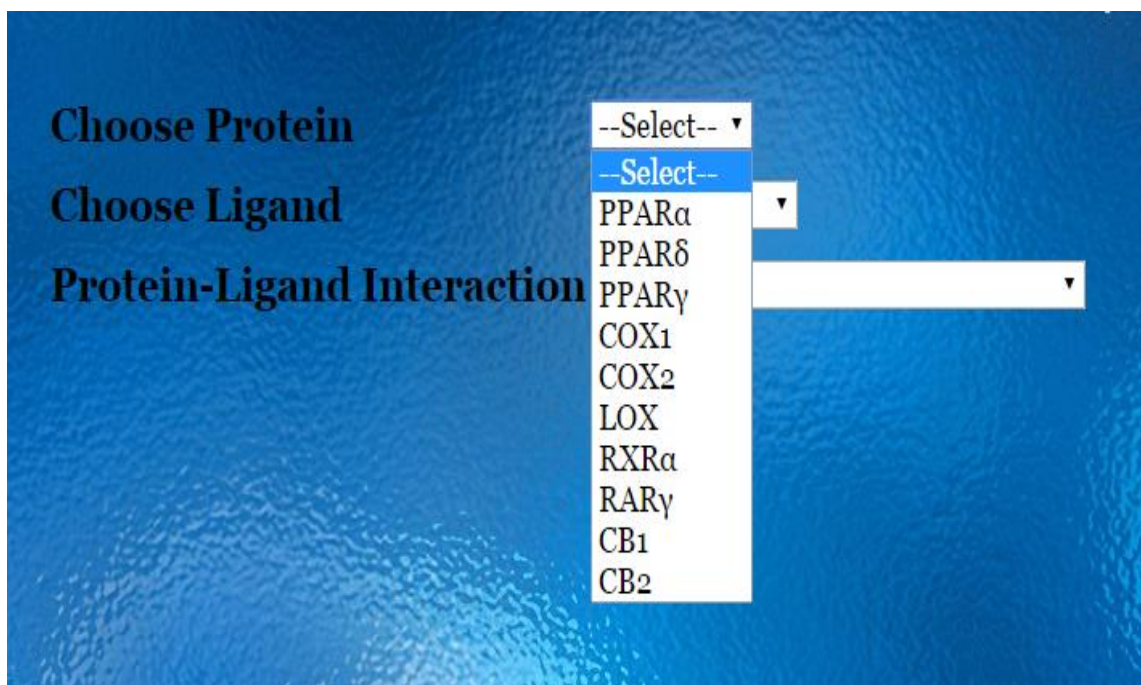


**Figure 8.7 List of proteins in the bioinformatic component of *Lipro Interact***

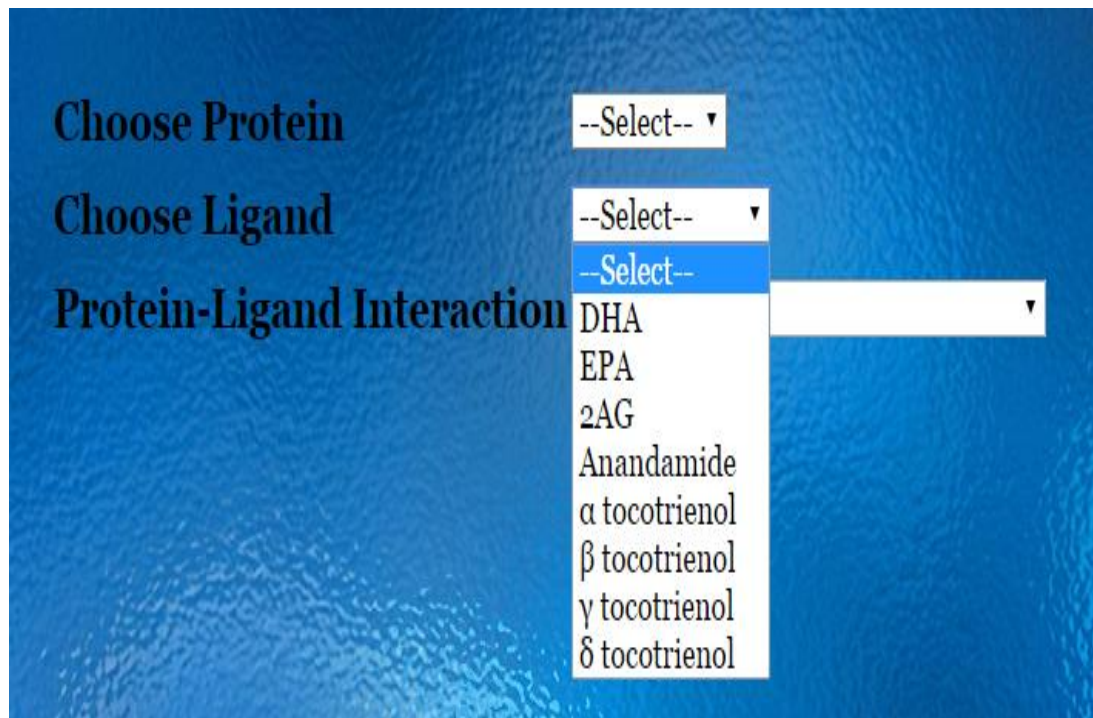


Figure 8.8 List of ligands in the bioinformatic component of *Lipro Interact*

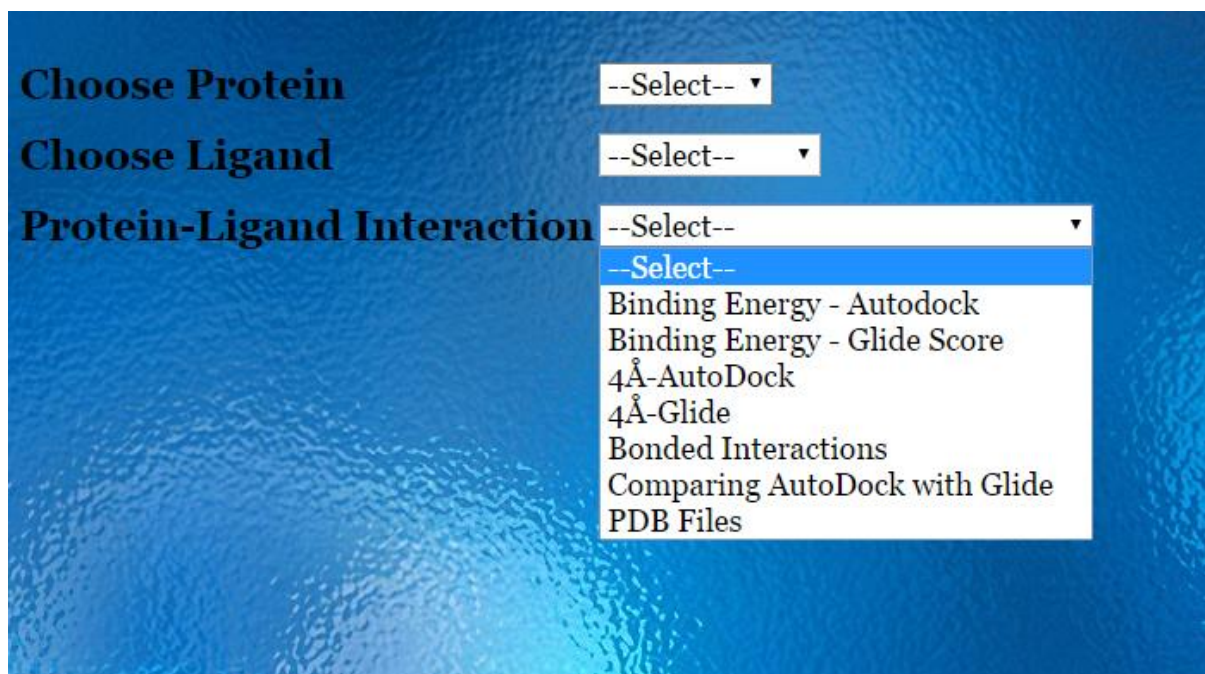
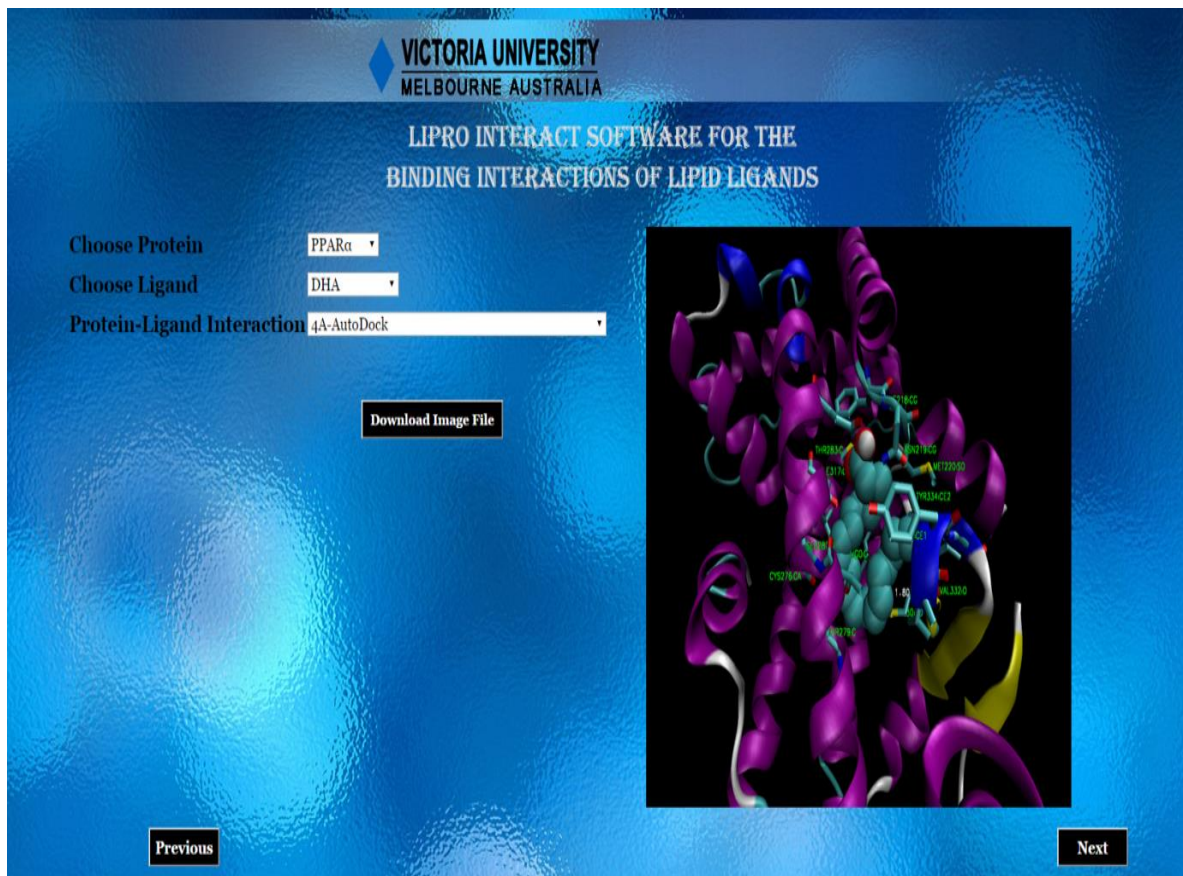


Figure 8.9 List of protein-ligand interactions in the bioinformatic component of *Lipro Interact*



## Figure 8.10 The Bioinformatic component of *Lipro Interact*

- **Biochemical Component:** The third page of *Lipro Interact* is about the experimental validation of bioinformatic results in page 2. There are five proteins included under the ‘Choose Protein’ option. Further, the validation was provided for both AutoDock and Glide results with SPA results. The results included in this page increase the accuracy of simulation results in the second page. The information from this page would help the users to validate AutoDock and Glide results in second page. The images which can be downloaded from this page further benefit the users to find out which docking tool (among AutoDock and Glide) is in close agreement with the wet laboratory experiment. Hence, the third page acts in support of the results included in second page. Figure 8.11 shows the list of proteins available in the third page of *Lipro Interact*. Different validation choices are listed in the Figure 8.12. Figure 8.13 shows

an example of selecting PPAR- $\alpha$  from the ‘Choose Protein’ option and AutoDock Vs SPA from the ‘Validation’ option.

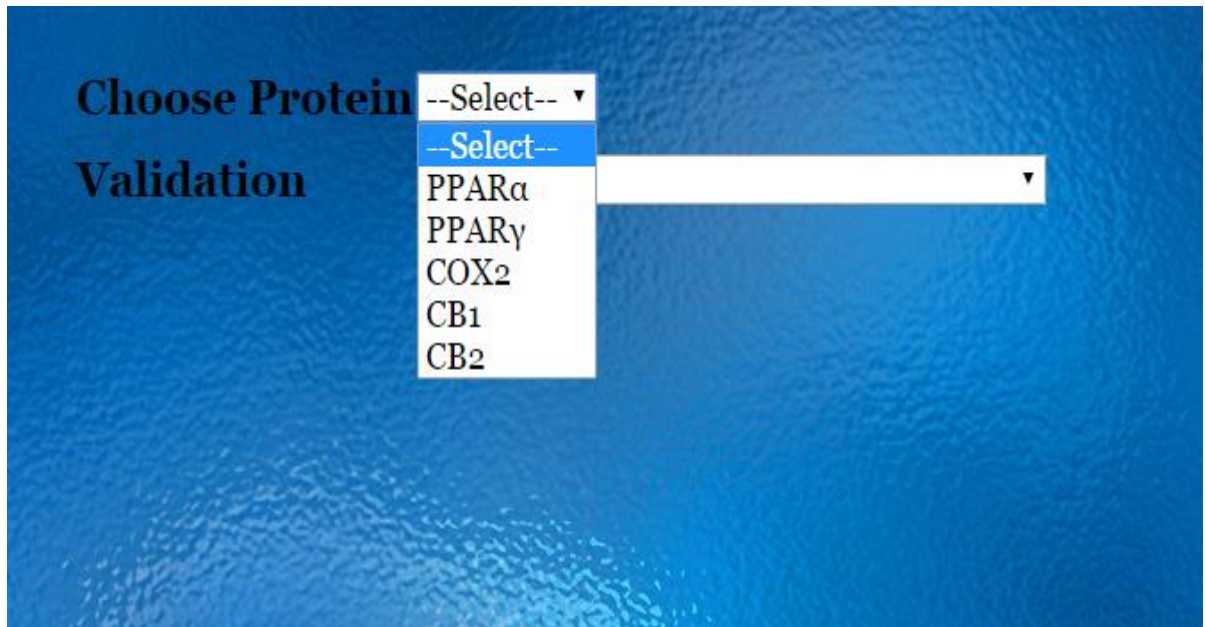


Figure 8.11 List of protein in the biochemical component of *Lipro Interact*

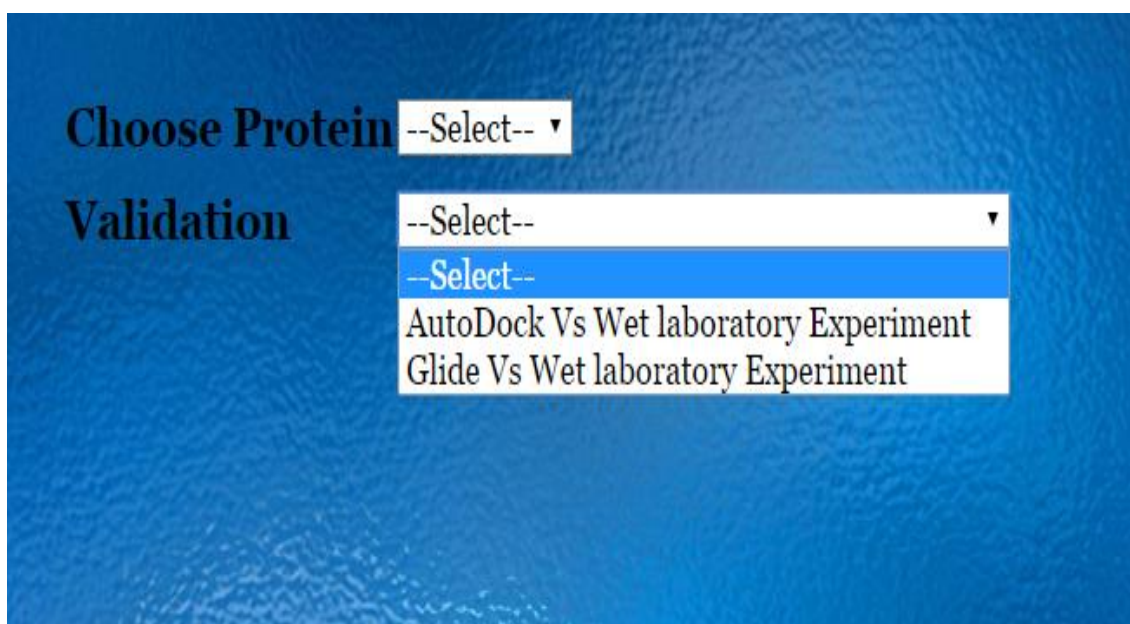
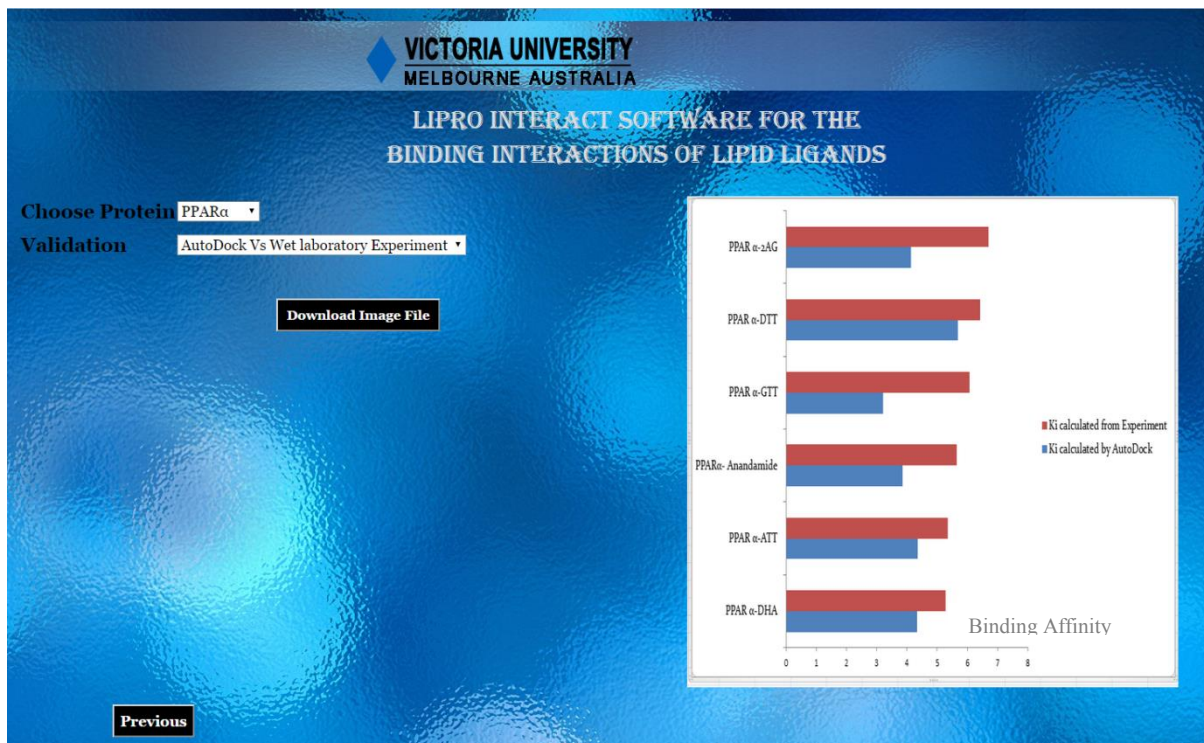


Figure 8.12 List of validated options in the biochemical component of *Lipro Interact*



**Figure 8.13 Experimental validation of *Lipro Interact***

- **Using *Lipro Interact***

To explain the use of *Lipro Interact*, the user, after reading the instructions on the first page, can navigate to the second page by clicking the ‘Next’ button. In the second page, the user can select any protein (out of ten proteins), and any ligand (out of eight ligands). Then by selecting the type of protein-ligand interaction (out of 7 options) the user can see the output generated from *Lipro Interact*.

For example, James Allan who is a biochemical drug designer, researching the interaction of PPARs with different ligands. He also wanted to compare the affinities of PPARs with different ligands. Then, he can simply access *Lipro Interact* and download the interacting images related to the binding of PPARs with all the available ligands. An example of accessing the image of interacting amino acids of PPAR- $\gamma$  within 4 Å from DHA is in

Figure 8.14. *Lipro Interact* helps James Allan in providing the related information and saves his time from studying these interactions again.

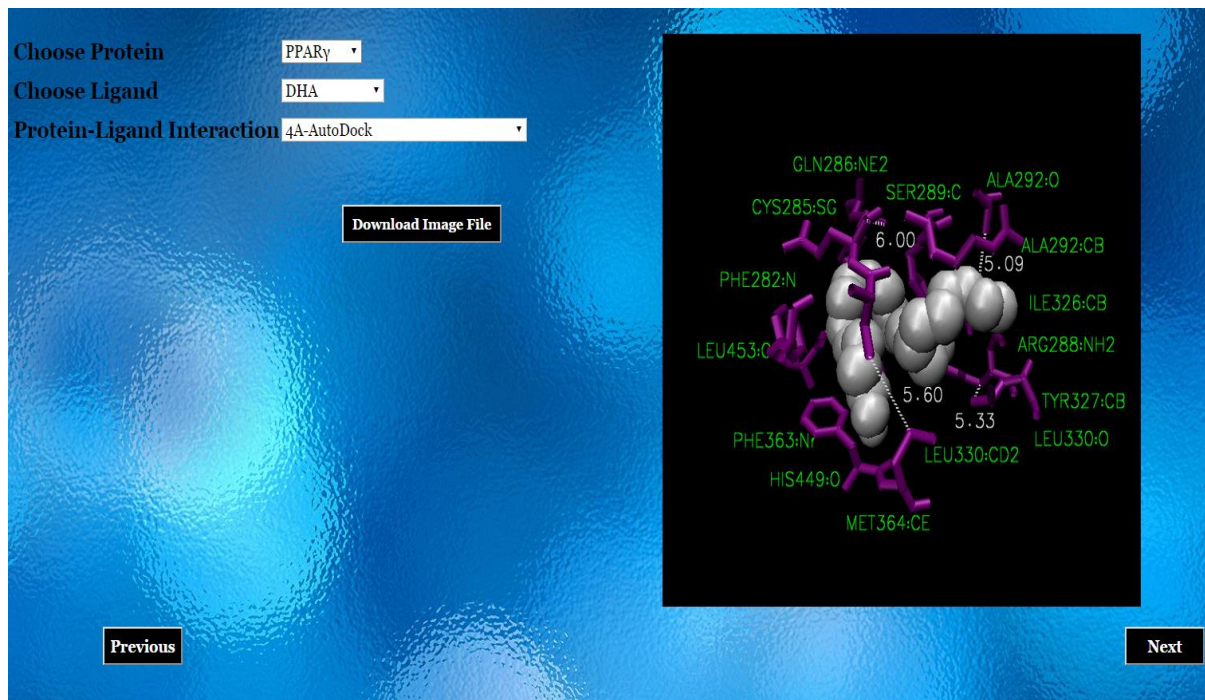


**Figure 8.14 Binding information about PPARs**

Dominic Clark, a biochemical student wants to perform molecular docking of cannabinoid receptors. He is confused of what docking program to use as there are many techniques available. In this instance, Dominic can access *Lipro Interact* and select the comparison studies of AutoDock and Glide for cannabinoid receptors as shown in Figure 8.15. Further, he can also check which tool is in close agreement with the wet laboratory experimental results prior to the selection of a specific tool. Nonetheless, *Lipro Interact* also provides the information on the active site of cannabinoid receptors. This way *Lipro Interact* helps Dominic in selecting a specific molecular docking tool and the active of the protein.

In another case, Kalpana Chawla a researcher in bioinformatics is looking for the PDB file of COX-2 bound to DHA. This PDB file is not available in protein data bank. Then, Kalpana can directly download this PDB file from *Lipro Interact* as shown in Figure 8.16.

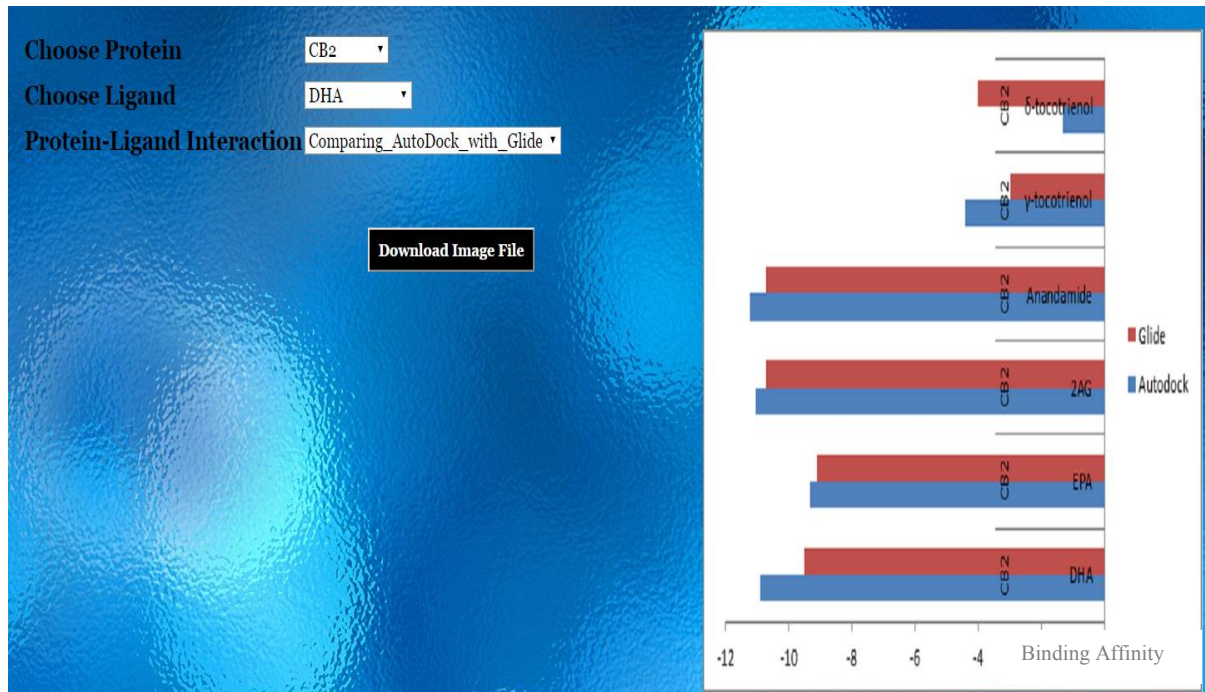


Figure 8.15 Comparing the AutoDock and Glide for Cannabinoid Receptors

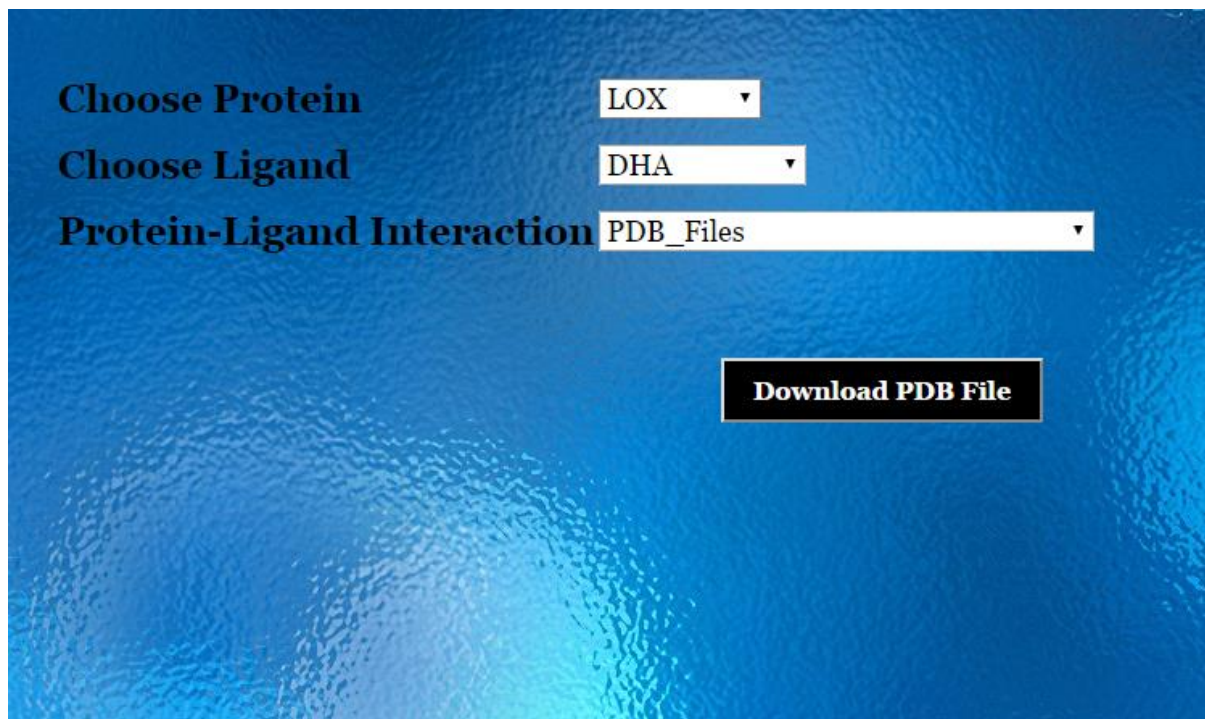


Figure 8.16 Downloading PDB files

### 8.4.3. Results Analysis in Bioinformatic Component

Under the bioinformatics component, the following AutoDock and Glide results were included. There are seven options included to study the protein-ligand interactions and these seven options were prepared as explained below.

#### Option 1. Binding energy:

After performing molecular docking of the protein and ligand, AutoDock calculates the binding affinity of that protein and ligand in kcal/mol. As explained in Chapter 3 in Section 3.4.4, AutoDock creates a DLG file with the docking results. This DLG file was opened with text editors, from which the lowest binding energy for the docked protein and ligand was recorded from the clustering histogram, as shown in Figure 8.17. This number is useful for the user to understand the binding strength between the selected protein and ligand.

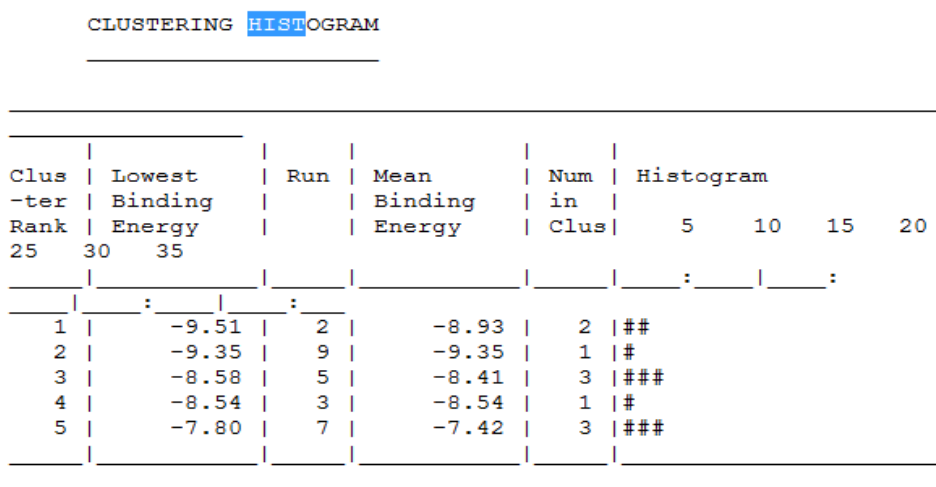


**Figure 8.17 Using AutoDock binding energy in *Lipro Interact***

#### Option 2. Glide Score:

Glide calculates the binding energy in terms of Glide Score. After successful docking of protein and ligand, the Glide score for each protein-ligand pair can be viewed as ‘Gscoore’

from the “XP visualizer window”, as shown in Figure 8.18. ‘Gscore’ is in the second column next to the ligand name, highlighted in a green colour in Figure 8.18.

Name	GScore
5282348	-8.0
92161	-7.2
5282280	-7.2
5282349	-7.1
5281969	-6.7
5282350	-6.2
446284	-5.8
445580	-5.5

**Figure 8.18 Using Glide Score as binding energy in *Lipro Interact***

### Option 3. 4Å -AutoDock:

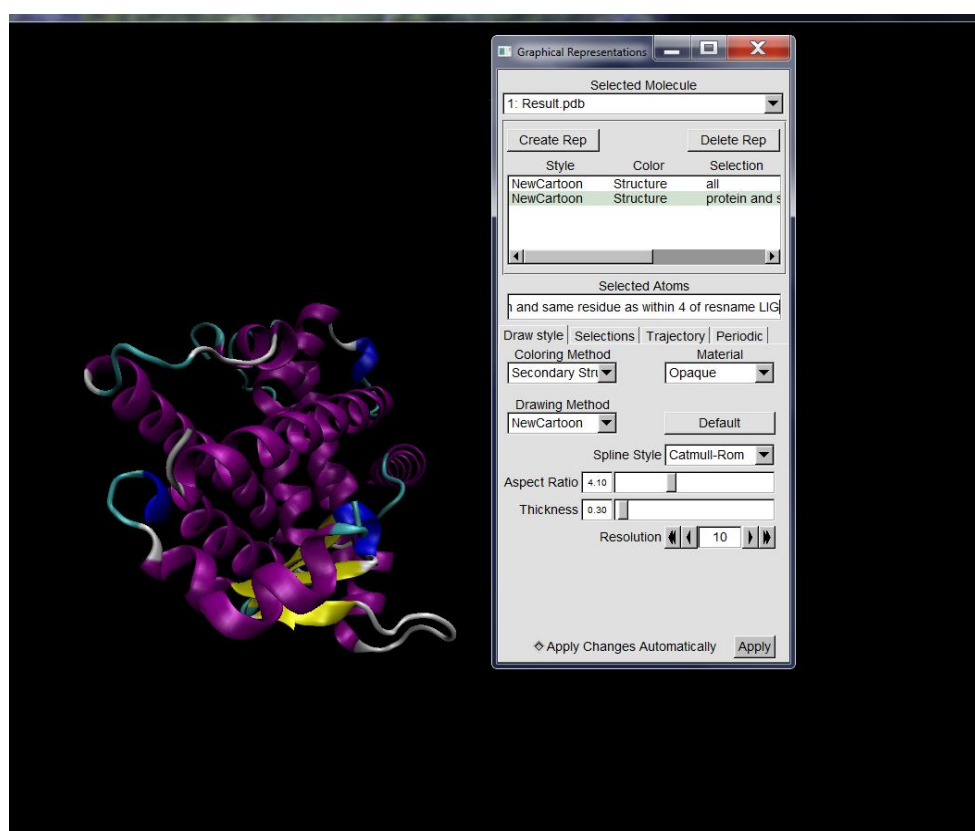


**Figure 8.19 Preparing the protein structure using VMD**

AutoDock generates a DLG file after a successful docking procedure. The lowest binding energy ligand pose was copied from the DLG file and pasted in the protein PDB files. Now, this protein-ligand PDB file was uploaded in VMD software to analyze the interacting amino acids. An example is shown in Figure 8.19. Then, new cartoon model was selected from the Graphical representation window to represent the protein structure, as shown in the following screenshot (Figure 8.19). The coloring method (Secondary Structure) and drawing method (new cartoon) were selected from the ‘Draw Style’ tab as shown in Figure 8.19. The other tabs such as ‘Selections’, ‘Trajectory’ and ‘Periodic’ were considered with the default values since they do not play a role in analyzing the lipid-protein interaction. Figure 8.20 shows the available drawing methods within VMD.

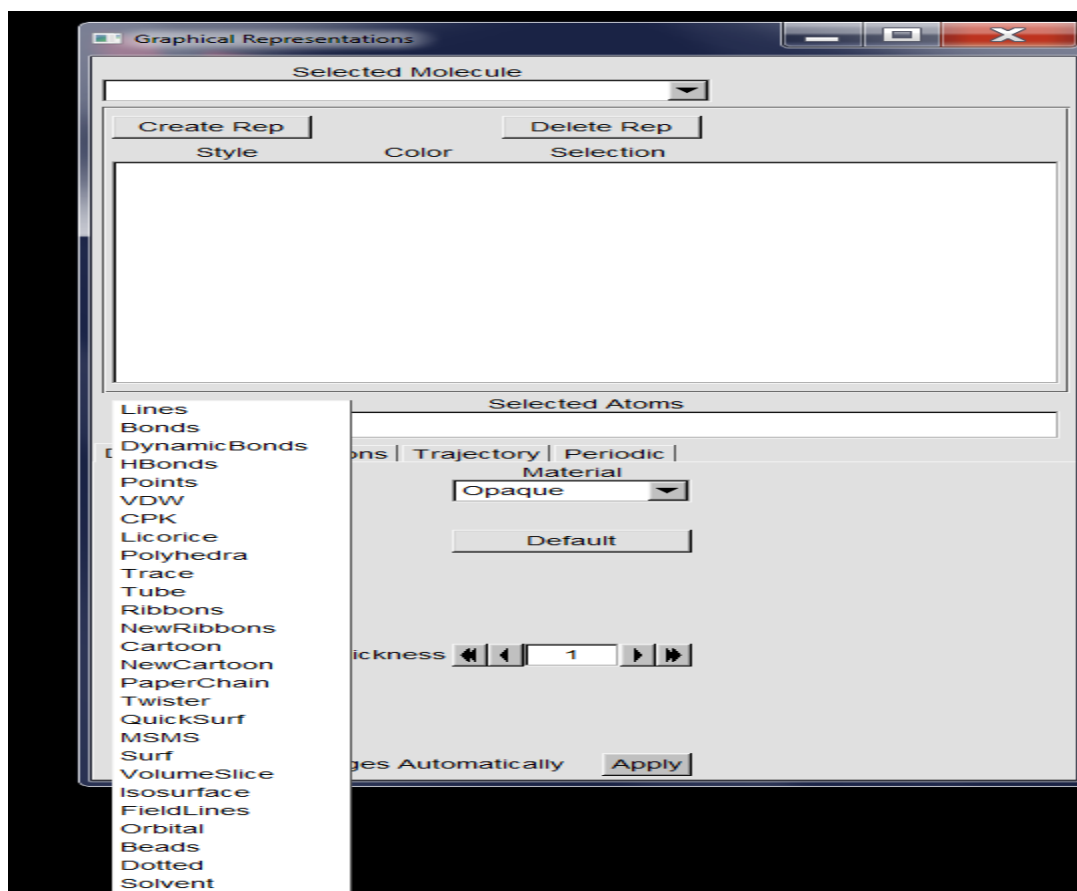


**Figure 8.20 Different drawing methods of VMD**

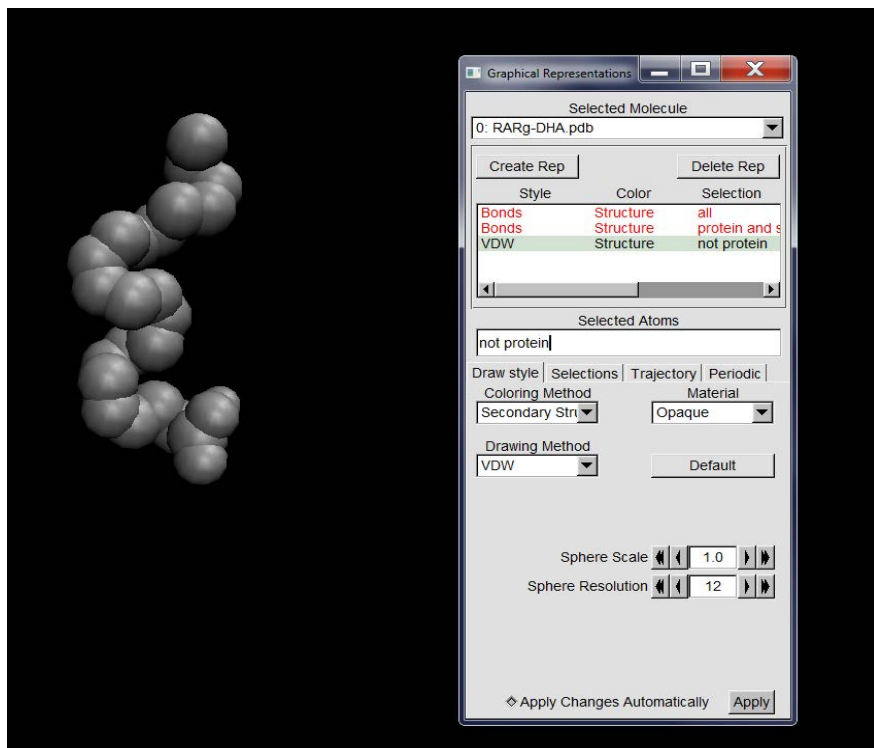


**Figure 8.21 Preparing ligand structure using VMD**

Another representation was created by clicking on the Create Rep button, as shown in Figure 8.21. Next, to select the ligand structure without protein, the protein structure was disabled (shown in a red colour in Figure 8.21). The representation van der Waal (VDW) was selected for the ligand structure.

One more representation was created, as shown in Figure 8.22. Then, the amino acids of the protein around a 4Å distance from the ligand were selected by typing ‘protein and same residue as within 4 of resname LIG’ under Selected Atoms shown in Figure 8.22. For these amino acids, the ‘Bonds’ representation was selected as shown in Figure 8.22. ‘Delete Rep’ button was used to delete any unnecessary representations. The style, color and selection of the representation were generated from VMD. The default values were considered for ‘Sphere Scale’ and ‘Sphere Resolution’ as they do not have an effect on the image.

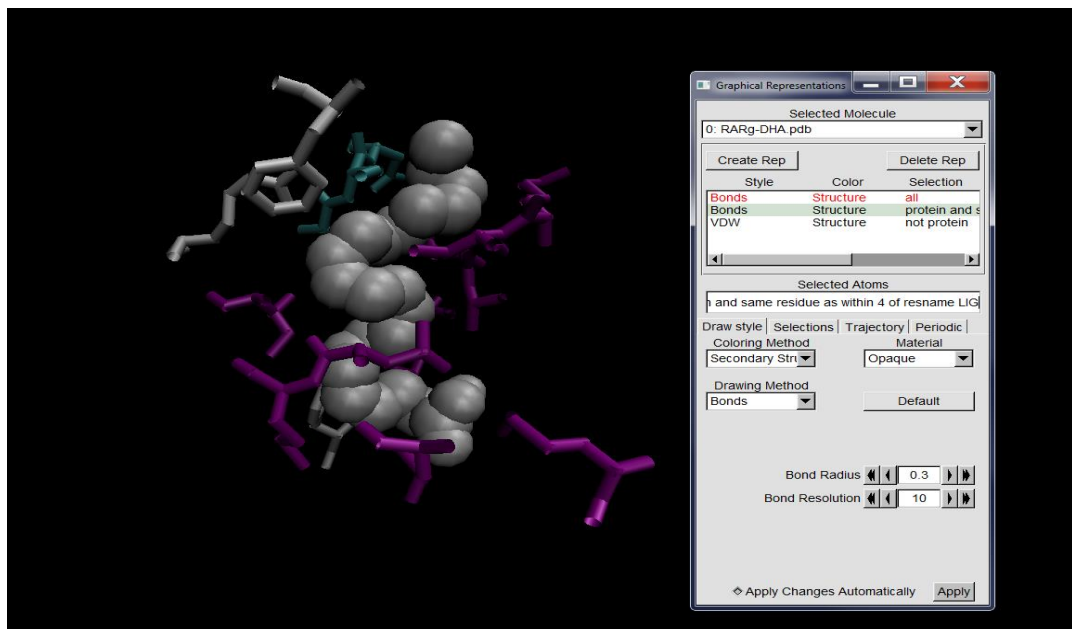


**Figure 8.22 Interacting amino acids of protein with ligand**

Later, the amino acids around a 4Å distance from the ligand were named by typing number 1 and clicking near the amino acid residues. The names of amino acids were adjusted by a simple mouse drag. Figure 8.23 shows the main window of VMD in the top left corner, and in the bottom left-hand side the Labels window is shown. The Labels window was used to adjust the labels of all the amino acids of the protein and the atoms of the ligand. The bond distances were adjusted using the same window. The default values were considered for ‘Bond Radius’ and ‘Bond Resolution’, because they do not play a role in analyzing the result of lipid-protein interactions.

The distance between the ligand and atoms were drawn by typing number 2. Then, the amino acid residues and the bond distances were adjusted for a better view, as shown in Figure 8.24, using the properties option from the Labels window (bottom left corner), which was selected from the main window. The Show and Hide buttons from the Labels window also provides an option of showing and hiding the atom names and bond distances. These images were prepared in the same way for all 80 lipid-protein interactions. However, there is no favorable

binding for few of the combinations and hence, the user is provided with the information instead of an image.

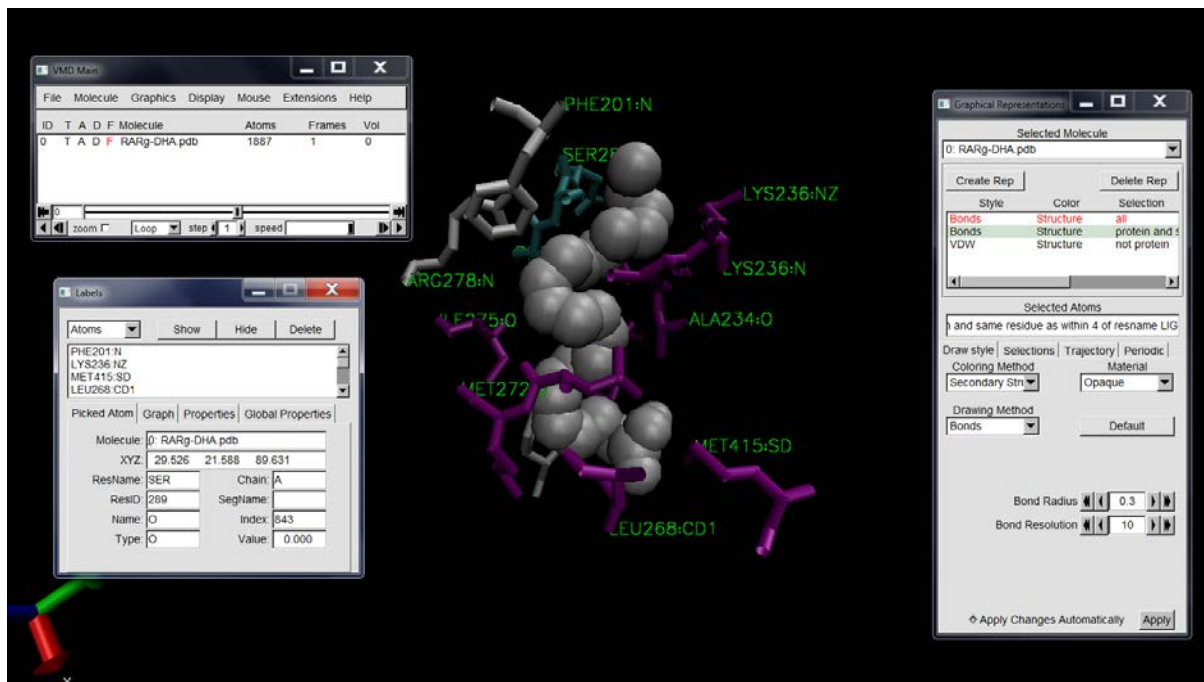


**Figure 8.23** Labelling the atoms of protein and ligand

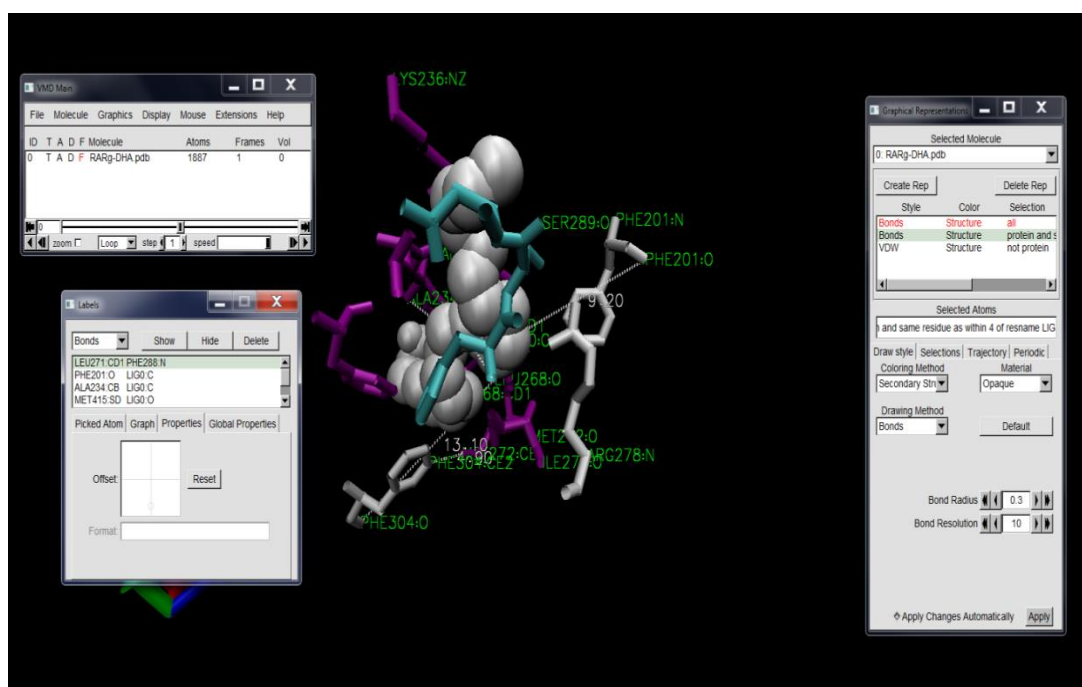


**Figure 8.24** Adjusting the image lay out

### Option 4. 4Å -Glide:

Glide generates a PV file with docking results. When this PV file was loaded in Maestro (Chapter 3, Section 3.5.2), the project table (window is shown in a yellow colour in Figure 8.25) displays all the ligands that were docked with the protein.

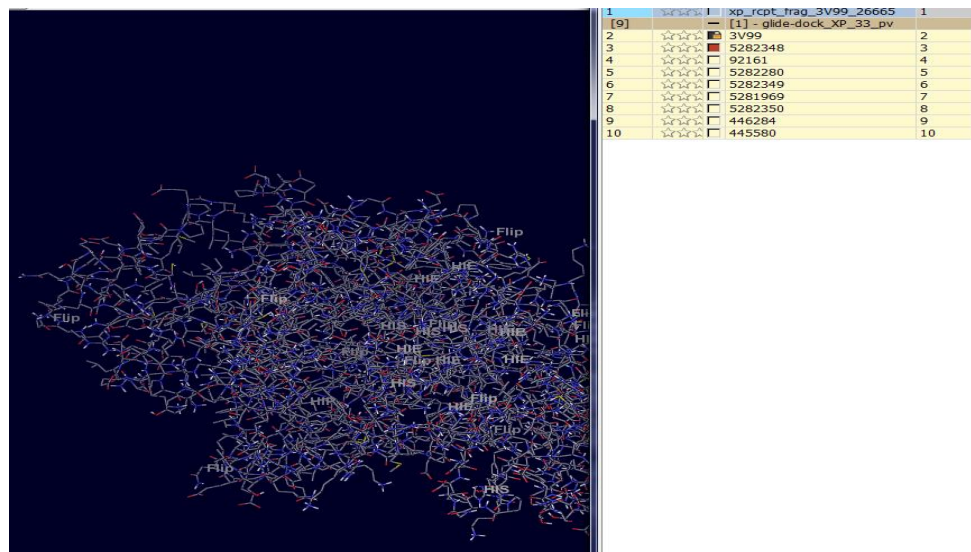


**Figure 8.25 Importing the protein-ligand docked structure into Maestro suite**

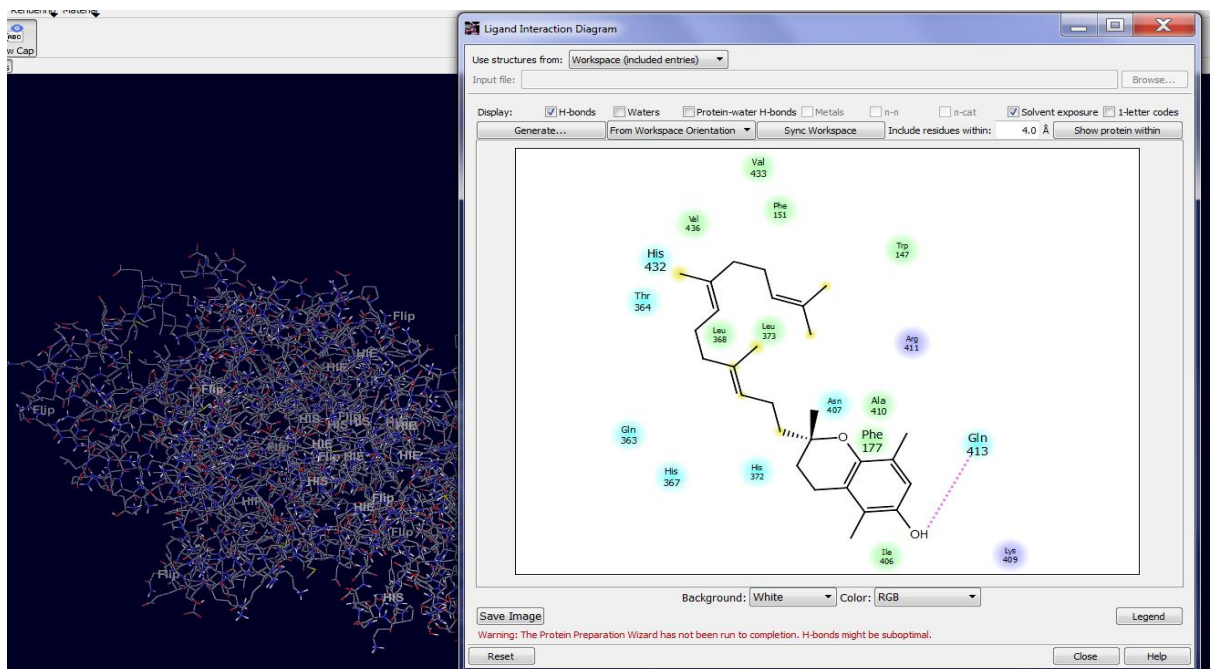


**Figure 8.26 Generating the ligand interaction diagram**

The protein was selected with each ligand from the project table, and a ligand interaction diagram (shown in Figure 8.26) was generated for each pair of protein and ligand.

#### Option 5. Interactions:

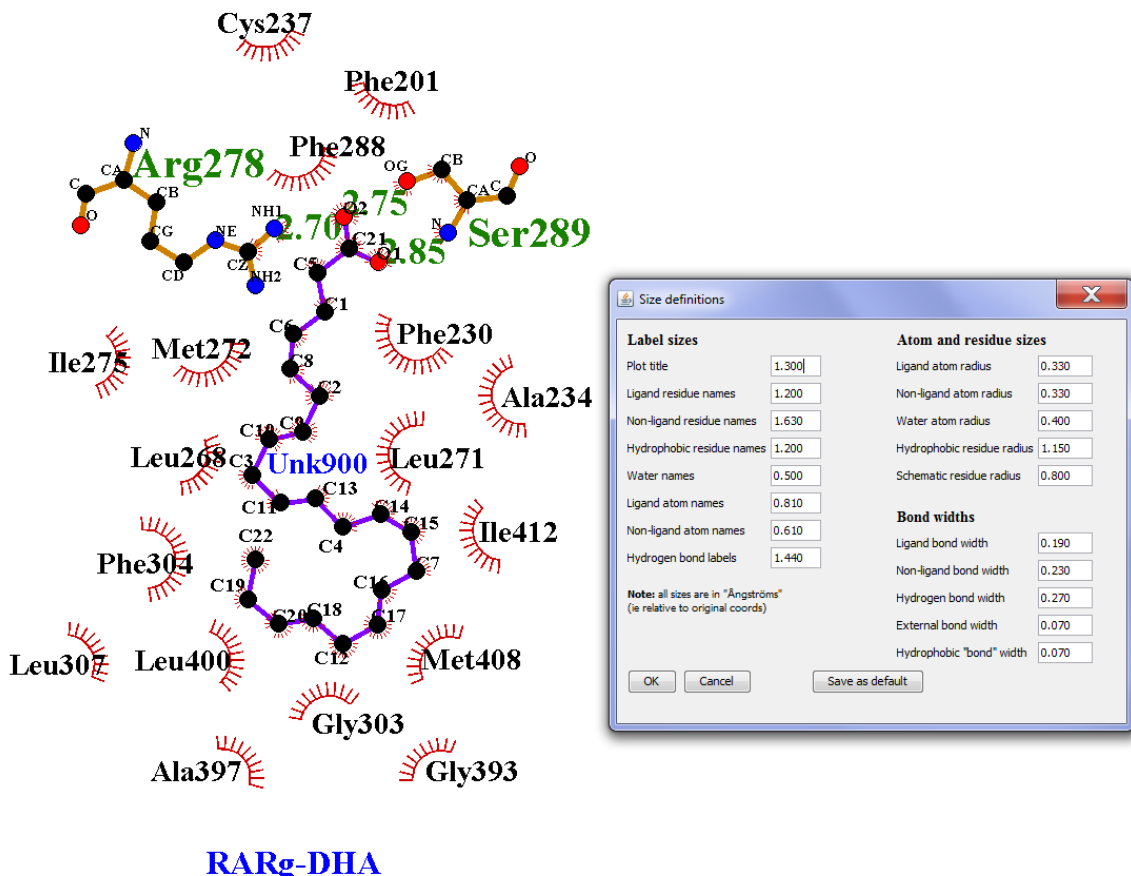


Figure 8.27 Preparing the image using LigPlot

Further, the PDB files were created after docking results were analyzed using LigPlot software. The hydrogen bond distances and hydrophobic interactions were studied using LigPlot. The size of the ligand atom names and the residue names were adjusted using the Size definitions (shown in Figure 8.27) window of LigPlot. The Size definitions window contains the adjustment settings for label size, atom and residue sizes and bond width. The values for these settings are shown in Figure 8.27. These values were set as default by clicking ‘Save as default’ button shown in Figure 8.27. After setting the default values for

one pair of protein and ligand the same values were applied for all the remaining lipid-protein interactions. By clicking ‘OK’ button the values were applied for the selected PDB file and the button ‘Cancel’ was used to cancel the settings.

#### **Option 6. Comparing AutoDock and Glide results:**

The binding affinities yielded by AutoDock and Glide were copied into Microsoft Excel, as shown in Figure 8.28. Then a bar chart was drawn from the data and was uploaded into *Lipro Interact*.

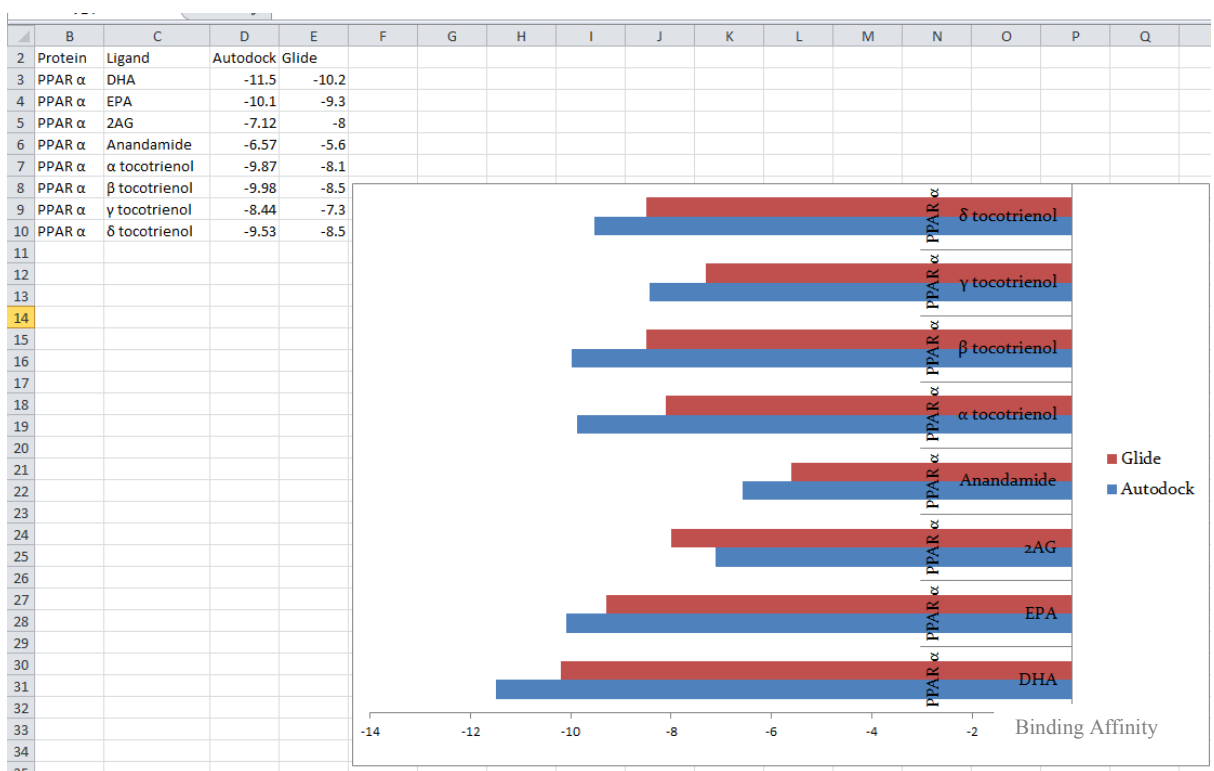


**Figure 8.28 Preparing the bar chart using Excel sheet**

#### **Option 7. PDB files:**

These PDB files were the docking result files that are made available to download from *Lipro Interact*. These PDB files (with the target receptor protein and ligand) are not available on any other website, making them a unique feature of *Lipro Interact*. Once

downloaded from *Lipro Interact*, they are ready to use further for molecular docking, MD simulation, or any other computational binding studies of the specified proteins and ligands.

#### **8.4.4. Results Analysis in Biochemical Component**

Furthermore, *Lipro Interact* provides the validation of AutoDock and Glide results with the wet laboratory experiment (SPA). Since, SPA was conducted for only five proteins; this page provides the information about the five proteins studied. There are two options included to validate the results of AutoDock and Glide. These two options were prepared using the following steps.

##### **Option 1. SPA Vs AutoDock:**

The  $K_i$  values calculated by both AutoDock and Glide were copied into MS. Excel, and a bar chart was drawn to compare the results, as shown in Figure 8.29.

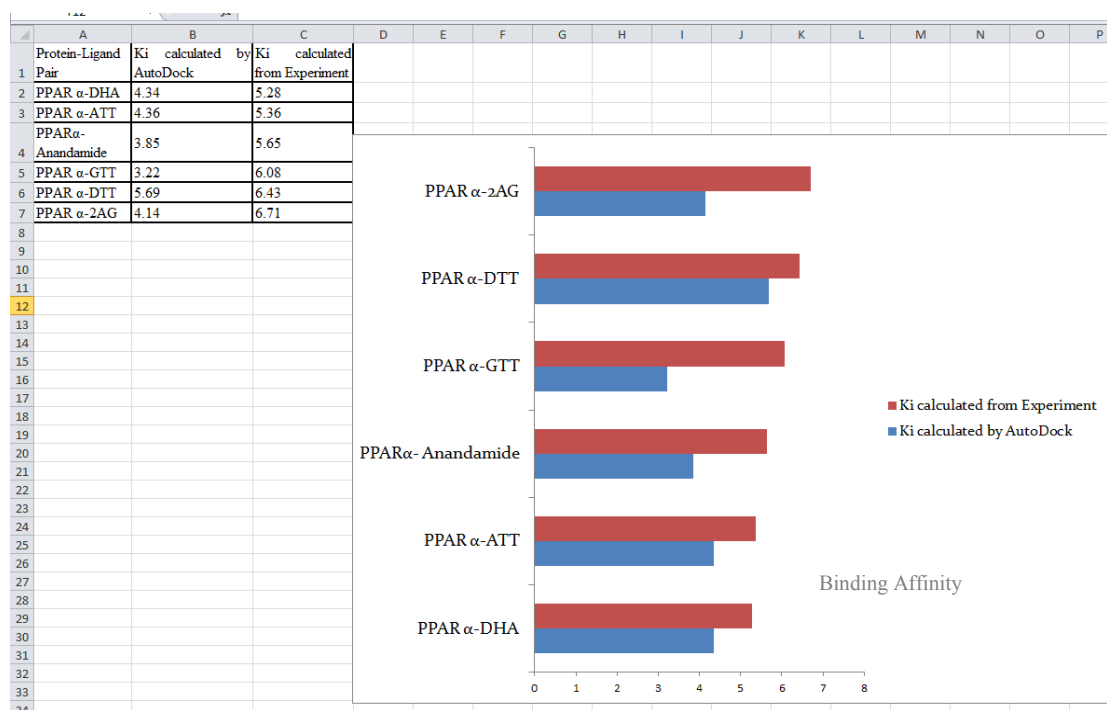


**Figure 8.29 Comparison of AutoDock results with SPA**

## Option 2. SPA Vs Glide:

Unlike AutoDock, Glide does not calculate  $K_d$  or  $K_i$  which can be compared with the wet laboratory experiment. Hence, the results of both SPA and Glide were ranked according to their lowest binding affinities. The bar chart is drawn for the rankings using Excel, as shown in Figure 8.30.

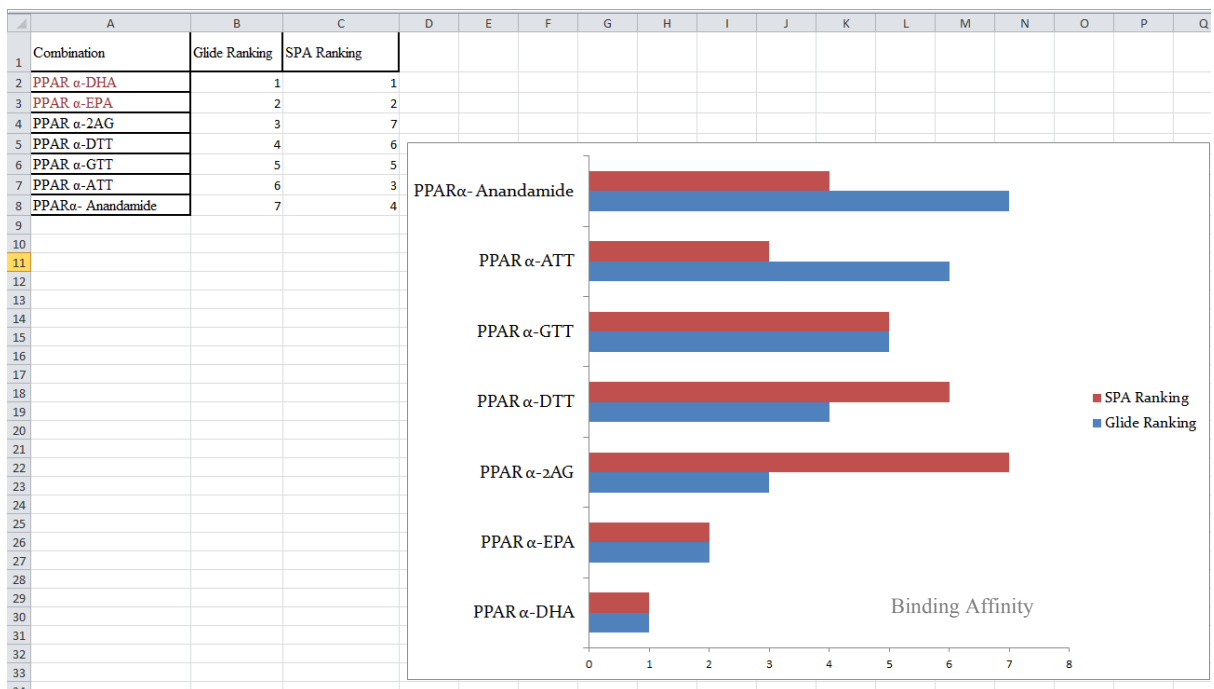


**Figure 8.30 Comparison of Glide results with SPA**

### 8.4.5. Code Used to Develop *Lipro Interact*

*Lipro Interact* was developed with the concept that the results of the author's study can be accessed globally by the researchers, drug designers, students and whoever is interested in studying the lipid-protein interactions. To provide easier accessibility, the results formed into images (using different software tools such as VMD, LigPlot) which show the microscopic association of two biomolecules (lipid and protein in this context). For this all 80 lipid-protein interactions were analyzed and prepared in image format as described in Sections 8.5.3 and 8.5.4. Further, PDB files were prepared for each interacting lipid and protein from

the author's study, so that PDB files can be readily used for future research studies on these lipid-protein interactions. Then, the images, PDB files and the binding energy information from AutoDock, Glide and SPA were transferred into XML data as a first step in developing *Lipro Interact*. The sample XML data for the protein PPAR- $\alpha$  and the ligand DHA is shown in Figures 8.31. The same format was followed for the remaining nine proteins and seven ligands. The complete XML data source is included in Appendix-L.

```

<Details>
<Protein val="PPAR $\alpha$ ">
    <Ligand val="DHA">
        <Protien_Ligand_Interactions>
            <Autodock>-11.5 Kcal/m</Autodock>
            <Glide_Score>-10.2 Kcal/m</Glide_Score>
            <Bonded_Interactions>PPAR $\alpha$ -DHA.PNG</Bonded_Interactions>
            <AutoDock>PPAR $\alpha$ -DHA.PNG</AutoDock>
            <Glide>PPAR $\alpha$ -DHA.PNG</Glide>
            <Comparing_AutoDock_with_Glide>Comparing AutoDock and Glide-
                PPAR $\alpha$ .PNG</Comparing_AutoDock_with_Glide>
            <PDB_Files>PPAR $\alpha$ -DHA.pdb</PDB_Files>
        </Protien_Ligand_Interactions>
    </Ligand>
    |
    |
    |
</Protein>
|
|
|
<Details>

```

**Figure 8.31 XML Source code**

```
_dstMain.ReadXml(Server.MapPath("~/Data/Data.xml"));
```

(a)

```
ViewState["_dstMain"] = _dstMain;
```

```
drpprotein.Items.Add("--Select--");
drpprotein.Items.Add("PPAR $\alpha$ ");
drpprotein.Items.Add("PPAR $\delta$ ");
drpprotein.Items.Add("PPAR $\gamma$ ");
drpprotein.Items.Add("COX1");
drpprotein.Items.Add("COX2");
drpprotein.Items.Add("LOX");
drpprotein.Items.Add("RXR $\alpha$ ");
drpprotein.Items.Add("RAR $\gamma$ ");
drpprotein.Items.Add("CB1");
drpprotein.Items.Add("CB2");
```

(b)

```
DataRow[] bdrow = _dstMain.Tables[2].Select("Ligand_id=" + Ligand_id);
```

```
if (bdrow.Length > 0)
{
    if (drpinteraction.SelectedItem.Value.ToString().Trim().CompareTo("Binding Energy - Autodock") == 0)
    {
        imginteraction.Visible = false;

        lblbindingenergy.Visible = true;
        lblbindingenergyvalue.Visible = true;
        lblbindingenergyvalue.Text = bdrow[0][1].ToString();
        btndownload.Visible = false;
        btndwnpdb.Visible = false;
    }
}
```

}

(c)

**Figure 8.32 Code used to develop *Lipro Interact***

The next step is to design a GUI that can be used to access and download the result data set from *Lipro Interact*. This was achieved through three steps. The first step is to bind the XML data to the data set of lipid-protein interactions which is completed by the code shown in Figure 8.32 a. The second step is to create a data set with all the proteins, ligands and the type of protein-ligand interactions. In Figure 8.32b a sample code is shown to add the GUI

controls (drop down boxes, buttons and labels) to add all ten proteins. The same code is followed for all the 8 ligands and 7 options of Protein-ligand interactions explained Section 8.5.3. Finally, the task is to generate output from *Lipro Interact* based on the user selection of protein, ligand and protein-ligand interaction. This is achieved by the code shown in Figure 8.32c. The complete project code is included in Appendix-M

#### **8.4.6. Data Exceptions**

Some protein-ligand pairs did not show favorable binding. For these combinations, the information was provided instead of an image. They are as follows:

- RXR- $\alpha$  did not produce considerable binding poses with  $\alpha$ -,  $\beta$ - and  $\delta$ -tocotrienols.
- RAR- $\gamma$  did not produce considerable binding poses with  $\alpha$ -tocotrienol.
- CB2 did not produce considerable binding poses with  $\alpha$ - and  $\beta$ -tocotrienols.
- COX-1 did not produce considerable binding poses with  $\alpha$ - and  $\gamma$ -tocotrienols.

Hence, with the selection of above mentioned protein-ligand pairs, *Lipro Interact* displays a message instead of the result. Otherwise, for all other combinations of proteins and ligands, *Lipro Interact* displays either the image, or the binding data.

#### **8.5. Structure of *Lipro Interact***

Out of all 80 Lipid-protein interactions, excluding the above data of lipid-protein interactions, *Lipro Interact* provides a total of 72 downloadable images for each of the options 3, 4, and 5, whereas for the option six there are ten images available. This is because the comparison is made of all ten proteins with all the ligands in the same image. Option 7 allows the user to download PDB files. Likewise, Option 1 in page 3 provides five images for SPA Vs AutoDock, as well as five images for the option SPA Vs Glide. Finally,

- *Lipro Interact* provides the binding affinities for 72 pairs of lipid-protein interactions in both AutoDock and Glide.
- 216 images are available for download that provide the information of bonded amino acids of the protein with the ligand, the hydrogen and hydrophobic bonds between the proteins, and ligands for all 72 lipid-protein interactions.
- 10 downloadable images are available to compare two widely used docking programs, AutoDock and Glide.
- 72 PDB files can be downloaded.
- 10 downloadable images can be obtained that validate the docking results with the wet laboratory experiment.
- As a whole, there are 236 images and 72 PDB files to download.

## **8.6. Conclusion**

Ten proteins and eight lipid ligands were selected from the literature review based on the need for research and their biological significance. Each protein was docked with each ligand in order to study their interaction. The docking results were analyzed in terms of the microscopic interaction between the protein and ligand. Further, the results were studied to observe the hydrogen and hydrophobic interactions of the protein with the ligand. The LigPlot software tool was used to study the interactions between the protein and ligand. AutoDock results were also analyzed using VMD. The results of both AutoDock and Glide were compared in terms of common interacting amino acids of protein within 4 $\text{\AA}$  distance from the ligand. The binding affinities between protein and ligand were studied through both AutoDock and Glide.

Later, the molecular docking results were validated using the wet laboratory experiment (SPA). After checking the accuracy of results, finally, the whole study of 80 lipid-protein

interactions was considered to develop *Lipro Interact*. *Lipro Interact* was developed using Microsoft Visual Studio 2010, C# programming language and ASP.NET. Since there are many images that can explain the interaction between studied lipid ligands and proteins, they are made available for the future research through the development of *Lipro Interact*. The binding data of ten proteins and eight lipid ligands is included in *Lipro Interact*. This data is in the form of binding affinities, images that provide the information on closely interacting amino acids of proteins with ligand atoms. *Lipro Interact* facilitates the users with downloading the image files and PDB files. Furthermore, *Lipro Interact* provides the validation of AutoDock and Glide with wet laboratory experimental results.

The author's study was completed with the development of *Lipro Interact*. The conclusion from the thesis study and further prospective work is discussed in Chapter 9.

# Chapter 9

## Conclusions and Future work

### ***9.1. Introduction***

Ligand-receptor interactions play a significant role in inducing biological response thereby playing an important role in the drug discovery. The affinity of eight lipid ligands with ten proteins was studied. The binding of eight lipid ligands with ten proteins was studied and compared with each other. The eight lipid ligands were compared in terms of their relative affinities with target proteins.

Wet laboratory experiments are useful in the study of binding affinities of ligands with proteins. However, the microscopic atomic interactions cannot be studied in these experimental procedures. Molecular docking and virtual simulation experiments were used to study the microscopic atomic interactions. Still they need experimental validations as the simulation techniques have some limitations. Hence, the author's study was focused on studying the ligand-receptor interactions using both bioinformatic and biochemical techniques. Bioinformatic techniques were used to study the microscopic atomic interactions between the ligand and protein. Further, these interactions were also examined and validated with the wet laboratory experiment.

The ten proteins were examined for potential ligands. The eight lipid ligands were compared for the strong binding affinities and bonded interactions with the protein. Each protein-

ligand interaction was studied to observe the microscopic atomic interactions between the protein and ligand. Different bioinformatic tools such as Chimera, VMD, LigPlot and Pymol were used to analyze the bonded interactions between ligand and protein. The analyzed results were transformed into images which provide the information about target ligand-protein interactions. The virtual results were validated with the wet laboratory experimental results. Finally, the bioinformatic experimental results and wet laboratory validations were used to develop *Lipro Interact* software.

The author's research presents novel *Lipro Interact* software which comprises the study of 80 lipid-protein interactions. Considering the lack of such software that can provide the binding data of lipid-protein interactions, *Lipro Interact* was developed as a timely contribution to the literature discussed in Chapter 2. Advantageously, *Lipro Interact* is simple to access and easy to use. *Lipro Interact* was designed in such a way that it can be accessed by the research scholars, drug designers and whoever else is interested in studying the lipid-protein interactions. Since *Lipro Interact* was developed from the results of both bioinformatics and biochemical methods, the software would receive much attention in research circles.

Apart from developing *Lipro Interact*, the major contribution of the author's study is the observation of naturally occurring lipid ligands as the new series of potential ligands of biologically significant proteins. As the author's project work involves the binding mechanism of eight lipid ligands with ten proteins, this research has revealed many facts about these lipid ligands and proteins. Interestingly, the three groups of lipid ligands have expressed similar binding affinities and favorable binding interactions. The binding studies are not just limited to the binding affinity between the lipid and protein. Binding affinity provides the basic information on the strength of binding between the protein and lipid ligand. In order to consider a lipid ligand as a molecular target of a protein or an enzyme,

more should be known about the atomic interaction between the lipid and protein to study the significance of that particular lipid-protein interaction. Hence, the author's study has examined the microscopic interaction of these lipid ligands with the target proteins. In order to provide this study of atomic lipid-protein interactions to all the future researchers, *Lipro Interact* facilitates the download of images that explain the binding mechanism of all eight lipid ligands with ten proteins. The validation of virtual molecular docking results with the wet laboratory experiment further improved the accuracy of the experimental findings.

In this Chapter, Section 9.2 illustrates the major contributions of the author's study of the thesis. Section 9.3 explains the possible future work on this project.

## ***9.2. Key Contributions of the Research***

It is known so far that tocotrienols are chemically more active than tocopherols. However, the author's study of the thesis explored that tocotrienols bind to PPARs and hence can be the pharmacological targets. All four types of tocotrienols have exhibited strong binding with all the three isomers of PPARs. Both tocotrienols and PPARs play an important role in the treatment of diseases like cancer, atherosclerosis, and hence, their association is further significant. The interaction of tocotrienols with RAR- $\gamma$  and RXR- $\alpha$  is interesting.  $\beta$ -,  $\gamma$ - and  $\delta$ -tocotrienols have shown a favorable interaction with RAR- $\gamma$  whereas  $\alpha$ -tocotrienol did not express considerable binding with RAR- $\gamma$ . In contrast, RXR- $\alpha$  has exhibited a strong affinity with  $\gamma$ -tocotrienol and not with the other three tocotrienols.

Interestingly, all the three isomers of PPARs have shown strong binding affinity with DHA followed by EPA in both SPA and molecular docking experiments. Hence, the author's study proposes DHA and EPA as potential drug candidates of PPARs. Even though the binding affinity of 2AG and anandamide is less compared to DHA and EPA, the strong association of 2AG and anandamide with PPARs is considerable. DHA was identified as a potential ligand

of both RAR- $\gamma$  and RXR- $\alpha$ . Comparatively DHA has expressed strong affinity with RAR- $\gamma$  and RXR- $\alpha$  than the other lipid ligands tested in the author's study. Next to DHA, EPA has shown favorable binding interactions with RAR- $\gamma$  and RXR- $\alpha$ . The endocannabinoids, 2AG and anandamide also have exhibited similar binding affinities with RAR- $\gamma$  and RXR- $\alpha$ . Finally, the author's study has identified a series of ligands for the nuclear receptors PPARs, RAR- $\gamma$  and RXR- $\alpha$ . Omega 3 fatty acids (DHA, EPA) followed by endocannabinoids and tocotrienols are the new drug candidates of nuclear receptors, PPARs, RAR- $\gamma$  and RXR- $\alpha$ .

Along with proteins, including three enzymes—COX-1, COX-2 and LOX—as target receptors for the binding studies makes the author's study unique. It is worthwhile to compare the mechanism of enzyme action with proteins and the same lipid ligands. In virtual experiments, there is not much difference in the action of enzymes with that of proteins. The wet laboratory experiment has determined the rapid action of the enzyme as the reaction rate of the enzyme progressed by the time. Conducting SPA with the enzymatic system is another interesting aspect of the author's study. The methodology of performing SPA in the enzymatic system can be used as a guideline for the future research in conducting SPA with enzymes.

COX-1 has shown strong binding affinity with EPA than with DHA. Next to the group of omega 3 fatty acids, endocannabinoids have shown strong affinity with COX-1. Comparatively, tocotrienols have expressed less affinity with COX-1. In spite of little difference in binding affinities, all the three groups of lipid ligands have shown favorable interactions with COX-1. Unlike other enzymes and targets, LOX has expressed strong binding affinity with tocotrienols. All four isomers of tocotrienols have expressed strong binding with the enzyme LOX. Omega 3 fatty acids and endocannabinoids have occupied the second and third rank respectively in the binding affinities with LOX.

Considering the biological significance of COX-2, the molecular docking findings of the author's study on COX-2 were further evaluated using the wet laboratory experiment. The wet laboratory results are in strong agreement with the virtual docking results. Both the bioinformatic and biochemical experiments have strongly indicated that DHA followed by EPA have exhibited strong binding with COX-2. The binding affinities of 2AG and anandamide are very similar to DHA and EPA. The difference in the binding affinities between these two groups with COX-2 is considerably less. Depending on the binding affinities of the three groups of lipids with COX-2, omega 3 fatty acids are ranked as, number one followed by endocannabinoids and tocotrienols.

Another group of biologically significant proteins, cannabinoid receptors have strong affinity with 2AG and anandamide followed by DHA and EPA. The author's study has revealed that DHA and EPA could be the ligands of cannabinoids receptors. Tocotrienols occupy the third position followed by endocannabinoids and omega 3 fatty acids according to their binding affinity with CB1 and CB2. The findings from molecular docking experiment indicate that  $\beta$ -tocotrienol binds to CB1 and did not bind to CB2. Hence, the author's study found that  $\beta$ -tocotrienol acts as a selective ligand of CB1. The author's study also has identified the three groups of lipid ligands as a new generation of drug candidates for both CB1 and CB2.

The comparison studies were performed for all the ten proteins individually with the eight lipid ligands. The comparison studies were also conducted between the virtual docking experiments and wet laboratory experiment. This information is ready to download from *Lipro Interact*. The author's study has generated PDB files for each lipid-protein interaction examined and the PDB files are downloadable for future use from *Lipro Interact*.

*Lipro Interact* is the innovative software developed by the author for the future studies of lipid-protein interactions. All the 80 lipid-protein interactions are put together in the form of

*Lipro Interact* software. The bioinformatic component of the author's study has revealed all the microscopic interactions of each lipid and protein, whereas the biochemical experiment has further validated the bioinformatic results.

Molecular docking is useful in the study of ligand-receptor interactions as the docking programs could analyze the microscopic atomic interactions between the ligand and receptor. However, docking has some limitation as the results depend on the structure of ligand and receptor. Further, the computational capability is limited to follow the exact modeling of the flexibility available to protein during binding process. Sometimes, inaccuracies in the energy models used to score potential ligand-receptor complexes lead to the differences in binding energies. Some docking experiments might fail due to the inability of docking method to account for conformational changes that occur during the binding process of ligand and protein (Teodoro et al., 2001). Molecular docking techniques never predict the binding energies accurately. The main advantage of molecular docking is the speed and the guidance it provides to perform wet laboratory experiments. The microscopic atomic interactions can be studied in much better way even though they do not produce accurate binding energies.

In some instances, AutoDock failed to identify the difference between similar atomic structures. For example, 2AG and anadamide yielded same binding fifties with CB1. The difference between the structures of 2AG and anandamide was not recognized by AutoDock. The Glide score or docking score is an estimate of the binding affinity and is accurate up to only few kcal/mol. Glide has been designed to achieve docking accuracy and it is difficult to produce strong correlations with experimental binding energies because of the approximations used in Glide. MD simulations are helpful to study the stability of docked complexes. However, the results of MD simulations will be realistic only if the potential energy mimics the forces experienced by the real atoms. In order to speed up the evolution of forces potential should have a simple functional form.

### 9.3. Future Work

The proposed ligands of PPARs, DHA and EPA can be further examined to design PPAR-based drugs. As the interaction of tocotrienols is determined in both wet laboratory experiment and *in silico* experiments, further work can be done to prove tocotrienols as pharmacological ligands of PPARs. The biological interaction of all the eight lipid ligands with RAR- $\gamma$  and RXR- $\alpha$  has yet to be studied using the wet laboratory experiment. The detailed binding analysis of these lipid ligands with RAR- $\gamma$  and RXR- $\alpha$  might reveal new potential targets of RAR- $\gamma$ , RXR- $\alpha$  and why all the isomers of tocotrienols did not bind to RAR- $\gamma$  and RXR- $\alpha$ .

The binding of lipid ligands with the enzymes COX-1 and LOX can be examined with a wet laboratory experiment. The virtual molecular docking experiments conducted by the author have laid a foundation for the future research on COX-1 and LOX. Further, biological experiments on COX-1 would confirm the author's findings about the selective inhibition of  $\alpha$ -tocotrienol. The author's study has demonstrated that DHA and EPA have strong binding affinity with COX-2. Hence, the potential of DHA and EPA to be the pharmacological targets can be further examined.

The binding of CB1 with the lipid ligands can be further tested in wet laboratory experiment. It is interesting to examine in wet laboratory if  $\beta$ -tocotrienol binds to CB2 as it did not produce considerable binding poses in virtual molecular docking experiments. This would further confirm the selective inhibition of  $\beta$ -tocotrienol with CB1. The potential of DHA, EPA, 2AG and anandamide to be the pharmacological ligands in the design of a new generation of cannabinoid-based drugs can be examined.

The affinity of all eight lipid ligands with ten receptors was studied during this study. The efficacy of these ligands with the target proteins can be tested in the future. The efficacy and affinity together would determine the potency of the studied ligand-receptor interactions.

The future enhancements would further develop *Lipro Interact* in different aspects. Initially, the  $K_d$  and  $K_i$  values generated from the wet laboratory experiment can be incorporated into *Lipro Interact*. At the moment, *Lipro Interact* contains only validation images in comparison of SPA with AutoDock and Glide. In future, this can be preceded by the incorporation of SPA results (such as  $K_d$  and  $K_i$  values for each protein with each ligand and graphs used to generate these values) for each protein and lipid ligand combination. Further, *Lipro Interact* can be updated with the wet laboratory experimental findings from other five proteins (COX-1, LOX, RXR- $\alpha$ , RAR- $\gamma$  and PPAR- $\delta$ ). In this case, *Lipro Interact* helps the users to find out the comparison between  $K_d$  and  $K_i$  values calculated by SPA with the binding affinities generated from AutoDock and Glide.

In order to consider the above lipid-protein interactions for the drug designing, the metabolism and mechanism of each lipid-protein interaction has to be analysed further *in vivo*. Then the action of lipid ligand over the existing drug candidate has to be compared to examine the side effects (if there are any). The side effects after the administration of drug have to be studied. For example, to consider DHA as lipid ligand for PPAR- $\gamma$  in the treatment of diabetes, the metabolism of DHA-PPAR- $\gamma$  interaction should be studied. Then, the action of DHA on PPAR- $\gamma$  has to be examined *in vivo*. If it is proved that DHA is not causing adverse side effects in the treatment of diabetes, then DHA can be used as a drug candidate for PPAR- $\gamma$  in the treatment of diabetes. Likewise, DHA and EPA can be examined further for their metabolism and inhibitory action on cyclooxygenases. The author's research has laid a foundation on the binding affinities and microscopic atomic interactions of these lipid

ligands on the target proteins. These lipid-protein interactions could be tested further to study if the ligands are acting as agonist or antagonists of the target proteins.

Basically *Lipro Interact* is useful to study the molecular mechanism of 80 lipid-protein interactions. Also, *Lipro Interact* can be updated in such a way that the software calculates the binding affinity for any protein and ligand uploaded by the users. This way, *Lipro Interact* would not limit only to ten proteins and eight lipid ligands. The type of protein-ligand interactions involved in *Lipro Interact* can also be increased with the ligand binding pocket of proteins, the three dimensional structures of lipids and proteins, etc.

MD simulation results couldn't be included in the current version of *Lipro Interact*, because MD simulation studies were performed only for the top ranked docked poses. However, in the future version the significance of *Lipro Interact* can be enormously increased by adding the MD simulation studies of all the proteins with ligands. The results from MD simulation studies include the RMSD and RMSF values for the simulated protein-ligand complexes. The MD simulation studies are useful to analyze the stability of protein structures.

Further, the improvement of *Lipro Interact* can be achieved by discussing the usability of this tool with the researchers in the field of biomedicine. Usability testing is evaluating the software with the real users. In the case of *Lipro Interact* the real users are biochemical students, researchers, drug designers and the others who wanted to study lipid-protein interactions. Usability testing can be conducted with the researchers who benefit from *Lipro Interact*. This way the usability of *Lipro Interact* can be understood and improved further. Usability evaluation is helpful to determine the extent of usability of *Lipro Interact* among the researchers and to know if there are still any gaps between ideals and realities. Then *Lipro Interact* can be modified to close these gaps. *Lipro Interact* can be improved with the results of usability testing. An evaluation study with the related researchers can be conducted to

know if *Lipro Interact* is fulfilling the purpose of its development. This study is helpful to determine the relevance of *Lipro Interact* to the user's requirements.

# Abbreviations

1. Molecular Dynamic Simulations (MD simulations)
2. Thiazolidinediones (TZDs)
3. Nonsteroidal Anti-inflammatory Drugs (NSAIDs)
4. Retinoid Xenobiotic Receptor (RXR)
5. Peroxisome Proliferator Activated Receptor (PPAR)
6. Cyclooxygenase (COX)
7. Lipoxygenase (LOX)
8. Docosahexaenoic acid (DHA)
9. Acquired Immune Deficiency Syndrome (AIDS)
10. Eicosapentanoic acid (EPA)
11. 2 Arachidonyl Glycerol (2AG)
12. Retinoic Acid Receptor (RAR- $\gamma$ )
13. Cannabinoid Receptor1 (CB1)
14. Cannabinoid Receptor2 (CB2)
15. Ligand Binding Pocket (LBP)
16. Tocotrienol Rich Fraction (TRF)
17.  $\alpha$ -Tocopherol Transport Protein ( $\alpha$ -TTP)
18. Steroid Xenobiotic Receptor (SXR)
19. Adenosine Triphosphate (ATP)
20. Farnesoid Xenobiotic Receptor (FXR)
21. PolyUnsaturated Fatty Acids (PUFAs)
22. Transient Receptor Potential Vanilloid Receptor (TRPV1)

23. Fatty Acid Amide Hydrolase (FAAH)
24.  $\Delta 9$ -tetrahydrocannabinol ( $\Delta 9$ -THC)
25. National Centre for Biotechnology Information (NCBI)
26. Research Collaboratory for Structural Bioinformatics (RCSB)
27. Standard Precession (SP)
28. Extra Precession (XP)
29. Scintillation Proximity Assay (SPA)
30. Lamarckian Genetic Algorithm (LGA)
31. Root Mean Square Deviation (RMSD)
32. Visual Molecular Dynamics (VMD)
33. AutoDock Tools (ADT)
34. Ligand Binding Domain (LBD)
35. Cutaneous T-Cell Lymphoma (CTCL)
36. N-methyl-D-aspartic Acid (NMDA)
37. Inositol Triphosphate (IP<sub>3</sub>)
38. G-protein coupled receptors (GPCRs)
39. Wheat Germ Agglutinin (WGA)
40. Graphical User Interface (GUI)

# References

- Adams, I., Compton, D., & Martin, B. (1998). Assessment of anandamide interaction with the cannabinoid brain receptor: SR 141716A antagonism studies in mice and autoradiographic analysis of receptor binding in rat brain. *Journal of Pharmacology and Experimental Therapeutics*, 284(3), 1209-1217.
- Adeniyi, A.A., & Ajibade, P.A. (2013). Comparing the suitability of autodock, gold and glide for the docking and predicting the possible targets of ru (ii)-based complexes as anticancer agents. *Molecules*, 18(4), 3760-3778.
- Aggarwal, B.B., Sundaram, C., Prasad, S., & Kannappan, R. (2010). Tocotrienols, the vitamin E of the 21st century: Its potential against cancer and other chronic diseases. *Biochemical Pharmacology*, 80(11), 1613-1631.
- Agostini, M., Schoenmakers, E., Mitchell, C., Szatmari, I., Savage, D., Smith, A., et al. (2006). Non-DNA binding, dominant-negative, human PPAR<sup>3</sup> mutations cause lipodystrophic insulin resistance. *Cell Metabolism*, 4(4), 303-311.
- Ahn, K.S., Sethi, G., Krishnan, K., & Aggarwal, B.B. (2007).  $\gamma$ -tocotrienol inhibits nuclear factor- $\kappa$ b signaling pathway through inhibition of receptor-interacting protein and tak1 leading to suppression of antiapoptotic gene products and potentiation of apoptosis. *Journal of Biological Chemistry*, 282(1), 809-820.
- Alder, B.J., & Wainwright, T.E. (1957). Phase transition for a hard sphere system. *The Journal of Chemical Physics*, 27(5), 1208-1209.
- Ali, H.I., Nagamatsu, T., & Akaho, E. (2011). Structurebased drug design and AutoDock study of potential protein tyrosine kinase inhibitors. *Bioinformation*, 5(9), 368.
- Allen, M.P. (2004). Introduction to molecular dynamics simulation. *Computational Soft Matter: From Synthetic Polymers to Proteins*, 23, 1-28.
- Altucci, L., Leibowitz, M.D., Ogilvie, K.M., de Lera, A.R., & Gronemeyer, H. (2007). RAR and RXR modulation in cancer and metabolic disease. *Nature Reviews Drug Discovery*, 6(10), 793-810.
- Anderson A. C. (2003). The process of structure-based drug design. *Chemistry & Biology*, 10(9), 787-797.
- Aparoy P., Reddy, K. K., et al. (2012). Structure and ligand based drug design strategies in the development of novel 5-LOX inhibitors. *Current Medicinal Chemistry*, 19(22), 3763.
- Appa, Y. (1999). Retinoid therapy: compatible skin care. *Skin Pharmacology and Physiology*, 12(3), 111-119.
- ASP.NET vs PHP (2015). Retrieved 13/07, 2015.
- Auld D.S., Farmen MW, Kahl S.D., et al. Receptor binding assays for HTS and drug discovery. 2012 May 1 [Updated 2012 Oct 1]. In: Sittampalam GS, Coussens NP, Nelson H, et al., editors. Assay Guidance Manual [Internet]. Bethesda (MD): Eli Lilly & Company and

the National Center for Advancing Translational Sciences; 2004-. Available from: <http://europepmc.org/books/NBK91992;jsessionid=oDaowiUovTn01bY15Do4.3>

Balvers, M.G.J., Verhoeckx, K.C.M., Plastina, P., Wortelboer, H.M., Meijerink, J., & Witkamp, R.F. (2010). Docosahexaenoic acid and eicosapentaenoic acid are converted by 3T3-L1 adipocytes to N-acyl ethanolamines with anti-inflammatory properties. *Biochimica et Biophysica Acta (BBA) - Molecular and Cell Biology of Lipids*, 1801(10), 1107-1114.

Barroso, I., Gurnell, M., Crowley, V., Agostini, M., Schwabe, J., Soos, M., *et al.* (1999). Dominant negative mutations in human PPAR $\gamma$  associated with severe insulin resistance, diabetes mellitus and hypertension. *Nature*, 402(6764), 880-883.

Bass, R., Engelhard, D., Trembovler, V., & Shohami, E. (1996). A novel nonpsychotropic cannabinoid, HU-211, in the treatment of experimental pneumococcal meningitis. *Journal of Infectious Diseases*, 173(3), 735-738.

Belloni, P. N., & Klaus, M. (2001). Treatment of emphysema using RAR $\gamma$  selective retinoid agonists: U.S. Patent No. 6,300,350. Washington, DC: U.S. Patent and Trademark Office.

Berry, J., Price-Jones, M., & Killian, B. (2012). Use of Scintillation Proximity Assay to measure radioligand binding to immobilized receptors without separation of bound from free ligand. *Receptor Binding Techniques*, 897, 79-94.

Binda, C., Li, M., Hubálek, F., Restelli, N., Edmondson, D.E., & Mattevi, A. (2003). Insights into the mode of inhibition of human mitochondrial monoamine oxidase B from high-resolution crystal structures. *Proceedings of the National Academy of Sciences*, 100(17), 9750-9755.

Bíró, T., Tóth, B.I., Haskó, G., Paus, R., & Pacher, P. (2009). The endocannabinoid system of the skin in health and disease: novel perspectives and therapeutic opportunities. *Trends in Pharmacological Sciences*, 30(8), 411-420.

Bissantz, C., Folkers, G., & Rognan, D. (2000). Protein-Based Virtual Screening of Chemical Databases. 1. Evaluation of Different Docking/Scoring Combinations. *Journal of Medicinal Chemistry*, 43 (25), 4759-4767.

Bongrand, P. (1999). Ligand-receptor interactions. *Reports on Progress in Physics*, 62, 921-968.

Bouaboula, M., Hilairet, S., Marchand, J., Fajas, L., Fur, G.L., & Casellas, P. (2005). Anandamide induced PPAR $\gamma$  transcriptional activation and 3T3-L1 preadipocyte differentiation. *European Journal of Pharmacology*, 517(3), 174-181.

Bowers, K.J., Chow, E., Xu, H., Dror, R.O., Eastwood, M.P., Gregersen, B.A., *et al.* (2006). Scalable algorithms for molecular dynamics simulations on commodity clusters. Paper presented at the SC 2006 Conference, Proceedings of the ACM/IEEE.

Brash, A.R. (1999). Lipoxygenases: occurrence, functions, catalysis, and acquisition of substrate. *Journal of Biological Chemistry*, 274(34), 23679-23682.

Brown, I., Cascio, M.G., Wahle, K.W., Smoum, R., Mechoulam, R., Ross, R.A., *et al.* (2010). Cannabinoid receptor-dependent and-independent anti-proliferative effects of omega-3 ethanolamides in androgen receptor-positive and-negative prostate cancer cell lines. *Carcinogenesis*, 31(9), 1584-1591.

Brown, J.R., & DuBois, R.N. (2005). COX-2: A Molecular Target for Colorectal Cancer Prevention. *Journal of Clinical Oncology*, 23(12), 2840-2855.

Buaud, B., Esterle, L., Vaysse, C., Alfos, S., Combe, N., Higueret, P., et al. (2010). A high-fat diet induces lower expression of retinoid receptors and their target genes GAP-43/neuromodulin and RC3/neurogranin in the rat brain. *British Journal of Nutrition*, 103(12), 1720-1729.

Burke, S. (2014). Using the Microsoft .NET Framework to Create Windows-based Applications. *Microsoft Developer Network* Retrieved 23/11/2014, 2014, from <http://msdn.microsoft.com/en-us/library/ms973883.aspx>

Burnett, B.P., & Levy, R.M. (2012). 5-Lipoxygenase metabolic contributions to NSAID-induced organ toxicity. *Advances in Therapy*, 29(2), 79-98.

Buzko, O., Bishop, A., & Shokat, K. (2002). Modified AutoDock for accurate docking of protein kinase inhibitors. *Journal of Computer-Aided Molecular Design*, 16(2), 113-127.

Caffrey, M., & Hogan, J. (1992). LIPIDAT: A database of lipid phase transition temperatures and enthalpy changes. DMPC data subset analysis. *Chemistry and Physics of Lipids*, 61(1), 1-109.

Calder, P.C. (2006). Long-chain polyunsaturated fatty acids and inflammation. *Food & Nutrition Research*, 50, 54-61.

Calignano, A., La Rana, G., Giuffrida, A., & Piomelli, D. (1998). Control of pain initiation by endogenous cannabinoids. *Nature*, 394(6690), 277-281.

Cannabis Oil : Raided for helping their son. (2014). Sunday Night. Melbourne, Australia: Channel 7.

Cer, R.Z., Mudunuri, U., Stephens, R., & Lebeda, F.J. (2009). IC50-to-Ki: a web-based tool for converting IC50 to Ki values for inhibitors of enzyme activity and ligand binding. *Nucleic Acids Research*, 37(suppl 2), W441-W445.

Chang, Y., Ganesh, T., Horton, J.R., Spannhoff, A., Liu, J., Sun, A., et al. (2010). Adding a lysine mimic in the design of potent inhibitors of histone lysine methyltransferases. *Journal of Molecular Biology*, 400(1), 1-7.

Chávez, A.E., Chiu, C.Q., & Castillo, P.E. (2010). TRPV1 activation by endogenous anandamide triggers postsynaptic long-term depression in dentate gyrus. *Nature Neuroscience*, 13(12), 1511-1518.

ChemSketch. (1996). Retrieved from [www.acdlabs.com](http://www.acdlabs.com)

Chen, K., James Adelstein, S., & Kassis, A.I. (2004). Molecular simulation of ligand-binding with DNA: implications for 125I-labeled pharmaceutical design. *International Journal of Radiation Biology*, 80(11-12), 921-926.

Chen, S., Costa, C.H.R.M., Nakamura, K., Ribeiro, R.C.J., & Gardner, D.G. (1999). Vitamin D-dependent suppression of human atrial natriuretic peptide gene promoter activity requires heterodimer assembly. *Journal of Biological Chemistry*, 274(16), 11260-11266.

- Cheng Y.C., Prosooff W.H. (1973). Relationship between the inhibition constant and the concentration of inhibitor which causes 50 per cent inhibition of an enzymatic reaction. *Biochemical Pharmacology*, 22(23), 3099-3108.
- Chomienne, C., Ballerini, P., Balirand, N., Amar, M., François Bernard, J., Boivin, P., et al. (1989). Retinoic acid therapy for promyelocytic leukaemia. *The Lancet*, 334(8665), 746-747.
- Clark, W.F., Parbtani, A., Naylor, C.D., Levinton, C., Muirhead, N., Spanner, E., et al. (1993). Fish oil in lupus nephritis: clinical findings and methodological implications. *Kidney International*, 44, 75-75.
- Collino, M., Patel, N.S.A., & Thiemermann, C. (2008). Review: PPARs as new therapeutic targets for the treatment of cerebral ischemia/reperfusion injury. *Therapeutic Advances in Cardiovascular Disease*, 2(3), 179-197.
- Colombo, G., Agabio, R., Diaz, G., Lobina, C., Reali, R., & Gessa, G.L. (1998). Appetite suppression and weight loss after the cannabinoid antagonist SR 141716. *Life Sciences*, 63(8), PL113-PL117.
- Colovos, C., & Yeates, T.O. (1993). Verification of protein structures: patterns of nonbonded atomic interactions. *Protein Science*, 2(9), 1511-1519.
- Comitato, R., Nesaretnam, K., Leoni, G., Ambra, R., Canali, R., Bolli, A., et al. (2009). A novel mechanism of natural vitamin E tocotrienol activity: involvement of ER $\beta$  signal transduction. *American Journal of Physiology-Endocrinology and Metabolism*, 297(2), E427-E437.
- Connors, R.V., Wang, Z., Harrison, M., Zhang, A., Wanska, M., Hiscock, S., et al. (2009). Identification of a PPAR $\delta$  agonist with partial agonistic activity on PPAR $\gamma$ . *Bioorganic & Medicinal Chemistry Letters*, 19(13), 3550-3554.
- Cory, J. (2014). Structured Systems Analysis and Design Method Retrieved from <http://www.techopedia.com/about/contact.aspx>
- Cotter, D., Maer, A., Guda, C., Saunders, B., & Subramaniam, S. (2006). LMPD: Lipid maps proteome database. *Nucleic Acids Research*, 34(suppl 1), D507-D510.
- Cottin, S., Sanders, T., & Hall, W. (2011). The differential effects of EPA and DHA on cardiovascular risk factors. *Proceedings of the Nutrition Society*, 70(02), 215-231.
- Cramer, F. (1994). Emil Fischer's Lock-and-Key Hypothesis after 100 years-Towards a Supracellular Chemistry'. Perspectives in Supramolecular Chemistry: The Lock-and-Key Principle, 1, 1-23.
- Crespi, V., Galstyan, A., & Lerman, K. (2005). Comparative analysis of top-down and bottom-up methodologies for multi-agent system design. Paper presented at the Proceedings of the fourth international joint conference on Autonomous agents and multiagent systems.
- Cross, J.B., Thompson, D.C., Rai, B.K., Baber, J.C., Fan, K.Y., Hu, Y., et al. (2009). Comparison of Several Molecular Docking Programs: Pose Prediction and Virtual Screening Accuracy. *Journal of Chemical Information and Modeling*, 49(6), 1455-1474.
- Crowe, D., & Chandraratna, R. (2004). A retinoid X receptor (RXR)-selective retinoid reveals that RXR- $\alpha$  is potentially a therapeutic target in breast cancer cell lines, and that it

potentiates antiproliferative and apoptotic responses to peroxisome proliferator-activated receptor ligands. *Breast Cancer Research*, 6(5), 1-10.

Davies, S.N., Pertwee, R.G., & Riedel, G. (2002). Functions of cannabinoid receptors in the hippocampus. *Neuropharmacology*, 42(8), 993-1007.

de Lera, A.R., Bourguet, W., Altucci, L., & Gronemeyer, H. (2007). Design of selective nuclear receptor modulators: RAR and RXR as a case study. *Nature Reviews Drug Discovery*, 6(10), 811-820.

Deb, P.K., Sharma, A., Piplani, P., & Akkinepally, R.R. (2012). Molecular docking and receptor-specific 3D-QSAR studies of acetylcholinesterase inhibitors. *Molecular Diversity*, 16(4), 803-823.

Deckelbaum, R.J., Worgall, T.S., & Seo, T. (2006). n-3 fatty acids and gene expression. *The American Journal of Clinical Nutrition*, 83(6), S1520-1525S.

Deeb, S.S., Fajas, L., Nemoto, M., Pihlajamäki, J., Mykkänen, L., Kuusisto, J., et al. (1998). A Pro12Ala substitution in PPAR $\gamma$ 2 associated with decreased receptor activity, lower body mass index and improved insulin sensitivity. *Nature Genetics*, 20(3), 284-287.

Deng, W., & Verlinde, C.L. (2008). Evaluation of different virtual screening programs for docking in a charged binding pocket. *Journal of Chemical Information and Modeling*, 48(10), 2010-2020.

Desmond. (2012). Schrodinger (Version 3.1). New York: D.E.Shaw Reserach

Deutsch, D.G., & Chin, S.A. (1993). Enzymatic synthesis and degradation of anandamide, a cannabinoid receptor agonist. *Biochemical Pharmacology*, 46(5), 791-796.

DeWitt, D.L. (1999). Cox-2-Selective Inhibitors: The New Super Aspirins. *Molecular Pharmacology*, 55(4), 625-631.

Di Marzo, V., Bifulco, M., & De Petrocellis, L. (2004). The endocannabinoid system and its therapeutic exploitation. *Nature Reviews Drug Discovery*, 3(9), 771-784.

Di Marzo, V., Breivogel, C.S., Tao, Q., Bridgen, D.T., Razdan, R.K., Zimmer, A.M., et al. (2000). Levels, metabolism, and pharmacological activity of anandamide in CB1 cannabinoid receptor knockout mice. *Journal of Neurochemistry*, 75(6), 2434-2444.

Di Pasquale, E., Chahinian, H., Sanchez, P., & Fantini, J. (2009). The insertion and transport of anandamide in synthetic lipid membranes are both cholesterol-dependent. *PLoS One*, 4(3), e4989.

Ding, X.-Z., Hennig, R., & Adrian, T. (2003). Lipoxygenase and cyclooxygenase metabolism: new insights in treatment and chemoprevention of pancreatic cancer. *Molecular Cancer*, 2(1), 1-12.

Doyle, D.F., Braasch, D.A., Jackson, L.K., Weiss, H.E., Boehm, M.F., Mangelsdorf, D.J., et al. (2001). Engineering orthogonal ligand-receptor pairs from "near drugs". *Journal of American Chemical Society*, 123(46), 11367-11371.

- Egea, P.F., Mitschler, A., Rochel, N., Ruff, M., Chambon, P., & Moras, D. (2000). Crystal structure of the human RXR $\alpha$  ligand-binding domain bound to its natural ligand: 9-cis retinoic acid. *The EMBO Journal*, 19(11), 2592-2601.
- Evans, D., Aberle, J., Wendt, D., Wolf, A., Beisiegel, U., & Mann, W. (2001). A polymorphism, L162V, in the peroxisome proliferator-activated receptor  $\alpha$  (PPAR  $\alpha$ ) gene is associated with lower body mass index in patients with non-insulin-dependent diabetes mellitus. *Journal of Molecular Medicine*, 79(4), 198-204.
- Evans, R.M., Barish, G.D., & Wang, Y.-X. (2004). PPARs and the complex journey to obesity. *Nature Medicine*, 10(4), 355-361.
- Ewing, T.J., Makino, S., Skillman, A.G., & Kuntz, I.D. (2001). DOCK 4.0: search strategies for automated molecular docking of flexible molecule databases. *Journal of Computer-Aided Molecular Design*, 15(5), 411-428.
- Fahy, E., Sud, M., Cotter, D., & Subramaniam, S. (2007). LIPID MAPS online tools for lipid research. *Nucleic Acids Research*, 35(suppl 2), W606-W612.
- Fairus, S., Nor, R.M., Cheng, H.M., & Sundram, K. (2006). Postprandial metabolic fate of tocotrienol-rich vitamin E differs significantly from that of  $\alpha$ -tocopherol. *The American Journal of Clinical Nutrition*, 84(4), 835-842.
- Fang, F., Kang, Z., & Wong, C. (2010). Vitamin E tocotrienols improve insulin sensitivity through activating peroxisome proliferator-activated receptors. *Molecular Nutrition & Food Research*, 54(3), 345-352.
- Fattore, L., & Fratta, W. (2011). Beyond THC: the new generation of cannabinoid designer drugs. *Frontiers in Behavioral Neuroscience*, 5.
- Felder, C.C., Joyce, K.E., Briley, E.M., Glass, M., Mackie, K.P., Fahey, K.J., et al. (1998). LY320135, a novel cannabinoid CB1 receptor antagonist, unmasks coupling of the CB1 receptor to stimulation of cAMP accumulation. *Journal of Pharmacology and Experimental Therapeutics*, 284(1), 291-297.
- Fowler, C.J. (2007). The contribution of cyclooxygenase-2 to endocannabinoid metabolism and action. *British Journal of Pharmacology*, 152(5), 594-601.
- Francis, G., Li, G., Casey, R., Wang, J., Cao, H., Leff, T., et al. (2006). Peroxisomal proliferator activated receptor- $\gamma$  deficiency in a Canadian kindred with familial partial lipodystrophy type 3 (FPLD3). *BMC Medical Genetics*, 7(1), 1-7.
- Friesner, R., Banks, J., Murphy, R., Halgren, T., Klicic, J., Mainz, D., et al. (2004). Glide: a new approach for rapid, accurate docking and scoring. 1. Method and assessment of docking accuracy. *Journal of Medicinal Chemistry*, 47, 1739 - 1749.
- Friesner, R.A., Murphy, R.B., Repasky, M.P., Frye, L.L., Greenwood, J.R., Halgren, T.A., et al. (2006). Extra precision glide: docking and scoring incorporating a model of hydrophobic enclosure for protein-ligand complexes. *Journal of Medicinal Chemistry*, 49(21), 6177-6196.
- Fu, J.-Y., Che, H.-L., Tan, D., & Teng, K.-T. (2014). Bioavailability of tocotrienols: evidence in human studies. *Nutrition Metabolism*, 11(1), 5.

- Funahashi, H., Satake, M., Hasan, S., Sawai, H., Newman, R.A., Reber, H.A., et al. (2008). Opposing effects of n-6 and n-3 polyunsaturated fatty acids on pancreatic cancer growth. *Pancreas*, 36(4), 353-362.
- Furse, K.E., Pratt, D.A., Porter, N.A., & Lybrand, T.P. (2006). Molecular dynamics simulations of arachidonic acid complexes with cox-1 and cox-2: insights into equilibrium behavior. *Biochemistry*, 45(10), 3189-3205.
- Gaddipati, R.S., Raikundalia, G.K., & Mathai, M.L. (2012). *Towards the Design of PPAR based Drugs using tocotrienol as natural ligands-A Docking Analysis*. Paper presented at the International Conference on Engineering and Applied Sciences, Beijing.
- Gaddipati, R.S., Raikundalia, G.K., & Mathai, M.L. (2014a). Comparison of AutoDock and Glide towards the Discovery of PPAR Agonists. *International Journal of Bioscience, Biochemistry and Bioinformatics*, 4(2), 100-105.
- Gaddipati, R.S., Raikundalia, G.K., & Mathai, M.L. (2014). Dual and selective lipid inhibitors of cyclooxygenases and lipoxygenase: a molecular docking study. *Medicinal Chemistry Research*, 23(7), 3389-3402.
- Gan, T.J. (2010). Diclofenac: an update on its mechanism of action and safety profile. *Current Medical Research & Opinion*, 26(7), 1715-1731.
- Gani, & Sylte. (2008). Molecular recognition of Docosahexaenoic acid by peroxisome proliferator-activated receptors and retinoid-X receptor  $\alpha$ . *Journal of Molecular Graphics and Modelling*, 27(2), 217-224.
- Gee, P.T. (2011). Vitamin E—essential knowledge for supplementation. *Lipid Technology*, 23(4), 79-82.
- Germain, P., Chambon, P., Eichele, G., Evans, R.M., Lazar, M.A., Leid, M., et al. (2006a). International union of pharmacology. LX. retinoic acid receptors. *Pharmacological Reviews*, 58(4), 712-725.
- Germain, P., Chambon, P., Eichele, G., Evans, R.M., Lazar, M.A., Leid, M., et al. (2006b). International union of pharmacology. LXIII. retinoid X receptors. *Pharmacological Reviews*, 58(4), 760-772.
- Germain, P., Kammerer, S., Perez, E., Peluso-Iltis, C., Tortolani, D., Zusi, F.C., et al. (2004). Rational design of RAR-selective ligands revealed by RAR $\beta$  crystal structure. *EMBO reports*, 5(9), 877-882.
- Glaser, F., Morris, R.J., Najmanovich, R.J., Laskowski, R.A., & Thornton, J.M. (2006). A method for localizing ligand binding pockets in protein structures. *Proteins: Structure, Function, and Bioinformatics*, 62(2), 479-488.
- Glide. (2011). Schrodinger (Version 5.7). New York: LLC.
- Gonsiorek, W., Lunn, C., Fan, X., Narula, S., Lundell, D., & Hipkin, R.W. (2000). Endocannabinoid 2-arachidonoyl glycerol is a full agonist through human type 2 cannabinoid receptor: antagonism by anandamide. *Molecular Pharmacology*, 57(5), 1045-1050.
- Goodsell, D.S. (2000). The molecular perspective: cyclooxygenase-2. *The Oncologist*, 5(2), 169-171.

- Grether, U., Bénardeau, A., Benz, J., Binggeli, A., Blum, D., Hilpert, H., *et al.* (2009). Design and biological evaluation of novel, balanced dual PPAR $\alpha/\gamma$  agonists. *ChemMedChem*, 4(6), 951-956.
- Griffin, G., Wray, E.J., Tao, Q., McAllister, S.D., Rorrer, W.K., Aung, M., *et al.* (1999). Evaluation of the cannabinoid CB2 receptor-selective antagonist, SR144528: further evidence for cannabinoid CB2 receptor absence in the rat central nervous system. *European Journal of Pharmacology*, 377(1), 117-125.
- Guo, Z., Mohanty, U., Noehre, J., Sawyer, T.K., Sherman, W., & Krilov, G. (2010). Probing the  $\alpha$ -Helical Structural Stability of Stapled p53 Peptides: Molecular Dynamics Simulations and Analysis. *Chemical Biology & Drug Design*, 75(4), 348-359.
- Guthrie, N., Gapor, A., Chambers, A.F., & Carroll, K.K. (1997). Inhibition of Proliferation of Estrogen Receptor-Negative MDA-MB-435 and -Positive MCF-7 Human Breast Cancer Cells by Palm Oil Tocotrienols and Tamoxifen, Alone and in Combination. *The Journal of Nutrition*, 127(3), 544S-548S.
- Guzman, M.F. (2015). Pharmacodynamics animation: full agonists, partial agonists, inverse agonists, competitive antagonists and irreversible antagonists. Retrieved 27/04/2015, 2015, from <http://pharmacologycorner.com/pharmacodynamics-animation-full-agonists-partial-agonists-inverse-agonists-competitive-antagonists-and-irreversible-antagonists/>
- Hansson T., Oostenbrink, C., & Van Gunsteren, W. (2002). Molecular dynamics simulations. *Current Opinion in Structural Biology*, 12, 190-196.
- Harris, C.R., & Brown, A. (2013). Synthetic cannabinoid intoxication: a case series and review. *The Journal of Emergency Medicine*, 44(2), 360-366.
- Hart, H.E., & Greenwald, E.B. (1979). Scintillation Proximity Assay (SPA)—A new method of immunoassay: Direct and inhibition mode detection with human albumin and rabbit antihuman albumin. *Molecular Immunology*, 16(4), 265-267.
- Hawcroft, G., Loadman, P.M., Belluzzi, A., & Hull, M.A. (2010). Effect of Eicosapentaenoic Acid on E-type Prostaglandin Synthesis and EP4 Receptor Signaling Human Colorectal Cancer Cells. *Neoplasia*, 12(8), 618-IN612.
- Hayes, J.M., Skamnaki, V.T., Archontis, G., Lamprakis, C., Sarrou, J., Bischler, N., *et al.* (2011). Kinetics, in silico docking, molecular dynamics, and MM-GBSA binding studies on prototype indirubins, KT5720, and staurosporine as phosphorylase kinase ATP-binding site inhibitors: The role of water molecules examined. *Proteins: Structure, Function, and Bioinformatics*, 79(3), 703-719.
- Hendrich, S., Lee, K.W., Xu, X., Wang, H.J., & Murphy, P.A. (1994). Defining Food components as new nutrients. *The Journal of Nutrition*, 124(9 Suppl), 1789S-1792S.
- Hetényi, C., & van der Spoel, D. (2002). Efficient docking of peptides to proteins without prior knowledge of the binding site. *Protein science*, 11(7), 1729-1737.
- Hillard, C.J., & Jarrahian, A. (2005). Accumulation of anandamide: evidence for cellular diversity. *Neuropharmacology*, 48(8), 1072-1078.

- Hincha, D.K. (2008). Effects of  $\alpha$ -tocopherol (vitamin E) on the stability and lipid dynamics of model membranes mimicking the lipid composition of plant chloroplast membranes. *FEBS Letters*, 582(25–26), 3687-3692.
- Hohmann, A.G., Farthing, J.N., Zvonok, A.M., & Makriyannis, A. (2004). Selective activation of cannabinoid CB<sub>2</sub> receptors suppresses hyperalgesia evoked by intradermal capsaicin. *Journal of Pharmacology and Experimental Therapeutics*, 308(2), 446-453.
- Howlett, A., Barth, F., Bonner, T., Cabral, G., Casellas, P., Devane, W., et al. (2002). International Union of Pharmacology. XXVII. Classification of cannabinoid receptors. *Pharmacological Reviews*, 54(2), 161-202.
- Howlett, A., Johnson, M.R., Melvin, L., & Milne, G. (1988). Nonclassical cannabinoid analgetics inhibit adenylate cyclase: development of a cannabinoid receptor model. *Molecular Pharmacology*, 33(3), 297-302.
- Howlett, A.C. (1995). Pharmacology of cannabinoid receptors. *Annual Review of Pharmacology and Toxicology*, 35(1), 607-634.
- Hu, F.B., Bronner, L., & Willett, W.C. (2002). Fish and omega-3 fatty acid intake and risk of coronary heart disease in women. *The Journal of American Medical Association*, 287(14), 1815-1821.
- Huang, N., Shoichet, B.K., & Irwin, J.J. (2006). Benchmarking Sets for Molecular Docking. *Journal of Medicinal Chemistry*, 49(23), 6789-6801.
- Huber W., & Mueller, F. (2006). Biomolecular interaction analysis in drug discovery using surface plasmon resonance technology. *Current Pharmaceutical Design*, 12(31), 3999-4021.
- Hudson, N., Balsitis, M., Everitt, S., & Hawkey, C. (1993). Enhanced gastric mucosal leukotriene B<sub>4</sub> synthesis in patients taking non-steroidal anti-inflammatory drugs. *Gut*, 34(6), 742-747.
- Huss, U., Ringbom, T., Perera, P., Bohlin, L., & Vasänge, M. (2002). Screening of ubiquitous plant constituents for COX-2 inhibition with a scintillation proximity based assay. *Journal of Natural Products*, 65(11), 1517-1521.
- Hustert, E., Zibat, A., Presecan-Siedel, E., Eiselt, R., Mueller, R., Fuß, C., et al. (2001). Natural protein variants of pregnane X receptor with altered transactivation activity toward CYP3A4. *Drug Metabolism and Disposition*, 29(11), 1454-1459.
- ido.net. (2010). Advantages of ASP.Net Framework Retrieved 21/11/2014, from <http://www.ido.net>ShowArticle/54/advantages-of-aspnet-framework>
- Imaiizumi, M., Suzuki, H., Yoshinari, M., Sato, A., Saito, T., Sugawara, A., et al. (1998). Mutations in the E-domain of RAR $\alpha$  portion of the PML/RAR $\alpha$  chimeric gene may confer clinical resistance to all-transretinoic acid in acute promyelocytic leukemia. *Blood*, 92(2), 374-382.
- Impref. (2011). Schrodinger (Version Impact version 5.7). New York: LLC.
- Iwata, M., Haruta, T., Usui, I., Takata, Y., Takano, A., Uno, T., et al. (2001). Pioglitazone ameliorates tumor necrosis factor- $\alpha$ -induced insulin resistance by a mechanism independent

of adipogenic activity of peroxisome proliferator-activated receptor- $\gamma$ . *Diabetes*, 50(5), 1083-1092.

Iwata, Y., Miyamoto, S., Takamura, M., Yanagisawa, H., & Kasuya, A. (2001). Interaction between peroxisome proliferator-activated receptor  $\gamma$  and its agonists: docking study of oximes having 5-benzyl-2, 4-thiazolidinedione. *Journal of Molecular Graphics and Modelling*, 19(6), 536-542.

Jeninga, E.H., van Beekum, O., van Dijk, A.D.J., Hamers, N., Hendriks-Stegeman, B.I., Bonvin, A.M.J.J., et al. (2007). Impaired peroxisome proliferator-activated receptor  $\gamma$  function through mutation of a conserved salt bridge (R425C) in familial partial lipodystrophy. *Molecular Endocrinology*, 21(5), 1049-1065.

Jhaveri, M., Richardson, D., & Chapman, V. (2007). Endocannabinoid metabolism and uptake: novel targets for neuropathic and inflammatory pain. *British Journal of Pharmacology*, 152(5), 624-632.

Jonsson, K.-O., Holt, S., & Fowler, C.J. (2006). The endocannabinoid system: current pharmacological research and therapeutic possibilities. *Basic & Clinical Pharmacology & Toxicology*, 98(2), 124-134.

Kalva, S., Vadivelan, S., & Jagarlapudi, S. (2011). *Pharmacophore design, homology and docking studies on 5-lipoxygenase inhibitors*. Paper presented at the International Conference on Bioscience, Biochemistry and Bioinformatics.

Kano, M., Ohno-Shosaku, T., Hashimotodani, Y., Uchigashima, M., & Watanabe, M. (2009). Endocannabinoid-mediated control of synaptic transmission. *Physiological Reviews*, 89(1), 309-380.

Kastner, P., Mark, M., & Chambon, P. (1995). Nonsteroid nuclear receptors: what are genetic studies telling us about their role in real life? *Cell*, 83(6), 859-869.

Katz, H.I., Waalen, J., & Leach, E.E. (1999). Acitretin in psoriasis: an overview of adverse effects. *Journal of the American Academy of Dermatology*, 41(3), S7-S12.

Kellenberger, E., Rodrigo, J., Muller, P., & Rognan, D. (2004). Comparative evaluation of eight docking tools for docking and virtual screening accuracy. *Proteins: Structure, Function, and Bioinformatics* 57(2), 225-242.

Keriel, A., Stary, A., Sarasin, A., Rochette-Egly, C., & Egly, J.M. (2002). XPD mutations prevent tfiIih-dependent transactivation by nuclear receptors and phosphorylation of RARalpha. *Cell*, 109(1), 125-135.

Khan, Akhtar, S., Al-Sagair, O.A., & Arif, J.M. (2011). Protective effect of dietary tocotrienols against infection and inflammation-induced hyperlipidemia: an in vivo and in silico study. *Phytotherapy Research*, 25(11), 1586-1595.

Khan, M., Khan, M., Siddiqui, M., & Arif, J. (2011). An in vivo and in silico approach to elucidate the Tocotrienol-mediated fortification against infection and inflammation induced alterations in antioxidant defense system. *European Review for Medical and Pharmacological Sciences*, 15(8), 916-930.

Khanna, S., Roy, S., Ryu, H., Bahadduri, P., Swaan, P.W., Ratan, R.R., et al. (2003). Molecular basis of vitamin E Action: tocotrienol modulates 12-lipoxygenase, a key mediator

of glutamate-induced neurodegeneration. *Journal of Biological Chemistry*, 278(44), 43508-43515.

Klaholz, B., Renaud, J.-P., Mitschler, A., Zusi, C., Chambon, P., Gronemeyer, H., et al. (1998). Conformational adaptation of agonists to the human nuclear receptor RAR $\gamma$ . *Nature Structural & Molecular Biology*, 5(3), 199-202.

Kliewer, S.A., Sundseth, S.S., Jones, S.A., Brown, P.J., Wisely, G.B., Koble, C.S., et al. (1997). Fatty acids and eicosanoids regulate gene expression through direct interactions with peroxisome proliferator-activated receptors  $\alpha$  and  $\gamma$ . *Proceedings of the National Academy of Sciences*, 94(9), 4318-4323.

Koshland, D.E. (1995). The key-lock theory and the induced fit theory. *Angewandte Chemie International Edition in English*, 33(23-24), 2375-2378.

Koyano, S., Kurose, K., Saito, Y., Ozawa, S., Hasegawa, R., Komamura, K., et al. (2004). Functional characterization of four naturally occurring variants of human pregnane X receptor (PXR): one variant causes dramatic loss of both DNA binding activity and the transactivation of the CYP3A4 promoter/enhancer region. *Drug Metabolism and Disposition*, 32(1), 149-154.

Kozak, K.R., Prusakiewicz, J.J., & Marnett, L.J. (2004). Oxidative metabolism of endocannabinoids by COX-2. *Current Pharmaceutical Design*, 10(6), 659-667.

Kozak, K.R., Rowlinson, S.W., & Marnett, L.J. (2000). Oxygenation of the endocannabinoid, 2-arachidonylglycerol, to glyceryl prostaglandins by cyclooxygenase-2. *Journal of Biological Chemistry*, 275(43), 33744-33749.

Kramer, B., Rarey, M., & Lengauer, T. (1999). Evaluation of the FLEXX incremental construction algorithm for protein-ligand docking. *Proteins: Structure, Function, and Bioinformatics*, 37(2), 228-241.

Kroemer, R.T., Vulpetti, A., McDonald, J.J., Rohrer, D.C., Trosset, J.-Y., Giordanetto, F., et al. (2004). assessment of docking poses: interactions-based accuracy classification (IBAC) versus crystal structure deviations. *Journal of Chemical Information and Computer Sciences*, 44(3), 871-881.

Krönke, G., Katzenbeisser, J., Uderhardt, S., Zaiss, M. M., Scholtysek, C., Schabbauer, G., et al. (2009). 12/15-Lipoxygenase Counteracts Inflammation and Tissue Damage in Arthritis. *The Journal of Immunology*, 183(5), 3383-3389.

Krovat, E. M., Steindl, T., & Langer, T. (2005). Recent advances in docking and scoring. *Current Computer - Aided Drug Design*, 1(1), 93-102.

Kuhn, H. (2005). Biologic relevance of lipoxygenase isoforms in atherosclerosis. *Expert Review of Cardiovascular Therapy*, 3(6), 1099-1110.

Kuntz, I.D., Blaney, J.M., Oatley, S.J., Langridge, R., & Ferrin, T.E. (1982). A geometric approach to macromolecule-ligand interactions. *Journal of Molecular Biology*, 161(2), 269-288.

Kuzmanic, A., & Zagrovic, B. (2010). Determination of ensemble-average pairwise root mean-square deviation from experimental B-factors. *Biophysical Journal*, 98(5), 861-871.

- Lafourcade, M., Larrieu, T., Mato, S., Duffaud, A., Sepers, M., Matias, I., et al. (2011). Nutritional omega-3 deficiency abolishes endocannabinoid-mediated neuronal functions. *Nature Neuroscience*, 14(3), 345-350.
- Lape, M., Elam, C., & Paula, S. (2010). Comparison of current docking tools for the simulation of inhibitor binding by the transmembrane domain of the sarco/endoplasmic reticulum calcium ATPase. *Biophysical Chemistry*, 150(1–3), 88-97.
- Larsson, M. (2004). Predicting quality attributes in component-based software systems: Mälardalen University.
- Laskowski, R.A., & Swindells, M.B. (2011). LigPlot+: multiple ligand–protein interaction diagrams for drug discovery. *Journal of Chemical Information and Modeling*, 51(10), 2778-2786.
- Lavigne, A.-C., Mengus, G., Gangloff, Y.-G., Wurtz, J.-M., & Davidson, I. (1999). Human TAFII55 Interacts with the Vitamin D<sub>3</sub> and Thyroid Hormone Receptors and with Derivatives of the Retinoid X Receptor That Have Altered Transactivation Properties. *Molecular and Cellular Biology*, 19(8), 5486-5494.
- Lazareno, S., & Birdsall, N. (1993). Estimation of antagonist from inhibition curves in functional experiments: alternatives to the Cheng-Prusoff equation. *Trends in Pharmacological Sciences*, 14(6), 237-239.
- Le Foll, B., Gorelick, D.A., & Goldberg, S.R. (2009). The future of endocannabinoid-oriented clinical research after CB1 antagonists. *Psychopharmacology*, 205(1), 171-174.
- Lee, J.Y., & Hwang, D.H. (2002). Docosahexaenoic acid suppresses the activity of peroxisome proliferator-activated receptors in a colon tumor cell line. *Biochemical and Biophysical Research Communications*, 298(5), 667-674.
- Lee, S.-K., Lee, B., & Lee, J.W. (2000). Mutations in Retinoid X Receptor that impair heterodimerization with specific nuclear hormone receptor. *Journal of Biological Chemistry*, 275 (43), 33522-33526.
- Lengqvist, J., de Urquiza, A. M., Bergman, A.-C., Willson, T. M., Sjövall, J., Perlmann, T., et al. (2004). Polyunsaturated fatty acids including docosahexaenoic and arachidonic acid bind to the retinoid X receptor  $\alpha$  ligand-binding domain. *Molecular & Cellular Proteomics*, 3(7), 692-703.
- Leval, X. d., Julemont, F., Delarge, J., Pirotte, B., & Dogne, J. M. (2002). New Trends in Dual 5-LOX / COX Inhibition. *Current Medicinal Chemistry*, 9(9), 941-962.
- Li, H., Ruan, X.Z., Powis, S.H., Fernando, R., Mon, W.Y., Wheeler, D.C., et al. (2005). EPA and DHA reduce LPS-induced inflammation responses in HK-2 cells: Evidence for a PPAR- $\gamma$ -dependent mechanism. *Kidney International*, 67(3), 867-874.
- Li, J. (2005). Basic molecular dynamics Handbook of Materials Modeling (pp. 565-588): Springer.
- Lim, Y.P., & Huang, J.D. (2007). Pregnan X receptor polymorphism affects CYP3A4 induction via a ligand-dependent interaction with steroid receptor coactivator-1. *Pharmacogenetics and Genomics*, 17(5), 369-382.

- Lindert, S., Zhu, W., Liu, Y.L., Pang, R., Oldfield, E., & McCammon, J.A. (2013). Farnesyl diphosphate synthase inhibitors from in silico screening. *Chemical Biology & Drug Design*, 81(6), 742-748.
- Ling, M. T., Luk, S. U., Al-Ejeh, F., & Khanna, K. K. (2012). Tocotrienol as a potential anticancer agent. *Carcinogenesis*, 33(2), 233-239.
- Lowe, M., & Plosker, G. (2000). Bexarotene. *American Journal of Clinical Dermatology*, 1(4), 245-250.
- Lüdtke, A., Buettner, J., Schmidt, H.H.-J., & Worman, H.J. (2007). New PPARG mutation leads to lipodystrophy and loss of protein function that is partially restored by a synthetic ligand. *Journal of Medical Genetics*, 44(9), e88.
- Luquet, S., Gaudel, C., Holst, D., Lopez-Soriano, J., Jehl-Pietri, C., Fredenrich, A., et al. (2005). Roles of PPAR delta in lipid absorption and metabolism: a new target for the treatment of type 2 diabetes. *Biochimica et Biophysica Acta (BBA)-Molecular Basis of Disease*, 1740(2), 313-317.
- Lynch, D., & Reggio, P. (2005). Molecular dynamics simulations of the endocannabinoid N-arachidonylethanolamine (anandamide) in a phospholipid bilayer: probing structure and dynamics. *Journal of Medicinal Chemistry*, 48, 4824 - 4833.
- Mackie, K. (2006). Cannabinoid receptors as therapeutic targets. *Annual Reviews of Pharmacology and Toxicology*, 46, 101-122.
- Madeswaran A., Umamaheswari, M., et al. (2012). Docking studies: In silico lipoxygenase inhibitory activity of some commercially available flavonoids. *Bangladesh Journal of Pharmacology* 6(2), 133-138.
- Mahmoudian, M. (1997). The cannabinoid receptor: computer-aided molecular modeling and docking of ligand. *Journal of Molecular Graphics and Modelling*, 15(3), 149-153.
- Malapaka, R. R. V., Khoo, S., Zhang, J., Choi, J. H., Zhou, X. E., Xu, Y., et al. (2012). Identification and mechanism of 10-carbon fatty acid as modulating ligand of peroxisome proliferator-activated receptors. *Journal of Biological Chemistry*, 287(1), 183-195.
- Malaviya, A., & Sylvester, P.W. (2013). Mechanisms mediating the effects of  $\gamma$ -tocotrienol when used in combination with ppar $\gamma$  agonists or antagonists on mcf-7 and mda-mb-231 breast cancer cells. *International Journal of Breast Cancer*, 2013.
- Malaviya, A., & Sylvester, P.W. (2014). Synergistic antiproliferative effects of combined  $\gamma$ -tocotrienol and PPAR $\gamma$  antagonist treatment are mediated through PPAR $\gamma$ -independent mechanisms in breast cancer cells. *PPAR Research*, 2014.
- Mallari, R., Swearingen, E., Liu, W., Ow, A., Young, S.W., & Huang, S.-G. (2003). A generic high-throughput screening assay for kinases: protein kinase a as an example. *Journal of Biomolecular Screening*, 8(2), 198-204.
- Mangelsdorf, D. J., Thummel, C., Beato, M., Herrlich, P., Schütz, G., Umesono, K., et al. (1995). The nuclear receptor superfamily: the second decade. *Cell*, 83(6), 835-839.

- Mangoni, M., Roccatano, D., & Di Nola, A. (1999). Docking of flexible ligands to flexible receptors in solution by molecular dynamics simulation. *Proteins: Structure, Function, and Bioinformatics*, 35(2), 153-162.
- Mark, M., Ghyselinck, N. B., & Chambon, P. (2006). Function of retinoid nuclear receptors: lessons from genetic and pharmacological dissections of the retinoic acid signaling pathway during mouse embryogenesis. *Annual Reviews of Pharmacology and Toxicology*, 46, 451-480.
- Marshall, T.G., Lee, R.E., & Marshall, F.E. (2006). Theoretical biology and medical modelling. *Theoretical Biology and Medical Modelling*, 3, 1.
- Matsuyama, M., & Yoshimura, R. (2009). Arachidonic acid pathway: A molecular target in human testicular cancer (Review). *Molecular Medicine Reports*, 2(4), 527-531.
- McAinch, A., Aguila, J., Cornall, L., & Mathai, M. (2012). The effects of CB2 antagonism and tocotrienols on markers of inflammation/fibrosis in H9C2 cardiac myoblast cells. *Obesity Research & Clinical Practice*, 6, Supplement 1(0), 68.
- Meirhaeghe, A., Fajas, L., Helbecque, N., Cottet, D., Lebel, P., Dallongeville, J., et al. (1998). A genetic polymorphism of the peroxisome proliferator-activated receptor  $\gamma$  gene influences plasma leptin levels in obese humans. *Human Molecular Genetics*, 7(3), 435-440.
- Meller, J.A. (2001). Molecular Dynamics Encyclopedia of Life Sciences: Nature Publishing Group.
- Mifflin, R. C., & Powell, D. W. (2001). The Cyclooxygenase Reaction. *Cyclooxygenases*, 8.
- Modica, S., Gadaleta, R. M., & Moschetta, A. (2009). Deciphering the nuclear bile acid receptor FXR paradigm. *Nuclear Receptor Signaling*, 8, e005-e005.
- Moise, A. R., Noy, N., Palczewski, K., & Blaner, W. S. (2007). Delivery of retinoid-based therapies to target tissues. *Biochemistry*, 46(15), 4449-4458.
- Monajemi, H., Zhang, L., Li, G., Jeninga, E.H., Cao, H., Maas, M., et al. (2007). Familial Partial Lipodystrophy Phenotype Resulting from a Single-Base Mutation in Deoxyribonucleic Acid-Binding Domain of Peroxisome Proliferator-Activated Receptor- $\gamma$ . *Journal of Clinical Endocrinology & Metabolism*, 92(5), 1606-1612.
- Montero, C., Campillo, N. E., Goya, P., & Páez, J. A. (2005). Homology models of the cannabinoid CB1 and CB2 receptors. A docking analysis study. *European Journal Of Medicinal Chemistry*, 40(1), 75-83.
- Moreira, F. A., & Crippa, J. A. S. (2009). The psychiatric side-effects of rimonabant. *Revista brasileira de psiquiatria*, 31(2), 145-153.
- Morris, G. M., Huey, R., Lindstrom, W., Sanner, M. F., Belew, R. K., Goodsell, D. S., et al. (2009). AutoDock4 and AutoDockTools4: Automated docking with selective receptor flexibility. *Journal of Computational Chemistry*, 30(16), 2785-2791.
- Morris, G.M., Goodsell, D.S., Halliday, R.S., Huey, R., Hart, W.E., Belew, R.K., et al. (1998). Automated docking using a Lamarckian genetic algorithm and an empirical binding free energy function. *Journal of Computational Chemistry*, 19(14), 1639-1662.

- Motulsky, H. (1996). The GraphPad Guide to Analyzing Radiligand Binding Data Retrieved 02-06-2014, from <http://www2.uah.es/farmamol/Public/GraphPad/radiolig.htm>
- Motulsky, H., & Neubig, R. (2001). Analyzing radioligand binding data. *Current Protocols in Protein Science*, A-3H.
- Mouchon, A., Delmotte, M.-H., Formstecher, P., & Lefebvre, P. (1999). Allosteric regulation of the discriminative responsiveness of retinoic acid receptor to natural and synthetic ligands by Retinoid X Receptor and DNA. *Molecular and Cellular Biology*, 19(4), 3073-3085.
- Murphy, G. J., & Holder, J. C. (2000). PPAR- $\gamma$  agonists: therapeutic role in diabetes, inflammation and cancer. *Trends in pharmacological sciences*, 21(12), 469-474.
- Naef, M., Curatolo, M., Petersen-Felix, S., Arendt-Nielsen, L., Zbinden, A., & Brenneisen, R. (2003). The analgesic effect of oral delta-9-tetrahydrocannabinol (THC), morphine, and a THC-morphine combination in healthy subjects under experimental pain conditions. *Pain*, 105(1), 79-88.
- Nesaretnam, K., & Meganathan, P. (2011). Tocotrienols: inflammation and cancer. *Annals of the New York Academy of Sciences*, 1229(1), 18-22.
- Nesaretnam, K., Gomez, P.A., Selvaduray, K.R., & Razak, G. (2007). Tocotrienol levels in adipose tissue of benign and malignant breast lumps in patients in Malaysia. *Asia Pacific Journal of Clinical Nutrition*, 16(3), 498.
- Nesto, R.W., Bell, D., Bonow, R.O., Fonseca, V., Grundy, S.M., Horton, E.S., et al. (2003). Thiazolidinedione use, fluid retention, and congestive heart failure: a consensus statement from the american heart association and american diabetes association. *Circulation*, 108(23), 2941-2948.
- Ng, P.C., & Henikoff, S. (2002). Accounting for human polymorphisms predicted to affect protein function. *Genome Research*, 12(3), 436-446.
- Ngah, W.Z., Jarien, Z., San, M.M., Marzuki, A., Top, G.M., Shamaan, N.A., et al. (1991). Effect of tocotrienols on hepatocarcinogenesis induced by 2-acetylaminofluorene in rats. *The American Journal of Clinical Nutrition*, 53(4), 1076S-1081S.
- Nielsen, J. (1995). 10 Usability heuristics for user interface design. nielsen norman group: evidence-based user experience research, training, and consulting. Retrieved from <http://www.nngroup.com/articles/ten-usability-heuristics/>.
- Noble, S.M., Carnahan, V.E., Moore, L.B., Luntz, T., Wang, H., Ittoop, O.R., et al. (2006). Human PXR forms a tryptophan zipper-mediated homodimer. *Biochemistry*, 45(28), 8579-8589.
- Nohara, A., Kawashiri, M.-a., Claudel, T., Mizuno, M., Tsuchida, M., Takata, M., et al. (2007). High frequency of a retinoid x receptor  $\gamma$  gene variant in familial combined hyperlipidemia that associates with atherogenic dyslipidemia. *Arteriosclerosis, Thrombosis, and Vascular Biology*, 27(4), 923-928.
- Noyes, R., Brunk, S.F., Avery, D., & Canter, A. (1975). The analgesic properties of delta-9-tetrahydrocannabinol. *Clinical Pharmacology & Therapeutics*, 18(1), 84-89.

Oh, D.Y., Talukdar, S., Bae, E.J., Imamura, T., Morinaga, H., Fan, W., *et al.* (2010). GPR120 is an omega-3 fatty acid receptor mediating potent anti-inflammatory and insulin-sensitizing effects. *Cell*, 142(5), 687-698.

Ooms, F., Frédéric, R., Durant, F., Petzer, J.P., Castagnoli Jr, N., Van der Schyf, C.J., *et al.* (2003). Rational approaches towards reversible inhibition of type B monoamine oxidase. Design and evaluation of a novel 5H-Indeno pyridazin-5-one derivative. *Bioorganic & Medicinal Chemistry Letters*, 13(1), 69-73.

Ortega-Gutiérrez, S., Hawkins, E.G., Viso, A., López-Rodríguez, M.L., & Cravatt, B.F. (2004). Comparison of anandamide transport in FAAH wild-type and knockout neurons: evidence for contributions by both FAAH and the CB1 receptor to anandamide uptake. *Biochemistry*, 43(25), 8184-8190.

Östberg, T., Bertilsson, G., Jendeberg, L., Berkenstam, A., & Uppenberg, J. (2002). Identification of residues in the PXR ligand binding domain critical for species specific and constitutive activation. *European Journal of Biochemistry*, 269(19), 4896-4904.

Ostrowski, J., Hammer, L., Roalsvig, T., Pokornowski, K., & Reczek, P.R. (1995). The N-terminal portion of domain E of retinoic acid receptors alpha and beta is essential for the recognition of retinoic acid and various analogs. *Proceedings of the National Academy of Sciences*, 92(6), 1812-1816.

O'Sullivan, S.E., Kendall, D.A., & Randall, M.D. (2009). Time-dependent vascular effects of endocannabinoids mediated by peroxisome proliferator-activated receptor gamma. *PPAR Research*, 2009.

Oyama, T., Toyota, K., Waku, T., Hirakawa, Y., Nagasawa, N., Kasuga, J.-i., *et al.* (2009). Adaptability and selectivity of human peroxisome proliferator-activated receptor (PPAR) pan agonists revealed from crystal structures. *Acta Crystallographica Section D*, 65(8), 786-795.

Pacher, P., & Kunos, G. (2013). Modulating the endocannabinoid system in human health and disease – successes and failures. *FEBS Journal*, 280(9), 1918-1943.

Pacher, P., Bátkai, S., & Kunos, G. (2006). The endocannabinoid system as an emerging target of pharmacotherapy. *Pharmacological Reviews*, 58(3), 389-462.

Packer, L., Weber, S.U., & Rimbach, G. (2001). Molecular aspects of  $\alpha$ -tocotrienol antioxidant action and cell signalling. *The Journal of Nutrition*, 131(2), 369S-373S.

Padgett, L., Howlett, A., & Shim, J.-Y. (2008). Binding mode prediction of conformationally restricted anandamide analogs within the CB1 receptor. *Journal of Molecular Signaling*, 3(1), 5.

Parnes, S.M., & Chuma, A.V. (2000). Acute effects of antileukotrienes on sinonasal polyposis and sinusitis. *Ear, Nose, & Throat Journal*, 79(1), 18-20, 24-15.

Pavlopoulos, S., Thakur, G.A., Nikas, S.P., & Makriyannis, A. (2006). Cannabinoid receptors as therapeutic targets. *Current Pharmaceutical Design*, 12(14), 1751-1769.

Peet, D.J., Doyle, D.F., Corey, D.R., & Mangelsdorf, D.J. (1998). Engineering novel specificities for ligand-activated transcription in the nuclear hormone receptor RXR. *Chemistry & Biology*, 5(1), 13-21.

- Pérez, E., Bourguet, W., Gronemeyer, H., & de Lera, A.R. (2012). Modulation of RXR function through ligand design. *Biochimica et Biophysica Acta (BBA) - Molecular and Cell Biology of Lipids*, 1821(1), 57-69.
- Pertwee, R.G. (2007). Cannabinoids and multiple sclerosis. *Molecular Neurobiology*, 36(1), 45-59.
- Pertwee, R.G. (2009). Emerging strategies for exploiting cannabinoid receptor agonists as medicines. *British Journal of Pharmacology*, 156(3), 397-411.
- Pertwee, R.G. (2012). Targeting the endocannabinoid system with cannabinoid receptor agonists: pharmacological strategies and therapeutic possibilities. *Philosophical Transactions of the Royal Society B: Biological Sciences*, 367(1607), 3353-3363.
- Pettersen, E.F., Goddard, T.D., Huang, C.C., Couch, G.S., Greenblatt, D.M., Meng, E.C., *et al.* (2004). UCSF Chimera—a visualization system for exploratory research and analysis. *Journal of Computational Chemistry*, 25(13), 1605-1612.
- Pommery, N., Taverne, T., Telliez, A., Goossens, L., Charlier, C., Pommery, J., *et al.* (2004). New COX-2/5-LOX inhibitors: apoptosis-inducing agents potentially useful in prostate cancer chemotherapy. *Journal of Medicinal Chemistry*, 47(25), 6195-6206.
- Porro, G.B., Caruso, I., Petrillo, M., Montrone, F., & Ardizzone, S. (1991). A double-blind gastroscopic evaluation of the effects of etodolac and naproxen on the gastrointestinal mucosa of rheumatic patients. *Journal of Internal Medicine*, 229(1), 5-8.
- Pymol. (Version 1.5.0.4). The PyMOL Molecular Graphics System,.
- Qin, S.-S., Yu, Z.-W., & Yu, Y.-X. (2009). Structural and kinetic properties of  $\alpha$ -tocopherol in phospholipid bilayers, a molecular dynamics simulation study. *The Journal of Physical Chemistry B*, 113(52), 16537-16546.
- Qureshi, A.A., Bradlow, B.A., Salser, W.A., & Brace, L.D. (1997). Novel tocotrienols of rice bran modulate cardiovascular disease risk parameters of hypercholesterolemic humans. *The Journal of Nutritional Biochemistry*, 8(5), 290-298.
- Qureshi, A.A., Qureshi, N., Wright, J.J., Shen, Z., Kramer, G., Gapor, A., Chong, Y.H., DeWitt, G., Ong, A., Peterson, D.M. (1991). Lowering of serum cholesterol in hypercholesterolemic humans by tocotrienols (palmvitene). *The American Journal of Clinical Nutrition*, 53(4), 1021S-1026S.
- Rafat, A.S., Saame, R.S., Laura, A.S., Heidi, R.Y., William, S., & Gary, P.Z. (2004). Omega 3-fatty acids: health benefits and cellular mechanisms of action. *Mini Reviews in Medicinal Chemistry*, 4(8), 859-871.
- Rainsford, K. (1987). The effects of 5-lipoxygenase inhibitors and leukotriene antagonists on the development of gastric lesions induced by nonsteroidal antiinflammatory drugs in mice. *Agents and Actions*, 21(3-4), 316-319.
- Rainsford, K. (1993). Leukotrienes in the pathogenesis of NSAID-induced gastric and intestinal mucosal damage. *Agents and Actions*, 39(1), C24-C26.

- Rainsford, K. (1999). Profile and mechanisms of gastrointestinal and other side effects of nonsteroidal anti-inflammatory drugs (NSAIDs). *The American Journal of Medicine*, 107(6), 27-35.
- Ramamoorthy, D., Turos, E., & Guida, W.C. (2013). Identification of a new binding site in *E. coli* FabH using molecular dynamics simulations: Validation by computational alanine mutagenesis and docking studies. *Journal of Chemical Information and Modeling*, 53(5), 1138-1156.
- Reggio, P.H. (2010). Endocannabinoid Binding to the Cannabinoid Receptors: What Is Known and What Remains Unknown. *Current Medicinal Chemistry*, 17(14), 1468-1486.
- Reiss, C.S. (2010). Cannabinoids and viral infections. *Pharmaceuticals*, 3(6), 1873-1886.
- Richard, B.J. (2014). Tocotrienols: Twenty Years of Dazzling Cardiovascular and Cancer Research, *Health News*.
- Rinaldi-Carmona, M., Barth, F., Héaulme, M., Shire, D., Calandra, B., Congy, C., et al. (1994). SR141716A, a potent and selective antagonist of the brain cannabinoid receptor. *FEBS Letters*, 350(2–3), 240-244.
- Ristow, M., Müller-Wieland, D., Pfeiffer, A., Krone, W., & Kahn, C.R. (1998). Obesity associated with a mutation in a genetic regulator of adipocyte differentiation. *New England Journal of Medicine*, 339(14), 953-959.
- Rizo, R. (2015). MD Simulation: Protein in Water. Rizo lab research group Retrieved 29/04/2015, 2015, from [http://ringo.ams.sunysb.edu/index.php/MD\\_Simulation:\\_Protein\\_in\\_Water\\_\(Pt.\\_2\)#RMSD](http://ringo.ams.sunysb.edu/index.php/MD_Simulation:_Protein_in_Water_(Pt._2)#RMSD)
- Rizvi, N.A., Marshall, J.L., Dahut, W., Ness, E., Truglia, J.A., Loewen, G., et al. (1999). A Phase I Study of LGD1069 in Adults with Advanced Cancer. *Clinical Cancer Research*, 5(7), 1658-1664.
- Romani, R., Galeazzi, R., Rosi, G., Fiorini, R., Pirisinu, I., Ambrosini, A., et al. (2011). Anandamide and its congeners inhibit human plasma butyrylcholinesterase. Possible new roles for these endocannabinoids. *Biochimie*, 93(9), 1584-1591.
- Ross, R.A., Craib, S.J., Stevenson, L.A., Pertwee, R.G., Henderson, A., Toole, J., et al. (2002). Pharmacological characterization of the anandamide cyclooxygenase metabolite: prostaglandin E2 ethanolamide. *Journal of Pharmacology and Experimental Therapeutics*, 301(3), 900-907.
- Rowlinson, S.W., Crews, B.C., Lanzo, C.A., & Marnett, L.J. (1999). The binding of arachidonic acid in the cyclooxygenase active site of mouse prostaglandin endoperoxide synthase-2 (COX-2): a putative l-shaped binding conformation utilizing the top channel region. *Journal of Biological Chemistry*, 274(33), 23305-23310.
- Roy, A., Kucukural, A., & Zhang, Y. (2010). I-TASSER: a unified platform for automated protein structure and function prediction. *Nature Protocols*, 5(4), 725-738.
- Roy, A., Yang, J., & Zhang, Y. (2012). Cofactor: an accurate comparative algorithm for structure-based protein function annotation. *Nucleic Acids Research*, gks372.

- Ruxton, C.H.S., Reed, S.C., Simpson, M.J.A., & Millington, K.J. (2004). The health benefits of omega-3 polyunsaturated fatty acids: a review of the evidence. *Journal of Human Nutrition and Dietetics*, 17(5), 449-459.
- Sarfaraz, S., Adhami, V.M., Syed, D.N., Afaq, F., & Mukhtar, H. (2008). Cannabinoids for cancer treatment: progress and promise. *Cancer Research*, 68(2), 339-342.
- Sarraf, P., Mueller, E., Smith, W.M., Wright, H.M., Kum, J.B., Aaltonen, L.A., *et al.* (1999). Loss-of-function mutations in ppar<sup>3</sup> associated with human colon cancer. *Molecular Cell*, 3(6), 799-804.
- Schlicker, E., & Kathmann, M. (2001). Modulation of transmitter release via presynaptic cannabinoid receptors. *Trends in Pharmacological Sciences*, 22(11), 565-572.
- Schneider, G., & Böhm, H.-J. (2002). Virtual screening and fast automated docking methods. *Drug Discovery Today*, 7, Supplement 1(0), 64-70.
- Schulz-Gasch, T., & Stahl, M. (2003). Binding site characteristics in structure-based virtual screening: evaluation of current docking tools. *Journal of Molecular Modeling*, 9(1), 47-57.
- Sen, C.K., Khanna, S., & Roy, S. (2006). Tocotrienols: vitamin E beyond tocopherols. *Life Sciences*, 78(18), 2088-2098.
- Serhan, C.N., Arita, M., Hong, S., & Gotlinger, K. (2004). Resolvins, docosatrienes, and neuroprotectins, novel omega-3-derived mediators, and their endogenous aspirin-triggered epimers. *Lipids*, 39(11), 1125-1132.
- Sethi, S., Ziouzenkova, O., Ni, H., Wagner, D.D., Plutzky, J., & Mayadas, T.N. (2002). Oxidized omega-3 fatty acids in fish oil inhibit leukocyte-endothelial interactions through activation of PPARα. *Blood*, 100(4), 1340-1346.
- Shearman, L., Rosko, K., Fleischer, R., Wang, J., Xu, S., Tong, X., *et al.* (2003). Antidepressant-like and anorectic effects of the cannabinoid CB1 receptor inverse agonist AM251 in mice. *Behavioural Pharmacology*, 14(8), 573-582.
- Shirode, A.B., & Sylvester, P.W. (2010). Synergistic anticancer effects of combined γ-tocotrienol and celecoxib treatment are associated with suppression in Akt and NFκB signaling. *Biomedicine & Pharmacotherapy*, 64(5), 327-332.
- Shivakumar, D., Williams, J., Wu, Y., Damm, W., Shelley, J., & Sherman, W. (2010). Prediction of absolute solvation free energies using molecular dynamics free energy perturbation and the OPLS force field. *Journal of Chemical Theory and Computation*, 6(5), 1509-1519.
- Shoichet, B.K. (2004). Virtual Screening of Chemical Libraries. *Nature*, 432, 862-865.
- Shu, M., Lin, Z., Zhang, Y., Wu, Y., Mei, H., & Jiang, Y. (2011). Molecular dynamics simulation of oseltamivir resistance in neuraminidase of avian influenza H5N1 virus. *Journal of Molecular Modeling*, 17(3), 587-592.
- Shureiqi, I., & Lippman, S.M. (2001). Lipoxygenase modulation to reverse carcinogenesis. *Cancer Research*, 61(17), 6307-6312.

- Shureiqi, I., Chen, D., Lee, J.J., Yang, P., Newman, R.A., Brenner, D.E., *et al.* (2000). 15-LOX-1: a novel molecular target of nonsteroidal anti-inflammatory drug-induced apoptosis in colorectal cancer cells. *Journal of the National Cancer Institute*, 92(14), 1136-1142.
- Sidhu, R.S., Lee, J.Y., Yuan, C., & Smith, W.L. (2010). Comparison of cyclooxygenase-1 crystal structures: cross-talk between monomers comprising cyclooxygenase-1 homodimers. *Biochemistry*, 49(33), 7069-7079.
- Sierra, M.L., Beneton, V., Boullay, A.-B., Boyer, T., Brewster, A.G., Donche, F., *et al.* (2007). Substituted 2-[(4-Aminomethyl)phenoxy]-2-methylpropionic acid PPAR $\alpha$  Agonists. 1. discovery of a novel series of potent HDLc raising agents. *Journal of Medicinal Chemistry*, 50(4), 685-695.
- Simmons, D.L., Botting, R.M., & Hla, T. (2004). Cyclooxygenase isozymes: the biology of prostaglandin synthesis and inhibition. *Pharmacological Reviews*, 56(3), 387-437.
- Simons, K., & Toomre, D. (2000). Lipid rafts and signal transduction. *Nature reviews Molecular Cell Biology*, 1(1), 31-39.
- Simopoulos, A.P. (1991). Omega-3 fatty acids in health and disease and in growth and development. *The American Journal of Clinical Nutrition*, 54(3), 438-463.
- Simopoulos, A.P. (2002). Omega-3 Fatty Acids in Inflammation and Autoimmune Diseases. *Journal of the American College of Nutrition*, 21(6), 495-505.
- Simopoulos, A.P. (2003). Omega-3 Fatty Acids and Cancer. *Indoor and Built Environment*, 12(6), 405-412.
- Sittampalam, G.S., Gal-Edd, N., Arkin, M., Auld, D., Austin, C., Bejcek, B., *et al.* (2012). Calculations and instrumentation used for radioligand binding assays. Retrieved from <http://www.ncbi.nlm.nih.gov/books/NBK91997/>.
- Skelly, M., & Hawkey, C. (2003). COX-LOX inhibition: current evidence for an emerging new therapy. *International Journal of Clinical Practice*, 57(4), 301-304.
- Smith, W.L., DeWitt, D.L., & Garavito, R.M. (2000). Cyclooxygenases: structural, cellular, and molecular biology. *Annual Review of Biochemistry*, 69(1), 145-182.
- Sousa, S.F., Fernandes, P.A., & Ramos, M.J. (2006). Protein-ligand docking: current status and future challenges. *Proteins: Structure, Function, and Bioinformatics*, 65(1), 15-26.
- Staels, B., & Fruchart, J.-C. (2005). Therapeutic roles of peroxisome proliferator-activated receptor agonists. *Diabetes*, 54(8), 2460-2470.
- Steele, N., Gralla, R., Braun Jr, D., & Young, C. (1979). Double-blind comparison of the antiemetic effects of nabilone and prochlorperazine on chemotherapy-induced emesis. *Cancer Treatment Reports*, 64(2-3), 219-224.
- Stoll, A.L., Locke, C.A., Marangell, L.B., & Severus, W.E. (1999). Omega-3 fatty acids and bipolar disorder: a review. *Prostaglandins, Leukotrienes and Essential Fatty Acids*, 60(5-6), 329-337.
- Stone, W.L., Krishnan, K., & Campbell, S. (2005). Tocotrienols and prostate cancer: DTIC Document. East Tennessee State Univ Johnson City.

- Strange, P. (2008). Agonist binding, agonist affinity and agonist efficacy at G protein-coupled receptors. *British Journal of Pharmacology*, 153(7), 1353-1363.
- Subbaramaiah, K., & Dannenberg, A.J. (2003). Cyclooxygenase 2: a molecular target for cancer prevention and treatment. *Trends in Pharmacological Sciences*, 24(2), 96-102.
- Sudha, A., Manikandan, R., Arulvasu, C., & Srinivasan, P. (2011). Molecular docking studies of 1, 2 disubstituted idopyranose from vitex negundo with anti-diabetic activity of type 2 diabetes. *Bioinformatics*, 2(1).
- Sugiura, T., Kondo, S., Kishimoto, S., Miyashita, T., Nakane, S., Kodaka, T., et al. (2000). Evidence that 2-arachidonoylglycerol but not N-palmitoylethanolamine or anandamide is the physiological ligand for the cannabinoid CB<sub>2</sub> receptor Comparison of the agonistic activities of various cannabinoid receptor ligands in HL-60 cells. *Journal of Biological Chemistry*, 275(1), 605-612.
- Suite 2011. (Maestro Version 9.2). LLC, New York.
- Sun, S., Almaden, J., Carlson, T.J., Barker, J., & Gehring, M.R. (2005). Assay development and data analysis of receptor-ligand binding based on scintillation proximity assay. *Metabolic Engineering*, 7(1), 38-44.
- Sun, Y., & Bennett, A. (2007). Cannabinoids: a new group of agonists of PPARs. *PPAR Research*, 2007.
- Suleyman, H., Demircan, B., & Karagoz, Y. (2007). Anti-inflammatory and side effects of cyclooxygenase inhibitors. *Pharmacol Rep*, 59(3), 247-258.
- Tan, G.D., Savage, D.B., Fielding, B.A., Collins, J., Hodson, L., Humphreys, S.M., et al. (2008). Fatty acid metabolism in patients with PPAR $\gamma$  mutations. *Journal of Clinical Endocrinology & Metabolism*, 93(11), 4462-4470.
- Tate, B.F., & Grippo, J.F. (1995). Mutagenesis of the ligand binding domain of the human retinoic acid receptor identifies critical residues for 9-cis-retinoic acid binding. *Journal of Biological Chemistry*, 270(35), 20258-20263.
- Teodoro, M.L., Phillips Jr, G.N., & Kavraki, L.E. (2001). Molecular docking: A problem with thousands of degrees of freedom. Paper presented at the Robotics and Automation, 2001. Proceedings 2001 ICRA. IEEE International Conference on.
- Thai, T., & Lam, H. (2003). . *.NET framework essentials*: " O'Reilly Media, Inc.".
- Tiwari, R., Mahasenan, K., Pavlovicz, R., Li, C., & Tjarks, W. (2009). Carborane clusters in computational drug design: a comparative docking evaluation using AutoDock, FlexX, Glide, and Surflex. *Journal of Chemical Information and Modeling*, 49(6), 1581-1589.
- Tollenaere, J. (1996). The role of structure-based ligand design and molecular modelling in drug discovery. *Pharmacy World and Science*, 18(2), 56-62.
- Tomeo, A.C., Geller, M., Watkins, T.R., Gapor, A., & Bierenbaum, M.L. (1995). Antioxidant effects of tocotrienols in patients with hyperlipidemia and carotid stenosis. *Lipids*, 30(12), 1179-1183.

- Ton, M.N., Chang, C., Carpentier, Y.A., & Deckelbaum, R.J. (2005). In vivo and in vitro properties of an intravenous lipid emulsion containing only medium chain and fish oil triglycerides. *Clinical Nutrition*, 24(4), 492-501.
- Toprakçı, M., & Yelekçi, K. (2005). Docking studies on monoamine oxidase-B inhibitors: estimation of inhibition constants of a series of experimentally tested compounds. *Bioorganic & Medicinal Chemistry Letters*, 15(20), 4438-4446.
- Tripathi, S., Selvaraj, C., Singh, S., & Reddy, K. (2012). Molecular docking, QPLD, and ADME prediction studies on HIV-1 integrase leads. *Medicinal Chemistry Research*, 21(12), 4239-4251.
- Udenfriend, S., Gerber, L., & Nelson, N. (1987). Scintillation proximity assay: a sensitive and continuous isotopic method for monitoring ligand/receptor and antigen/antibody interactions. *Analytical Biochemistry*, 161(2), 494-500.
- Umamaheswari, A. (2011). Docking and Molecular Dynamic Simulations of *Legionella pneumophila* MurB Reductase for Potential Inhibitor Design. *Biochemistry & Analytical Biochemistry*.
- Upadhyay, J., Misra, K. (2009). Towards the interaction mechanism of tocopherols and tocotrienols (vitamin E) with selected metabolizing enzymes. *Bioinformation*, 3(8), 326-331.
- Van Sickle, M.D., Duncan, M., Kingsley, P.J., Mouihate, A., Urbani, P., Mackie, K., et al. (2005). Identification and functional characterization of brainstem cannabinoid CB<sub>2</sub> receptors. *Science*, 310(5746), 329-332.
- Vane, J., Bakhle, Y., & Botting, R. (1998). Cyclooxygenases 1 and 2. *Annual Review of Pharmacology and Toxicology*, 38(1), 97-120.
- Vasanthi , H., , P., R, & K Das, D. (2011). Tocotrienols and its role in cardiovascular health-a lead for drug design. *Current Pharmaceutical Design*, 17(21), 2170-2175.
- Vass, M., Tarcsay, Á., & Keserű, G.M. (2012). Multiple ligand docking by Glide: implications for virtual second-site screening. *Journal of Computer-Aided Molecular Design*, 26(7), 821-834.
- Vecchio, A.J., Simmons, D.M., & Malkowski, M.G. (2010). Structural Basis of Fatty Acid Substrate Binding to Cyclooxygenase-2. *Journal of Biological Chemistry*, 285(29), 22152-22163.
- Verdonk, M.L., Cole, J.C., Hartshorn, M.J., Murray, C.W., & Taylor, R.D. (2003). Improved protein-ligand docking using GOLD. *Proteins: Structure, Function, and Bioinformatics*, 52(4), 609-623.
- Vetrivel, U., Ravichandran, S., Kuppan, K., Mohanlal, J., Das, U., & Narayanasamy, A. (2012). Agonistic effect of polyunsaturated fatty acids (PUFAs) and its metabolites on brain-derived neurotrophic factor (BDNF) through molecular docking simulation. *Lipids in Health and Disease*, 11(1), 109.
- W3Schools. (1999-2013). OS Platform Statistics. Retrieved from [http://www.w3schools.com/browsers/browsers\\_os.asp](http://www.w3schools.com/browsers/browsers_os.asp).

- Wahn, H., Wolf, J., Kram, F., Frantz, S., & Wagner, J.A. (2005). The endocannabinoid arachidonyl ethanolamide (anandamide) increases pulmonary arterial pressure via cyclooxygenase-2 products in isolated rabbit lungs. *American Journal of Physiology-Heart and Circulatory Physiology*, 289(6), H2491-H2496.
- Wallace, A., Laskowski, R., & Thornton, J. (1995). LIGPLOT a program to generate schematic diagrams of protein-ligand interactions. *Protein Engineering*, 8, 127 - 134.
- Wan, H., Dawson, M.I., Hong, W.K., & Lotan, R. (1998). Overexpressed Activated Retinoid X Receptors Can Mediate Growth Inhibitory Effects of Retinoids in Human Carcinoma Cells. *Journal of Biological Chemistry*, 273(41), 26915-26922.
- Wang, L., Deng, Y., Knight, J.L., Wu, Y., Kim, B., Sherman, W., et al. (2013). Modeling local structural rearrangements using fep/rest: application to relative binding affinity predictions of cdk2 inhibitors. *Journal of Chemical Theory and Computation*, 9(2), 1282-1293.
- Wang, S., Lai, K., Moy, F.J., Bhat, A., Hartman, H.B., & Evans, M.J. (2006). The nuclear hormone receptor farnesoid x receptor (FXR) is activated by androsterone. *Endocrinology*, 147(9), 4025-4033.
- Wang, Y., Xu, A., Pearson, R.B., & Cooper, G.J.S. (1999). Insulin and insulin antagonists evoke phosphorylation of P20 at serine 157 and serine 16 respectively in rat skeletal muscle. *FEBS Letters*, 462(1–2), 25-30.
- Watanabe K., Yasugi E., Oshima M. (2000). How to search the glycolipid data in LIPIDBANK for Web: the newly developed lipid database. *Trends in Glycoscience and Glycotechnology*, 12, 175-184.
- Watkins, R.E., Wisely, G.B., Moore, L.B., Collins, J.L., Lambert, M.H., Williams, S.P., et al. (2001). The human nuclear xenobiotic receptor PXR: structural determinants of directed promiscuity. *Science*, 292(5525), 2329-2333.
- Webdeveloper.com. (2014). The main advantages of .NET framework. Retrieved from <http://www.webdeveloper.com/forum/showthread.php?278141-The-main-advantages-of-.NET-framework>.
- Web Hosting, Design, & Coding. (2015). Retrieved 13/07, 2015
- Wu, S., & Liu, B. (2005). Application of scintillation proximity assay in drug discovery. *BioDrugs*, 19(6), 383-392.
- Xu, H.E., Lambert, M.H., Montana, V.G., Parks, D.J., Blanchard, S.G., Brown, P.J., et al. (1999). Molecular recognition of fatty acids by peroxisome proliferator activated receptors. *Molecular cell*, 3(3), 397-403.
- Yang, P., Chan, D., Felix, E., Cartwright, C., Menter, D.G., Madden, T., et al. (2004). Formation and antiproliferative effect of prostaglandin E3 from eicosapentaenoic acid in human lung cancer cells. *Journal of Lipid Research*, 45(6), 1030-1039.
- Yue, L., Ye, F., Xu, X., Shen, J., Chen, K., Shen, X., et al. (2005). The conserved residue Phe273(282) of PPAR $\alpha(\gamma)$ , beyond the ligand-binding site, functions in binding affinity through solvation effect. *Biochimie*, 87(6), 539-550.

- Zhang, C., & Duvic, M. (2003). Retinoids: therapeutic applications and mechanisms of action in cutaneous T-cell lymphoma. *Dermatologic Therapy*, 16(4), 322-330.
- Zhang, J., & Chen, C. (2008). Endocannabinoid 2-arachidonoylglycerol protects neurons by limiting COX-2 elevation. *Journal of Biological Chemistry*, 283(33), 22601-22611.
- Zhang, J., Kuehl, P., Green, E.D., Touchman, J.W., Watkins, P.B., Daly, A., et al. (2001). The human pregnane X receptor: genomic structure and identification and functional characterization of natural allelic variants. *Pharmacogenetics and Genomics*, 11(7), 555-572.
- Zhang, X.K., Salbert, G., Lee, M.O., & Pfahl, M. (1994). Mutations that alter ligand-induced switches and dimerization activities in the retinoid X receptor. *Molecular and Cellular Biology*, 14(6), 4311-4323.
- Zhang, Y. (2008). I-TASSER server for protein 3D structure prediction. *BMC Bioinformatics*, 9(40).
- Zhang, Y., & Skolnick, J. (2004). Scoring function for automated assessment of protein structure template quality. *Proteins: Structure, Function, and Bioinformatics*, 57(4), 702-710.
- Zhao, A., Yu, J., Lew, J.-L., Huang, L., Wright, S.D., & Cui, J. (2004). Polyunsaturated fatty acids are FXR ligands and differentially regulate expression of FXR targets. *DNA and Cell Biology*, 23(8), 519-526.
- Zheng, M., Zhang, Z., Zhu, W., Liu, H., Luo, X., Chen, K., et al. (2006). Essential structural profile of a dual functional inhibitor against cyclooxygenase-2 (COX-2) and 5-lipoxygenase (5-LOX): molecular docking and 3D-QSAR analyses on DHMBF analogues. *Bioorganic & Medicinal Chemistry*, 14(10), 3428-3437.
- Zhou, X.-P., Smith, W.M., Gimm, O., Mueller, E., Gao, X., Sarraf, P., et al. (2000). Overrepresentation of PPAR $\gamma$  sequence variants in sporadic cases of glioblastoma multiforme: preliminary evidence for common low penetrance modifiers for brain tumour risk in the general population. *Journal of Medical Genetics*, 37(6), 410-414.

# Appendices

## Appendix-A

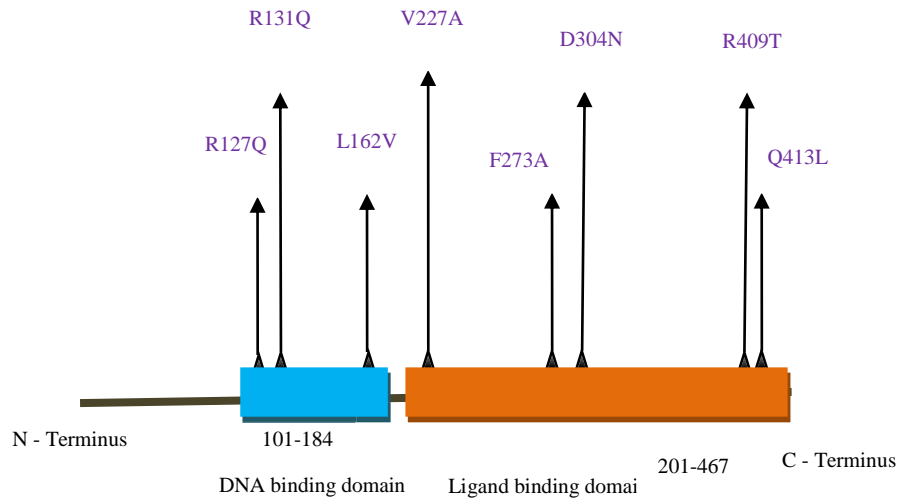


**Figure1. Mutations in PPAR alpha**

**Table 1. Mutations in PPAR alpha**

Serial Number	Mutation	Type	Effect	Literature Review Source
1.	L162V	Missense	Lower body mass index in non-insulin dependent diabetes	(Evans D, 2001)
2.	F273A	Missense	Decrease binding affinity of the ligands to the receptors	(Yue et al., 2005)
3.	R127Q	Missense	Changes in fatty acid metabolism	(Ng & Henikoff, 2002)
4.	V227A	Missense	Changes in fatty acid metabolism	(Ng et al., 2002)
5.	D304N	Missense	Changes in fatty acid metabolism	(Ng et al., 2002)
6.	R409T	Missense	Changes in fatty acid metabolism	(Ng et al., 2002)
7.	R131Q	Missense	Changes in fatty acid metabolism	(Ng et al., 2002)
8.	Q413L	Missense	Changes in fatty acid metabolism	(Ng et al., 2002)

## Appendix-B

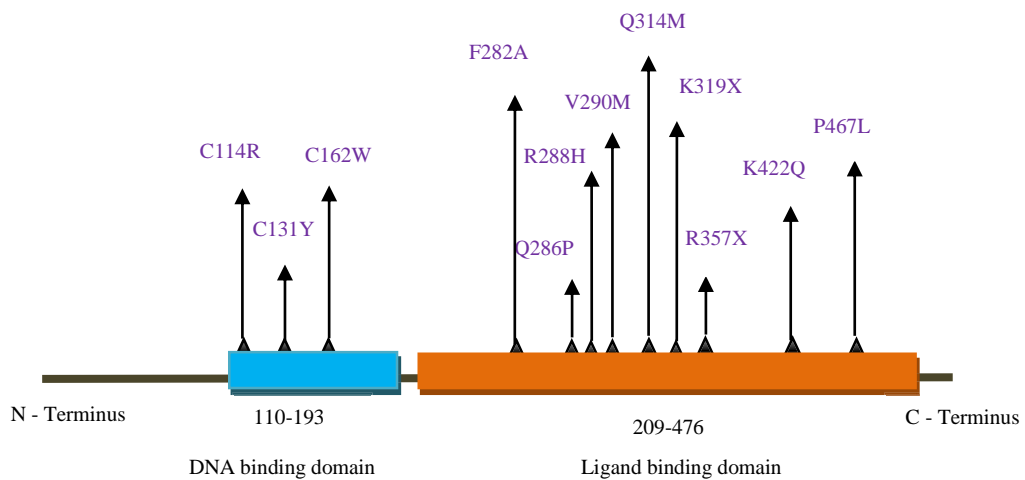


**Figure 1. Mapping Mutations in PPAR gamma isoform1**

**Table 1. Mutations in PPAR gamma isoform1**

Serial Number	Mutation	Type	Effect	Literature Review Source
1.	C114R	Point	Partial lipodystrophy and severe insulin resistance	(Tan et al., 2008)
2.	C131Y	Point	Partial lipodystrophy and severe insulin resistance	(Tan et al., 2008)
3.	C162W	Point	Partial lipodystrophy and severe insulin resistance	(Tan et al., 2008)
4.	V290M	Point	Reduced transcriptional activity	(Tan et al., 2008)
5.	Q314M	Point	Colon Cancer, loss of ligand binding	(Tan et al., 2008)
6.	R357X	Point	Partial lipodystrophy and severe insulin resistance	(Tan et al., 2008)
7.	P467L	Point	Reduced transcriptional activity	(Tan et al., 2008)
8.	Q286P	Missense	inactive transcription	(Sarraf et al., 1999)
9.	K319X	Missense	inactive transcription	(Sarraf et al., 1999)
10.	R288H	Point	Decreased transcription and binding	(Sarraf et al., 1999)
11.	F282A	Point	Enlarged binding pocket and reduced binding affinity	(Sarraf et al., 1999)
12.	K422Q	Point	Expressed in colon cancer cells	Sarraf et al., 1999

## **Appendix-C**

**Table 1 Mutations in PPAR gamma isoform 2**

<b>Serial Number</b>	<b>Mutation</b>	<b>Type</b>	<b>Effect</b>	<b>Literature Review Source</b>
1.	P495L	Point	Diabetes Mellitus	(Barroso et al., 1999)
2.	P113Q	Missense	Obesity severe	(Ristow et al., 1998)
3.	P12A	Missense	Observed variability in body mass index and insulin sensitivity	(Deeb et al., 1998)
4.	S112A	Experimental mutation	Increase adipogenic activity	(Iwata et al., 2001)
5.	H449H	Insertion	Insulin resistance	(Zhou et al., 2000)
6.	FS315X	Frame shift	Inactive transcription	(Agostini et al., 2006)
7.	C190S	Missense	Partial lipodystrophy and severe insulin resistance	(Lüdtke et al., 2007)
8.	R194W	Point	Partial lipodystrophy and severe insulin resistance	(Monajemi et al., 2007)
9.	D424N	Point	Partial lipodystrophy and severe insulin resistance	(Lüdtke et al., 2007)
10.	R425C	Point	Partial lipodystrophy and severe insulin resistance	(Jeninga et al., 2007)
11.	F388L	Point	Partial lipodystrophy and severe insulin resistance	(Jeninga et al., 2007)
12.	R316H	Point	Colon cancer	(Sarraf et al., 1999)
13.	V318M	Point	Diabetes Mellitus	(Barroso et al., 1999)
14.	C142R	Missense	Insulin resistance	(Agostini et al., 2006)
15.	C159Y	Missense	Insulin resistance	(Agostini et al., 2006)
16.	C190W	Missense	Insulin resistance	(Agostini et al., 2006)
17.	Y355X	Nonsense	Partial lipodystrophy	(Francis et al., 2006)
18.	R385X	Missense	Insulin resistance	(Agostini et al., 2006)
19.	H477H	Missense	Increased Body mass index	(Meirhaeghe et al., 1998)

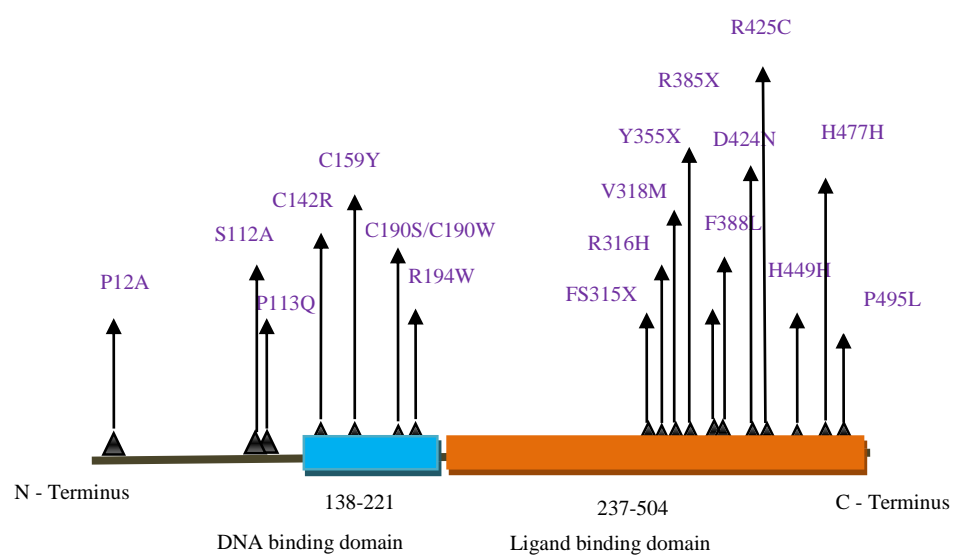


**Figure 1 Mapping Mutations in PPAR gamma isoform 2**

## **Appendix-D**

**Table 1 Mutations in Steroid Xenobiotic Receptor**

Serial Number	Mutation	Type	Effect	Literature Source	Review
1.	R98C	Missense	Reduced transcriptional activity	(Koyano et al., 2004)	
2.	R148Q	Missense	Reduced transcriptional activity	(Koyano et al., 2004)	
3.	R381W	Missense	Reduced transcriptional activity	(Koyano et al., 2004)	
4.	I403V	Missense	Reduced transcriptional activity	(Koyano et al., 2004)	
5.	R122Q	Missense	Attenuated ligand activation	(Zhang et al., 2001)	
6.	V140M	Missense	Altered basal or induced transactivation	(Hustert et al., 2001)	
7.	Q158K	Missense	Low levels of promoter activity	(Lim & Huang, 2007)	
8.	D163G	Missense	Altered basal or induced transactivation	(Fang et al., 2010)	
9.	A370T	Missense	Altered basal or induced transactivation	(Fang et al., 2010)	
10.	R410A	Experimental substitution	Increased basal transcriptional activity	(Watkins et al., 2001)	
11.	E321A	Experimental substitution	Decreased basal transcriptional activity	(Watkins et al., 2001)	
12.	G36R	Missense	Altered basal or induced transactivation	(Fang et al., 2010)	
13.	R413A	Experimental substitution	Reduced transcriptional activity	(Watkins et al., 2001)	
14.	D205A	Experimental substitution	Reduced transcriptional activity	(Watkins et al., 2001)	
15.	P27S	Missense	Altered basal or induced transactivation	(Watkins et al., 2001)	
16.	E18K	Missense	Altered basal or induced transactivation	(Watkins et al., 2001)	
17.	W223A	Missense	No basal transcriptional activity	(Noble et al., 2006)	
18.	T225A	Missense	No basal transcriptional activity	(Noble et al., 2006)	
19.	Q285A	Point	Less pronounced role in receptor activity	(Östberg et al., 2002)	
20.	H407A	Point	High level of constitutive activity	(Östberg et al., 2002)	
21.	H407Q	Point	Lower fold induction	(Östberg et al., 2002)	

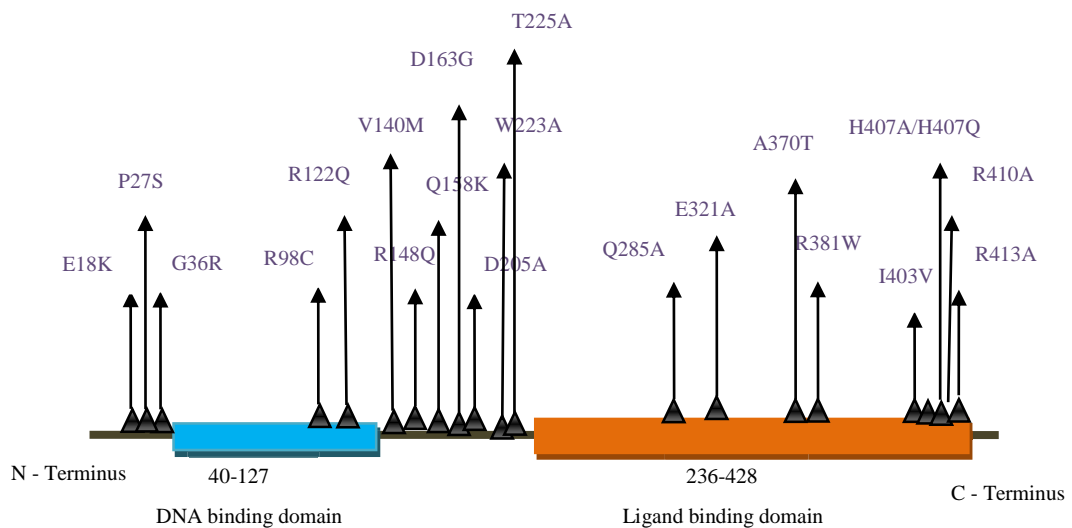


**Figure 1 Mapping Mutations in SXR**

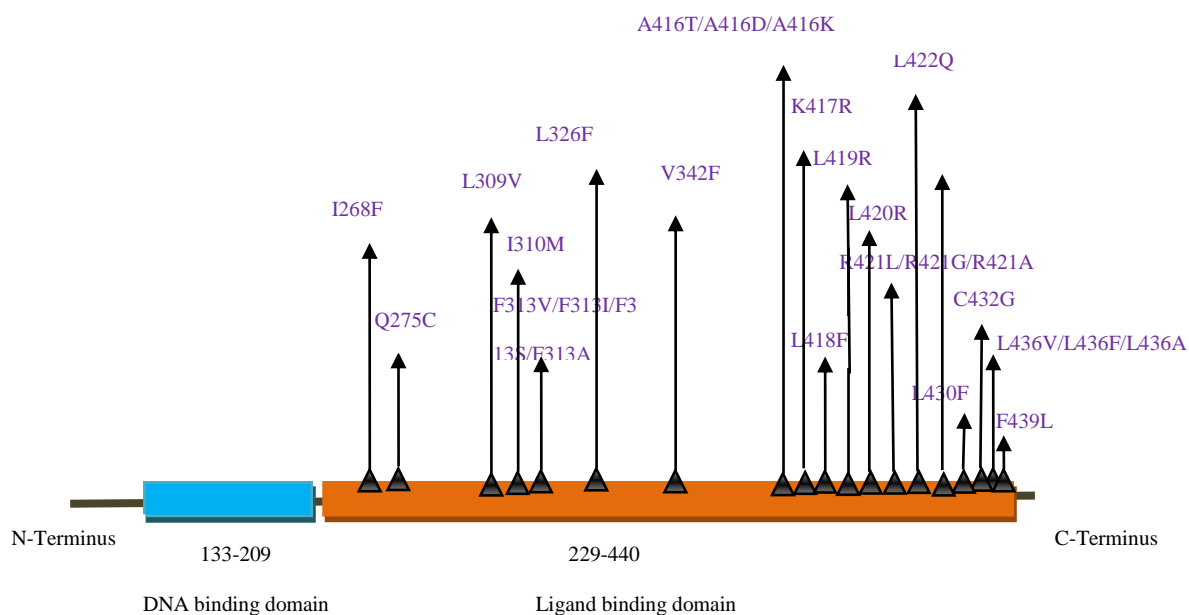
## **Appendix-E**

**Table 1 Mutations in RXR alpha**

<b>Serial Number</b>	<b>Mutation</b>	<b>Type</b>	<b>Effect</b>	<b>Literature Review Source</b>
1.	F313V	Experimental substitution	Decreased activation by 9CRA and increased activation by synthetic ligands	(Peet et al., 1998)
2.	F313I	Experimental substitution	Poor activation by ligands	(Doyle et al., 2001)
3.	Q275C	Experimental substitution	No considerable effect	(Doyle et al., 2001)
4.	I310M	Experimental substitution	Increased activation by ligands	(Doyle et al., 2001)
5.	L309V	Experimental substitution	Decreased activation	(Doyle et al., 2001)
6.	L436V	Experimental substitution	Decreased activation	(Doyle et al., 2001)
7.	I268F	Experimental substitution	No considerable effect	(Doyle et al., 2001)
8.	C432G	Experimental substitution	No considerable effect	(Doyle et al., 2001)
9.	L326F	Experimental substitution	No activation by all trans retinoic acid	(Doyle et al., 2001)
10.	V342F	Experimental substitution	Increased activation by ligands	(Doyle et al., 2001)
11.	F439L	Experimental substitution	Increased activation by ligands	(Doyle et al., 2001)
12.	F313S	Experimental substitution	Poor activation by ligands	(Peet et al., 1998)
13.	F313A	Missense	Increased constitutional activity & inhibition of DNA synthesis	(Zhang et al., 2001)
14.	A416T	Experimental Substitution	No effect on receptor interaction with PPAR, RAR & Thyroid hormone Receptor	(Lee et al., 2000)
15.	A416D	Missense	Impaired interaction with TR	(Lee et al., 2000)
16.	R421L	Experimental Substitution	Impaired interaction with TR	(Lee et al., 2000)
17.	A416K	Missense	Impaired interaction with both TR and RA	(Lee et al., 2000)
18.	K417R	Experimental Substitution	No effect on receptor interaction with PPAR, RAR & TR	(Lee et al., 2000)
19.	R421G	Experimental Substitution	No effect on receptor interaction with PPAR, RAR, & TR	(Lee et al., 2000)

**Table 1(Continued)**

Serial Number	Mutation	Type	Effect	Literature Review Source
20.	R421A	Missense	Loss of heterodimerization with PPAR, TR & RAR	(Chen et al., 1999)
21.	L419R	Missense	Poor heterodimerization with PPAR, TR & RAR	(Chen et al., 1999)
22.	L420R	Missense	Poor heterodimerization with PPAR, TR & RAR	(Chen et al., 1999)
23.	L430F	Point	Decreased RXR alpha heterodimerization	(Wan et al., 1998)
24.	L436F	Experimental Substitution	Activated by 9CRA but not responded by synthetic ligands	(Peet et al., 1998)
25.	L436A	Experimental Substitution	No activation with all ligands	(Peet et al., 1998)
26.	L422Q	Amino acid substitution	Altered homodimer DNA binding activity	(Zhang et al., 1994)
27.	L418F	Amino acid substitution	Inhibition of homodimer DNA binding	(Zhang et al., 1994)
28.	L425Q	Amino acid substitution	Inhibition of homodimer DNA binding	(Fang et al., 2010)

**Figure 1 Mapping Mutations in RXR alpha**

## Appendix-F

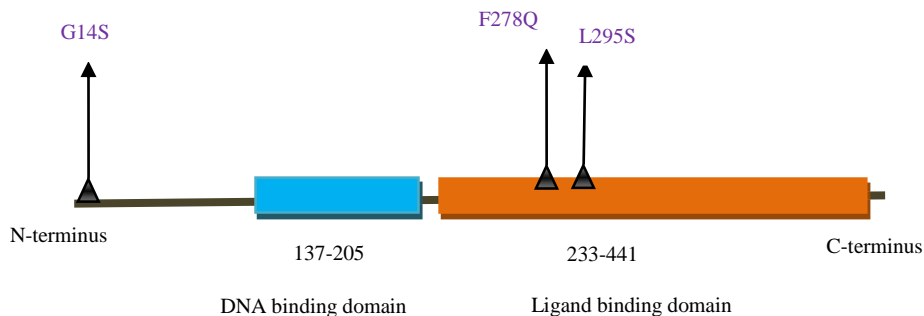


**Figure 1 Mapping Mutations in RXR alpha**

**Table 1 Mutations in RXR gamma**

Serial Number	Mutation	Type	Effect	Literature Review Source
1.	G14S	Missense	Hyperlipidemia	(Nohara et al., 2007)
2.	F278Q	Missense	Low interaction with ligands	(Lavigne et al., 1999)
3.	L295S	Missense	Low interaction with ligands	(Lavigne et al., 1999)

## **Appendix-G**

**Table 1 Mutations in RAR alpha**

<b>Serial Number</b>	<b>Mutation</b>	<b>Type</b>	<b>Effect</b>	<b>Literature Review Source</b>
1.	S232A	Experimental Substitution	Ability to bind RAR beta specific retinoid	(OstrowsK <sub>d</sub> et al., 1995)
2.	T239I	Experimental Substitution	Ability to bind RAR beta specific retinoid	(OstrowsK <sub>d</sub> et al., 1995)
3.	K244A	Silent	Impaired or diminished binding	(Mouchon et al., 1999)
4.	K262A	Silent	Impaired or diminished binding	(Mouchon et al., 1999)
5.	S388A	Experimental Substitution	No effect on phosphate content of hRAR alpha	(Wang et al., 1999)
6.	I410A	Experimental Substitution	No binding with 9 cis-RA	(Tate & Grippo, 1995)
7.	M406A	Experimental Substitution	No binding with 9 cis-RA	(Tate et al., 1995)
8.	S115A	Experimental Substitution	No binding with 9 cis-RA	(Tate et al., 1995)
9.	S115G	Experimental Substitution	No binding with 9 cis-RA	(Tate et al., 1995)
10.	S157D	Experimental Substitution	No binding with 9 cis-RA	(Tate et al., 1995)
11.	S157A	Experimental Substitution	No binding with 9 cis-RA	(Tate et al., 1995)
12.	S77E	Experimental Substitution	Mimics phosphorylated RAR alpha	(Keriel et al., 2002)
13.	R272G	Missense	Inhibits the ligand binding function	(Imaizumi et al., 1998)
14.	M297L	Missense	Decreased ligand dependent transcription	(Imaizumi et al., 1998)

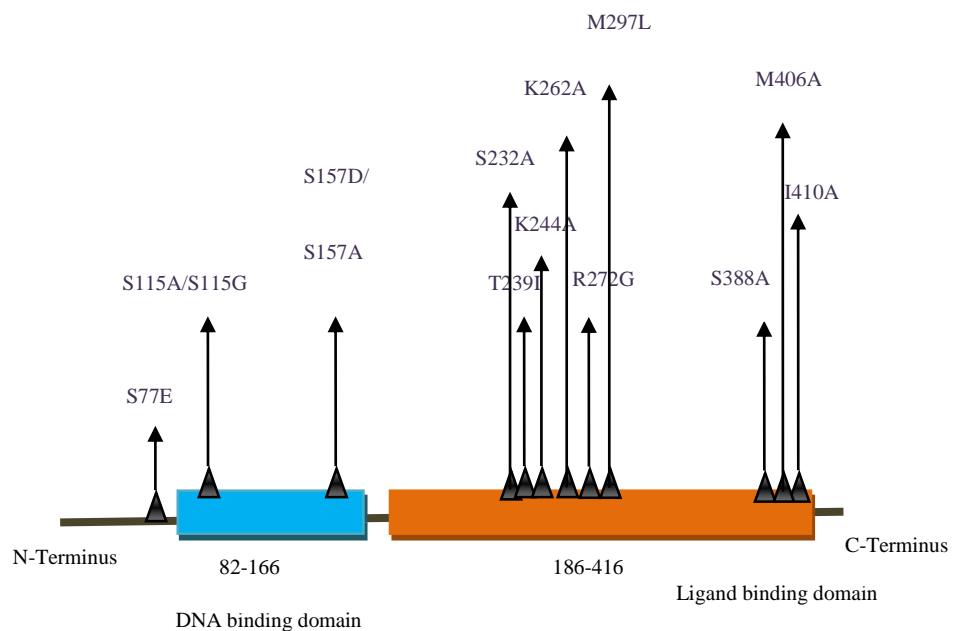


**Figure 1 Mutations in RAR alpha**

## **Appendix-H**

**Table 1 Mutations in FXR**

<b>Serial Number</b>	<b>Mutation</b>	<b>Type</b>	<b>Effect</b>	<b>Literature Review Source</b>
1.	A291S	Missense	Reduced activation by the ligands	(Wang et al., 2006)
2.	L348A	Missense	Reduced activation by the ligands	(Wang et al., 2006)
3.	W469F	Missense	Reduced activation by the ligands	(Wang et al., 2006)
4.	M290V	Missense	Diminished the level of protein expression	(Wang et al., 2006)
5.	M328I	Missense	Diminished the level of protein expression	(Wang et al., 2006)
6.	I352S	Missense	Diminished the level of protein expression	(Wang et al., 2006)
7.	I357H	Missense	Diminished the level of protein expression	(Wang et al., 2006)
8.	F366S	Missense	Diminished the level of protein expression	(Wang et al., 2006)
9.	L451Y	Missense	Diminished the level of protein expression	(Wang et al., 2006)
10.	L465F	Missense	Diminished the level of protein expression	(Wang et al., 2006)
11.	Y369Q	Missense	Diminished the level of protein expression	(Wang et al., 2006)
12.	H249S	Missense	Not activated by the ligand	(Wang et al., 2006)
13.	S332V	Missense	Not activated by the ligand	(Wang et al., 2006)
14.	R351H	Missense	Not activated by the ligand	(Wang et al., 2006)
15.	Y361F	Missense	Not activated by the ligand	(Wang et al., 2006)

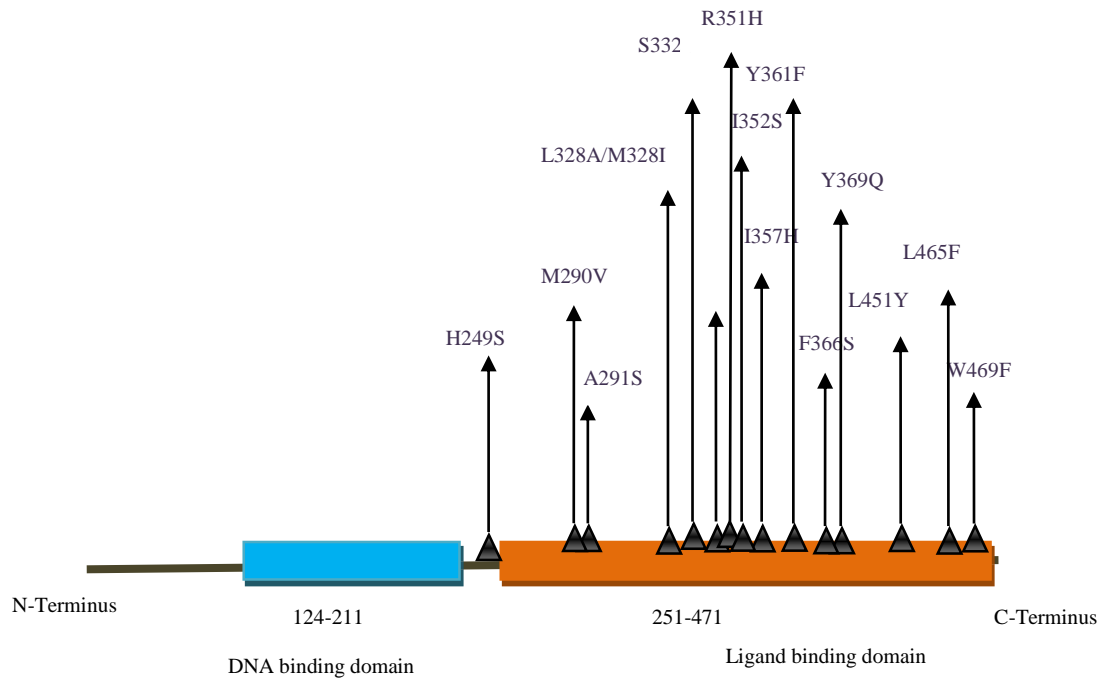


**Figure 1 Mutations in FXR**

## ***Appendix-I***

### **Preparation of Assay Buffer**

- 10% Glycerol - 20ml of Glycerol in 180ml of distilled water
- 25mM HEPES -0.005moles of HEPES in 238.3grams/mole.
- 12.5mM MgCl<sub>2</sub>- 0.50825grams of MgCl<sub>2</sub> in 180ml of water
- 50mM KCl – 0.7455grams of Kcl in 180ml of water.
- 1mM DTT- 0.03085grams of DTT in 180ml of water.

All the above solutions are mixed together and the pH is adjusted to 7.6 and the final volume is made up to 1000ml.

## Appendix-J

### Saturation Binding Analysis

The results of saturation binding analysis are as follows:

#### 1. PPAR- $\alpha$ with $C^{14}$ Labeled DHA

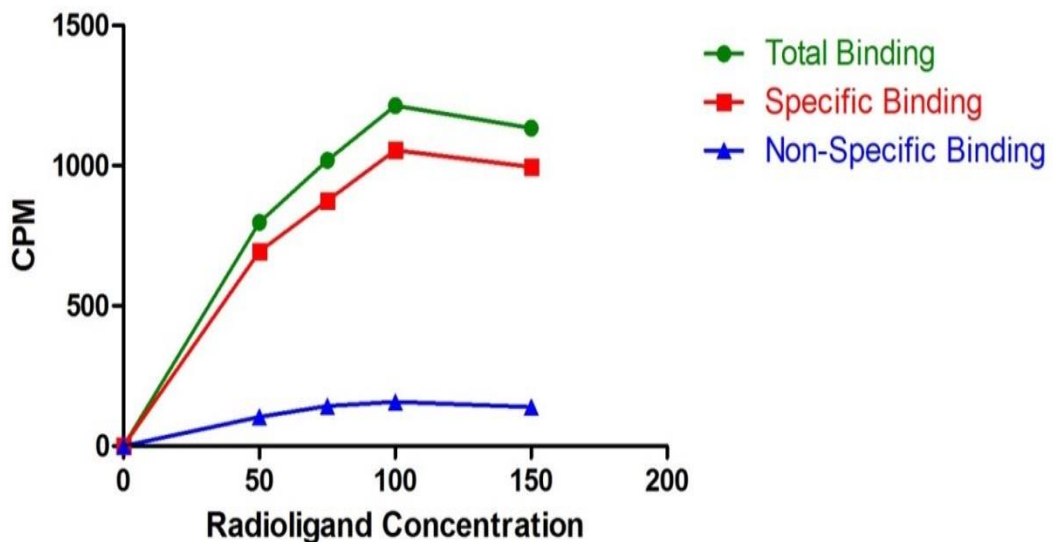


Figure 1 Total binding of PPAR- $\alpha$  with DHA

Table 1 Total binding of PPAR- $\alpha$  with DHA

Radio ligand Concentration (nM)	Total Binding (CPM)	Specific Binding (CPM)	Nonspecific Binding (CPM)
50	801	656	145
75	1028	840	188
100	1230	1045	185
150	1190	936	254

**Table 2 Specific binding of PPAR- $\alpha$  with DHA**

Radio ligand Concentration (nM)	Specific Binding (CPM)	Specific Binding ( $\mu$ M)	Specific Binding ( $\mu$ M/mg)
50	656	0.059	0.050
75	840	0.076	0.064
100	1045	0.095	0.081
150	936	0.087	0.074

1. 656CPM/ 0.10989 CPM/fmol /0.1ml

$$= 596967 \text{ pM or } 0.059 \mu\text{M}$$

2. 840CPM/ 0.10989 CPM/fmol /0.1ml

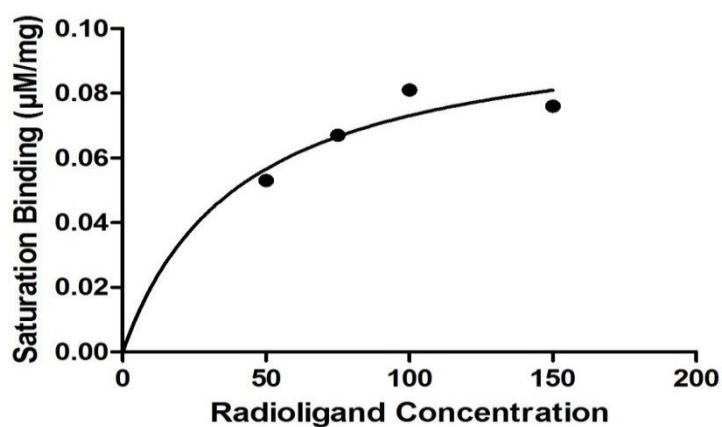
$$= 76440 \text{ pM or } 0.076 \mu\text{M}$$

3. 1045CPM/ 0.10989 CPM/fmol /0.1ml

$$= 95095 \text{ pM or } 0.095 \mu\text{M}$$

4. 936CPM/ 0.10989 CPM/fmol /0.1ml

$$= 85176 \text{ pM or } 0.087 \mu\text{M}$$

**Figure 2 Specific binding of PPAR- $\alpha$  with DHA**

## 2. CB1 with H<sup>3</sup> Labeled Anandamide

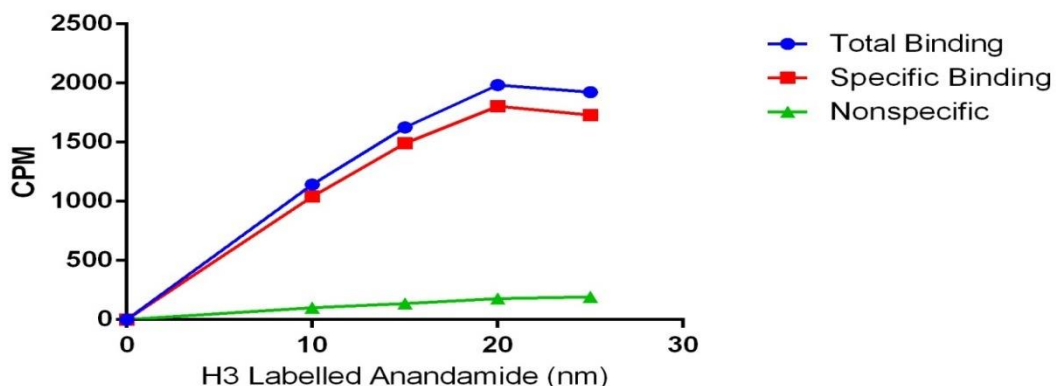


**Figure 3 Total binding of CB1 with H<sup>3</sup>Anandamide**

**Table 3 Total binding of CB1 with H<sup>3</sup> Anandamide**

Radio ligand Concentration (nM)	Total Binding (CPM)	Specific Binding (CPM)	Nonspecific Binding (CPM)
10	1142	1040	102
15	1627	1491	136
20	1985	1806	179
25	1923	1730	193

The specific activity of H<sup>3</sup> labelled Anandamide is 200ci/mmol.

Efficiency calculated by microbeta during normalization of the sample is 0.95.

Converting it into CPM/fmol = SA × Eff × 2.22

$$= 421.8 \text{ CPM/fmol}$$

The specific activity of H<sup>3</sup> labelled Anandamide is 421.8CPM/fmol

Equation to convert CPM to pM :

pM = CPM/SA (CPM in fmol) / Vol (in ml). Total volume is a 100μl aliquot of a stock mix.

The specific binding in CPM from Table 3 is converted into the specific binding in  $\mu\text{M}/\text{mg}$  as shown in Table 4.

**Table 4 Specific binding of CB1 with  $\text{H}^3\text{Anandamide}$**

Radio ligand Concentration (nM)	Specific Binding (CPM)	Specific Binding (pM/mg)
10	1040	24.67
15	1491	35.34
20	1806	42.81
25	1730	41.01

1.  $1040\text{CPM} / 421.8 \text{ CPM/fmol} / 0.1\text{ml}$   
 $= 24.67\text{pM}$
2.  $1491\text{CPM} / 421.8 \text{ CPM/fmol} / 0.1\text{ml}$   
 $= 35.34\text{pM}$
3.  $1806\text{CPM} / 421.8 \text{ CPM/fmol} / 0.1\text{ml}$   
 $= 42.81\text{pM}$
4.  $1730\text{CPM} / 421.8 \text{ CPM/fmol} / 0.1\text{ml}$   
 $= 41.01\text{pM}$

Graph Pad calculates the best fit  $B_{\max}$  as 75.50 pM/mg and  $K_d$  as 18.21nM from the graph shown in Figure 4.

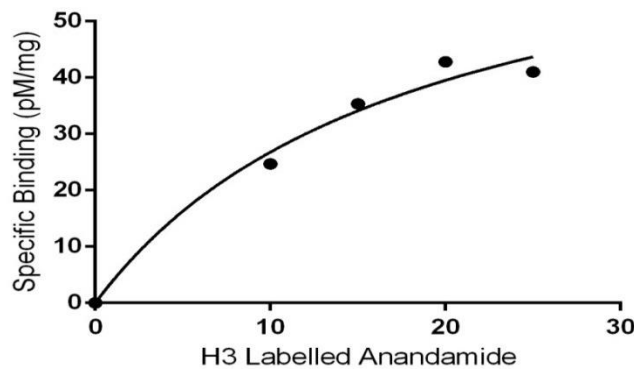


**Figure 4 Specific binding of CB1 with  $\text{H}^3\text{Anandamide}$**

### 3. CB2 with H<sup>3</sup> Labeled Anandamide

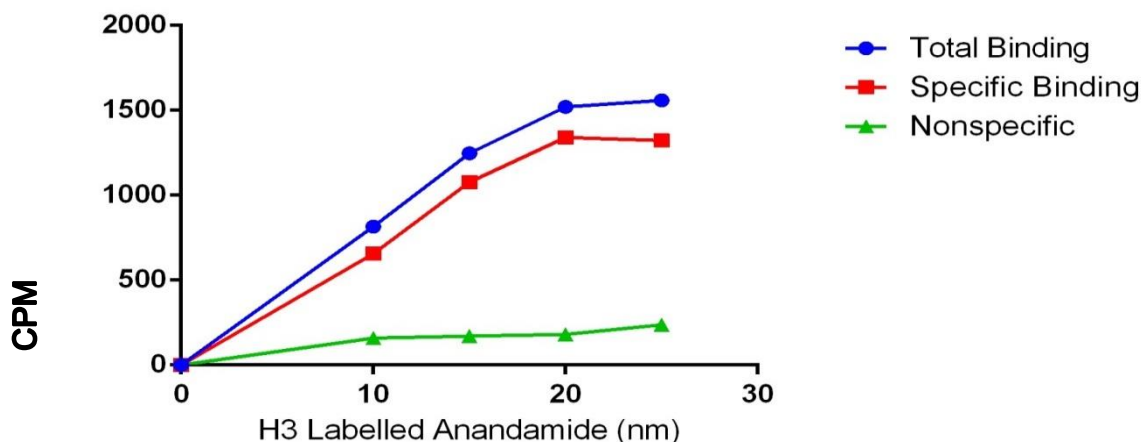


**Figure 5 Total Binding of CB2 with Anandamide**

Figure 5 represents the total, specific and nonspecific bindings of CB2 with H<sup>3</sup> labeled anandamide.

**Table 5 Total Binding of CB2 with Anandamide**

Radio ligand Concentration (nM)	Total Binding (CPM)	Specific Binding (CPM)	Nonspecific Binding (CPM)
50	815	656	159
75	1248	1078	170
100	1520	1340	180
150	1559	1322	237

The specific activity of H<sup>3</sup> labelled Anandamide is 200ci/mmol.

Efficiency calculated by microbeta during normalization of the sample is 0.95.

Converting it into CPM/fmol = SA × Eff × 2.22

$$= 421.8 \text{ CPM/fmol.}$$

The specific activity of H<sup>3</sup> labelled Anandamide is 421.8CPM/fmol.

Equation to convert CPM to pM:

$$\text{pM} = \text{CPM/SA (CPM in fmol) / Vol (in ml)}$$

Total volume is a 100 $\mu\text{l}$  aliquot of a stock mix.

**Table 6 Specific binding of CB2 with Anandamide**

Radio ligand Concentration (nM)	Specific Binding (CPM)	Specific Binding (pM/mg)
10	656	15.55
15	1078	25.55
20	1340	31.76
25	1322	31.34

The specific binding in CPM from Table 5 is converted into the specific binding in  $\mu\text{M}/\text{mg}$  as shown in Table 6.

1.  $656\text{CPM} / 421.8 \text{ CPM/fmol} / 0.1\text{ml}$

$$= 15.55\text{pM}$$

2.  $1078\text{CPM} / 421.8 \text{ CPM/fmol} / 0.1\text{ml}$

$$= 25.55$$

3.  $1340\text{CPM} / 421.8 \text{ CPM/fmol} / 0.1\text{ml}$

$$= 31.76\text{pM}$$

4.  $1322\text{CPM} / 421.8 \text{ CPM/fmol} / 0.1\text{ml}$

$$= 31.34\text{pM}$$

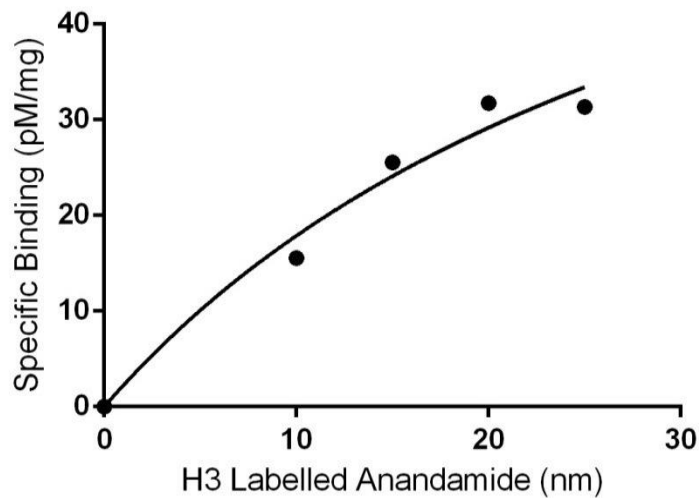


Figure 6 Specific binding of CB2 with Anandamide

#### 4. PPAR $\gamma$ with C<sup>14</sup>EPA

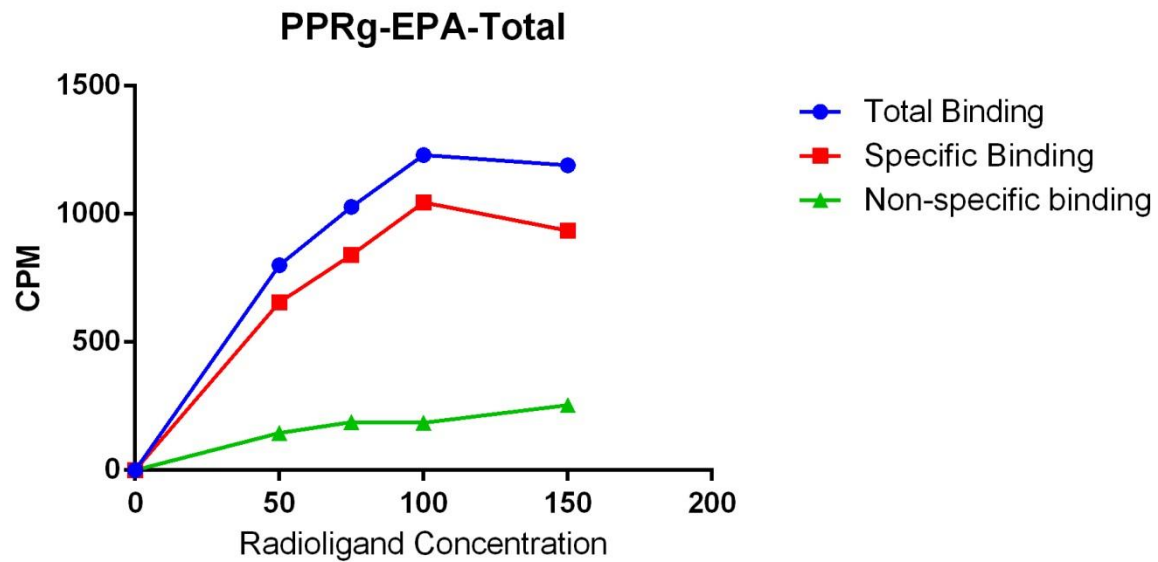


Figure 7 Total binding of PPAR- $\gamma$  with C<sup>14</sup>EPA

**Table 7 Total binding of PPAR- $\gamma$  with C<sup>14</sup>EPA**

<b>Radio ligand Concentration (nM)</b>	<b>Total Binding in CPM</b>	<b>Specific Binding in CPM</b>	<b>Non-Specific Binding in CPM</b>
50	801	656	145
75	1028	840	188
100	1230	1045	185
150	1190	936	254

Converting Specific binding into  $\mu\text{M}/\text{mg}$

**Table 8 Specific binding of PPAR- $\gamma$  with C<sup>14</sup>EPA**

<b>Radio ligand Concentration (nM)</b>	<b>Specific Binding in CPM</b>	<b>Specific Binding in <math>\mu\text{M}</math></b>	<b>Specific Binding in <math>\mu\text{M}/\text{mg}</math></b>
50	656	0.059	0.050
75	840	0.076	0.064
100	1045	0.095	0.081
150	936	0.087	0.074

$$1. \quad 656\text{CPM} / 0.10989 \text{ CPM/fmol} / 0.1\text{ml}$$

$$= 596967 \text{ pM or } 0.059 \mu\text{M}$$

$$2. \quad 840\text{CPM} / 0.10989 \text{ CPM/fmol} / 0.1\text{ml}$$

$$= 76440 \text{ pM or } 0.076 \mu\text{M}$$

$$3. \quad 1045\text{CPM} / 0.10989 \text{ CPM/fmol} / 0.1\text{ml}$$

$$= 95095 \text{ pM or } 0.095 \mu\text{M}$$

$$4. \quad 936\text{CPM} / 0.10989 \text{ CPM/fmol} / 0.1\text{ml}$$

$$= 85176 \text{ pM or } 0.087 \mu\text{M}$$

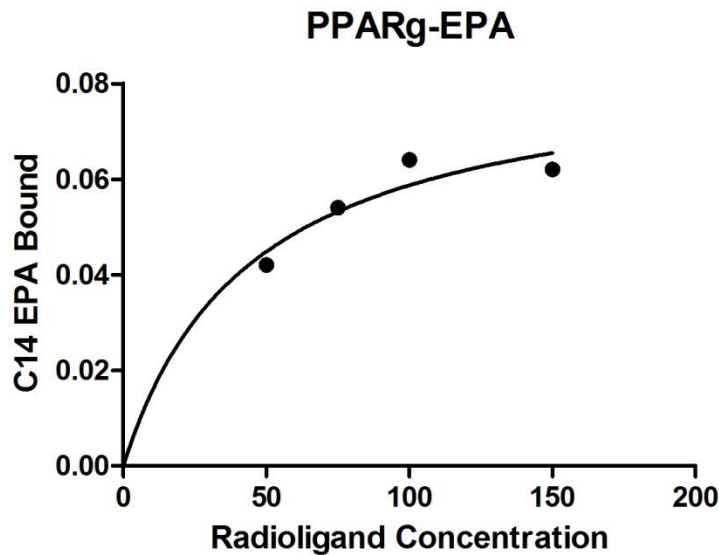


Figure 8 Specific binding of PPAR- $\gamma$  with  $C^{14}$ EPA

##### 5. PPAR- $\alpha$ with DHA

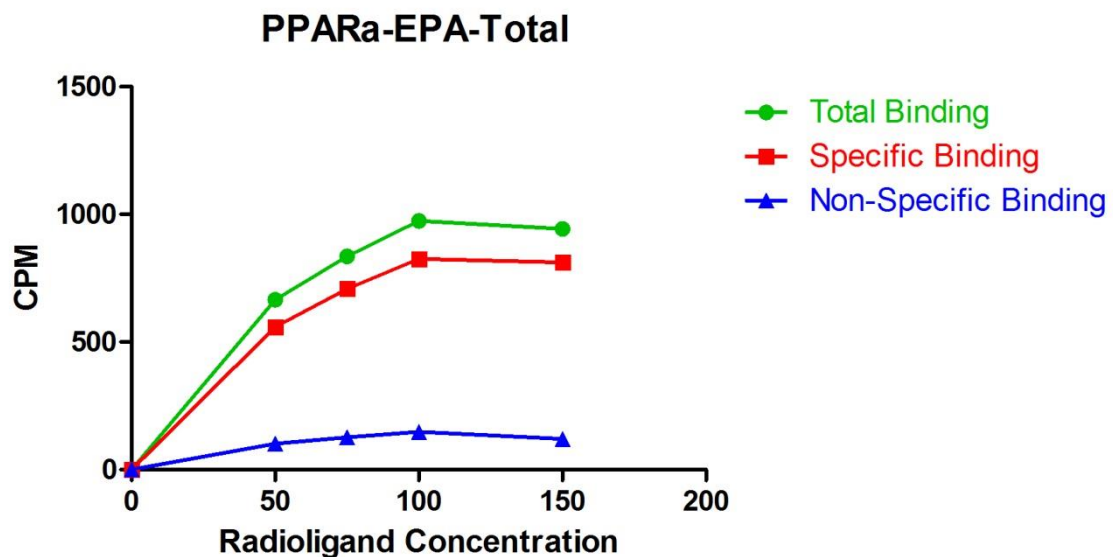


Figure 9 Total binding of PPAR- $\alpha$  with  $C^{14}$ DHA

**Table 9 Total binding of PPAR- $\alpha$  with C14DHA**

<b>Radio ligand Concentration (nM)</b>	<b>Total Binding in CPM</b>	<b>Specific Binding in CPM</b>	<b>Nonspecific Binding in CPM</b>
50	798	694	104
75	1019	876	143
100	1214	1056	158
150	1134	995	139

Converting the specific binding into  $\mu\text{mol}/\text{mg}$

**Table 10 Specific binding of PPAR- $\alpha$  with C14DHA**

<b>Radio ligand Concentration (nM)</b>	<b>Specific Binding in CPM</b>	<b>Specific Binding in <math>\mu\text{M}</math></b>	<b>Specific Binding in <math>\mu\text{M}/\text{mg}</math></b>
50	694	0.063	0.053
75	876	0.079	0.067
100	1056	0.095	0.081
150	995	0.090	0.076

$$1. \quad 694\text{CPM} / 0.10989 \text{ CPM/fmol} / 0.1\text{ml}$$

$$= 63154 \text{ pM or } 0.063 \text{ } \mu\text{M}$$

$$2. \quad 876\text{CPM} / 0.10989 \text{ CPM/fmol} / 0.1\text{ml}$$

$$= 79716 \text{ pM or } 0.079 \text{ } \mu\text{M}$$

$$3. \quad 1056\text{CPM} / 0.10989 \text{ CPM/fmol} / 0.1\text{ml}$$

$$= 96096 \text{ pM or } 0.095 \text{ } \mu\text{M}$$

$$4. \quad 995\text{CPM} / 0.10989 \text{ CPM/fmol} / 0.1\text{ml}$$

$$= 90545 \text{ pM or } 0.090 \text{ } \mu\text{M}$$

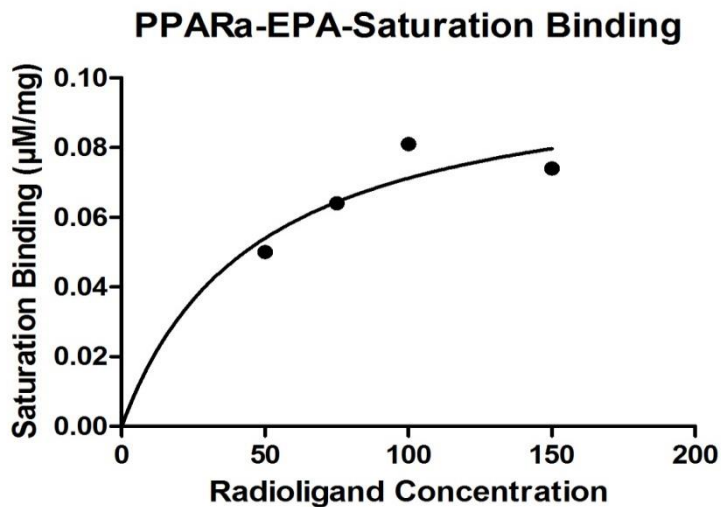


**Figure 10 Specific binding of PPAR- $\alpha$  with C14DHA**

#### 6. CB1 with 2AG

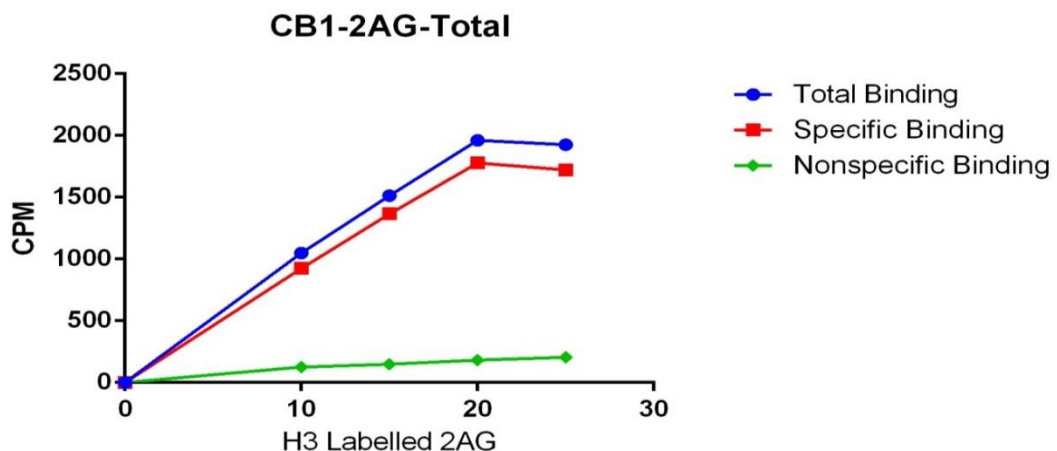


**Figure 11 Total binding of CB1 with H<sup>3</sup>2AG**

**Table 11 Total binding of CB1 with H<sup>3</sup>2AG**

Radio ligand Concentration (nM)	Total Binding in CPM	Specific Binding in CPM	Nonspecific Binding in CPM
10	1049	923	126
15	1513	1365	148
20	1961	1778	183
25	1926	1721	205

Converting CPMs of Specific binding into pM/mg

**Table 12 Specific binding of CB1 with H<sup>3</sup>2AG**

Radio ligand Concentration (nM)	Specific Binding in CPM	Specific Binding in pM/mg
10	923	109.4
15	1365	161.8
20	1778	210.7
25	1721	204.0

1. 923CPM/ 84.36CPM/fmol /0.1ml

$$= 109.41 \text{ pM}$$

2. 1365CPM/ 84.36 CPM/fmol /0.1ml

$$= 161.8 \text{ pM}$$

3. 1778CPM/ 84.36 CPM/fmol /0.1ml

$$= 210.7 \text{ pM}$$

4. 1721CPM/ 421.8 CPM/fmol /0.1ml

$$= 204.0 \text{ pM}$$

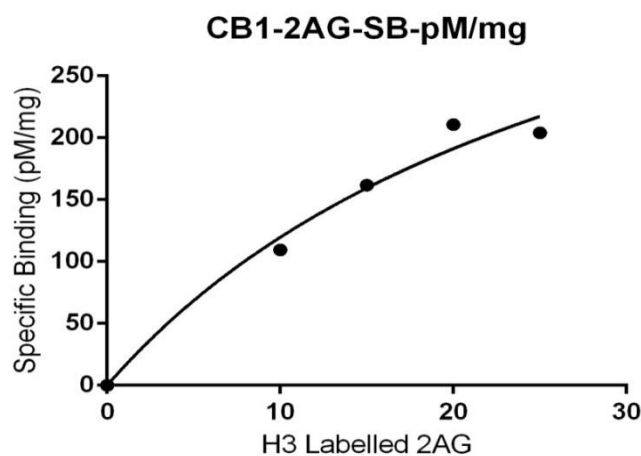


**Figure 12 Specific binding of CB1 with H<sup>3</sup>2AG**

$B_{max} = 477.1 \text{ pM/mg}$

$K_d = 29.90 \text{ nM}$

## 7. CB1 with $C^{14}$ DHA

**Table 13 Total binding of CB1 with  $C^{14}$ DHA**

Radio ligand Concentration (nM)	Total Binding in CPM	Specific Binding in CPM	Nonspecific Binding in CPM
50	1201.	1089.	112.
75	1469.	1334.	135.
100	1735.	1567.	168.
150	1713.	1521.	192.

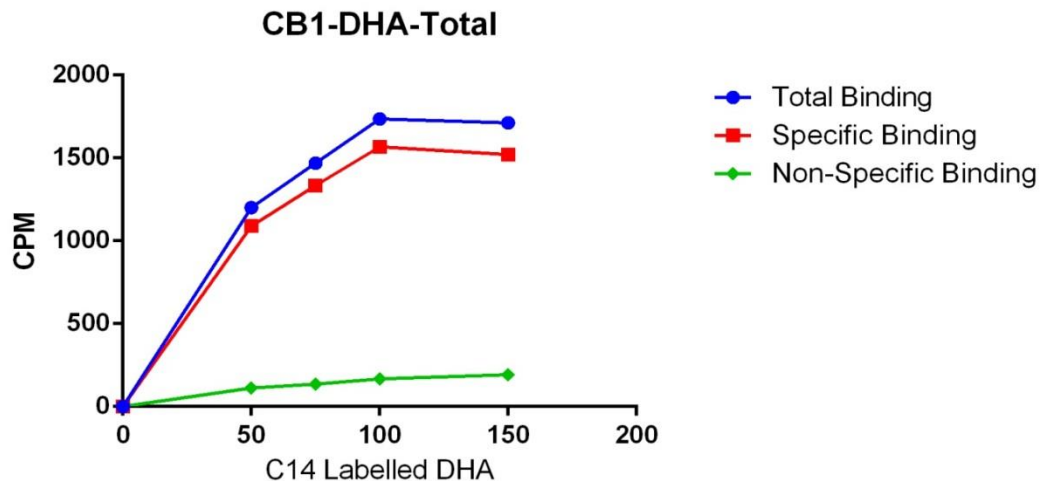


**Figure 13 Total binding of CB1 with  $C^{14}$ DHA**

Converting CPMs into pM

**Table 14 Specific binding of CB1 with  $C^{14}$ DHA**

Unlabeled Ligand in $\mu\text{M}$	Specific Binding in CPM	Specific Binding in $\mu\text{M}$
0	1089	0.099
5	1334	0.121
10	1567	0.142
20	1521	0.138

1.  $1089\text{CPM} / 0.10989 \text{ CPM/fmol} / 0.1\text{ml}$

$$= 99099\text{pM} \text{ or } 0.099\mu\text{M}$$

2.  $1334 / 0.10989 \text{ CPM/fmol} / 0.1\text{ml}$

$$= 121394\text{pM} \text{ or } 0.121 \mu\text{M}$$

3.  $1567 / 0.10989 \text{ CPM/fmol} / 0.1\text{ml}$

$$= 142597\text{pM} \text{ or } 0.142 \mu\text{M}$$

4.  $1521 / 0.10989 \text{ CPM/fmol} / 0.1\text{ml}$

$$= 138411\text{pM} \text{ or } 0.138 \mu\text{M}$$

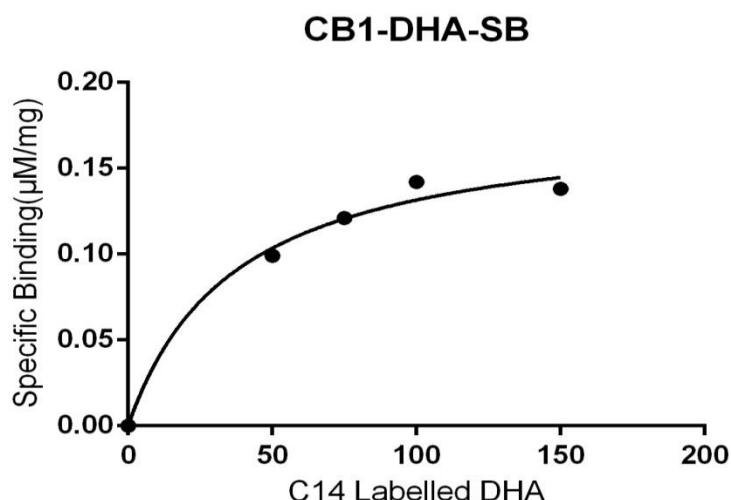


**Figure 14 Specific binding of CB1 with C<sup>14</sup>DHA**

$$B_{\max} = 0.1805$$

$$K_d = 37.22$$

### 8. CB1 with C<sup>14</sup>EPA

**Table 15 Total binding of CB1 with C<sup>14</sup> EPA**

Radio ligand Concentration (nM)	Total Binding in CPM	Specific Binding in CPM	Nonspecific Binding in CPM
50	1203.	1094.	109.
75	1591.	1456.	135.
100	1816.	1648.	168.
150	1794.	1598.	196.

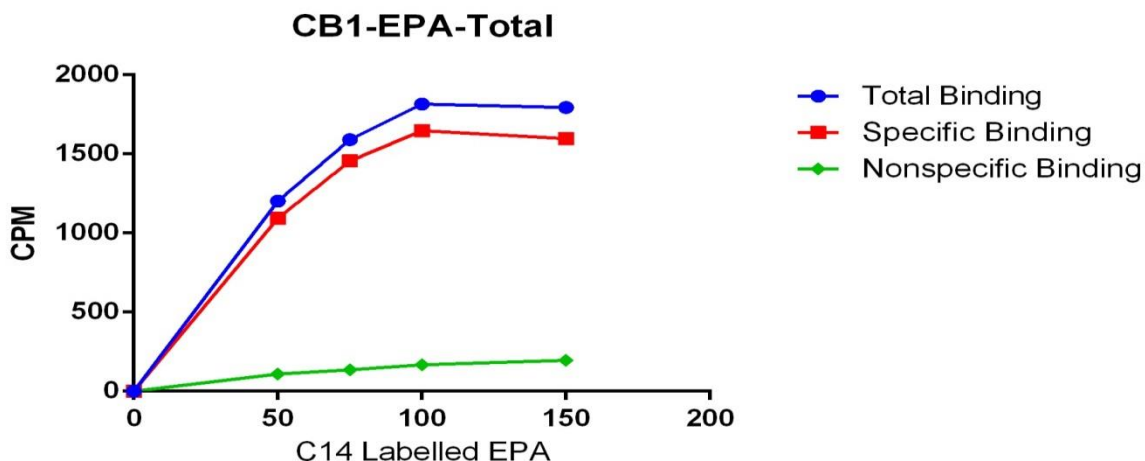


**Figure 15 Total binding of CB1 with C<sup>14</sup> EPA**

Converting CPMs into pM

**Table 16 Specific binding of CB1 with C<sup>14</sup> EPA**

Unlabeled Ligand in μM	Specific Binding in CPM	Specific Binding in μM
50	1094.	0.099
75	1456.	0.132
100	1648.	0.149
150	1598.	0.145

$$1. \frac{1094 \text{ CPM}}{0.10989 \text{ CPM/fmol}} / 0.1 \text{ ml}$$

$$= 99554 \text{ pM} \text{ or } 0.099 \mu\text{M}$$

$$2. \frac{1456}{0.10989} \text{ CPM/fmol} / 0.1 \text{ ml}$$

$$= 132496 \text{ pM} \text{ or } 0.132 \mu\text{M}$$

$$3. \frac{1648}{0.10989} \text{ CPM/fmol} / 0.1 \text{ ml}$$

$$= 149968 \text{ pM} \text{ or } 0.149 \mu\text{M}$$

$$4. \frac{1598}{0.10989} \text{ CPM/fmol} / 0.1 \text{ ml}$$

$$= 145418 \text{ pM} \text{ or } 0.145 \mu\text{M}$$

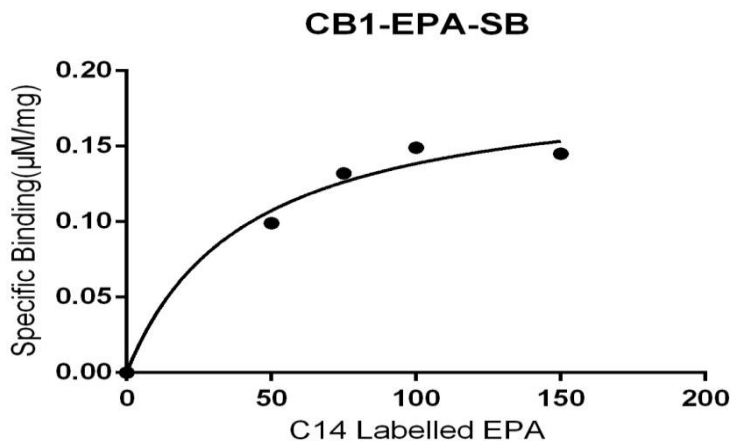


**Figure 16 Specific binding of CB1 with C<sup>14</sup> EPA**

$$B_{max} = 0.1952 \mu\text{M}/\text{mg}$$

$$K_d = 40.95 \text{nM}$$

#### 9. CB2 with H<sup>3</sup> Labelled 2AG

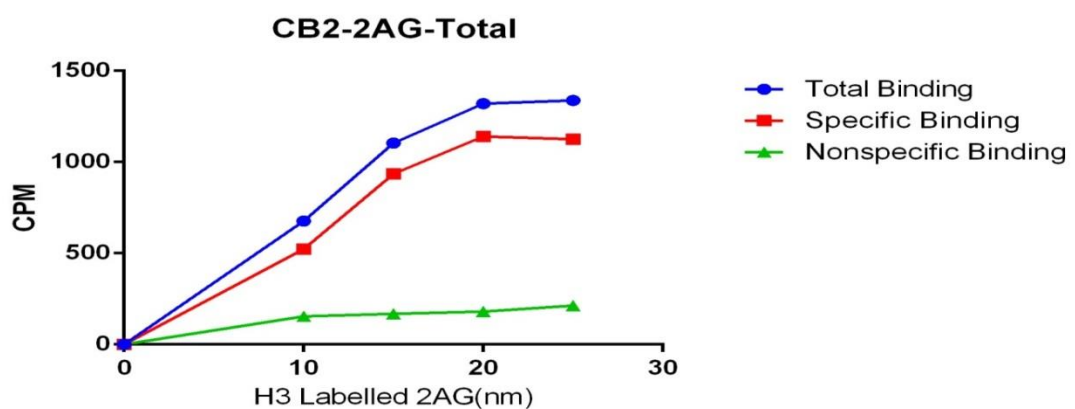


**Figure 17 Total binding of CB2 with 2AG**

**Table 17 Total binding of CB2 with 2AG**

Radio ligand Concentration (nM)	Total Binding in CPM	Specific Binding in CPM	Nonspecific Binding in CPM
50	677	523	154
75	1104	936	168
100	1321	1140	181
150	1338	1125	213

Converting CPMs of Specific binding into pM/mg

Converting it into CPM/fmol = SA \* Eff \* 2.22

$$= 40 * 0.95 * 2.22$$

$$= 84.36 \text{ CPM/fmol}$$

The specific activity of H<sup>3</sup> labelled Anandamide is 84.36CPM/fmol

**Table 18 Specific binding of CB2 with 2AG**

Radio ligand Concentration (nM)	Specific Binding in CPM	Specific Binding in pM/mg
10	523	61.99
15	936	110.95
20	1140	135.13
25	1125	133.35

1. 523CPM/ 84.36 CPM/fmol /0.1ml

$$= 61.99 \text{ pM}$$

2. 936CPM/ 84.36 CPM/fmol /0.1ml

$$= 110.95 \text{ pM}$$

3. 1140CPM/ 84.36 CPM/fmol /0.1ml

$$= 135.13 \text{ pM}$$

4. 1125CPM/ 84.36 CPM/fmol /0.1ml

$$= 133.35 \text{ pM}$$

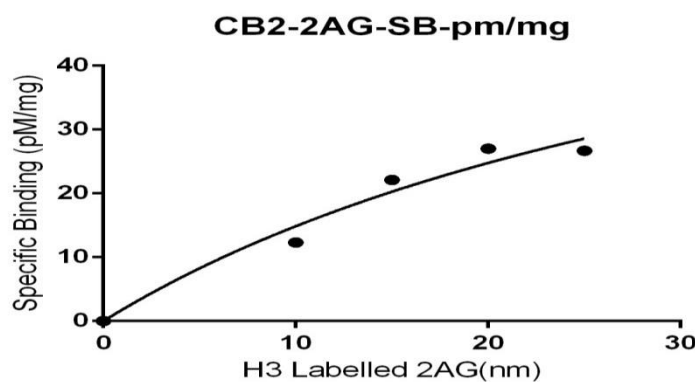


**Figure 18 Specific binding of CB2 with 2AG**

Bmax = 365.1pm/mg

K<sub>d</sub> = 38.86nM

#### **10. CB2 with C<sup>14</sup> labelled DHA**

**Table 19 Total binding of CB2 with DHA**

<b>Radio ligand Concentration (nM)</b>	<b>Total Binding in CPM</b>	<b>Specific Binding in CPM</b>	<b>Nonspecific Binding in CPM</b>
50	1385	1063	322
75	1763	1361	402
100	2083	1618	465
150	2134	1596	538

Converting CPMs into pM

**Table 20 Specific binding of CB2 with DHA**

<b>Unlabeled Ligand in μM</b>	<b>Specific Binding in CPM</b>	<b>Specific Binding in μM</b>
0	1083	0.098
5	1361	0.123
10	1618	0.147
20	1596	0.145

$$1. \quad 1063 \text{ CPM} / 0.10989 \text{ CPM/fmol} / 0.1 \text{ ml}$$

$$= 98553 \text{ pM or } 0.098 \mu\text{M}$$

$$2. \quad 1361 / 0.10989 \text{ CPM/fmol} / 0.1 \text{ ml}$$

$$= 123851 \text{ pM or } 0.123 \mu\text{M}$$

$$3. \quad 1618 / 0.10989 \text{ CPM/fmol} / 0.1 \text{ ml}$$

$$= 1472381 \text{ pM or } 0.147 \mu\text{M}$$

$$4. \quad 1596 / 0.10989 \text{ CPM/fmol} / 0.1 \text{ ml}$$

$$= 145236 \text{ pM or } 0.145 \mu\text{M}$$

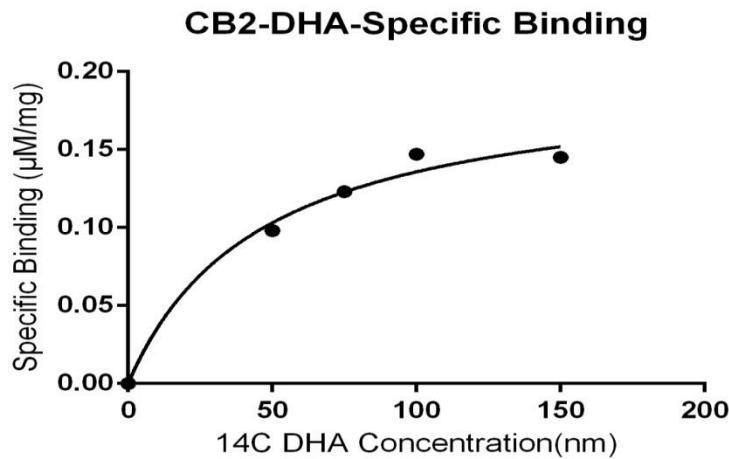


**Figure 20 Specific binding of CB2 with DHA**

$$B_{max} = 0.1989 \mu M/mg$$

$$K_d = 46.51 nM$$

### 11. CB2 with $C^{14}$ labelled EPA

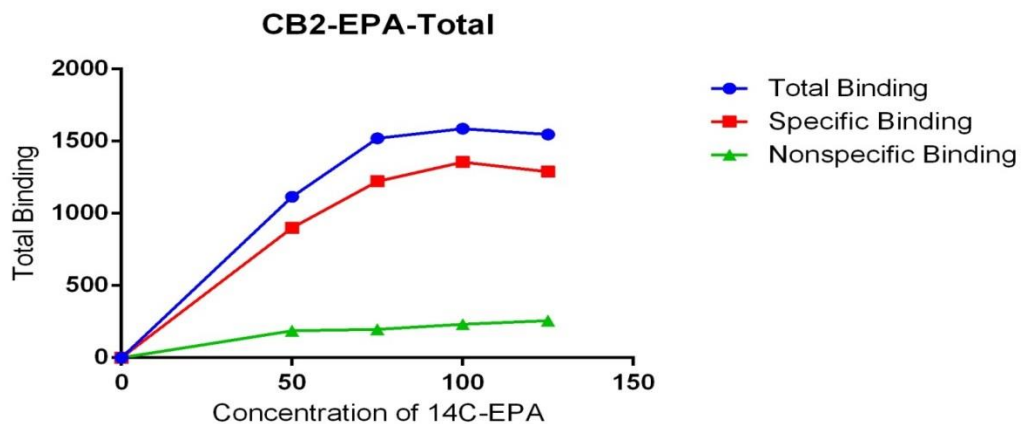


**Figure 21 Total binding of CB2 with EPA**

**Table 21 Total binding of CB2 with EPA**

Radio ligand Concentration (nM)	Total Binding in CPM	Specific Binding in CPM	Nonspecific Binding in CPM
50	1115	901	188
75	1520	1223	197
100	1588	1356	232
150	1547	1289	258

## Converting CPMs into pM

**Table 22 Specific binding of CB2 with EPA**

Unlabeled Ligand in $\mu\text{M}$	Specific Binding in CPM	Specific Binding in $\mu\text{M}$
50	804	0.073
75	1223	0.111
100	1356	0.123
150	1289	0.117

1.  $901\text{CPM} / 0.10989 \text{ CPM/fmol} / 0.1\text{ml}$

$$= 73164\text{pM or } 0.073\mu\text{M}$$

2.  $1223 / 0.10989 \text{ CPM/fmol} / 0.1\text{ml}$

$$= 111293\text{pM or } 0.111 \mu\text{M}$$

3.  $1356 / 0.10989 \text{ CPM/fmol} / 0.1\text{ml}$

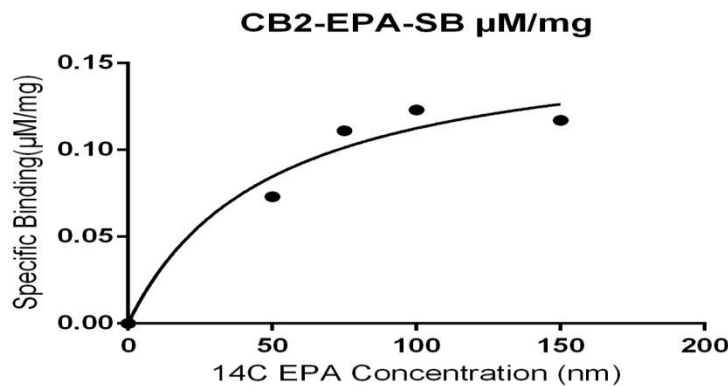
$$= 123396\text{pM or } 0.123 \mu\text{M}$$

4.  $1289 / 0.10989 \text{ CPM/fmol} / 0.1\text{ml}$

$$= 117299\text{pM or } 0.117 \mu\text{M}$$

$$B_{\max} = 0.1678\mu\text{m/mg}$$

$$K_d = 49.19\text{nM}$$

**Figure 22 Specific binding of CB2 with EPA**

## **Appendix-K**

### **Competitive Binding Analysis**

#### **1. $K_i$ of PPAR- $\alpha$ with C<sup>14</sup> Labeled DHA and Unlabeled DHA**

The radio ligand concentration is 50nM (because K<sub>d</sub> from the saturation binding analysis is 41.23nM). The unlabeled ligand concentration is taken as 100 times of the radio ligand concentration (Sittampalam et al., 2012). Table 1 shows the nonspecific binding in CPM and the conversion of nonspecific binding into  $\mu\text{M}/\text{mg}$ .

**Table 1 Binding of C<sup>14</sup>DHA to PPAR- $\alpha$  in presence of unlabeled DHA**

<b>Unlabeled Ligand in <math>\mu\text{M}</math></b>	<b>Nonspecific Binding in CPM</b>	<b>Nonspecific Binding in <math>\mu\text{M}</math></b>	<b>Nonspecific Binding in <math>\mu\text{M}/\text{mg}</math></b>
2.5	3527	0.294	0.251
5	2943	0.267	0.22
10	2526	0.229	0.195
15	1378	0.125	0.106
25	983	0.089	0.076
40	767	0.069	0.058

$$1. \quad 3527 \text{ CPM} / 0.10989 \text{ CPM/fmol} / 0.1\text{ml} \quad (100\mu\text{l} \text{ aliquot of stock mix})$$

$$= 321754 \text{ pM} \quad \text{or} \quad 0.321 \mu\text{M}$$

$$2. \quad 2943 \text{ CPM} / 0.10989 \text{ CPM/fmol} / 0.1\text{ml}$$

$$= 267813 \text{ pM} \quad \text{or} \quad 0.267 \mu\text{M}$$

$$3. \quad 2526 \text{ CPM} / 0.10989 \text{ CPM/fmol} / 0.1\text{ml}$$

$$= 229866 \text{ pM} \quad \text{or} \quad 0.229 \mu\text{M}$$

$$4. \quad 1378 \text{ CPM} / 0.10989 \text{ CPM/fmol} / 0.1\text{ml}$$

$$= 125398 \text{ pM} \quad \text{or} \quad 0.125 \mu\text{M}$$

$$5. \quad 983 \text{ CPM} / 0.10989 \text{ CPM/fmol} / 0.1\text{ml}$$

= 89453 pM or 0.089 μM

6.  $767\text{CPM}/0.10989 \text{ CPM/fmol} / 0.1\text{ml}$

= 69797 pM or 0.069 μM

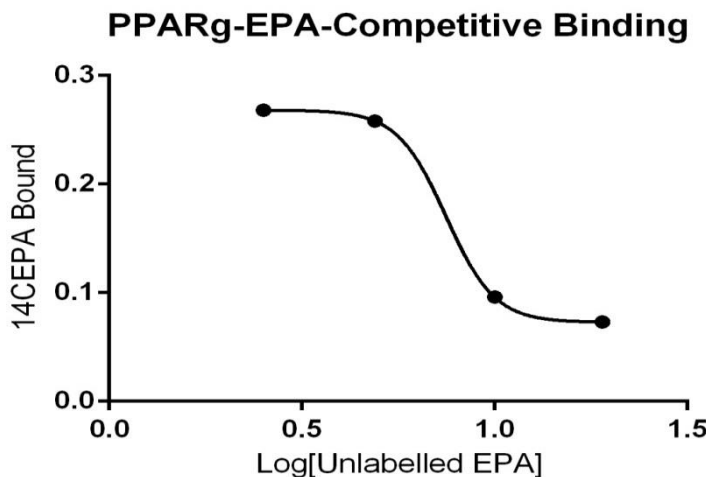


**Figure 1 Binding of  $\text{C}^{14}\text{EPA}$  to PPAR- $\gamma$  in presence of unlabelled EPA**

$\text{EC}_{50}$  and  $K_i$  values are calculated from the graph shown in Figure 7.15.

$$\text{EC}_{50} = 11.69$$

$$K_i = 11.69 / 2.21$$

$$= 5.28 \mu\text{M}.$$

## 2. $K_i$ of PPAR $\gamma$ with Radiolabelled EPA and Unlabelled EPA

**Table 2 Binding of  $\text{C}^{14}\text{EPA}$  to PPAR- $\gamma$  in presence of unlabelled EPA**

Unlabelled Ligand in $\mu\text{M}$	Non-Specific Binding in CPM	Non-Specific Binding in $\mu\text{M}$	Non-Specific Binding in $\mu\text{M}/\text{mg}$
0	3461	0.314	0.268
5	3324	0.302	0.258
10	1242	0.113	0.096
20	946	0.104	0.073

1.  $3461 \text{ CPM} / 0.10989 \text{ CPM/fmol} / 0.1\text{ml}$  ( $100\mu\text{l}$  aliquot of stock mix)

$$= 314951 \text{ pM} \text{ or } 0.314 \mu\text{M}$$

2.  $3324 \text{ CPM} / 0.10989 \text{ CPM/fmol} / 0.1\text{ml}$

$$= 302484 \text{ pM} \text{ or } 0.302 \mu\text{M}$$

3.  $1242 \text{ CPM} / 0.10989 \text{ CPM/fmol} / 0.1\text{ml}$

$$= 113022 \text{ pM} \text{ or } 0.113 \mu\text{M}$$

4.  $946 \text{ CPM} / 0.10989 \text{ CPM/fmol} / 0.1\text{ml}$

$$= 86086 \text{ pM} \text{ or } 0.086$$

$$\text{EC}_{50} = 7.4$$

$$K_i = 7.4 / 2.06$$

$$= 3.59 \mu\text{M}$$

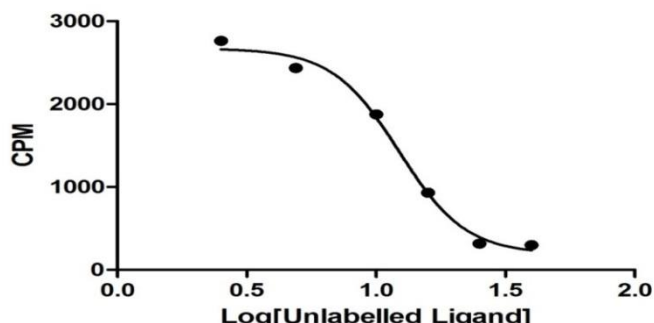


**Figure 2 Binding of C¹⁴DHA to PPAR-α in presence of unlabeled DHA**

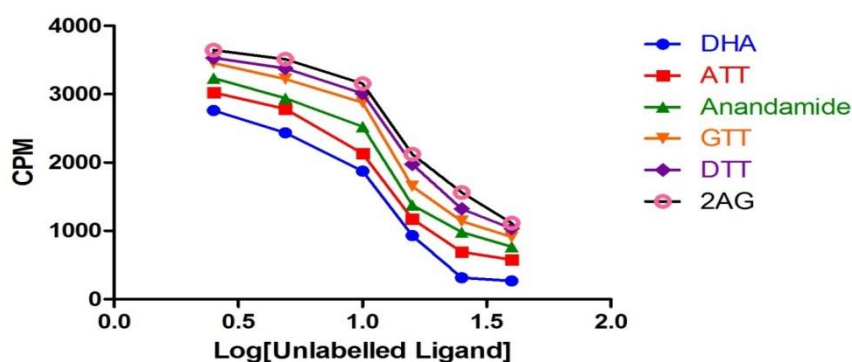


**Figure 3 Binding of C¹⁴DHA to PPAR-α in presence of unlabeled DHA**

### 3. *K<sub>i</sub> of CB1 with H<sup>3</sup> Labeled Anandamide and Unlabeled Anandamide*

The stock concentration of anandamide is 1ml/1mg. So dividing by 1 gives the same number.

Table 7.13 shows the binding of CB2 to H<sup>3</sup> Labeled Anandamide in CPM and in pM/mg.

**Table 3 Binding of H<sup>3</sup>Anandamide to CB1 in presence of unlabeled anandamide**

Unlabeled Anandamide(μM)	Binding of CB2 in presence of Unlabeled Anandamide (CPM)	Binding of CB2 in presence of Unlabeled Anandamide (pM/mg)
2.5	1758	41.67
5	1662	39.40
10	1125	26.67
15	521	12.35
25	302	7.15
40	157	3.72

$$1. \quad 1758 \text{ CPM} / 421.8 \text{ CPM/fmol} / 0.1 \text{ ml}$$

$$= 41.67 \text{ pM}$$

$$2. \quad 1662 \text{ CPM} / 421.8 \text{ CPM/fmol} / 0.1 \text{ ml}$$

$$= 39.40 \text{ pM}$$

$$3. \quad 1125 \text{ CPM} / 421.8 \text{ CPM/fmol} / 0.1 \text{ ml}$$

$$= 26.67 \text{ pM}$$

$$4. \quad 521 \text{ CPM} / 421.8 \text{ CPM/fmol} / 0.1 \text{ ml}$$

$$= 12.35 \text{ pM}$$

$$5. \quad 302 \text{ CPM} / 421.8 \text{ CPM/fmol} / 0.1 \text{ ml}$$

$$= 7.15 \text{ pM}$$

$$6. \quad 157 \text{ CPM} / 421.8 \text{ CPM/fmol} / 0.1 \text{ ml}$$

$$= 3.72 \text{ pM}$$

$$K_i = EC_{50} / [1 + ([L] / K_d)]$$

$$EC_{50} = 11.22 \text{ (calculated from the graph shown in Figure 7.17).}$$

$K_d$  calculated from saturation binding is 18.21nM.

Hot ligand concentration  $L = 20\text{nM}$ .

$$K_i = 11.22 / [1 + (20 / 18.21)]$$

$$= 11.22 / [1 + 1.09]$$

$$= 11.22 / 2.09$$

$$= 5.36 \mu\text{M}.$$

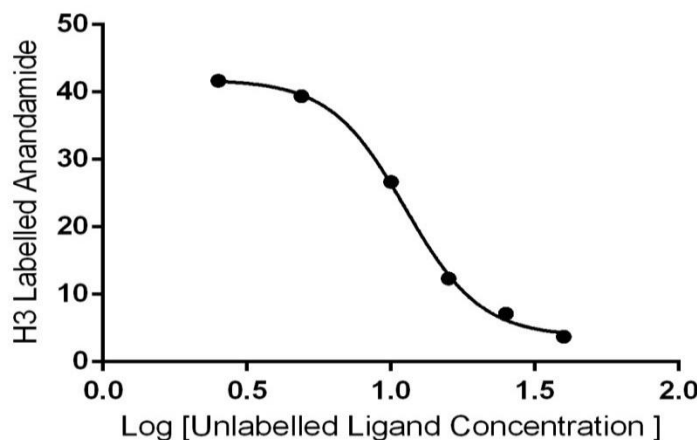


**Figure 4 Binding of  $\text{H}^3\text{Anandamide}$  to CB1 in presence of unlabeled Anandamide**

#### 4. $K_i$ of COX-2 with $\text{C}^{14}$ Labeled DHA and Unlabeled EPA

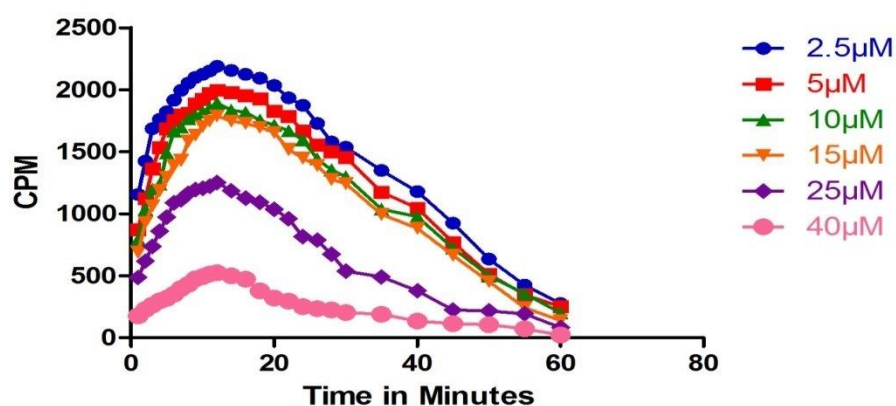


**Figure 5 Time dependent Binding of  $\text{C}^{14}\text{DHA}$  to COX-2 in presence of unlabeled EPA**

**Table 4 Binding of C<sup>14</sup>DHA to COX-2 in presence of unlabeled EPA**

Unlabeled Ligand ( $\mu\text{M}$ )	Nonspecific Binding (CPM)	Nonspecific Binding ( $\mu\text{M}$ )	Nonspecific Binding ( $\mu\text{M}/\text{mg}$ )
2.5	2189	0.199	0.90
5	1996	0.186	0.84
10	1392	0.126	0.57
15	789	0.071	0.32
25	552	0.050	0.22
40	525	0.047	0.21

Figure 5 shows the binding of COX-2 with C<sup>14</sup> labeled DHA in presence of unlabeled EPA.

Table 4 represents this binding in CPM and in  $\mu\text{M}/\text{mg}$ .

1. 2189CPM/ 0.10989 CPM/fmol /0.1ml (100 $\mu\text{l}$  aliquot of stock mix)

$$= 199199 \text{ pM} \text{ or } 0.199 \mu\text{M}$$

2. 1996CPM/ 0.10989 CPM/fmol /0.1ml

$$= 181636 \text{ pM} \text{ or } 0.186 \mu\text{M}$$

3. 1392CPM/0.10989 CPM/fmol /0.1ml

$$= 126672 \text{ pM} \text{ or } 0.126 \mu\text{M}$$

4. 789CPM/0.10989 CPM/fmol /0.1ml

$$= 71799 \text{ pM} \text{ or } 0.071 \mu\text{M}$$

5. 552CPM/0.10989 CPM/fmol /0.1ml

$$= 50232 \text{ pM} \text{ or } 0.050 \mu\text{M}$$

6. 525CPM/0.10989 CPM/fmol /0.1ml

$$= 47775 \text{ pM} \text{ or } 0.047 \mu\text{M}$$

$\text{IC}_{50} = 10.29$  (calculated from the graph shown Figure 7.24)

$$K_i = \frac{\text{IC}_{50}}{[S/(K_m + 1)]} \quad (\text{Cer et.al, 2009})$$

$$[S/(K_m + 1)]$$

Substituting IC<sub>50</sub>, Substrate Concentration and Km in the above equation:

$$= \frac{10.29}{[75/(30.66+1)]}$$

$$= \frac{10.29}{(75/31.66)}$$

$$= 10.29 / 2.36$$

$$= 4.36\mu M.$$

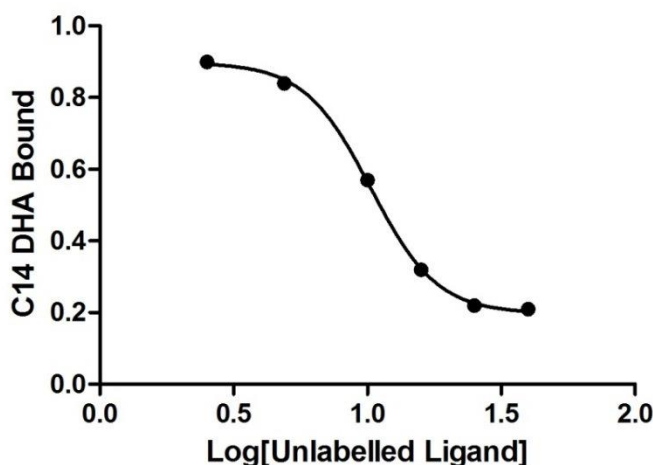


**Figure 6 Binding of C<sup>14</sup>DHA to COX-2 in presence of unlabeled EPA**

### 7. *K<sub>i</sub> of PPAR γ with Radiolabelled EPA and Unlabelled α-tocotrienol*

**Table 5 Binding of C<sup>14</sup>EPA to PPAR-γ in presence of unlabelled α-tocotrienol**

Unlabelled Ligand in μM	Non-Specific Binding in CPM	Non-Specific Binding in μM	Non-Specific Binding in μM/mg
0	3945	0.358	0.305
5	3753	0.341	0.291
10	1537	0.139	0.118
20	1052	0.090	0.081

1. 3945CPM/ 0.10989 CPM/fmol /0.1ml (100μl aliquot of stock mix)

$$= 358995 \text{ pM} \text{ or } 0.358\mu M$$

2.  $3753 \text{ CPM} / 0.10989 \text{ CPM/fmol} / 0.1\text{ml}$   
 $= 341523 \text{ pM or } 0.341 \mu\text{M}$

3.  $1537 \text{ CPM} / 0.10989 \text{ CPM/fmol} / 0.1\text{ml}$   
 $= 139867 \text{ pM or } 0.139 \mu\text{M}$

4.  $1092 \text{ CPM} / 0.10989 \text{ CPM/fmol} / 0.1\text{ml}$   
 $= 95732 \text{ pM or } 0.095 \mu\text{M}$

$\text{EC}_{50} = 7.667$

$K_i = 7.667 / 2.06 = 3.72 \mu\text{M}$

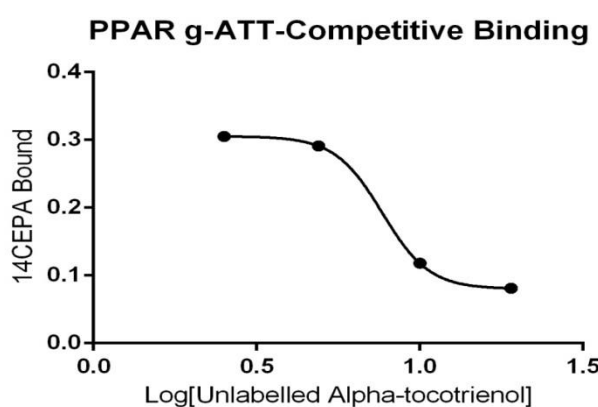


**Figure 7 Binding of  $\text{C}^{14}\text{EPA}$  to PPAR- $\gamma$  in presence of unlabelled  $\alpha$ -tocotrienol**

#### 6. $K_i$ of PPAR $\gamma$ with Radiolabelled EPA and Unlabelled $\gamma$ -tocotrienol

**Table 6 Binding of  $\text{C}^{14}\text{EPA}$  to PPAR- $\gamma$  in presence of unlabelled  $\gamma$ -tocotrienol**

Unlabelled Ligand in $\mu\text{M}$	Non-Specific Binding in CPM	Non-Specific Binding in $\mu\text{M}$	Non-Specific Binding in $\mu\text{M}/\text{mg}$
0	4131	0.375	0.320
5	3992	0.363	0.310
10	1784	0.162	0.138
20	1265	0.115	0.098

1.  $4131 \text{ CPM} / 0.10989 \text{ CPM/fmol} / 0.1\text{ml} (100\mu\text{l aliquot of stock mix})$   
 $= 375921 \text{ pM or } 0.375 \mu\text{M}$

2.  $3992 \text{ CPM} / 0.10989 \text{ CPM/fmol} / 0.1\text{ml}$  ( $100\mu\text{l}$  aliquot of stock mix)

$$= 363272 \text{ pM} \text{ or } 0.363\mu\text{M}$$

3.  $1784 \text{ CPM} / 0.10989 \text{ CPM/fmol} / 0.1\text{ml}$  ( $100\mu\text{l}$  aliquot of stock mix)

$$= 162344 \text{ pM} \text{ or } 0.162\mu\text{M}$$

4.  $1265 \text{ CPM} / 0.10989 \text{ CPM/fmol} / 0.1\text{ml}$  ( $100\mu\text{l}$  aliquot of stock mix)

$$= 115115 \text{ pM} \text{ or } 0.115\mu\text{M}$$

$$\text{EC}_{50} = 7.904$$

$$K_i = 7.904/2.06$$

$$= 3.952 \mu\text{M}$$

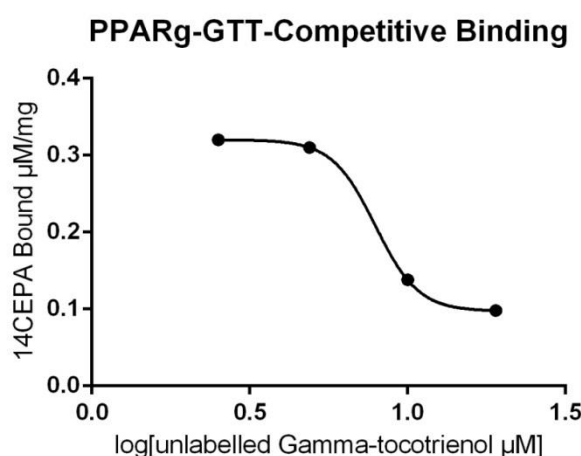


**Figure 8 Binding of  $\text{C}^{14}\text{EPA}$  to PPAR- $\gamma$  in presence of unlabelled  $\gamma$ -tocotrienol**

### 7. $K_i$ of PPAR $\gamma$ with Radiolabelled EPA and Unlabelled $\delta$ -tocotrienol

**Table 7 Binding of  $\text{C}^{14}\text{EPA}$  to PPAR- $\gamma$  in presence of unlabelled  $\delta$ -tocotrienol**

Unlabelled Ligand in $\mu\text{M}$	Non-Specific Binding in CPM	Non-Specific Binding in $\mu\text{M}$	Non-Specific Binding in $\mu\text{M}/\text{mg}$
0	4354	0.396	0.338
5	4068	0.370	0.316
10	2037	0.185	0.165
20	1302	0.118	0.100

1. 4354 CPM/ 0.10989 CPM/fmol /0.1ml (100 $\mu$ l aliquot of stock mix)

$$= 396214 \text{ pM} \text{ or } 0.396\mu\text{M}$$

2. 4068CPM/ 0.10989 CPM/fmol /0.1ml (100 $\mu$ l aliquot of stock mix)

$$= 370188 \text{ pM} \text{ or } 0.370\mu\text{M}$$

3. 2037CPM/ 0.10989 CPM/fmol /0.1ml

$$= 185367 \text{ pM} \text{ or } 0.185\mu\text{M}$$

4. 1302CPM/ 0.10989 CPM/fmol /0.1ml (100 $\mu$ l aliquot of stock mix)

$$= 11842 \text{ pM} \text{ or } 0.118\mu\text{M}$$

$$\text{EC}_{50} = 8.15$$

$$K_i = 8.15/2.06$$

$$= 3.95 \mu\text{M}$$

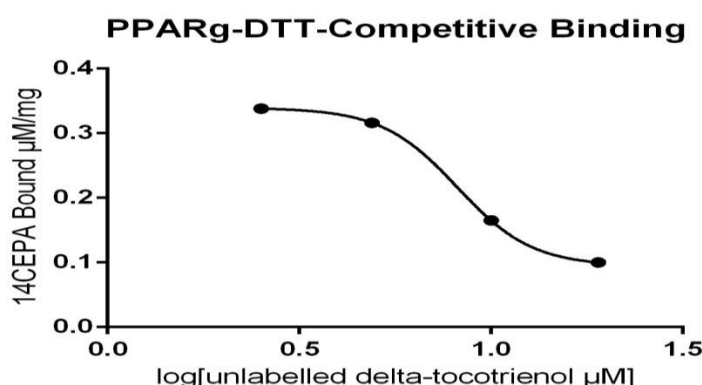


**Figure 9 Binding of C<sup>14</sup>EPA to PPAR- $\gamma$  in presence of unlabelled  $\delta$ -tocotrienol**

### 8. $K_i$ of PPAR- $\alpha$ with Radiolabelled DHA and Unlabelled $\alpha$ -tocotrienol

**Table 8 Binding of C<sup>14</sup>DHA to PPAR- $\alpha$  in presence of unlabelled  $\alpha$ -tocotrienol**

Unlabelled Ligand in $\mu\text{M}$	Non-Specific Binding in CPM	Non-Specific Binding in $\mu\text{M}$	Non-Specific Binding in $\mu\text{M}/\text{mg}$
2.5	3026.	0.321	0.275
5	2784.	0.253	0.216
10	2132.	0.194	0.165
15	1174.	0.106	0.090
25	692.	0.062	0.52
40	579.	0.052	0.044

1.  $3026 \text{ CPM} / 0.10989 \text{ CPM/fmol} / 0.1\text{ml}$  (100 $\mu\text{l}$  aliquot of stock mix)  
 $= 275366 \text{ pM}$  or  $0.275 \mu\text{M}$
2.  $2784 \text{ CPM} / 0.10989 \text{ CPM/fmol} / 0.1\text{ml}$   
 $= 25344 \text{ pM}$  or  $0.253 \mu\text{M}$
3.  $2132 \text{ CPM} / 0.10989 \text{ CPM/fmol} / 0.1\text{ml}$   
 $= 194012 \text{ pM}$  or  $0.194 \mu\text{M}$
4.  $1174 \text{ CPM} / 0.10989 \text{ CPM/fmol} / 0.1\text{ml}$   
 $= 106834 \text{ pM}$  or  $0.106 \mu\text{M}$
5.  $692 \text{ CPM} / 0.10989 \text{ CPM/fmol} / 0.1\text{ml}$   
 $= 62972 \text{ pM}$  or  $0.062 \mu\text{M}$
6.  $579 \text{ CPM} / 0.10989 \text{ CPM/fmol} / 0.1\text{ml}$   
 $= 52689 \text{ pM}$  or  $0.052 \mu\text{M}$

$$\text{EC}_{50} = 11.86$$

$$K_i = 11.86 / 2.21$$

$$= 5.36 \mu\text{M}$$

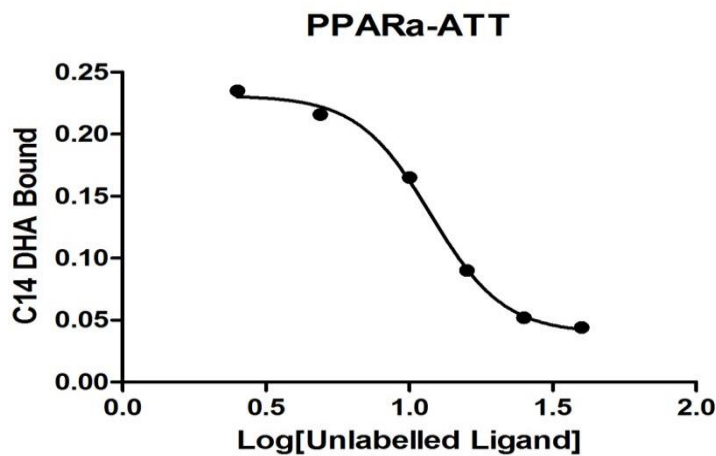


**Figure 10 Binding of C<sup>14</sup>DHA to PPAR- $\alpha$  in presence of unlabelled  $\alpha$ -tocotrienol**

**9.  $K_i$  of PPAR- $\alpha$  with Radiolabelled DHA and Unlabelled Anandamide**

**Table 9 Binding of C<sup>14</sup>DHA to PPAR- $\alpha$  in presence of unlabelled anandamide**

Unlabelled Ligand in $\mu\text{M}$	Non-Specific Binding in CPM	Non-Specific Binding in $\mu\text{M}$	Non-Specific Binding in $\mu\text{M}/\text{mg}$
2.5	2763.	0.251	0.214
5	2435.	0.221	0.180
10	1876.	0.170	0.145
15	932.	0.084	0.071
25	315.	0.028	0.023
40	298.	0.027	0.019

1. 2763CPM/ 0.10989 CPM/fmol /0.1ml (100 $\mu\text{l}$  aliquot of stock mix)

$$= 251433\text{pM} \text{ or } 0.251 \mu\text{M}$$

2. 2435CPM/ 0.10989 CPM/fmol /0.1ml (100 $\mu\text{l}$  aliquot of stock mix)

$$= 221585\text{pM} \text{ or } 0.221 \mu\text{M}$$

3. 1876CPM/ 0.10989 CPM/fmol /0.1ml (100 $\mu\text{l}$  aliquot of stock mix)

$$= 170716\text{pM} \text{ or } 0.170 \mu\text{M}$$

4. 932CPM/ 0.10989 CPM/fmol /0.1ml

$$= 84812\text{pM} \text{ or } 0.084 \mu\text{M}$$

5. 315CPM/ 0.10989 CPM/fmol /0.1ml

$$= 28665\text{pM} \text{ or } 0.028 \mu\text{M}$$

6. 298CPM/ 0.10989 CPM/fmol /0.1ml

$$= 27118\text{pM} \text{ or } 0.023 \mu\text{M}$$

$$\text{So } K_i = 12.49 / [1 + (50/41.23)]$$

$$= 12.49 / 1+1.21$$

$$= 12.49 / 2.21$$

$$= 5.65\mu\text{M}$$

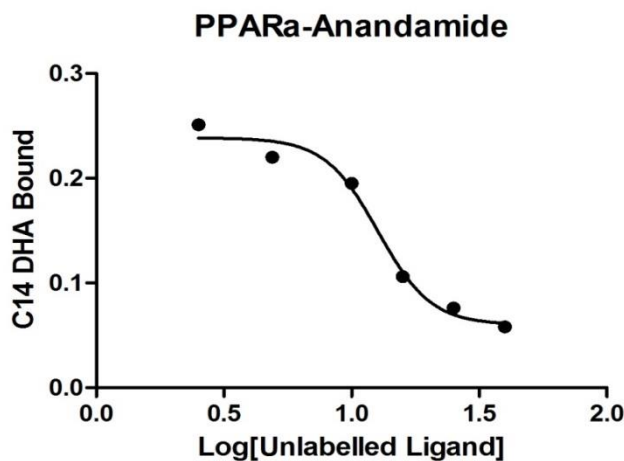


**Figure 11 Binding of C<sup>14</sup>DHA to PPAR- $\alpha$  in presence of unlabelled Anandamide**

**10.  $K_i$  of PPAR- $\alpha$  with Radiolabelled DHA and Unlabelled  $\gamma$ -tocotrienol**

**Table 10 Binding of C<sup>14</sup>DHA to PPAR- $\alpha$  in presence of unlabelled  $\gamma$ -tocotrienol**

Unlabelled Ligand in $\mu\text{M}$	Non-Specific Binding in CPM	Non-Specific Binding in $\mu\text{M}$	Non-Specific Binding in $\mu\text{M}/\text{mg}$
2.5	3456.	0.314	0.26
5	3223.	0.293	0.25
10	2878.	0.261	0.223
15	1652.	0.150	0.128
25	1143.	0.104	0.088
40	912.	0.082	0.07

1. 3456 CPM/ 0.10989 CPM/fmol /0.1ml (100 $\mu\text{l}$  aliquot of stock mix)

$$= 314496 \text{ pM} \text{ or } 0.314 \mu\text{M}$$

2. 3223CPM/ 0.10989 CPM/fmol /0.1ml (100 $\mu\text{l}$  aliquot of stock mix)

$$= 293293 \text{ pM} \text{ or } 0.293 \mu\text{M}$$

3. 2878CPM/ 0.10989 CPM/fmol /0.1ml (100 $\mu\text{l}$  aliquot of stock mix)

$$= 261898 \text{ pM} \text{ or } 0.261 \mu\text{M}$$

4. 1652CPM/ 0.10989 CPM/fmol /0.1ml (100 $\mu\text{l}$  aliquot of stock mix)

$$= 150332 \text{ pM} \text{ or } 0.150 \mu\text{M}$$

5.  $1143 \text{ CPM} / 0.10989 \text{ CPM/fmol} / 0.1\text{ml}$

$$= 104013 \text{ pM} \text{ or } 0.104 \mu\text{M}$$

6.  $912 \text{ CPM} / 0.10989 \text{ CPM/fmol} / 0.1\text{ml}$

$$= 82992 \text{ pM} \text{ or } 0.082 \mu\text{M}$$

$$\text{EC}_{50} = 13.45$$

$$K_i = 13.45 / 2.21$$

$$= 6.08 \mu\text{M}$$

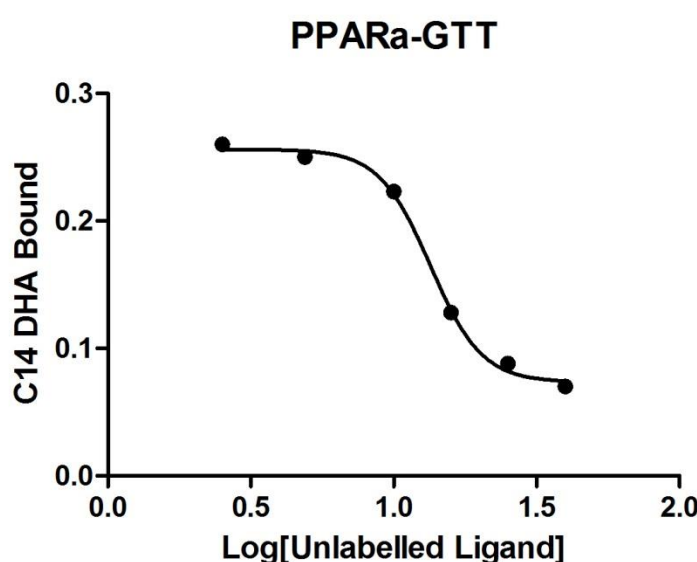


**Figure 12 Binding of C<sup>14</sup>DHA to PPAR- $\alpha$  in presence of unlabelled  $\gamma$ -tocotrienol**

### **11. *K<sub>i</sub> of PPAR- $\alpha$ with Radiolabelled DHA and Unlabelled $\delta$ -tocotrienol***

**Table 11 Binding of C<sup>14</sup>DHA to PPAR- $\alpha$  in presence of unlabelled  $\delta$ -tocotrienol**

Unlabelled Ligand in $\mu\text{M}$	Non-Specific Binding in CPM	Non-Specific Binding in $\mu\text{M}$	Non-Specific Binding in $\mu\text{M}/\text{mg}$
2.5	3531.	0.321	0.274
5	3378.	0.307	0.262
10	3012.	0.274	0.234
15	1976.	0.179	0.152
25	1323.	0.120	0.102
40	1036.	0.094	0.08

1. 3531 CPM/ 0.10989 CPM/fmol /0.1ml (100 $\mu$ l aliquot of stock mix)

= 321321 pM or 0.321 $\mu$ M

2. 3378CPM/ 0.10989 CPM/fmol /0.1ml (100 $\mu$ l aliquot of stock mix)

= 307398 pM or 0.307 $\mu$ M

3. 3012CPM/ 0.10989 CPM/fmol /0.1ml (100 $\mu$ l aliquot of stock mix)

= 274092 pM or 0.274 $\mu$ M

4. 1976CPM/ 0.10989 CPM/fmol /0.1ml

= 179816 pM or 0.179 $\mu$ M

5. 1323CPM/ 0.10989 CPM/fmol /0.1ml

= 120393 pM or 0.120 $\mu$ M

6. 1036CPM/ 0.10989 CPM/fmol /0.1ml

= 94276 pM or 0.094 $\mu$ M

$EC_{50}$  = 14.22

$K_i$  = 14.22/2.21

= 6.43  $\mu$ M

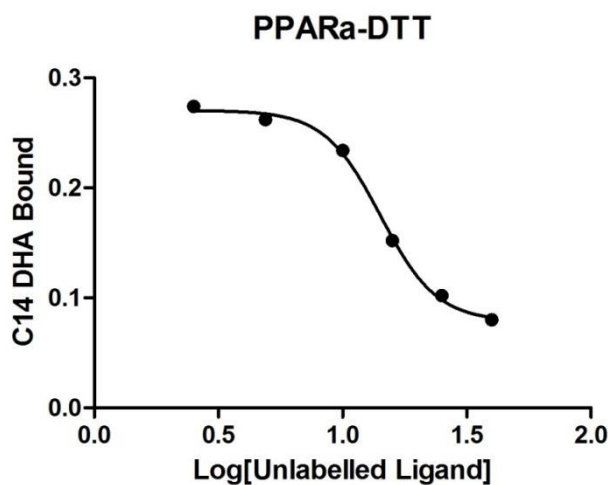


**Figure 13 Binding of C<sup>14</sup>DHA to PPAR- $\alpha$  in presence of unlabelled  $\delta$ -tocotrienol**

**12. *K<sub>i</sub>of PPAR-α with Radiolabelled DHA and Unlabelled 2AG***

1. 3645 CPM/ 0.10989 CPM/fmol /0.1ml (100μl aliquot of stock mix)

= 331695 pM or 0.331μM

2. 3513CPM/ 0.10989 CPM/fmol /0.1ml (100μl aliquot of stock mix)

= 319683 pM or 0.319μM

3. 3156CPM/ 0.10989 CPM/fmol /0.1ml

= 287196 pM or 0.287μM

4. 2123CPM/ 0.10989 CPM/fmol /0.1ml

= 193193 pM or 0.193μM

5. 1562CPM/ 0.10989 CPM/fmol /0.1ml

= 142143 pM or 0.142μM

6. 1114CPM/ 0.10989 CPM/fmol /0.1ml

= 101374 pM or 0.101μM

$EC_{50}$  = 14.83

$K_i$  = 14.83/2.21

= 6.71 μM

**Table 12 Binding of C<sup>14</sup>DHA to PPAR-α in presence of unlabelled 2AG**

Unlabelled Ligand in μM	Non-Specific Binding in CPM	Non-Specific Binding in μM	Non-Specific Binding in μM/mg
2.5	3645.	0.331	0.282
5	3513.	0.319	0.272
10	3156.	0.287	0.245
15	2123.	0.193	0.164
25	1562.	0.142	0.121
40	1114.	0.101	0.086

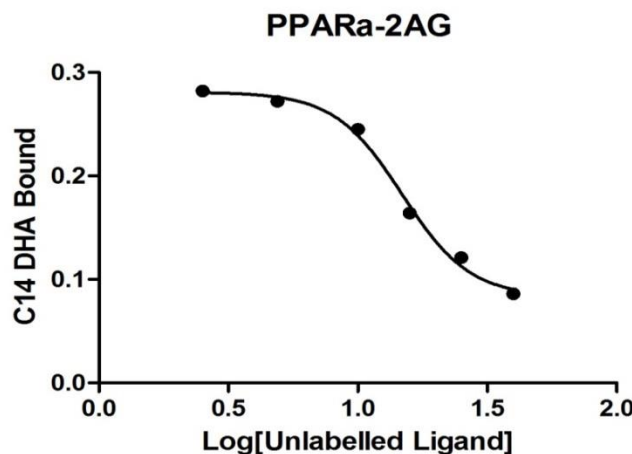


**Figure 14 Binding of C<sup>14</sup>DHA to PPAR- $\alpha$  in presence of unlabelled 2AG**

### 13. $K_i$ of CB1 with Radiolabelled Anandamide and Unlabelled $\alpha$ -tocotrienol

**Table 13 Binding of H<sup>3</sup>Anandamide to CB1 in presence of unlabelled  $\alpha$ -tocotrienol**

Unlabelled Anandamide in $\mu\text{M}$	Binding of CB2 in presence of Unlabelled Anandamide in CPM	Binding of CB2 in presence of Unlabelled Anandamide in pM/mg
2.5	1803.	42.74
5	1756.	41.63
10	1297.	30.74
15	676.	16.02
25	353.	8.36
40	202.	4.78

1. 1803CPM/ 421.8 CPM/fmol /0.1ml  
= 42.74pM
2. 1756CPM/ 421.8 CPM/fmol /0.1ml  
= 41.63pM
3. 1297CPM/ 421.8 CPM/fmol /0.1ml  
= 30.74pM
4. 676CPM/ 421.8 CPM/fmol /0.1ml  
= 16.02pM
5. 353CPM/ 421.8 CPM/fmol /0.1ml  
= 8.36pM

6. 202CPM/ 421.8 CPM/fmol /0.1ml  
 $= 4.78\text{pM}$

$$\text{EC}_{50} = 12.48$$

$$K_i = 12.48/2.09 \\ = 5.97\mu\text{M}$$

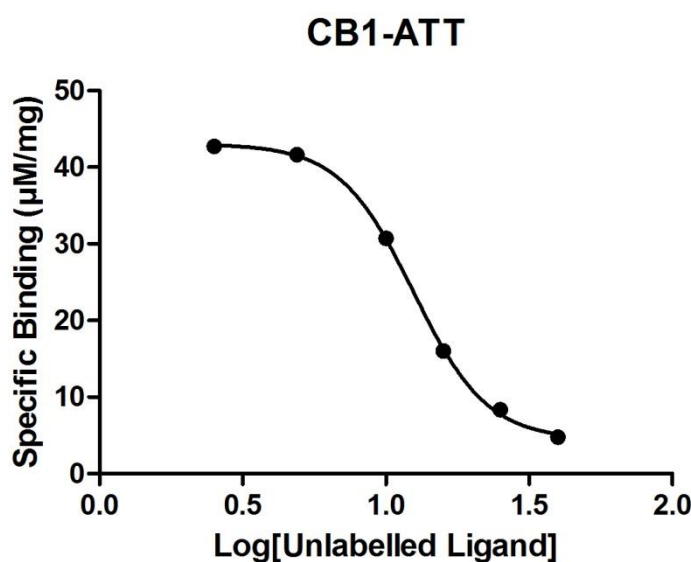


Figure 15 Binding of  $\text{H}^3\text{Anandamide}$  to CB1 in presence of unlabelled  $\alpha$ -tocotrienol

#### 14. $K_i$ of CB1 with Radiolabelled Anandamide and Unlabelled $\gamma$ -tocotrienol

Table 14 Binding of  $\text{H}^3\text{Anandamide}$  to CB1 in presence of unlabelled  $\gamma$ -tocotrienol

Unlabelled Anandamide in μM	Binding of CB2 in presence of Unlabelled Anandamide in CPM	Binding of CB2 in presence of Unlabelled Anandamide in pM/mg
2.5	2034.	48.22
5	1968.	46.55
10	1512.	35.84
15	921.	21.83
25	689.	16.33
40	345.	8.17

1. 2034CPM/ 421.8 CPM/fmol /0.1ml  
= 48.22pM
2. 1968CPM/ 421.8 CPM/fmol /0.1ml  
= 46.65pM
3. 1512CPM/ 421.8 CPM/fmol /0.1ml  
= 35.84pM
4. 921CPM/ 421.8 CPM/fmol /0.1ml  
= 21.83pM
5. 689CPM/ 421.8 CPM/fmol /0.1ml  
= 16.33pM
6. 345CPM/ 421.8 CPM/fmol /0.1ml  
= 8.17pM

$$EC_{50} = 13.39$$

$$K_i = 13.39/2.09$$

$$= 6.4 \mu M$$

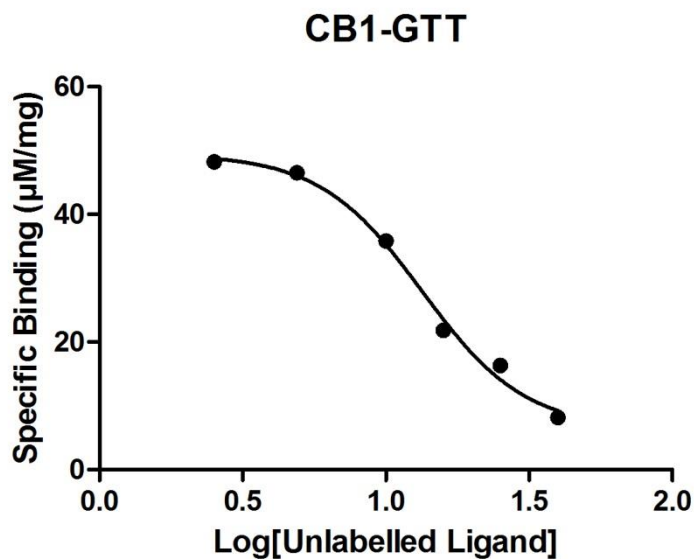


**Figure 16 Binding of H<sup>3</sup>Anandamide to CB1 in presence of unlabelled γ-tocotrienol**

**15.  $K_i$  of CB1 with Radiolabelled Anandamide and Unlabelled  $\delta$ -tocotrienol****Table 15 Binding of H<sup>3</sup>Anandamide to CB1 in presence of unlabelled  $\gamma$ -tocotrienol**

Unlabelled Anandamide in $\mu\text{M}$	Binding of CB2 in presence of Unlabelled Anandamide in CPM	Binding of CB2 in presence of Unlabelled Anandamide in pM/mg
2.5	2213.	52.46
5	2167.	51.37
10	1603.	38.00
15	1092.	25.88
25	851.	20.17
40	428.	10.14

1. 2213CPM/ 421.8 CPM/fmol /0.1ml

$$= 52.46\text{pM}$$

2. 2167CPM/ 421.8 CPM/fmol /0.1ml

$$= 51.37\text{pM}$$

3. 1603CPM/ 421.8 CPM/fmol /0.1ml

$$= 38.00\text{pM}$$

4. 1092CPM/ 421.8 CPM/fmol /0.1ml

$$= 25.88\text{pM}$$

5. 851CPM/ 421.8 CPM/fmol /0.1ml

$$= 20.17\text{pM}$$

6. 428CPM/ 421.8 CPM/fmol /0.1ml

$$= 10.14\text{pM}$$

$$\text{EC}_{50} = 14.08$$

$$K_i = 14.08/2/09$$

$$= 6.73\mu\text{M}$$

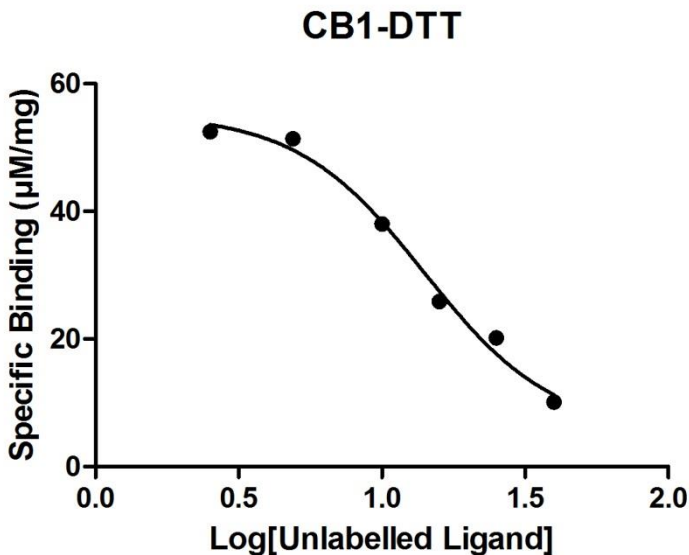


**Figure 17 Binding of H<sup>3</sup>Anandamide to CB1 in presence of unlabelled  $\gamma$ -tocotrienol**

#### 16. $K_i$ of CB2 with H<sup>3</sup>Labeled Anandamide and Unlabeled Anandamide

Radiolabeled ligand-H<sup>3</sup> labeled anandamide competed with the unlabeled anandamide, 2AG, DHA and EPA. Since tocotrienols did not produce satisfactory results during molecular docking, they were not tested in the competitive binding analysis. The concentration of H<sup>3</sup> labeled anandamide is constant (20nM) with various unlabeled ligand concentrations in both homologous and heterologous binding assays.

**Table 16 Binding of H<sup>3</sup>Anandamide to CB2 in presence of unlabeled Anandamide**

Unlabeled Anandamide in μM	Binding of CB2 in presence of Unlabeled Anandamide in CPM	Binding of CB2 in presence of Unlabeled Anandamide in pM/mg
2.5	1925	45.63
5	1775	42.08
10	1350	32.00
15	622	14.74
25	255	6.04
40	176	4.17

1. 1925CPM/ 421.8 CPM/fmol /0.1ml  
= 45.63pM
2. 1775CPM/ 421.8 CPM/fmol /0.1ml  
= 42.08pM
3. 1350CPM/ 421.8 CPM/fmol /0.1ml  
= 32.00pM
4. 622CPM/ 0.10989 CPM/fmol /0.1ml  
= 14.74pM
5. 255CPM/ 421.8 CPM/fmol /0.1ml  
= 6.04pM
6. 176CPM/ 421.8 CPM/fmol /0.1ml  
= 4.17pM

Anandamide stock concentration is 1ml/1mg. So dividing by 1 gives the same number. The binding of H<sup>3</sup> labeled anandamide to CB2 in presence of unlabeled anandamide is shown in Table 16 in both CPM and in pM/mg.

$$K_i = EC_{50} / [1 + ([L] / K_d)]$$

$$EC_{50} = 12.28$$

$$K_i \text{ calculated from saturation binding is } 34.43\text{nM.}$$

$$\text{Hot ligand concentration } L = 20\text{nM.}$$

$$K_i = 12.28 / [1 + (20 / 34.43)]$$

$$= 12.28 / [1 + 0.58]$$

$$= 12.28 / 1.58$$

$$= 7.77 \mu\text{M}$$

The logarithmic values of unlabeled ligand concentration is taken on X-axis and the amount of H<sup>3</sup>labeled anandamide bound is taken on Y- axis as shown in Figure 18.

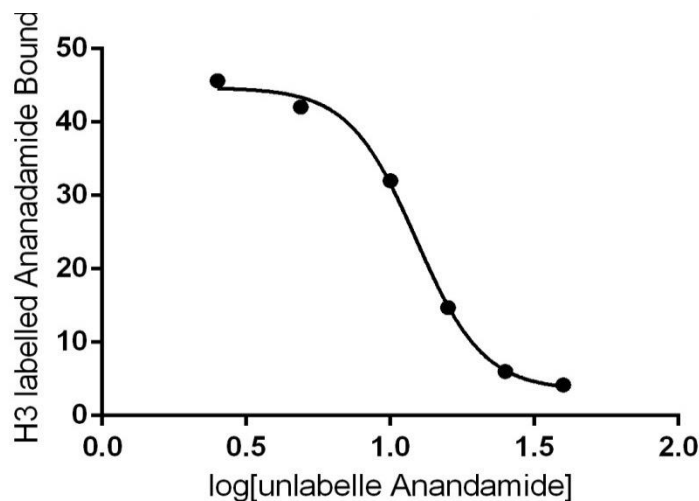


**Figure 18 Binding of H<sup>3</sup>Anandamide to CB2 in presence of unlabeled Anandamide**

The binding of unlabeled  $\alpha$ ,  $\gamma$  and  $\delta$ -tocotrienols is compared with the binding of unlabelled Anandamide and is shown in Figure 18.

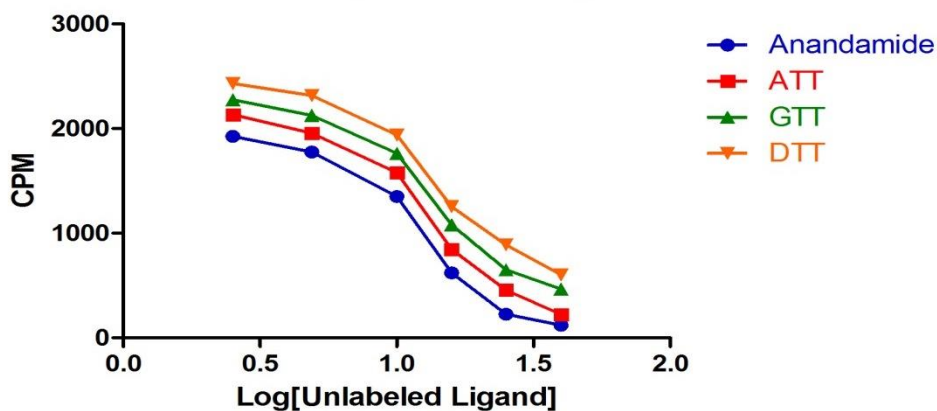


**Figure 19 Competitive Binding of CB2**

- EC<sub>50</sub> of CB2- $\alpha$ -tocotrienol = 13.30 and K<sub>i</sub> = 8.41  $\mu$ M.
- EC<sub>50</sub> of CB2- $\gamma$ -tocotrienol = 13.48 and K<sub>i</sub> = 8.53  $\mu$ M.
- EC<sub>50</sub> of CB2- $\delta$ -tocotrienol = 13.87 and K<sub>i</sub> = 8.77  $\mu$ M.

From the above data, it is concluded that tocotrienols have strong potential with CB1 than with CB2.

### 17. $K_i$ of CB2 with Radiolabelled Anandamide and Unlabelled $\alpha$ -tocotrienol

**Table 17 Binding of  $H^3$ Anandamide to CB2 in presence of unlabelled  $\alpha$ -tocotrienol**

Unlabelled Anandamide in $\mu M$	Binding of CB2 in presence of Unlabelled Anandamide in CPM	Binding of CB2 in presence of Unlabelled Anandamide in pM/mg
2.5	2134	50.59
5	1957	46.39
10	1578	37.41
15	845	20.03
25	456	10.81
40	224	5.31

$$1. \quad 2134 \text{ CPM} / 421.8 \text{ CPM/fmol} / 0.1 \text{ ml}$$

$$= 50.59 \text{ pM}$$

$$2. \quad 1957 \text{ CPM} / 421.8 \text{ CPM/fmol} / 0.1 \text{ ml}$$

$$= 46.39 \text{ pM}$$

$$3. \quad 1578 \text{ CPM} / 421.8 \text{ CPM/fmol} / 0.1 \text{ ml}$$

$$= 37.41 \text{ pM}$$

$$4. \quad 845 \text{ CPM} / 421.8 \text{ CPM/fmol} / 0.1 \text{ ml}$$

$$= 20.03 \text{ pM}$$

$$5. \quad 456 \text{ CPM} / 421.8 \text{ CPM/fmol} / 0.1 \text{ ml}$$

$$= 10.81 \text{ pM}$$

$$6. \quad 224 \text{ CPM} / 421.8 \text{ CPM/fmol} / 0.1 \text{ ml}$$

$$= 5.31 \text{ pM}$$

$$EC_{50} = 13.30$$

$$K_i = 13.30 / 1.58$$

$$= 8.41 \mu M$$

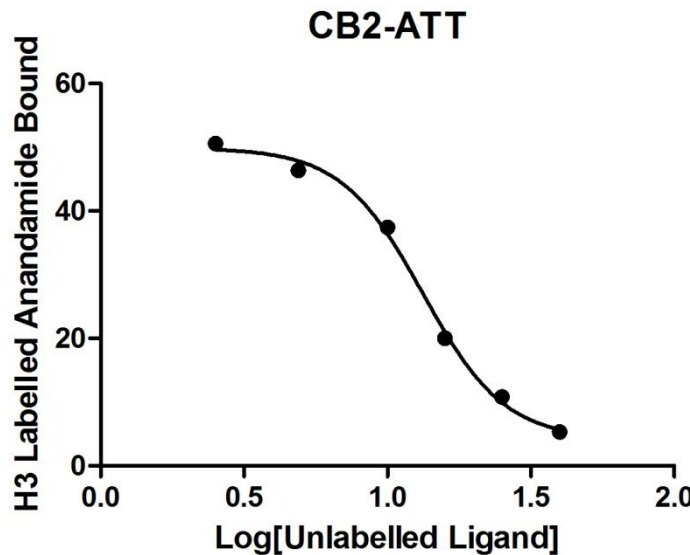


**Figure 19 Binding of H<sup>3</sup>Anandamide to CB2 in presence of unlabelled  $\alpha$ -tocotrienol**

**18. *K<sub>i</sub> of CB2 with Radiolabelled Anandamide and Unlabelled  $\gamma$ -tocotrienol***

**Table 18 Binding of H<sup>3</sup>Anandamide to CB2 in presence of unlabelled  $\gamma$ -tocotrienol**

Unlabelled Anandamide in $\mu\text{M}$	Binding of CB2 in presence of Unlabelled Anandamide in CPM	Binding of CB2 in presence of Unlabelled Anandamide in pM/mg
2.5	2275	53.93
5	2127	50.42
10	1763	41.79
15	1080	25.60
25	650	15.41
40	467	11.07

$$1. \quad 2275 \text{ CPM} / 421.8 \text{ CPM/fmol} / 0.1 \text{ ml}$$

$$= 53.93 \text{ pM}$$

$$2. \quad 2127 \text{ CPM} / 421.8 \text{ CPM/fmol} / 0.1 \text{ ml}$$

$$= 50.42 \text{ pM}$$

$$3. \quad 1763 \text{ CPM} / 421.8 \text{ CPM/fmol} / 0.1 \text{ ml}$$

$$= 41.79 \text{ pM}$$

4. 1080CPM/ 421.8 CPM/fmol /0.1ml

$$= 25.60 \text{ pM}$$

5. 650CPM/ 421.8 CPM/fmol /0.1ml

$$= 15.41 \text{ pM}$$

6. 467CPM/ 421.8 CPM/fmol /0.1ml

$$= 11.07 \text{ pM}$$

$$\text{EC}_{50} = 13.48$$

$$K_i = 13.48/1.58$$

$$= 8.53 \mu\text{M}$$

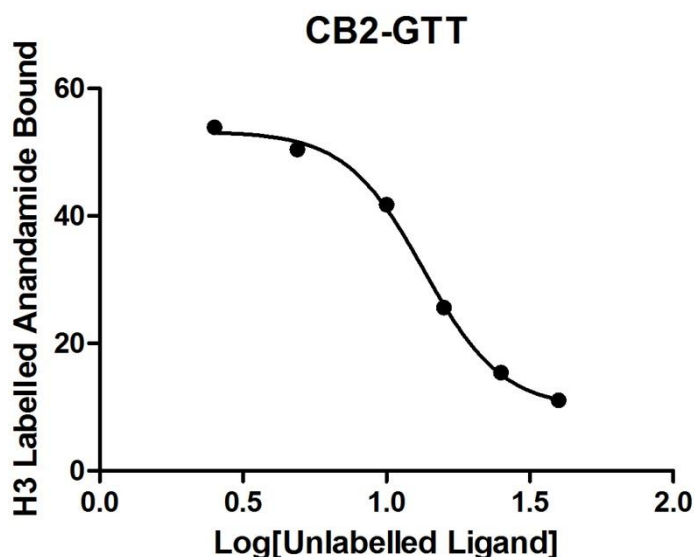


**Figure 20 Binding of H<sup>3</sup>Anandamide to CB2 in presence of unlabelled  $\gamma$ -tocotrienol**

**19.  $K_i$  of CB2 with Radiolabelled Anandamide and Unlabelled  $\delta$ -tocotrienol****Table 19 Binding of H<sup>3</sup>Anandamide to CB2 in presence of unlabelled  $\delta$ -tocotrienol**

Unlabelled Anandamide in $\mu\text{M}$	Binding of CB2 in presence of Unlabelled Anandamide in CPM	Binding of CB2 in presence of Unlabelled Anandamide in pM/mg
2.5	2432	57.65
5	2317	54.93
10	1958	46.42
15	1253	29.70
25	889	21.07
40	603	14.29

1. 2432CPM/ 421.8 CPM/fmol /0.1ml

$$= 57.65\text{pM}$$

2. 2317CPM/ 421.8 CPM/fmol /0.1ml

$$= 54.93\text{pM}$$

3. 1958CPM/ 421.8 CPM/fmol /0.1ml

$$= 46.42\text{pM}$$

4. 1253CPM/ 421.8 CPM/fmol /0.1ml

$$= 29.70\text{pM}$$

5. 889CPM/ 421.8 CPM/fmol /0.1ml

$$= 21.07\text{pM}$$

6. 603CPM/ 421.8 CPM/fmol /0.1ml

$$= 14.29\text{pM}$$

$$\text{EC}_{50} = 13.87$$

$$K_i = 13.87/1.58$$

$$= 8.77\mu\text{M}$$

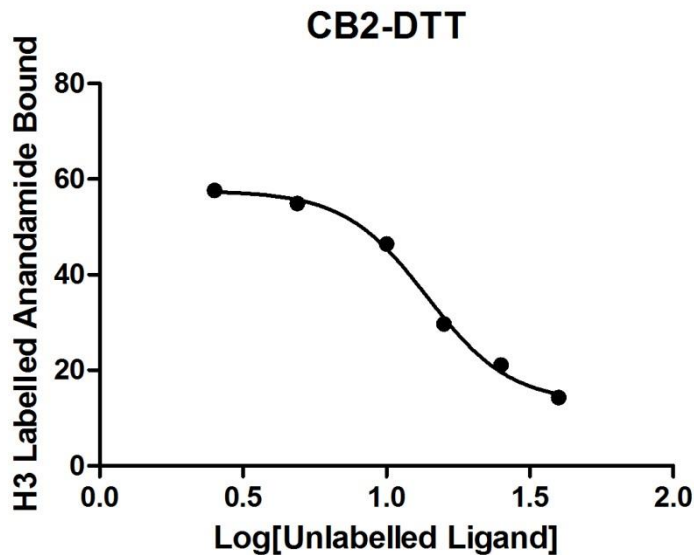


**Figure 21 Binding of H<sup>3</sup>Anandamide to CB2 in presence of unlabelled δ-tocotrienol**

**20. *K<sub>i</sub> of COX-2 with Radiolabelled DHA and Unlabelled Anandamide***

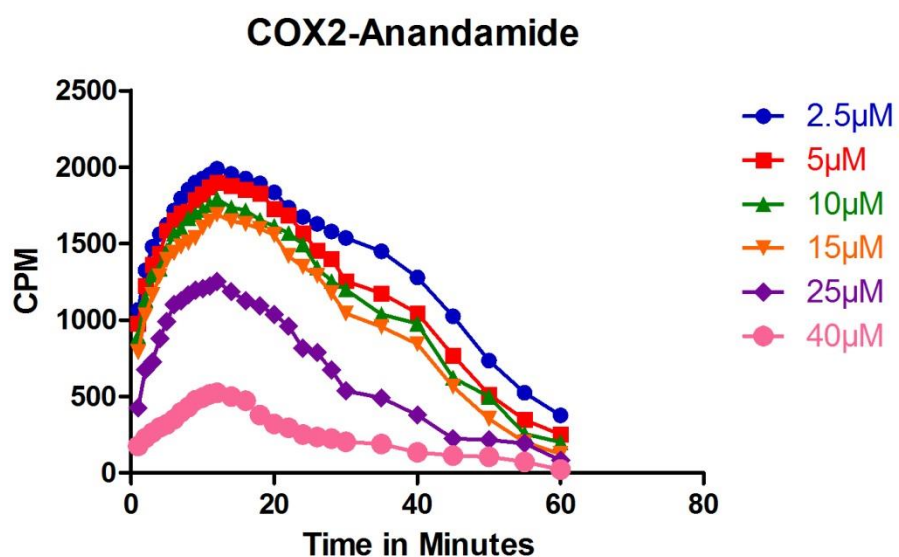


**Figure 22 Binding of C<sup>14</sup>DHA to COX-2 in presence of unlabelled Anandamide**

**Table 21 Binding of C<sup>14</sup>DHA to COX-2 in presence of unlabelled Anandamide**

Unlabelled Ligand in $\mu\text{M}$	Non-Specific Binding in CPM	Non-Specific Binding in $\mu\text{M}$	Non-Specific Binding in $\mu\text{M}/\text{mg}$
2.5	2834.	0.257	1.16
5	2619.	0.238	1.08
10	2035.	0.185	0.84
15	1022.	0.093	0.42
25	782.	0.071	0.32
40	518.	0.047	0.21

1. 2834CPM/ 0.10989 CPM/fmol /0.1ml (100 $\mu\text{l}$  aliquot of stock mix)

$$= 257894 \text{ pM} \text{ or } 0.257 \mu\text{M}$$

2. 2619CPM/ 0.10989 CPM/fmol /0.1ml

$$= 238329 \text{ pM} \text{ or } 0.238 \mu\text{M}$$

3. 2035CPM/0.10989 CPM/fmol /0.1ml

$$= 18585 \text{ pM} \text{ or } 0.185 \mu\text{M}$$

4. 1022CPM/0.10989 CPM/fmol /0.1ml

$$= 93002 \text{ pM} \text{ or } 0.093 \mu\text{M}$$

5. 782CPM/0.10989 CPM/fmol /0.1ml

$$= 71162 \text{ pM} \text{ or } 0.071 \mu\text{M}$$

6. 518CPM/0.10989 CPM/fmol /0.1ml

$$= 47138 \text{ pM} \text{ or } 0.047 \mu\text{M}$$

$$\text{IC 50} = 11.75$$

$$K_i = 11.75/2.36$$

$$= 4.97$$

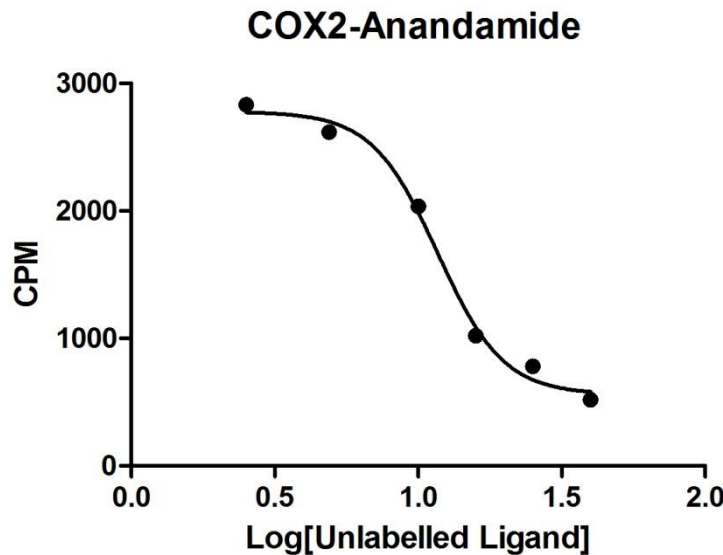


**Figure 23 Binding of C<sup>14</sup>DHA to COX-2 in presence of unlabelled Anandamide**

**21. *K<sub>i</sub> of COX-2 with Radiolabelled DHA and Unlabelled α-tocotrienol***

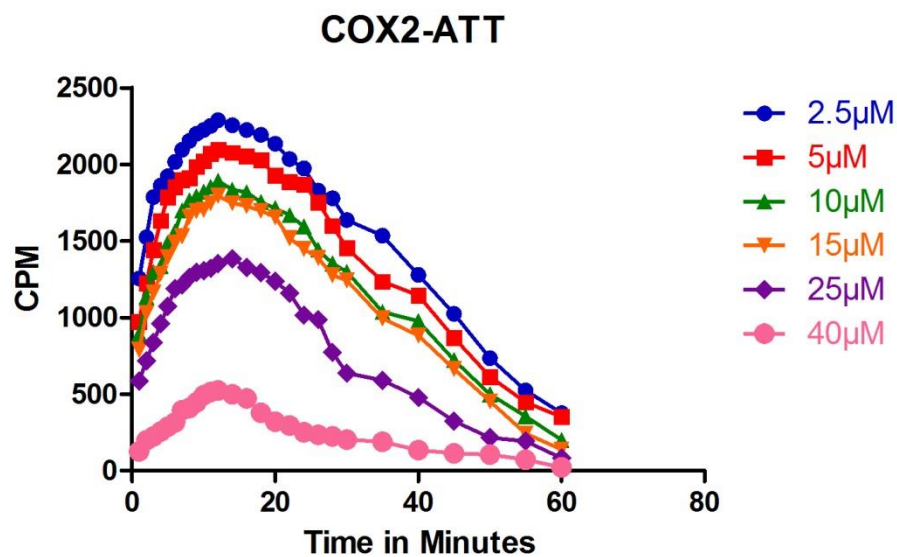


**Figure 24 Binding of C<sup>14</sup>DHA to COX-2 in presence of unlabelled α-tocotrienol**

**Table 21 Binding of C<sup>14</sup>DHA to COX-2 in presence of unlabelled  $\alpha$ -tocotrienol**

Unlabelled Ligand in $\mu\text{M}$	Non-Specific Binding in CPM	Non-Specific Binding in $\mu\text{M}$	Non-Specific Binding in $\mu\text{M}/\text{mg}$
2.5	3165.	0.288	1.30
5	2873.	0.261	1.18
10	2251.	0.204	0.92
15	1447.	0.131	0.59
25	942.	0.857	0.38
40	766.	0.069	0.31

1. 3165CPM/ 0.10989 CPM/fmol /0.1ml (100 $\mu\text{l}$  aliquot of stock mix)

$$= 288015 \text{ pM} \text{ or } 0.288 \mu\text{M}$$

2. 2873CPM/ 0.10989 CPM/fmol /0.1ml

$$= 261443 \text{ pM} \text{ or } 0.261 \mu\text{M}$$

3. 2251CPM/0.10989 CPM/fmol /0.1ml

$$= 204841 \text{ pM} \text{ or } 0.204 \mu\text{M}$$

4. 1447CPM/0.10989 CPM/fmol /0.1ml

$$= 131677 \text{ pM} \text{ or } 0.131 \mu\text{M}$$

5. 942CPM/0.10989 CPM/fmol /0.1ml

$$= 85722 \text{ pM} \text{ or } 0.857 \mu\text{M}$$

6. 766CPM/0.10989 CPM/fmol /0.1ml

$$= 69706 \text{ pM} \text{ or } 0.069 \mu\text{M}$$

$$\text{IC}_{50} = 12.02$$

$$K_i = 12.02/2.36$$

$$= 5.09$$

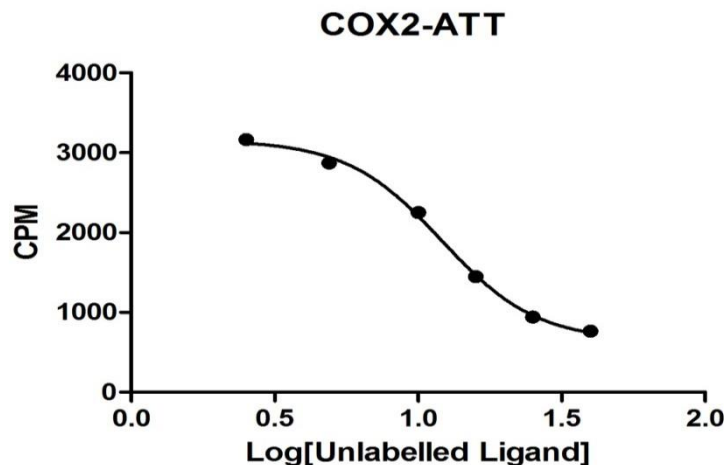


Figure 25 Binding of C¹⁴DHA to COX-2 in presence of unlabelled  $\alpha$ -tocotrienol

## 22. *K<sub>i</sub> of COX-2 with Radiolabelled DHA and Unlabelled 2AG*

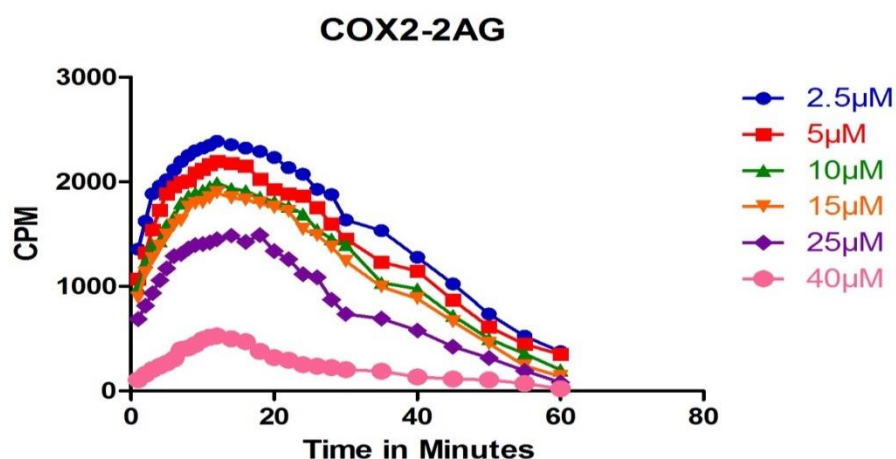


Figure 26 Binding of C¹⁴DHA to COX-2 in presence of unlabelled 2AG

Table 22 Binding of C¹⁴DHA to COX-2 in presence of unlabelled 2AG

Unlabelled Ligand in $\mu\text{M}$	Non-Specific Binding in CPM	Non-Specific Binding in $\mu\text{M}$	Non-Specific Binding in $\mu\text{M}/\text{mg}$
2.5	3231.	0.294	1.33
5	2972.	0.270	1.22
10	2428.	0.220	1.00
15	1576.	0.143	0.65
25	1278.	0.116	0.52
40	867.	0.078	0.35

1.  $3231 \text{ CPM} / 0.10989 \text{ CPM/fmol} / 0.1\text{ml}$  ( $100\mu\text{l}$  aliquot of stock mix)

$$= 294021 \text{ pM} \text{ or } 0.294 \mu\text{M}$$

2.  $2972 \text{ CPM} / 0.10989 \text{ CPM/fmol} / 0.1\text{ml}$

$$= 270452 \text{ pM} \text{ or } 0.270 \mu\text{M}$$

3.  $2428 \text{ CPM} / 0.10989 \text{ CPM/fmol} / 0.1\text{ml}$

$$= 220948 \text{ pM} \text{ or } 0.220 \mu\text{M}$$

4.  $1576 \text{ CPM} / 0.10989 \text{ CPM/fmol} / 0.1\text{ml}$

$$= 143416 \text{ pM} \text{ or } 0.143 \mu\text{M}$$

5.  $1278 \text{ CPM} / 0.10989 \text{ CPM/fmol} / 0.1\text{ml}$

$$= 116298 \text{ pM} \text{ or } 0.116 \mu\text{M}$$

6.  $867 \text{ CPM} / 0.10989 \text{ CPM/fmol} / 0.1\text{ml}$

$$= 78897 \text{ pM} \text{ or } 0.078 \mu\text{M}$$

$$\text{IC}_{50} = 12.89$$

$$K_i = 12.89 / 2.36$$

$$= 5.46$$

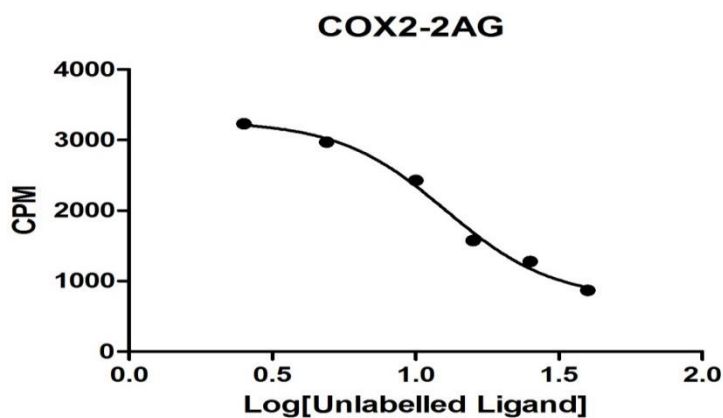


**Figure 27 Binding of C<sup>14</sup>DHA to COX-2 in presence of unlabelled 2AG**

**23.  $K_i$  of COX-2 with Radiolabelled DHA and Unlabelled  $\gamma$ -tocotrienol**

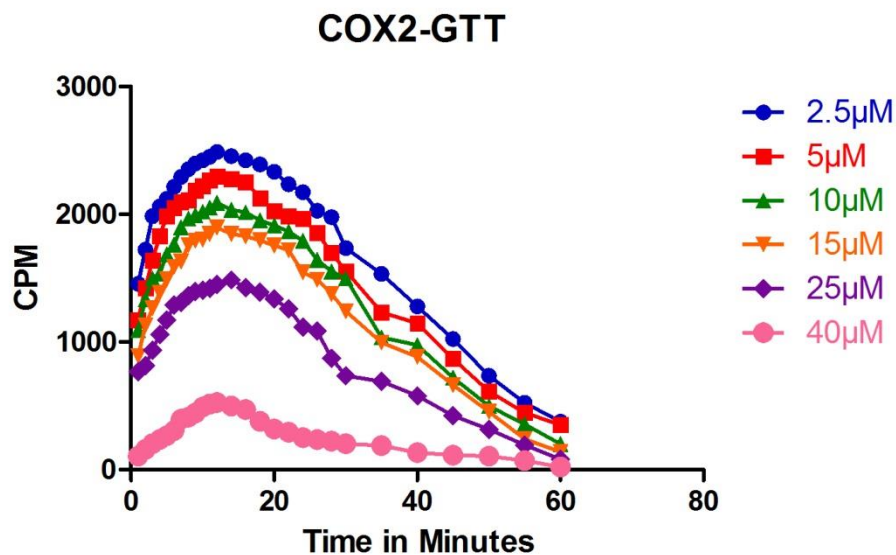


**Figure 28 Binding of C<sup>14</sup>DHA to COX-2 in presence of unlabelled  $\gamma$ -tocotrienol**

**Table 23 Binding of C<sup>14</sup>DHA to COX-2 in presence of unlabelled  $\gamma$ -tocotrienol**

Unlabelled Ligand in $\mu$ M	Non-Specific Binding in CPM	Non-Specific Binding in $\mu$ M	Non-Specific Binding in $\mu$ M/mg
2.5	3345.	0.304	1.38
5	3113.	0.283	1.28
10	2665.	0.242	1.1
15	1689.	0.153	0.69
25	924.	0.084	0.38
40	906.	0.082	0.37

1. 3345CPM/ 0.10989 CPM/fmol /0.1ml (100 $\mu$ l aliquot of stock mix)

$$= 304395 \text{ pM} \text{ or } 0.304 \mu\text{M}$$

2. 3113CPM/ 0.10989 CPM/fmol /0.1ml

$$= 283283 \text{ pM} \text{ or } 0.283 \mu\text{M}$$

3. 2665CPM/0.10989 CPM/fmol /0.1ml

$$= 242515 \text{ pM} \text{ or } 0.242 \mu\text{M}$$

4.  $1689 \text{ CPM} / 0.10989 \text{ CPM/fmol} / 0.1\text{ml}$

$$= 153699 \text{ pM or } 0.153 \mu\text{M}$$

5.  $924 \text{ CPM} / 0.10989 \text{ CPM/fmol} / 0.1\text{ml}$

$$= 84084 \text{ pM or } 0.084 \mu\text{M}$$

6.  $906 \text{ CPM} / 0.10989 \text{ CPM/fmol} / 0.1\text{ml}$

$$= 82446 \text{ pM or } 0.082 \mu\text{M}$$

$$\text{IC}_{50} = 13.41$$

$$K_i = 13.41 / 2.36$$

$$= 5.68$$

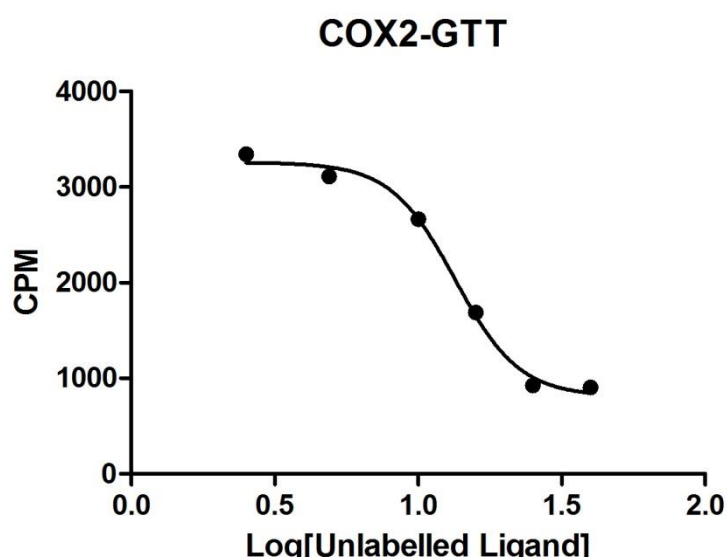


Figure 29 Binding of C<sup>14</sup>DHA to COX-2 in presence of unlabelled  $\gamma$ -tocotrienol

## **Appendix-L**

### **XML Data Source**

```

<Details>
  <Protein val="PPAR $\alpha$ ">
    <Ligand val="DHA">
      <Binding_Energy>
        <Autodock>-11.5 Kcal/mol</Autodock>
        <Glide_Score>-10.2 Kcal/mol</Glide_Score>
        <Bonded_Interactions>PPAR $\alpha$ -DHA.PNG</Bonded_Interactions>
        <AutoDock>PPAR $\alpha$ -DHA.PNG</AutoDock>
        <Glide>PPAR $\alpha$ -DHA.PNG</Glide>
        <Binding_Pocket>PPAR $\alpha$ -DHA.PNG</Binding_Pocket>
        <Comparing_AutoDock_with_Glide>Comparing AutoDock
        and Glide-PPAR $\alpha$ .PNG</Comparing_AutoDock_with_Glide>
        <PDB_Files>PPAR $\alpha$ -DHA.pdb</PDB_Files>
      </Binding_Energy>
    </Ligand>
    <Ligand val="EPA">
      <Binding_Energy>
        <Autodock>-10.1 Kcal/mol</Autodock>
        <Glide_Score>-9.3 Kcal/mol</Glide_Score>
        <Bonded_Interactions>PPAR $\alpha$ -EPA.PNG</Bonded_Interactions>
        <AutoDock>PPAR $\alpha$ -EPA.PNG</AutoDock>
        <Glide>PPAR $\alpha$ -EPA.PNG</Glide>
        <Binding_Pocket>PPAR $\alpha$ -EPA.PNG</Binding_Pocket>
        <Comparing_AutoDock_with_Glide>Comparing AutoDock
        and Glide-PPAR $\alpha$ .PNG</Comparing_AutoDock_with_Glide>
        <PDB_Files>PPAR $\alpha$ -EPA.pdb</PDB_Files>
      </Binding_Energy>
    </Ligand>
    <Ligand val="2AG">
      <Binding_Energy>
        <Autodock>-7.69 Kcal/mol</Autodock>
        <Glide_Score>-8.0 Kcal/mol</Glide_Score>
        <Bonded_Interactions>PPAR $\alpha$ -2AG.PNG</Bonded_Interactions>
        <AutoDock>PPAR $\alpha$ -2AG.PNG</AutoDock>
      </Binding_Energy>
    </Ligand>
  </Protein>
</Details>

```

```

<Glide>PPARa-2AG.PNG</Glide>
<Binding_Pocket>PPARA-2AG.PNG</Binding_Pocket>
<Comparing_AutoDock_with_Glide>Comparing AutoDock
and Glide-PPARa.PNG</Comparing_AutoDock_with_Glide>
    <PDB_Files>PPARa-2AG.pdb</PDB_Files>
    </Binding_Energy>
</Ligand>
<Ligand val="Anandamide">
    <Binding_Energy>
        <Autodock>-6.57 Kcal/mol</Autodock>
        <Glide_Score>-5.6 Kcal/mol</Glide_Score>
        <Bonded_Interactions>PPARa-
Anan.PNG</Bonded_Interactions>
    <AutoDock>PPARa-Anan.PNG</AutoDock>
    <Glide>PPARa-Anan.PNG</Glide>
    <Binding_Pocket>PPARA-Anan.PNG</Binding_Pocket>
    <Comparing_AutoDock_with_Glide>Comparing AutoDock
and Glide-PPARa.PNG</Comparing_AutoDock_with_Glide>
    <PDB_Files>PPARa-Anan.pdb</PDB_Files>
    </Binding_Energy>
</Ligand>
<Ligand val="α tocotrienol">
    <Binding_Energy>
        <Autodock>-9.87 Kcal/mol</Autodock>
        <Glide_Score>-7.1 Kcal/mol</Glide_Score>
        <Bonded_Interactions>PPARa-
aTT.PNG</Bonded_Interactions>
    <AutoDock>PPARa-aTT.PNG</AutoDock>
    <Glide>PPARa-aTT.PNG</Glide>
    <Binding_Pocket>PPARA-aTT.PNG</Binding_Pocket>
    <Comparing_AutoDock_with_Glide>Comparing AutoDock
and Glide-PPARa.PNG</Comparing_AutoDock_with_Glide>
    <PDB_Files>PPARa-aTT.pdb</PDB_Files>
    </Binding_Energy>
</Ligand>
<Ligand val="β tocotrienol">
    <Binding_Energy>
        <Autodock>-9.98 Kcal/mol</Autodock>
        <Glide_Score>-7.5 Kcal/mol</Glide_Score>
        <Bonded_Interactions>PPARa-
bTT.PNG</Bonded_Interactions>
    <AutoDock>PPARa-bTT.PNG</AutoDock>
    <Glide>PPARa-bTT.PNG</Glide>
    <Binding_Pocket>PPARA-bTT.PNG</Binding_Pocket>

```

```

<Comparing_AutoDock_with_Glide>Comparing      AutoDock
and Glide-PPARa.PNG</Comparing_AutoDock_with_Glide>
    <PDB_Files>PPARa-bTT.pdb</PDB_Files>
        </Binding_Energy>
    </Ligand>
    <Ligand val="γ tocotrienol">
        <Binding_Energy>
            <Autodock>-8.44 Kcal/mol</Autodock>
            <Glide_Score>-7.3 Kcal/mol</Glide_Score>
            <Bonded_Interactions>PPARa-
gTT.PNG</Bonded_Interactions>
        <AutoDock>PPARa-gTT.PNG</AutoDock>
        <Glide>PPARa-gTT.PNG</Glide>
        <Binding_Pocket>PPARA-gTT.PNG</Binding_Pocket>
        <Comparing_AutoDock_with_Glide>Comparing      AutoDock
and Glide-PPARa.PNG</Comparing_AutoDock_with_Glide>
    <PDB_Files>PPARa-gTT.pdb</PDB_Files>
        </Binding_Energy>
    </Ligand>
    <Ligand val="δ tocotrienol">
        <Binding_Energy>
            <Autodock>-9.53 Kcal/mol</Autodock>
            <Glide_Score>-7.5 Kcal/mol</Glide_Score>
            <Bonded_Interactions>PPARa-
dTTPNG</Bonded_Interactions>
        <AutoDock>PPARa-dTT.PNG</AutoDock>
        <Glide>PPARa-dTT.PNG</Glide>
        <Binding_Pocket>PPARA-dTT.PNG</Binding_Pocket>
        <Comparing_AutoDock_with_Glide>Comparing      AutoDock
and Glide-PPARa.PNG</Comparing_AutoDock_with_Glide>
    <PDB_Files>PPARa-dTT.pdb</PDB_Files>
        </Binding_Energy>
    </Ligand>
</Protein>
<Protein val="PPARδ">
    <Ligand val="DHA">
        <Binding_Energy>
            <Autodock>-11.5 Kcal/mol</Autodock>
            <Glide_Score>-10.2 Kcal/mol</Glide_Score>
            <Bonded_Interactions>PPARD-
DHA.PNG</Bonded_Interactions>
        <AutoDock>PPARD-DHA.PNG</AutoDock>
        <Glide>PPARD-DHA.PNG</Glide>
        <Binding_Pocket>PPARD-DHA.PNG</Binding_Pocket>

```

AutoDock

```

<Comparing_AutoDock_with_Glide>Comparing
and Glide-PPARd.PNG</Comparing_AutoDock_with_Glide>
    <PDB_Files>PPARd-DHA.pdb</PDB_Files>
        </Binding_Energy>
    </Ligand>
    <Ligand val="EPA">
        <Binding_Energy>
            <Autodock>-10.1 Kcal/mol</Autodock>
            <Glide_Score>-9.3 Kcal/mol</Glide_Score>
            <Bonded_Interactions>PPARd-
EPA.PNG</Bonded_Interactions>
        <AutoDock>PPARd-EPA.PNG</AutoDock>
        <Glide>PPARd-EPA.PNG</Glide>
        <Binding_Pocket>PPARd-EPA.PNG</Binding_Pocket>
        <Comparing_AutoDock_with_Glide>Comparing      AutoDock
and Glide-PPARd.PNG</Comparing_AutoDock_with_Glide>
    <PDB_Files>PPARd-EPA.pdb</PDB_Files>
        </Binding_Energy>
    </Ligand>
    <Ligand val="2AG">
        <Binding_Energy>
            <Autodock>-7.69 Kcal/mol</Autodock>
            <Glide_Score>-8.0 Kcal/mol</Glide_Score>
            <Bonded_Interactions>PPARd-
2AG.PNG</Bonded_Interactions>
        <AutoDock>PPARd-2AG.PNG</AutoDock>
        <Glide>PPARd-2AG.PNG</Glide>
        <Binding_Pocket>PPARd-2AG.PNG</Binding_Pocket>
        <Comparing_AutoDock_with_Glide>Comparing      AutoDock
and Glide-PPARd.PNG</Comparing_AutoDock_with_Glide>
    <PDB_Files>PPARd-2AG.pdb</PDB_Files>
        </Binding_Energy>
    </Ligand>
    <Ligand val="Anandamide">
        <Binding_Energy>
            <Autodock>-6.57 Kcal/mol</Autodock>
            <Glide_Score>-5.6 Kcal/mol</Glide_Score>
            <Bonded_Interactions>PPARd-
Anan.PNG</Bonded_Interactions>
        <AutoDock>PPARd-Anan.PNG</AutoDock>
        <Glide>PPARd-Anan.PNG</Glide>
        <Binding_Pocket>PPARd-Anan.PNG</Binding_Pocket>
        <Comparing_AutoDock_with_Glide>Comparing      AutoDock
and Glide-PPARd.PNG</Comparing_AutoDock_with_Glide>

```

```

<PDB_Files>PPARd-Anan.pdb</PDB_Files>
</Binding_Energy>
</Ligand>
<Ligand val="α tocotrienol">
    <Binding_Energy>
        <Autodock>-9.87 Kcal/mol</Autodock>
        <Glide_Score>-7.1 Kcal/mol</Glide_Score>
        <Bonded_Interactions>PPARd-
aTT.PNG</Bonded_Interactions>
    <AutoDock>PPARd-aTT.PNG</AutoDock>
    <Glide>PPARd-aTT.PNG</Glide>
    <Binding_Pocket>PPARd-aTT.PNG</Binding_Pocket>
    <Comparing_AutoDock_with_Glide>Comparing AutoDock
and Glide-PPARd.PNG</Comparing_AutoDock_with_Glide>
    <PDB_Files>PPARd-aTT.pdb</PDB_Files>
    </Binding_Energy>
</Ligand>
<Ligand val="β tocotrienol">
    <Binding_Energy>
        <Autodock>-9.98 Kcal/mol</Autodock>
        <Glide_Score>-7.5 Kcal/mol</Glide_Score>
        <Bonded_Interactions>PPARd-
bTT.PNG</Bonded_Interactions>
    <AutoDock>PPARd-bTT.PNG</AutoDock>
    <Glide>PPARd-bTT.PNG</Glide>
    <Binding_Pocket>PPARd-bTT.PNG</Binding_Pocket>
    <Comparing_AutoDock_with_Glide>Comparing AutoDock
and Glide-PPARd.PNG</Comparing_AutoDock_with_Glide>
    <PDB_Files>PPARd-bTT.pdb</PDB_Files>
    </Binding_Energy>
</Ligand>
<Ligand val="γ tocotrienol">
    <Binding_Energy>
        <Autodock>-8.44 Kcal/mol</Autodock>
        <Glide_Score>-7.3 Kcal/mol</Glide_Score>
        <Bonded_Interactions>PPARd-
gTT.PNG</Bonded_Interactions>
    <AutoDock>PPARd-gTT.PNG</AutoDock>
    <Glide>PPARd-gTT.PNG</Glide>
    <Binding_Pocket>PPARd-gTT.PNG</Binding_Pocket>
    <Comparing_AutoDock_with_Glide>Comparing AutoDock
and Glide-PPARd.PNG</Comparing_AutoDock_with_Glide>
    <PDB_Files>PPARd-gTT.pdb</PDB_Files>
    </Binding_Energy>

```

```

</Ligand>
<Ligand val="δ tocotrienol">
    <Binding_Energy>
        <Autodock>-9.53 Kcal/mol</Autodock>
        <Glide_Score>-7.5 Kcal/mol</Glide_Score>
        <Bonded_Interactions>PPARd-
dT.T.PNG</Bonded_Interactions>
        <AutoDock>PPARd-dTT.PNG</AutoDock>
        <Glide>PPARd-dTT.PNG</Glide>
        <Binding_Pocket>PPARd-dTT.PNG</Binding_Pocket>
        <Comparing_AutoDock_with_Glide>Comparing AutoDock
and Glide-PPARd.PNG</Comparing_AutoDock_with_Glide>
        <PDB_Files>PPARd-dTT.pdb</PDB_Files>
    </Binding_Energy>
</Ligand>
</Protein>
<Protein val="PPARγ">
    <Ligand val="DHA">
        <Binding_Energy>
            <Autodock>-11.5 Kcal/mol</Autodock>
            <Glide_Score>-10.2 Kcal/mol</Glide_Score>
            <Bonded_Interactions>PPARG-
DHA.PNG</Bonded_Interactions>
            <AutoDock>PPARG-DHA.PNG</AutoDock>
            <Glide>PPARG-DHA.PNG</Glide>
            <Binding_Pocket>PPARG-DHA.PNG</Binding_Pocket>
            <Comparing_AutoDock_with_Glide>Comparing AutoDock
and Glide-PPARG.PNG</Comparing_AutoDock_with_Glide>
            <PDB_Files>PPARG-DHA.pdb</PDB_Files>
        </Binding_Energy>
    </Ligand>
    <Ligand val="EPA">
        <Binding_Energy>
            <Autodock>-10.1 Kcal/mol</Autodock>
            <Glide_Score>-9.3 Kcal/mol</Glide_Score>
            <Bonded_Interactions>PPARG-
EPA.PNG</Bonded_Interactions>
            <AutoDock>PPARG-EPA.PNG</AutoDock>
            <Glide>PPARG-EPA.PNG</Glide>
            <Binding_Pocket>PPARG-EPA.PNG</Binding_Pocket>
            <Comparing_AutoDock_with_Glide>Comparing AutoDock
and Glide-PPARG.PNG</Comparing_AutoDock_with_Glide>
            <PDB_Files>PPARG-EPA.pdb</PDB_Files>
        </Binding_Energy>
    </Ligand>
</Protein>

```

```

</Ligand>
<Ligand val="2AG">
    <Binding_Energy>
        <Autodock>-7.69 Kcal/mol</Autodock>
        <Glide_Score>-8.0 Kcal/mol</Glide_Score>
        <Bonded_Interactions>PPARg-
2AG.PNG</Bonded_Interactions>
        <AutoDock>PPARg-2AG.PNG</AutoDock>
        <Glide>PPARg-2AG.PNG</Glide>
        <Binding_Pocket>PPARg-2AG.PNG</Binding_Pocket>
        <Comparing_AutoDock_with_Glide>Comparing AutoDock
and Glide-PPARg.PNG</Comparing_AutoDock_with_Glide>
        <PDB_Files>PPARg-2AG.pdb</PDB_Files>
    </Binding_Energy>
</Ligand>
<Ligand val="Anandamide">
    <Binding_Energy>
        <Autodock>-6.57 Kcal/mol</Autodock>
        <Glide_Score>-5.6 Kcal/mol</Glide_Score>
        <Bonded_Interactions>PPARg-
Anan.PNG</Bonded_Interactions>
        <AutoDock>PPARg-Anan.PNG</AutoDock>
        <Glide>PPARg-Anan.PNG</Glide>
        <Binding_Pocket>PPARg-Anan.PNG</Binding_Pocket>
        <Comparing_AutoDock_with_Glide>Comparing AutoDock
and Glide-PPARg.PNG</Comparing_AutoDock_with_Glide>
        <PDB_Files>PPARg-Anan.pdb</PDB_Files>
    </Binding_Energy>
</Ligand>
<Ligand val="α tocotrienol">
    <Binding_Energy>
        <Autodock>-9.87 Kcal/mol</Autodock>
        <Glide_Score>-7.1 Kcal/mol</Glide_Score>
        <Bonded_Interactions>PPARg-
aTT.PNG</Bonded_Interactions>
        <AutoDock>PPARg-aTT.PNG</AutoDock>
        <Glide>PPARg-aTT.PNG</Glide>
        <Binding_Pocket>PPARg-aTT.PNG</Binding_Pocket>
        <Comparing_AutoDock_with_Glide>Comparing AutoDock
and Glide-PPARg.PNG</Comparing_AutoDock_with_Glide>
        <PDB_Files>PPARg-aTT.pdb</PDB_Files>
    </Binding_Energy>
</Ligand>
<Ligand val="β tocotrienol">

```

```

<Binding_Energy>
    <Autodock>-9.98 Kcal/mol</Autodock>
    <Glide_Score>-7.5 Kcal/mol</Glide_Score>
    <Bonded_Interactions>PPARg-
bTT.PNG</Bonded_Interactions>
    <AutoDock>PPARg-bTT.PNG</AutoDock>
    <Glide>PPARg-bTT.PNG</Glide>
    <Binding_Pocket>PPARg-bTT.PNG</Binding_Pocket>
    <Comparing_AutoDock_with_Glide>Comparing AutoDock
and Glide-PPARg.PNG</Comparing_AutoDock_with_Glide>
    <PDB_Files>PPARg-bTT.pdb</PDB_Files>
    </Binding_Energy>
</Ligand>
<Ligand val="γ tocotrienol">
    <Binding_Energy>
        <Autodock>-8.44 Kcal/mol</Autodock>
        <Glide_Score>-7.3 Kcal/mol</Glide_Score>
        <Bonded_Interactions>PPARg-
gTT.PNG</Bonded_Interactions>
    <AutoDock>PPARg-gTT.PNG</AutoDock>
    <Glide>PPARg-gTT.PNG</Glide>
    <Binding_Pocket>PPARg-gTT.PNG</Binding_Pocket>
    <Comparing_AutoDock_with_Glide>Comparing AutoDock
and Glide-PPARg.PNG</Comparing_AutoDock_with_Glide>
    <PDB_Files>PPARg-gTT.pdb</PDB_Files>
    </Binding_Energy>
</Ligand>
<Ligand val="δ tocotrienol">
    <Binding_Energy>
        <Autodock>-9.53 Kcal/mol</Autodock>
        <Glide_Score>-7.5 Kcal/mol</Glide_Score>
        <Bonded_Interactions>PPARg-
dTTPNG</Bonded_Interactions>
    <AutoDock>PPARg-dTT.PNG</AutoDock>
    <Glide>PPARg-dTT.PNG</Glide>
    <Binding_Pocket>PPARg-dTT.PNG</Binding_Pocket>
    <Comparing_AutoDock_with_Glide>Comparing AutoDock
and Glide-PPARg.PNG</Comparing_AutoDock_with_Glide>
    <PDB_Files>PPARg-dTT.pdb</PDB_Files>
    </Binding_Energy>
</Ligand>
</Protein>
<Protein val="COX-1">
    <Ligand val="DHA">

```

```

<Binding_Energy>
    <Autodock>-11.5 Kcal/mol</Autodock>
    <Glide_Score>-10.2 Kcal/mol</Glide_Score>
    <Bonded_Interactions>COX-1-
DHA.PNG</Bonded_Interactions>
    <AutoDock>COX-1-DHA.PNG</AutoDock>
    <Glide>COX-1-DHA.PNG</Glide>
    <Binding_Pocket>COX-1-DHA.PNG</Binding_Pocket>
    <Comparing_AutoDock_with_Glide>Comparing AutoDock
and Glide-COX-1.PNG</Comparing_AutoDock_with_Glide>
    <PDB_Files>COX-1-DHA.pdb</PDB_Files>
</Binding_Energy>
</Ligand>
<Ligand val="EPA">
    <Binding_Energy>
        <Autodock>-10.1 Kcal/mol</Autodock>
        <Glide_Score>-9.3 Kcal/mol</Glide_Score>
        <Bonded_Interactions>COX-1-
EPA.PNG</Bonded_Interactions>
    <AutoDock>COX-1-EPA.PNG</AutoDock>
    <Glide>COX-1-EPA.PNG</Glide>
    <Binding_Pocket>COX-1-EPA.PNG</Binding_Pocket>
    <Comparing_AutoDock_with_Glide>Comparing AutoDock
and Glide-COX-1.PNG</Comparing_AutoDock_with_Glide>
    <PDB_Files>COX-1-EPA.pdb</PDB_Files>
</Binding_Energy>
</Ligand>
<Ligand val="2AG">
    <Binding_Energy>
        <Autodock>-7.69 Kcal/mol</Autodock>
        <Glide_Score>-8.0 Kcal/mol</Glide_Score>
        <Bonded_Interactions>COX-1-
2AG.PNG</Bonded_Interactions>
    <AutoDock>COX-1-2AG.PNG</AutoDock>
    <Glide>COX-1-2AG.PNG</Glide>
    <Binding_Pocket>COX-1-2AG.PNG</Binding_Pocket>
    <Comparing_AutoDock_with_Glide>Comparing AutoDock
and Glide-COX-1.PNG</Comparing_AutoDock_with_Glide>
    <PDB_Files>COX-1-2AG.pdb</PDB_Files>
</Binding_Energy>
</Ligand>
<Ligand val="Anandamide">
    <Binding_Energy>
        <Autodock>-6.57 Kcal/mol</Autodock>

```

```

<Glide_Score>-5.6 Kcal/mol</Glide_Score>
<Bonded_Interactions>COX-1-
Anan.PNG</Bonded_Interactions>
    <AutoDock>COX-1-Anan.PNG</AutoDock>
    <Glide>COX-1-Anan.PNG</Glide>
    <Binding_Pocket>COX-1-Anan.PNG</Binding_Pocket>
    <Comparing_AutoDock_with_Glide>Comparing AutoDock
and Glide-COX-1.PNG</Comparing_AutoDock_with_Glide>
    <PDB_Files>COX-1-Anan.pdb</PDB_Files>
    </Binding_Energy>
</Ligand>
<Ligand val=" $\alpha$  tocotrienol">
    <Binding_Energy>
        <Autodock>-9.87 Kcal/mol</Autodock>
        <Glide_Score>-7.1 Kcal/mol</Glide_Score>
        <Bonded_Interactions>COX-1-
aTT.PNG</Bonded_Interactions>
    <AutoDock>COX-1-aTT.PNG</AutoDock>
    <Glide>COX-1-aTT.PNG</Glide>
    <Binding_Pocket>COX-1-aTT.PNG</Binding_Pocket>
    <Comparing_AutoDock_with_Glide>Comparing AutoDock
and Glide-COX-1.PNG</Comparing_AutoDock_with_Glide>
    <PDB_Files>COX-1-aTT.pdb</PDB_Files>
    </Binding_Energy>
</Ligand>
<Ligand val=" $\beta$  tocotrienol">
    <Binding_Energy>
        <Autodock>-9.98 Kcal/mol</Autodock>
        <Glide_Score>-7.5 Kcal/mol</Glide_Score>
        <Bonded_Interactions>COX-1-
bTT.PNG</Bonded_Interactions>
    <AutoDock>COX-1-bTT.PNG</AutoDock>
    <Glide>COX-1-bTT.PNG</Glide>
    <Binding_Pocket>COX-1-bTT.PNG</Binding_Pocket>
    <Comparing_AutoDock_with_Glide>Comparing AutoDock
and Glide-COX-1.PNG</Comparing_AutoDock_with_Glide>
    <PDB_Files>COX-1-bTT.pdb</PDB_Files>
    </Binding_Energy>
</Ligand>
<Ligand val=" $\gamma$  tocotrienol">
    <Binding_Energy>
        <Autodock>-8.44 Kcal/mol</Autodock>
        <Glide_Score>-7.3 Kcal/mol</Glide_Score>

```

```

        <Bonded_Interactions>COX-1-
gTT.PNG</Bonded_Interactions>
        <AutoDock>COX-1-gTT.PNG</AutoDock>
        <Glide>COX-1-gTT.PNG</Glide>
        <Binding_Pocket>COX-1-gTT.PNG</Binding_Pocket>
        <Comparing_AutoDock_with_Glide>Comparing      AutoDock
and Glide-COX-1.PNG</Comparing_AutoDock_with_Glide>
        <PDB_Files>COX-1-gTT.pdb</PDB_Files>
        </Binding_Energy>
    </Ligand>
    <Ligand val="δ tocotrienol">
        <Binding_Energy>
            <Autodock>-9.53 Kcal/mol</Autodock>
            <Glide_Score>-7.5 Kcal/mol</Glide_Score>
            <Bonded_Interactions>COX-1-
dTT.PNG</Bonded_Interactions>
            <AutoDock>COX-1-dTT.PNG</AutoDock>
            <Glide>COX-1-dTT.PNG</Glide>
            <Binding_Pocket>COX-1-dTT.PNG</Binding_Pocket>
            <Comparing_AutoDock_with_Glide>Comparing      AutoDock
and Glide-COX-1.PNG</Comparing_AutoDock_with_Glide>
            <PDB_Files>COX-1-dTT.pdb</PDB_Files>
            </Binding_Energy>
        </Ligand>
    </Protein>
    <Protein val="COX-2">
        <Ligand val="DHA">
            <Binding_Energy>
                <Autodock>-11.5 Kcal/mol</Autodock>
                <Glide_Score>-10.2 Kcal/mol</Glide_Score>
            <Bonded_Interactions>COX-2-
DHA.PNG</Bonded_Interactions>
            <AutoDock>COX-2-DHA.PNG</AutoDock>
            <Glide>COX-2-DHA.PNG</Glide>
            <Binding_Pocket>COX-2-DHA.PNG</Binding_Pocket>
            <Comparing_AutoDock_with_Glide>Comparing      AutoDock
and Glide-COX-2.PNG</Comparing_AutoDock_with_Glide>
            <PDB_Files>COX-2-DHA.pdb</PDB_Files>
            </Binding_Energy>
        </Ligand>
        <Ligand val="EPA">
            <Binding_Energy>
                <Autodock>-10.1 Kcal/mol</Autodock>
                <Glide_Score>-9.3 Kcal/mol</Glide_Score>

```

```

<Bonded_Interactions>COX-2-
EPA.PNG</Bonded_Interactions>
    <AutoDock>COX-2-EPA.PNG</AutoDock>
    <Glide>COX-2-EPA.PNG</Glide>
    <Binding_Pocket>COX-2-EPA.PNG</Binding_Pocket>
    <Comparing_AutoDock_with_Glide>Comparing AutoDock
and Glide-COX-2.PNG</Comparing_AutoDock_with_Glide>
    <PDB_Files>COX-2-EPA.pdb</PDB_Files>
    </Binding_Energy>
</Ligand>
<Ligand val="2AG">
    <Binding_Energy>
        <Autodock>-7.69 Kcal/mol</Autodock>
        <Glide_Score>-8.0 Kcal/mol</Glide_Score>
        <Bonded_Interactions>COX-2-
2AG.PNG</Bonded_Interactions>
    <AutoDock>COX-2-2AG.PNG</AutoDock>
    <Glide>COX-2-2AG.PNG</Glide>
    <Binding_Pocket>COX-2-2AG.PNG</Binding_Pocket>
    <Comparing_AutoDock_with_Glide>Comparing AutoDock
and Glide-COX-2.PNG</Comparing_AutoDock_with_Glide>
    <PDB_Files>COX-2-2AG.pdb</PDB_Files>
    </Binding_Energy>
</Ligand>
<Ligand val="Anandamide">
    <Binding_Energy>
        <Autodock>-6.57 Kcal/mol</Autodock>
        <Glide_Score>-5.6 Kcal/mol</Glide_Score>
        <Bonded_Interactions>COX-2-
Anan.PNG</Bonded_Interactions>
    <AutoDock>COX-2-Anan.PNG</AutoDock>
    <Glide>COX-2-Anan.PNG</Glide>
    <Binding_Pocket>COX-2-Anan.PNG</Binding_Pocket>
    <Comparing_AutoDock_with_Glide>Comparing AutoDock
and Glide-COX-2.PNG</Comparing_AutoDock_with_Glide>
    <PDB_Files>COX-2-Anan.pdb</PDB_Files>
    </Binding_Energy>
</Ligand>
<Ligand val="α tocotrienol">
    <Binding_Energy>
        <Autodock>-9.87 Kcal/mol</Autodock>
        <Glide_Score>-7.1 Kcal/mol</Glide_Score>
        <Bonded_Interactions>COX-2-
aTT.PNG</Bonded_Interactions>

```

```

<AutoDock>COX-2-aTT.PNG</AutoDock>
<Glide>COX-2-aTT.PNG</Glide>
<Binding_Pocket>COX-2-aTT.PNG</Binding_Pocket>
<Comparing_AutoDock_with_Glide>Comparing AutoDock
and Glide-COX-2.PNG</Comparing_AutoDock_with_Glide>
    <PDB_Files>COX-2-aTT.pdb</PDB_Files>
        </Binding_Energy>
    </Ligand>
    <Ligand val="β tocotrienol">
        <Binding_Energy>
            <Autodock>-9.98 Kcal/mol</Autodock>
            <Glide_Score>-7.5 Kcal/mol</Glide_Score>
            <Bonded_Interactions>COX-2-
bTT.PNG</Bonded_Interactions>
        <AutoDock>COX-2-bTT.PNG</AutoDock>
        <Glide>COX-2-bTT.PNG</Glide>
        <Binding_Pocket>COX-2-bTT.PNG</Binding_Pocket>
        <Comparing_AutoDock_with_Glide>Comparing AutoDock
and Glide-COX-2.PNG</Comparing_AutoDock_with_Glide>
    <PDB_Files>COX-2-bTT.pdb</PDB_Files>
        </Binding_Energy>
    </Ligand>
    <Ligand val="γ tocotrienol">
        <Binding_Energy>
            <Autodock>-8.44 Kcal/mol</Autodock>
            <Glide_Score>-7.3 Kcal/mol</Glide_Score>
            <Bonded_Interactions>COX-2-
gTT.PNG</Bonded_Interactions>
        <AutoDock>COX-2-gTT.PNG</AutoDock>
        <Glide>COX-2-gTT.PNG</Glide>
        <Binding_Pocket>COX-2-gTT.PNG</Binding_Pocket>
        <Comparing_AutoDock_with_Glide>Comparing AutoDock
and Glide-COX-2.PNG</Comparing_AutoDock_with_Glide>
    <PDB_Files>COX-2-gTT.pdb</PDB_Files>
        </Binding_Energy>
    </Ligand>
    <Ligand val="δ tocotrienol">
        <Binding_Energy>
            <Autodock>-9.53 Kcal/mol</Autodock>
            <Glide_Score>-7.5 Kcal/mol</Glide_Score>
            <Bonded_Interactions>COX-2-
dTTPNG</Bonded_Interactions>
        <AutoDock>COX-2-dTT.PNG</AutoDock>
        <Glide>COX-2-dTT.PNG</Glide>

```

```

<Binding_Pocket>COX-2-dTT.PNG</Binding_Pocket>
<Comparing_AutoDock_with_Glide>Comparing      AutoDock
and Glide-COX-2.PNG</Comparing_AutoDock_with_Glide>
<PDB_Files>COX-2-dTT.pdb</PDB_Files>
</Binding_Energy>
</Ligand>
</Protein>
<Protein val="LOX">
  <Ligand val="DHA">
    <Binding_Energy>
      <Autodock>-11.5 Kcal/mol</Autodock>
      <Glide_Score>-10.2 Kcal/mol</Glide_Score>
      <Bonded_Interactions>LOX-
DHA.PNG</Bonded_Interactions>
      <AutoDock>LOX-DHA.PNG</AutoDock>
      <Glide>LOX-DHA.PNG</Glide>
      <Binding_Pocket>LOX-DHA.PNG</Binding_Pocket>
      <Comparing_AutoDock_with_Glide>Comparing      AutoDock
and Glide-LOX.PNG</Comparing_AutoDock_with_Glide>
      <PDB_Files>LOX-DHA.pdb</PDB_Files>
    </Binding_Energy>
  </Ligand>
  <Ligand val="EPA">
    <Binding_Energy>
      <Autodock>-10.1 Kcal/mol</Autodock>
      <Glide_Score>-9.3 Kcal/mol</Glide_Score>
      <Bonded_Interactions>LOX-
EPA.PNG</Bonded_Interactions>
      <AutoDock>LOX-EPA.PNG</AutoDock>
      <Glide>LOX-EPA.PNG</Glide>
      <Binding_Pocket>LOX-EPA.PNG</Binding_Pocket>
      <Comparing_AutoDock_with_Glide>Comparing      AutoDock
and Glide-LOX.PNG</Comparing_AutoDock_with_Glide>
      <PDB_Files>LOX-EPA.pdb</PDB_Files>
    </Binding_Energy>
  </Ligand>
  <Ligand val="2AG">
    <Binding_Energy>
      <Autodock>-7.69 Kcal/mol</Autodock>
      <Glide_Score>-8.0 Kcal/mol</Glide_Score>
      <Bonded_Interactions>LOX-
2AG.PNG</Bonded_Interactions>
      <AutoDock>LOX-2AG.PNG</AutoDock>
      <Glide>LOX-2AG.PNG</Glide>

```

```

<Binding_Pocket>LOX-2AG.PNG</Binding_Pocket>
<Comparing_AutoDock_with_Glide>Comparing AutoDock
and Glide-LOX.PNG</Comparing_AutoDock_with_Glide>
<PDB_Files>LOX-2AG.pdb</PDB_Files>
</Binding_Energy>
</Ligand>
<Ligand val="Anandamide">
<Binding_Energy>
<Autodock>-6.57 Kcal/mol</Autodock>
<Glide_Score>-5.6 Kcal/mol</Glide_Score>
<Bonded_Interactions>LOX-
Anan.PNG</Bonded_Interactions>
<AutoDock>LOX-Anan.PNG</AutoDock>
<Glide>LOX-Anan.PNG</Glide>
<Binding_Pocket>LOX-Anan.PNG</Binding_Pocket>
<Comparing_AutoDock_with_Glide>Comparing AutoDock
and Glide-LOX.PNG</Comparing_AutoDock_with_Glide>
<PDB_Files>LOX-Anan.pdb</PDB_Files>
</Binding_Energy>
</Ligand>
<Ligand val="α tocotrienol">
<Binding_Energy>
<Autodock>-9.87 Kcal/mol</Autodock>
<Glide_Score>-7.1 Kcal/mol</Glide_Score>
<Bonded_Interactions>LOX-aTT.PNG</Bonded_Interactions>
<AutoDock>LOX-aTT.PNG</AutoDock>
<Glide>LOX-aTT.PNG</Glide>
<Binding_Pocket>LOX-aTT.PNG</Binding_Pocket>
<Comparing_AutoDock_with_Glide>Comparing AutoDock
and Glide-LOX.PNG</Comparing_AutoDock_with_Glide>
<PDB_Files>LOX-aTT.pdb</PDB_Files>
</Binding_Energy>
</Ligand>
<Ligand val="β tocotrienol">
<Binding_Energy>
<Autodock>-9.98 Kcal/mol</Autodock>
<Glide_Score>-7.5 Kcal/mol</Glide_Score>
<Bonded_Interactions>LOX-bTT.PNG</Bonded_Interactions>
<AutoDock>LOX-bTT.PNG</AutoDock>
<Glide>LOX-bTT.PNG</Glide>
<Binding_Pocket>LOX-bTT.PNG</Binding_Pocket>
<Comparing_AutoDock_with_Glide>Comparing AutoDock
and Glide-LOX.PNG</Comparing_AutoDock_with_Glide>
<PDB_Files>LOX-bTT.pdb</PDB_Files>

```

```

        </Binding_Energy>
    </Ligand>
    <Ligand val="γ tocotrienol">
        <Binding_Energy>
            <Autodock>-8.44 Kcal/mol</Autodock>
            <Glide_Score>-7.3 Kcal/mol</Glide_Score>
            <Bonded_Interactions>LOX-gTT.PNG</Bonded_Interactions>
            <AutoDock>LOX-gTT.PNG</AutoDock>
            <Glide>LOX-gTT.PNG</Glide>
            <Binding_Pocket>LOX-gTT.PNG</Binding_Pocket>
            <Comparing_AutoDock_with_Glide>Comparing AutoDock
            and Glide-LOX.PNG</Comparing_AutoDock_with_Glide>
            <PDB_Files>LOX-gTT.pdb</PDB_Files>
        </Binding_Energy>
    </Ligand>
    <Ligand val="δ tocotrienol">
        <Binding_Energy>
            <Autodock>-9.53 Kcal/mol</Autodock>
            <Glide_Score>-7.5 Kcal/mol</Glide_Score>
            <Bonded_Interactions>LOX-dTT.PNG</Bonded_Interactions>
            <AutoDock>LOX-dTT.PNG</AutoDock>
            <Glide>LOX-dTT.PNG</Glide>
            <Binding_Pocket>LOX-dTT.PNG</Binding_Pocket>
            <Comparing_AutoDock_with_Glide>Comparing AutoDock
            and Glide-LOX.PNG</Comparing_AutoDock_with_Glide>
            <PDB_Files>LOX-dTT.pdb</PDB_Files>
        </Binding_Energy>
    </Ligand>
</Protein>
<Protein val="RXRα">
    <Ligand val="DHA">
        <Binding_Energy>
            <Autodock>-12.06 Kcal/mol</Autodock>
            <Glide_Score>-15.4 Kcal/mol</Glide_Score>
            <Bonded_Interactions>RXRa-DHA.PNG</Bonded_Interactions>
            <AutoDock>RXRa-DHA.PNG</AutoDock>
            <Glide>RXRa-DHA.PNG</Glide>
            <Binding_Pocket>RXRa-DHA.PNG</Binding_Pocket>
            <Comparing_AutoDock_with_Glide>Comparing AutoDock
            and Glide-RXRα.PNG</Comparing_AutoDock_with_Glide>
            <PDB_Files>RXRa-DHA.pdb</PDB_Files>
        </Binding_Energy>
    </Ligand>

```

```

<Ligand val="EPA">
    <Binding_Energy>
        <Autodock>-11.92 Kcal/mol</Autodock>
        <Glide_Score>-14.3 Kcal/mol</Glide_Score>
        <Bonded_Interactions>RXRa-
EPA.PNG</Bonded_Interactions>
    <AutoDock>RXRa-EPA.PNG</AutoDock>
    <Glide>RXRa-EPA.PNG</Glide>
    <Binding_Pocket>RXRa-EPA.PNG</Binding_Pocket>
    <Comparing_AutoDock_with_Glide>Comparing AutoDock
and Glide-RXRa.PNG</Comparing_AutoDock_with_Glide>
    <PDB_Files>RXRa-EPA.pdb</PDB_Files>
</Binding_Energy>
</Ligand>
<Ligand val="2AG">
    <Binding_Energy>
        <Autodock>-8.24 Kcal/mol</Autodock>
        <Glide_Score>-9.6 Kcal/mol</Glide_Score>
        <Bonded_Interactions>RXRa-
2AG.PNG</Bonded_Interactions>
    <AutoDock>RXRa-2AG.PNG</AutoDock>
    <Glide>RXRa-2AG.PNG</Glide>
    <Binding_Pocket>RXRa-2AG.PNG</Binding_Pocket>
    <Comparing_AutoDock_with_Glide>Comparing AutoDock
and Glide-RXRa.PNG</Comparing_AutoDock_with_Glide>
    <PDB_Files>RXRa-2AG.pdb</PDB_Files>
</Binding_Energy>
</Ligand>
<Ligand val="Anandamide">
    <Binding_Energy>
        <Autodock>-9.15 Kcal/mol</Autodock>
        <Glide_Score>-11.6 Kcal/mol</Glide_Score>
        <Bonded_Interactions>RXRa-
Anan.PNG</Bonded_Interactions>
    <AutoDock>RXRa-Anan.PNG</AutoDock>
    <Glide>RXRa-Anan.PNG</Glide>
    <Binding_Pocket>RXRa-Anan.PNG</Binding_Pocket>
    <Comparing_AutoDock_with_Glide>Comparing AutoDock
and Glide-RXRa.PNG</Comparing_AutoDock_with_Glide>
    <PDB_Files>RXRa-Anan.pdb</PDB_Files>
</Binding_Energy>
</Ligand>
<Ligand val="α tocotrienol">
    <Binding_Energy>

```

<Autodock>RXR  $\alpha$  did not generate any binding poses with  $\alpha$ -tocotrienol</Autodock>  
 <Glide\_Score>RXR  $\alpha$  did not generate any binding poses with  $\alpha$ -tocotrienol</Glide\_Score>  
 <Bonded\_Interactions>RXRa-aTT.PNG</Bonded\_Interactions>  
 <AutoDock>RXRa-aTT.PNG</AutoDock>  
 <Glide>RXRa-aTT.PNG</Glide>  
 <Binding\_Pocket>RXRa-aTT.PNG</Binding\_Pocket>  
 <Comparing\_AutoDock\_with\_Glide>Comparing AutoDock  
 and Glide-RXRa.PNG</Comparing\_AutoDock\_with\_Glide>  
 <PDB\_Files>RXRa-aTT.pdb</PDB\_Files>  
 </Binding\_Energy>  
 </Ligand>  
 <Ligand val=" $\beta$  tocotrienol">  
 <Binding\_Energy>  
 <Autodock>RXR  $\alpha$  did not generate any binding poses with  $\beta$ -tocotrienol</Autodock>  
 <Glide\_Score>RXR  $\alpha$  did not generate any binding poses with  $\beta$ -tocotrienol</Glide\_Score>  
 <Bonded\_Interactions>RXRa-bTT.PNG</Bonded\_Interactions>  
 <AutoDock>RXRa-bTT.PNG</AutoDock>  
 <Glide>RXRa-bTT.PNG</Glide>  
 <Binding\_Pocket>RXRa-bTT.PNG</Binding\_Pocket>  
 <Comparing\_AutoDock\_with\_Glide>Comparing AutoDock  
 and Glide-RXRa.PNG</Comparing\_AutoDock\_with\_Glide>  
 <PDB\_Files>RXRa-bTT.pdb</PDB\_Files>  
 </Binding\_Energy>  
 </Ligand>  
 <Ligand val=" $\gamma$  tocotrienol">  
 <Binding\_Energy>  
 <Autodock>-8.63 Kcal/mol</Autodock>  
 <Glide\_Score>-10.9 Kcal/mol</Glide\_Score>  
 <Bonded\_Interactions>RXRa-gTT.PNG</Bonded\_Interactions>  
 <AutoDock>RXRa-gTT.PNG</AutoDock>  
 <Glide>RXRa-gTT.PNG</Glide>  
 <Binding\_Pocket>RXRa-gTT.PNG</Binding\_Pocket>  
 <Comparing\_AutoDock\_with\_Glide>Comparing AutoDock  
 and Glide-RXRa.PNG</Comparing\_AutoDock\_with\_Glide>  
 <PDB\_Files>RXRa-gTT.pdb</PDB\_Files>  
 </Binding\_Energy>  
 </Ligand>

```

<Ligand val="δ tocotrienol">
    <Binding_Energy>
        <Autodock>RXR α did not generate any binding poses with δ-tocotrienol</Autodock>
        <Glide_Score>RXR α did not generate any binding poses with δ-tocotrienol</Glide_Score>
        <Bonded_Interactions>RXRa-dTT.PNG</Bonded_Interactions>
            <AutoDock>RXRa-dTT.PNG</AutoDock>
            <Glide>RXRa-dTT.PNG</Glide>
            <Binding_Pocket>RXRa-dTT.PNG</Binding_Pocket>
            <Comparing_AutoDock_with_Glide>Comparing AutoDock and Glide-RXRa.PNG</Comparing_AutoDock_with_Glide>
            <PDB_Files>RXRa-dTT.pdb</PDB_Files>
        </Binding_Energy>
    </Ligand>
</Protein>
<Protein val="RARγ">
    <Ligand val="DHA">
        <Binding_Energy>
            <Autodock>-12.51 Kcal/mol</Autodock>
            <Glide_Score>-16.0 Kcal/mol</Glide_Score>
            <Bonded_Interactions>RARg-DHA.PNG</Bonded_Interactions>
            <AutoDock>RARg-DHA.PNG</AutoDock>
            <Glide>RARg-DHA.PNG</Glide>
            <Binding_Pocket>RARg-DHA.PNG</Binding_Pocket>
            <Comparing_AutoDock_with_Glide>Comparing AutoDock and Glide-RARg.PNG</Comparing_AutoDock_with_Glide>
            <PDB_Files>RARg-DHA.pdb</PDB_Files>
        </Binding_Energy>
    </Ligand>
    <Ligand val="EPA">
        <Binding_Energy>
            <Autodock>-10.18 Kcal/mol</Autodock>
            <Glide_Score>-14.7 Kcal/mol</Glide_Score>
            <Bonded_Interactions>RARg-EPA.PNG</Bonded_Interactions>
            <AutoDock>RARg-EPA.PNG</AutoDock>
            <Glide>RARg-EPA.PNG</Glide>
            <Binding_Pocket>RARg-EPA.PNG</Binding_Pocket>
            <Comparing_AutoDock_with_Glide>Comparing AutoDock and Glide-RARg.PNG</Comparing_AutoDock_with_Glide>
            <PDB_Files>RARg-EPA.pdb</PDB_Files>

```

```

        </Binding_Energy>
    </Ligand>
    <Ligand val="2AG">
        <Binding_Energy>
            <Autodock>-10.73 Kcal/mol</Autodock>
            <Glide_Score>-12.9 Kcal/mol</Glide_Score>
            <Bonded_Interactions>RARg-
2AG.PNG</Bonded_Interactions>
            <AutoDock>RARg-2AG.PNG</AutoDock>
            <Glide>RARg-2AG.PNG</Glide>
            <Binding_Pocket>RARg-2AG.PNG</Binding_Pocket>
            <Comparing_AutoDock_with_Glide>Comparing      AutoDock
and Glide-RARg.PNG</Comparing_AutoDock_with_Glide>
            <PDB_Files>RARg-2AG.pdb</PDB_Files>
        </Binding_Energy>
    </Ligand>
    <Ligand val="Anandamide">
        <Binding_Energy>
            <Autodock>-10.84 Kcal/mol</Autodock>
            <Glide_Score>-10.7 Kcal/mol</Glide_Score>
            <Bonded_Interactions>RARg-
Anan.PNG</Bonded_Interactions>
            <AutoDock>RARg-Anan.PNG</AutoDock>
            <Glide>RARg-Anan.PNG</Glide>
            <Binding_Pocket>RARg-Anan.PNG</Binding_Pocket>
            <Comparing_AutoDock_with_Glide>Comparing      AutoDock
and Glide-RARg.PNG</Comparing_AutoDock_with_Glide>
            <PDB_Files>RARg-Anan.pdb</PDB_Files>
        </Binding_Energy>
    </Ligand>
    <Ligand val="α tocotrienol">
        <Binding_Energy>
            <Autodock>RAR γ did not generate any binding poses with α-
tocotrienol</Autodock>
            <Glide_Score>RAR γ did not generate any binding poses with
α-tocotrienol</Glide_Score>
            <Bonded_Interactions>RARg-
aTT.PNG</Bonded_Interactions>
            <AutoDock>RARg-aTT.PNG</AutoDock>
            <Glide>RARg-aTT.PNG</Glide>
            <Binding_Pocket>RARg-aTT.PNG</Binding_Pocket>
            <Comparing_AutoDock_with_Glide>Comparing      AutoDock
and Glide-RARg.PNG</Comparing_AutoDock_with_Glide>
            <PDB_Files>RARg-aTT.pdb</PDB_Files>

```

```

        </Binding_Energy>
    </Ligand>
    <Ligand val="β tocotrienol">
        <Binding_Energy>
            <Autodock>-12.15 Kcal/mol</Autodock>
            <Glide_Score>-10.3 Kcal/mol</Glide_Score>
            <Bonded_Interactions>RARg-
bTT.PNG</Bonded_Interactions>
            <AutoDock>RARg-bTT.PNG</AutoDock>
            <Glide>RARg-bTT.PNG</Glide>
            <Binding_Pocket>RARg-bTT.PNG</Binding_Pocket>
            <Comparing_AutoDock_with_Glide>Comparing      AutoDock
and Glide-RARg.PNG</Comparing_AutoDock_with_Glide>
            <PDB_Files>RARg-bTT.pdb</PDB_Files>
        </Binding_Energy>
    </Ligand>
    <Ligand val="γ tocotrienol">
        <Binding_Energy>
            <Autodock>-11.42 Kcal/mol</Autodock>
            <Glide_Score>-11.2 Kcal/mol</Glide_Score>
            <Bonded_Interactions>RARg-
gTT.PNG</Bonded_Interactions>
            <AutoDock>RARg-gTT.PNG</AutoDock>
            <Glide>RARg-gTT.PNG</Glide>
            <Binding_Pocket>RARg-gTT.PNG</Binding_Pocket>
            <Comparing_AutoDock_with_Glide>Comparing      AutoDock
and Glide-RARg.PNG</Comparing_AutoDock_with_Glide>
            <PDB_Files>RARg-gTT.pdb</PDB_Files>
        </Binding_Energy>
    </Ligand>
    <Ligand val="δ tocotrienol">
        <Binding_Energy>
            <Autodock>-9.03 Kcal/mol</Autodock>
            <Glide_Score>-12.1 Kcal/mol</Glide_Score>
            <Bonded_Interactions>RARg-
dTT.PNG</Bonded_Interactions>
            <AutoDock>RARg-dTT.PNG</AutoDock>
            <Glide>RARg-dTT.PNG</Glide>
            <Binding_Pocket>RARg-dTT.PNG</Binding_Pocket>
            <Comparing_AutoDock_with_Glide>Comparing      AutoDock
and Glide-RARg.PNG</Comparing_AutoDock_with_Glide>
            <PDB_Files>RARg-dTT.pdb</PDB_Files>
        </Binding_Energy>
    </Ligand>

```

```

    </Protein>
    <Protein val="CB1">
        <Ligand val="DHA">
            <Binding_Energy>
                <Autodock>-10.55 Kcal/mol</Autodock>
                <Glide_Score>-9.9 Kcal/mol</Glide_Score>
                <Bonded_Interactions>CB1-
                    DHA.PNG</Bonded_Interactions>
                <AutoDock>CB1-DHA.PNG</AutoDock>
                <Glide>CB1-DHA.PNG</Glide>
                <Binding_Pocket>CB1-DHA.PNG</Binding_Pocket>
                <Comparing_AutoDock_with_Glide>Comparing      AutoDock
            and Glide-CB1.PNG</Comparing_AutoDock_with_Glide>
                <PDB_Files>CB1-DHA.pdb</PDB_Files>
            </Binding_Energy>
        </Ligand>
        <Ligand val="EPA">
            <Binding_Energy>
                <Autodock>-10.46 Kcal/mol</Autodock>
                <Glide_Score>-9.8 Kcal/mol</Glide_Score>
                <Bonded_Interactions>CB1-EPA.PNG</Bonded_Interactions>
                <AutoDock>CB1-EPA.PNG</AutoDock>
                <Glide>CB1-EPA.PNG</Glide>
                <Binding_Pocket>CB1-EPA.PNG</Binding_Pocket>
                <Comparing_AutoDock_with_Glide>Comparing      AutoDock
            and Glide-CB1.PNG</Comparing_AutoDock_with_Glide>
                <PDB_Files>CB1-EPA.pdb</PDB_Files>
            </Binding_Energy>
        </Ligand>
        <Ligand val="2AG">
            <Binding_Energy>
                <Autodock>-11.28 Kcal/mol</Autodock>
                <Glide_Score>-10.2 Kcal/mol</Glide_Score>
                <Bonded_Interactions>CB1-2AG.PNG</Bonded_Interactions>
                <AutoDock>CB1-2AG.PNG</AutoDock>
                <Glide>CB1-2AG.PNG</Glide>
                <Binding_Pocket>CB1-2AG.PNG</Binding_Pocket>
                <Comparing_AutoDock_with_Glide>Comparing      AutoDock
            and Glide-CB1.PNG</Comparing_AutoDock_with_Glide>
                <PDB_Files>CB1-2AG.pdb</PDB_Files>
            </Binding_Energy>
        </Ligand>
        <Ligand val="Anandamide">
            <Binding_Energy>

```

```

<Autodock>-11.83 Kcal/mol</Autodock>
<Glide_Score>-10.1 Kcal/mol</Glide_Score>
<Bonded_Interactions>CB1-
Anan.PNG</Bonded_Interactions>
    <AutoDock>CB1-Anan.PNG</AutoDock>
    <Glide>CB1-Anan.PNG</Glide>
    <Binding_Pocket>CB1-Anan.PNG</Binding_Pocket>
    <Comparing_AutoDock_with_Glide>Comparing AutoDock
and Glide-CB1.PNG</Comparing_AutoDock_with_Glide>
    <PDB_Files>CB1-Anan.pdb</PDB_Files>
    </Binding_Energy>
</Ligand>
<Ligand val="α tocotrienol">
    <Binding_Energy>
        <Autodock>-8.35 Kcal/mol</Autodock>
        <Glide_Score>-7.5 Kcal/mol</Glide_Score>
        <Bonded_Interactions>CB1-aTT.PNG</Bonded_Interactions>
        <AutoDock>CB1-aTT.PNG</AutoDock>
        <Glide>CB1-aTT.PNG</Glide>
        <Binding_Pocket>CB1-aTT.PNG</Binding_Pocket>
        <Comparing_AutoDock_with_Glide>Comparing AutoDock
and Glide-CB1.PNG</Comparing_AutoDock_with_Glide>
    <PDB_Files>CB1-aTT.pdb</PDB_Files>
    </Binding_Energy>
</Ligand>
<Ligand val="β tocotrienol">
    <Binding_Energy>
        <Autodock>-9.76 Kcal/mol</Autodock>
        <Glide_Score>-7.8 Kcal/mol</Glide_Score>
        <Bonded_Interactions>CB1-bTT.PNG</Bonded_Interactions>
        <AutoDock>CB1-bTT.PNG</AutoDock>
        <Glide>CB1-bTT.PNG</Glide>
        <Binding_Pocket>CB1-bTT.PNG</Binding_Pocket>
        <Comparing_AutoDock_with_Glide>Comparing AutoDock
and Glide-CB1.PNG</Comparing_AutoDock_with_Glide>
    <PDB_Files>CB1-bTT.pdb</PDB_Files>
    </Binding_Energy>
</Ligand>
<Ligand val="γ tocotrienol">
    <Binding_Energy>
        <Autodock>-9.46 Kcal/mol</Autodock>
        <Glide_Score>-8.6 Kcal/mol</Glide_Score>
        <Bonded_Interactions>CB1-gTT.PNG</Bonded_Interactions>
        <AutoDock>CB1-gTT.PNG</AutoDock>

```

```

<Glide>CB1-gTT.PNG</Glide>
<Binding_Pocket>CB1-gTT.PNG</Binding_Pocket>
<Comparing_AutoDock_with_Glide>Comparing AutoDock
and Glide-CB1.PNG</Comparing_AutoDock_with_Glide>
    <PDB_Files>CB1-gTT.pdb</PDB_Files>
</Binding_Energy>
</Ligand>
<Ligand val="δ tocotrienol">
    <Binding_Energy>
        <Autodock>-9.11 Kcal/mol</Autodock>
        <Glide_Score>-8.0 Kcal/mol</Glide_Score>
        <Bonded_Interactions>CB1-dTT.PNG</Bonded_Interactions>
        <AutoDock>CB1-dTT.PNG</AutoDock>
        <Glide>CB1-dTT.PNG</Glide>
        <Binding_Pocket>CB1-dTT.PNG</Binding_Pocket>
        <Comparing_AutoDock_with_Glide>Comparing AutoDock
and Glide-CB1.PNG</Comparing_AutoDock_with_Glide>
    <PDB_Files>CB1-dTT.pdb</PDB_Files>
</Binding_Energy>
</Ligand>
</Protein>
<Protein val="CB2">
    <Ligand val="DHA">
        <Binding_Energy>
            <Autodock>-10.88 Kcal/mol</Autodock>
            <Glide_Score>-9.5 Kcal/mol</Glide_Score>
            <Bonded_Interactions>CB2-
DHA.PNG</Bonded_Interactions>
            <AutoDock>CB2-DHA.PNG</AutoDock>
            <Glide>CB2-DHA.PNG</Glide>
            <Binding_Pocket>CB2-DHA.PNG</Binding_Pocket>
            <Comparing_AutoDock_with_Glide>Comparing AutoDock
and Glide-CB2.PNG</Comparing_AutoDock_with_Glide>
    <PDB_Files>CB2-DHA.pdb</PDB_Files>
</Binding_Energy>
</Ligand>
<Ligand val="EPA">
    <Binding_Energy>
        <Autodock>-9.33 Kcal/mol</Autodock>
        <Glide_Score>-9.1 Kcal/mol</Glide_Score>
        <Bonded_Interactions>CB2-EPA.PNG</Bonded_Interactions>
        <AutoDock>CB2-EPA.PNG</AutoDock>
        <Glide>CB2-EPA.PNG</Glide>
        <Binding_Pocket>CB2-EPA.PNG</Binding_Pocket>

```

<Comparing\_AutoDock\_with\_Glide>Comparing AutoDock  
 and Glide-CB2.PNG</Comparing\_AutoDock\_with\_Glide>  
     <PDB\_Files>CB2-EPA.pdb</PDB\_Files>  
     </Binding\_Energy>  
 </Ligand>  
 <Ligand val="2AG">  
     <Binding\_Energy>  
         <Autodock>-11.03 Kcal/mol</Autodock>  
         <Glide\_Score>-10.7 Kcal/mol</Glide\_Score>  
         <Bonded\_Interactions>CB2-2AG.PNG</Bonded\_Interactions>  
         <AutoDock>CB2-2AG.PNG</AutoDock>  
         <Glide>CB2-2AG.PNG</Glide>  
         <Binding\_Pocket>CB2-2AG.PNG</Binding\_Pocket>  
         <Comparing\_AutoDock\_with\_Glide>Comparing AutoDock  
 and Glide-CB2.PNG</Comparing\_AutoDock\_with\_Glide>  
     <PDB\_Files>CB2-2AG.pdb</PDB\_Files>  
     </Binding\_Energy>  
 </Ligand>  
 <Ligand val="Anandamide">  
     <Binding\_Energy>  
         <Autodock>-11.24 Kcal/mol</Autodock>  
         <Glide\_Score>-10.7 Kcal/mol</Glide\_Score>  
         <Bonded\_Interactions>CB2-  
         Anan.PNG</Bonded\_Interactions>  
         <AutoDock>CB2-Anan.PNG</AutoDock>  
         <Glide>CB2-Anan.PNG</Glide>  
         <Binding\_Pocket>CB2-Anan.PNG</Binding\_Pocket>  
         <Comparing\_AutoDock\_with\_Glide>Comparing AutoDock  
 and Glide-CB2.PNG</Comparing\_AutoDock\_with\_Glide>  
     <PDB\_Files>CB2-Anan.pdb</PDB\_Files>  
     </Binding\_Energy>  
 </Ligand>  
 <Ligand val="α tocotrienol">  
     <Binding\_Energy>  
         <Autodock>CB2 did not generate any binding poses with α-tocotrienol</Autodock>  
         <Glide\_Score>CB2 did not generate any binding poses with α-tocotrienol</Glide\_Score>  
         <Bonded\_Interactions>CB2-aTT.PNG</Bonded\_Interactions>  
         <AutoDock>CB2-aTT.PNG</AutoDock>  
         <Glide>CB2-aTT.PNG</Glide>  
         <Binding\_Pocket>CB2-aTT.PNG</Binding\_Pocket>  
         <Comparing\_AutoDock\_with\_Glide>Comparing AutoDock  
 and Glide-CB2.PNG</Comparing\_AutoDock\_with\_Glide>

```

<PDB_Files>CB2-aTT.pdb</PDB_Files>
</Binding_Energy>
</Ligand>
<Ligand val="β tocotrienol">
    <Binding_Energy>
        <Autodock>CB2 did not generate any binding poses with β-tocotrienol</Autodock>
        <Glide_Score>-3.0 Kcal/mol</Glide_Score>
        <Bonded_Interactions>CB2-bTT.PNG</Bonded_Interactions>
        <AutoDock>CB2-bTT.PNG</AutoDock>
        <Glide>CB2-bTT.PNG</Glide>
        <Binding_Pocket>CB2-bTT.PNG</Binding_Pocket>
        <Comparing_AutoDock_with_Glide>Comparing AutoDock and Glide-CB2.PNG</Comparing_AutoDock_with_Glide>
        <PDB_Files>CB2-bTT.pdb</PDB_Files>
    </Binding_Energy>
</Ligand>
<Ligand val="γ tocotrienol">
    <Binding_Energy>
        <Autodock>-4.42 Kcal/mol</Autodock>
        <Glide_Score>-3.0 Kcal/mol</Glide_Score>
        <Bonded_Interactions>CB2-gTT.PNG</Bonded_Interactions>
        <AutoDock>CB2-gTT.PNG</AutoDock>
        <Glide>CB2-gTT.PNG</Glide>
        <Binding_Pocket>CB2-gTT.PNG</Binding_Pocket>
        <Comparing_AutoDock_with_Glide>Comparing AutoDock and Glide-CB2.PNG</Comparing_AutoDock_with_Glide>
        <PDB_Files>CB2-gTT.pdb</PDB_Files>
    </Binding_Energy>
</Ligand>
<Ligand val="δ tocotrienol">
    <Binding_Energy>
        <Autodock>-1.33 Kcal/mol</Autodock>
        <Glide_Score>-4.01 Kcal/mol</Glide_Score>
        <Bonded_Interactions>CB2-dTT.PNG</Bonded_Interactions>
        <AutoDock>CB2-dTT.PNG</AutoDock>
        <Glide>CB2-dTT.PNG</Glide>
        <Binding_Pocket>CB2-dTT.PNG</Binding_Pocket>
        <Comparing_AutoDock_with_Glide>Comparing AutoDock and Glide-CB2.PNG</Comparing_AutoDock_with_Glide>
        <PDB_Files>CB2-dTT.pdb</PDB_Files>
    </Binding_Energy>
</Ligand>
</Protein>

```

&lt;/Details&gt;

## **Appendix-M**

### **Complete Project Code**

#### **Welcome Page: Design**

```
//Design page for LIPRO INTERACT SOFTWARE FOR THEBINDING
INTERACTIONS OF LIPID LIGANDS

<%@ Page Language="C#" AutoEventWireup="true" CodeFile="Welcome.aspx.cs"
Inherits="Welcome" %>

<!DOCTYPE html PUBLIC "-//W3C//DTD XHTML 1.0 Transitional//EN"
"http://www.w3.org/TR/xhtml1/DTD/xhtml1-transitional.dtd">

<html xmlns="http://www.w3.org/1999/xhtml">
<head id="Head1" runat="server">
    <title></title>
    <link rel="stylesheet" type="text/css" href="css/style.css" />
    <style type="text/css">
        .style1
        {
            width: 114px;
        }
    </style>
</head>
<body>
    <form id="form1" runat="server">
        <div>

            <div id="Div1" style="width:100%; text-align:center" >
                <br/>
                <asp:Image ID="Image2" ImageUrl="~/Images/BG3.png" runat="server"
                    Height="85px" Width="100%" />
                <br />
                <%--<asp:Image ID="Image2" ImageUrl="~/Images/Title.png"
runat="server" />--%>
                <asp:Image ID="Image4" ImageUrl="~/Images/1234.png"
runat="server" style="position: absolute; top: 22px; left: 496px;">
                    ImageAlign="Middle"/>
                <br />
            </div>
        </form>
    </body>
</html>
```

```
<div id="Div2" style="width:100%; text-align:center;font-family:Algerian;font-size:x-large">
```

LIPRO INTERACT SOFTWARE FOR THE<br>  
BINDING INTERACTIONS OF LIPID LIGANDS

```
<br />
```

```
</div>
```

```
<div style="font-family:Georgia;font-size:large;color:Black;font-weight:bold">
<asp:Image ID="Image3" runat="server" ImageUrl="~/Images/FLIP.png"
```

<ol style="position: absolute; top: 194px; left: 50px; right: 30px; line-height: 30px">

<li>Select protein and ligand from ‘Choose protein’ and ‘Choose Ligand’, respectively.

</li>

<li>Select the type of interaction you are interested in.</li>

<li>Binding energy provides the affinity between the selected protein and ligand as a result of AutoDock and Glide.</li>

<li>4A-AutoDock : The interacting amino acids of the selected protein with the selected ligand within 4A distance in AutoDock.

The images are drawn using VMD ([www.VMD.com](http://www.VMD.com)) software. A new cartoon model is selected to represent the protein structure and VDW is selected for the ligand structure.</li>

<li>4A-Glide : The interacting amino acids of the selected protein with the selected ligand within 4A distance in Glide.</li>

<li>Interactions: For the selected protein and ligand, this option displays the hydrophobic interactions and hydrogen bonds between them obtained from LigPlot

software. Hydrogen bonds are represented using dashes.

Hydrophobic interactions are represented by an arc with a spike pointing towards the ligand

atoms.</li>

<li>Comparison of AutoDock and Glide: This option compares AutoDock and Glide from

which the user can choose the best suitable docking technique for the selected protein

and ligand.</li>

<li>PDB files: The PDB files are generated after docking the protein with lipid ligand. This PDB files can be downloaded which reflect the interaction between protein and ligand.

These PDB files are ready to use further molecular docking or molecular dynamic simulations.</li>

</ol>  
</div>

</div>

```
<div runat="server" id="divref2" visible="true"
      style="position: absolute; left: 10px; font-family: Georgia; font-
      size: large; color: White; font-weight: bold; top: 544px; height: 198px;">
<br/>
<br/>
<br/>
<br/>
<br />
```

References:<br/>

1. Gaddipati, R.S, Raikundalia, G. K, & Mathai, ML. (2014). Comparison of AutoDock and Glide towards the Discovery of PPAR Agonists.

International Journal of Bioscience, Biochemistry and Bioinformatics, 4(2), 100-105.<br/>

2. Gaddipati, R. S., Raikundalia, G. K, & Mathai, ML. (2014).

Dual and selective lipid inhibitors of cyclooxygenases and lipoxygenase: a molecular docking study. Medicinal Chemistry Research, 1-14.<br/>

3. Gaddipati, R. S., Raikundalia GK, Mathai ML. (2012).

Towards the Design of PPAR based Drugs using tocotrienol as natural ligands-A Docking Analysis.

Paper presented at the International Conference on Engineering and Applied Sciences, Beijing.

<br/>  
<br/>  
<br/>

Contact:<br/>

Rajyalakshmi Gaddipati <br/>  
rajyalakshmi.gaddipati@live.vu.edu.au

</div>

```
<table style="position: absolute; top: 820px; left: 1482px">
<tr>
<td>
<asp:Button ID="Button1" runat="server" Text="Next" onclick="Button1_Click"
```

```

        Font-Size="Large"    Height="40px"    Width="100px"    Font-Names="Georgia"
BackColor="Black" Font-Bold="True" ForeColor="White" />
</td>
</tr>

</table>
</form>
</body>
</html>

```

## Welcome Page: Code-behind file

```

using System;
using System.Collections.Generic;
using System.Linq;
using System.Web;
using System.Web.UI;
using System.Web.UI.WebControls;

public partial class Welcome : System.Web.UI.Page
{
    protected void Page_Load(object sender, EventArgs e)
    {

    }
    protected void Button1_Click(object sender, EventArgs e)
    {
        Response.Redirect("Software.aspx");
    }
}

```

## Second Page-Design

*//Design page for Lipro Interact Software For the Binding Interactions of Lipid Ligands*

```

<%@ Page Language="C#" AutoEventWireup="true" CodeFile="Software.aspx.cs"
Inherits="_Default" %>

<!DOCTYPE html PUBLIC "-//W3C//DTD XHTML 1.0 Transitional//EN"
"http://www.w3.org/TR/xhtml1/DTD/xhtml1-transitional.dtd">

```

```

<html xmlns="http://www.w3.org/1999/xhtml">
<head runat="server">
    <title></title>
    <link rel="stylesheet" type="text/css" href="css/style.css" />
    <style type="text/css">
        .style1
        {
            width: 114px;
        }
    </style>
</head>
<body>
    <form id="form1" runat="server">
        <div>

            <div id="Div1" style="width:100%; text-align:center" >
                <br/>
                <asp:Image ID="Image2" ImageUrl "~/Images/BG3.png" runat="server"
                    Height="85px" Width="100%" />
                <br />
                <%--<asp:Image ID="Image2" ImageUrl "~/Images/Title.png"
runat="server" /--%>
                    <asp:Image ID="Image4" ImageUrl "~/Images/1234.png"
runat="server" style="position: absolute; top: 22px; left: 496px;"'
ImageAlign="Middle"/>
                <br />
            </div>

            <div id="Div2" style="width:100%; text-align:center;font-family:Algerian;font-size:xx-large">
                LIPRO INTERACT SOFTWARE FOR THE<br>
                BINDING INTERACTIONS OF LIPID LIGANDS
            </div>

        </div>

        <table style="position: absolute; top: 200px; left: 86px;">
            <tr>
                <td style="height:20px">
                </td></tr>

            <tr>
                <td>
                    <asp:Label ID="Label1" runat="server" Font-Bold="True" font-size="X-Large"
                        Text="Choose Protein" ForeColor="Black"
                        Font-Italic="False" Font-Names="Georgia"></asp:Label>
                </td>
                <td>

```

```

<asp:DropDownList ID="DropDownList1" runat="server"
    onselectedindexchanged="DropDownList1_SelectedIndexChanged"
    CssClass="style_Normal_Dropdown" AutoPostBack="true" font-size="Large"
    Font-Names="Georgia">
</asp:DropDownList>

</td>
</tr>
<tr>
<td style="height:10px">
</td></tr>
<tr>

<td>
    <asp:Label ID="Label2" runat="server" Font-Bold="True" Text="Choose Ligand"
        ForeColor="Black" font-size="X-Large" Font-Names="Georgia"></asp:Label>
</td>
<td>
    <asp:DropDownList ID="DropDownList2" runat="server"
        onselectedindexchanged="DropDownList2_SelectedIndexChanged"
        AutoPostBack="true" font-size="Large"
        Font-Names="Georgia">
        </asp:DropDownList>
</td>
</tr>
<tr>
<td style="height:10px">
</td></tr>
<tr>

<td>
    <asp:Label ID="Label3" runat="server" Font-Bold="True" Text="Protein-Ligand
    Interaction"
        ForeColor="Black" font-size="X-Large" Font-Names="Georgia"></asp:Label>
</td>
<td>
    <asp:DropDownList ID="DropDownList3" runat="server"
        onselectedindexchanged="DropDownList3_SelectedIndexChanged"
        AutoPostBack="true" font-size="Large"
        Font-Names="Georgia">
        </asp:DropDownList>
</td>
</tr>
</table>
<table style="position: absolute; top: 342px; left: 0px;">
<tr style="height:50px">
<td></td>
</tr>

```

```

<tr>
<td style="width:425px"></td>
<td>
<asp:Label ID="Label4" runat="server" Font-Bold="True" Visible="False"
    ForeColor="Black" Text="Binding Energy" font-size="X-Large"
    Font-Names="Georgia"></asp:Label>
</td>
<td style="width:20px"></td>
<td>
<asp:Label ID="Label5" runat="server" Font-Bold="True" Visible="False"
    ForeColor="Black" font-size="X-Large"
    Font-Names="Georgia"></asp:Label>
</td>
</tr>
<tr>
    <td style="position: absolute; left: 500px;">
        <asp:Button Visible="false" ID="btndwnpdb" runat="server"
            Text="Download PDB File" onclick="btndwnpdb_Click"
            BackColor="Black" Font-Bold="True"
            ForeColor="White" Font-Size="Medium"
            Height="40px" Width="200px" Font-Names="Georgia" />
    <%-- </td>
    <td> --%> <asp:Button Visible="false" ID="btndownload" runat="server"
        Text="Download Image File"
        onclick="btndownload_Click"
        BackColor="Black" Font-Bold="True" Font-Size="Medium" ForeColor="White"
        Height="40px" Width="200px" Font-Names="Georgia" />
    </td>
    </tr>
    </table>

<table style="position: absolute; top: 200px; left: 900px;">
<tr>
    <td>
        &nbsp;</td>
    </tr>
    <tr>
        <td>
            <asp:Image Height="600px" Width="600px" ID="Image1" Visible="false"
runat="server" />
        </td>
    </tr>
    <tr>
        <td>

```

```

</td>
</tr>

</table>
</div>

<table >
<tr>
<td style="position: absolute; top: 850px;left: 200px;font-family:Georgia">
<asp:Button ID="Button2" runat="server" Text="Previous" Font-Size="Large"
    Height="40px" Width="100px" onclick="Button2_Click" Font-Names="Georgia"
    BackColor="Black" Font-Bold="True" ForeColor="White" />
</td>
<td style="position: absolute; top: 850px;left: 1482px;font-family:Georgia">
<asp:Button ID="Button1" runat="server" Text="Next" onclick="Button1_Click"
    Font-Size="Large" Height="40px" Width="100px" Font-Names="Georgia"
    BackColor="Black" Font-Bold="True" ForeColor="White" />
</td>
</tr>

</table>

</form>

```

```

</body>
</html>

```

## Second Page-Code-behind

```

using System;
using System.Collections.Generic;
using System.Linq;
using System.Web;
using System.Web.UI;
using System.Web.UI.WebControls;
using System.Data;
using System.Data.SqlClient;

public partial class _Default : System.Web.UI.Page
{
    DataSet _dstMain = new DataSet();
    //int Protein_id, Ligand_id;
    string Protein_id = string.Empty;
}

```

```

string Ligand_id = string.Empty;
string Binding_Energy_val = string.Empty;
string filePath = string.Empty;
string fileName = string.Empty;

protected void Page_Load(object sender, EventArgs e)
{
    try
    {
        if (!Page.IsPostBack)
        {
            //divref2.Visible = false;

```

**//Code to load XML data in the dataset**

```
_dstMain.ReadXml(Server.MapPath("~/Data/Data.xml"));
```

```
ViewState["_dstMain"] = _dstMain;
```

**//Code to bind dropdown values for Protein**

```

DropDownList1.Items.Add("--Select--");
DropDownList1.Items.Add("PPAR $\alpha$ ");
DropDownList1.Items.Add("PPAR $\delta$ ");
DropDownList1.Items.Add("PPAR $\gamma$ ");
DropDownList1.Items.Add("COX1");
DropDownList1.Items.Add("COX2");
DropDownList1.Items.Add("LOX");
DropDownList1.Items.Add("RXR $\alpha$ ");
DropDownList1.Items.Add("RAR $\gamma$ ");
DropDownList1.Items.Add("CB1");
DropDownList1.Items.Add("CB2");
```

**//Code to bind dropdown values for Ligand**

```

DropDownList2.Items.Add("--Select--");
DropDownList2.Items.Add("DHA");
DropDownList2.Items.Add("EPA");
DropDownList2.Items.Add("2AG");
DropDownList2.Items.Add("Anandamide");
DropDownList2.Items.Add(" $\alpha$  tocotrienol");
DropDownList2.Items.Add(" $\beta$  tocotrienol");
DropDownList2.Items.Add(" $\gamma$  tocotrienol");
DropDownList2.Items.Add(" $\delta$  tocotrienol");
```

```

//Code to bind dropdown values for Protein- Ligand Interaction

DropDownList3.Items.Add("--Select--");
DropDownList3.Items.Add("Binding Energy - Autodock");
DropDownList3.Items.Add("Binding Energy - Glide Score");
DropDownList3.Items.Add("4A-AutoDock");
//modified on 19/7/14
//DropDownList3.Items.Add("4A-Glide");
DropDownList3.Items.Add("4A-Glide");
//DropDownList3.Items.Add("Binding_Pocket");
DropDownList3.Items.Add("Bonded_Interactions");
DropDownList3.Items.Add("Comparing_AutoDock_with_Glide");
//DropDownList3.Items.Add("Molecular Dynamic Simulation");
DropDownList3.Items.Add("PDB_Files");
}

}

catch (Exception ex)
{
}

protected void DropDownList1_SelectedIndexChanged(object sender, EventArgs e)
{
    try
    {
//Code to be executed if protein is selected from the dropdown

        //if (DropDownList1.SelectedIndex == 0)
        //{
            DropDownList2.SelectedIndex = 0;
            DropDownList3.SelectedIndex = 0;

            Label4.Visible = false;
            Label5.Visible = false;
            btndownload.Visible = false;
            btndwnpdb.Visible = false;
            Image1.Visible = false;
        //}

    }

    catch (Exception ex)
    {
}

}

protected void DropDownList2_SelectedIndexChanged(object sender, EventArgs e)
{
//Code to be executed if ligand is selected from the dropdown

```

```

{
    //DropDownList2.SelectedIndex = 0;
    DropDownList3.SelectedIndex = 0;
    Label4.Visible = false;
    Label5.Visible = false;
    btndownload.Visible = false;
    btndwnpdb.Visible = false;
    Image1.Visible = false;
}
catch (Exception ex)
{
}

}

protected void DropDownList3_SelectedIndexChanged(object sender, EventArgs e)
{
//Code to be executed if protein-ligand interaction is selected from the dropdown

try
{
    #region commented
    ////if (DropDownList3.SelectedItem.Value.ToString().CompareTo("Binding Energy - Autodock") == 0)
    ////{
    ////    Label4.Visible = true;
    ////    Label5.Visible = true;
    ////    Label5.Text = "-11.5 Kcal/mol";
    ////}
    ////else if (DropDownList3.SelectedItem.Value.ToString().CompareTo("Binding Energy - Glide Score") == 0)
    ////{
    ////    Label4.Visible = true;
    ////    Label5.Visible = true;
    ////    Label5.Text = "-10.2 Kcal/mol";
    ////}
    ////else
    ////{
    ////    Label4.Visible = false;
    ////    Label5.Visible = false;
    ////}
    ////if (DropDownList2.SelectedItem.Value.ToString().CompareTo("DHA") == 0 && DropDownList3.SelectedItem.Value.ToString().CompareTo("Interactions") == 0)
    ////{
    ////    Image1.Visible = true;
    ////    Image1.ImageUrl = "~/Images/DHA.jpg";
    ////}
    ////else
    ////{
}

```

```

//// Image1.Visible = false;
///}
#endregion

if (DropDownList1.SelectedIndex != 0 && DropDownList2.SelectedIndex != 0 &&
DropDownList3.SelectedIndex != 0)
{
    _dstMain = (DataSet)ViewState["_dstMain"];

    //to fetch protein id
    DataRow[] pdrow = _dstMain.Tables[0].Select("val      =      ''      +
DropDownList1.SelectedItem.Value.ToString().Trim() + """);

    if (pdrow.Length > 0)
    {
        Protein_id = pdrow[0][0].ToString();
    }

    //to fetch respective ligand id
    DataRow[] ldrow = _dstMain.Tables[1].Select("val      =      ''      +
DropDownList2.SelectedItem.Value.ToString().Trim() + '' and Protein_id=" + Protein_id);

    if (ldrow.Length > 0)
    {
        Ligand_id = ldrow[0][0].ToString();
    }

    //to fetch binding energy
    DataRow[] bdrow = _dstMain.Tables[2].Select("Ligand_id=" + Ligand_id);

    if (bdrow.Length > 0)
    {
        //Ligand_id = ldrow[0][0].ToString();
//code to be executed if Binding Energy - Autodock is selected in Protein- Ligand Interaction
        if (DropDownList3.SelectedItem.Value.ToString().Trim().CompareTo("Binding
Energy - Autodock") == 0)
        {
            Image1.Visible = false;

            Label4.Visible = true;
            Label5.Visible = true;
            Label5.Text = bdrow[0][1].ToString();
            btndownload.Visible = false;
            btndwnpdb.Visible = false;

        }
//code to be executed if Binding Energy - Glide Score is selected in Protein- Ligand Interaction
    }
}

```

```

        if (DropDownList3.SelectedItem.Value.ToString().Trim().CompareTo("Binding
Energy - Glide Score") == 0)
    {
        Image1.Visible = false;

        Label4.Visible = true;
        Label5.Visible = true;
        Label5.Text = bdrow[0][2].ToString();
        btndownload.Visible = false;
        btndwnpdb.Visible = false;

    }

//code to be executed if 4A-AutoDock is selected in Protein- Ligand Interaction

        if      (DropDownList3.SelectedItem.Value.ToString().Trim().CompareTo("4A-
AutoDock") == 0)
    {
        Label4.Visible = false;
        Label5.Visible = false;

        Image1.Visible = true;
        Image1.ImageUrl      =      "~/SW-input      files/4A-AutoDock/"      +
bdrow[0][3].ToString();
        ViewState["FileName"] = bdrow[0][3].ToString();

        //check file exists
        if (!System.IO.File.Exists(Server.MapPath(Image1.ImageUrl)))
        {
            Label5.Visible = true;
            Label5.Text  =  DropDownList1.SelectedValue.ToString() + " did not
produce considerable binding poses with " + DropDownList2.SelectedValue.ToString();
            btndownload.Visible = false;
            btndwnpdb.Visible = false;
            Image1.Visible = false;
            return;
        }
        else
        {
            Label5.Visible = false;
            btndownload.Visible = true;
            btndwnpdb.Visible = false;
            //divref2.Visible = true
            //divref1.Visible = false;
        }
    }

//modified 19/7 based on drop down value
//code to be executed if 4A-Glide is selected in Protein- Ligand Interaction

```

```

if      (DropDownList3.SelectedItem.Value.ToString().Trim().CompareTo("4A-
Glide") == 0)
{
    Label4.Visible = false;
    Label5.Visible = false;

    Image1.Visible = true;
    Image1.ImageUrl = "~/SW-input files/4A-Glide/" + bdrow[0][5].ToString();
    ViewState["FileName"] = bdrow[0][5].ToString();
    //check file exists
    if (!System.IO.File.Exists(Server.MapPath(Image1.ImageUrl)))
    {
        Label5.Visible = true;
        Label5.Text = DropDownList1.SelectedValue.ToString() + " did not
produce considerable binding poses with " + DropDownList2.SelectedValue.ToString();
        btndownload.Visible = false;
        btndwnpdb.Visible = false;
        Image1.Visible = false;
        return;
    }
    else
    {
        Label5.Visible = false;
        btndownload.Visible = true;
        btndwnpdb.Visible = false;
        //divref2.Visible = true
        //divref1.Visible = false;
    }
}
//if
(DropDownList3.SelectedItem.Value.ToString().Trim().CompareTo("Binding_Pocket") ==
0)
//code to be executed if Bonded_Interactions is selected in Protein- Ligand Interaction

if
(DropDownList3.SelectedItem.Value.ToString().Trim().CompareTo("Bonded_Interactions") ==
0)
{
    Label4.Visible = false;
    Label5.Visible = false;

    Image1.Visible = true;
    Image1.ImageUrl =     "~/SW-input     files/Bonded_Interactions/" +
bdrow[0][3].ToString();
    ViewState["FileName"] = bdrow[0][3].ToString();
    //check file exists
    if (!System.IO.File.Exists(Server.MapPath(Image1.ImageUrl)))
    {
        Label5.Visible = true;
    }
}

```

```

Label5.Text = DropDownList1.SelectedValue.ToString() + " Did not
produce considerable binding poses with " + DropDownList2.SelectedValue.ToString();
btndownload.Visible = false;
btndwnpdb.Visible = false;
Image1.Visible = false;
return;
}
else
{
    Label5.Visible = false;
    btndownload.Visible = true;
    btndwnpdb.Visible = false;
    //divref2.Visible = true
    //divref1.Visible = false;
}
}

//Code to be executed if Comparing_AutoDock_with_Glide is selected in Protein- Ligand
Interaction

if
(DropDownList3.SelectedItem.Value.ToString().Trim().CompareTo("Comparing_AutoDock
_with_Glide") == 0)
{
    Label4.Visible = false;
    Label5.Visible = false;

    Image1.Visible = true;
    Image1.ImageUrl = "~/SW-input files/Comparing_AutoDock_with_Glide/" +
bdrow[0][7].ToString();
    ViewState["FileName"] = bdrow[0][7].ToString();
    //check file exists
    if (!System.IO.File.Exists(Server.MapPath(Image1.ImageUrl)))
    {
        Label5.Visible = true;
        Label5.Text = DropDownList1.SelectedValue.ToString() + " Did not
produce considerable binding poses with " + DropDownList2.SelectedValue.ToString();
        btndownload.Visible = false;
        btndwnpdb.Visible = false;
        Image1.Visible = false;
        return;
    }
    else
    {
        Label5.Visible = false;
        btndownload.Visible = true;
        btndwnpdb.Visible = false;
        //divref2.Visible = true
        //divref1.Visible = false;
    }
}

```

```

//if
(DropDownList3.SelectedItem.Value.ToString().Trim().CompareTo("Molecular_Dynamic_Simulation") == 0)
//{
//  Label4.Visible = false;
//  Label5.Visible = false;

//  Image1.Visible = true;
//  Image1.ImageUrl = "~/SW-input files/Molecular Dynamic Simulation/" +
bdrow[0][7].ToString();
//  ViewState["FileName"] = bdrow[0][7].ToString();
// //check file exists
// if (!System.IO.File.Exists(Server.MapPath(Image1.ImageUrl)))
// {
//   Label5.Visible = true;
//   Label5.Text = DropDownList1.SelectedValue.ToString() + " did not
produce considerable binding poses with " + DropDownList2.SelectedValue.ToString();
//   btndownload.Visible = false;
//   btndwnpdb.Visible = false;
//   Image1.Visible = false;
//   return;
// }
// else
// {
//   Label5.Visible = false;
//   btndownload.Visible = true;
//   btndwnpdb.Visible = false;
// }
//}
//code to be executed if PDB_Files is selected in Binding Ligand Interation

```

```

if
(DropDownList3.SelectedItem.Value.ToString().Trim().CompareTo("PDB_Files") == 0)
{
  Label4.Visible = false;
  Label5.Visible = false;

  filePath = Server.MapPath("~/SW-input files/PDB_Files/");
  fileName = bdrow[0][8].ToString();

  //check file exists
  if (!System.IO.File.Exists(filePath + fileName))
  {
    Label5.Visible = true;
    Label5.Text = DropDownList1.SelectedValue.ToString() + " Did not
produce considerable binding poses with " + DropDownList2.SelectedValue.ToString();
    btndownload.Visible = false;
    Image1.Visible = false;
    return;
  }
}

```

```

        }
    else
    {
        ViewState["PDBFilePath"] = filePath;
        ViewState["PDBFileName"] = fileName;

        Label5.Visible = false;
        btndownload.Visible = false;
        Image1.Visible = false;
        btndwnpdb.Visible = true;
    }

}

}
else
{
    Label4.Visible = false;
    Label5.Visible = false;

    Image1.Visible = false;

}

}

catch (Exception ex)
{
    Response.Write(ex.Message);
}

protected void btndownload_Click(object sender, EventArgs e)
{
//code to be executed if Download Button is clicked. On clicking Lipro Interact will download respective image file

try
{
    byte[] bytes = System.IO.File.ReadAllBytes(Server.MapPath(Image1.ImageUrl));

    Response.Clear();
    //Response.ContentType = "image/png";
    Response.Cache.SetCacheability(HttpCacheability.Private);
    Response.Expires = -1;
    Response.Buffer = true;
    Response.AddHeader("Content-Disposition", string.Format("{0};FileName=\"{1}\"", "attachment", ViewState["FileName"].ToString()));
    Response.BinaryWrite(bytes);
    Response.End();
}

catch (Exception ex)

```

```

        {
    }
}
protected void btndwnpdb_Click(object sender, EventArgs e)
{
//code to be executed if Download PDB File Button is clicked.On clicking Lipro Interact
//will download respective PDBfile

    try
    {
        byte[] bytes = System.IO.File.ReadAllBytes(ViewState["PDBFilePath"].ToString() +
ViewState["PDBFileName"].ToString());
        Response.Clear();
        Response.ContentType = "application/pdb";
        Response.Cache.SetCacheability(HttpCacheability.Private);
        Response.Expires = -1;
        Response.Buffer = true;
        Response.AddHeader("Content-Disposition", string.Format("{0};FileName=\"{1}\"",
"attachment", ViewState["PDBFileName"].ToString()));
        Response.BinaryWrite(bytes);
        Response.End();
    }
    catch (Exception ex)
    {
    }
}
protected void Button1_Click(object sender, EventArgs e)
{
    Response.Redirect("Experiment.aspx");
}
protected void Button2_Click(object sender, EventArgs e)
{
    Response.Redirect("Welcome.aspx");
}
}

```

### Third Page-Design

*//Design page for Lipro Interact Software for the Binding Interactions of Lipid Ligands*

```

<%@ Page Language="C#" AutoEventWireup="true" CodeFile="Experiment.aspx.cs"
Inherits="Software1" %>

<!DOCTYPE html PUBLIC "-//W3C//DTD XHTML 1.0 Transitional//EN"
"http://www.w3.org/TR/xhtml1/DTD/xhtml1-transitional.dtd">

<html xmlns="http://www.w3.org/1999/xhtml">
<head id="Head1" runat="server">
<title></title>

```

```

<link rel="stylesheet" type="text/css" href="css/style.css" />
<style type="text/css">
    .style1
    {
        width: 114px;
    }
</style>
</head>
<body>
    <form id="form1" runat="server">
        <div>

            <div id="Div1" style="width:100%; text-align:center" >
                <br/>
                <asp:Image ID="Image2" ImageUrl="~/Images/BG3.png" runat="server"
                    Height="85px" Width="100%" />
                <br />
                <%--<asp:Image ID="Image2" ImageUrl="~/Images/Title.png" 
runat="server" /%>-->
                    <asp:Image ID="Image4" ImageUrl="~/Images/1234.png"
                    runat="server" style="position: absolute; top: 22px; left: 496px;" 
                    ImageAlign="Middle"/>
                <br />
            </div>

            <div id="Div2" style="width:100%; text-align:center;font-family:Algerian;font-size:xx-
large">
                LIPRO INTERACT SOFTWARE FOR THE</br>
                BINDING INTERACTIONS OF LIPID LIGANDS
            </div>

            <table style="position: absolute; top: 200px; left: 86px;">
                <tr>
                    <td style="height:20px">
                    </td></tr>

                <tr>
                    <td>
                        <asp:Label ID="Label1" runat="server" Font-Bold="True" font-size="X-Large"
                            Text="Choose Protein" ForeColor="Black"
                            Font-Italic="False" Font-Names="Georgia"></asp:Label>
                    </td>
                    <td>

                        <asp:DropDownList ID="DropDownList1" runat="server"
                            onselectedindexchanged="DropDownList1_SelectedIndexChanged"
                            CssClass="style_Normal_Dropdown" AutoPostBack="true" font-size="Large"
                            Font-Names="Georgia">

```

```

</asp:DropDownList>

</td>
</tr>
<tr>
<td style="height:10px">
</td></tr>
<tr>

<td>
<asp:Label ID="Label2" runat="server" Font-Bold="True" Text="Validation"
    ForeColor="Black" font-size="X-Large" Font-Names="Georgia"></asp:Label>
</td>
<td>
    <asp:DropDownList ID="DropDownList2" runat="server"
        onselectedindexchanged="DropDownList2_SelectedIndexChanged"
        AutoPostBack="true" font-size="Large"
        Font-Names="Georgia">
        </asp:DropDownList>
    </td>
</tr>
<tr>
<td style="height:10px">
</td></tr>
<%-- <tr>

<td>
    <asp:Label ID="Label3" runat="server" Font-Bold="True" Text="Protein-Ligand
Interaction"
        ForeColor="Black" font-size="X-Large" Font-Names="Georgia"></asp:Label>
</td>
<td>
    <asp:DropDownList ID="DropDownList3" runat="server"
        onselectedindexchanged="DropDownList3_SelectedIndexChanged"
        AutoPostBack="true" font-size="Medium" Font-Names="Calibri">
        </asp:DropDownList>
    </td>
</tr>--%>
</table>
<table style="position: absolute; top: 342px; left: 0px;">
<%-- <tr>
<td style="width:300px"></td>
<td>
    <asp:Label ID="Label4" runat="server" Font-Bold="True" Visible="False"
        ForeColor="Black" Text="Binding Energy" font-size="Large" Font-
Names="Calibri"></asp:Label>
    </td>
<td>
    <asp:Label ID="Label5" runat="server" Font-Bold="True" Visible="False"

```

```

    ForeColor="Black" Font-Names="Calibri" font-size="Large">></asp:Label>
</td>
</tr>--%>
<tr>
    <td style="position: absolute; left: 400px;">
        <%--<asp:Button Visible="false" ID="btndwnpdb" runat="server"
            Text="Download PDB File" onclick="btndwnpdb_Click" font-size="Medium"
            Font-Names="Calibri" BackColor="Black" Font-Bold="True"
            ForeColor="White" />--%>
<%--      </td>
<td> --%>           <asp:Button Visible="false" ID="btndownload" runat="server"
Text="Download Image File"
            onclick="btndownload_Click" font-size="Medium"
            BackColor="Black"   Font-Bold="True"   ForeColor="White"   Height="40px"
Width="200px"   Font-Names="Georgia" />

</td>
</tr>
</table>

<table style="position: absolute; top: 200px; left: 900px;">
<tr>
    <td>
        &nbsp;</td>
    </tr>
    <tr>
        <td>
            <asp:Image   Height="600px"   Width="600px"   ID="Image1"   Visible="false"
runat="server" />
        </td>
    </tr>
    <tr>
        <td>
            </td>
        </tr>
    </table>
</div>

<table >
    <tr>
        <td style="position: absolute; top: 850px;left: 200px">
            <asp:Button ID="Button2" runat="server" Text="Previous" Font-Size="Large"

```

```

    Height="40px" Width="100px" onclick="Button2_Click" Font-Names="Georgia"
    BackColor="Black" Font-Bold="True" ForeColor="White" />
  </td>

</tr>

</table>

</form>

</body>
</html>
```

### **Third Page-Code-behind file**

```

using System;
using System.Collections.Generic;
using System.Linq;
using System.Web;
using System.Web.UI;
using System.Web.UI.WebControls;
using System.Data;
using System.Data.SqlClient;

public partial class Software1 : System.Web.UI.Page
{
  DataSet _dstMain = new DataSet();
  //int Protein_id, Ligand_id;
  string Protein_id = string.Empty;
  string Ligand_id = string.Empty;
  string Binding_Energy_val = string.Empty;
  string filePath = string.Empty;
  string fileName = string.Empty;

  protected void Page_Load(object sender, EventArgs e)
  {
    try
    {
      if (!Page.IsPostBack)
      {
        //divref2.Visible = false;

//Code to read the content from XML file and store in dataset.

      _dstMain.ReadXml(Server.MapPath("~/Data/Data.xml"));

      ViewState["_dstMain"] = _dstMain;

//Code to bind data to protein dropdown.
```

```

DropDownList1.Items.Add("--Select--");
DropDownList1.Items.Add("PPAR $\alpha$ ");
DropDownList1.Items.Add("PPAR $\gamma$ ");
DropDownList1.Items.Add("COX2");
DropDownList1.Items.Add("CB1");
DropDownList1.Items.Add("CB2");

```

**//Code to bind data to validation dropdown.**

```

DropDownList2.Items.Add("--Select--");
DropDownList2.Items.Add("AutoDock Vs Wet laboratory Experiment");
DropDownList2.Items.Add("Glide Vs Wet laboratory Experiment");

}

}

catch (Exception ex)
{
}

}

```

```

protected void DropDownList1_SelectedIndexChanged(object sender, EventArgs e)
{
}

```

**//Code to be executed if Protein is selected.**

```

try
{
}

DropDownList2.SelectedIndex = 0;
btndownload.Visible = false;
Image1.Visible = false;

}

catch (Exception ex)
{
}
}

```

```

protected void DropDownList2_SelectedIndexChanged(object sender, EventArgs e)
{
}

```

**//Code to be executed if Validation is selected.**

```

try
{
    if (DropDownList2.SelectedIndex == 0)
    {
        btndownload.Visible = false;
        Image1.Visible = false;
        return;
    }
}

```

```

}

//Code to be executed if PPARα as Protein

if (DropDownList1.SelectedIndex != 0 && DropDownList2.SelectedIndex != 0)
{
    if (DropDownList1.SelectedItem.Value.ToString().Trim().CompareTo("PPARα")
== 0)
    {
//Code to be executed if AutoDock Vs Wet laboratory Experiment from validation
        if
(DropDownList2.SelectedItem.Value.ToString().Trim().CompareTo("AutoDock     Vs     Wet
laboratory Experiment") == 0)
        {
            Image1.Visible = true;
            Image1.ImageUrl = "~/SW-input files/SPA Vs AutoDock/PPARα.png";
            btndownload.Visible = true;
            ViewState["FileName"] = "PPARα.png";
        }
//Code to be executed if Glide Vs Wet laboratory Experiment from validation
        else
if
(DropDownList2.SelectedItem.Value.ToString().Trim().CompareTo("Glide     Vs     Wet
laboratory Experiment") == 0)
        {
            Image1.Visible = true;
            Image1.ImageUrl = "~/SW-input files/SPA Vs Glide/PPARα.png";
            btndownload.Visible = true;
            ViewState["FileName"] = "PPARα.png";
        }
    }

//Code to be executed if PPARγ from protein

else
if
(DropDownList1.SelectedItem.Value.ToString().Trim().CompareTo("PPARγ") == 0)
{
//Code to be executed if AutoDock Vs Wet laboratory Experiment from validation
    if
(DropDownList2.SelectedItem.Value.ToString().Trim().CompareTo("AutoDock     Vs     Wet
laboratory Experiment") == 0)
    {
        Image1.Visible = true;
        Image1.ImageUrl = "~/SW-input files/SPA Vs AutoDock/PPARγ.png";
        btndownload.Visible = true;
        ViewState["FileName"] = "PPARγ.png";
    }
//Code to be executed if Glide Vs Wet laboratory Experiment from validation
}
}

```

```

        else if
(DropDownList2.SelectedItem.Value.ToString().Trim().CompareTo("Glide Vs Wet laboratory Experiment") == 0)
{
    Image1.Visible = true;
    Image1.ImageUrl = "~/SW-input files/SPA Vs Glide/PPARg.png";
    btndownload.Visible = true;
    ViewState["FileName"] = "PPARg.png";
}
}

//Code to be executed if COX2 from protein

else if
(DropDownList1.SelectedItem.Value.ToString().Trim().CompareTo("COX2") == 0)
{
}

//Code to be executed if AutoDock Vs Wet laboratory Experiment from validation

if
(DropDownList2.SelectedItem.Value.ToString().Trim().CompareTo("AutoDock Vs Wet laboratory Experiment") == 0)
{
    Image1.Visible = true;
    Image1.ImageUrl = "~/SW-input files/SPA Vs AutoDock/COX2.png";
    btndownload.Visible = true;
    ViewState["FileName"] = "COX2.png";
}

//Code to be executed if Glide Vs Wet laboratory Experiment from validation

else if
(DropDownList2.SelectedItem.Value.ToString().Trim().CompareTo("Glide Vs Wet laboratory Experiment") == 0)
{
    Image1.Visible = true;
    Image1.ImageUrl = "~/SW-input files/SPA Vs Glide/COX2.png";
    btndownload.Visible = true;
    ViewState["FileName"] = "COX2.png";
}

//Code to be executed if CB1from protein

else if (DropDownList1.SelectedItem.Value.ToString().Trim().CompareTo("CB1") == 0)
{
}

//Code to be executed if AutoDock Vs Wet laboratory Experiment from validation

if
(DropDownList2.SelectedItem.Value.ToString().Trim().CompareTo("AutoDock Vs Wet laboratory Experiment") == 0)

```

```

{
    Image1.Visible = true;
    Image1.ImageUrl = "~/SW-input files/SPA Vs AutoDock/CB1.png";
    btndownload.Visible = true;
    ViewState["FileName"] = "CB1.png";
}
//Code to be executed if Glide Vs Wet laboratory Experiment from validation

else if (DropDownList2.SelectedItem.Value.ToString().Trim().CompareTo("Glide      Vs      Wet
laboratory Experiment") == 0)
{
    Image1.Visible = true;
    Image1.ImageUrl = "~/SW-input files/SPA Vs Glide/CB1.png";
    btndownload.Visible = true;
    ViewState["FileName"] = "CB1.png";
}
}
//Code to be executed if CB2from protein

else if (DropDownList1.SelectedItem.Value.ToString().Trim().CompareTo("CB2") == 0)
{
//Code to be executed if AutoDock Vs Wet laboratory Experiment from protein

if (DropDownList2.SelectedItem.Value.ToString().Trim().CompareTo("AutoDock      Vs      Wet
laboratory Experiment") == 0)
{
    Image1.Visible = true;
    Image1.ImageUrl = "~/SW-input files/SPA Vs AutoDock/CB2.png";
    btndownload.Visible = true;
    ViewState["FileName"] = "CB2.png";
}
}
//Code to be executed if Glide Vs Wet laboratory Experiment from protein

else if (DropDownList2.SelectedItem.Value.ToString().Trim().CompareTo("Glide      Vs      Wet
laboratory Experiment") == 0)
{
    Image1.Visible = true;
    Image1.ImageUrl = "~/SW-input files/SPA Vs Glide/CB2.png";
    btndownload.Visible = true;
    ViewState["FileName"] = "CB2.png";
}
}
}
}

catch (Exception ex)

```

```
{  
}  
}  
  
protected void btndownload_Click(object sender, EventArgs e)  
{  
    //code to be executed to download respective Image file  
    try  
    {  
        byte[] bytes = System.IO.File.ReadAllBytes(Server.MapPath(Image1.ImageUrl));  
  
        Response.Clear();  
        //Response.ContentType = "image/png";  
        Response.Cache.SetCacheability(HttpCacheability.Private);  
        Response.Expires = -1;  
  
        Response.Buffer = true;  
        Response.AddHeader("Content-Disposition", string.Format("{0};FileName=\"{1}\\"",  
        "attachment", ViewState["FileName"].ToString()));  
        Response.BinaryWrite(bytes);  
        Response.End();  
    }  
    catch (Exception ex)  
    {  
    }  
}  
  
protected void Button2_Click(object sender, EventArgs e)  
{  
    //code to be executed to redirect to software.aspx page  
    Response.Redirect("Software.aspx");  
}
```